eman ta zabal zazu

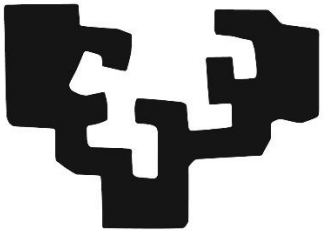

Universidad del País Vasco

Euskal Herriko Unibertsitatea

Click Reactions: An Efficient Tool Towards Biofunctional Materials

Klik Erreakzioak: Material Biofuntzionalen Biderako Metodo Eraginkorra

Julia Sánchez Bodón

2024

Directores: Dra. Isabel Moreno Benítez

Prof. José Luis Vilas Vilela

eman ta zabal zazu

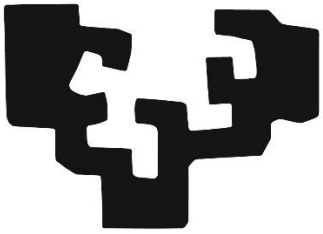

Universidad del País Vasco

Euskal Herriko Unibertsitatea

Click Reactions: An Efficient Tool Towards Biofunctional Materials

Klik Erreakzioak: Material Biofuntzionalen Biderako Metodo Eraginkorra

Julia Sánchez Bodón

2024

Supervisors: Dra. Isabel Moreno Benítez

Prof. José Luis Vilas Vilela

A mi ama

A Shei

to my mom

to Shei

Como no estás experimentado en las cosas del mundo, todas las cosas que tienen algo de dificultad, te parecen imposibles. Confía en el tiempo, que suele dar dulces salidas, a muchas amargas dificultades.

Miguel de Cervantes Saavedra

Don Quijote de la Mancha. SXVII

Table of contents

Abstract

Biomaterials are defined as substrates that actively interact with biological systems, serving purposes like assessment, treatment, healing or the replacement of tissues. Beyond biocompatibility, every biomaterial device must meet fundamental functional requirements, including safety, durability and biofunctionality. In recent decades, the development of biomedical materials capable of establishing enduring and remarkable interactions with human cells and proteins, while simultaneously preventing bacterial contamination has been extensively studies. Among biomedical materials, three main types are recognized: ceramics, polymers and metals. Despite their appealing characteristics, such as hardness, ductility or excellent mechanical properties, they still present some limitations. Indeed, many biomedical devices are susceptible to bacterial infection and often lack efficient biointegration. It has to be noted that numerous studies have concluded that a rapid integration of the implant could avoid bacterial adhesion and colonization. In fact, the competition of host cell and bacteria, known as "race for the surface" is a critical factor for the successful integration of biomaterials into host tissues.

Additionally, studies have affirmed that surface characteristics encompassing factors such as a topography, wettability, charge and chemical properties, play a pivotal role in governing the adhesion and growth of proteins, cells and bacteria. Consequently, these properties exert a profound influence on hemo- and biocompatibility. Recognizing the paramount importance of these surface attributes, researchers have underscored the need for modifying implants to optimize the hemo- and bio-integration, thereby mitigating inflammatory responses and bacterial adhesion. Recent research delving into enhancements in host tissue response and antibacterial properties of diverse materials has highlighted the potential efficacy of surface modification technologies. These approaches are essential to restrict and prevent bacterial contamination, while promoting proper cells and proteins adhesion. It is noteworthy that both physical treatments, like patterning, and chemical, such as hydrolysis, aminolysis, or functionalization, alongside with strategies such as drug delivery and bioactive molecules immobilization, have proven to be effective methodologies in achieving the mentioned objective. These approaches can directly or indirectly influence the activity of components within the immune system, presenting promising avenues for improving overall biomaterial performance.

At the intersection of chemistry and molecular biology, bioconjugation involves covalently linking biomolecule structures to synthetic or natural labels. This interdisciplinary field focuses on biocompatible reactions, such as click reactions, that rapidly, efficiently and selectively connect biomolecules with substrates. Challenges,

such as attaching small molecular probes (e.g., fluorescent dyes, radical probes or affinity tags) to biopolymers or linking complex carbohydrates with peptides, can be addressed through click reactions. Overall, the concept of Click Chemistry described the formation of C-heteroatom and C-C bond reactions that produce products with exceptional efficiency and selectivity. This innovative approach has proved to be a versatile and invaluable method for the seamless construction of complex structures by effectively combining smaller molecules through a limited set of highly efficient reactions.

This Doctoral Thesis extensively explores the application of diverse click reactions, notably encompassing the Copper (I) Catalyzed Azide Alkyne Cycloaddition and its activated acetylene copper-free variant, alongside innovative amino-yne and thiol-yne click reactions. These powerful tools have been employed for the precise bioconjugation of various drugs, including anti-inflammatory, antibiotic and anticoagulant biomolecules, onto both polymer and metal surfaces. These research includes several chemical functionalization strategies, including hydrolysis, amidation reactions, plasma treatments and self-assembled monolayer (SAM) formation, in order to facilitate the efficient binding of the drugs to the surfaces. A comprehensive understanding of the state-of-the-art surface analysis techniques has ensured rigorous characterization of each modified surface. This in-depth exploration not only contributed to the advancement of Click Chemistry applications, but also provides valuable insights into the tailored functionalization of surfaces for enhanced biomedical applications.

Resumen

Los biomateriales se definen como sustratos que interactúan activamente con los sistemas biológicos, sirviendo para fines como el diagnóstico, el tratamiento, la curación o el reemplazo de tejidos. Más allá de la biocompatibilidad, todo biomaterial debe cumplir varios requisitos fundamentales, que incluyen la seguridad, durabilidad y biofuncionalidad. En las últimas décadas, se ha realizado un estudio exhaustivo centrado en el desarrollo de materiales biomédicos capaces de establecer interacciones prolongadas y adecuadas con células y proteínas humanas, mientras previene la contaminación bacteriana. Entre los materiales biomédicos, se reconocen tres tipos de materiales principales: cerámicos, polímeros y metales. A pesar de sus características atractivas como las propiedades mecánicas, todavía presentan algunas limitaciones. Muchos de los dispositivos biomédicos son susceptibles a la infección bacteriana y a menudo carecen de una eficiente biointegración. Es más, numerosos estudios han demostrado la importancia de una rápida integración para evitar así la adhesión y colonización bacteriana. De hecho, la competencia entre las células del huésped y las bacterias, conocida como "carrera por la superficie", es un factor crítico para la integración exitosa de los implantes en los tejidos del huésped.

Numerosos estudios han afirmado que características superficiales, tales como la topografía, la humectabilidad, la carga y las propiedades químicas, desempeñan un papel fundamental a la hora de regular la adhesión y el crecimiento de proteínas, células y bacterias. Por consiguiente, estas propiedades ejercen una profunda influencia en la hemo- y biocompatibilidad. Reconociendo la importancia primordial de estos atributos superficiales, los investigadores han subrayado la necesidad de modificar los implantes para optimizar la hemo- y bio-integración, mitigando así las respuestas inflamatorias y la adhesión bacteriana. Investigaciones recientes sobre la mejora de la respuesta del tejido huésped y las propiedades antibacterianas de diversos materiales han puesto de relieve la eficacia potencial de las tecnologías de modificación de superficies. Estos enfoques son esenciales para restringir y prevenir la contaminación bacteriana, al mismo tiempo que promueven la correcta adhesión de células y proteínas. Cabe destacar que tanto los tratamientos físicos (modelización), como los químicos (hidrólisis, aminólisis o funcionalización), junto con estrategias como la administración de fármacos y la inmovilización de moléculas bioactivas, han demostrado ser metodologías eficaces para lograr el objetivo mencionado anteriormente. Estas estrategias pueden influir directa o indirectamente en la actividad de los componentes del sistema inmunitario, lo que supone una vía prometedora para la mejora del rendimiento general de los biomateriales.

La bioconjugación, que consiste en unir covalentemente biomoléculas con otros materiales sintéticos o naturales, se encuentra en la frontera entre la Química y la Biología Molecular. Este campo interdisciplinar se centra en reacciones biocompatibles, como las reacciones click, que conectan biomoléculas con sustratos de forma rápida, eficaz y selectiva. Las reacciones click permiten afrontar retos como la unión de pequeñas sondas moleculares (por ejemplo, tintes fluorescentes, sondas radicales o etiquetas de afinidad) a biopolímeros o la unión de carbohidratos complejos con péptidos. En general, el concepto de química click describe reacciones de formación de enlaces C-heteroátomo y C-C que producen productos con una eficacia y selectividad excepcionales. Este enfoque innovador ha demostrado ser un método versátil e inestimable para la construcción de estructuras complejas mediante la combinación eficaz de moléculas más pequeñas a través de un conjunto limitado de reacciones altamente eficientes.

Esta Tesis Doctoral se enfoca en la aplicación de diversas reacciones de click, como la Cicloadición entre Azida y Alquino Catalizada por Cobre (I), así como su última variante, la reacción entre azida y alquino activo en ausencia de catalizador, junto con las innovadoras reacciones click amino-ino y tiol-ino. Estas reacciones se han empleado para la bioconjugación precisa de diversos fármacos, antiinflamatorios, antibióticas y anticoagulantes, entre otros, sobre superficies poliméricas y metálicas. Estas investigaciones incluyen varias estrategias de funcionalización química, como hidrólisis, reacciones de amidación, tratamientos con plasma y formación de monocapas autoensambladas (SAM), para facilitar la unión eficaz de los fármacos a las superficies. Un conocimiento exhaustivo de las técnicas más avanzadas de análisis de superficies ha garantizado una caracterización rigurosa de cada superficie modificada. Esta exploración en profundidad no sólo ha contribuido al avance de las aplicaciones de la Química del Click, sino que, además, proporciona valiosos conocimientos sobre la precisa funcionalización de superficies para su mejora en aplicaciones biomédicas.

Laburpena

Biomaterialak sistema biologikoekin aktiboki elkar egiten duten substratu gisa definitzen dira. Izan ere, zenbait helburuetarako erabiltzen dira: ehunen ebaluazioa, tratamendua, sendaketa edo ordezkapena. Biobateragarritasunaz gain, oro har biomaterial batek oinarrizko eginkizun batzuk bete behar ditu, besteak beste, segurtasuna, iraunkortasuna eta biofuntzionalizazioa. Azken hamarkadetan, bakterioen kutsadura saihesten duten eta giza zelula eta proteinekin elkarrekintza iraunkorrak eta nabarmenak sortzeko gai diren material biomedikoen garapena sakonki ikertu egin da. Material biomedikoen artean, hiru bereizten dira nagusiki: zeramikoak, polimeroak eta metalak. Ezaugarri erakargarriak izan arren, hala nola, gogortasuna, harikortasuna edo propietate mekaniko bikainak, zenbait muga aurkezten dituzte. Oraindik ere, gailu biomediko askok infekzio bakterianoa jasan dezakete eta, sarritan, ez dute beharrezko biointegrazioa pairatzen. Gainera, hainbat ikerketen arabera, biomaterialaren integrazioa azkarrak bakterioen atxikimendua eta kolonizazioa saihes dezake. Izan ere, ostalariaren zelulen eta bakterioen arteko lehia, "gainazalaren aldeko lasterketa" bezala ezagutzen dena, inplanteak ostalariaren ehunetan arrakastaz integratzeko faktore kritikoa da.

Ikerketa ugarik adierazi dutenez, gainazaleko propietateek, hala nola, topografiak, bustigarritasunak, kargak eta propietate kimikoak, funtsezko zeregina dute proteina, zelula eta bakterioen atxikimendua eta hazkundea arautzeko orduan. Izan ere, propietate horiek hemo- eta biobateragarritasunean eragin sakona erakutsi dute. Gainazaleko ezaugarri horien funtsezko garrantzia kontuan hartuz, ikertzaileek inplanteen eraldaketen beharra azpimarratu dute hemo-eta bio-integrazioa hobetzeko, hanturazko erantzuna eta bakterioen atxikimendua arintzen dirn bitartean. Ehun ostalariaren erantzuna hobetu duten inplanteen eta bakterioen aurkako propietateak dituzten materialen buruzko azken ikerketek agerian utzi dute gainazalak eraldatzeko teknologien eraginkortasuna. Hala, ikuspegi horiek funtsezkoak baitira bakterioen kutsadura murrizteko eta prebenitzeko, zelulen eta proteinen atxikimendua sustatzen duten bitartean. Azpimarratzekoa da, bai tratamendua fisikoa (modelizazioa), bai kimikoa (hidrolisia, aminolisia edo funtzionalizazioa), bai farmakoen askapena eta molekula bioaktiboen immobilizazioa estrategia eraginkorrak direla aipatutako helburua lortzeko. Estrategia horiek zuzenean edo zeharka sistema immunearen osagaien jardueretan eragin ditzakete, etorkizun handiko bidea izanik biomaterialen errendimendua hobetzeko.

Kimika eta biologia molekularraren elkargunearen artean biokonjugazioa kokatzen da, hau da, biomolekulak beste material sintetiko edo natural batekin kobalenteki lotzeari biokonjugazioa deitzen zaio. Diziplina arteko eremu honek erreakzio

biobateragarriak ditu ardatz, hala nola, klik erreakzioak. Izan ere, biomolekulak substratuekin azkar, eraginkortasunez eta modu selektiboan konektatzen dituzten erreakzioak dira. Klik erreakzioek hainbat erronkari aurre egiteko aukera ematen dute: zuntza molekular txikiak (adibidez, tinta fluoreszenteak, zuntz erradikalak edo afinitate etiketak) biopolimeroei lotzea edo karbohidrato konplexuak peptidoekin lotzea. Oro har, Klik Kimika C-heteroatomo eta C-C loturen eraketa deskribatzen duten erreakzioak dira, baina hauek produktuen ekoizpena eraginkortasunez eta modu oso selektiboki lortzen dute. Estrategia berritzaile hau oso moldakorra da eta, molekula txikiagoak modu eraginkorrean konbinatuz, egitura konplexuak eraikitzen ditu hausturarik gabe.

Doktoretza-tesi hau hainbat klik erreakzioen aplikazioan oinarritzen da, hala nola, kobrez (I) katalizaturiko azida eta alkinoaren arteko zikloadizioa, edota, bere azken bertsioa, aktibatutako alkino taldearen bidezko kobre gabeko azida eta alkinoaren arteko erreakzioa, hauekin batera amino-ino eta tiol-ino klik erreakzioak ere aztertu egin dira. Erreakzio hauek gainazal polimeriko eta metalikoen gainean zenbait farmako, anti-inflamatorioa, antibiotiko eta antikoagulatzailea, besteak beste, biokonjugatzeko erabili dira. Farmakoak gainazalean modu eraginkorrean lotu daitezen, funtzionalizazio kimikoan oinarritzen diren zenbait estrategia erabili dira, hala nola, hidrolisia, amidazio-erreakzioak, plasmaren bidezko tratamenduak eta monokapa automuntatzaileen eraketa (SAM). Gainazalak aztertzeko ezagutzen diren teknika aurreratuen ikasketa zehatza burutu da, gainazal bakoitzaren karakterizazio zorrotza bermatzeko. Sakoneko azterketa hauek Klik Kimikaren aplikazioen aurrerapena suposatzeaz gain, gainazalen funtzionalizazio zehatzari buruzko ezagutza baliotsuak ematen ditu biomaterialen aplikazio biomedikoen hobekuntzarako.

CONTRIBUTIONS/*EKARPENAK*

PUBLICATIONS OF THIS THESIS/*TESI ARGITALPENAK*

Julia Sánchez-Bodón, Maria Diaz-Galbarriatu, Rebeca Sola-Llano, Leire Ruiz-Rubio, José Luis Vilas-Vilela 1,3 and Isabel Moreno-Benítez. Catalyst-Free Amino-Yne Click Reaction: An Efficient Way for Immobilizing Amoxicillin onto Polymeric Surfaces. *Polymers*, **2024**, 16, 246. DOI: https://doi.org/10.3390/polym16020246

Julia Sánchez-Bodón, Maria Diaz-Galbarriatu, Leyre Pérez-Álvarez, Isabel Moreno-Benítez and José Luis Vilas-Vilela. Strategies to Enhance Biomedical Device Performance and Safety: A Comprehensive Review. *Coatings*, **2023**, *13*, 1981. DOI: https://doi.org/10.3390/coatings13121981

Julia Sánchez-Bodón, Jon Andrade del Olmo, José María Alonso, Isabel Moreno-Benítez, José Luis Vilas-Vilela and Leyre Pérez-Álvarez. Bioactive Coatings on Titanium: A Review on Hydroxylation, Self-Assembled Monolayers (SAMs) and Surface Modification Strategies. *Polymers*, **2022**, *14*, 165. DOI: https://doi.org/10.3390/polym14010165

Julia Sánchez-Bodón, Leire Ruiz-Rubio, Estíbaliz Hernáez-Laviña, José Luis Vilas-Vilela and Mª Isabel Moreno-Benítez. Poly(L-lactide)-Based Anti-Inflammatory Responsive Surfaces for Surgical Implants. *Polymers*, **2021**, *13*, 34. DOI: https://dx.doi.org/10.3390/polym13010034

Publications in Basque/*Euskerazko argitalpenak*

Julia Sánchez-Bodón, Isabel Moreno-Benítez, Leyre Pérez-Álvarez, Leire Ruiz-Rubio, José Luis Vilas-Vilela. Click erreakzioa erabiliz aktibitate biologikoa erakusten duten sistema polimerikoen garapena. *Ekaia*, **2020**, *37*, 103-116. DOI: *https://doi.org/10.1387/ekaia.20847*

Julia Sánchez Bodón, Ane Garcia, Maria Diaz Galbarriatu, Ana Catarina Lopes, Isabel Moreno Benítez eta Jose Luis Vilas Vilela. Nobel Saridun Klik erreakzioaren baliagarritasuna konposatu biologikoak eransteko polimero gainazalean. *Inguma*, **2023**, *54*, 401-407. DOI: https://dx.doi.org/10.26876/ikergazte.v.05.51

In preparation/Prestatzen

Julia Sánchez-Bodón, Isabel Moreno-Benitez, José Manuela Laza, Asier Larrea-Sebal, Cesar Martin, Igor Irastorza, Unai Silvan, José Luis Vilas-Vilela. Multifunctional Curcumin-Based Polymer Coating: a promising platform against bacteria, inflammation and coagulation.

Julia Sánchez-Bodón, Maria Diaz-Galbarriatu, Ane García-García, Leire Ruiz-Rubio, José Luis Vilas-Vilela and Isabel Moreno-Benítez. Propiolic based copper-free click chemistry: A promising tool for bioconjugation onto PLLA surfaces.

Julia Sánchez-Bodón, Isabel Moreno-Benítez, Leire Ruiz-Rubio, Leyre Pérez-Álvarez, José Manuel Laza, José Luis Vilas-Vilela. Smart titanium surfaces for improving antibacterial properties. *Elsevier*. **2024**

Maria Diaz-Galbarriatu, Julia Sánchez-Bodón, Isabel Moreno-Benítez, José Luis Vilas-Vilela. Klik kimika, erabilera askotariko konposatuak eratzen dituen Nobel saridun erreakzioa. *Ekaia*, **2024**

OTHER PUBLICATIONS/*BESTE PUBLIKAZIOAK*

Silvia Soledad Rosales-Murillo, Julia Sánchez-Bodón, Saray L. Hernández Olmos, María Fernanda Ibarra-Vázquez, Luis Guillermo Guerrero-Ramírez, Leyre Pérez-Álvarez and José Luis Vilas-Vilela. Anthocyanin-Loaded Polymers as Promising Nature-Based, Responsive, and Bioactive Materials. *Polymers*, **2024**, *16*, 163. DOI: https://doi.org/10.3390/polym16010163

Cristina Monteserin, Miren Blanco, Nerea Uranga, Julia Sánchez, José Manuel Laza, José Luis Vilas, Estibaliz Aranzabe. Sustainable biobased epoxy thermosets with covalent dynamic imine bonds for green composite development. *Polymer*, **2023**, *285*, 126339. DOI: https://doi.org/10.1016/j.polymer.2023.126339

Alejandro Fidel Alba, Roberto Fernández-de Luis, Joseba Totoricaguena-Gorriño, Leire Ruiz-Rubio, Julia Sánchez, José Luis Vilas-Vilela, Senentxu Lanceros-Méndez, Francisco Javier del Campo. Understanding electrogenerated chemiluminescence at graphite screen-printed electrodes. *Journal of Electroanalytical Chemistry*, **2022**, *914*, 116331. DOI: https://doi.org/10.1016/j.jelechem.2022.116331

José Manuel Laza, Antonio Veloso-Fernández, Julia Sánchez-Bodón, Ane Martín, Amaia M. Goitandia, Cristina Monteserín, Xabier Mendibil, Karmele Vidal, Jon Lambarri, Estibaliz Aranzabe, Miren Blanco, José Luis Vilas-Vilela. Analysis of the influence of microencapsulated phase change materials on the behavior of a new

generation of thermo-regulating shape memory polyurethane fibers. *Polymer Testing*, **2022**, *116*, 107807. DOI: https://doi.org/10.1016/j.polymertesting.2022.107807

Leire Ruiz-Rubio, Julia Sánchez-Bodón, Isabel Moreno, Leyre Pérez-Álvarez, José Luis Vilas-Vilela. 7 Polyester-based biodegradable polymers for commodities. Sustainability of Polymeric Materials. De Gruyter. **2020**, Berlin/Boston. 135-172.

Leire Ruiz-Rubio, Leyre Pérez-Álvarez, Julia Sánchez-Bodón, Valeria Arrighi and José Luis Vilas-Vilela. The Effect of the Isomeric Chlorine Substitutions on the Honeycomb-Patterned Films of Poly(x-chlorostyrene)s/Polystyrene Blends and Copolymers via Static Breath Figure Technique. *Materials*, **2019**, *12*, 167. DOI: https://doi.org/10.3390/ma12010167

Basque publications/*Euskerazko argitalpenak*

Ane Araiz-Márquez, Julia Sánchez-Bodón, Antonio Veloso-Fernández, Leire Ruiz-Rubio, Isabel Moreno-Benítez, José Luis Vilas-Vilela. Eugenola: polimero jasangarrien biomasatik erauzitako lehengaia. *Ekaia*, **2023**, *43*, 27-40. DOI: https://doi.org/10.1387/ekaia.23782

CONGRES/*KONGRESUAK*

Oral Communications/*Ahozko Komunikazioa*

XXVI Encontro Galego Portugués de Química, **2022**. *Cómo minimizar el rechazo de implantes empleando la química click*. Julia Sánchez-Bodón, Isabel Moreno-Benítez, Leire Ruiz-Rubio, Leyre Pérez-Álvarez, Ana Catarina-Lopes, José Luis Vilas-Vilela.

XVI Reunión del Grupo Especializado de Polímeros – GEP 2022 y XVII Simposio Latinoamericano de Polímeros - SLAP 2022, **2022**. *Anti-inflammatory Poly(L-Lactide)-based biocoating for surgical Implants*. Julia Sánchez Bodón, Isabel Moreno Benítez, Leire Ruiz Rubio, José Luis Vilas Vilela**.**

XII Jornadas de Jóvenes Investigadores en Física Atómica y Molecular. **2020**. *Drugs Immobilization by Click reaction: A way to minimize implant rejection*. Julia Sánchez Bodón, Isabel Moreno Benítez, Leire Ruiz Rubio, and José Luis Vilas Vilela.

VI Jornadas de investigación de la Facultad de Ciencia y Tecnología. **2018**. *Azide-alkyne "click" reaction: A suitable methodology for drug immobilizationin polymeric materials*. Julia Sánchez Bodón, Isabel Moreno Benítez and José Luis Vilas Vilela.

Oral communications in Basque/*Euskerazko ahozko komunikazioak*

IkerGazte: Nazioarteko ikerketa euskaraz Kongresua. **2023**. *Nobel Saridun Klik erreakzioaren baliagarritasuna konposatu biologikoak eransteko polimero gainazalean*. Julia Sánchez Bodón, Ane Garcia, Maria Diaz Galbarriatu, Ana Catarina Lopes, Isabel Moreno Benítez and Jose Luis Vilas Vilela.

Materialen Zientzia eta Teknologia V. Kongresua. **2021**. *Antiinflammatorio baten immobilizazio kobalentea gainestaldura biodegradagarrien inplante kirurgikoen errefusa minimizatzeko*. Julia Sánchez-Bodón, Isabel Moreno-Benítez, Antonio Veloso, Leire Ruiz-Rubio, José Luis Vilas-Vilela.

Poster Communications/*Poster komunikazioak*

XVI Reunión del Grupo Especializado de Polímeros – GEP 2022 y XVII Simposio Latinoamericano de Polímeros - SLAP 2022, **2022**. *Anti-inflammatory Poly(L-Lactide)-based biocoating for surgical Implants*. Julia Sánchez Bodón, Isabel Moreno Benítez, Leire Ruiz Rubio, José Luis Vilas Vilela**.**

VII Jornadas de Investigación de la Facultad de Ciencia y Tecnología. **2020**. *The Chemistry of Polymers*.

3rd Biennial Young Researchers Workshop on Biomaterials and Applications. **2019**. *Drug immobilization by Click reaction: a way to minimize implant rejection*. Julia Sánchez Bodón, Isabel Moreno Benítez, Leire Ruiz Rubio, and José Luis Vilas Vilela.

Workshop: New Materials for a Better Life: Porous Structures as Key Enabling Materials for Advanced Technologies. **2018**. *Azide-alkyne "click" reaction: A suitable methodology for drug immobilization in polymeric surfaces*. Julia Sánchez Bodón, Leire Ruiz Rubio, Leyre Pérez Álvarez, Isabel Moreno Benítez and José Luis Vilas Vilela.

Poster communications in Basque/ Poster Komunikazioak euskeraz

IkerGazte: Nazioarteko ikerketa euskaraz Kongresua. **2021**. *Polimero biobateragarrien garapena biomedikuntzan erabiltzeko*. Julia Sánchez-Bodón, Antonio Veloso, Leire Ruiz-Rubio, Leyre Pérez-Álvarez, José Manuel Laza, Isabel Moreno-Benítez eta José Luis Vilas-Vilela.

II Jornadas Doctorales de la UPV/EHU. **2019**. *Farmako desberdinen gainazal immobilizazioa click erreakzioaren bidez inplanteen errefusa minimizatzeko*. Julia Sánchez Bodón, Isabel Moreno Benítez, Leyre Perez Álvarez, Leire Ruiz Rubio, José Luis Vilas Vilela.

CURSOS/*KURTSOAK*

COMUNICACIÓN VISUAL APLICADA A LA CIENCIA. (12 h) **2018**.

FUNDAMENTOS Y APLICACIONES DE LA ESPECTROSCOPÍA FOTOELECTRÓNICA DE RAYOS X (XPS). (20 h) **2019**.

IMAGEN DIGITAL EN MICROSCOPÍA (20 h). **2021**.

Abbreviations and acronyms

6-APA 6-aminopenicilanic acid
ALG Alginate
ALP Alkaline phosphate
AMP Antimicrobial peptide
APP Atmospheric Pressure Plasma
APTES (3-aminopropyl)triethoxysilane
Arg Arginine
AS Salicylic acid
ASA Acetyl salicylic acid
ASm Salicylic acid derivative **6a**
ATR-FTIR Attenuated Total Reflectance Fourier Transform Infrared
BF Before Christ
BG Biactive glass
BMS Bare-metal stents
BMTS Bacterial microtubules
BTMS bromotrimethylsilane
CFU Colony Forming Units
CHI Chitosan
Col I Collagen type I
COX Cyclooxygenase
CPTES (3-chloropropyl)triethoxysilane
CS Chondroitin
CuAAC Copper (I) Catalyzed Azide Alkyne Cycloaddition
Cur Curcumin
DCC N,N'-Dicyclohexylcarbodiimide
DEX Dexamethasone
DIBO dibenzocyclooctyne
DIFO Difluorinated cyclooctyne
DIPEA N,N'-Diisopropylethylamine
DMAP 4-dimethylaminopyridine
DMEM Dulbecco's Modified Eagle Medium
DMF N,N'-Dimethylformamide
DMSO Dimethyl sullfoxide
DMTA Differential Mechanical Thermal Analysis
Dns Dansyl
DSA Drop Shape Analysis System
DSC Differential Scanning Calorimetry
DSSD N,N'-(disulfanediylbis(ethane-2,1-diyl))bis(5-(dimethylamino)naphthalene-1-sulfonamide
EC Endotelial cell
ECM Extracelular amtrix
EDC·HCl 1-Ethyl-3-(3-dimethylaminopropyl)carbodiimide hydrochloride
ELISA Enzyme-linked immunosorbent assay
EPD Electrophoretic deposition

EPS Extracelular polymeric substances
Eq. Equivalents
ETDA Ethylendiamine
EtOAc Ethyl acetate
EtOH Ethanol
FBGC Foreign body giant cell
FBR Foreign body response
FBS Fetal Bovine Serum
FDA Food and Drug Agency
FTIR Fourier Transform Infrared Spectroscopy
GAGs Glycosaminoglycans
HA Hyaluronic acid
Hap hydroxyapatite
HDPE High-density polyethylene
HEP Heparin
HexVP N-hexylpyridinium bromide
HIV Human immunodeficiency virus
HOBT Hydrobenzotriazole
HUVEC Human umbilical vein endothelial cell
IAI Implanted-associate infection
IL-1β Interleukin 1 beta
IL-4 Interleukin 4
IL-6 Interleukin 6
Indo Indomethacin
J Coupling constant
LBL Layer by layer
LF1-11 Lactoferrin peptide
Lys Lysine
MAPK mitogen-activated protein kinase
MOFO Monofluorinated cyclooctyne
MSC Mesenchymal Stem Cell
MTS 3-(4,5-dimethylthiazol-2-yl)-5-(3-carboxymethoxyphenyl)-2-(4-sulfophenyl)-2H-tetrazolium
NHS N-hydyroxysuccinimide
NMR Nuclear Magnetic Resonance
NTAPPJ Non-Thermal Atmospheric Pressure Plasma Jet
Nu nucleophil
OCN Oseocalcin
Oct Cyclooctyne
PA Pathway A
PAA Polyacrylic acid
PB Pathway B
PBS Phosphate buffer solution
PCL Polycaprolactone
PDLA Poly-D-lactic acid
PEC Polyelectrolyte complex
PEG Polyethylen glucol

PEI Polyethyleneimine
PET Polyethyelene terephthalate
PHEMA Poly(hydroxyethyl methacrylate)
PLA Poly(lactic acid)
PLLA Poly-L-lactic acid
PMDETA N,N,N-pentamethylethylenetetramine
PMMA Polymethylmethacrylate
PP Polyproprylene
PPy Polypyrrolidine
PU Polyurethane
r.t. Room temperature
REDV Tetrapeptide Arg-Glu-Asp-Val
Ref. References
RF Radiofrecuency
RF-MS Rafiofrecuency magnetrón sputtering
RPMI Roswell Park Memorial Institute Medium
RUNX2 Runt-Related
SAM Self-Assembled Monolayer
SAR Structure Activity Relationship
SEM Scanning Electron Microscope
Ser Serine
SMC Smooth muscle cell
SN2 Bimolecular nucleophilic substitution
SPAAC Strain-Promoted Azide-Alkyne Cycloaddition
TBO Toluidine Blue O
TCP Tricalcium phosphate
Tg Glass transition temperature
Thr threonine
Ti Titanium
TLC Thin Layer Chromatography
Tm Melting temperature
TNF-α Tumor necrosis factor alpha
TNT Anti-inflammatory nanotubes
TRP Tryptophan
Tyr tyrosine
UV-Vis Vitamin K epoxide reductase
VBP vinylbenzylphosphonate
VKOR Vitamin K epoxide reductase
VP 4-vinylpyridine
Warf Warfarin
WCA Water Contact Angle
XPS X-ray Photoelectron Spectroscopy
YSZ Yttria-stabilized zirconia

LABURDURAK ETA AKRONIMOAK

ALG	Alginatoa
ALP	Alkaline fosfatoa
AMP	Mikrobioen aurkako peptidoa
APTES	(3-aminopropil)trietoxisilanoa
Arg	Arginina
AS	Azido salizilikoa
ASA	Azido azetil salizilikoa
ASm	Azido salizilikoaren deribatua 6a
FTIR	Fourier Transformatutako Infragorria
BG	Kristal bioaktiboak
BMS	Metalezko *stent*-ak
BMTS	Mikrotubulu bakteriarra
BTMS	bromotrimetilsilanoa
CFU	Eratutako kolonia unitatea
CHI	Kitosanoa
Col I	Kolageno mota I
COX	Ziklooxigenasa
CPTES	(3-kloropropil)trietoxisilanoa
CS	Kondroitin sulfatoa
CuAAC	Kobre (I) katalizatzailearen bidezko azida eta alkinoaren arteko zikloadizioa
DEX	Dexametasona
DIBO	dibentzoziklooktinoa
DIFO	dilfuoroziklooktinoa
DIPEA	N,N'-Diisopropiletilamina
Dns	Dansil
DSC	Ekorketazko kalorimetria diferentziala
EC	Zelula endoteliala
ECM	Zelula kanpoko matrizea
EDC·HCl	1-Etil-3-(3-dimetilaminopropil)karbodiimida
EPD	Jalkitze elektroforetikoa
EPS	Zelula kanpoko substantzia polimerikoa
Bal.	Baliokideak
FBGC	Gorputz arrotzen zelula erraldoiak
FBR	Gorputz arrotzaren erantzuna
FDA	Elikagai eta Sendagaien Administrazioa
GAGs	Glikosaminoglikanoak
HA	Azido hialuronikoa
Hap	hidroxiapatita
HDPE	Dentsitate altuko polietilenoa
HEP	Heparina
HexVP	*N*-hexilpiridin bromuroa
HUVEC	Giza zainaren zelula endoteliala

IL-1β Interleukina 1 beta
IL-4 Interleukina 4
IL-6 Interleukina 6
J Akoplamendu konstantea
LF1-11 Laktoferrin peptidoa
Lis Lisina
MAPK Mitogeno aktibatutako proteína kinasa
MOFO monofluorurozikloktinoa
MSC Zelula ama mesenkimiala
NHS *N*-hidroxisukzinimida
EMN Erresonantzia
NTAPPJ Presio atmosferikoko plasma zorrotada ez termikoa
Nu nukleozalea
OCN Oseokalzin
Okt Zikloktinoak
PAA Azido poliakrilikoa
PBS Fosfato
PCL Polikaprolaktona
PDLA Azido poli-D-laktikoa
PEC Polieketrolito konplexua
PEG Polietilen glikola
PEI Polietilenimina
PET Polietilen tereftalatoa
PHEMA Poli(hidroximetil metakrilatoa)
PLA Azido polilaktikoa
PLLA Azido poli-L-laktikoa
PMDETA N,N,N-pentametiletilentetramina
PMMA Polimetilmetakrilatoa
PP Polipropilenoa
PPy Polipirrolidina
PU Poliuretanoa
i.t. Inguru temperatura
REDV Arg-Glu-Asp-Bal peptidoa
Erref. Erreferentzia
Sar. Sarrera
RF Radiofrekuentzia
SAM Monogeruza Automuntzailea
SAR Egitura Jarduera Erlazioa
SEM Ekorketazko Mikrokopia Elektronikoa
Ser Serina
SMC muskulu-zelula leuna
SN2 Ordezkapen nukleozale bimolekularra
SPAAC Tentsioaren bidezko azida eta alkinoaren arteko zikloadizioa
TCP Trikaltzio fosfatoa
Tg Beira trantsizio tenperatura

Thr	Treonina
Ti	Titanioa
GFK	Geruza Fineko Kromatografia
Tm	Fusio tenperatura
Tyr	Tirosina
UM-Ikus	Ultramore Ikuskorra
VBP	Binilbentzilfosfatoa
VP	4-binilpiridina
WCA	Uraren kontaktu angelua
XPS	X-izpien bidezko Fotoelektroi Espektroskopia
YSZ	Ytrioz egonkortutako zirconioa

CHAPTER 1

INTRODUCTION

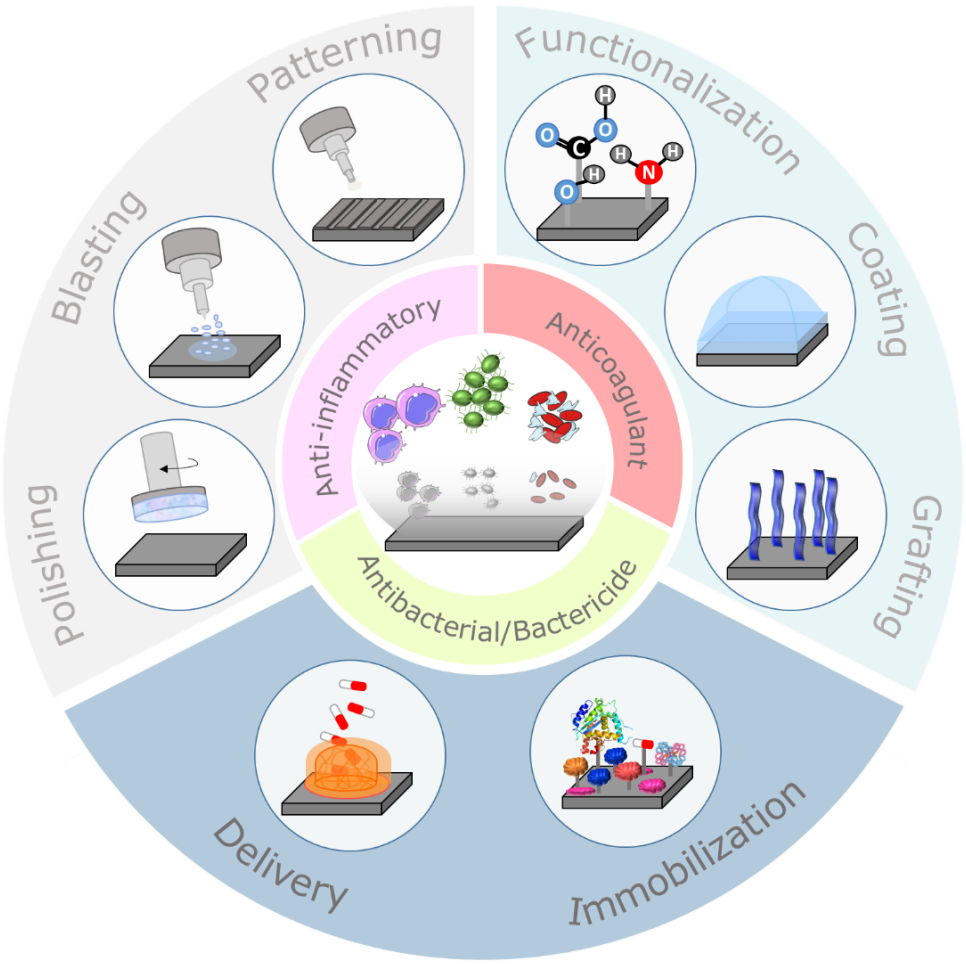

This chapter aims to explore the utilization of biomedical devices and shed light on their inherent limitations, including issues such as biofilm formation and challenges related to biointegration. Strategies to combat these issues will be discussed, encompassing approaches such as surface modifications, bioactive coatings and targeted drug delivery or drug immobilization techniques. In fact, potential solutions to enhance biointegration and promote better patient outcomes will be explained. In addition to addressing these devices related challenges, this chapter will delve into the concept of click chemistry and its application in the immobilization of drugs. Furthermore, the fundamentals of click chemistry, including the types of reactions involved and the key principles guiding its application will be described. Finally, the global objectives of this work will be presented as well as the work plan.

.

CHAPTER 1

INTRODUCTION

1.1. Introduction to biomaterials

In 1987, the European Society for Biomaterials coined the term "biomaterial", defining it as a non-biological material used in medical devices with the specific purpose of interacting with biological systems [1]. Over time, this definition of biomaterial has evolved, adapting to various contexts. Currently, biomaterials are described as materials that actively interact with biological system to assess, treat, promote healing or even replace any tissue or body function [2,3].

The main characteristic of a biomaterial is its biocompatibility, which refers to the ability of the material to elicit an appropriate response from the host in a specific situation [4–6]. Again, the interpretation of biocompatibility varies based on the required performance or function of the material. Chen *et al.* defined biocompatibility as a factor that can be assessed through parameters such as cell viability, tissue response, tumor formation, genetic integrity, immune reaction, and blood clotting potential [7]. Acknowledging this wide spectrum of considerations, the Food and Drug Administration (FDA) agency has stipulated that to consider a material biocompatible [8], it must not cause harm to the patient. Consequently, evaluating the biocompatibility of a medical device involves considering not only the biological compatibility of the materials used, but also other factors such as its design, including

geometry, electric control, and mechanical performance [7,9]. A comprehensive assessment of these aspects ensures the safety and efficacy of the medical device in its intended application, prioritizing patient well-being.

Beside biocompatibility, as described by Reinwald and collaborators, every biomaterial device must fulfil some functional requirements: safety, which is the most crucial aspect of a medical device; durability, in order to minimize the number of surgical interventions; and bio-functionality, as the biomaterial should be functionally optimized for its intended purpose, ensuring seamless performance without any interferences that could compromise its efficacy. Biodegradable biomaterials naturally break down over time, potentially eliminating the need for device removal. Thus, in certain applications, biodegradability can offer significant benefits by enhancing biocompatibility and reducing negative immune responses in the patient [10].

Regarding toxicology, biomaterials can be categorized based on their different types of responses [2]. These categories include: (I) toxic biomaterials, which can lead to cell death or damage in the surrounding and contiguous tissues; (II) non-toxic and biologically inactive biomaterials, which refers to materials that do not elicit toxic responses but, instead, trigger the formation of fibrous tissue with varying thickness at the implant site; (III) non-toxic and biologically active biomaterials, which provide a formation of a strong bonding at the interface zone between the implant and surrounding tissues; and (IV) non-toxic and biodegradable, because as the biomaterial degrades, the surrounding tissue replaces the implant [2,11,12].

Over the past few decades, the development of biomedical materials that can establish good long-term interactions with human cells has been extensively explored [10,13,14]. These advancements have revolutionized various aspects of human healthcare, offering a multitude of applications. Biomedical devices have become increasingly prevalent and are used in non-implanted forms, such as surgical tools, glucose meters, pulse oximeters, as well as implants like sutures, catheters, dental and cardiovascular devices, including stents, heart valves or vascular grafts [15,16]. Whereas orthopedic materials aid in the stabilization and healing of bone fractures and other musculoskeletal conditions, fixation screws provide robust support and secure alignment during the healing process. Similarly, implants like sutures, catheters and dental or cardiovascular devices serve diverse purposes, ranging from wound closure to the restoration of bodily functions.

The continuous development and refinement of biomedical materials have led to remarkable improvements in patient care. These materials possess unique properties that enable them to interact with human cells in a controlled and beneficial manner.

Moreover, the constant exploration and innovation in biomedical materials have paved the way for novel applications and improved patient outcomes across various medicals fields. Researchers and engineers are continuously striving to enhance the biocompatibility, mechanical strength and longevity of these materials, ensuring their suitability for long-term interactions with the human body.

The meticulous selection of materials is of outmost importance when designing biomedical devices, as they must meet a diverse range of demanding criteria. As commented, these materials should exhibit exceptional durability, promote favorable interaction with tissue cells, elicit no immunological or allergic responses, possess mechanical properties appropriated to the required function and demonstrate corrosion resistance, among other essential characteristics. To fulfill these requirements, the manufacturing of such devices predominantly relies on the use of three types of materials: ceramics, polymers and metals and their alloys. Ceramics possess desirable hardness, biocompatibility and resistance to wear, making them suitable for load-bearing applications, whereas polymers offer versatility, ease of processing and excellent biocompatibility. Metals and their alloys exhibit remarkable mechanical properties, ductility and biocompatibility, making them indispensable for numerous biomedical devices. In summary, the selection of materials for biomedical use is a critical process that needs careful consideration of various demanding properties. **Table 1.1.** summarizes the main groups of biomaterials currently employed, their main characteristics and applications [17].

Table 1.1. Classification of biomaterials based on their material, characteristics and applications [2].

Material	Advantages	Disadvantages	Applications
Ceramics	High biocompatibility, corrosion resistance, inert, low thermal and electrical conductivity	Low impact strength, difficult to reproduce properties, difficult manufacturing and processing	Coatings, medical equipment and tools, bone filling
Metals	Ductility, high resistance to wear and impact	Low biocompatibility, low resistance to corrosion in physiological environment	Staples, plates and wires, joint prostheses, dental implants, cranial plaques
Polymers	Easy production, low density	Low mechanical resistance, easily degradable	Sutures, arteries, veins, artificial tendons, implants
Composites	High biocompatibility, inert, corrosion resistance	Inconsistent and difficult replication	Heart valves, implants, artificial joints

This Doctoral Thesis is centered on metals and polymers due to their essential roles in modern material science and engineering. In fact, these materials have been meticulously chosen for their attributes and their suitability for functionalization. Therefore, hereunder an exhaustive review of these materials will be presented.

1.2. Metals and alloys

Over the centuries, metallic biomaterials have played a crucial role in the field of surgery. Early surgical devices such as screws and pins were crafted from metals like iron, gold, silver or platinum among others [7,18]. Over two centuries ago, the use of alloys in surgical implants emerged, with steel being among the earliest metal alloys employed. Later, with advancements in material science and engineering, the variety of metallic biomaterials expanded significantly. In this context, innovation brought forth sophisticated alloys like stainless steel, cobalt-chromium alloys, nickel

alloys and titanium alloys among others, all specifically tailored to meet the demanding requirements of medical applications.

1.2.1. Ti6Al4V alloy

Titanium (Ti) remains as principal material for surgical implants, especially in orthopedics or dentistry due to its excellent properties. So, its excellent resistance to corrosion in physiological conditions ensures the stability and longevity of the implant guarantying its structural integrity over time and its bio-inert nature as well as its capacity to osseointegration. Moreover, Ti possesses good fatigue strength (300 MPa at 10^7 cycles) and its low elastic modulus (113 GPa) reduces the risk of stress shielding. Last, but no least, due to its low density (4.51 g/cm^3) this metal is light weight. All these outstanding properties make Ti one of the most biocompatible materials [19]. Additionally, the phenomenon of osseointegration, which refers to the formation of an interface between implant surface and bones, enhance Ti implants to form a strong bond with adjacent bone tissue, providing another pivotal aspect on biocompatibility [20]. This fusion with bone enhances the stability and functionality of the implant, creating a reliable and lasting connection that facilitates healing and load-bearing capacities [21].

The superiority of Ti alloys over other metals is underscored by their remarkable versatility, offering a diverse range of microstructures attainable through alloy chemistry and thermal/mechanical processing methods. As a result, these alloys can precisely be tailored to meet specific application requirements, activating the desired properties with precision [22]. The microstructure and phase of the Ti-alloys at room temperature are primarily governed by two key factors: the chemical composition, particularly the percentage of α and β stabilizers, and the processing of the material, including thermal and mechanical treatments. By carefully adjusting the chemical composition, it can be find the balance between α and β phases, which are vital contributors to the mechanical and functional characteristics of the material [23]. Moreover, the combination of thermal and mechanical processing methods allows for meticulous control over the microstructure, paving the way for customized material properties. Facilitating clear categorization and selection, Ti alloys are grouped into distinct grades based on their microstructural orientation and phases, specifically α, β and α+β [24]. These classification enable a comprehensive understanding of the capabilities and limitations of the material, assisting the scientist in choosing the most suitable alloys for a given application.

It is crucial to emphasize that no implant material has demonstrated a completely adverse-effect free profile. Specifically, the release of vanadium and aluminum ions from Ti6Al4V implants has been associated with potential toxicity issue. These ions can accumulate in the adjacent/host tissue, leading to inflammatory and hypersensitivity problems. However, when compared to stainless steel and Co-Cr alloys, Ti and its alloys showcase superior performance in term of osseointegration, making it highly desirable for medical applications [25]. Furthermore, a stable TiO_2 layer naturally forms on the surface of Ti alloys contributes to the biocompatibility of the material. This TiO_2 layer enhances the interaction between the implant and surrounding biological environment, fostering an integration and supporting successful surgical outcomes [26,27].

1.3. Polymers

Polymeric biomaterials have emerged as indispensable components in a diverse range of medical devices, diagnostic systems and pharmaceutical formulations [28]. Over the past decades, due to the rapid progress in tissue engineering and regenerative medicine, polymeric biomaterial field has experienced remarkable growth. The development of numerous novel polymeric biomaterials, comprising biodegradable synthetic polymers and natural macromolecules, has paved the way for significant advancements in tissue regeneration [13,28]. The versatility of polymeric biomaterials allows for tailoring their properties to suit specific applications, such as wound dressings, tissue grafts and drug delivery systems among others. Moreover, most of these materials possess desirable characteristics like biocompatibility, biodegradability and tuneable mechanical properties, which make them suitable for safe and effective medical interventions [29].

1.3.1. Poly-L-lactic acid (PLLA)

Polylactic acid (PLA), also known as polylactide, is an aliphatic polyester derived from lactic acid, (2-hydroxypropanoic acid), which is obtained from starch. Polylactide is a highly versatile biodegradable polymer and has become one of the most important material due to its adaptive properties [30–33]. It is not a new polymer, in fact it was first prepared in 1932 by Carothers Dupont and, since then, extensive research has been carried out to develop new ways of obtaining and optimizing its properties. As lactic acid is a chiral molecule existing in L and D isomers, the term poly-lactic acid refers to a family of polymers, including pure poly-L-lactic acid (PLLA), pure poly-D-lactic acid (PDLA) and poly-D,L-lactic acid (PDLLA) (**Figure 1.1**) [34,35]. The L-isomer is a biological metabolite and constitutes the main component of PLA

derived from renewable sources since the majority of lactic acid from biological sources exists in this form. Depending on the composition of the optically active L- and D,L-enantiomers, PLA can crystallize in three forms (α,β,ɣ).

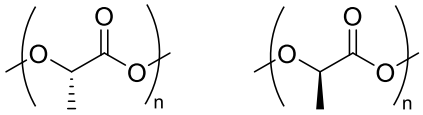

PLLA PDLA

Figure 1.1. PLLA and PDLA schematic representation.

In this way, PLLA has garnered significant attention due to its remarkable biocompatibility and mechanical properties. However, it needs extended periods of time to degrade and combined with the high crystallinity of its fragments, can potentially induce inflammatory reactions in the body. The degradation rate can be enhanced by incorporating DL-lactic acid mitigating the potential inflammatory response caused by prolonged degradation and crystalline fragments accumulation [31,36].

Regarding properties of PLA, the crystallinity of PLA is directly affected by factors such as stereochemistry and thermal properties. When L-isomer content (PLLA) in PLA exceeds 90 %, the material tends to exhibit a crystalline structure, whereas lower levels of optical purity result in amorphous PLA. Likewise, the melting temperature (T_m) and glass transition temperature (T_g) of PLA are directly related to the amount of PLLA present. As the PLLA content decreases, both T_m and T_g of PLA decrease as well. The transition temperature of PLA plays a crucial role in determining its physical characteristics including density, heat capacity, and mechanical an rheological properties. Consequently, PLAs with properties tailored to different applications can be achieved through careful control of the stereochemistry in the polymerization reaction [30,34].

Regarding PLA degradation, it primarily undergoes hydrolytic decomposition, taking, typically, several months in the presence of moisture. This degradation process occurs in two stages: (I) random non-enzymatic chain scission of the ester groups leads to a reduction in the molecular weight of the polymer, (II) in the subsequent stage, the molecular weight further decreases as generated lactic acid and low molecular weight oligomers are naturally metabolized by microorganisms to yield carbon dioxide and water [37]. The rate of polymer degradation is mainly influenced by the reactivity of the polymer with water and catalyst. Several factors affect this reactivity and accessibility, including particle size and shape, temperature, moisture

levels, crystallinity, % isomer content, residual lactic acid concentration, molecular weight, water diffusion and catalyst impurities. The degradation behaviour of polylactide surgical implants has been extensively evaluated both *in vivo* and *in vitro*. *In vitro* studies have shown that the pH of the surrounding environment plays a key role in the degradation process [38].

1.3.2. Poly(ethylene terephthalate) (PET)

Poly(ethylene terephthalate) (PET) (**Figure 1.2**) is a cost-effective polymer known for its impressive mechanical properties and moderate biocompatibility. Its remarkable properties, including hardness, stiffness, bio- and chemical stability, make this polymer highly promising for biomedical uses. Indeed, it presents medical applications, such as vascular and urinary catheters, heart valves and sutures, among others [39,40]. However, despite its utility, the high rate of infections associated with its use has limited its applicability as a biomaterial. As PET surfaces are hydrophobic, bacterial adhesion and, therefore, infection occurs before proper tissue integration takes place [41].

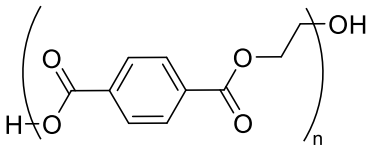

PET

Figure 1.2. Chemical structure of PET.

The presence of aromatic rings and polar groups into the main chain of PET contributes to its improved thermal stability and stiffness. This enhancement is demonstrated by its remarkable melting point (T_m) in the range of 255-265 °C for semy-crystalline PET, which is notably high for a polymeric material. Additionally, T_g value varies based on the crystallinity and orientation of PET. Amorphous PET presents a T_g of approximately 67 °C, while semi-crystalline PET exhibits a T_g around 80 °C. Crystalline and oriented PET chains show a further increase in T_g, reaching approximately to 125 °C. This tendency affirms that higher degrees of order within the polymer structure result in elevated T_g values [42].

Regarding chemical and mechanical stability, PET shows to be inert toward numerous solvents and reactants. However, this polymers is unstable in the presence of bases, even weak ones, strong acids, and hydrocarbons. Its mechanical performance is significantly influenced by various factors, including polymer crystallinity, processing

and shaping (bottles, films, fibers). In general, PET exhibits exceptional mechanical strength compared to traditional polymers (HDPE, PP), achieving a high Young modulus of approximately 3.0 GPa. Moreover, it has been proved that crystallinity degree is an important factor in the elongation of the polymer, resulting in higher elongation values when PET with lower crystalline degrees are employed [42].

PET, as a polyester, is susceptible to hydrolysis reactions when it is exposed to moisture at temperatures higher than its T_g. The hydrolytic degradation primarily affects the ester bonds present in the amorphous section of the main chain [43]. This process induces the scission of ester bonds, leading to the formation of acid and alcoholic functionalities and, consequently, resulting in polymers with lower molecular weight. This hydrolytic reaction occurs due to the polymer permeability to water molecules. The presence of crystalline phases within PET acts as a barrier, making it impermeable to water molecules and, thereby, mitigating the hydrolysis process. However, it is noteworthy that this process can be accelerated when PET is exposed to acidic or alkaline mediums [42].

Dracon® is the commercial name of biomedical PET. It is a versatile polymer and its biostability is primarily attributed to the presence of hydrophobic aromatic groups with high crystallinity, which effectively hinders hydrolytic degradation. However, the main limitation of Dracon® is its lack of polar functional groups on the surface, restricting its potential in tissue engineering applications [44]. Several research studies have focused on surface functionalization techniques to enhance the properties of PET. In fact, numerous attempts have been made to overcome the limitations derived from its hydrophobic nature. The ultimate goal is to create PET-based biomaterials with reduced infections rates and improved integration with the body's tissue, thus, enhancing patient outcomes and expanding the potential of this polymer in medical applications.

Polymers have made a significant impact on biomedical research and their role as the primary driving force behind biomaterials will continue growing in this 21st century. The current applications of polymeric materials represent merely the tip of the iceberg, as ongoing advancements promise even greater potential in this field. By delving deeper into the biological responses to existing biomaterials and gaining comprehensive understanding of human composition, function, biomechanics and disease etiology, chemist and polymer scientist must collaborate with biologists, physicians and engineers to obtain tailor-made polymers for specific biomedical applications. The future will be dominated by bioactive, biomimetic and smart polymers, which will take center stage in biomedical applications. These polymers

will not only interact with the body, but also actively respond to its needs, revolutionizing medical treatments and therapies.

Although polymers can be found in different forms such as surfaces, fibers, hydrogels, nanoparticles, among others, this chapter will explored the progress and challenges of functionalizing polymers surfaces for better performance as biomaterial.

1.4. Problems related to biomaterials

Biomedical implants encompassing prosthetics, catheters and an array of other devices, have undoubtedly revolutionized modern medicine, significantly improving the quality of life for countless patients. However, their integration with the human body does come with an inherent risk, an increased susceptibility to infections [45–47]. In fact, implant-related infections and limited biointegration represent the most prevalent and severe complications associated with the utilization of biomaterials. Infections can lead to various complications, ranging from localized discomfort to systemic health issues, potentially needing additional medical interventions and compromising patient outcomes [48].

Upon implantation of any biomaterial into the body, it elicits a response from the host tissue, commonly referred to as the host response [49]. This response occurs regardless of the method used to introduce the biomaterial, whether by injection or through surgery. The presence of a foreign biomaterial disrupts the local host tissue environment [49]. The magnitude of the host response depends on the extent to which the normal state of the equilibrium, known as homeostasis, is disturbed by the injury caused during implantation. This disruption, along with the introduction of the foreign object, determines the biocompatibility of the material. While numerous biomaterials and medical devices have been successfully implanted in humans, currently there is no material that can completely evade the highly efficient surveillance system of the human body. The host response is initiated by the adsorption of proteins on the surface of the material, leading to the formation of a dense collagenous capsule around the implant [11,50]. This encapsulation impedes further interaction of the implant with the surrounding tissue, a process often referred to as biofouling [49,51].

The various stages of foreign body response (FBR) are a dynamic process involving multiple intricate events. These stages include injury, blood-material interactions, provisional matrix formation, acute inflammation, chronic inflammation, granular tissue development and fibrous capsule development (**Figure 1.3**) [49]. Blood compatibility or hemocompatibility refers to a material's ability to regulate the

thrombotic and inflammatory responses induced by the foreign surface upon contact with blood. This attribute is an essential requirement for materials designed for blood–contact applications [52]. Such interactions between blood and medical devices trigger a complex series of events, including protein adsorption, platelet adhesion and activation, coagulation and thrombosis. The rapid absorption of plasma protein into the surface of biomaterial represents the initial event in blood/material interaction. This adsorption results in activated proteins that can catalyze, mediate or moderate subsequent biological response to the biomaterial [51]. Surface-induced thrombosis is the main problem impeding the development of long-term blood contacting devices. Thrombus formation on device surfaces is a consequence of two key factors: platelet-mediated reactions and coagulation of blood plasma [52].

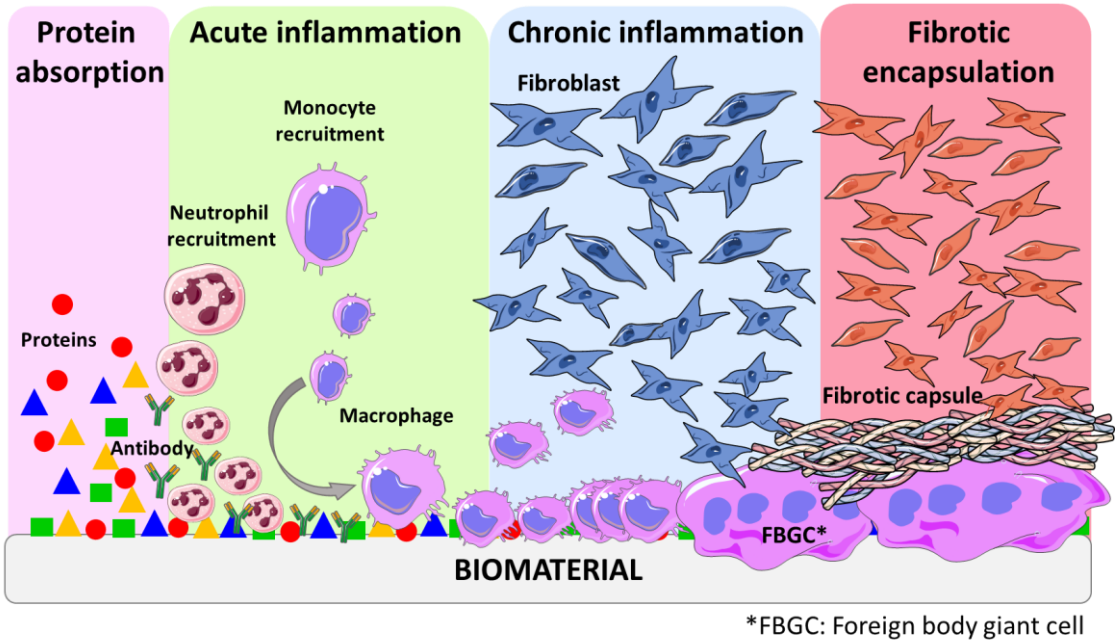

Figure 1.3. Schematic representation of some stages of the host tissue response.

Throughout this process, a complex interplay of inflammatory cells, mitogens, chemo-attractants, cytokines and other bioactive agents plays also a key role in orchestrating the response [11]. Understanding each of these events is essential as they contribute significantly to the overall outcome of FBR. Delicate interaction between the immune system and the foreign material leads to the formation of provisional matrices which trigger acute inflammation. This initial inflammatory response paves the way of chronic inflammation and subsequent granular tissue development. Ultimately, the formation of a fibrous capsule encapsulates the foreign material aiming to isolate and protect the surrounding tissue from potential harm [6].

Over the years, the concept of a "race to the surface" has been proposed to describe the competition between host cells and contaminating bacteria for occupying biomaterial surfaces [53]. The successful integration of biomaterials into host tissues is crucial for the effectiveness of many implants. Moreover, most studies conclude that rapid integration is also essential for preventing bacterial adhesion and colonization. In orthopedics, the healing of bone tissue around the implant leads to the apposition of bone, facilitating the integration of the implant into the bone tissue, a process known as osseointegration [54]. *In vitro* studies with osteosarcoma cells demonstrated that pre-colonizing bacteria significantly alter and compromise host cell adhesion to material surfaces. It is important to note that if bacterial adhesion occurs before tissue repair takes place, the defense mechanism of the host may not able to prevent surface colonization and subsequent biofilm formation [47,55].

In this chapter, our primary focus is on orthopedic implants, as these prosthetics that remain in the body are particularly susceptible to thrombosis, inflammation and, mostly infections, presenting significant challenges. In fact, these complications associated with these implants frequently lead to device failure, requiring, in some cases, replacement, and even can result in chronic diseases. Identifying and diagnosing orthopedic implant infections, including determining the infectious agent and its antimicrobial sensitivity, poses significant difficulties. Moreover, treating these infections can be complicated due to various factors, such as antimicrobial resistance, tolerance and/or persistence. Although *Staphylococcus aureus* is the most common bacteria around orthopedic implant infection [47,48], it is essential to recognize that many other pathogens can also be responsible for causing such infections.

Implant infections are complex processes involving interactions among the pathogens, biomaterial, and the response of the host immune system. In the absence of foreign bodies, opportunistic pathogens are typically cleared by the defenses of the immune system. However, as commented previously, in the case of implant-associated infections, the biomaterial triggers a localized tissue response, leading to acute and chronic inflammation, foreign body reaction, granulation tissue formation, and eventual fibrous encapsulation. This unique environment creates a niche of immune depression, known as a *locus minoris resistentiae*, which makes the implant more susceptible to microbial colonization and infection. Furthermore, the biomaterial serves as a substrate for bacterial adhesion and biofilm formation [47]. Bacterial adhesion is the initial step in biomaterial-related infections and serves as a foundation for subsequent implant colonization. Once attached, pathogens form micro-colonies and develop protective biofilms, allowing them to persist in the hostile host environment. Thus, adhesion and biofilm formation are critical processes that enable

pathogens to establish and maintain infections in implant sites. Understanding these complex interactions is essential for developing effective strategies to prevent and treat implant-associated infections [56,57].

Bacterial adhesion is a multi-stage process that can be divided into two main phases (**Figure 1.4**). The first stage involves the primary unspecific reversible attachment, while the second stage comprises specific irreversible attachment. When bacteria initially adhere to abiotic surfaces, such as those found in implants, the attachment is typically unspecific [47]. However, their attachment involves specific interactions facilitated by lectins or adhesins. When a bare material surface comes into contact with physiological fluids like blood and interstitial fluids, it rapidly becomes covered by extracellular matrix (ECM) proteins and immune components within nanoseconds. This process is influenced by the surface chemistry and wettability of the implant surface. Hence, adhesins play a crucial role as the primary mechanism for bacterial attachment to the implant surface within the body. Both *Staphylococcus aureus* and *Staphylococcus epidermis* possess multiple mechanism for attachment and biofilm formation, significantly contributing to their virulence in chronic implant infections [47]. The process of biofilm formation encompasses several stages (**Figure 1.4**): (I) adhesion, which is the initial stage, (II) micro-colony, where bacterial cells form aggregations and extracellular polymeric substances (EPS) are produced, (III) macro-colony formation, which undergoes further remodeling and maturation, resulting in the development of macro-colonies that appear as towers within the biofilm structure, and (IV) biofilm dispersal, which is the final stage, wherein some bacteria revert to a planktonic lifestyle, potentially colonizing new areas and initiating the biofilm formation process elsewhere [47].

Biological responses and bacterial adhesion are intricate processes influenced by numerous factors, but it is widely accepted that these responses are significantly affected by the surface properties [58]. In fact, various surface characteristics including chemistry, topography, surface free energy, elasticity, and charge play essential roles in modulating protein and cell interactions, and, consequently, host response.

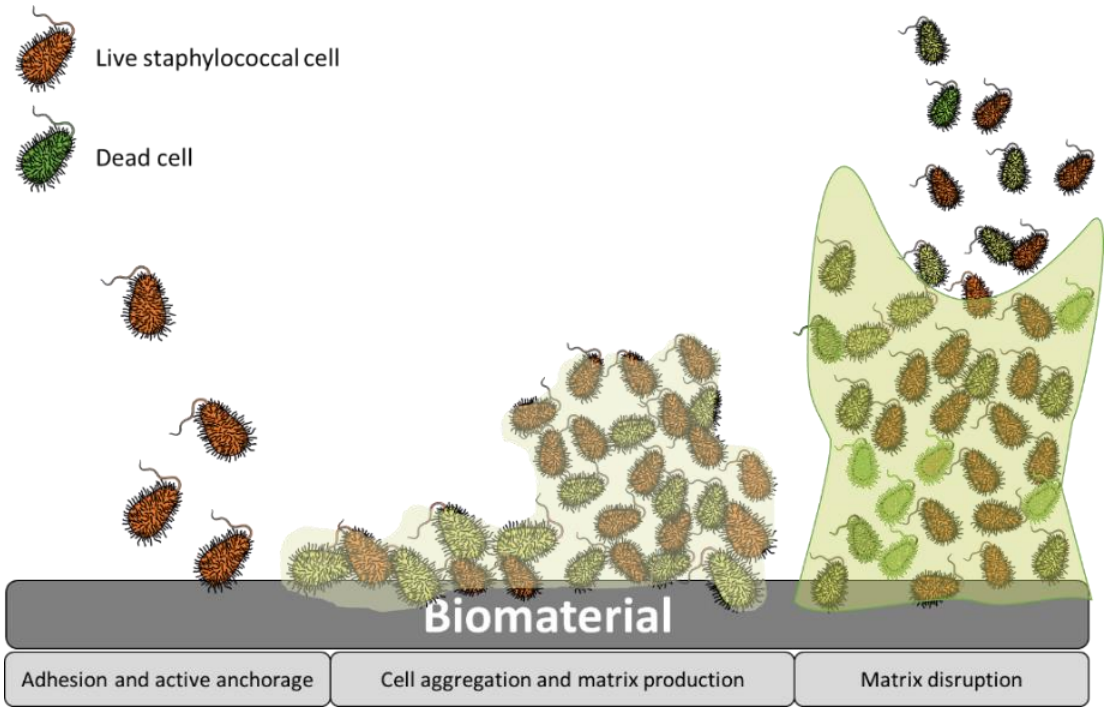

Figure 1.4. Stages of *staphylococcal* biofilm formation.

1.5. Biomaterial surface properties

As commented, several studies concluded that surface characteristic such as topography, wettability, charge and chemical properties play a key role in proteins, cells, and bacterial adhesion and growth and, consequently, they influence in hemo- and biocompatibility. This section will delve into the crucial attributes of a surface, providing an in-depth exploration of the key factors necessary for optimal biointegration. It will also expose the desirable properties required to foster a favourable response from the body and establish robust protection against bacteria.

Regarding surface topography and roughness, they play a crucial role in determining the biological responses to foreign materials and bacterial adhesion. Extensive research has shown that surfaces with micro- and nanoscale structures significantly impact various cells and bacteria behaviours. Surface patterning serves as a key determinant influencing both the contact area and the adhesion force between bacteria, proteins or cells, and the substrate. Indeed, these surface features can modulate cell orientation, morphology, adhesion, proliferation, and even regulate cellular functions and gene expression [59]. For instance, Yang *et al*. compared the adhesion of both Gram-positive and Gram-negative bacteria on different patterned surfaces (**Figure 1.5**) [60]. Factors such as the geometry, size, and the height of the patterned surface impact on the interaction of bacterial and surfaces. Nanostructures with a high-aspect-ratio, such as nanopillars and nanospikes, exhibited exceptional

bactericidal activity. Indeed, when bacterial attachment occurs, the cell membrane of the bacteria lies within these nanostructured patterns cavities until the membrane breaks. On the other hand, both nanotubes and nanoripples have demonstrated efficacy in diminishing bacterial adhesion. Furthermore, enhanced bacterial reduction is obtained with larger diameters for nanotubes and reduced contact within the structure array for both nanotubes and nanoripples. Similarly, microscale patterned surfaces including micro wells, sub micro pillars, micro pillars, and micro protrusions present significant bacterial growth and colonization inhibition [61]. In fact, they trap bacteria within deep valleys, shielding them from the shear force of fluid. Contrary, a smooth surface facilitates the movement of attached bacteria, thereby increasing the probability of bacterial adhesion [60].

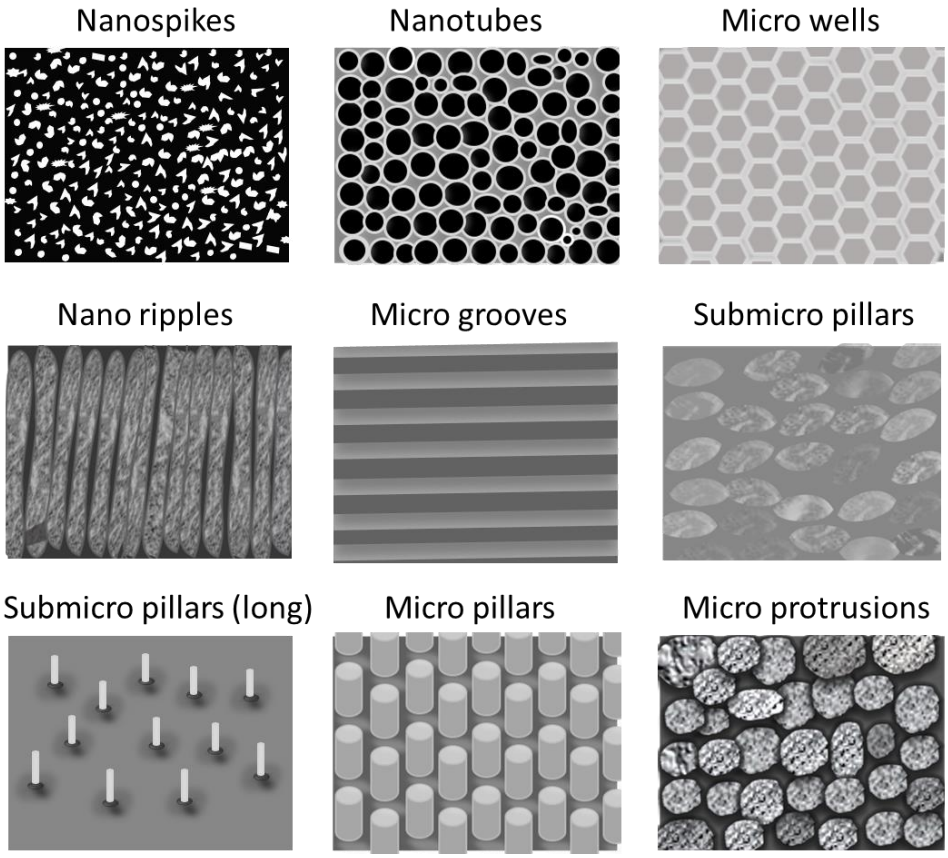

Figure 1.5. Schematic representation of the different patterned surfaces.

As commented, bacteria are not the only elements that are influenced by the topography. Surface texturing serves as a strategic approach to modulate protein uptake on surfaces as well. This technique requires precise control over total protein adsorption levels, influencing the ratio of various proteins, spatial distribution, protein conformation, and surface binding affinity. The impact of nanoscale topographies on protein adsorption is particularly significant when the surface features align with the

dimensions of the proteins. Conversely, interactions with topographies significantly larger than dimensions of proteins, such as micrometer-scale patterning, are generally perceived by proteins as a flat surface [62]. Moreover, smooth and flat implant surfaces have shown to induce the adhesion of foreign body giant cell (FBGC), which provokes the fibrotic capsule formation [63].

Concerning roughness, under static culture conditions, bacteria exhibit preference for smoother surfaces when the average roughness (Ra) value is low, ranging between 0.23 and 6.13 nm. Conversely, as these values increase within the range of 6–30 nm, bacteria tend to adhere to rougher surfaces [60,64]. This roughness adaptability was studied by Mu *et al*., who prepared quartz surfaces with different roughness and treated with *Salmonella enterica* culture [65]. The impact of the surface roughness on bacterial adhesion is evident from the findings illustrated in **Figure 1.6**. When the roughness is low (root-mean-square (RMS) < ≈ 10 nm), isolated microcolonies are formed, hosting a relatively sparse population of adherent bacteria with a low overall areal density. Progressing to intermediate roughness values (RMS between 10 and 40 nm), a substantial increase in adherent bacteria is observed, replacing isolated microcolonies with loosely connected bacterial monolayers. Additionally, the bacteria exhibited a more pronounced deformation/flattening ratio on these surfaces, suggesting a heightened attraction between bacteria and surfaces. Conversely, at high roughness values (RMS > 45 nm), the areal density of adhering bacteria is exceeding low, and no microcolonies are observed. Bacteria predominantly exist as individual isolated organisms on these surfaces with a small fraction forming dimeric and trimeric aggregates [65].

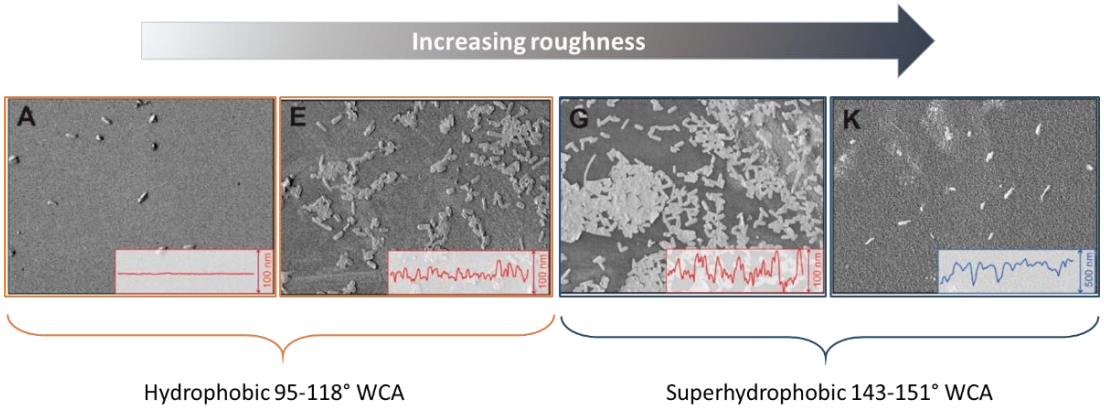

Figure 1.6. Adapted SEM micrographs displaying bacterial adhesion trends on hydrophobically modified quartz surfaces roughness for *Salmonella*. Adapted with permission from Influence of Surface Roughness, Nanostructure, and Wetting on Bacterial Adhesion. Copyright 2023 American Chemical Society [65].

Surface wettability is governed by both roughness and the chemistry of the surface jointly influencing its capability. It must be noted that the water contact angle (WCA) of rough surfaces (known as "apparent" WCA) differs from smooth surfaces (called "intrinsic" WCA). According to the Wenzel model, a rough hydrophilic surface exhibits an apparent WCA value lower than its intrinsic WCA value. Conversely, a rough hydrophobic surface displays an apparent WCA higher than its inherent WCA [66]. Some studies concluded that bacteria prefer to adhere to hydrophobic surfaces rather than hydrophilic ones. However, both superhydrophilic and superhydrophobic surfaces have demonstrated antibacterial behaviour [67,68]. In fact, superhydrophobic surfaces, characterized by an apparent WCA exceeding 150°, require the entrapment of air bubbles within nanostructures or microstructures, as outlined by the Cassie and Bexter model [68]. Regarding proteins and macrophages, hydrophobic materials exhibit increased protein adsorption but also enhanced macrophage adhesion [47,48], potentially contributing to the initiation of fibrotic encapsulation. Conversely, in the case of hydrophilic materials, macrophages demonstrate heightened adhesion to positively charged implants in comparison to anionic or nonionic alternatives [63].

To address this critical challenge, extensive research and advancements in material science and implant design are continuously pursued.

1.6. Modification of physicochemical properties of biomaterials

As described in detail in *Section 1.5*, physicochemical properties of biomaterials, such as surface topography, wettability, charge density and surface chemistry play a crucial role in protein adsorption and subsequent cellular behaviour as well in bacterial adhesion. Consequently, researches have recognized the significance of modifying these surface properties in implanted biomaterials to achieve enhanced biocompatibility and hemocompatibilty and reduce both inflammatory response and bacterial adhesion.

Recent studies exploring the improvements on host tissue response and antibacterial properties of various materials have highlighted the potential of surface modification technologies in limiting and preventing bacterial contamination, as well as to promote proper adhesion of cells and proteins [69,70]. Notably, both physical and chemical modifications of biomaterial, drug delivery as well as immobilization of bioactive molecules, which can directly or indirectly control the activity of components of the immune system, have emerged as effective approaches in this regard.

When discussing strategies for antibacterial surfaces, a recognize classification is widely employed, distinguishing two main types of approaches related to surface capability: biopassive and bioactive surfaces. Biopassive surfaces prevent the adhesion by repelling bacteria but without killing them, whereas bioactive surfaces are capable of killing bacteria before the adhesion takes place [58]. Considering these definitions, it is possible to further expand these terms to encompass strategies that not only combat bacteria, but also aim to improve biocompatibility and hemocompatibility along with reduce inflammation. In this work, this overarching classification will also extrapolate to surfaces with anti-inflammatory and anti-coagulant properties. Biopassive surfaces will also be considered those whose methods do not inactivate or kill cells or proteins responsible for inflammatory and coagulations processes, instead, they indirectly influence the adhesion, differentiation or growth of these biomolecules. Conversely, surfaces that actively inhibit any metabolic process or suppress elements involved in the synthesis of inflammatory and coagulation factors will be termed as bioactive surfaces (**Figure 1.7**).

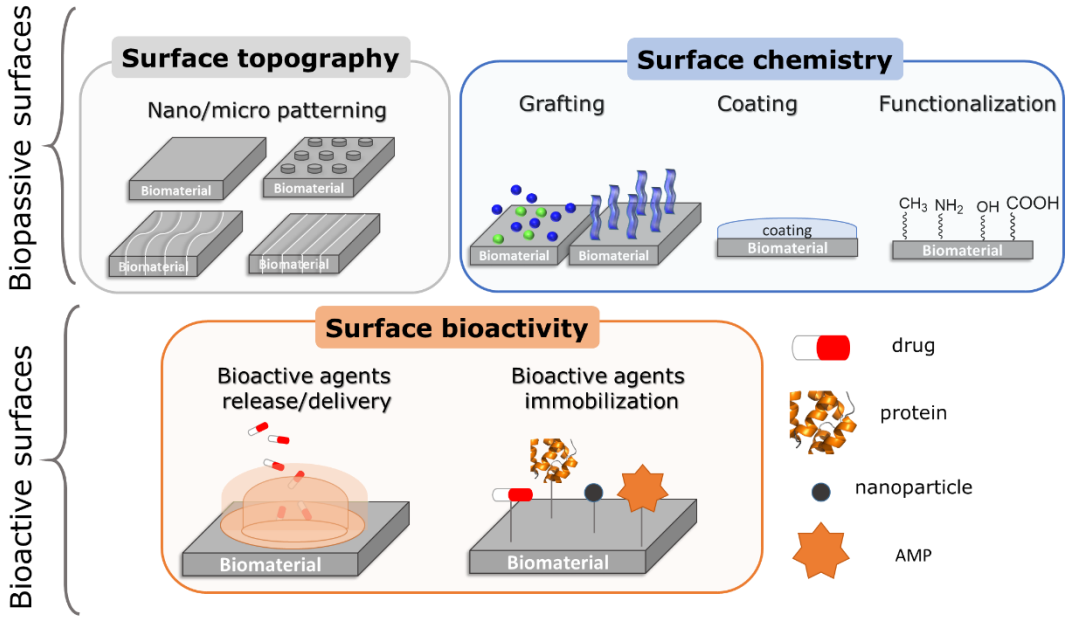

Figure 1.7. Schematic representation of biopassive and bioactive surfaces.

Among physical and chemical modifications, there is a wide range of approaches, including nano- and micro-structuration, grafting, coatings and surface functionalization. Indeed, surface topography modification offers a straightforward method to provide anti-adhesive properties to polymeric or metal materials [71,72]. By modifying surface characteristics like roughness, hydrophilicity and surface energy, these materials become less prone to bacterial, cellular or protein adhesion.

However, for more comprehensive protection to bacterial adhesion and inflammation response, both anti-adhesive/fouling and biocidal modifications and anti-inflammatory behaviours are achievable through other methods, such as drug delivery or drug immobilization, depending on the specific technologies and chemicals employed. Additionally, grafting and coating methodologies have demonstrated significant antibacterial and anti-inflammatory activity and improvements in biocompatibility, but there is still some advancements to do [73,74]. In fact, although any type of surface modification techniques will affect surface chemistry and morphology, and, in consequence, substrate mechanical, optical, adhesive, electrical, and morphological properties, these changes should occur in small depth to ensure that the bulk properties of the material remain unchanged.

1.6.1. Biopassive surfaces

1.6.1.1. Surface topography

Physical approaches for altering surface topography and roughness have demonstrated remarkable effectiveness in modulation of macrophage phenotype and function, while also providing an effective means to prevent bacterial adhesion [75,76].

It has long been known that macrophages prefer to adhere to rough surfaces rather than flat [77]. More recently, Refai *et al.* studied the influence of surface roughness on macrophage activation and secretion of interleukin (IL)-1β, IL-6 and tumour necrosis factor (TNF)-α, which are pro-inflammatory cytokines [78]. For this purpose, they employed four different topographies onto Ti surfaces, including mechanically polishing, coarse sand blasting, acid etching and sandblasting and acid etching. Additionally, they performed different assays with pristine Ti samples and Ti plus lipopolysaccharide (LPS) samples in order to have a negative and positive control, respectively. In the absence of LPS, sandblasting and acid etching roughened Ti surfaces increased TNF-α secretion, whereas LPS stimulated roughened Ti surfaces showed high levels of IL-1β, IL6 and TNF-α when the combination of sandblasting and acid etching was employed. Additionally, surface topography also modulated the secretion of chemoattractant monocyte chemotactic protein 1 (MCP-1) and macrophage inflammatory protein-1α (MIP-1α) in RAW264.7 macrophages. In this case, when no LPS was employed, the production of these chemoattractants decreased, while LPS stimulated surfaces proved to upregulate the production. It is worth to note that the enhanced secretion resulting from surface roughness was generally observed at later time points, specifically at 24 h and 48 h, but not at an

earlier 6 h time point. This suggests a temporal dependence of the topographical effect, indicating that the influence of surface roughness on RAW264.7 macrophage secretion may vary over time.

Similarly, in regard with macrophage behaviour, Chen *et al*. induced topography changes close to biological scale by imprinting lines about 250 nm^{-2} width on poly(ε-caprolactone) (PCL), PLA and poly(dimethylsiloxane)(PDMS) [79]. For this purpose, RAW 264.7 cells were used and they observed that the adhesion and elongation of these cells were the most pronounced on 500 nm graftings compared to planar controls. Notably, TNF-α and Vascular endothelial growth factor (VEGF) exhibited the greatest sensitivity to topographical effects. In fact, a discernible reduction of these cytokines was observed on larger sizes after 48 h. Furthermore, a remarkable decrease in macrophage adhesion density and a diminished extent of pronounced cell fusion on 2 μm topographical surfaces were observed in *in vivo* studies at 21 days. Thus, these results concluded that, on all surfaces examined and regarding the foreign body response, topography profoundly impacts on macrophage behaviour.

Regarding antibacterial properties, Wang *et al.* suggested that the micropatterning, obtained by quartz photomask, conducted on a scale comparable to the dimension of bacteria, exerts a profound influence on the adhesive behaviour of cells on PET surfaces. Furthermore, and more importantly, they concluded that the topography of the surface had greater influence on cell adhesion that the contact angle and, consequently, the surface wetting characteristic [80].

1.6.1.2. Chemical modifications

Chemically based surface modifications encompass a wide range of complexities, ranging from simple alterations or introductions of a single functional group to more intricate multi-step surface grafting reactions. These grafting strategies often involve a preliminary surface activation step, where reactive functional groups, such as hydroxyl, amines, or carboxylic acids among others, are introduced, followed by subsequent reaction to covalently link the molecule of interest to the surface.

A wide array of chemically based methods can be employed to introduce reactive functional groups onto biomaterial surfaces, effectively "activating" them for subsequent grafting reactions. Interestingly, many of these treatments can also independently alter specific material surface properties, leading to modifications in cell-material interactions as well as bacterial-substrate interactions. For instance, techniques that generate polarized hydroxyl, carboxyl or amino groups arouse changes in hydrophilicity/hydrophobicity and surface charge, influencing protein,

cellular and bacterial adhesion [81,82]. The most commonly used chemically based surface functionalization methods involve partial surface hydrolysis, oxidation, aminolysis and plasma treatment (**Table 1.2**.). Each of these techniques offers unique advantages and can be tailored to suit specific biomaterial requirements.

Table 1.2. Description of different techniques used for surface modification in metal, ceramic, and polymers materials.

Technique	Surface	Treatment	Advantage	Ref.*
Hydrolysis and aminolysis	PCL nanofibers	NaOH solution and ethylendiamine/isopropanol solution	Improved cytocompatibility Heightened cell attachment, spreading, and proliferation	[83]
	Ti6Al4V	Acidic and alkaline piranha	Excellent biocompatibility, cell proliferation and excellent hemocompatibility Enhanced antibiofilm activity	[84]
Oxidation	Ti	Ultraviolet (UV)/ozone	Improved antibacterial activity and bone regeneration	[85]
	Ti6Al7Nb	Electrochemical anodization	Enhanced adhesion and proliferation of human bone marrow mesenchymal stem cells	[86]
Plasma	Ti	Plasma polymerization with allylamine	Increased cell adhesion capability	[87]
	Ti	Oxygen plasma immersion	Promoted blood clotting and enhanced resistance to bacterial adhesion	[88]
	Polyurethane (PU)	Plasma immersion of nitrogen ions	Decreased bacterial adhesion: both Gram-positive (*Staphylococcus*) and Gram-negative (*Escherichia coli*) bacteria decreased	[89]
	Ti	Atmospheric pressure plasma (APP)	Provide both adhesion and osteogenic differentiation of cells culture	[90]
	Ti	Plasma fluoride ion release	Bactericidal properties	[91]

* Ref.: References.

Hydrolysis

Surface hydrolysis *via* acid or base treatment is a commonly employed method to modify aliphatic polyesters, such as PLA, poly(glycolic acid) (PGA) or PET, and metallic substrates, including Ti6Al4V. However, it is important to note that the mechanism underlying the hydrolysis of polymers and metal substrates are inherently distinct. In polymers, hydrolysis induces random chemical cleavage of the ester bonds on the polymer backbone, generating hydroxyl and carboxyl groups at the polymer surface. On the other hand, in Ti and its alloys, the hydrolysis only affects the passivated TiO_2 coatings previously generated on the metallic surface, introducing, by oxidation, hydroxyl groups. In any case, on both substrates, chemical acid and alkali treatments are the most used in industry due to their versatility, simplicity and effectiveness. A wide range of different treatments and mixtures can be employed, including basic or alkaline solutions (NH_4/H_2O_2, NaOH, KOH…) and acid solutions (HCl, HCl/H_2O_2, H_2SO_4/H_2O_2, H_2SO_4/HCl…) [16,84]. Nevertheless, there are some concerns associated with this wet chemical technique. For polymers, it is important to ensure that the concentration and treatment duration of the acidic/alkali solution do not significantly alter the bulk properties of the underlying polymer. And, in both cases, the nonspecific nature of the treatment can lead to irregular surface degradation, potentially affecting the overall surface integrity and properties of the modified material. Therefore, careful optimization of the hydrolysis process is essential to achieve desired modifications while preserving the core properties of the substrate. Nonetheless, these newly produced functional groups offer valuable attachment points for covalently linking other molecules to the polymer surface through various conjugation strategies. Although, it should be noted that hydrolysis itself has proved to increase cellular attachment to various polyesters and Ti alloys, as it increases material hydrophilicity and surface roughness, changing the wettability properties of the surface.

In this context, it has been demonstrated that the formation of Ti-OH after hydrolysis process enhance the hydrophilicity of the surface, thus improving cytocompatibility and cell proliferation among other. In fact, Andrade *et al*. prepared different chemical wet treatments based on acidic and alkali solutions, including H_2SO_4:H_2O_2, HCl:H_2O_2, NH_4OH: H_2O_2 and NaOH treatments [84]. They demonstrated that HCl:H_2O_2 treatment displayed the most effective surface activation without producing topographical changes, while improving biological functionalizations.

Oxidation

The introduction of peroxide groups onto polymers or metallic surfaces for subsequent grafting reactions can be accomplished through various strategies and techniques, such as photo-oxidation by UV light or ozone oxidation. While UV light can discompose hydroperoxide groups onto reactive oxygen and hydroxyl radicals, ozone treatment produces peroxides, carboxyl, and carbonyl groups that can be further employed to initialize surface polymerizations or grafting reactions [92]. However, both approaches can degrade the polymer, thus, it is important to control and minimize significant changes of the bulk properties of the substrates [93]. Conversely, in the case of metals, electrochemical anodic oxidation has stood as the method of choice for over a decade to grow a thick and uniform oxide layer on metal surfaces [94]. This technique has been demonstrated to significantly enhance the biocompatibility of metal implants, as detailed by Huang *et al*. [86]. In this work, an efficient electrochemical anodization treatment was employed, which led to the formation of a nanoporous oxide layer free of aluminum onto Ti-6Al-7Nb surface. By oxidating the surface, notable improvements in corrosion resistance were achieved. In fact, reduction in both corrosion rate and passive current were observed when surfaces were immersed in simulated blood plasma. Additionally, the presence of the nanoporous oxide layer exhibited a positive impact on cell behaviour. Specifically, it enhanced adhesion and proliferation of human bone marrow mesenchymal stem cells, providing significant importance in biomedical applications. It is worth to note that the development of an orderly oxide layer can be tailored by regulating parameters such as the choice of electrolyte, applied current density, electrolyte concentration, electrolyte temperature, stirring rate, and the ratio of cathode-to-anode surface areas [95].

Aminolysis

Similarly, aminolysis aims to introduce reactive amine groups onto polymer and metallic surfaces. For this modification, polymers such as polyurethane (PU), poly(caprolactone) (PCL), or PLA are submerged onto diamines solutions such as 1,6-hexanediamine or ethylendiamine, forming amides and obtaining free amino-end groups onto polymer surfaces [83,96]. Conversely, the introduction of amino groups into metallic substrates is usually more complex and it is generally necessary to use stronger conditions such as plasma. Nevertheless, similar to hydrolysis approaches, aminolysis can cause polymer degradation by increasing polymer roughness and wettability, which can alter subsequent protein, cell and even bacterial–material interactions [81,97].

An example of this was described by Yaseri *et al*.[83]. In this work applicability of PCL nanofibers in tissue engineering was analyzed employing surface treatments strategies including hydrolysis and aminolysis. It was observed that both treatments predominantly influenced the surface properties of PCL nanofibers without compromising their bulk properties. Beside minor morphological changes and a moderate reduction in mechanical performance, a notably enhancement in hydrophilicity was observed in most modified samples. It is worth to note that *in vitro* studies showed that the surface modifications of PCL nanofibers presented non-cytotoxicity as well as provided an ideal substrate for cell attachment, spreading, and proliferation when cultured L929 cells were employed.

Plasma treatment

Plasma treatment offers a versatile method for introducing functional groups onto inert polymeric and metallic surfaces, both directly and indirectly. The process involves exciting a low-pressure gas, such as ammonia, oxygen or argon, in a chamber through various energy sources such as electric discharge, alternating/direct current, radio-frequency energy, microwaves, or heat [98,99]. This partial ionization of the gas leads to charged molecules that bombard the material surface by modifying its chemical and physical properties. The type of functionality introduced on the surface of the substrate depends on the choice of plasma gas and the operating parameters, such as pressure, power, gas flow rate, and time. For instance, reactive NH_3 plasma introduces amines, O_2 plasma produces a mixture of OH and COOH functionalities, and argon plasma creates radicals. Similarly to other approaches, these functional groups can be effectively employed in combination with other surface grafting methods. As other approaches, plasma treatments can directly enhance surface hydrophilicity and cellular adhesion, offering advantages in biomedical applications [100–102].

In this regard, Ujino *et al*. employed atmospheric pressure plasma treatment to increase the hydrophilicity of pure Ti surfaces [90]. The main goal of this study was to evaluate the impact of the hydrophilicity surfaces on the initial adhesion of the material to rat bone marrow and its subsequent differentiation into hard tissue. After applying plasma to 30 s, superhydrophilicity was induced on pure Ti surfaces. The results suggested that a notable enhancement in both adhesion and osteogenic differentiation of cells culture was obtained on plasma-treated samples in comparison with untreated disks.

Similarly, Mian Chen *et al*. developed a fluorinated surface by plasma treatment of Ti surfaces [91]. The experiments involved various fluorine chemical compositions

applied as coatings. *In vitro* antibacterial studies were evaluated using *Staphylococcus aureus* and cell compatibility was studied employing MC3T3-E1 cells. The results suggested that both fluorocarbon coatings and metal fluorides coatings provided hydrophilicity with a nano-scaled roughness. Interestingly, the coating consisting of metal fluorides exhibited excellent bactericidal properties and demonstrated exceptional cytocompatibility. It has to be noted that antibacterial activity was attributed to the presence of metal fluorides and the release of fluoride ions.

In this context, Lee *et al.* conducted a comprehensive investigation into the antibacterial properties of Ti samples by treating the surface with non-thermal atmospheric pressure plasma jet (NTAPPJ) [103]. They studied two different bacterial cell wall structures of both Gram-positive and Gram-negative bacteria. To achieve this objective, they employed compressed air plasma, resulting in a notable increase of hydroxyl and carboxylate-related ions, including ^{-}OH and COO^{-}, respectively. Consequently, this treatment substantially enhanced the hydrophilicity and surface energy of the treated Ti samples without compromising topographical features. Fluorescent imaging technique concluded that the alterations in Ti surface, such as surface energy, chemical composition and reductive potential induced by NTAPPH treatment, led to a significantly lower number of adhered bacteria and a decreased rate of biofilm formation. Additionally, in their comparative analysis of Gram-positive and Gram-negative bacteria, it was observed that both adhesion and the biofilm formation rate were significantly lower in the case of Gram-negative bacteria when the samples were subjected to longer durations of the NTAPPJ treatment. These results suggest that NTAPPJ treatment can be considered a promising and effective strategy to prevent bacterial adhesion and biofilm formation on Ti dental implant surfaces.

Grafting

Various strategies have been proposed to develop coatings that exhibit enhanced physical and chemical resistance. However, these approaches are often constrained by the type of bonding between the coating and the substrate. A promising alternative method involves grafting, where covalent immobilization of compound takes place to create a resilient film on the material surface. Currently, two main grafting methods are employed: "grafting to" and "grafting from" [104].

In the "grafting to" method, polymer chains are attached to the surface, providing a means to modify the properties of the material. Conversely, in the case of "grafting from" methodology monomers are bonded to the surface where subsequent

polymerization takes place (**Figure 1.8**). This last approach offers greater control over the structure of the coating and properties. By employing grafting techniques, it is possible to obtain coatings with tailored functionalities, such as improved resistance to wear, corrosion and environmental degradation. Additionally, covalently immobilizing the polymers ensures better adhesion and durability, resulting in coatings that withstand harsh conditions over extended periods.

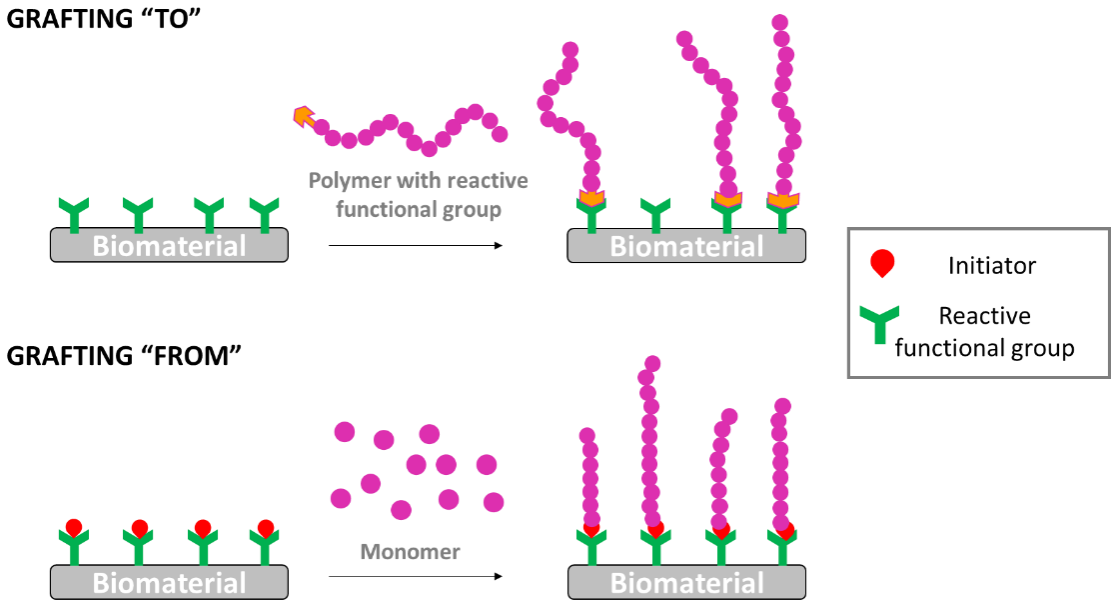

Figure 1.8. Representative scheme of grafting "to" and grafting "from" strategies.

In this context, Huh *et al.* performed different experiments using oxygen plasma glow discharge onto PET samples [105]. As a consequence of the plasma, the texture of PET surfaces was enhanced, resulting in the formation of peroxides on its surfaces. These peroxides were employed as catalysts for the grafting and polymerization of acrylic acid in order to introduce carboxylic acids onto the surfaces. Subsequently, neutral and quaternized chitosan were coupled with the previously introduced carboxyl groups, leading to chitosan-grafted PET and quaternized chitosan-grafted PET. To assess the antibacterial activity of the modified PET textures, a shake flask method was employed. After shaking for 6 h, it was observed that PET with covalently grafted chitosan and quaternized chitosan showed significant inhibition of bacterial growth. Even after PET texture laundering, the inhibition of bacterial growth remained in the range 48–58 %, demonstrating the durability and effectiveness of the chitosan grafted PET textures against washing.

Other strategy than can be classified as grafting is the formation of self-assembled structures. In this context, Blodgett *et al.* described in 1935 the preparation of organic thin films by depositing long-chain carboxylic acids onto solid surfaces [106].

Based on that previous work, one decade later, Zisman *et al.* modified platinum and pyrex surfaces through the establishment of self-assembled structures of long-chain hydrocarbons containing polar groups [107]. However, the term "self-assembled monolayers" (SAMs) was not introduced until 1983 by Jacob Sagiv, who described these SAMs as highly oriented and ideally ordered two-dimensional molecular assemblies that are formed on material surfaces due to the specific interactions between the monomers and the surface. While sulphur-containing molecules on gold and alkylsilanes on oxides are among the most well-known examples of SAMs, a diverse range of self-assembled systems have been reported. In fact, due to the physical and chemical robustness of this type of formation, this methodology allows for precise tailoring of surface properties in a controllable manner. As a result, this methodology finds extensive applications in various fields, such as biomaterials [108] or electronics [109,110].

SAMs involve amphiphilic molecules encompassing three essential components. Firstly, the anchoring group, which exhibits a specific affinity for the substrate and plays a crucial role in arranging the molecules orderly and laterally. Secondly, the molecular spacer, which is located between the head and the terminal group, determines the thickness of the SAM based on its length, typically ranging from 1 to 3 nm [16,108]. Finally, at the opposite end of the amphiphilic molecule, the free functional group remains available for subsequent modifications, dictating the physical and chemical properties of the modified substrate. This terminal functional group proved invaluable for fine-tuning surface characteristics such as conductivity, chemical reactivity, wettability, friction, corrosion resistance and, most significantly, in the context of this work, biocompatibility. SAMs offer a versatile approach to modify the properties of various substrates, including glass, silica, polymers and metals by skilfully tailoring the terminal functional group [111]. In fact, these surfaces have been successfully transformed to meet specific requirements for various applications.

SAMs can be categorized into six groups based on the primary coupling chemistry group employed for attachment: carboxylates, alkenes/alkynes, amines, silanes, phosphonates and catechols. Although carboxylates, alkene/alkynes, amines and catechols have also been extensively used in the preparation of SAMs [111], in this chapter, only silanes and phosphonates, used in this Doctoral Thesis, will be described.

a) Silanes

Surface modification with alkylsilanes is a highly interesting technique for creating monolayers on oxide surfaces. These organosilanes, involving compounds such as $RSiX_3$, R_2SiX_2 or R_3SiX; where R represents an alkyl group and X a leaving group like chloride, alkoxy or hydride, have found versatile application in various fields [108,112]. The key advantage of employing silanes monolayer formation on oxide surfaces lies in the rapid establishment of a covalent bond between the substrate and the anchoring group. This covalent linkage confers stability to the monolayer while facilitating chemical modifications without compromising its integrity [113]. A comprehensive understanding of these monolayers properties, such as their chemical composition, thickness, orientation and the lateral order of the alkyl chain, has been studied across a diverse range of surfaces, Ti and polymer based surfaces included.

Two different pathways can be followed to introduce a functional end group on Ti surfaces: the direct linkage to the metallic surface of pre-functionalized organosilane, or the chemical modification after SAM is formed. This second strategy has been revealed to be a better route due to several reasons. Firstly, the order of the monolayer is not affected by additional surface modifications, as long as the immobilized SAM is stable enough and, consequently, also the post-functionalization prompts. Secondly, different chemical reactions can be employed to modify the same surface, which offers more options for introducing various functional groups. In addition, this methodology is extremely simple and there is no need to synthesize and purify new tailor-made precursors since the most employed molecular precursors that form well-defined monolayers are easily accessible.

The first step in the formation of silane SAM is the hydrolysis of the organosilane by water molecules that are adsorbed onto the surface (**Scheme 1.1**). Later, in the second step, the formed hydroxysilanes bond to the polar oxide surface through Van der Waals forces. Once aggregated, the condensation of the Si-OH takes place, forming a new bond is formed, Si-O-Si. This new bond occurs between the silane and the surface and with the neighboring silanol groups, generating a cross-linked network between the silanes. The main advantage of this methodology lies in the great variability of commercially available silanes that allow subsequent reactions without compromising the stability of the monolayer. Monofunctional organosilanes having only one leaving group, typically, $R(CH_3)_2SiX$, are advantageous in terms of reproducibility because only one type of surface-binding bond is possible. The only disadvantage of these derivatives is that the volume of the two methyl groups limits the surface of the Ti covered. Conversely, in the case of trifunctional organosilanes

($RSiX_3$) all three leaving groups can be hydrolyzed yielding the intra-monolayer cross-linking and, as a consequence, increasing the stability. However, in this case, simultaneously or even prior, to covalent bonding with the surface, oligopolymerization reactions in solution may take place due to homocondensation giving rise to disordered structures.

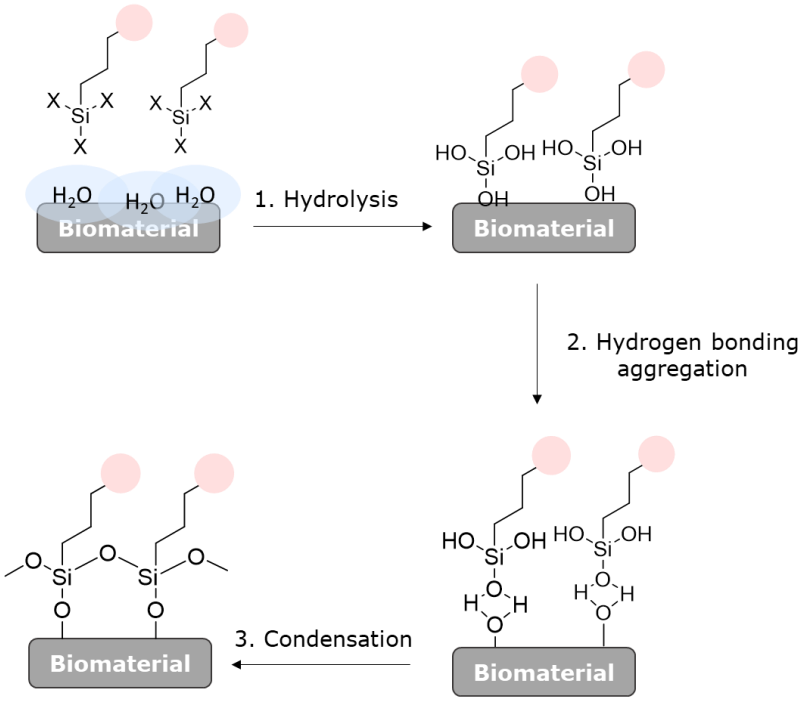

Scheme 1.1. Schematic representation of the mechanism of silanizated based SAMs generation.

On the other hand, alkyl chains are, by far, the most widely used spacers. The primary reason for this is the ease with which alkyl chains self-organize, in fact, this effect is widely manifested in biological structures involving lipid molecules. The length of the alkyl chains is a determining factor in achieving stable and well-organized SAMs through the Van de Waals interactions established between them [114,115].

The end functional group will determine the properties of the SAM as their chemical reactivity, conductivity, wettability, friction, adhesion and subsequent uses of the surface [116]. Concerning the introduction of these terminal functional groups in the monolayer, there are two general approaches. The main difference between them is at what point in the synthesis takes place the bonding to the Ti surface (**Figure 1.9**). The first approach (A approach in **Figure 1.9**) consists in carrying out the adsorption of a previously synthetized precursor. The main disadvantage of this protocol is the need to optimize the self-assembly step with each derivative synthesized. In contrast,

the second methodology (B approach in **Figure 1.9**) consists of forming the SAM in the first step, and then carrying out the necessary reactions to achieve the desired functionality. This methodology requires reactions with high selectivities and yields and the absence of secondary processes that give rise to impurities, since the possibilities of purification are limited. On the other hand, the main advantage of this approach is its simplicity. In fact, in this case, the silanes used are those in which the good results in their bonding to the surface and in the effective formation of monolayers are well established. Indeed, once the monolayer is formed, its stability will not be influenced by the subsequent reactions that must be carried out later to achieve the appropriate functionality [115].

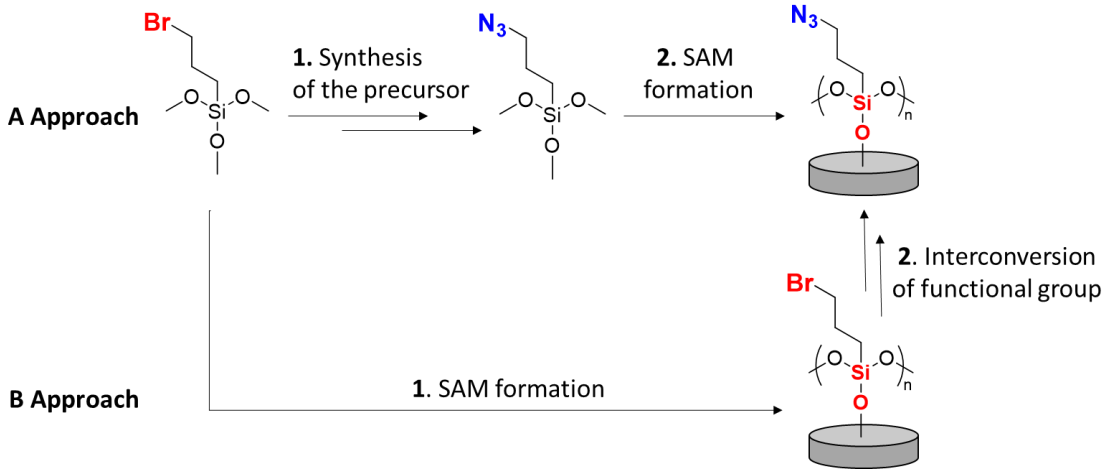

Figure 1.9. Two different approaches to obtain the desired end terminated SAM.

In this context, Hasan *et al.* conducted a study on the preparation of silanized coating and their impact on the antibacterial activity on Ti surfaces [117]. They successfully generated Ti6Al4V surfaces with a wide range of wettability by forming hydrophilic (carboxylic and amine), hydrophobic (Octyl) and moderately hydrophobic (mixed and hybrid) SAMs. A comprehensive comparative analysis was carried out to assess protein adsorption, cell adhesion and antimicrobial activity on the modified surfaces. The results revealed a close correlation between microbial adhesion and surface hydrophobicity. Amine functionalized surface, protonated under physiological pH, exhibited a positive charge that attracted bacterial cells due to their negatively charged cell walls. This led to maximum adhesion of both *Escherichia coli* (Gram-positive) and *Staphylococcus aureus* (Gram-negative) bacteria. As the hydrophobicity of the surfaces increased, bacterial adhesion drastically reduced, therefore, the highly hydrophobic octyl surface showed the least bacterial attachment.

Another example of silane activity was reported by Abraham Rodriguez and coworkers [118]. They presented a reproducible methodology to obtain a cross-linked polymer-type brush structure of covalently-bonded aminoalkylsilane chains on Ti6Al4V. They functionalized Ti6Al4V alloy with 3-aminopropyltrimethoxysilane (APTMS) achieving a high density coated surface, which could be resilanized. They studied *Staphylococcus* adhesion and biofilm formation compared to the pristine Ti6Al4V oxidized surface. Biological tests showed that the modified Ti-alloy is appropriate for biomedical implants and prostheses. According to human primary osteoblast behaviour, aminosilanized samples displayed a similar cytocompatibility to that of the alloy. Moreover, bacterial assays with *Staphylococcus epidermidis* cultures indicated that aminosilane layers exhibited protection against adhesion.

b) Phosphonates

Phosphonic acids ($R\text{-}PO_3H_2$), similar to silanes, are considered attractive anchoring groups for hydroxylated surfaces. In fact, ever since Ries and Cook's pioneering work in 1954, the use of these derivatives to form monolayers has made significant progress. In a comparative study conducted by Silverman *et al.* between phosphonates and silanes as anchoring groups [119], it was demonstrated that the former exhibit greater hydrolytic stability than the latter, especially under basic or physiological conditions. This characteristic renders phosphonic acids much more appealing for medical-related applications. In fact, the robustness of P-O-Ti bonds and their resistance to hydrolysis make this type of monolayer comparable to those based on catechol, alkenes or alkynes, in terms of stability and functionality. These findings highlight the potential of phosphonic acid-based monolayers for various practical applications, particularly in the medical field [120,121].

The most common technique used to obtain alkyl phosphonate-based monolayers is immersion or dip coating, which involves liquid-phase reaction conditions. Immersion times typically range from a few minutes to several hours or even days [16].

Various factors influence the chemisorption mechanism of phosphorus derivatives on metal surfaces, including temperature, pH value, concentration or solvent. Due to the Lewis acid character of previously activated Ti surfaces, the initial bonding step occurs through the coordination of the phosphorus atom. As a result, the electrophilicity of phosphorus increases, leading to a condensation reaction with the hydroxyl groups present on the metallic surface. This process results in a robust covalent anchoring of the monolayer. It is worth noting that not only phosphonic acid, but also phosphonate esters undergo similar condensation reactions under mild conditions, which is surprising giving that P-O-C bond cleavage in solution usually

requires comparatively drastic conditions (**Scheme 1.2**). In any case, the number of hydroxyl groups on the metal surface plays a key role in the successful binding of the phosphonates [111,120].

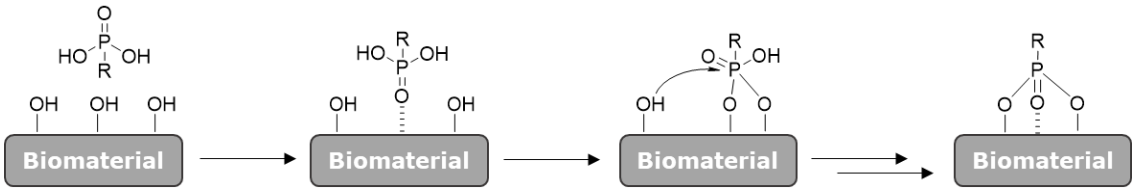

Scheme 1.2. Phosphonate SAM formation mechanism.

An example of this approach is described by Callies *et al*. In this work they presented the synthesis of copolymeros using 4-vinylpyridine (VP) in combination with vinylbenzylphosphonate (VBP) or dimethyl(2-methacryloyloxyethyl) phosphonate (DMMEP) through free radical polymerization [122]. Subsequently, *N*-alkylation with 1-bromohexane was carried out to introduce *N*-hexylpyridinium bromide groups (HexVP). The copolymers were then attached to Ti oxide surfaces using the phosphonates as linker groups. This coating process resulted in the formation of ultrathin polymer films at the nanometer scale, with thicknesses ranging between 3 and 11 nm. The study showed distinct distribution patterns for *Staphylococcus epidermis* and *Staphylococcus aureus* on the coated surfaces compared to blank Ti controls. These results clearly demonstrated the antimicrobial effect of coatings with a higher proportion of DMMEP, which is a relatively hydrophilic monomer and yields homopolymer with non-fouling properties. The presence of DMMEP in the copolymers contributed to increased antimicrobial activity of the coatings, indicating the potential of these materials in developing effective antimicrobial surfaces.

1.6.1.3. Coatings

Polymeric and ceramic coatings have become interesting subjects for biomedical applications (**Table 1.3**). These coatings provide a number of valuable advantageous properties attributed to the underlying material, such as enhanced biocompatibility, improved mechanical robustness, increased wear and corrosion resistance, and enhanced functional capabilities.

Table 1.3. Classification of most used ceramic and polymer coatings in the field of biomaterials.

Coating	Approach/Material	Advantage/Activity	Ref.
Ceramic	Calcium phosphate	Superior osseintegration rate Corrosion resistance Boosted cell adhesion	[123–128]
	Hydroxyapatite	Favourated cell adhesion and proliferation Enhanced osteoconductivity Improved osteointegration	[129–132]
	Bioactive glasses (BGs)	Excellente osteoconductivity and osteoinductivity properties	[133,134]
Polymer	Chitosan Collagen Hyaluronic acid PEG	Antibacterial and antifouling properties Improved osteogenesis Enhanced biofilm prevention	[135–141]

Ceramic Coatings

Ceramic coatings are thin layers of ceramic materials that are applied to the surface of various substrates, such as metal, glass, or ceramics to enhance their properties or provide specific functionalities. These coatings are commonly used in a wide range of industrial and technological applications due to their unique combination of properties, which can include high temperature resistance, wear resistance, corrosion resistance, electrical insulation, thermal insulation, and biocompatibility [142].

Among ceramic coatings, calcium phosphates (CaPs) are the most commonly employed due to their remarkable similarity to bone tissue. Indeed, they represent

highly promising materials in the field of bone regeneration, providing compelling substitutes for auto- and allografts in facilitating and reinforcing tissue regeneration within critically-sized bone defect [143]. Their exceptional biocompatibility and biodegradability make them especially well-suited for this purpose, owing to their resemblance to the mineral phase found in natural bone. Numerous studies have been dedicated to the development of CaP ceramic coatings on metallic substrates with the goal of replicating the biological properties of bulk bone tissue and improving the durability and stability of implants.

Biomineral formation and the adhesion of cells and proteins can be effectively regulated by tailoring the surface properties such as roughness and porosity of CaP materials [143]. On the other hand, it should be noted that different phosphates, such as hydroxyapatite (Hap) or tricalcium phosphate (TCP) have different biocompatibility due to differences in crystallinity, solubility, stability, ion release, and mechanical properties.

As commented, among CaPs, HAp deserves special attention, as it constitutes the primary inorganic component of bone tissue. In fact, recent advancements in materials science and processing have enabled the production of hydroxyapatite-based grafts in various forms, satisfying the demand for a wide range of clinical applications. Moreover, these innovations have obtained promising results in both *in vitro* and *in vivo* studies [143].

In this context, Chen *et al*. introduced a method for electrodepositing a nanostructured HAp coating onto Ti surface [132]. To enhance the adhesion between the HAp coating and the Ti surface, they employed chemical etching and oxidation treatments, generating a thin TiO_2 layer which served as an interlayer that mitigated thermal stress and prevented the formation of cracks in the coating. After electrodepositing HAp, uniform and crack free HAp nanostructured coating was successfully generated onto the Ti surface. Additionally, *in vitro* MSCs cell culture experiments demonstrated the excellent biocompatibility and bioactivity of HAp-Ti nanostructured surface. The MSCs exhibited enhanced proliferation on Ti surfaces with HAp coating compared to pristine Ti surfaces.

Similarly, Hui Du *et al*. fabricated a coating composed of calcium silicate and calcium phosphate onto Mg-Zn-Mn-Ca alloy through a chemical reaction involving $NaSiO_3$ and $Ca(NO_3)_2$ [128]. *In vitro* cell studies concluded that osteoblasts exhibited good cell adhesion, high growth rates and proliferation characteristics. These results indicated a significance enhancement in surface cytocompatibility attributed to the presence of calcium phosphate coating.

Other type of ceramic materials are zirconia-based coatings (ZrO_2). This type of material can withstand high temperatures and elevated stresses. Its uses span across dental implants, including the application of protective coatings on metallic implants to enhance their resistance to corrosion. ZrO_2 ceramics offer a multitude of advantages, encompassing robust mechanical strength, chemical stability, biocompatibility, and superior wear resistance. Additionally, zirconia stabilized with yttria (YSZ) has gained prominence as a dental implant material. YSZ coatings exhibit superior hardness and scratch resistance when compared to HAp coatings. Furthermore, Saravan *et al*. revealed that YSZ-coated Ti substrates exhibit enhanced hemocompatibility, stimulating blood platelets to develop pseudopods [144].

Bioactive glasses (BGs) constitute another type of promising ceramic material, mainly due to their osteoinductive and bioresorbable properties, which make them suitable materials for bone tissue engineering applications. Ideally, bioactive implants used in clinical applications should exhibit similar properties as the host tissue, while establishing robust interfacial connections with both hard and soft tissues. Owing to the inorganic composition and mechanical attributes of the bioactive glasses, which closely mimic those of "hard" bone tissue, there has been considerable interest in their application in bone and teeth-based implants. However, their inadequate mechanical properties considerably hinder their use in load-bearing situations [142,145]. Indeed, the majority of BGs present lower fracture toughness when compared to natural load-bearing cortical bone, with BGs ranging between 0.2 and 0.6 MPa, while cortical bone registers a range from 2 to 12 MPa in terms of fracture toughness [146]. Therefore, the use of a BG coating emerges as a viable strategy to not only bolster the osseointegration of metallic implants but also mitigate the inherent brittleness of BGs. BG and glass-ceramic coatings on metallic implants can be produced by different techniques, including thermal spraying, radiofrequency magnetron sputtering (RF-MS) deposition, pulser lasered deposition (PLD), sol gel coating, and electrophoretic deposition (EPD) [147].

In this context, Bargavi *et al*. presented a thin film coating based on zirconia incorporated on a BG matrix and deposited onto commercially pure Ti (Cp-Ti) substrates [148]. The incorporation of Zr, in different concentrations, aimed to enhance the mechanical stability of the coating. Hemocompatibility studies revealed excellent compatibility, with a favorable hemolysis rate of less than 2%. Furthermore, *in vitro* cytocompatibility assays employing MG-63 osteoblast cell lines demonstrated a noteworthy enhancement in cell viability. Additionally, according to antibacterial assays, when Bg-Zr composites with high contents of Zr were used to coat Cp-Ti substrates, reduced biofilm formation was observed presumably due to the increase

in surface roughness. Consequently, surface modification of Cp-Ti implant materials using BG-Zr coating exhibited improved bioactivity and enhanced osseointegration, making this type of coatings suitable for orthopedic applications.

Polymer Coatings

Another type of coatings with a crucial role in biomedical applications are polymeric coatings. In fact, these types of coatings are commonly used to improve the performance, biocompatibility and functionality of biomedical devices. Furthermore, while providing these specific benefits, these type of polymers can improve interactions with tissues and biological fluids [57,74]. In this context, it is worth noting the widely employed strategy of covering a surface with a polymer with antifouling properties.

Another widely employed strategy to alter surface characteristics involves the passivation of biomaterials through surface coatings with antifouling behaviour. For instance, polyethyelene glycol (PEG), poly(hydroxyethyl methacrylate) (PHEMA), and phosphatidylcholine polymers [149–151], among others, constitute prominent examples of polymeric materials employed in this regard. These coatings exhibit robust steric repulsion and instigate hydration forces that effectively avoid protein and bacterial adsorption. By employing these mechanisms, these coatings protect the material from the host immune system and, consequently, limit leukocyte adhesion and the host inflammatory response. Moreover, these highly hydrophilic coatings offer a straightforward solution for repelling bacteria and enhancing a more favorable host–material interaction.

In this context, Ungureanu and coworkers electrodeposited a composite coating based on polypyrrole (PPy) and polyethyelene glycol (PEG) onto Ti alloy [152]. Three different concentrations of PEG were employed, specifically 0.5%, 2%, and 4%. When testing antibacterial properties of the coatings, the best effect was found for the coating with 2% PEG concentration, which had hydrophilic character and minor roughness. Such results were in concordance with the mechanism of biomaterial–bacteria interaction, which involves as factors affecting bacterial adhesion and growth an initial physicochemical interaction stage, where roughness and wettability are factors that can regulate bacterial adhesion and biofilm deposition.

In recent years, the layer-by-layer (LBL) methodology has gained widespread popularity as a versatile and effective technique for depositing polymeric materials on a surface. This innovative method involves the sequential deposition of cationic and anionic polyelectrolyte layers, which can be firmly bonded through ionic

interactions to create a thin and precisely controlled coating film. This process relies on the positive and negative charges that each polymer acquired under specific pH conditions. The LBL approach offers exceptional flexibility, allowing the creation of coating with diverse functionalities and tailored properties [153]. By varying the types and sequences of polyelectrolytes used, it is possible to achieve specific surface characteristics, such as charge, hydrophilicity, or bioactivity. This technique has found application in various fields, including biomedical engineering, drug delivery systems and surface modification of medical implants [154–157]. Its ability to produce thin and uniform coatings with controlled release capabilities has opened new avenues for enhancing biocompatibility and functionality of biomaterials.

An example of this is described by Del Hoyo-Gallego and coworkers [141]. They reported the successful coating of PET film by positively charged chitosan (CHI) and negatively charged hyaluronic acid (HA). A layer by layer technique was employed to introduce each polymer onto the surface, fabricating a nanometer-scale thickness coating and producing a potentially antifouling surface by electrostatic interactions. While CHI contributed to contact-killing properties, HA hydrophilicity facilitated bacteria repellence through a steric effect generated by water absorption.

Various strategies have been proposed to develop coatings that exhibit enhanced physical and chemical resistance. However, these approaches are often constrained by the type of bonding between the coating and the substrate, as the coatings discussed so far are physically placed on top of the material, without any stable, covalent interaction between the two systems. Studies including drug delivery and drug immobilization have proved valuable effectiveness to eliminate bacteria and promote good blood contact interaction. By focusing on optimizing these surface modification techniques, highly effective antibacterial, anti-inflammatory and anticoagulant material for various applications can be achieved, including medical devices, implants and surfaces in healthcare settings.

1.6.2. Bioactive surfaces

1.6.2.1. Drug release

A promising strategy to develop bioactive surfaces involves the controlled release of various active agents, such as drugs, growth factors, proteins, peptides, nucleic acids and even silver nanoparticles [16]. This controlled release occurs from a variety of platforms, including hydrogels and nanogels, polymer multilayers and cyclodextrines [158–160]. These structures, which are built upon polymers and proteins, serve as

remarkably versatile reservoirs capable of releasing bioactive molecules. This controlled release mechanism enables the desired surface response.

As commented before, an alternative and versatile approach to creating coatings with self-controlled active agent release ability is through the use of multilayer systems. While multi-layered coatings may have lower drug loading capacity compared to hydrogels, they present excellent control in chemical composition, structure, thickness, homogeneity, and responsiveness [161]. To achieve effective loading and sustained release of active compounds, it is essential to have intermediate strength bonds or interactions between polymers and the active agents. Similar to hydrogels, the release of active agents from multilayer coatings typically occurs through diffusion and multilayer degradation processes [162].

Implants associated infection in orthopaedic surgeries represent a critical concern due to their potential to impede bone healing, induce implant failure and even escalate to osteomyelitis. The concept of drug-eluting implants, designed for localized antibiotic delivery at surgical sites holds promise in mitigating these infections. In the study presented by Li *et al.* vancomycin, an antibiotic, was encapsulated within a PEG based hydrogel film [163]. This hydrogel was covalently bound to Ti implants and subsequently enveloped by a PEG-(poly(lactic-co-caprolactone) (PEG-PCL) membrane. Additionally, crosslinked starch was incorporated into the hydrogel due to its porous microstructure, which effectively curbed hydrogel swelling and consequently regulated drug release. The release kinetics of vancomycin were found to be controllable, dependent on both the drug loading and the thickness of the coating. Notably, the vancomycin-loaded Ti samples exhibited a sustained drug release profile, with no initial burst release. *In vitro* experiments demonstrated continuous drug release for nearly 3 weeks, while *in vivo* testing extended this period to over 4 weeks. Furthermore, a rabbit model subjected to *Staphylococcus aureus* infections exhibited a significant reduction in the inflammatory response and demonstrated robust antimicrobial property when implants containing 4 mg of vancomycin were used. Therefore, this approach holds promise as an effective strategy for the treatment and prevention of localized bone infections.

Similarly, Karakurt *et al.* presented two different strategies for creating a combined saccharide coating onto PLLA with the aim to develop antibacterial biomaterial surfaces [164]. Initially, PLLA samples were exposed to low-pressure plasma treatment and were then reacted with acrylic acid solution to obtain COOH and OH reactive functional groups. Subsequently, a "grafting from" approach was employed to create polyacrilic acid (PAA) brushes on PLLA surface. In addition, chitosan was

introduced to the surface by either covalently by carbodiimide coupling reactions or by direct coating method with electrostatic interactions. Following this, lomefloxacin-containing chondroitin sulfate saccharide was coated onto the previously mentioned surface, resulting in a polyelectrolyte complex (PEC). The coatings with the PEC formation between CS-ChS exhibited enhanced antibacterial activity against bacterial strains compared to individual coatings. Furthermore, these interactions increased the amount of lomefloxacin adhered to the film coatings and extended the drug release profile. Finally, the zone of inhibition test confirmed that the CS-ChS coating showed a contact killing mechanism, whereas drug-loaded films demonstrated a dual killing mechanism, encompassing both contact and release-based antibacterial actions.

Another example regarding antibacterial properties is described by Chen *et al.* [165]. They developed successfully a cost-effective strategy to obtain antibacterial 3D-printed PLA disks. They employed the direct adsorption of two antibiotic agent, ampicillin and vancomycin, onto the PLA disk surfaces. They observed the maximum adsorption capacities of ampicillin and vancomycin on the PLA disk surfaces to be approximately 75 mg/g of PLA and 65 mg/g of PLA, respectively. As they varied the concentration of the antibiotic agents in the aqueous solution, they noted a corresponding decrease in the amount of antibiotic agents absorbed on the sample surfaces. When they employed an antibiotic agent concentration of 50 mg/mL in the aqueous solution for absorption onto the samples, they achieved stable drug release profiles. These profiles consistently maintained antibiotic agent concentration in the buffer solution above the minimum inhibitory concentration (MIC90) for *Staphylococcus aureus*. Furthermore, the drug release kinetics of the antibiotic agents from the samples closely followed the Korsmeyer–Peppas model. The bioactivity of ampicillin and vancomycin, when suitably absorbed onto the sample surfaces, remained effective for at least 28 days. In practical terms, the PLA disk with directly absorbed antibiotic agents reduced the relative optical density of *Staphylococcus aureus* in a solution with a concentration of 106 colony-forming units per milliliter (CFU/mL) to 40 %, compared to a solution with only *Staphylococcus aureus* under the same conditions.

Several remarkable examples of multilayer coatings on Ti6Al4V substrates with potential bioactive properties based on the release of active agents have been reported in the literature. In this context, Valverde *et al.* developed a hyaluronic acid (HA)-chitosan (CHI) multilayer coating onto different micropatterned Ti6Al4V samples [166]. For this purpose, they employed smooth and laser patterned samples that were preactivated with acid hydrolysis employing H_2SO_4/H_2O_2 mix and

subsequent silanization with APTES. Once the amino functional end groups were obtained, they deposited 5 bilayers of HA and CHI. Triclosan, the antibacterial agent, was incorporated into the polysaccharide coating after every dipping process of the layers. Furthermore, this modification transformed these initially highly hydrophobic surfaces to be remarkably hydrophilic, as demonstrated by the significant reduction in contact angle values of the micropatterned surfaces. On the other hand, the topographic characteristics of the initial materials were maintained after the surface modification. Moreover, both smooth and patterned multilayers can perform as effective potential reservoirs for bactericides, facilitating their controlled release after implantation. Indeed, these multilayers were capable of releasing approximately 25% of the loaded triclosan within the initial 10 hours. This control makes them interesting materials for inhibiting bacterial adhesion and proliferation during the critical post-implantation period. This efficacy has been confirmed through testing against the bacterial strain *Staphylococcus aureus*.

On the other hand, as mentioned before, regulating macrophage response to biomaterials is a pivotal factor in mitigating inflammation after implantation. In this context, Shen and coworkers [167] designed a sustained release system from TiO_2 nanotubes (TNTs) to enhance osteogenesis on Ti implants with anti-inflammatory properties. The process involved the fabrication of TNTs on Ti surfaces *via* anodization. These TNTs were subsequently loaded with the anti-inflammatory drug, dexamethasone (DEX), and then covered by chitosan (CHI) multilayer films. Regarding, *in vitro* experiments, primary osteoblast and macrophage (RAW 264.7) cells were cultured on both untreated and treated Ti surfaces. Osteoblasts cultivated on CHI-coated Dex-filled TNTs surfaces exhibited elevated alkaline phosphatase (ALP) and enhanced mineralization, which was consistent with qRT-PCR analysis of osteoblastic genes including collagen type I (Col I), osteocalcin (OCN), osteopontin (OPN) and runt related transcription factor 2 (Runx2). Conversely, protein levels of nitric oxide (NO) and proinflammatory cytokines (TNF-α and IL-1β) produced by macrophages on Dex-filled TNTs, CHI-coated TNTs and CHI-coated Dex-filled TNTs were notably lower. This reduction was particularly pronounced on CHI-coated Dex-filled TNTs surfaces when compared to Ti and TNTs. These results indicated that CHI-coated Dex-filled TNTs not only promoted osteoblast differentiation, but also decreased the inflammatory response of macrophages. This innovative approach provides new insight into the modification of TNTs for the development of Ti-based implants.

As commented, vascularization is still a significant challenge in the field of tissue engineering. When the biomaterial is introduced in the human body, the own body

elicit an immune response, which can profoundly impact the process of angiogenesis, which refers to the formation of new blood vessels. Yin *et al* proposed the release of an interleukin to prevent this event [168]. Indeed, they introduced an innovative multilayer coating for T43BL-G Ti implant surface, employing chitosan and alginate as its key components. This advance coating demonstrated the capability to efficiently encapsulate interleukin-4 (IL-4) cytokine. Notably, the controlled release of IL4-facilitated robust osteogenesis both *in vitro* and *in vivo*, leading to enhanced bone formation. The ALG/CS multilayer films on TNTs facilitated the adhesion and spreading of HUVECs, but did not significantly affect cell proliferation, migration and tube formation. IL-4 released from ALG/CS multilayer films further improved angiogenic behaviour of HUVECs, as well as up-regulated the expression of early vascular markers. Moreover, material-induced polarized macrophages (either M1 or M2) significantly elevated the expression of late vascular markers in HUVECs. Thus, the material properties and material-induced macrophages may affect different stages of angiogenesis. In the in vivo study, the IL-4-loaded implant induced abundant new blood vessels in a short period; at the later stage, the surrounding tissue of IL-4-loaded implant was generally recovered to a normal state. Therefore, the IL-4-loaded implant exhibited an outstanding ability to promote angiogenesis and tissue repair *via* both direct stimulation of endothelial cells and indirect induction of favourable macrophage phenotypes.

1.6.2.2. Drug immobilization

In this approach, the biomolecule or bioactive agent is effectively anchored to the surface of the material through covalent immobilization. With regards to the antibacterial behaviour, bactericidal agents like low molecular antibiotics, bacteriophagues, cationic antimicrobial peptides, lysozyme or quaternary ammonium polymers can cause bacterial death upon contact [57,169]. Typically, the death of bacteria occurs by either the disruption of the bacterial membrane, or from specific interactions of the immobilized agent with target biomolecules on the bacterial surface. Similarly, anti-inflammatory and anticoagulant properties can be obtained by immobilizing agents with the corresponding activity. However, the mechanisms behind these actions are intricate and depend on the specific agent involved. For instance, anti-inflammatory biomolecules like glycosaminoglycans (GAGs), including heparin (HEP), chondroitin sulphate (CS) or hyaluronic acid (HA)[138,170], which have demonstrated significant anti-inflammatory potency in numerous experimental studies and clinical trials, play different mechanism to induce anti-inflammatory response. These linear and negatively charged polysaccharides have a notable capacity to interact and bind with various proteins, encompassing ECM adhesive

proteins like collagen and fibronectin, along with chemokines, cytokines, growth factors and enzymes integral to biological processes such as cell migration, growth and differentiation. This ability enables them to modulate events connected with inflammation.

In order to carry out the immobilization of these agents on the different materials, it is necessary to previously modify or activate their surface. For this purpose, it is common to use the aforementioned strategies such as grafting and functionalization. After the introduction of functional groups, conjugation reactions including amidation, esterification or more valuable reactions such as click reactions are carried out to anchor the biomolecules.

Next, representative examples of antibacterial behaviour of various samples by immobilizing different antibiotics or bioactive agents will be presented.

The covalent immobilization of antimicrobial peptides onto Ti surfaces has indeed been a well-established approach to prevent bacterial adhesion and biofilm formation. However, it remains uncertainty regarding the necessity of using a spacer to bind the peptide onto the surface in order to promote antibacterial adhesion, while maintaining excellent biocompatibility. In a study by Nie and coworkers [171], the antibacterial properties and the inflammatory response elicited by Ti and PEGylated Ti surfaces (surfaces coated with PEG) were investigated. These surfaces were subsequently covalently functionalized with KR-12 peptide, which is a derived peptide from LL-37, a substance known for its bactericidal and bacteriostatic properties in solution. For this purpose, Ti surfaces were initially activated with NaOH alkali solution to introduce OH functional groups on the surface and then sinalized with 3-(2-aminoethylamino)propyltrimethoxysilane. For PEG conjugation, EDC and NHS coupling agents were employed. Finally, KR-12 peptide was immobilized onto silanizated Ti surfaces and PEGylated Ti surfaces using, again, EDC and NHS as coupling agents. The introduction of KR-12 affected profoundly on bacterial adhesion. Indeed, a significant decrease of bacterial adhesion was achieved on both surfaces. In addition, PEGylated surfaces demonstrated a marked enhancement in antimicrobial efficacy, resulting in a notable reduction *in vitro* adhesion and biofilm formation of *Staphylococcus epidermis* compared to non-PEGylated Ti surfaces. Furthermore, both PEGylated and non-PEGylated Ti surfaces exhibited a significant decrease in TNF-α and IL-1β secretion, leading to macrophages remaining in an inactive rounded state. Therefore, this study confirmed the potential of grafting of a PEG spacer to immobilize KR-12 peptide that promote improved antibacterial

properties and provided reduced macrophage activation, which can decrease overall inflammatory response.

On the other hand, Andras Heijink and coworkers proposed to enhance the surface of Ti implants by functionalizing them with the Arg-Gly-Aps tripeptide (RGD) [172]. Their objective was to facilitate the attachment of osteoblasts, a key step in achieving improved implant fixation. This study encompassed a comprehensive examination of the histomorphometric and mechanical performance of Ti implants, exploring two different approaches for RGD immobilization: one involving self-assembled monolayers of phosphonates (RGD/SAMPS) and the other employing the more conventional thiolate-gold interface (RGD/thiolate-gold). The results suggested that RGD/SAMP-coated implants exhibited a substantially greater affinity for bone growth and superior implant fixation compared to their RGD/thiolate-gold-coated surfaces.

In this context, Hoyos-Nogues and collaborators employed a dual peptide approach and PEG coating strategy onto commercially pure Ti samples [173]. They presented a method for the development of a trifunctional coating designed to repel bacterial contamination, kill adhering bacteria and promote osteoblast adhesion. For this purpose, they initiated the functionalization of metallic surfaces through the electrodeposition of an antifouling PEG layer, followed by the binding of a peptide platform, which contained RGD and LF1-11 that provide both cell-adhesive and bactericidal properties. As results suggested, the deposition of the PEG coating and the immobilization of the biomolecules did not alter the morphology and topography of Ti samples. Additionally, PET coated and peptide immobilized samples demonstrated a significant efficacy in preventing protein adsorption and hindered the attachment of osteoblast cells. However, the introduction of cell adhesive domains rescued osteoblast adhesion, resulting in significantly higher levels of cell attachment and spreading when compared to control samples. Regarding antibacterial properties, the presence of PEG layers led to a substantial reduction in bacterial attachment on the surface and the addition of the bactericidal peptide further improved this antibacterial behaviour, decreasing bacterial adhesion levels below 0.2 %. As commented on the Introduction Section, the balance between the risk of infection and the optimal osseointegration of a biomaterial is often described as “the race for the surface”, in which contaminating bacteria and host tissue cells compete to colonize the implant. In this study, they successfully developed a multifunctional coating for Ti surfaces, since not only promoted the attachment and spreading of osteoblast cells, but also effectively inhibited bacterial colonization.

Regarding anticoagulant effect, Tan and coworkers[174] grafted heparin (HEP) and phosphorylcholine groups (PC) onto the polyurethane (PU) surface in order to enhance biocompatibility and impart anticoagulant properties. After grafting polyethylenimine (PEI) on PU surface, primary free amino groups were displayed on PU surface. Heparin was then covalently anchored to the free amino groups on the surface by an amidation reaction involving the carboxyl groups of the heparine. Simultaneously, PC groups were covalently immobilized on the PU-PEI surface through the condensation between the amino group and the aldehyde group of phosphorylcholine glyceraldehyde (PCGA). The resulted PU-HEP and PU-PC composite films exhibited significant reduction in platelet adhesion, underscoring the efficacy in minimizing thrombotic events. Moreover, these materials exhibited exceptional antithrombogenicity and blood compatibility, rendering them as versatile candidates with potential applications in many fields, including artificial blood vessels, artificial heart valve prosthesis or heart stents Furthermore, this surface modifications significantly enhanced hydrophilicity and hemocompatibility. These results suggested that the PU-HEP and PU-PC composite films are promising candidates for blood contacting tissue engineering.

Similarly, Ozaltin and coworkers employed direct current air plasma treatment onto PET in order to create an oxidative layer to bind the marine-derived anticoagulant sulphated polysaccharide, fucoidan [175]. To optimize the chemical bonding behaviour and, consequently, the anticoagulant performance, this immobilization process was meticulously conducted at various pH values from 3-7. They concluded that pH 5 was the optimal for fucoidan immobilization onto PET surface post-plasma treatment. Under this conditions, the immobilized fucoidan exhibited exceptional anticoagulant activity, surpassing the crucial threshold of 100 s. This remarkable performance serves as clear evidence of the complete suitability of these PET-based materials for designing devices for direct contact with blood.

1.7. Click Chemistry

Click Chemistry, originally introduced by Sharpless *et al.* in 2001, can be defined as C-heteroatom and C-C bond forming reactions that yield products with high efficiency and selectivity [176]. This new concept emerged as a versatile and valuable approach for constructing complex structures seamlessly combining smaller molecules through a limited set of highly efficient reactions [177]. Generally, to consider a chemical transformation as click reaction, it has to gather the following characteristics [176]:

1. Wide substrate scope. These reactions accept a broad range of substrates, including small molecules, polymers, biomolecules and surfaces. This versatility enables the construction of diverse molecular assemblies and facilitates the integration of Click Chemistry in various research areas.
2. Simple reaction conditions. Click reactions typically employ mild reaction conditions, such as room temperature, air media, aqueous solvent and, even, physiological conditions. These gentle reaction conditions contribute to the wide applicability of Click Chemistry in various fields, including bioconjugation and materials science.
3. High efficiency. Click reactions are known for their exceptional conversion rates and high yields, allowing rapid formation of desired products.
4. Selectivity. These reactions demonstrate excellent selectivity targeting the desired product without generating undesired byproducts. In general, these reactions are addition or cycloadditions, which do not imply the formation of any secondary product, or condensations, being water, in this case, the only byproduct. In this context, it is worth noting that in the last decade a new term has been coined to refer to the complete chemoselectivity of click reactions: orthogonality.

Despite finding considerable variety of chemical reactions that could meet these criteria, the most outstanding examples are described below (**Figure 1.10**) [178]:

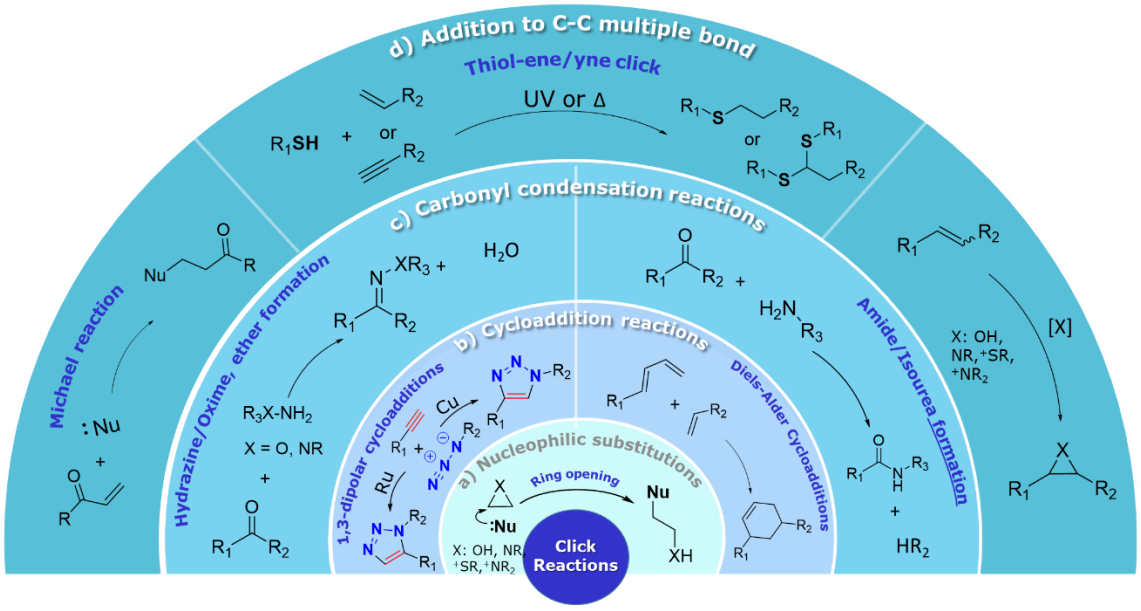

Figure 1.10. Schematic representation of the most used click reactions.

1. Nucleophilic ring opening reactions

The nucleophilic ring-opening reactions predominantly involve 3 member heterocycles, including epoxy derivatives, aziridines, cyclic sulfates, cyclic sulphamides, aziridinium ions, cyclosulfonium ions and more. These reactions, during the ring-opening process, effectively release the internal tension energy presented in these heterocyclic compounds (**Figure 1.10**) [176].

2. Cycloaddition reaction

Cycloaddition reaction are particularly suited for implementing the concept of Click Chemistry, as they enable the formation of diverse five and six-membered heterocycles by joining unsaturated reactants (**Figure 1.10**). The most significant example of these reactions is the reaction between azide and alkyne, firstly described by Huisgen in 1960 [179].

3. Carbonyl condensation reactions

Carbonyl condensation reactions encompass different processes that have found widespread application in organic synthesis. Notably, the reaction of aldehydes and ketones with 1,3-diols leading to the formation of 1,3-dioxolanes, the reaction of aldehydes with hydrazines or hydroxylamine ethers resulting in hydrazones or oximes, and the reaction of α,β-carbonyl aldehydes and ketones with esters to produces heterocyclic compounds are among the most widely utilized carbonyl condensation reactions (**Figure 1.10**). These versatile reactions offer an efficient route to construct a diverse array of valuable chemical scaffolds with various functional groups, making them indispensable in the synthesis of complex molecules including natural products [176].

4. Addition reaction of carbon-carbon multibonds

Thiol-ene/yne click reaction represents the typical addition reaction involving C-C multiple bonds (**Figure 1.10**), which was discovered subsequent to the Huisgen reaction. Generally, this reaction is carried out under UV irradiation, using a photoinitiator, which initiates the click reaction between unsaturated bond and thiol [180,181]. This Click Chemistry approach exhibits a remarkably broad scope of applications. Notably, the thiol-ene click reaction has emerged as a simple, and metal free catalyzed process, which can be employed as an efficient tool in curing reactions and polymer modification [182,183]. Additionally, alkynyl compounds are ideal substrates for Click Chemistry due to their ability to form diverse structure and their stability under standard conditions. The versatility and reliability of these click

reactions have made them indispensable in various fields, spanning from materials science to biomedical research, enabling the facile and controlled synthesis of complex molecules and polymers with tailored properties [184].

The common characteristics and variety of reactions mentioned above contribute to the broad utility and popularity of Click Chemistry as a synthetic tool. By providing efficient and reliable method for the assembly of complex structures, Click Chemistry has become an indispensable strategy in fields such as drug discovery, materials science and bioconjugation.

1.7.1. Copper Catalyzed Azide Alkyne Cycloaddition reaction (CuAAC)

Among many reactions, the 1,3-dipolar cycloaddition between azides and alkynes has been established as the prototype reaction among those classified as "click" reaction. This reaction was first described by Huisgen in 1960 and has proven to be the most efficient route to synthesize 1,2,3-triazoles [179]. The 1,3-dipolar cycloaddition between azides and alkynes is thermodynamically favorable, but it typically requires high temperatures and refluxing conditions in solvents such as toluene or carbon tetrachloride (CCl_4) [179]. The reaction is often carried out over prolonged periods, ranging from 12 to 60 hours, in order to achieve complete conversion. Under these thermal conditions, both regioisomers of the 1,2,3-triazole product (1,4 and 1,5 regioisomer) are formed in an almost equimolecular ration (**Scheme 1.3**). However, it is possible to obtain certain levels of regioselectivity by carefully controlling reaction conditions. In fact, the regioselectivity of the reaction can be influenced by the electronic properties of the reacting moieties. Electron deficient acetylenes increase the electrophilicity of the triple bond carbon, favoring nucleophilic attack at the more substituted carbon (1,4 addition). On the contrary, electron-rich acetylenes, leads to nucleophilic attack at the less hindered carbon (1,5 addition). So, the use of highly electron-deficient acetylenes tends to favor the formation of the 1,4-regioisomer, while the use of electron-deficient azides favors the production of the 1,5 isomer [185].

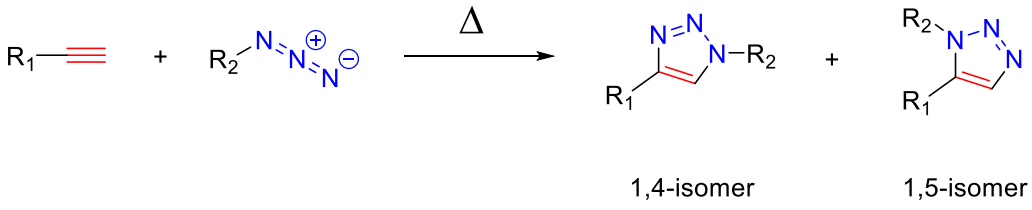

Scheme 1.3. Azide and alkyne Huisgen reaction.

Both alkynes and azides possess a relatively high energy content. However, these functional groups are considered to be among the least reactive in organic chemistry. Once a 1,2,3-triazole is formed through the 1,3-dipolar cycloaddition, these heterocycles exhibit remarkable stability and remain unaltered throughout subsequent chemical reactions. The kinetic stability of the resulting triazole enable it to withstand a wide range of reaction conditions, making it highly versatile in various organic and biological settings [176,177]. These heterocycle rings demonstrate exceptional tolerance towards biomolecules, oxygen, water and most experimental conditions encountered in organic and biological media. Moreover, the inertness of alkynes and azides towards various environmental factors and reactive species makes them suitable for applications in biological systems. They can coexist harmoniously with biomolecules, such as proteins or nucleic acids, without causing significant interference or detrimental effects. This compatibility has paved the way for the use of Click Chemistry in bioconjugation and biocompatible materials development [186,187]. Additionally, the physicochemical and biological properties of the 1,2,3-triazole structural block make this structure an excellent peptide bond mimetic, but with the advantage of being inactive to enzymatic hydrolysis. Indeed, in the 1,2,3-triazole linkage the carbon atoms remain linked to 1- and 4- positions, resulting in a distance of 5.0 Å, whereas amide typical linkage places the carbon atoms only at 3.8 Å. Moreover, the nitrogen atoms present in the 1,2,3-triazole at 2- and 3-positions show weak hydrogen bond-accepting properties. Similarly to amides (**Figure 1.11**), and due to the inherent dipole moment of the heterocyclic ring, triazoles can be hydrogen bond donors and acceptors [186,188].

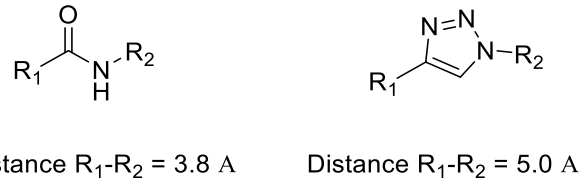

Figure 1.11. Electronic and topologic similarities between amide ad 1,2,3-triazole.

Although the practical value lies mainly in the ease of introduction of azide and alkyne groups into organic compounds, the great impact of this reactions came after the discovery of the copper (I) catalyzed process. In fact, the introduction of copper (I) catalysis revolutionized the field of Click Chemistry and significantly enhanced the efficiency and scope of the 1,3-dipolar cycloaddition reaction. Copper (I) ions serve as catalysts that facilitate the reaction between azides and alkynes, promoting faster reaction rates and improved regioselectivity. Indeed, the use of copper (I) increases the reaction rate up to 10^7, and absolute regioselectivity is obtained with the

exclusive formation of the 1,4 isomer. For instance, Meldal *et al.* demonstrated these benefits in 2002 by using CuI and *N,N*-diisopropylethylamine (DIPEA) for the synthesis of various 1,2,3-triazoles in different solvents using alkynes immobilized on a solid phase [189]. This discovery was also observed by Sharpless, Fokin and co-workers. Indeed, they described the use of $CuSO_4 \cdot 5H_2O$ and sodium ascorbate in water to carry out the cycloaddition between unactivated terminal alkynes and alkyl/aryl azides. As the reaction is extremely exothermic, the possibility of carrying out the reaction in water facilitates the large-scale production of the cycloadducts. In fact, the water itself acts as a coolant, dispersing the heat of the reaction. Moreover, it avoids interference from protic functional groups such as alcohols, carboxylic acids, amines and amides, which are present in numerous biologically active organic molecules [190]. These mild reaction conditions are highly advantageous, in fact, the potential for side reactions is reduced and, in consequence, the reaction is fully compatible with a broad range of substrates, including sensitive biomolecules and functional groups. In fact, its simple purification method, generally filtration of the precipitated product and washing, low sensitivity to steric effects and biocompatibility of the reagents make this reaction as one of the most powerful methods to carry out the irreversible binding of two building blocks in a fast and efficient way.

As previously mentioned, this reaction is carried out between azides and alkynes under the copper catalysis. Therefore, the study of the sources of these reagents is interesting and demanding.

Regarding alkyne sources, the main used approach introduce a terminal alkyne moiety into organic compounds derived from propargylic amines, alcohols or halides is the propargyl group. Indeed, propargylation of phenols can be easily achieved by Wiliamson reactions [191].

On the other hand, the copper (I) catalyst required for CuAAC reaction can be achieved by three different strategies: (1) *in situ* reduction of Cu (II) salts, for example, $CuSO_4 \cdot 5H_2O$ and sodium ascorbate is a typical duo that have demonstrated efficacy in CuAAC reactions even in the presence of oxygen [191,192]. (2) Oxidation of metallic copper, for this methodology it is essential the use of Cu (II) salts. In fact, copper metal act as a reducing agent, facilitating the conversion of Cu (II) ions to Cu (I) ions [191–193]. (3) the use of already prepared Cu (I) salts, this methodology describes the direct addition of Cu (I) salts tipycally optimized by the incorporation of specific nitrogen bases, such as trimethylamine (Et_3N), pyridine (Py), 2,2-bipyridine, 2,6-ludidine, DIPEA or *N,N,N*-pentamethylethylenetetramine (PMDETA) [186,191–193].

In this Doctorate Thesis, the first strategy has been chosen, as the catalyst obtained from the *in situ* reduction of Cu (II) salts is often than CuI salts and Cu (II) salts are commercially more available. Furthermore, in the case of $CuSO_4 \cdot 5H_2O$, sodium ascorbate has proven to be an excellent reductant, since it allows the preparation of a broad spectrum of 1,4-disubstituted triazole products in high yields and purity with low catalytic loadings. Although most experiments have been performed at near neutral pH values, the catalysis appears to proceed well at pH values ranging from about 4 to 12.

Numerous investigations have demonstrated a complex dependence of the reaction mechanism on the concentration, nature of the solvent, employed ligand and the Cu(I) source used. Density Functional Theory (DFT) calculations on monomeric copper-acetylene complexes indicate that a concerted mechanism of azide-alkyne cycloaddition is strongly disfavored over a stepwise mechanism in the case of the Cu(I)-catalyzed process. The lowest energy barrier described for a concerted process is 23.7 kcal/mol. However, a stepwise cycloaddition process catalyzed by a monomeric Cu(I) species is 11 kcal/mol, justifying that the rate improvement is due to a stepwise process that reduces the transition energy [194].

The proposed catalytic cycle (**Scheme 1.4**) consists of 5 stages [190]. The initial step is the formation of the copper (I) acetylide complex (**I**). In organic solvents, such as acetonitrile, the formation of this complex requires the dissociation of the terminal alkynes in this reaction. Formation of this complex requires endothermic dissociation of the ligand (0.6 kcal/mol). However, in aqueous solution the formation of copper acetylide is exothermic (11.7 kcal/mol), which justifies the increased reaction rate discussed above. Theoretical calculations also indicate that the coordination of copper significantly reduces the pKa of the alkyne (CH), which allows the deprotonation of acetylene in aqueous systems without the addition of a base. In fact, these copper acetylides have even been identified at acidic aqueous solutions. Once formed the copper acetylide, the displacement of a ligand by the azide generates a copper acetylide-azide complex (**II**). Due to the complexation of the azide, the nucleophilic attack of the N3 nitrogen on the internal carbon of the acetylide is promoted, thus, generating the metallocycle (**III**). Subsequently, a transannular contraction generating the triazole-copper metallocycle (**IV**), which evolves by an acid-base process into the desired 1,4-disubstituted triazole product (**V**) and the catalyst is regenerated to initiate a new cycle. Several studies have shown that triazole-Cu intermediates (**IV or V**) can have a significant half-life even in aqueous solution.

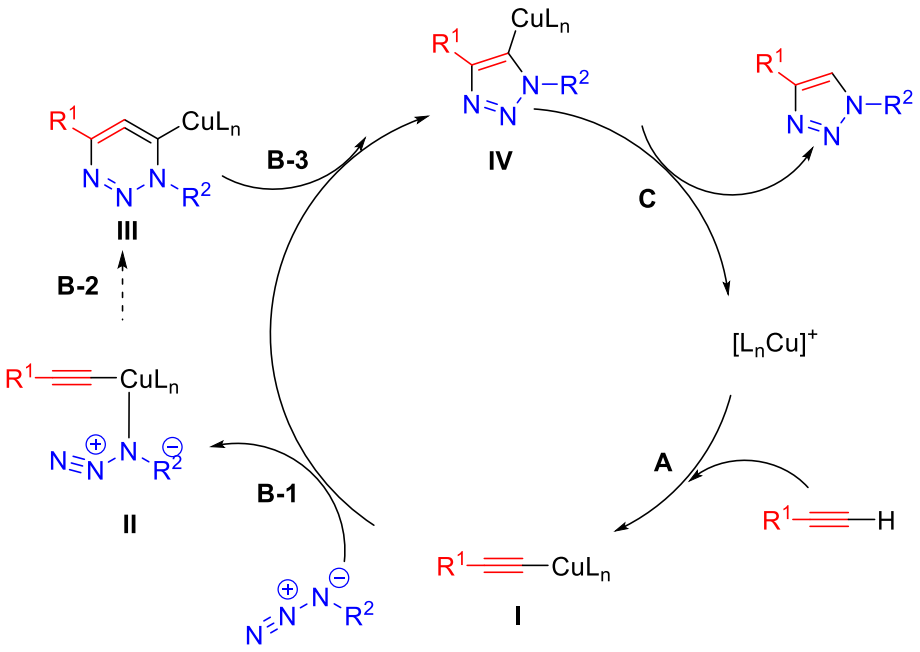

Scheme 1.4. Mechanism of copper catalyzed azide alkyne click reaction.

According to several kinetic studies the process obeys a second order catalysis on copper. At present, the role of the second copper atom is not well known, it could act either by activating the azide function or in a subsequent complexation of copper acetylide I, which would substantially increase the reactivity towards cycloaddition, due to the decrease of the charge density on the acetylene and properly orienting the substrate [195]. On the other hand, under conditions of excess copper, the order of the reaction can be treated between one and two on the alkyne. When higher concentrations of alkyne are used the Cu (I) sphere is saturated inhibiting the reaction. Thus, commercial copper acetylides, which are already saturated in acetylene, do not show any catalytic activity, which emphasizes the importance of ligand dissociation during catalysis. Although there are doubts as to the exact nature of the active complex involved in the catalytic process, the most recent results indicate that it is a species with two metal centers, one or two alkynes as ligands, and an azide group.

Recently, it has been shown that this cycloaddition can be carried out at room temperature catalyzed by metal salts such as Ru, Ni, Pb and Pt. The use of these new catalysts is very promising since some of them, especially Ru, favor the formation of the 1,5-disubstituted triazole adduct instead of the 1,4-disubstituted regioisomer obtained by Cu(I) catalysis [188].

1.7.2. Catalyst free azide-yne cycloaddition reactions

1.7.2.1. Strain promoted cycloaddition reactions (SPAAC)

The strain-promoted cycloaddition of cyclooctynes with azides represents copper-free alternative to the widely used CuAAC click reaction [196]. The strategic attachment of a suitable handle to the cyclooctyne was a result of logical reasoning, as it would facilitate conjugation with any organic azide in any solvent of choice [197]. Significantly, it became evident that the copper catalyzed azide-alkyne cycloaddition (CuAAC) showed significant limitations in biological media due to the toxicity of the inevitable copper (I) species to living cells and organisms [188].

The spontaneous reaction between cycloalkynes and organic azides is a captivating organic chemical transformation due to its simplicity. With just mixing and stirring and no need of catalyst or precise reaction conditions, a stable triazole product is rapidly and selectively formed through the cycloaddition of cycloalkyne with azide. This strain promoted reaction has firmly established itself as a powerful chemical process with extensive academic and commercial applications. The main focus of this chemistry lies in the highly strained, medium-sized cyclic alkyne and, in particular, cyclooctynes. The stability of cyclic alkynes decreases rapidly as the ring size increases. This instability is directly related to the C-C triple bond angle, which, due to the cyclic structure can not achieve the ideal 180º bond angle that corresponds to in sp-hybridized carbon atoms [196,198]. It is worth noting that cyclooctyne is the smallest isolable cycloalkyne and exhibits an acetylene bond angle of 163°, still significantly deviating from linearity. Unlike linear acetylenes, the deformation of the carbon-carbon triple bond of a cyclooctyne allows the spontaneous reaction with azide compound despite its poor ability to act as 1,3-dipolar acceptor. Experimental data indicates that cyclooctyne possess a ring strain of approximately 18 kcal/mol, while, on the contrary, saturated cyclooctane has a ring strain of 12.1 kcal/mol. Consequently, the intrinsically low stability of medium-sized cyclic alkynes can be attributed to the presence of significant ring strain [198].

As discussed above, this fast and spontaneous reaction between cycloalkyne and azide could be carried out by the highly enthalpic release of the ring deformation, which transforms from strain ring to favourable fused ring [199]. This second ring contains a bond with sp^2 hybridized carbon atoms, because of the triazole, so the angle formed is favourable for that type of bond. This type of reaction was originally developed for application in biorthogonal chemistry, which refers to any chemical reaction that can carried out inside of the living systems without compromising native biochemical processes. It has to be noted that biorthogonal terminology was firstly

introduced by Bertozzi *et al.* This concept of biorthogonal reactions is rooted in earlier methodologies that leverage the distinct reactivity of functional groups found on amino acid side chain, such as lysine and cysteine. While this approach remains widely used in bioconjugation, their applicability for *in vitro* purposed is restricted due to the natural occurrence of these functional groups in multiple compounds [200,201]. Although, SPAAC reactions have proven to be an effective tool in additional areas of science such as bioconjugation processes, hybrid and block polymers, high-performance and self-healing materials, metabolic engineering of biological systems and more [202–204]. One of the keys to the success of SPAAC is the readily accessible, small and stable azide component of the reaction. However, in recent years the power of cyclooctyne chemistry beyond cycloaddition with organic azides has been pleasingly demonstrated. Although early experiments were performed with unmodified cyclooctynes, the use of electron attracting groups favour this reaction. The first employed cyclooctyne (Oct) (**Figure 1.12**), developed as biorthogonal reagent, showed a second order rate constant of $2.4x10^{-3}$ $M^{-1}{\cdot}s^{-1}$ when was reacted with benzyl azide. Additionally, this rate was enhanced to $4.3x10^{-3}$ $M^{-1}{\cdot}s^{-1}$ when monofluorinated cyclooctyne (MOFO) (**Figure 1.12**) was used and continued increasing with the addition of two fluorine atoms (difluorinated cyclooctyne DIFO) (**Figure 1.12**) at the propargylic position, showing a rate constant of $7.6x10^{-2}$ $M^{-1}s^{-1}$, one order faster that Oct. This is why in recent years the synthesis of derivatized cyclooctynes has increased considerably. Indeed, this last decade dibenzocylooctyne (DIBO) (**Figure 1.12)** and its derivatives, which demonstrated faster rate constant than Oct, have been widely explored. However, these materials are expensive and difficult to synthesize, so the design of other strategies is of great importance [198,205–207].

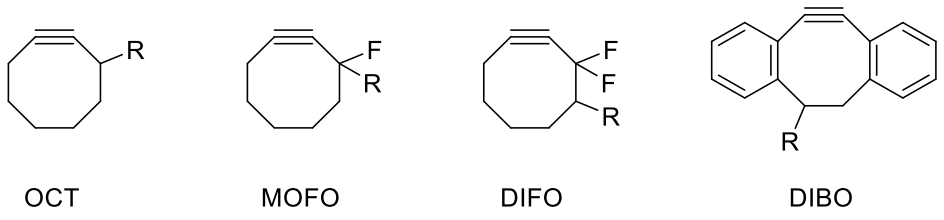

Figure 1.12. Most employed cyclooctyne derivatives.

1.7.2.2. Activated acetylene cycloaddition reactions

The previously mentioned poor ability of azide compounds to participate as dipolarophiles would be compensated, not by strain as in Bertozzi's proposal, but by electronic effects. Therefore, modifying alkyne groups and becoming more reactive can be a promising alternative.

The use of alkyne derived compounds with electron-attracting groups, such as propiolic acid and its derivatives, has been shown to be a fast and efficient way of promoting the reaction between azide and alkynes, reducing the activation energy required for the reaction (**Scheme 1.5**). This novel methodology was firstly studied by Ju *et al.* in solution, where they reported the first 1,3-dipolar cycloaddition reaction between azides and electron-deficient alkynes in water [208]. When the alkyne (either terminal or internal) had at least one neighbouring electron-withdrawing functional group, such as propiolic acid, the triazole formation was achieved even in water at room temperature without any catalysts. Despite the great versatility of this promising alternative to SPAAC, there are only few examples where this type of copper free reactions are used. For instance, it has been employed in the synthesis of hydrogels [209], foams or polymers [210,211]. Although its great potential, the use of alkyne derived compound with electron-attracting groups in bio-conjugation or immobilization of compounds on materials is still not widely known. While it has been shown to be a similar strategy to other copper-free click reactions, such as SPAAC, its application in these fields is still relatively new and unexplored. However, as more research is con-ducted and the methodology is further optimized, it has the potential to become valuable tool in the modification of polymeric surfaces for biomedical use.

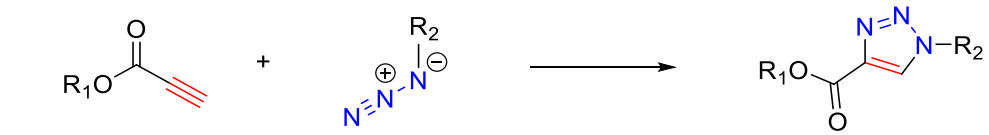

propiolic acid derivative

Scheme 1.5. Copper free cycloaddition reaction between activated alkyne and azide.

1.7.3. Catalyst free amino-yne reaction

The amino-yne Michael reaction is a versatile chemical transformation that shares similarities with above mentioned thiol-yne reaction. In this Michael reaction, a primary or secondary amine attacks the β-carbon of an electron-deficient alkyne. However, the main difference between these two reaction lies in catalysis, as many amino-yne reactions occur spontaneously at ambient temperature without the need for an additional catalyst or stimuli [212]. This remarkable reactivity is attributed to the excellent nucleophilicity of the amine functionality, which often leads to even superior reaction efficiency compared to thiol-yne Michael additions. Consequently, the amino-yne reaction has found wide applications in material and biological

sciences. Additionally, the resulting enamine Michael adducts exhibit high reactivity and versatility, making them valuable intermediates in organic synthesis [213].

The first amino-yne nucleophilic addition was reported in 1899 by Ruhemann and coworkers [213,214]. They observed violent exothermic reactions between diethylamine (or piperidine) and diethylacetylene dicarboxylate, as well as phenylpropiolate. Interestingly, these reactions occurred spontaneously without the need for a catalyst at ambient temperatures.

The amino-yne Michael reaction offers a straightforward and efficient method for producing regio- and stereoregular products in excellent yields, without the need for a catalyst [212]. By simply mixing alkynes and amines at room temperature, the reaction proceeds smoothly, as depicted in **Scheme 1.6**. Furthermore, the reaction mechanism is well understood and can be briefly discusses as follows: In the nucleophilic addition step, the electron-pair of the nitrogen attacks the end carbon of the ethynyl group. This occurs due to the electron withdrawal effect of the carbonyl, which enhances the electrophilic character of the triple bond. As a result, the reaction exhibits regioselectivity, favouring the addition at the end carbon of the ethynyl. In the proton transfer step, the *E*-isomers are found to be more thermodynamically stable than *Z*-isomers. This stability arises from the geometric arrangement of the substituents around the double bond. However, it is worth noting that at room temperature, the *Z*-isomers can undergo a transformation into the more stable *E*-isomers. This transformation occurs through a single transition state known as "nitrogen-activated double bond reaction", leading to a stereoselectivity in the reaction [212].

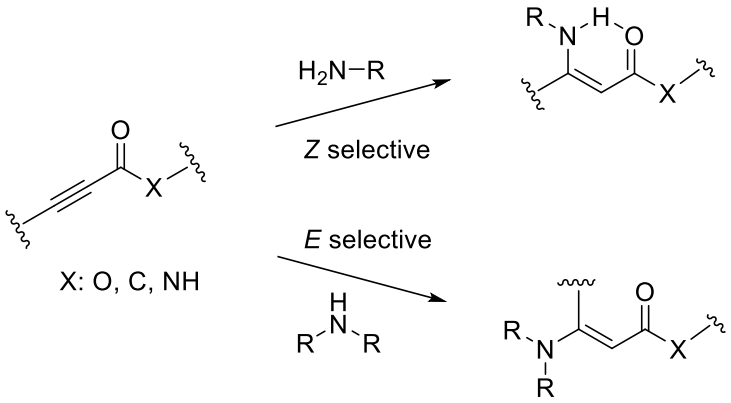

Scheme 1.6. Generic scheme of 1,4-conjugate addition of 1 and 2 amine nucleophiles to carbonyl containing Michael acceptors.

1.7.4. Catalyst free thiol-yne reaction

In 2009, Bowman and coworkers introduced the radical mediated thiol-yne coupling procedure as means to develop highly cross-linked polymer networks [180]. Their inspiration came from overlooked studies on multiple radical additions of thiols to alkynes. This innovative approach combines the easily accessible building blocks of the copper (I) azide-alkyne reaction and thiol-ene chemistry, allowing for the creation of multifunctional materials under mild reaction conditions [184].

The thiol-yne coupling procedure offers several advantages [215]. Firstly, it enables the coupling of two thiols with one alkyne, a process that can be facilitated by a chemical radical source, UV irradiation or even sunlight at ambient temperature [188]. This versatility and the ability to operate under mild conditions make the thiol-yne procedure highly attractive. One of the key features of this reaction is its radical mechanism, which imparts robustness and versatility to the method [180].

Thiol-yne radical reactions share a similar initiation step with thiol-ene reactions (**Scheme 1.7**). This process begins with the formation of thiyl radical and its addition to an alkyne, forming a vinyl radical with a β-thioether function. Subsequently, a hydrogen atom is captured from another thiol molecule, generating new thiyl radical. This thiyl radical is add to the vinyl thioether, creating another carbon radical, which, in turn, abstracts a hydrogen atom from another thiol molecule again, resulting in the formation of a 1,2-dithioether. The generated thiyl radical continues the chain process, completing the cycle. In this radical click reaction, the addition of the first thiol to the alkyne is the rate-limiting step. In fact, the subsequent addition of the second thiol to the intermediate thiol-alkene is a faster step, approximately three times faster than the initial addition [180,188].

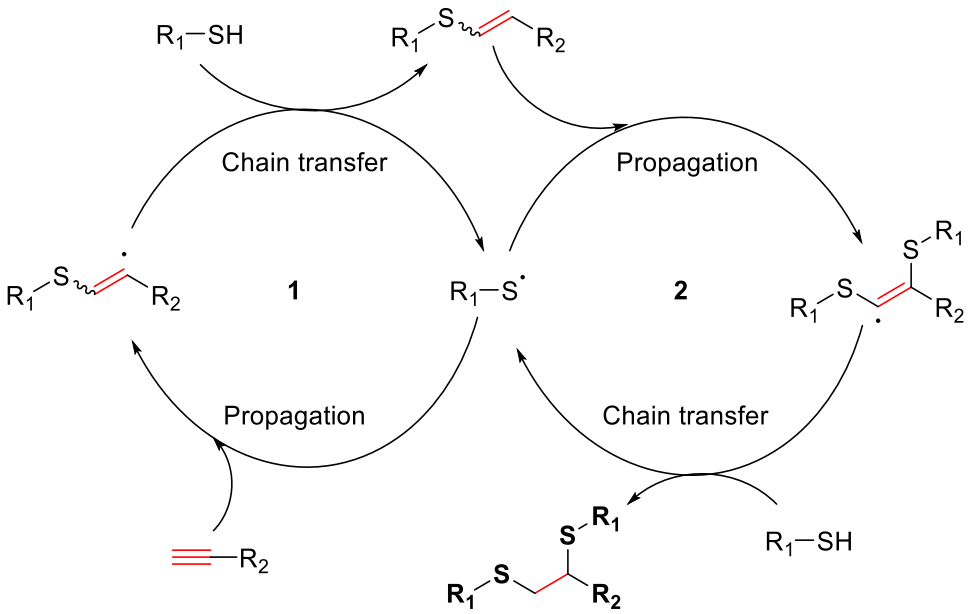

Scheme 1.7. The reaction mechanism of thiol-yne addition reaction.

In summary, the thiol-yne click reaction involves the double addition of thiols onto an alkyne, leading to the formation of a 1,2-dithioether. This reaction has found extensive use in creating multifunctional polymer structures [181,182]. By employing repetitive thiol-yne reactions, multifunctional molecules are generated, which can be further employed to construct dendrimers or hyperbranched polymers. This versatile reaction offers exciting possibilities for the design and synthesis of diverse polymeric architectures with tailored functionalities [213,216]. Additionally, this radical mediated pathway tolerated a wide range of functional groups, allowing for the incorporation of diverse chemical moieties into the resulting polymer networks. However, it is important to note that as it is a radical reaction, the presence of oxygen should be avoided to ensure optimal reaction outcomes [217].

1.8. General objectives and work plan

This Doctoral Thesis aims to develop surfaces and materials with bioactive properties, including antibacterial, anti-inflammatory or/and anticoagulant functionalities. The surfaces and materials will be diverse, and various strategies will be employed to achieve these bioactive properties. However, a common thread throughout the research is the utilization of click reactions for the bioconjugation of drugs or active biomolecules. By employing Click Chemistry, this Thesis aims to facilitate precise and efficient binding of the desired bioactive compounds to polymers (PLLA and PET) and Ti6Al4V metal alloy, enhancing their therapeutic potential. This approach offers versatility and control, enabling the development of novel biomaterials with tailored bioactive functionalities. The research endeavors to contribute to the advancement of biomedical applications by providing innovative solutions for improving biocompatibility and therapeutic efficacy of various materials, minimizing the disadvantages that the use of these devices usually present.

The structure of this document follows the development of materials and approaches used to immobilize the desired drugs. *Chapter 1* provided an overview of the current state of the art, encompassing all types of biomaterials and their principal challenges, including biocompatibility, hemocompatibility and bacterial infection. Special emphasis has been on strategies to prevent bacterial adhesion and biofilm formation, as well as advancements in biocompatibility to mitigate adverse host tissue responses. The chapter also focused on the versatility of Click Chemistry reactions, with particular attention to the copper-catalyzed azide-alkyne cycloaddition reaction. In summary, by following this sequence, the document aims to present a coherent and informative narrative, showcasing the materials and strategies in the pursuit of developing bioactive surfaces with enhanced biomedical applications.

Chapter 2 delves into the bioconjugation of diverse agents including indomethacin and amoxicillin onto PLLA employing different click reactions. For this purpose, the chapter provides a comprehensive understanding of the drug candidates and their potential efficacy in the context of bioactive materials under development, by delving into the essential pharmacological characteristics of the drugs employed and explores the relationship between their structure and activity. Indeed, this section will be divided in 5 section according to the click reaction used. In this chapter, the use of copper-catalyzed click reaction between azides and alkynes is described, showcasing its ability to immobilize various compounds and even enable double sequential functionalization. Additionally, novel copper-free click strategies involving activated acetylene are discussed. A suitable activated alkyne group has been employed to

carry out copper-free click reactions, such as azide-alkyne, amine-alkyne, and thiol-alkyne reactions.

Chapter 3 is dedicated to exploring the utilization of PET and strategies to improve the biological activity of its surface. The key approach involves surface functionalization, which includes hydrolysis and subsequent reactions to immobilize the multiactive curcumin derivative using the copper catalyzed azide-alkyne reaction. By detailing these methods, the chapter describes the bioactivity enhance of PET surfaces, especially anti-inflammatory, anticoagulant and antibacterial properties, making these surfaces more suitable for biomedical applications. The functionalization process plays a pivotal role in optimizing the surface properties and creating a platform for the successful immobilization of the curcumin derivatives. The chapter provides valuable insights into the step-by-step procedures involved, contributing to the development of bioactive PET surfaces with potential therapeutic applications such as coating, fibers or even, biomedical implants.

Chapter 4 focuses on the utilization of Ti6Al4V as the primary substrate. In this case, two significant strategies are distinguished: silane based and phosphonate-based SAMs. In both cases, the Ti alloy is carefully prepared in advance to facilitate subsequent functionalizations. Additionally, this chapter explores the conventional CuAAc reaction, which enables the immobilization of salicylic acid derivative onto the surface. Again, through these distinct approaches, the chapter aims to enhance the versatility of the click reaction in different substrate and anti-inflammatory and anticoagulant behaviour of the fabricated surfaces.

The final chapter of this Thesis, *Chapter 5*, serves as a platform for presenting the overall conclusions derived from this research. It offers a comprehensive summary of the key findings and insights obtained throughout the study. Additionally, *Chapter 5* provides valuable suggestions for potential improvements or modifications to existing materials, offering insightful perspective for future research endeavors.

1.9. Bibliography

1. Williams, D.F. On the nature of biomaterials. *Biomaterials* **2009**, *30*, 5897–5909, doi:10.1016/j.biomaterials.2009.07.027.

2. Festas, A.J.; Ramos, A.; Davim, J.P. Medical devices biomaterials – A review. *Proc. Inst. Mech. Eng. Part L J. Mater. Des. Appl.* **2020**, *234*, 218–228, doi:10.1177/1464420719882458.

3. Crawford, L.; Wyatt, M.; Bryers, J.; Ratner, B. Biocompatibility Evolves: Phenomenology to Toxicology to Regeneration. *Adv. Healthc. Mater.* **2021**, *10*, 1–21, doi:10.1002/adhm.202002153.

4. Black, J. *Biological Performance of Materials: Fundamentals of Biocompatibility, Fourth Edition*; 2005; ISBN 9781420057843.

5. Ludovica Parisi; Carlo Galli; Alberto Neri; Andrea Toffoli; Elena Calciolari; Edoardo Manfredi; Simone Lumetti; Guido M Macaluso; Federico Rivara; Claudio Macaluso Aptamers improve the bioactivity of biomaterials. *Aptamers* **2017**, *1*, 3–12.

6. Williams, D.F. On the mechanisms of biocompatibility. *Biomaterials* **2008**, *29*, 2941–2953, doi:10.1016/j.biomaterials.2008.04.023.

7. Chen, Q.; Thouas, G.A. Metallic implant biomaterials. *Mater. Sci. Eng. R Reports* **2015**, *87*, 1–57, doi:10.1016/j.mser.2014.10.001.

8. Cber, C. FDA Guidance Document, 2023, Use of the International Standard ISO 10993-1, dated September 8, 2023 (Docket No. FDA-2013-D-0350) 2023, 1–66.

9. Ghasemi-Mobarakeh, L.; Kolahreez, D.; Ramakrishna, S.; Williams, D. Key terminology in biomaterials and biocompatibility. *Curr. Opin. Biomed. Eng.* **2019**, *10*, 45–50, doi:10.1016/j.cobme.2019.02.004.

10. Reinwald, Y.; Shakesheff, K.; Howdle, S. *Biomedical Devices*; 2011; ISBN 9780470390849.

11. Velnar, T.; Bunc, G.; Klobucar, R.; Gradisnik, L. Biomaterials and host versus graft response: A short review. *Bosn. J. Basic Med. Sci.* **2016**, *16*, 82–90, doi:10.17305/bjbms.2016.525.

12. BaoLin, GUO; MA, P.X. Synthetic biodegradable functional polymers for tissue engineering: a brief review. *Sci. China Chem.* **2014**, *57*, 490–500, doi:10.1007/s11426-014-5086-y.

13. Dang, T.T.; Nikkhah, M.; Memic, A.; Khademhosseini, A. *Polymeric Biomaterials for Implantable Prostheses*; Elsevier Inc., 2014; ISBN 9780123969835.

14. Wendels, S.; Avérous, L. Biobased polyurethanes for biomedical applications. *Bioact. Mater.* **2021**, *6*, 1083–1106, doi:10.1016/j.bioactmat.2020.10.002.

15. Guo, J.; Chai, R.; Li, H.; Sun, S. *Hearing Loss: Mechanisms, Prevention and Cure*; 2019; Vol. 1130; ISBN 978-981-13-6122-7.

16. Sánchez-Bodón, J.; Andrade-Del Olmo, J.; Alonso, J.M.; Moreno-Benítez, I.; Vilas-Vilela, J.L.; Pérez-Alvarez, L. Bioactive Coatings on Titanium: A Review on Hydroxylation, Self-Assembled Monolayers (SAMs) and Surface Modification Strategies. *Polymers (Basel).* **2022**, *14*, 165, doi:10.3390/polym14010165.

17. Sáenz, A.; Rivera-muñoz, E.; Brostow, W.; Castaño, V.M. Ceramic Biomaterials : an Introductory Overview. *J. Mater. Educ.* **1999**, *21*, 297–306.

18. Sidambe, A.T. Biocompatibility of advanced manufactured titanium implants-A review. *Materials (Basel).* **2014**, *7*, 8168–8188, doi:10.3390/ma7128168.

19. Özcan, M.; Hämmerle, C. Titanium as a reconstruction and implant material in dentistry: Advantages and pitfalls. *Materials (Basel).* **2012**, *5*, 1528–1545, doi:10.3390/ma5091528.

20. Liu, Y.; Rath, B.; Tingart, M.; Eschweiler, J. Role of implants surface modification in osseointegration: A systematic review. *J. Biomed. Mater. Res. - Part A* **2020**, *108*, 470–484, doi:10.1002/jbm.a.36829.

21. W. Nicholson, J. Titanium Alloys for Dental Implants: A Review. *Prosthesis* **2020**, *2*, 100–116, doi:10.3390/prosthesis2020011.

22. Sarraf, M.; Rezvani Ghomi, E.; Alipour, S.; Ramakrishna, S.; Liana Sukiman, N. A state-of-the-art review of the fabrication and characteristics of titanium and its alloys for biomedical applications. *Bio-Design Manuf.* **2022**, *5*, 371–395, doi:10.1007/s42242-021-00170-3.

23. Shen, X.; Shukla, P. A Review of Titanium Based Orthopaedic Implants (Part-

I): Physical Characteristics , Problems and the need for Surface Modification. *Int. J. Peen. Sci. Technol.* **2020**, *1*, 301–332.

24. Chopplet, M.; Theirry, J.P. *Biomedical materials*; 1990; Vol. 5; ISBN 9783030492052.

25. Eliaz, N. Corrosion of metallic biomaterials: A review. *Materials (Basel).* **2019**, *12*, doi:10.3390/ma12030407.

26. Wang, G.; Wan, Y.; Wang, T.; Liu, Z. Corrosion Behavior of Titanium Implant with different Surface Morphologies. *Procedia Manuf.* **2017**, *10*, 363–370, doi:10.1016/j.promfg.2017.07.006.

27. Karpagavalli, R.; Zhou, A.; Chellamuthu, P.; Nguyen, K. Corrosion behavior and biocompatibility of nanostructured TiO 2 film on Ti6Al4V. *J. Biomed. Mater. Res. Part A* **2007**, *83A*, 1087–1095, doi:10.1002/jbm.a.31447.

28. He, W.; Benson, R. *Polymeric Biomaterials*; Elsevier Inc., 2014; ISBN 9780323221696.

29. Teo, A.J.T.; Mishra, A.; Park, I.; Kim, Y.J.; Park, W.T.; Yoon, Y.J. Polymeric Biomaterials for Medical Implants and Devices. *ACS Biomater. Sci. Eng.* **2016**, *2*, 454–472, doi:10.1021/acsbiomaterials.5b00429.

30. Narayanan, G.; Vernekar, V.N.; Kuyinu, E.L.; Laurencin, C.T. Poly (Lactic Acid)-Based Biomaterials for Orthopaedic Regenerative Engineering. **2017**, 247–276, doi:10.1016/j.addr.2016.04.015.Poly.

31. Taib, N.A.A.B.; Rahman, M.R.; Huda, D.; Kuok, K.K.; Hamdan, S.; Bakri, M.K. Bin; Julaihi, M.R.M. Bin; Khan, A. *A review on poly lactic acid (PLA) as a biodegradable polymer*; Springer Berlin Heidelberg, 2022; ISBN 0123456789.

32. Gilding, D.K.; Reed, A.M. Biodegradable polymers for use in surgery-polyglycolic/poly(actic acid) homo- and copolymers: 1. *Polymer (Guildf).* **1979**, *20*, 1459–1464, doi:10.1016/0032-3861(79)90009-0.

33. Li, J.; Liu, F.; Qin, Y.; He, J.; Xiong, Z.; Deng, G.; Li, Q. crossmark. *J. Memb. Sci.* **2017**, *523*, 505–514, doi:10.1016/j.memsci.2016.10.027.

34. Garlotta, D. A Literature Review of Poly (Lactic Acid). *J. Polym. Environ.* **2019**, *9*, 63–84.

35. Mehta, R.; Kumar, V.; Bhunia, H.; Upadhyay, S.N. Synthesis of poly(lactic acid): A review. *J. Macromol. Sci. - Polym. Rev.* **2005**, *45*, 325–349, doi:10.1080/15321790500304148.

36. Lorenzo, M.L. Di; Androsch, R. *Industrial Applications of Poly(lactic acid)*; 2018; ISBN 9783319754581.

37. da Silva, D.; Kaduri, M.; Poley, M.; Adir, O.; Krinsky, N.; Shainsky-Roitman, J.; Schroeder, A. Biocompatibility, biodegradation and excretion of polylactic acid (PLA) in medical implants and theranostic systems. *Chem. Eng. J.* **2018**, *340*, 9–14, doi:10.1016/j.cej.2018.01.010.

38. Bone, P.-L.P. Long-term in vivo Degradation of Poly-. *21*, 395–411, doi:10.1177/0885328206065125.

39. Bhouri, N.; Debbabi, F.; Merghni, A.; Rohleder, E.; Mahltig, B.; Ben Abdessalem, S. New manufacturing process to develop antibacterial dyed polyethylene terephthalate sutures using plasma functionalization and chitosan immobilization. *J. Ind. Text.* **2021**, *0*, 1–24, doi:10.1177/15280837211050525.

40. Swar, S.; Zajícová, V.; Rysová, M.; Lovětinská-Šlamborová, I.; Voleský, L.; Stibor, I. Biocompatible surface modification of poly(ethylene terephthalate) focused on pathogenic bacteria: Promising prospects in biomedical applications. *J. Appl. Polym. Sci.* **2017**, *134*, 1–11, doi:10.1002/app.44990.

41. Çaykara, T.; Sande, M.G.; Azoia, N.; Rodrigues, L.R.; Silva, C.J. Exploring the potential of polyethylene terephthalate in the design of antibacterial surfaces. *Med. Microbiol. Immunol.* **2020**, *209*, 363–372, doi:10.1007/s00430-020-00660-8.

42. Nisticò, R. Polyethylene terephthalate (PET) in the packaging industry. *Polym. Test.* **2020**, *90*, 106707, doi:10.1016/j.polymertesting.2020.106707.

43. Lasoski, W. Kinetics of hydrolysis of polyethylese terephthalate filris. *J. Phys. Chem* **1960**, *64*, 895–898.

44. Subramaniam, A.; Sethuraman, S. *Biomedical Applications of Nondegradable Polymers*; Elsevier Inc., 2014; ISBN 9780123969835.

45. Agrawal, R.; Kumar, A.; Mohammed, M.K.A.; Singh, S. Biomaterial types, properties, medical applications, and other factors: a recent review. *J. Zhejiang*

Univ. Sci. A **2023**, doi:10.1631/jzus.A2200403.

46. Schierholz, J.M.; Beuth, J. Implant infections : a haven for opportunistic bacteria. **2001**, 87–93, doi:10.1053/jhin.2001.1052.

47. Arciola, C.R.; Campoccia, D. Implant infections: adhesion, biofilm formation and immune evasion. *Nat. Rev. Microbiol.* **2018**, *16*, doi:10.1038/s41579-018-0019-y.

48. Campoccia, D.; Montanaro, L.; Renata, C. The significance of infection related to orthopedic devices and issues of antibiotic resistance. *Biomaterials* **2006**, *27*, 2331–2339, doi:10.1016/j.biomaterials.2005.11.044.

49. Chandorkar, Y.; Ravikumar, K.; Basu, B. The Foreign Body Response Demystified. *ACS Biomater. Sci. Eng.* **2019**, *5*, 19–44, doi:10.1021/acsbiomaterials.8b00252.

50. Sheikh, Z.; Brooks, P.J.; Barzilay, O.; Fine, N.; Glogauer, M. Macrophages, foreign body giant cells and their response to implantable biomaterials. *Materials (Basel).* **2015**, *8*, 5671–5701, doi:10.3390/ma8095269.

51. Zhou, G.; Groth, T. Host Responses to Biomaterials and Anti-Inflammatory Design—a Brief Review. *Macromol. Biosci.* **2018**, *18*, 1–15, doi:10.1002/mabi.201800112.

52. Franz, S.; Rammelt, S.; Scharnweber, D.; Simon, J.C. Immune responses to implants - A review of the implications for the design of immunomodulatory biomaterials. *Biomaterials* **2011**, *32*, 6692–6709, doi:10.1016/j.biomaterials.2011.05.078.

53. Subbiahdoss, G.; Kuijer, R.; Grijpma, D.W.; van der Mei, H.C.; Busscher, H.J. Microbial biofilm growth vs. tissue integration: "The race for the surface" experimentally studied. *Acta Biomater.* **2009**, *5*, 1399–1404, doi:10.1016/j.actbio.2008.12.011.

54. López-Valverde, A.; López-Valverde, N.; Flores-Fraile, J. The unknown process osseointegration. *Biology (Basel).* **2020**, *9*, 1–3, doi:10.3390/biology9070168.

55. Stones, D.H.; Krachler, A.M. Against the tide: The role of bacterial Adhesion in host colonization. *Biochem. Soc. Trans.* **2016**, *44*, 1571–1580, doi:10.1042/BST20160186.

56. Benčina, M.; Mavrič, T.; Junkar, I.; Bajt, A.; Krajnović, A.; Lakota, K.; Žigon, P.; Sodin-Šemrl, S.; Kralj-Iglič, V.; Iglič, A. The Importance of Antibacterial Surfaces in Biomedical Applications. *Adv. Biomembr. Lipid Self-Assembly* **2018**, *28*, 115–165, doi:10.1016/bs.abl.2018.05.001.

57. Olmo, J.A. Del; Ruiz-Rubio, L.; Pérez-Alvarez, L.; Sáez-Martínez, V.; Vilas-Vilela, J.L. Antibacterial coatings for improving the performance of biomaterials. *Coatings* **2020**, *10*, doi:10.3390/coatings10020139.

58. Chouirfa, H.; Bouloussa, H.; Migonney, V.; Falentin-Daudré, C. Review of titanium surface modification techniques and coatings for antibacterial applications. *Acta Biomater.* **2019**, *83*, 37–54, doi:10.1016/j.actbio.2018.10.036.

59. Wu, S.; Zhang, B.; Liu, Y.; Suo, X.; Li, H. Influence of surface topography on bacterial adhesion: A review (Review). *Biointerphases* **2018**, *13*, 1–11, doi:10.1116/1.5054057.

60. Yang, K.; Shi, J.; Wang, L.; Chen, Y.; Liang, C.; Yang, L.; Wang, L.N. Bacterial anti-adhesion surface design: Surface patterning, roughness and wettability: A review. *J. Mater. Sci. Technol.* **2022**, *99*, 82–100, doi:10.1016/j.jmst.2021.05.028.

61. Francone, A.; Merino, S.; Retolaza, A.; Ramiro, J.; Alves, S.A.; de Castro, J.V.; Neves, N.M.; Arana, A.; Marimon, J.M.; Torres, C.M.S.; et al. Impact of surface topography on the bacterial attachment to micro- and nano-patterned polymer films. *Surfaces and Interfaces* **2021**, *27*, 101494, doi:10.1016/j.surfin.2021.101494.

62. Luong-Van, E.; Rodriguez, I.; Low, H.Y.; Elmouelhi, N.; Lowenhaupt, B.; Natarajan, S.; Lim, C.T.; Prajapati, R.; Vyakarnam, M.; Cooper, K. Review: Micro-and nanostructured surface engineering for biomedical applications. *J. Mater. Res.* **2013**, *28*, 165–174, doi:10.1557/jmr.2012.398.

63. Hernandez, J.L.; Park, J.; Yao, S.; Blakney, A.K.; Nguyen, H. V; Katz, B.H.; Jensen, J.T.; Woodrow, K.A. Effect of tissue microenvironment on fibrous capsule formation to biomaterial-coated implants. *Biomaterials* **2021**, *273*, 120806, doi:10.1016/j.biomaterials.2021.120806.

64. Crawford, R.J.; Webb, H.K.; Truong, V.K.; Hasan, J.; Ivanova, E.P. Surface topographical factors influencing bacterial attachment. *Adv. Colloid Interface*

Sci. **2012**, *179–182*, 142–149, doi:10.1016/j.cis.2012.06.015.

65. Mu, M.; Liu, S.; DeFlorio, W.; Hao, L.; Wang, X.; Salazar, K.S.; Taylor, M.; Castillo, A.; Cisneros-Zevallos, L.; Oh, J.K.; et al. Influence of Surface Roughness, Nanostructure, and Wetting on Bacterial Adhesion. *Langmuir* **2023**, *39*, 5426–5439, doi:10.1021/acs.langmuir.3c00091.

66. Ubuo, E.E.; Udoetok, I.A.; Tyowua, A.T.; Ekwere, I.O.; Al-Shehri, H.S. The direct cause of amplified wettability: Roughness or surface chemistry? *J. Compos. Sci.* **2021**, *5*, 1–9, doi:10.3390/jcs5080213.

67. Ellinas, K.; Kefallinou, D.; Stamatakis, K.; Gogolides, E.; Tserepi, A. Is There a Threshold in the Antibacterial Action of Superhydrophobic Surfaces? *ACS Appl. Mater. Interfaces* **2017**, *8*, 39781–39789, doi:10.1021/acsami.7b11402.

68. Zhang, X.; Wang, L.; Levänen, E. Superhydrophobic surfaces for the reduction of bacterial adhesion. *RSC Adv.* **2013**, *3*, 12003–12020, doi:10.1039/c3ra40497h.

69. Mariani, E.; Lisignoli, G.; Maria, R.; Pulsatelli, L. Biomaterials : Foreign Bodies or Tuners for the Immune Response? *Int. J. Mol* **2019**, *20*, 636–678, doi:10.3390/ijms20030636.

70. Anderson, J.M. Exploiting the inflammatory response on biomaterials research and development. *J. Mater. Sci. Mater. Med.* **2015**, *26*, 1–2, doi:10.1007/s10856-015-5423-5.

71. Hotchkiss, K.M.; Reddy, G.B.; Hyzy, S.L.; Schwartz, Z.; Boyan, B.D.; Olivares-Navarrete, R. Titanium surface characteristics, including topography and wettability, alter macrophage activation. *Acta Biomater.* **2016**, *31*, 425–434, doi:10.1016/j.actbio.2015.12.003.

72. Bhagwat, G.; O'Connor, W.; Grainge, I.; Palanisami, T. Understanding the Fundamental Basis for Biofilm Formation on Plastic Surfaces: Role of Conditioning Films. *Front. Microbiol.* **2021**, *12*, 1–10, doi:10.3389/fmicb.2021.687118.

73. Nathanael, A.J.; Oh, T.H. Biopolymer coatings for biomedical applications. *Polymers (Basel).* **2020**, *12*, 1–26, doi:10.3390/polym12123061.

74. Song, J.; Winkeljann, B.; Lieleg, O. Biopolymer-Based Coatings : Promising Strategies to Improve the Biocompatibility and Functionality of Materials Used

in Biomedical Engineering. **2020**, *2000850*, doi:10.1002/admi.202000850.

75. Mcwhorter, F.Y.; Davis, C.T.; Liu, W.F. Physical and mechanical regulation of macrophage phenotype and function. *Cell. Mol. Life Sci.* **2015**, *72*, 1303–1316, doi:10.1007/s00018-014-1796-8.Physical.

76. McNamara, L.E.; Burchmore, R.; Riehle, M.O.; Herzyk, P.; Biggs, M.J.P.; Wilkinson, C.D.W.; Curtis, A.S.G.; Dalby, M.J. The role of microtopography in cellular mechanotransduction. *Biomaterials* **2012**, *33*, 2835–2847, doi:10.1016/j.biomaterials.2011.11.047.

77. Rich, A.; Harris, A.K. Anomalous preferences of cultured macrophages for hydrophobic and roughened substrata. *J. Cell Sci.* **1981**, *50*, 1–7, doi:10.1242/jcs.50.1.1.

78. Refai, A.K.; Textor, M.; Brunette, D.M.; Waterfield, J.D. Effect of titanium surface topography on macrophage activation and secretion of proinflammatory cytokines and chemokines. *J. Biomed. Mater. Res. - Part A* **2004**, *70*, 194–205, doi:10.1002/jbm.a.30075.

79. Chen, S.; Jones, J.A.; Xu, Y.; Low, H.Y.; Anderson, J.M.; Leong, K.W. Characterization of topographical effects on macrophage behavior in a foreign body response model. *Biomaterials* **2010**, *31*, 3479–3491, doi:10.1016/j.biomaterials.2010.01.074.

80. Wang, L.; Chen, W.; Terentjev, E. Effect of micro-patterning on bacterial adhesion on polyethylene terephthalate surface. *J. Biomater. Appl.* **2015**, *29*, 1351–1362, doi:10.1177/0885328214563998.

81. Zhu, Y.; Mao, Z.; Gao, C. Aminolysis-based surface modification of polyesters for biomedical applications. *RSC Adv.* **2013**, *3*, 2509–2519, doi:10.1039/c2ra22358a.

82. Stewart, C.; Akhavan, B.; Wise, S.G.; Bilek, M.M.M. Progress in Materials Science A review of biomimetic surface functionalization for bone- integrating orthopedic implants : Mechanisms , current approaches , and future directions. *Prog. Mater. Sci.* **2019**, *106*, 100588, doi:10.1016/j.pmatsci.2019.100588.

83. Yaseri, R.; Fadaie, M.; Mirzaei, E.; Samadian, H.; Ebrahiminezhad, A. Surface modification of polycaprolactone nanofibers through hydrolysis and aminolysis: a comparative study on structural characteristics, mechanical properties, and

cellular performance. *Sci. Rep.* **2023**, *13*, 1–17, doi:10.1038/s41598-023-36563-w.

84. Andrade del Olmo, J.; Alonso, J.M.; Ronco-Campaña, A.; Sáez-Martínez, V.; Pérez-González, R.; Rothnie, A.J.; Tighe, B.J.; Vilas-Vilela, J.L.; Pérez-Álvarez, L. Effectiveness of physicochemical techniques on the activation of Ti6Al4V surface with improved biocompatibility and antibacterial properties. *Surf. Coatings Technol.* **2022**, *447*, doi:10.1016/j.surfcoat.2022.128821.

85. Yang, Y.; Zhang, H.; Komasa, S.; Morimoto, Y.; Sekino, T.; Kawazoe, T.; Okazaki, J. UV/ozone irradiation manipulates immune response for antibacterial activity and bone regeneration on titanium. *Mater. Sci. Eng. C* **2021**, *129*, 112377, doi:10.1016/j.msec.2021.112377.

86. Huang, H.H.; Wu, C.P.; Sun, Y.S.; Lee, T.H. Improvements in the corrosion resistance and biocompatibility of biomedical Ti-6Al-7Nb alloy using an electrochemical anodization treatment. *Thin Solid Films* **2013**, *528*, 157–162, doi:10.1016/j.tsf.2012.08.063.

87. Huang, M.S.; Wu, C.Y.; Ou, K.L.; Huang, B.H.; Chang, T.H.; Endo, K.; Cho, Y.C.; Lin, H.Y.; Liu, C.M. Preparation of a biofunctionalized surface on titanium for biomedical applications: Surface properties, wettability variations, and biocompatibility characteristics. *Appl. Sci.* **2020**, *10*, 1438–1449, doi:10.3390/app10041438.

88. Shiau, D.K.; Yang, C.H.; Sun, Y.S.; Wu, M.F.; Pan, H.; Huang, H.H. Enhancing the blood response and antibacterial adhesion of titanium surface through oxygen plasma immersion ion implantation treatment. *Surf. Coatings Technol.* **2019**, *365*, 173–178, doi:10.1016/j.surfcoat.2018.05.029.

89. Morozov, I.A.; Kamenetskikh, A.S.; Beliaev, A.Y.; Scherban, M.G.; Lemkina, L.M.; Eroshenko, D. V.; Korobov, V.P. The Effect of Damage of a Plasma-Treated Polyurethane Surface on Bacterial Adhesion. *Biophys. (Russian Fed.* **2019**, *64*, 410–415, doi:10.1134/S000635091903014X.

90. Ujino, D.; Nishizaki, H.; Higuchi, S.; Komasa, S.; Okazaki, J. Effect of plasma treatment of titanium surface on biocompatibility. *Appl. Sci.* **2019**, *9*, doi:10.3390/app9112257.

91. Chen, M.; Wang, X.Q.; Zhang, E.L.; Wan, Y.Z.; Hu, J. Antibacterial ability and biocompatibility of fluorinated titanium by plasma-based surface modification.

Rare Met. **2022**, *41*, 689–699, doi:10.1007/s12598-021-01808-y.

92. Diamanti, M.V.; del Curto, B.; Pedeferri, M. Anodic oxidation of titanium: From technical aspects to biomedical applications. *J. Appl. Biomater. Biomech.* **2011**, *9*, 55–69, doi:10.5301/JABB.2011.7429.

93. Celina, M.C. Review of polymer oxidation and its relationship with materials performance and lifetime prediction. *Polym. Degrad. Stab.* **2013**, *98*, 2419–2429, doi:10.1016/j.polymdegradstab.2013.06.024.

94. Huynh, V.; Ngo, N.K.; Golden, T.D. Surface Activation and Pretreatments for Biocompatible Metals and Alloys Used in Biomedical Applications. *Int. J. Biomater.* **2019**, *2019*, doi:10.1155/2019/3806504.

95. Minagar, S.; Berndt, C.C.; Wang, J.; Ivanova, E.; Wen, C. A review of the application of anodization for the fabrication of nanotubes on metal implant surfaces. *Acta Biomater.* **2012**, *8*, 2875–2888, doi:10.1016/j.actbio.2012.04.005.

96. Carmagnola, I.; Chiono, V.; Abrigo, M.; Ranzato, E.; Martinotti, S.; Ciardelli, G. Tailored functionalization of poly(L-lactic acid) substrates at the nanoscale to enhance cell response. *J. Biomater. Sci. Polym. Ed.* **2019**, *30*, 526–546, doi:10.1080/09205063.2019.1580954.

97. Jeznach, O.; Kołbuk, D.; Marzec, M.; Bernasik, A.; Sajkiewicz, P. Aminolysis as a surface functionalization method of aliphatic polyester nonwovens: impact on material properties and biological response. *RSC Adv.* **2022**, *12*, 11303–11317, doi:10.1039/d2ra00542e.

98. Mai-Prochnow, A.; Murphy, A.B.; McLean, K.M.; Kong, M.G.; Ostrikov, K. Atmospheric pressure plasmas: Infection control and bacterial responses. *Int. J. Antimicrob. Agents* **2014**, *43*, 508–517, doi:10.1016/j.ijantimicag.2014.01.025.

99. Cools, P.; De Geyter, N.; Vanderleyden, E.; Dubruel, P.; Morent, R. Surface analysis of titanium cleaning and activation processes: Non-thermal plasma versus other techniques. *Plasma Chem. Plasma Process.* **2014**, *34*, 917–932, doi:10.1007/s11090-014-9552-2.

100. Paredes, V.; Salvagni, E.; Rodriguez, E.; Gil, F.J.; Manero, J.M. Assessment and comparison of surface chemical composition and oxide layer modification

upon two different activation methods on a cocrmo alloy. *J. Mater. Sci. Mater. Med.* **2014**, *25*, 311–320, doi:10.1007/s10856-013-5083-2.

101. Pelleg, J. Surface Treatment. In *Structural Integrity*; 2022; Vol. 22, pp. 431–478 ISBN 9780323266987.

102. De Geyter, N.; Morent, R.; Desmet, T.; Trentesaux, M.; Gengembre, L.; Dubruel, P.; Leys, C.; Payen, E. Plasma modification of polylactic acid in a medium pressure DBD. *Surf. Coatings Technol.* **2010**, *204*, 3272–3279, doi:10.1016/j.surfcoat.2010.03.037.

103. Lee, M.; Kwon, J.; Jiang, H.B.; Choi, E.H.; Park, G.; Kim, K. The antibacterial effect of non- thermal atmospheric pressure plasma treatment of titanium surfaces according to the bacterial wall structure. *Sci. Rep.* **2019**, *9*, 1–13, doi:10.1038/s41598-019-39414-9.

104. Helary, G.; Migonney, V. *Bioactive polymer coatings to improve bone repair*; Woodhead Publishing Limited, 2009; ISBN 9781845693855.

105. Huh, M.W.; Kang, I.K.; Lee, D.H.; Kim, W.S.; Lee, D.H.; Park, L.S.; Min, K.E.; Seo, K.H. Surface characterization and antibacterial activity of chitosan-grafted poly(ethylene terephthalate) prepared by plasma glow discharge. *J. Appl. Polym. Sci.* **2001**, *81*, 2769–2778, doi:10.1002/app.1723.

106. Blodgett, B. Films Built by Depositing Successive Monomolecular Layers on a Solid Surface. *J. Am. Chem. Soc.* **1935**, *57*, 1007–1022.

107. Bigelow, W.C.; Pickett, D.L.; Zisman, W.A. Oleophobic monolayers: I. Films adsorbed from solution in non-polar liquids. *Joural Colloid Sci.* **1946**, *1*, 513–538.

108. Hasan, A.; Pandey, L.M. *Self-assembled monolayers in biomaterials*; Elsevier Ltd., 2018; ISBN 9780081007167.

109. Casalini, S.; Bortolotti, C.A.; Leonardi, F.; Biscarini, F. Self-assembled monolayers in organic electronics. *Chem. Soc. Rev.* **2017**, *46*, 40–71, doi:10.1039/c6cs00509h.

110. Kim, S.; Yoo, H. Self-assembled monolayers: Versatile uses in electronic devices from gate dielectrics, dopants, and biosensing linkers. *Micromachines* **2021**, *12*, doi:10.3390/mi12050565.

111. Pujari, S.P.; Scheres, L.; Marcelis, A.T.M.; Zuilhof, H. Covalent surface modification of oxide surfaces. *Angew. Chemie - Int. Ed.* **2014**, *53*, 6322–6356, doi:10.1002/anie.201306709.

112. Faucheux, N.; Schweiss, R.; Lützow, K.; Werner, C.; Groth, T. Self-assembled monolayers with different terminating groups as model substrates for cell adhesion studies. *Biomaterials* **2004**, *25*, 2721–2730, doi:10.1016/j.biomaterials.2003.09.069.

113. Sagiv, L.N. and J. A New Approach to Construction of Artificial Monolayer Assemblies. *J. Am. Chem. Soc.* **1983**, *105*, 674–676.

114. Singh, V.; Mondal, P.C.; Singh, A.K.; Zharnikov, M. Molecular sensors confined on SiOx substrates. *Coord. Chem. Rev.* **2017**, *330*, 144–163, doi:10.1016/j.ccr.2016.09.015.

115. Wang, L.; Schubert, U.S.; Hoeppener, S. Surface chemical reactions on self-assembled silane based monolayers. *Chem. Soc. Rev.* **2021**, *50*, 6507–6540, doi:10.1039/d0cs01220c.

116. Love, J.C.; Estroff, L.A.; Kriebel, J.K.; Nuzzo, R.G.; Whitesides, G.M. *Self-assembled monolayers of thiolates on metals as a form of nanotechnology*; 2005; Vol. 105; ISBN 2172440809.

117. Hasan, A.; Saxena, V.; Pandey, L.M. Surface Functionalization of Ti6Al4V via Self-assembled Monolayers for Improved Protein Adsorption and Fibroblast Adhesion. *Langmuir* **2018**, *34*, 3494–3506, doi:10.1021/acs.langmuir.7b03152.

118. Rodríguez-Cano, A.; Cintas, P.; Fernández-Calderón, M.C.; Pacha-Olivenza, M. ángel; Crespo, L.; Saldaña, L.; Vilaboa, N.; González-Martín, M.L.; Babiano, R. Controlled silanization-amination reactions on the Ti6Al4V surface for biomedical applications. *Colloids Surfaces B Biointerfaces* **2013**, *106*, 248–257, doi:10.1016/j.colsurfb.2013.01.034.

119. Silverman, B.M.; Wieghaus, K.A.; Schwartz, J. Comparative properties of siloxane vs phosphonate monolayers on a key titanium alloy. *Langmuir* **2005**, *21*, 225–228, doi:10.1021/la0482271.

120. Han, X.; Sun, X.; He, T.; Sun, S. Formation of highly stable self-assembled alkyl phosphonic acid monolayers for the functionalization of titanium surfaces

and protein patterning. *Langmuir* **2015**, *31*, 140–148, doi:10.1021/la504644q.

121. Adden, N.; Gamble, L.J.; Castner, D.G.; Hoffmann, A.; Gross, G.; Menzel, H. Phosphonic acid monolayers for binding of bioactive molecules to titanium surfaces. *Langmuir* **2006**, *22*, 8197–8204, doi:10.1021/la060754c.

122. Calliess, T.; Sluszniak, M.; Winkel, A.; Pfaffenroth, C.; Dempwolf, W.; Heuer, W.; Menzel, H.; Windhagen, H.; Stiesch, M. Antimicrobial surface coatings for a permanent percutaneous passage in the concept of osseointegrated extremity prosthesis. *Biomed. Tech.* **2012**, *57*, 467–471, doi:10.1515/bmt-2011-0041.

123. Cunningham, B.W.; Hu, N.; Zorn, C.M.; McAfee, P.C. Bioactive titanium calcium phosphate coating for disc arthroplasty: analysis of 58 vertebral end plates after 6- to 12-month implantation. *Spine J.* **2009**, *9*, 836–845, doi:10.1016/j.spinee.2009.04.015.

124. Katić, J.; Krivačić, S.; Petrović, Ž.; Mikić, D.; Marciuš, M. Titanium Implant Alloy Modified by Electrochemically Deposited Functional Bioactive Calcium Phosphate Coatings. *Coatings* **2023**, *13*, doi:10.3390/coatings13030640.

125. Farjam, P.; Luckabauer, M.; de Vries, E.G.; Rangel, V.R.; Hekman, E.E.G.; Verkerke, G.J.; Rouwkema, J. Bioactive calcium phosphate coatings applied to flexible poly(carbonate urethane) foils. *Surf. Coatings Technol.* **2023**, *470*, 129838, doi:10.1016/j.surfcoat.2023.129838.

126. Heimann, R.B. Osseoconductive and corrosion-inhibiting plasma-sprayed calcium phosphate coatings for metallic medical implants. *Metals (Basel).* **2017**, *7*, 1–19, doi:10.3390/met7110468.

127. Yang, F.; Wolke, J.G.C.; Jansen, J.A. Biomimetic calcium phosphate coating on electrospun poly(ε-caprolactone) scaffolds for bone tissue engineering. *Chem. Eng. J.* **2008**, *137*, 154–161, doi:10.1016/j.cej.2007.07.076.

128. Du, H.; Wei, Z.; Wang, H.; Zhang, E.; Zuo, L.; Du, L. Surface microstructure and cell compatibility of calcium silicate and calcium phosphate composite coatings on Mg-Zn-Mn-Ca alloys for biomedical application. *Colloids Surfaces B Biointerfaces* **2011**, *83*, 96–102, doi:10.1016/j.colsurfb.2010.11.003.

129. Lin, B.; Zhong, M.; Zheng, C.; Cao, L.; Wang, D.; Wang, L.; Liang, J.; Cao, B.

Preparation and characterization of dopamine-induced biomimetic hydroxyapatite coatings on the AZ31 magnesium alloy. *Surf. Coatings Technol.* **2015**, *281*, 82–88, doi:10.1016/j.surfcoat.2015.09.033.

130. Deplaine, H.; Lebourg, M.; Ripalda, P.; Vidaurre, A.; Sanz-Ramos, P.; Mora, G.; Prõsper, F.; Ochoa, I.; Doblaré, M.; Gõmez Ribelles, J.L.; et al. Biomimetic hydroxyapatite coating on pore walls improves osteointegration of poly(L-lactic acid) scaffolds. *J. Biomed. Mater. Res. - Part B Appl. Biomater.* **2013**, *101 B*, 173–186, doi:10.1002/jbm.b.32831.

131. Rigo, E.C.S.; Boschi, A.O.; Yoshimoto, M.; Allegrini, S.; Konig, B.; Carbonari, M.J. Evaluation in vitro and in vivo of biomimetic hydroxyapatite coated on titanium dental implants. *Mater. Sci. Eng. C* **2004**, *24*, 647–651, doi:10.1016/j.msec.2004.08.044.

132. Chen, F.; Lam, W.M.; Lin, C.J.; Qiu, G.X.; Wu, Z.H.; Luk, K.D.K.; Lu, W.W. Biocompatibility of Electrophoretical Deposition of Nanostructured Hydroxyapatite Coating on Roughen Titanium Surface : In Vitro Evaluation Using Mesenchymal Stem Cells. *J. Biomed. Mater. Res.* **2006**, *82B*, 183–191, doi:10.1002/jbmb.

133. Yuan, H.; De Bruijn, J.D.; Zhang, X.; Van Blitterswijk, C.A.; De Groot, K. Bone induction by porous glass ceramic made from Bioglass® (45S5). *J. Biomed. Mater. Res.* **2001**, *58*, 270–276, doi:10.1002/1097-4636(2001)58:3<270::AID-JBM1016>3.0.CO;2-2.

134. El-Fiqi, A.; Kim, J.H.; Kim, H.W. Osteoinductive fibrous scaffolds of biopolymer/mesoporous bioactive glass nanocarriers with excellent bioactivity and long-term delivery of osteogenic drug. *ACS Appl. Mater. Interfaces* **2015**, *7*, 1140–1152, doi:10.1021/am5077759.

135. D'Almeida, M.; Attik, N.; Amalric, J.; Brunon, C.; Renaud, F.; Abouelleil, H.; Toury, B.; Grosgogeat, B. Chitosan coating as an antibacterial surface for biomedical applications. *PLoS One* **2017**, *12*, 1–11, doi:10.1371/journal.pone.0189537.

136. Palla-Rubio, B.; Araújo-Gomes, N.; Fernández-Gutiérrez, M.; Rojo, L.; Suay, J.; Gurruchaga, M.; Goñi, I. Synthesis and characterization of silica-chitosan hybrid materials as antibacterial coatings for titanium implants. *Carbohydr. Polym.* **2019**, *203*, 331–341, doi:10.1016/j.carbpol.2018.09.064.

137. Xing, C.M.; Meng, F.N.; Quan, M.; Ding, K.; Dang, Y.; Gong, Y.K. Quantitative fabrication, performance optimization and comparison of PEG and zwitterionic polymer antifouling coatings. *Acta Biomater.* **2017**, *59*, 129–138, doi:10.1016/j.actbio.2017.06.034.

138. Ao, H.; Zong, J.; Nie, Y.; Wan, Y.; Zheng, X. An in vivo study on the effect of coating stability on osteointegration performance of collagen/hyaluronic acid multilayer modified titanium implants. *Bioact. Mater.* **2018**, *3*, 97–101, doi:10.1016/j.bioactmat.2017.07.004.

139. Guarise, C.; Maglio, M.; Sartori, M.; Galesso, D.; Barbera, C.; Pavan, M.; Martini, L.; Giavaresi, G.; Sambri, V.; Fini, M. Titanium implant coating based on dopamine-functionalized sulphated hyaluronic acid: in vivo assessment of biocompatibility and antibacterial efficacy. *Mater. Sci. Eng. C* **2021**, *128*, 112286, doi:10.1016/j.msec.2021.112286.

140. Guarise, C.; Barbera, C.; Pavan, M.; Pluda, S.; Celestre, M.; Galesso, D. Dopamine-functionalized sulphated hyaluronic acid as a titanium implant coating enhances biofilm prevention and promotes osseointegration. *Biofouling* **2018**, *34*, 719–730, doi:10.1080/08927014.2018.1491555.

141. Del Hoyo-Gallego, S.; Pérez-Álvarez, L.; Gómez-Galván, F.; Lizundia, E.; Kuritka, I.; Sedlarik, V.; Laza, J.M.; Vila-Vilela, J.L. Construction of antibacterial poly(ethylene terephthalate) films via layer by layer assembly of chitosan and hyaluronic acid. *Carbohydr. Polym.* **2016**, *143*, 35–43, doi:10.1016/j.carbpol.2016.02.008.

142. Montazerian, M.; Hosseinzadeh, F.; Migneco, C.; Fook, M.V.L.; Baino, F. Bioceramic coatings on metallic implants: An overview. *Ceram. Int.* **2022**, *48*, 8987–9005, doi:10.1016/j.ceramint.2022.02.055.

143. Fiume, E.; Magnaterra, G.; Rahdar, A.; Vern, E. Hydroxyapatite for Biomedical Applications : A Short Overview. *Ceramics* **2021**, *4*, 542–563.

144. Kaliaraj, G.S.; Bavanilathamuthiah, M.; Kirubaharan, K.; Ramachandran, D.; Dharini, T.; Viswanathan, K.; Vishwakarma, V. Bio-inspired YSZ coated titanium by EB-PVD for biomedical applications. *Surf. Coatings Technol.* **2016**, *307*, 227–235, doi:10.1016/j.surfcoat.2016.08.039.

145. Sergi, R.; Bellucci, D.; Cannillo, V. A review of bioactive glass/natural polymer composites: State of the art. *Materials (Basel).* **2020**, *13*, 1–38,

doi:10.3390/ma13235560.

146. Kaur, G.; Kumar, V.; Baino, F.; Mauro, J.C.; Pickrell, G.; Evans, I.; Bretcanu, O. Mechanical properties of bioactive glasses, ceramics, glass-ceramics and composites: State-of-the-art review and future challenges. *Mater. Sci. Eng. C* **2019**, *104*, 109895, doi:10.1016/j.msec.2019.109895.

147. Sergi, R.; Bellucci, D.; Cannillo, V. A comprehensive review of bioactive glass coatings: State of the art, challenges and future perspectives. *Coatings* **2020**, *10*, doi:10.3390/COATINGS10080757.

148. Bargavi, P.; Chitra, S.; Durgalakshmi, D.; Radha, G.; Balakumar, S. Zirconia reinforced bio-active glass coating by spray pyrolysis: Structure, surface topography, in-vitro biological evaluation and antibacterial activities. *Mater. Today Commun.* **2020**, *25*, doi:10.1016/j.mtcomm.2020.101253.

149. Ishihara, K. Blood-Compatible Surfaces with Phosphorylcholine-Based Polymers for Cardiovascular Medical Devices. *Langmuir* **2019**, *35*, 1778–1787, doi:10.1021/acs.langmuir.8b01565.

150. Peng, L.; Chang, L.; Si, M.; Lin, J.; Wei, Y.; Wang, S.; Liu, H.; Han, B.; Jiang, L. Hydrogel-Coated Dental Device with Adhesion-Inhibiting and Colony-Suppressing Properties. *ACS Appl. Mater. Interfaces* **2020**, *12*, 9718–9725, doi:10.1021/acsami.9b19873.

151. Zare, M.; Bigham, A.; Zare, M.; Luo, H.; Ghomi, E.R. pHEMA : An Overview for Biomedical Applications. *Int. J. Mol. Sci.* **2021**, *22*, 6376–6384.

152. Ungureanu, C.; Pirvu, C.; Mindroiu, M.; Demetrescu, I. Antibacterial polymeric coating based on polypyrrole and polyethylene glycol on a new alloy TiAlZr. *Prog. Org. Coatings* **2012**, *75*, 349–355, doi:10.1016/j.porgcoat.2012.07.015.

153. Tang, J.; Yan, D.; Chen, L.; Shen, Z.; Wang, B.; Weng, S.; Wu, Z.; Xie, Z.; Fang, K.; Hong, C.; et al. Enhancement of local bone formation on titanium implants in osteoporotic rats by biomimetic multilayered structures containing parathyroid hormone (PTH)-related protein. *Biomed. Mater.* **2020**, *15*, 045011, doi:10.1088/1748-605X/ab7b3d.

154. Wang, B.; Ren, K.; Chang, H.; Wang, J.; Ji, J. Construction of Degradable Multilayer Films for Enhanced Antibacterial Properties. *ACS Appl. Mater. Interfaces* **2013**, *5*, 4136–4143, doi:10.1021/am4000547.

155. Wu, C.; Shao, X.; Lin, X.; Gao, W.; Fang, Y.; Wang, J. Surface modification of titanium with collagen/hyaluronic acid and bone morphogenetic protein 2/7 heterodimer promotes osteoblastic differentiation. *Dent. Mater. J.* **2020**, *39*, 1072–1079, doi:10.4012/dmj.2019-249.

156. Jacob, J.; Haponiuk, J.T.; Thomas, S.; Gopi, S. Biopolymer based nanomaterials in drug delivery systems: A review. *Mater. Today Chem.* **2018**, *9*, 43–55, doi:10.1016/j.mtchem.2018.05.002.

157. Criado-Gonzalez, M.; Mijangos, C.; Hernández, R. Polyelectrolyte multilayer films based on natural polymers: From fundamentals to Bio-Applications. *Polymers (Basel).* **2021**, *13*, 1–30, doi:10.3390/polym13142254.

158. Li, J.; Mooney, D.J. Designing hydrogels for controlled drug delivery. *Nat. Rev. Mater.* **2016**, *1*, 1–18, doi:10.1038/natrevmats.2016.71.

159. Zafar, M.S.; Fareed, M.A.; Riaz, S.; Latif, M.; Habib, S.R.; Khurshid, Z. Customized therapeutic surface coatings for dental implants. *Coatings* **2020**, *10*, 1–37, doi:10.3390/coatings10060568.

160. Li, X.; He, L.; Li, N.; He, D. Curcumin loaded hydrogel with anti-inflammatory activity to promote cartilage regeneration in immunocompetent animals. *J. Biomater. Sci. Polym. Ed.* **2023**, *34*, 200–216, doi:10.1080/09205063.2022.2113290.

161. Ariga, K.; McShane, M.; Lvov, Y.M.; Ji, Q.; Hill, J.P. Layer-by-layer assembly for drug delivery and related applications. *Expert Opin. Drug Deliv.* **2011**, *8*, 633–644, doi:10.1517/17425247.2011.566268.

162. Pahal, S.; Gakhar, R.; Raichur, A.M.; Varma, M.M. Polyelectrolyte multilayers for bio-applications: recent advancements. *IET Nanobiotechnology* **2017**, *11*, 903–908, doi:10.1049/iet-nbt.2017.0007.

163. Li, D.; Lv, P.; Fan, L.; Huang, Y.; Yang, F.; Mei, X.; Wu, D. The immobilization of antibiotic-loaded polymeric coatings on osteoarticular Ti implants for the prevention of bone infections. *Biomater. Sci.* **2017**, *5*, 2337–2346, doi:10.1039/c7bm00693d.

164. Karakurt, I.; Ozaltin, K.; Pištˇ, H.; Vesela, D.; Michael-lindhard, J.; Mozetiˇ, M. Effect of Saccharides Coating on Antibacterial Potential and Drug Loading and Releasing Capability of Plasma Treated Polylactic Acid Films. *Int. J. Mol.*

Sci **2022**, *23*, 8821.

165. Chen, C.; Yao, Y.; Tang, H.; Lin, T.; Chen, D.W.; Cheng, K. Long-term antibacterial performances of biodegradable polylactic acid materials with direct absorption of antibiotic agents. *RSC Adv.* **2018**, *8*, 16223–16231, doi:10.1039/C8RA00504D.

166. Valverde, A.; Pérez-Álvarez, L.; Ruiz-Rubio, L.; Pacha Olivenza, M.A.; García Blanco, M.B.; Díaz-Fuentes, M.; Vilas-Vilela, J.L. Antibacterial hyaluronic acid/chitosan multilayers onto smooth and micropatterned titanium surfaces. *Carbohydr. Polym.* **2019**, *207*, 824–833, doi:10.1016/j.carbpol.2018.12.039.

167. Shen, K.; Tang, Q.; Fang, X.; Zhang, C.; Zhu, Z.; Hou, Y.; Lai, M. The sustained release of dexamethasone from TiO 2 nanotubes reinforced by chitosan to enhance osteoblast function and anti-in fl ammation activity. *Mater. Sci. Eng. C* **2020**, *116*, 111241, doi:10.1016/j.msec.2020.111241.

168. Yin, X.; Li, Y.; Chen, Y.; Liu, P.; Feng, B.; Zhang, P.; Zeng, H. IL-4-loaded alginate/chitosan multilayer films for promoting angiogenesis through both direct and indirect means. *Int. J. Biol. Macromol.* **2023**, *232*, 123486, doi:10.1016/j.ijbiomac.2023.123486.

169. Birkett, M.; Dover, L.; Cherian Lukose, C.; Wasy Zia, A.; Tambuwala, M.M.; Serrano-Aroca, Á. Recent Advances in Metal-Based Antimicrobial Coatings for High-Touch Surfaces. *Int. J. Mol. Sci.* **2022**, *23*, doi:10.3390/ijms23031162.

170. Karakurt, I.; Ozaltin, K.; Vesela, D.; Lehocky, M.; Humpol, P. Antibacterial Activity and Cytotoxicity of Immobilized Glucosamine / Chondroitin Sulfate on Polylactic Acid Films. *Polymers (Basel).* **2019**, *11*, 1–12.

171. Nie, B.; Long, T.; Li, H.; Wang, X.; Yue, B. A comparative analysis of antibacterial properties and inflammatory responses for the KR-12 peptide on titanium and PEGylated titanium surfaces. *RSC Adv.* **2017**, *7*, 34321–34330, doi:10.1039/c7ra05538b.

172. Heijink, A.; Schwartz, J.; Zobitz, M.E.; Nicole Crowder, K.; Lutz, G.E.; Sibonga, J.D. Self-assembled monolayer films of phosphonates for bonding RGD to titanium. *Clin. Orthop. Relat. Res.* **2008**, *466*, 977–984, doi:10.1007/s11999-008-0117-7.

173. Hoyos-Nogués, M.; Buxadera-Palomero, J.; Ginebra, M.P.; Manero, J.M.; Gil,

F.J.; Mas-Moruno, C. All-in-one trifunctional strategy: A cell adhesive, bacteriostatic and bactericidal coating for titanium implants. *Colloids Surfaces B Biointerfaces* **2018**, *169*, 30–40, doi:10.1016/j.colsurfb.2018.04.050.

174. Tan, M.; Feng, Y.; Wang, H.; Zhang, L.; Khan, M.; Guo, J. Immobilized Bioactive Agents onto Polyurethane Surface with Heparin and Phosphorylcholine Group Immobilized Bioactive Agents onto Polyurethane Surface with Heparin and Phosphorylcholine Group. *Macromol. Res.* **2013**, *21*, 541–549, doi:10.1007/s13233-013-1028-3.

175. Ozaltin, K.; Lehocky, M.; Humpolicek, P.; Pelkova, J.; Di Martino, A.; Karakurt, I.; Saha, P. Anticoagulant polyethylene terephthalate surface by plasma-mediated fucoidan immobilization. *Polymers (Basel).* **2019**, *11*, 1–12, doi:10.3390/polym11050750.

176. Kolb, H.C.; Finn, M.G.; Sharpless, K.B. Click Chemistry : Diverse Chemical Function from a Few Good Reactions. *Angew. Chemie - Int. Ed.* **2001**, *40*, 2004–2021.

177. Devaraj, N.K.; Finn, M.G. Introduction: Click Chemistry. *Chem. Rev.* **2021**, *121*, 6697–6698, doi:10.1021/acs.chemrev.1c00469.

178. Amna, B.; Ozturk, T. Click chemistry: a fascinating method of connecting organic groups. *Org. Commun.* **2021**, *78*, 97–120, doi:10.25135/ACG.OC.100.21.03.2006.

179. Huisgen, R. 1,3-Dipolar Cycloadditions. *Angew. Chemie - Int. Ed.* **1963**, *2*, 565–598.

180. Fairbanks, B.D.; Scott, T.F.; Kloxin, C.J.; Anseth, K.S.; Bowman, C.N. Thiol - Yne Photopolymerizations : Novel Mechanism , Kinetics , and Step-Growth Formation of Highly Cross-Linked Networks. *Macromolecules* **2009**, *42*, 211–217.

181. Daglar, O.; Luleburgaz, S.; Baysak, E.; Gunay, U.S.; Hizal, G.; Tunca, U.; Durmaz, H. Nucleophilic Thiol-yne reaction in Macromolecular Engineering: From synthesis to applications. *Eur. Polym. J.* **2020**, *137*, 109926, doi:10.1016/j.eurpolymj.2020.109926.

182. Lowe, A.B. Thiol-yne 'click'/coupling chemistry and recent applications in polymer and materials synthesis and modification. *Polymer (Guildf).* **2014**, *55*,

5517–5549, doi:10.1016/j.polymer.2014.08.015.

183. Hensarling, R.M.; Doughty, V.A.; Chan, J.W.; Patton, D.L. "Clicking" polymer brushes with thiol-yne chemistry: Indoors and out. *J. Am. Chem. Soc.* **2009**, *131*, 14673–14675, doi:10.1021/ja9071157.

184. Lowe, A.B.; Hoyle, C.E.; Bowman, C.N. Thiol-yne click chemistry: A powerful and versatile methodology for materials synthesis. *J. Mater. Chem.* **2010**, *20*, 4745–4750, doi:10.1039/b917102a.

185. Huisgen, R. 1,3-Dipolar Cycloadditions Past and Future [*]. *Angew. Chemie - Int. Ed.* **1963**, *2*, 565–632, doi:10.1097/TP.0000000000001850.

186. Diaz Diaz, David; Finn, M.G; Sharpless, K.Barry, Fokin, Valery.V; Hawker, C.. Cicloadición 1,3-dipolar de azidas y alquinos. I: Principales aspectos sintéticos. *An. Química RSEQ* **2008**, *104*, 173–180.

187. Lutz, J. 1 , 3-Dipolar Cycloadditions of Azides and Alkynes : A Universal Ligation Tool in Polymer and Materials Science. *Angew. Chemie - Int. Ed.* **2007**, *46*, 1018–1025, doi:10.1002/anie.200604050.

188. Ramapanicker, R.; Chauhan, P. Click Chemistry : Mechanistic and Synthetic Perspectives. In *Click reactions in Organic Synthesis*; 2016; pp. 1–24.

189. Meldal, M.; Tornøe, C.W. Cu-Catalyzed Azide - Alkyne Cycloaddition. **2008**, 2952–3015.

190. Rostovtsev, V. V; Green, L.G.; Fokin, V. V; Sharpless, K.B. A Stepwise Huisgen Cycloaddition Process : Copper (i) -Catalyzed Regioselective ™ Ligation ∫ of Azides and Terminal Alkynes **. *Angew. Chemie - Int. Ed.* **2002**, *41*, 2596–2599.

191. Liang, L.; Astruc, D. The copper(I)-catalyzed alkyne-azide cycloaddition (CuAAC) "click" reaction and its applications. An overview. *Coord. Chem. Rev.* **2011**, *255*, 2933–2945, doi:10.1016/j.ccr.2011.06.028.

192. Molteni, G.; Bianchi, C.L.; Marinoni, G.; Santo, N.; Ponti, A. Cu/Cu-oxide nanoparticles as catalyst in the "click" azide-alkyne cycloaddition. *New J. Chem.* **2006**, *30*, 1137–1139, doi:10.1039/b604297j.

193. Himo, F.; Lovell, T.; Hilgraf, R.; Rostovtsev, V. V.; Noodleman, L.; Sharpless, K.B.; Fokin, V. V. Copper(I)-catalyzed synthesis of azoles. DFT study predicts

unprecedented reactivity and intermediates. *J. Am. Chem. Soc.* **2005**, *127*, 210–216, doi:10.1021/ja0471525.

194. Ben El Ayouchia, H.; Bahsis, L.; Anane, H.; Domingo, L.R.; Stiriba, S.E. Understanding the mechanism and regioselectivity of the copper(i) catalyzed [3 + 2] cycloaddition reaction between azide and alkyne: A systematic DFT study. *RSC Adv.* **2018**, *8*, 7670–7678, doi:10.1039/c7ra10653j.

195. Wang, C.; Ikhlef, D.; Kahlal, S.; Saillard, J.Y.; Astruc, D. Metal-catalyzed azide-alkyne "click" reactions: Mechanistic overview and recent trends. *Coord. Chem. Rev.* **2016**, *316*, 1–20, doi:10.1016/j.ccr.2016.02.010.

196. Agard, N.J.; Prescher, J.A.; Bertozzi, C.R. A Strain-Promoted [3 + 2] Azide - Alkyne Cycloaddition for Covalent Modification of Biomolecules in Living Systems. *J. Am. Chem. Soc.* **2004**, *126*, 15046–15047.

197. Best, M.D. Click Chemistry and Bioorthogonal Reactions: Unprecedented Selectivity in the Labeling of Biological Molecules. *Biochemistry* **2009**, *48*, 6571–6584, doi:10.1021/bi9007726.

198. Dommerholt, J.; Rutjes, F.P.J.T.; van Delft, F.L. Strain-Promoted 1,3-Dipolar Cycloaddition of Cycloalkynes and Organic Azides. *Top. Curr. Chem.* **2016**, *374*, 1–20, doi:10.1007/s41061-016-0016-4.

199. Bach, R.D. Ring strain energy in the cyclooctyl system. the effect of strain energy on [3 + 2] cycloaddition reactions with azides. *J. Am. Chem. Soc.* **2009**, *131*, 5233–5243, doi:10.1021/ja8094137.

200. Baskin, J.M.; Bertozzi, C.R. Bioorthogonal click chemistry: Covalent labeling in living systems. *QSAR Comb. Sci.* **2007**, *26*, 1211–1219, doi:10.1002/qsar.200740086.

201. Sletten, E.M.; Bertozzi, C.R. Bioorthogonal Chemistry : Fishing for Selectivity in a Sea of Functionality Angewandte. *Angew. Chemie - Int. Ed.* **2009**, *48*, 6974–6998, doi:10.1002/anie.200900942.

202. Vrabel, M.; Carell, T. *Cycloadditions in Bioorthogonal Chemistry*; 2016; ISBN 978-3-319-29684-5.

203. Kim, E.; Koo, H. Biomedical applications of copper-free click chemistry:: In vitro, in vivo, and ex vivo. *Chem. Sci.* **2019**, *10*, 7835–7851, doi:10.1039/c9sc03368h.

204. Wang, S.; Yang, X.; Zhu, W.; Zou, L.; Zhang, K.; Chen, Y.; Xi, F. Strain-promoted azide-alkyne cycloaddition " click " as a conjugation tool for building topological polymers. **2014**, *55*, 4812–4819, doi:10.1016/j.polymer.2014.08.003.

205. Li, W.; Zou, J.; Zhu, S.; Mao, X.; Tian, H.; Wang, X. Fluorodibenzocyclooctynes: A Trackable Click Reagent with Enhanced Reactivity. *Chem. - A Eur. J.* **2019**, *25*, 10328–10332, doi:10.1002/chem.201902834.

206. Gordon, C.G.; MacKey, J.L.; Jewett, J.C.; Sletten, E.M.; Houk, K.N.; Bertozzi, C.R. Reactivity of biarylazacyclooctynones in copper-free click chemistry. *J. Am. Chem. Soc.* **2012**, *134*, 9199–9208, doi:10.1021/ja3000936.

207. Sakata, Y.; Nabekura, R.; Hazama, Y.; Hanya, M.; Nishiyama, T.; Kii, I.; Hosoya, T. Synthesis of Functionalized Dibenzoazacyclooctynes by a Decomplexation Method for Dibenzo-Fused Cyclooctyne-Cobalt Complexes. *Org. Lett.* **2022**, doi:10.1021/acs.orglett.2c03832.

208. Li, Z.; Seo, T.S.; Ju, J. 1,3-Dipolar cycloaddition of azides with electron-deficient alkynes under mild condition in water. *Tetrahedron Lett.* **2004**, *45*, 3143–3146, doi:10.1016/j.tetlet.2004.02.089.

209. Truong, V.X.; Ablett, M.P.; Gilbert, H.T.J.; Bowen, J.; Richardson, S.M.; Hoyland, J.A.; Dove, A.P. In situ-forming robust chitosan-poly(ethylene glycol) hydrogels prepared by copper-free azide-alkyne click reaction for tissue engineering. *Biomater. Sci.* **2014**, *2*, 167–175, doi:10.1039/c3bm60159e.

210. Saric, I.; Peter, R.; Kolympadi Markovic, M.; Jelovica Badovinac, I.; Rogero, C.; Ilyn, M.; Knez, M.; Ambrožić, G. Introducing the concept of pulsed vapor phase copper-free surface click-chemistry using the ALD technique. *Chem. Commun.* **2019**, *55*, 3109–3112, doi:10.1039/c9cc00367c.

211. Šarić, I.; Kolympadi Markovic, M.; Peter, R.; Linić, P.; Wittine, K.; Kavre Piltaver, I.; Jelovica Badovinac, I.; Marković, D.; Knez, M.; Ambrožić, G. In-situ multi-step pulsed vapor phase surface functionalization of zirconia nanoparticles via copper-free click chemistry. *Appl. Surf. Sci.* **2021**, *539*, doi:10.1016/j.apsusc.2020.148254.

212. He, B.; Su, H.; Bai, T.; Wu, Y.; Li, S.; Gao, M.; Hu, R.; Zhao, Z.; Qin, A.; Ling, J.; et al. Spontaneous Amino-yne Click Polymerization: A Powerful Tool toward

Regio- and Stereospecific Poly(β-aminoacrylate)s. *J. Am. Chem. Soc.* **2017**, *139*, 5437–5443, doi:10.1021/jacs.7b00929.

213. Worch, J.C.; Stubbs, C.J.; Price, M.J.; Dove, A.P. Click Nucleophilic Conjugate Additions to Activated Alkynes: Exploring Thiol-yne, Amino-yne, and Hydroxyl-yne Reactions from (Bio)Organic to Polymer Chemistry. *Chem. Rev.* **2021**, *121*, 6744–6776, doi:10.1021/acs.chemrev.0c01076.

214. Ruhemann, Siegfried; Beddow, F. CII.—Condensation of phenols with esters of the acetylene series. Part II. Action of phenols on ethyl phenylpropiolate and ethyl acetylenedicarboxylat. *J. Chem. Soc., Trans.* **1900**, *77*, 1119–1125.

215. Yakubu, S.; Etim, E.E. Modern Advances in Click Reactions and applications. *J. Chem. React. Synth.* **2023**, *13*, 129–151.

216. Fu, X.; Qin, A.; Tang, B.Z. Dynamic covalent polymers generated from X-yne click polymerization. *J. Polym. Sci.* **2023**, 1–12, doi:10.1002/pol.20230383.

217. Fu, X.; Qin, A.; Tang, B.Z. X-yne click polymerization. *Aggregate* **2023**, *4*, 1–22, doi:10.1002/agt2.350.

CHAPTER 2

DESIGNING BIOFUNCTIONAL POLY-L-LACTIDE BASED SURFACES EMPLOYING DIVERSE CLICK REACTIONS

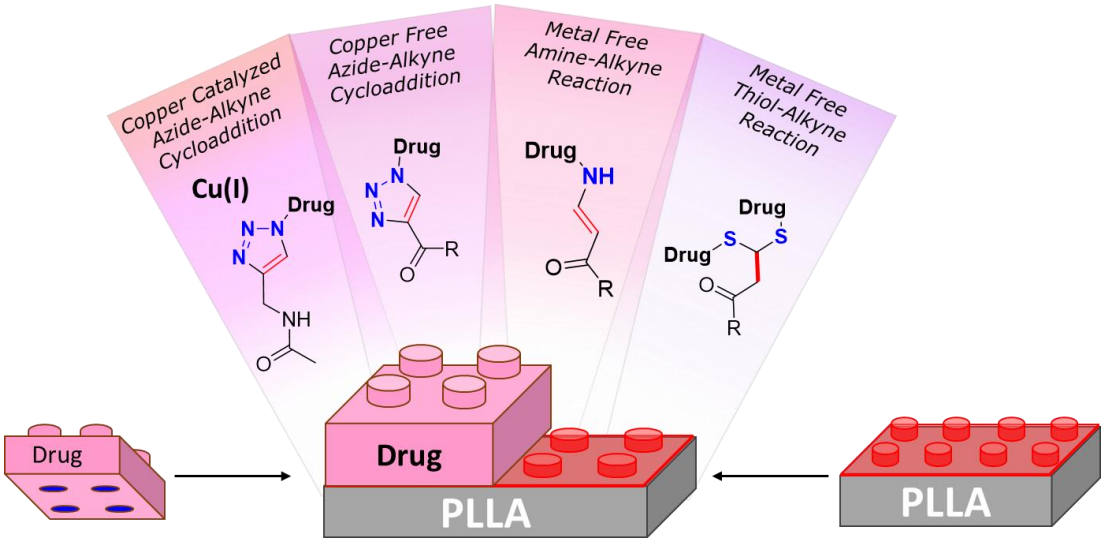

In the last few decades, surgical implants have become increasingly prevalent for restoring the functionality of damaged bones or joints. Nonetheless, it remains crucial to implement antibiotic or anti-inflammatory treatments in order to mitigate significant issues associated with these procedures. Such issues include the colonization of the implanted surface by bacteria or other microorganisms, as well as the occurrence of strong host inflammatory responses. This work presents the effectiveness of the Copper Catalyzed Alkyne-Azide Cycloaddition (CuAAC) reaction by the linkage of a fluorophore to the poly(L-lactide) (PLLA) surface. Moreover, this current work describes the covalent immobilization of the anti-inflammatory drug indomethacin on a PLLA surface. The CuAAC click reaction was selected to anchor the drug to the polymeric films.

CHAPTER 2

DESIGNING BIOFUNCTIONAL POLY-L-LACTIDE BASED SURFACES EMPLOYING DIVERSE CLICK REACTIONS

2.1. Introduction

Nowadays, ligament and tendon reconstructions or other surgical implants used in medicine have become attractive procedures to restore the functionality of affected joints [1]. Annually around 1 million hips are replaced worldwide and more than 250,000 knee replacements are provided. In addition, 30% of hospitalized patients have one or even more vascular catheters [2][3]. Along with the implantation of a surgical device different host responses appear. For example, contact can induce a negative response that enhances protein adhesion on the material surface, blood coagulation and complement activation.

Another drawback is the initial acute inflammatory, in this case neutrophils and monocytes are adsorbed in the site of inflammation [3,4]. Moreover, if no restoration of the tissue occurs, the initial inflammation may become to a chronic one and may develop a fibrotic encapsulation, which implies a premature failure of the implant [5,6]. The inflammation process of the biomaterial is mediated by a complex reaction, which involves protein adsorption, leukocyte recruitment and activation, secretion of

inflammatory mediators, and fibrous encapsulation of the implant [7]. In order to reduce macrophage adhesion at early stage and to block pro-inflammatory cytokine release chemical and physical modifications of biomaterials and immunomodulatory approaches have been developed [8,9].

Depending on the size and the surface properties of the material, the initial response of the living components of blood to the biomaterial may vary [10]. It is believed that the endothelialization of the blood-contacting device surface may overcome the problems. Therefore, it is essential a surface that enhances cell–material interaction and promotes the endothelialization at a shorter time. However, the modified surface may accelerate the aggregation of platelets before the formation of an endothelial monolayer and, because of that, a previous surface modification is required to provide anticoagulant and anti-inflammatory properties [11]. The ideal non-thrombogenic blood-contacting surface in blood vessels could be formed by a monolayer of healthy endothelial cells. The surface topography of materials, such as the presence of grooves, pores, or fibres, can also influence the behaviour of the cultured cells, for example, cell adhesion, orientation, movement, growth, and activation [12]. In the case of hemocompatibility regulation, it is essential to present a good regulation of blood-material interface in blood-contacting medical devices, such as vascular graft and stents, heart valves and intravascular catheters [13].

Metals and metal alloys, such as titanium and its alloys, are widely used on implants due to their biological security, biocompatibility and good mechanical strength. Nevertheless, thus organic coatings are frequently employed in order to enhance corrosion resistance, which is one of the main disadvantages of metals. In addition, these coatings show better thromboresistance, antimicrobial action, dielectric strength, wear properties and lubricity over metals [14]. Among organic coatings, polymeric ones are the most used materials due to the fact that they are inexpensive and environmentally friendly. Furthermore, polymer coatings can modify the negative effects caused by Ti6Al4V implants, such as the stress shielding effects [15,16]. Additionally, the stress that it is transferred by synthetic biodegradable polymers to the damaged tissue has shown to allow tissue healing comparing to metal implants [16]. On the other hand, polymer coatings provide large surface area-to-volume ratios [16]. Beside their suitable mechanical properties, polymeric biomaterials present different surface properties, such as surface chemistry, hydrophilicity, surface energy and charge density and their interactions with living tissue are necessary to ensure biocompatibility. All these properties can be adapted to the needs of each specific application. For example, poly(L-lactide) (PLLA) is one of the most promising biodegradable polymers and it is derived from natural feedstock such

as corn starch rice, potatoes and other natural resources [17,18]. The mechanical properties of PLLA are similar to those of synthetic polymers like polypropylene; in addition, raw materials for PLLA preparation are abundant and, consequently, PLLA is low cost [19,20]. Moreover, PLLA can offer some benefits to implantable devices as a coating due to its bioabsorbability and biocompatibility [21,22] and its hydrolytic degradation does not leave toxic by-products in the body fluid [23,24]. An increment of surface hydrophilicity by a simple functionalization with hydrophilic moieties could overcome the hydrophobicity that PLLA surface presents, in this way PLLA can be suitable for biomedical devices.

Not only to biomedical field, has PLLA revealed as a promise in the market due to its versatile applications, spanning from industrial to everyday use. Its appeal for mass production arises from its commendable attributes; for instance, PLLA boasts excellent physical properties suitable for crafting a wide array of plastic products, including fast-food containers and textiles used in both industrial and consumer setting. With its favorable tensile strength and ductility, PLLA lends itself to diverse processing methods such as melt-extrusion molding, inhection molding, blown film molding, foam and *vacuum* molding. Nonetheless, it has to be noted that its exceptional biocompatibility has increase its usage in the realm of biomedical applications. Indeed, it has been employed in different areas such as drug delivery systems[25], cardiovascular devices[26], tissue fixation devices[26] or wound dressings[27]. Nevertheless, despite having such promising features, PLLA has demonstrated that can cause an inflammation response, with limited cell adhesion and proliferation, due to its strong hydrophobicity and lack of active functional groups on surface capable to interact with cell surface receptors. These drawbacks limit the use of PLLA as biomedical device [28].

The low hemocompatibility represents another disadvantage of these biomaterials. Thus, a thrombus formation could occur on the material surface (namely, surface-induced thrombus formation) and may cause failure of the implanted material, vascular occlusion, heart attack and stroke [28]. Hence, it would be convenient to adhere to surface an anti-inflammatory agent in order to enhance hemocompatibility, which provides a faster endothelialization. As a consequence of the immobilization, a thrombogenic type surfaces may be avoided and so do the inflammation. Therefore, significant research efforts have focused on modifying material properties using various anti-inflammatory polymeric surface coatings to generate more biocompatible implants [29,30]. In order to have a bioactive surface a previous surface modification is required, for that two types of modification can be applied: (I) physical changed such as topography; (II) chemical modification of the surface to

obtain specific properties, for instance, by drug immobilization [31]. Therefore, several methods are known to improve the reactivity of the surfaces such as UV irradiation, ozone-induced treatment, plasma treatment or chemical modification, e.g., Click Chemistry.

Among a variety of techniques and methodologies, atmospheric pressure plasma (APP) has proven to be an effective strategy for modifying a wide variety of material surface such as ceramic, metal or polymer surfaces [29–31]. This solvent-free technique can be used to achieve active functional groups on any material, but in particular, non-active polymer surfaces. Therefore, properties like wettability, biocompatibility or surface chemistry can be enhanced, while the bulk properties of the polymers endure unaffected [30]. Indeed, this economical and easy-to-use technique is fast and highly adaptable, since different types of plasma gases (Ar, O_2, N_2) can be employed. APP has been mostly used itself to generate active surfaces capable of controlling or enhancing macrophage, cell or protein adhesion [30].

Despite the fact that APP technique could overcome the problem of wettability capacity of many materials, further modifications are usually required to obtain a good endothelization process. Nowadays, finding the appropriate surface that is able to capture endothelial cells from the bloodstream and to resist the processes of adhesion and proliferation is still a challenge. Therefore, one of the second strategy used involves the immobilization of some bioactive agent such as proteins, antibiotics, anti-inflammatory agents, nanoparticles (NP), among others.

In recent years, Click Chemistry has gained prominence for its advantageous capability to bioconjugate diverse systems onto any surface. This discovery not only made C-C or C-heteroatom bond formation reactions a reality, but also transformed chemistry into a limitless tool [32,33]. By addition of a catalyst, the reaction conducted a single regioisomer, particularly, 1,4-regioisomer of 1,2,3-triazole when copper (I) is employed [34,35]. Since the introduction of Cu(I), azide-alkyne cycloaddition reaction has been advanced remarkably over the last decade, and has now spread to almost all areas of chemistry, applied sciences and even biomedical fields [36–40]. Despite its exceptional features the CuAAC methodology presents a major drawback regarding the complete removal of the metallic catalyst. Indeed, in some cases related to biological or biomedical applications the CuAAC is not a suitable choice due to the cytotoxicity of the metal, which limits these reactions in living systems [41].

Nevertheless, in 2004 the term strain promoted [3+2] azide alkyne cycloaddition (SPAAC) reaction was introduced by Bertozzi *et al*., a novel strategy in which the use

of copper was excluded. Unlike linear acetylenes, the deformation of the carbon-carbon triple bond of a cyclooctyne (163°) allows the spontaneous reaction with azide compound despite its poor ability to act as 1,3-dipolar acceptor [42,43].

This methodology was used by the same authors to label different biomolecules in cellular environments, demonstrating not only the complete bioorthogonality of the process but also the survival of the cells in the reaction media [44,45]. This reaction has established itself as a powerful and versatile chemical reaction with wide academic and commercial applications, such as bioconjugation processes [46], hybrid and block polymers, high-performance and self-healing materials, metabolic engineering of biological systems and more [33,45,47,48]. However, these materials are expensive and difficult to synthesize, so the design of other strategies is of great importance.

In recent years, one of the priority lines of our research group has focused its attention on the bioconjugation of drugs to different polymeric surfaces in order to increase their biocompatibility and, thus, improve their applicability as biomedical devices [24]. In this context, we proposed the use of activated alkynes that favour the reaction between alkyne and azide without the use of copper catalyst. In fact, the previously mentioned poor ability of azide compounds to participate as dipolarophiles would be compensated, not by strain as in Bertozzi's proposal, but by electronic effects [25]. Therefore, modifying alkyne groups and becoming more reactive can be a promising alternative. The use of alkyne derived compounds with electron-attracting groups has been shown to be a fast and efficient way of promoting the reaction between azide and alkynes, reducing the activation energy required for the reaction. This novel methodology was firstly studied by Ju *et al*. in solution, where they reported the first 1,3-dipolar cycloaddition reaction between azides and electron-deficient alkynes in water [26]. When the alkyne (either terminal or internal) had at least one neighboring electron-withdrawing functional group, such as propiolic acid, the triazole formation was achieved even in water at room temperature without any catalysts. Despite the great versatility of this promising alternative to SPAAC, there are only few examples where this type of copper free reactions are used [26–28]. For instance, it has been employed in the synthesis of hydrogels, foams or polymers among others [29–31]. Although its great potential, the use of alkyne derived compound with electron-attracting groups in bioconjugation or immobilization of compounds on materials is still not widely known. While it has been shown to be a similar strategy to other copper-free click reactions, such as SPAAC, its application in these fields is still relatively new and unexplored. However, as more

research is conducted and the methodology is further optimized, it has the potential to become valuable tool in the modification of polymeric surfaces for biomedical use.

Another strategy that addresses the limitations associated with of the use of copper and has recently gained attention, particularly with the utilization of activated acetylene methodology, is the spontenaoeus amino-yne click reactions [49]. By simply combining electron deficient terminal alkynes with amines at room temperature without any catalyst, this reaction notably produces regio- and stereo-selective products, β-aminoacrylates, in excellent yields [49]. The mechanism underlying this reaction involves the electron-pair of the nitrogen and the terminal carbon of an activated ethynyl group. This occurs due to the electron-withdrawing nature ability of the ester functional group, facilitating a nucleophilic addition step that leads to a regioselectivity in the resulting product. From a thermodynamic point of view, *E*-isomers exhibit greater stability than *Z*-isomers during the proton transfer step. However, at room temperature *Z*-isomers can be transformed to *E*-isomers through a single transition state involving "nitrogen activated double bond rotation", thereby demonstrating the stereo-selectivity in the resulted enamine [50]. The amino-yne click reaction presents three additional advantages alongside the general benefits of click reactions: (I) it proceeds spontaneously at room temperature, requiring neither catalyst nor stimuli, thus simplifying the operational process. (II) amine are very economical and accessible reagents, and propiolate like compounds are easily synthesized from commercially available propiolic acid, and aromatic or aliphatic alcohols by esterification procedures under mild reaction conditions [49,51]. Moreover, the amino containing biomolecules do not required premodifications steps as amino functional groups is frequent in a wide range of compounds, facilitating the experimental process and paving the way for the widespread utilization of the amino-yne click reactions across various domains. (III) the β-aminoacrylate resulting from the amino-yne reaction can respond to particular stimuli, such as weak acid media, making the cleavage of the product and reobtaining the amino group, which make this type of reaction an interesting approach for designing materials that exhibit stimulus-triggered responses [50].

Similarly, another promising click reaction that does not required metal catalyst is thiol-yne click reaction. Thiols display versatile reactivity with a wide array of substrated and functional groups, often yielding high and easily traceable reactions. Many of these reactions occur under mild conditions, finding extensive use in routine organic synthesis, polymerization and surface modification. While their broad reactivity makes thiols excellent moieties for conjugation purposes, it also renders them prone to numerous side reactions. Sulfur-based cross-linking was firstly

described by Goodyear in 1839 using elementary sulfur. This reactions marked the inception of sulfur and thiols as accesible conjugation tools. Thiols' reaction, broadly categorized into radical and nucleophilic reactions, exhibit selectivity towards specific groups under varying conditions, accommodating numerous functional groups. The reaction of thiols with alkenes and alkyne progress smoothly in light or with a radical intiator, requiring no transition metals as catalysts. This method is highly favored in creating functional molecules for biological applicatios, forming stable thioether bonds resistant to stronsigs acids, bases and reducing conditions. These reactions find utility in tailoring solid surfaces, immobilizing macromolecules like proteins and surface engineering.

Bioconjugation can be considered as an intersection between chemistry and molecular biology, encompassing the covalent linking of synthetic or natural labels to biomolecular structures [52]. This interdisciplinary field focuses on biocompatible reactions that rapidly, efficiently and selectively join substrates with biomolecules. Indeed, challenges like attaching small molecular probes, such as fluorescent dyes, radical probes or affinity tags, to biopolymers or linking complex carbohydrates with peptides can be possible thanks to click reactions. However, the alteration of biomolecules can affect their specific biological functions, so maintaining their inherent bioactivity once attached onto the non-biological material represents a significant challenge [53]. Addressing this challenge, the bioconjugation of antibiotics, anti-inflammatories and anticoagulants onto various surfaces has garnered significant attention, aiming to design antimicrobial, anti-inflammatory and more hemocompaible surfaces that mitigate infection-related complications and biointegration failures associated with biomaterials implantation.

For the bioconjugation of anti-inflammatory, antibiotic, anticoagulant drugs and peptides a careful selection process has been carried out. These biomolecules were chosen based on their robust activity and the presence of readily modifiable moieties, enhancing both effectiveness and adaptability in the bioconjugation process. Next, the selected biomolecules and their activity will be described.

Indomethacin, or 1-(*p*-chlorobenzoyl)-5-mehoxy-2-methylindole-3-acetic acid (**Figure 2.1**) an extremely powerful non-steroidal anti-inflammatory drug, emerged over 50 years ago in the context of a research aimed at discovering effective anti-inflammatory and analgesic drugs [54]. In the 1960s, acetic acid derivatives were developed into indomethacin, diclofenac and sulindac, while propionic acid derivatives led to the generation of ibuprofen, naproxen and ketoprofen (**Figure**

2.1). Among these compounds, indomethacin was likely the most potent and one of the earliest to undergo clinical trials [55].

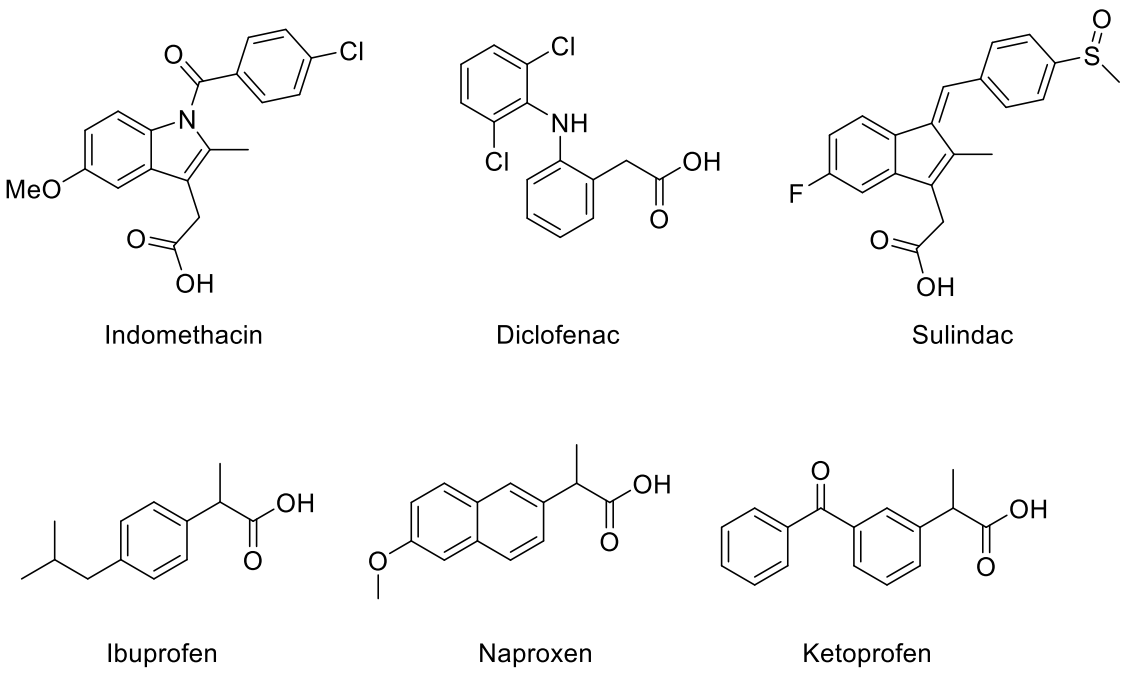

Figure 2.1. Acetic acid and propionic acid derivatives.

The mechanism of action of indomethacin, as well as that of other previously mentioned NSAIDs, was described for the first time in 1971. It acts as a non-selective inhibitor of cyclooxygenases (COX1 and COX2), which are enzymes involved in the synthesis of prostaglandins from arachidonic acid [56]. While COX1 is universally present in most body tissues and is involved in the synthesis of the prostaglandins and thromboxane A2, COX2 is expressed in response to injury or inflammation. Prostaglandins are hormone-like molecules naturally present in the body and they play a key role in the generation of pain, fever and inflammation [57]. By impeding the synthesis of prostaglandins, indomethacin can effectively alleviate pain, reduce fever and mitigate inflammation. Studies conducted both *in vitro* and *in vivo* have consistently demonstrated that the potency of compounds follows a specific order: indomethacin > naproxen > ibuprofen > phenylbutazone > aspirin. This ranking of relative potency provides valuable insight on why the first three drugs have gained popularity in the NSAID market [58].

Regarding the structure-activity relationship (SAR) of indomethacin, several studies concluded that indol structural moiety is necessary for inhibiting COX1 and COX2. Moreover, alterations to the halogen in benzoyl-indomethacin indicated that this substituent was not required for the potentiating activity of the compound. However,

when amide and ester indomethacin analogues were studied, it was observed that the transformation of the chloride moiety to bromide exhibited stronger effect against COX2 and weaker against COX1, indicating that bromide group improve selectivity effect of the drug [59]. Additionally, benzoyl indomethacin derivatives without methoxy moiety did not render the compound inactive. According to the selectivity of the activity, benzoyl indomethacin derivatives showed no significance difference in inhibiting COX1 and COX2, whereas *N*-benzyl indomethacin analogues were weak COX1 inhibitors, suggesting that the carbonyl group might be important for COX1 inhibition. Furthermore, it is worth noting that the alteration of acid group to amide or ester do not reduce the activity. In fact, these analogues continue being active on both COX, or even more effective to COX2, improving the selectivity of the drug [60]. This latest modification holds immense significance because carboxylic acids are functional moieties mainly employed for the derivatization and the introduction of interesting functional groups. Within this Doctoral Thesis, essential groups enabling the click reaction have been incorporated into the drug's structure *via* amidation reactions. Consequently, it is demonstrated that these alterations do not compromise the compound's pharmacological activity, and therefore the activity of the drug will remain, but further biological assays are essential to corroborate the activity (**Figure 2.2**) [61].

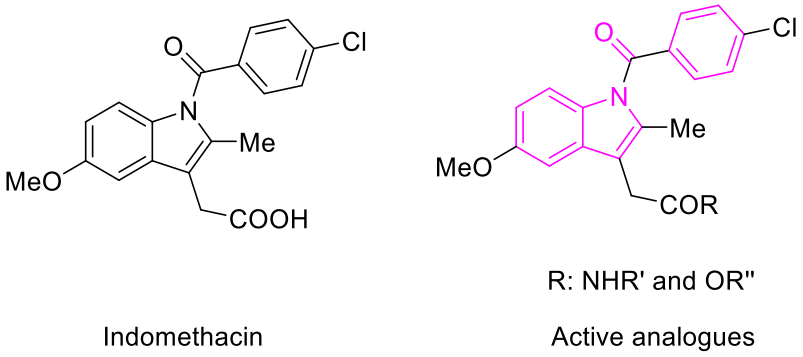

Figure 2.2. Indomethacin and its active analogues chemical structure.

A considerable percentage, ranging from 30 to 60% of patients who receive typical therapeutic doses of indomethacin experience adverse effects. Indeed, these effects can lead to discontinuation of the medication in approximately 10 to 20% of cases [54]. It is worth noting that most of these adverse effects are directly related to the administrated dose. These adverse effects could clearly overcome by the immobilization of the drug onto the required platforms, avoiding oral administration and providing anti-inflammatory effect at local damage tissue. Indeed, conjugation of drugs is a highly effective strategy for achieving targeted drug delivery while minimizing undesired side effects. This approach involves the covalent attachment of

drugs to other platforms, such as surfaces or molecules, resulting in numerous clinical advantages [62]. By forming a stable linkage, bioconjugation enhances disease-specific targeting, leading to improved therapeutic outcomes [56]. Furthermore, this approach offers benefits such as reduced toxicity, optimized pharmacokinetics and so increased efficacy, enhanced safety and improved tolerability. Overall, bioconjugation strategy holds great promise for advancing precision medicine and improving patient care.

Another potent drug with interesting antibacterial properties is amoxicillin. Amoxicillin (**Figure 2.3**) belongs to the group of β-lactam amino-penicillin drugs and is known for its wide action against both aerobic and anaerobic bacteria, with good absorption and tissue penetration [63]. Its mechanism of action involves disrupting the proper formation of the bacteria cell wall, leading to the death of susceptible microorganisms [64]. To achieve this, amoxicillin acts by inhibiting one or more enzymes, often referred to as penicillin-binding proteins (PBPs), which play a crucial role in the biosynthetic pathway of bacterial peptidoglycan [65]. As a result of this inhibition, the bacterial cell wall weakens commonly followed by cell lysis and subsequent death [66,67].

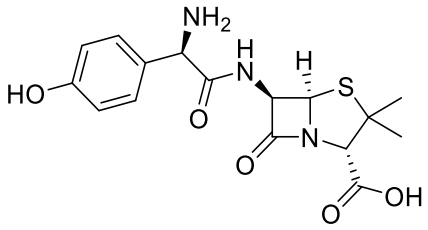

Amoxicillin

Figure 2.3. Amoxicillin chemical structure.

The comprehensive SAR studies have shown that the pharmacophore central to the activity of the drug is 6-APA (6-aminopenicillanic acid), while the amide moiety and the aromatic ring are essentials as well. Importantly, it should be noted that any substitution in the heteroaromatic ring tends to significantly diminish the activity of the drug, particularly when it comes to combating Gram-negative organisms like *Escherichia coli.* This information highlights the critical structural elements responsible for the effectives of amoxicillin and sheds light on the challenges posed by specific bacterial strains [68].

Although its excellent antimicrobial activity against both Gram-positive and Gram-negative bacteria, amoxicillin presents some disadvantages. Indeed, the primary

disadvantages of amoxicillin include potential side effects such as allergic reactions (ranging from mild rash to severe anaphylaxis), susceptibility to bacterial resistance development when used inappropriately or excessively, and the possibility of disrupting the balance of beneficial bacteria in the gut, leading to issues like antibiotic-associated diarrhoea. Additionally, some individuals may experience gastrointestinal upset, such as nausea, vomiting, or abdominal discomfort, as a result of taking amoxicillin. These common issues can be avoided by immobilizing amoxicillin onto substrates, given the typically low drug concentrations that are required in bioconjugation methodologies [63,65].

Similarly, antimicrobial peptides (AMPs) represent a diverse class of small peptides present in nature, constituting an integral component of the innate immune defense across various organisms. AMPs exhibit a remarkable array of inhibitory actions, showcasing potent effects against a spectrum of pathogens including bacteria, fungi, parasites, and viruses. This broad-spectrum activity significantly enhances the appeal of these peptides as possible candidates in addressing microbial threats [51]. In this way, Feng *et al.* [52] investigated the impact of tryptophan within truncated dCATHs peptides derived from animal sources and classified as AMPs. Their findings underscored the pivotal role of tryptophan (TRP), highlighting that peptides incorporating this amino acid exhibited notably heightened antibacterial efficacy. Conversely, peptides devoid of tryptophan showcased a lack of discernible antibacterial activity. TRP, an indispensable amino acid sourced from plants, is pivotal in the *in vivo* synthesis of proteins. Among the 20 naturally occurring amino acids crucial for animal and human nutrition, TRP stands out for its multifaceted roles [53]. Functioning as an essential amino acid vital for normal growth, TRP assumes a dynamic role as a precursor in the synthesis of various bioactive compounds. Notably, it serves as a starting compound for an array of important molecules, including nicotinamide (vitamin B6), serotonin, melatonin, tryptamine, kynurenine, 3-hydroxykynurenine, and quinolinic and xanthurenic acids [54]. As the most widely dispersed indole derivative in nature, tryptophan holds the distinction of being the first recognized essential amino acid for numerous animal species. The implications of tryptophan and its metabolites span across a broad spectrum of health-related fields [55]. Beside its notable antimicrobial effect, this amino acid is recognized for its ability to emit fluorescence [69]. Consequently, in this study, it has been employed as a flurophore for the validarion of the methodology, concurrently broadening the scope of the reaction.

Regarding anticoagulant activity, warfarin, discovered in 1939 by Karl Paul Link, remains a fundamental agent in preventing clot formation and prolonging existing

clots [70,71]. Its molecular structure allows for various tautomeric forms, with analysis revealing its prevalence existence as a mixture of cyclic hemiketal diasteroisomers/enantiomers and a small portion in an open-chain form (**Figure 2.4**). However, it has to be noted that the (S)-(-) enantiomer demonstrates six times greater anticoagulant activity than the (+) enantiomer. While its mechanism does not directly address clot removal or ischemic tissue damage reversal, its efficacy lies in impeding the intrinsic and extrinsic pathways of the clotting cascade. This interference occurs through the inhibition of vitamin K-dependent clotting factors (II, VII, IX, X) and anticoagulants proteins C and S. By disrupting the vitamin K oxidation-reduction cycle, crucial for clotting factor activation, warfarin decreases the availability of active vitamin K reserves. In fact, the reaction is exclusively carried out in the presence of sufficient levels of vitamin K hydroquinone. During the conversion process from glutamic acid moiety to a y-carboxyglutamic acid moiety, one molecule of vitamin K hydroquinone is employed, transforming into vitamin K 2,3-epoxide. This epoxide form required a two-step reduction process to transform to vitamin K quinone and subsequently to vitamin K hydroquinone for the cycle to resume. The enzyme used for these two reductions it vitamin K epoxide reducatse (VKOR), which is inhibited by warfarin [72]. This depletion prevents the formation of glutamic acid residues within clotting factors, rendering them inactive and incapable of participating in the clotting process. According to SAR studies, it has been concluded that 4-hydroxycoumarin moiety is essential for inhibiting VKOR. In fact, it has been shown that replacing the hydroxyl moiety for a chloride or a thiol led to ineffective analogues [72].

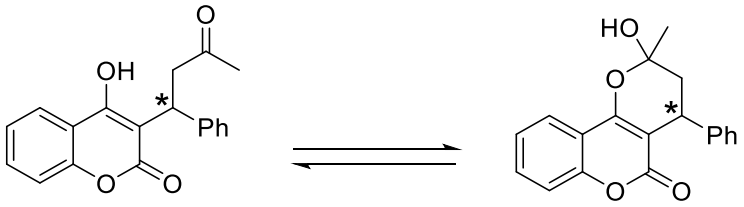

Figure 2.4. Warfarin tautomers.

Despite its isolation from spoiled sweet clover, warfarin stands as the most prescribed anticoagulant globally. However, due to its narrow therapeutic index, maintaining a precise anticoagulation range poses challenges, risking bleeding with overdoses or thrombotic events with insufficient doses [73].

As mentioned in *Chapter 1*, beside antibacterial or anti-inflammatory properties, promoting proper endothelization is essential for successful biointegration. REDV is a fibronectin-derived peptide known for its remarkable ability to specifically bind to

endothelial cells [74]. Studies have shown that the REDV sequence serve as a crucial recognition site for integrin α4β1, which is a receptor that describe cell-cell interactions that are critical for immune function, this receptor is abundant on endothelial cells (ECs), whereas scarce on smooth muscle cells (SMCs) [75]. The connexion of the peptide and this integrin receptor provides the interaction of fibronectin and endothelial cells. This remarkable property provides REDV with a unique ability to selectively promote the adhesion and proliferation of ECs, while showing minimal impact on SMCs [76]. This selective behaviour holds tremendous promise for various biomedical applications, particularly in tissue engineering and regenerative medicine, where targeted promotion of endothelial cell growth is crucial for enhancing vascularization and tissue repair.

Beside the drugs employed for the bioconjugation, the new generated triazole has gained attention these last years. Indeed, it has been studied that 1,2,3-triazole heteroaromatic ring exhibits a diverse array of pharmacological properties, making it another chemical structure highly valuable in biochemical and biomedical field. It has demonstrated significant potential as anticancer [77], anti-parasitic [78], antimicrobial [79], anti-HIV [80], antiviral and anti-inflammatory substance [81–84]. One key advantage is its exceptional stability under various conditions, including acidic or basic hydrolysis, as well as oxidative and reductive environments, primarily due to their high aromatic stabilization. This inherent stability enhances their potential for drug development and highlights their significance modern pharmacological research [83,85]. Furthermore, the stability of the resulting triazole ensured the permanent immobilization of the drug onto the substrate.

This Doctoral Thesis explores anti-inflammatory, antibiotic, and anticoagulant agents that offer easy modifications without compromising their pharmacological activity. These selected drugs have been extensively studied in oral systems but most of them often present drawbacks such as adverse effects or low bioavailability. The aim of this work is the use of click reactions to address these issues and enhance their efficacy, as well as obtaining PLLA based materials with promising biological activity for biomedical applications. Amonng these drugs, nonstereoidal anti-inflammatory indomethacin, broad spectrum antibiotic amoxicillin and potent anticoagulant warfarin can be found. Moreover, it has to be highlithed that most of these drugs exhibit also antioxidant, antipyretic and analgesic effect, which are also beneficial attributes for improving the biocompatibily of these materials.

2.2. Materials and Methods

2.2.1. Materials

Poly-L-lactide (PLLA) (Corbion, Amsterdam, The Netherlands) was used to prepare films. Chloroform ($CHCl_3$, >98% Macron Fine Chemicals, Gliwice, Poland), tert-butanol (^tBuOH, Macron Fine Chemicals, Bologna, Italy), ethanol (EtOH, 99.8%, Macron Fine Chemicals, Gliwice, Poland), methanol (MeOH, 98%, Macron Fine Chemicals, Gliwice, Poland), acetonitrinile (CH_3CN, 99%, Panreac, Darmstadt, Germany), dichloromethane (CH_2Cl_2, 98%, Macron Fine Chemicals, Gliwice, Poland), toluene (99%, Sigma Aldrich, St. Louis, MO, USA), *N*,*N*-dimethylformamide (DMF, 99%, Macron Fine Chemicals, Bologna, Italy), acetic acid (AcOH, Sigma Aldrich, St. Louis, MO, USA), deuterated chloroform ($CDCl_3$, 99.8% Sigma Aldrich, St. Louis, MO, USA) and Milli Q water were used as a solvents. Sodium hydroxide (99%, Panreac, Darmstadt, Germany), sodium hydrogen carbonate ($NaHCO_3$, 99%, Merck, Darmstadt, Germany), sodium carbonate (Na_2CO_3, 98%, Panreac, Darmstadt, Germany), *N*,*N*-dicyclohexylcarbodiimide (DCC, 99%, Sigma Aldrich, St. Louis, MO, USA), 1-hydroxybenzotriazole hydrate (HOBT, 97%, Sigma Aldrich, St. Louis, MO, USA), *N*-(3-dimethylaminopropyl)-*N*-ethylcarbodiimide hydrochloride (EDC·HCl, 98%, Sigma Aldrich, St. Louis, MO, USA), *N*-hydroxysuccinimide (NHS, 98%, Sigma Aldrich, St. Louis, MO, USA), *N*,*N*-diisopropylethylamine (DIPEA, 99%, Sigma Aldrich, St. Louis, MO, USA), ethylendiamine (99%, Sigma Aldrich, St. Louis, MO, USA), triethylamine (Et_3N, <99.5%, Sigma Aldrich, St. Louis, MO, USA), propargylamine (97.5%, Sigma Aldrich, St. Louis, MO, USA), propiolic acid (95%, Sigma Aldrich, St. Louis, MO, USA), 3-bromopropylamine hydrobromide (98%, Sigma Aldrich, St. Louis, MO, USA), sodium azide (NaN_3, 99.5%, Sigma Aldrich, St. Louis, MO, USA), copper (II) sulphate pentahydrate ($CuSO_4·5H_2O$, 98%, Sigma Aldrich, St. Louis, MO, USA), sodium ascorbate (98%, Sigma Aldrich, St. Louis, MO, USA), sodium sulfate anhydrous (Na_2SO_4, 96%, Panreac, Darmstadt, Germany), magnesium sulfate anhydrous (MgSO4, 96%, Panreac, Darmstadt, Germany), O-toluidine blue (TBO, dye content 80%, St. Louis, MO, USA), dansyl chloride (<99%, Sigma Aldrich, St. Louis, MO, USA), L-tryptophan (<98%, Sigma Aldrich, St. Louis, MO, USA), indomethacin (<99%, Sigma Aldrich, St. Louis, MO, USA), thionyl chloride (<99%, Sigma Aldrich, St. Louis, MO, USA), amoxicillin (98%, Sigma Aldrich, St. Louis, USA), warfarin (98%, Sigma Aldrich, St. Louis, EEUU),).

For plasma functionalization, chemicals were purchased from: EDC·HCl (Sigma-Aldrich, Tauf-kirchen, Germany), NHS (Sigma-Aldrich, Tauf-kirchen, Germany), PLLA (PolyScience, Warrington, UK), (3-aminopropyl)trimethoxysilane (APTES, SERVA

Feinbiochemica, Heidelberg, Germany), chloroform (Thermo Scientific, Karlsruhe, Germany), propiolic acid (Merck, Darmstadt, Germany) in p.a. quality or higher if not indicated differently.

For *in vitro* biological tests various reagents and solvents were employ: DMEM (Merck, Sigma-Aldrich, Darmstadt, Germany), fetal bovine serum (FBS) (Thermo Fisher Scientific, Carlsbad, CA, USA), streptomicyin (Thermo Fisher Scientific, Invitrogen, Carlsbad, CA, USA), penicillin (Thermo Fisher Scientific, Invitrogen, Carlsbad, CA, USA), L-glutamine (Thermo Fisher Scientific, Invitrogen, Carlsbad, CA, USA), HEK293 cells (Sarstedt, Hildesheim, Germany), phorbol myristate acetate (PMA) (Merck, Sigma-Aldrich, Darmstadt, Germany), RPMI-1640 medium (Merck, Sigma-Aldrich, Darmstadt, Germany).

2.2.2. Experimental procedure

2.2.2.1. General procedure for the synthesis of 3-azidopropan-1-amine

3-Bromopropan-1-amine hydrobromide (2.28, 10.4 mmol) was dissolved in H_2O/CH_3CN (1:1, 15 mL) and NaN_3 (2.78 g, 42.8 mmol) was added. The reaction mixture was heated at 80 °C for 48 h. After cooling to room temperature, the solution was basified by addition of 2 M NaOH solution, and the mixture was extracted with CH_2Cl_2 (3x10 mL). Finally, organic layers were collected, dried over anhydrous Na_2SO_4 and the solvent was evaporated to obtain 3-azidopropan-1-amine as a yellowish oil (0.77 g, 77%). ^{1}H-NMR (300 MHz, $CDCl_3$) (δ, ppm): 2.92 (t, *J* = 6.6 Hz, 2H, CH_2, H_3), 2.33 (t, *J* = 6.6 Hz, 2H, CH_2, H_1), 1.99 (bs, 2H, NH_2), 1.29 (q, *J* = 6.6 Hz, 2H, CH_2, H_2); ^{13}C-NMR (75 MHz, $CDCl_3$) (δ, ppm): 48.8 (N_3-CH_2, C_1), 38.5 (NH-CH_2, C_3), 31.5 (CH_2, C_2).

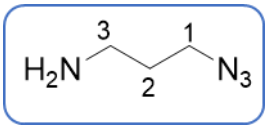

2.2.2.2. Synthesis of dansyl derivatives

a) Synthesis of dansyl derivative ***2a***

Dansyl chloride (2.00 g, 7.40 mmol) was dissolved in CH_2Cl_2 (20 mL) and 3-azidopropan-1-amine (0.75 g, 7.40 mmol) and Et_3N (0.75 g, 7.40 mmol) was added. The reaction was refluxed at 40 °C for 48 h. After cooling to room temperature, a portion of water was added to the reaction and the solution was extracted with CH_2Cl_2 (3x10 mL) and washed with a saturated solution of sodium chloride (2x10 mL). Organic layers were collected, dried over anhydrous Na_2SO_4 and the solvent was evaporated under vacuum to afford *N*-(3-azidopropyl)-5-

(dimethylamino)naphthalene-1-sulfonamide (**2a**) as a brownish oil (1.8 g, 94%). ^{1}H-NMR (300 MHz, $CDCl_3$) (δ, ppm): 8.53 (d, *J* = 8.5 Hz, 1H, CH_{arom}, H_7), 8.38 (d, *J* = 8.5 Hz, 1H, CH_{arom}, H_{12}), 8.22 (dd, *J* = 8.5 Hz, *J* =7.5 Hz, 1H, CH_{arom}, H_5), 7.49 (dd, *J* = 8.5 Hz, *J* =7.5 Hz, 2H, CH_{arom}, H_6, H_{11}), 7.16 (d, *J* = 7.5 Hz, 1H, CH_{arom}, H_{10}), 5.97 (s, 2H, NH_2), 3.27 (t, *J* = 5.7 Hz, 2H, CH_2, H_1), 2.94 (t, *J* = 5.7 Hz, 2H, CH_2, H_3), 2.86 (s, 6H, 3xCH_3), 1.57-1.54 (m, 2H, CH_2, H_2); ^{13}C-NMR (75 MHz, $CDCl_3$) (δ, ppm): 152.0 (C_{arom}-N, C_9), 134.5 (C_{arom}-S, C_4), 131.9 (C_{arom}-H, C_7), 130.6 (C_{arom}-H, C_6), 129.9 (C_{arom}-C, C_{13}), 128.5 (C_{arom}-H, C_{11}, C_5), 123.2 (C_{arom}-H, C_{12}), 118.7 (C_{arom}-C, C_8), 115.3 (C_{arom}-H, C_{10}), 48.4 (CH_2, C_1), 44.1 (N-CH_3), 39.4 (CH_2, C_3), 26.8 (CH_2, C_2).

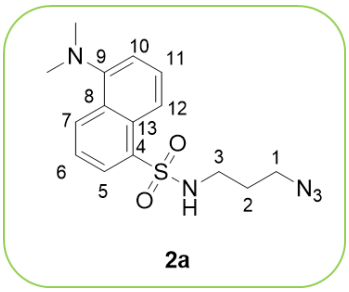

2a

b) Synthesis of dansyl derivative ***2b***

Dansyl chloride (2.00 g, 7.40 mmol) was dissolved in CH_2Cl_2 (20 mL) and propargylamine (0.48 mL, 7.40 mmol) and Et_3N (0.75 g, 7.40 mmol) were added. The reaction was refluxed for 48 h. After cooling to room temperature, a portion of water was added to the reaction and the solution was extracted with CH_2Cl_2 (3x10 mL) and washed with a saturated solution of sodium chloride (2x10 mL). Organic layers were collected, dried over anhydrous Na_2SO_4 and the solvent was evaporated under *vacuum* to afford 5-(dimethylamino)-*N*-(prop-2-yn-1-yl)naphthalene-1-sulfonamide (**2b**) as a yellowish oil (0.95 g, 89%). ^{1}H-NMR (300 MHz, $CDCl_3$) (δ, ppm): 8.52 (d, *J* = 8.5 Hz, 1H, CH_{arom}, H_7), 8.30-8.28 (m, 2H, CH_{arom}, H_5 and H_{12}), 7.54-7.51 (m, 2H, CH_{arom}, H_6 and H_{11}), 7.18 (dd, *J* = 7.5 Hz, *J* = 0.54 Hz, 1H, CH_{arom}, H_{10}), 5.26 (s,1H, NH), 3.77 (d, *J* = 2.5 Hz, 2H, CH_2, H_3), 2.86 (s, 6H, 2xCH_3), 1.91 (t, *J* = 2.5 Hz, 1H, ≡CH, H_1); ^{13}C-NMR (75 MHz, $CDCl_3$) (δ, ppm): 152.0 (C_{arom}-N, C_9), 135.5 (C_{arom}-S, C_4), 132.6 (C_{arom}-H, C_7), 131.3 (C_{arom}-C, C_{13}), 129.5 (C_{arom}-H, C_5), 129.2 (C_{arom}-H, C_6), 128.5 (C_{arom}-H, C_{11}), 123.2 (C_{arom}-H, C_{12}), 118.9 (C_{arom}-C, C_8), 115.3 (C_{arom}-H, C_{10}), 84.3 (C≡C, C_2), 71.2 (≡CH), 45.2 (N-$(CH_3)_2$), 33.2 (CH_2).

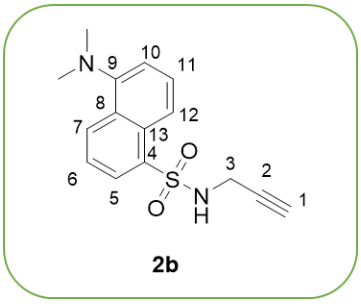

2b

c) Synthesis of dansyl derivative ***2c***

The synthesis of dansyl derivative **2c** was carried out in a two.step methodology.

i. Synthesis of *N,N'*-(disulfanediylbis(ethane-2,1-diyl))bis(5-(dimethylamino)naphthalene-1-sulfonamide) (DSSD)

Dansyl chloride (0.50 g, 1.85 mmol) was dissolved in acetone (51 mL) and water (2 mL). Then, previously prepared cysteamine hydrochloride (0.11 g, 0.93 mmol) in aqueous $NaHCO_3$ (0.1 M, 12 mL) solution was added in small portions. In addition, NaOH (0.5 M) was used to keep the solution at pH= 7.5. Then, the mixture was stirred for 90 mins at room temperature. After, chloroform (100 mL) was added to the solutions and layers were separated. The organic layer was washed with sodium bicarbonate solution (4x20 mL) and water (1x20 mL). Finally, the organic phase was collected, dried over anhydrous $MgSO_4$ and the solvent was evaporated under *vacuum* to afford *N,N'*-(disulfanediylbis(ethane-2,1-diyl))*bis*(5-(dimethylamino)naphthalene-1-sulfonamide) (DSSD), which was used in the next step without further purification. ^{1}H-NMR (300 MHz, $CDCl_3$) (δ, ppm): 8.54 (d, *J*= 8.5 Hz, 1H, CH_{arom}, H_7), 8.24-8.20 (m, 2H, CH_{arom}, H_5 and H_{12}), 7.56-7.52 (m, 2H, CH_{arom}, H_6 and H_{11}), 7.17 (d, *J*= 7.6 Hz, 1H, CH_{arom}, H_{10}), 5.24 (t, *J*= 6.3 Hz, 1H, NH), 3.09 (q, *J*= 6.3 Hz, 2H, $NHCH_2$, H_3), 2.88 (s, 6H, $2CH_3$), 2.48 (t, *J*= 6.3 Hz, 2H, $S\text{-}CH_2$, H_2); ^{13}C-NMR (75 MHz, $CDCl_3$) (δ, ppm): 152.2 (C_{arom}-N, C_9), 134.5 (C_{arom}-S, C4), 132.4 (C_{arom}-H, C_7), 130.8 (C_{arom}-C, C_{13}), 130.0 (C_{arom}-H, C_5), 129.8 (C_{arom}-H, C_6), 129.6 (C_{arom}-H, C_{11}), 123.3 (C_{arom}-H, C_{12}), 118.7 (C_{arom}-C, C_8), 115.4 (C_{arom}-H, C_{10}), 45.6 ($N(CH_3)_2$), 41.7 ($NHCH_2$, C_3), 37.9($S\text{-}CH_2$, C_2).

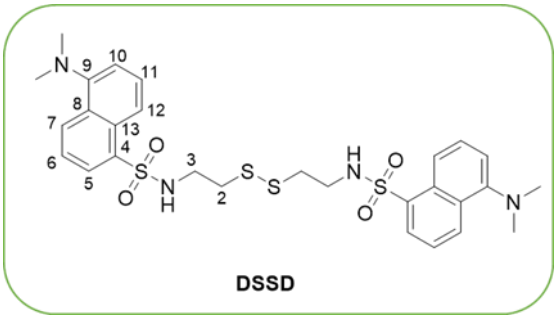

ii. Synthesis of 5-(dimethylamino)-*N*-(2-mercaptoethyl)naphthalene-1-sulfonamide (**2c**)

Previously synthesized DSSD (0.09 g, 0.16 mmol) was dissolved in THF (6 mL) and water (1 mL) at 0 ºC. Then, $NaBH_4$ (0.06 g, 1.63 mmol) was added in small portion. After, the reaction was vigorously stirred for 4 h at room temperature. Following, the solvent was evaporated under *vacuum* and the obtained solid was dissolved in water (10 mL). This last aqueous solution was extracted with diethyl ether (3x10 mL). Finally, organic layers were collected, dried over anhydrous Na_2SO_4 and solvent was evaporated under *vacuum* to afford 5-(dimethylamino)-*N*-(2-

mercaptoethyl)naphthalene-1-sulfonamide (**2c**). ^{1}H-NMR (300 MHz, $CDCl_3$) (δ, ppm): 8.56 (d, *J*= 8.5 Hz, 1H, CH_{arom}, H_7), 8.26-8.23 (m, 2H, CH_{arom}, H_5 and H_{12}), 7.55-7.52 (m, 2H, CH_{arom}, H_6 and H_{11}), 7.20 (d, *J*= 7.6 Hz, 1H, CH_{arom}, H_{10}), 5.18 (t, *J*= 6.3 Hz, 1H, NH), 3.10-3.07 (m, 2H, $NHCH_2$, H_3), 2.89 (s, 6H, $2xCH_3$), 2.51 (dt, *J*= 8.7, 6.4 Hz, 2H, $SHCH_2$, H_2), 1.21 (t, *J*= 8.7 Hz, 1H, SH, H_1); ^{13}C-NMR (75 MHz, $CDCl_3$) (δ, ppm): 152.1 (C_{arom}-N, C_9), 150.1 (C_{arom}-S, C_4), 134.6 (C_{arom}-H, C_7), 130.7 (C_{arom}-C, C_{13}), 129.9 (C_{arom}-H, C_5), 129.5 (C_{arom}-H, C_6 and C_{11}), 128.6 (C_{arom}-H, C_{12}), 123.2 (C_{arom}-H, C_{10}), 118.5 (C_{arom}-C, C_8), 115.3 (C_{arom}-H, C_{10}), 45.9 (NH-CH_2, C_3), 45.4 ($N(CH_3)_2$), 24.8 ($SHCH_2$, C_2).

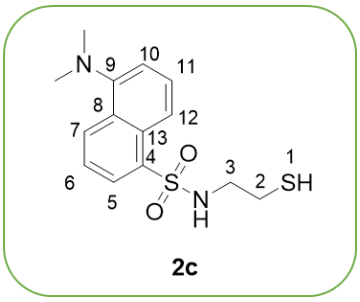

2c

*2.2.2.3. Synthesis of indomethacin derivative **3a***

Indomethacin (2.10 g, 5.60 mmol) was dissolved in CH_2Cl_2 (20 mL) and $SOCl_2$ (0.81 g, 6.20 mmol) was added. The reaction was refluxed during 2 h. After that, the excess of $SOCl_2$ was removed under *vacuum* and 3-azidopropan-1-amine (0.6 g, 6.2 mmol) dissolved in CH_2Cl_2 (5 mL) was added to the mixture along with additional CH_2Cl_2 (15 mL). Then, the reaction was stirred at room temperature or 72 h. After that time, the reaction was stopped by adding water and CH_2Cl_2, the phases were separated, and the aqueous phase was extracted with CH_2Cl_2 (3x20 mL) and the combined organic phases were washed with a sodium chloride saturated aqueoys solution (2 x 10 mL). Then, organic layers were dried over anhydrous Na_2SO_4 and, finally, the solvent was evaporated under *vacuum* to obtain *N*-(3-azidopropyl)-2-(1-(4-chlorobenzoyl)-5-methoxy-2-methyl-1H-indol-3-yl)acetamide (**3a**) as a yellowish oil (1.5 g, 71%). ^{1}H-NMR (300 MHz, $CDCl_3$) (δ, ppm): 7.61 (d, *J* = 8.5 Hz, 2H, CH_{arom}, H_{14} and H_{18}); 7.46 (d, *J* =8.5 Hz, 2H, CH_{arom}, H_{15} and H_{17}), 6.88 (d, *J* = 2.5 Hz, 1H, CH_{arom}, H_7), 6.84 (d, *J* = 9.0 Hz, 1H, CH_{arom}, H_{10}), 6.69 (dd, *J* = 9.0 Hz, *J* = 2.5 Hz, 1H, CH_{arom}, H_9), 6.21 (s, 1H, NH), 3.82 (s, 3H, OCH_3), 3.64 (s, 2H, CH_2, H_4), 3.27-3.26 (m, 4H, CH_2, H_1 and H_3), 2.38 (s, 3H, CH_3), 1.71-1.68 (m, 2H, CH_2, H_2); ^{13}C-NMR (75 MHz, $CDCl_3$) (δ, ppm): 171.2 (NHCO), 168.9 (NRCO), 156.1 (C_{arom}-C, C_8), 139.2 (C_{arom}-Cl, C_{15}), 136.0 (C_{arom}-C, C6), 124.2 (C_{arom}-C, C_{12}), 131.3 (C_{arom}-H, C_{14} and C_{18}), 131.0 (C_{arom}-C, C_{13}), 129.3 (C_{arom}-H, C_{15} and C_{17}), 129.3 (C_{arom}-C, C_{11}) 115.1 (C_{arom}-H, C_{10}), 112.3 (C_{arom}-H, C_9), 111.8 (C_{arom}-C, C_5) 102.3 (C_{arom}-H, C_7), 55.5 (OCH_3), 48.8 (CH_2, C_1), 38.5 (CH_2, C_3), 32.5 (CH_2, C_4), 28.8 (CH2, C2), 12.6 (CH_3).

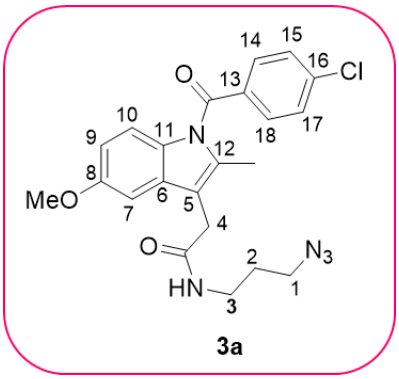

3a

*2.2.2.4. Synthesis of warfarin derivative **4a***

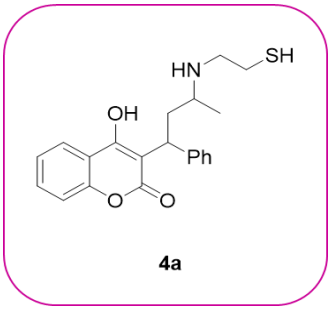

4a

Warfarin (0.50 g, 1.62 mmol) was dissolved in DMF (5 mL) and, then, CH_3COOH (0.1 mL)) was added. After, cysteamine hydrochloride (0.25 g, 3.18 mmol) was added along with DMF (3 mL). The reaction was stirred during 1 h at room temperature. After that, $NaBH_3CN$ (0.42 g, 6.26 mmol) were previously dissolved in DMF (2 mL) and added to the solution. The reactions was then stirred for 24-28 h and followed by thin layer chromatography (TLC). the phases were separated, and the organic phase was washed with a saturated solution of sodium chloride (3x20 mL).Then, organic layers were collected, dried over anhydrous Na_2SO_4 and, finally, the solvent was evaporated under *vacuum*. No desired product was obtained.

2.2.2.5. Preparation of PLLA Films

This procedure was employed in all type of PLLA surface functionalizations, except for plasma functionalization, where casting solvent was used to obtain PLLA surfaces. PLLA (1.00 g) was dissolved in $CHCl_3$ (50 mL) for 2 h under magnetic stirring. The solution was finally precipitated in an excess of cold distilled MeOH to isolate the product. Resulting materials were dried at 70 °C in *vacuum* for 48 h. Films were fabricated in a hydraulic hot press by compression moulding at 200 °C for 30 s under 0 MPa, then 1 min under 50 MPa and finally 3 min under a pressure of 150 MPa followed by water quenching [86].

Otherwise, different strategy was followed during my reaserach stay in Italy. The polymers films were prepared using the following procedure: PLLA (0.50 g) (PolyScience, Mw 300,000, Warrington, UK) was dissolved in 20 mL of $CHCl_3$ and poured into a glass petri dish (55 mm). The remaining solvent was evaporated obtaining 0.040 ± 0.014 mm thick films, measured by a thickness gauge. Finally, PLLA films were cut into 2x2 cm and prepared for further modifications.

2.2.2.6. Hydrolysis of PLLA Films

20 mm x 10 mm rectangular PLLA films were washed in MeOH/H_2O (1:1 v/v) solution for 1 h under sonication. Samples were dried overnight before surface modification. Hydrolysis was performed according to Lao *et al.* PLLA films were immersed in NaOH (0.25 M) at 52 °C under constant magnetic stirring during 30 min [87]. Samples were removed and washed with distilled water for 90 min and further dried at 30 °C before characterization.

2.2.2.7. Plasma mediated functionalization

PLLA samples, obtained by solvent casting, were treated by Argon plasma (Ar-plasma) in order to generate active radicals at the surface. Different generator power (10, 20 W) and time of plasma treatment (1, 2 min) were applied with a radiofrecuency (RF) plasma generator at a low pressure of 8 mbar in constant flow in order to optimize the method. After that, APTES plasma treatment was applied with varied flow rate (1 mL/min) in pulsed at diverse power (10, 20 W) and time (5, 10, 15 min). Eight different experiments were performed changing above-mentioned parameters.

2.2.2.8. Amidation of PLLA Films

a) PLLA amidation for copper catalyzed methodology

An acetic/acetate buffer solution (pH=5) was prepared and NHS (0.015 g, 0.13 mmol) and EDC·HCl (0.025 g, 0.13 mmol) were added. Then, PLLA films were submerged in the solution under constant stirring for 4 h at room temperature. After, they were immersed in another acetic/acetate buffer solution (pH= 5) and heated at 40 °C for 2 h. Then, another portion of EDC·HCl (0.028 g, 0.15 mmol) was added and films were left to react at room temperature for 24 h. After, they were washed in distilled water and dried at 30 °C under *vacuum* [86]. Once dried, the films were treated with thw corresponding amine, propargyl amine or 3-azidopropan-1-amine.

i. Propargylamine based amidation reaction (Pathway A, PA)

In pathway A (PA) the films were immersed in a solution of propargylamine (0.89 g, 16.1 mmol) for 48 h under room temperature. Then, modified films were cleaned with water and dried under *vacuum* at 30 °C before characterization, obtaining PLLA films with ending azide group (PLLA-N_3).

ii. 3-azidopropan-1-amine based amidation reaction (Pathway B, PB)

In pathway B (PB) the films were modified with 3-azidopropan-1-amine (2.00 g, 19.0 mmol) for 48 h under room temperature. Then, modified films were cleaned with water and dried under *vacuum* at 30 °C before characterization, obtaining PLLA films with ending alkyne group (PLLA-Alkyne).

b) PLLA amidation for copper free methodology

PLLA was initially cut in 20 mm x 10 mm rectangular films, then were washed in methanol/water (1:1 v/v) solution for 10 min and dried overnight before surface functionalization. Hydrolysis reaction was performed according to Lao *et al*. PLLA films were firslty immersed in NaOH (0.25 M) at 52 °C under constant magnetic stirring during 30 min [87]. After, hydrolyzed samples were washed with HCl (10%) and water. Finally, hydrolyzed PLLA (PLLA-COOH) substrates were dried at 30 °C before characterization. Subsequently, amidation of the films was carried out. For this purpose, two steps were involved: (I) EDC·HCl (0.025 g, 0.13 mmol) and NHS (0.015 g, 0.13 mmol) were dissolved in acetic/acetate buffer solution of pH 5. Then, hydrolyzed PLLA films were introduced into the prepared solution for 4 h under constant stirring at room temperature. After, they were immersed in a new EDC·HCl (0.028 g, 0.15 mmol) acetic/acetate buffer solution for 2 h at 40 ºC. Then, films were left to react at room temperature for 24 h. After 24 h, films were introduced in ethylendiamine (88 µL, 1.32 mmol) PBS buffer solution for 24 h at room temperature. Finally, samples were dried under *vacuum* for 24 h before second step. (II) Propiolic acid (83 µL, 1.33 mmol) is mixed with EDC·HCl (0.29 g, 1.50 mmol) and NHS (0.17 g, 1.50 mmol) in water (10 mL) for 4 h. Then, functionalized PLLA films were introduced into the solution for 24 h. Finally, samples were washed with water and dried under *vacuum* for 24 h.

c) PLLA amidation for plasma methodology

EDC·HCl/NHS approach was followed in order to perform the amidation reaction to incorporate propiolic acid. Several conditions were employ that are explained in *2.3. Results and Discussion section*.

2.2.2.9. Immobilization of different biological compounds onto PLLA films

*a) Conjugation of dansyl derivatives **2a** and **2b** onto PLLA surfaces via CuAAC*

Dansil derivative (**2a** or **2b**, 2.21 g, 6.69 or 7.59 mmol, respetively) was dissolved in a mix of ^{t}BuOH/H_2O (1:1 v/v, 10 mL) and $CuSO_4 \cdot 5H_2O$ (0.025 g, 0.10 mmol) and sodium ascorbate (0.025 g, 0.13 mmol) were added to the solution. Once the solution was homogeneous, previously prepared PLLA samples were immersed on it during 72 h at room temperature. After 72 h, samples were washed in EtOH under sonication. The reaction between dansyl derivative (**2a**) and PLLA-Alk was carried out through the pathway A (PA), whereas the reaction between dansyl derivative (**2b**) and PLLA-Azi was through pathway B (PB). Obtaining funtionalized PLLA-Dansyl-A and PLLA-Dansyl-B respectively.

*b) Bioconjugation of indomethacin derivative **3a** via CuAAC*

Indomethacin derivative **3a** (2.21 g, 5.02 mmol) was dissolved in a mix of EtOH/H_2O (1:1 v/v, 10 mL) and $CuSO_4 \cdot 5H_2O$ (0.025 g, 0.10 mmol) and sodium ascorbate (0.025 g, 0.13 mmol) were added to the solution. Once the solution was homogeneous, previously prepared PLLA-Alkyne samples were immersed on it during 72 h at room temperature. After 72 h, samples were washed in EtOH under sonication. Finally, biofuntionalized PLLA-Indo samples were dried at 30 °C under *vacuum* before characterization.

*c) Conjugation of dansyl derivative **2a** via copper free azide-yne click reaction*

Similarly to *section 2.2.10.1*, dansyl derivative **2a** (0.20 g, 0.61 mmol) was dissolved in EtOH:H_2O (1:1 v/v, 10 mL) and activated alkyne functionalized PLLA (PLLA-Alkyne) films were introduced onto the solution under constant stirring for 124 h at room temperature. Finally, dansylated PLLA (PLLA-Dns) films were washed with EtOH and dried under *vacuum* for 24 h.

d) Conjugation of trypthophan via copper free amino-yne click reaction

Similar to previous section, PLLA-Alkyne surfaces were further functionalized with triptophan (1.4 mmol equivalent to introduced propiolic acid) previously dissolved in Na_2CO_3 (0.1 M, 10 mL) solution under room temperature during 72 h. Then, the obtained PLLA-TRP surfaces were rinsed with water and ethanol and dried under *vacumm* for further characterization.

e) Bioconjugation of amoxicillin via copper free amino-yne click reaction

Similar to previous section, PLLA-Alkyne surfaces were further functionalized with amoxicillin (1.4 mmol equivalent to introduced propiolic acid) previously dissolved in Na_2CO_3 (0.1 M, 10 mL) solution under room temperature during 72 h. Then, the obtained PLLA-TRP surfaces were rinsed with water and ethanol and dried under *vacumm* for further characterization.

2.2.3. Characterization of synthesized compound and functionalized PLLA Samples

2.2.3.1. Nuclear Magnetic Resonance (NMR)

For the characterization of derivatized compound proton (^{1}H-NMR) and carbon thirteen (^{13}C-NMR) nuclear magnetic resonance spectra were performed, employing AV-300 spectrometer (300 MHz for ^{1}H and 75.4 MHz for ^{13}C) (Bruker, Rheinstetten,

Germany) at room temperature and using deuterated chloroform as solvent. Chemical shifts (δ) are expressed in parts per million (ppm) relative to TMS using the residual signal of the solvent [7.26 ppm (^{1}H) and 77.0 (^{13}C)] as internal reference. Coupling constants (*J*) are expressed in Hertz (Hz).

2.2.3.2. Fourier Transform Infrared Spectroscopy (FTIR)

FTIR has been used to analyze the vibrational bands of different bonds of the different synthesized drugs derivative, in order to visualize the functional groups generated after modification. For this purpose, NICOLET Nexus FT-IR spectrophotometer (Thermo Electron Corporation, Thermo Scientific, Loughborough, UK) was used and the conditions were used as follows: 32 scans, between 4000 – 500 cm^{-1} wavenumber, y 4 cm^{-1} resolution.

2.2.3.3. Attenuated Total Reflectance Fourier Transform Infrarred (ATR-FTIR)

Surface chemical modifications of pristine PLLA and functionalized PLLA were analyzed via FTIR by employing NICOLET Nexus 670 FT-IR spectrophotometer (Thermo Scientific, Loughborough, UK) equipped with an ATR employing 32 scans from 4000 cm^{-1} to 600 cm^{-1} within the wavenumber range and a resolution of 4 cm^{-1}.

PLLA surfaces treated with plasma: ATR-FTIR technique was performed in order to analyse surface chemical compounds after each surface treatment. ATR-FTIR spectra measurements were obtained using ThermoScientific Nicolet iS50 FTIR spectrometer equipped with a diamond crystal ATR accessory. Each measurement was performed from 4000 to 650 cm^{-1} wavenumber interval, at 4 cm^{-1} resolution and 32 scans. The spectra were analysed by Spectrum software.

2.2.3.4. Colorymetric methodology via UV-Vis

The amount of grafted carboxylic groups (–COOH) in the hydrolysis process was determined by a colorimetric method using TBO as a colorant. Chollet *et al.* proposed this method [88], which is based on an ionic interaction between the cationic colorant and the deprotonated carboxylate groups of the acid. Hydrolyzed PLLA films were immersed in a TBO 5 x 10^{4} M basic solution for 5 min. Then, the films were removed and washed in a NaOH 2M solution, so that the excess of TBO could be removed. Subsequently the films were immersed in an acetic acid (50%) aqueous solution in order to release the attached TBO and, the final solution was measured by UV-VIS (Shimadzu MultiSpec-1501 spectrophotometer, Kioto, Japan). The concentration of the carboxyl groups was determined using a calibration plot (Abs = 75,301xM; R2 = 0.9984) by measuring the optical absorbance at 633 nm and based on the

assumption that 1 mol of TBO reacts with 1 mol of carboxyl groups [89]. By means of this strategy, the amount of the reacted amine was calculated employing the following equation (1):

$$\% \text{ Surface Amidation} = \frac{\text{nPLLA-COOH-nPLLA-Amidated COOH}}{\text{nPLLA-COOH}} \text{x } 100 \quad (1)$$

Otherwise, PLLA sample surfaces with APTES plasma treatment were determined by Acid Orange II colorimetric method. The method is based on the adsorption and desorption of Orange II at different pH values. First, APTES plasma treated were dipped into 2 mL of Orange II acidic solution (pH 3, HCl 37%) overnight at room temperature. Then, HCl 37% was employed to wash (×3) the samples, until there was no more color release. After, they were submerged in 2 mL of NaOH 1 M (pH 12) (obtained by the addition of 1 M NaOH solution) for 30 min at room temperature to induce the release of electrostatically adsorbed AO molecules. Finally, the absorbance of the solution was measured at 485 nm (Perkin Elmer Instrument Lambda 40) and, the amount of adsorbed AO molecules was calculated, by a proper calibration curve (Abs= 23.768XM R2= 0.9653) assuming that AO's concentration is directly proportional to the concentration of amino groups on sample surface,

2.2.3.5. Water Contact Angle (WCA)

On the other hand, the changes in hydrophobicity in PLLA films caused by surface modifications were analyzed using static contact angle method (NEURTEK Instruments OCA 15 EC, Eibar, Spain). Milli-Q water was used as a testing liquid and sessile drop method (2 µL per drop) was carried out at room temperature to do the measurements. The average values were calculated using five measurements of each composition.

For surfaces treated with plasma, PLLA-PL-Si-NH_2: The wettability of samples was evaluated through static contact angle analysis using CAM 200 KSV instrument and Drop Shape Analysis System DSA 10 software after each surface modification. Measurements were performed at room temperature using drops of 2 µL volume collecting 3 frames per second. For each sample, contact angle was evaluated on two samples and using three drops per sample. Data are reported as mean value ± standard deviation.

2.2.3.6. X-ray Photoelectron Spectroscopy (XPS)

The elemental analysis of modified PLLA films was carried out by X-ray photoelectron spectroscopy SPECS system (XPS, SPECS Surface Nano Analysis, Berlin, Germany) using focus monochromatic radiation source 500 with dual anode Al/Ag and it is

equipped with a 150 1D-DLD analyzer (Phoibos, Berlin, Germany). PLLA samples were fixed with stainless steel holders and carbon tape during de measurements. Moreover, a carbon reference was used to do the measurements.

2.2.3.7. Fluorescence Microscopy

The fluorescence of the PLLA surface was analyzed before and after click reaction using an epifluorescence microscope Zeiss Axioskop (Jena, Germany).

2.2.3.8. Fluorescence spectroscopy

Emission spectra of the PLLA films were recorded exciting in the UV region using an Edinburgh Instruments spectrofluorimeter (FLSP920 model, Livingston, U.K.) in front-face configuration. Samples were positioned at 40° and 50° angles to the excitation and emission beams, respectively, and were tilted at a 30° angle relative to the plane formed by the direction of incidence and detection.

2.2.3.9. Scanning Electron Microscope (SEM)

Morphological observations were carried out onto functionalized PLLA surfaces employing electronic microscope HITACHI S-4800 (Singapore, Japan). Different voltages were applied on PLLA surfaces: an electron acceleration voltage of 1.5 kV over a distance of 7.1 mm x 5.00 k for pristine PLLA and PLLA-COOH surfaces, an electron acceleration voltage of 1.50 kV over a distance of 8.3 mm x 5.00 k for PLLA-NH_2 surface, 2.0 kV over a distance of 8.3 mm x 5.00 k for PLLA-Alkyne, 2.0 kV over a distance of 7.2 mm x 5.00 k for PLLA-TRP and PLLA-Dns and 1.5 kV over a distance of 6.0 mm x 5.00 k for PLLA-Amox surfaces.

2.2.3.10. Differential Scanning Calorimetry (DSC)

The glass transition temperature of the pristine PLLA and PLLA-COOH were measured by differential scanning calorimeter (DSC) with a DSC METTLER TOLEDO 822^e instrument (Greifensee, Switzerland) equipped with STAR© v14.0 software. The samples (~10 mg) were placed in 100 µL aluminum crucibles. Samples were heated from 0 °C to 200 °C, cooled from 200 °C to 0 °C and again heated from 0 °C to 200 °C employing a scanning rate of 10 °C·min^{-1} under a nitrogen atmosphere with a flow rate of 20 mL/min.

2.2.3.11. In vitro cytotoxicity assay

HEK293 cells (40 $\times 10^3$) in DMEM supplemented with 10% FBS (v/v), 100 µg/mL streptomycin, 100 U/mL penicillin and L-glutamine were seeded by adding a 50 µL drop in the different pristine PLLA and PLLA-indo surfaces (2 mm diameter) and allowed to attach during 1 h at 37 ˚C and at 5% CO_2. Then, pristine PLLA and PLLA-indo were transferred to a 96-well culture plate and cells were maintained for 48 h in complete DMEM 150 µL/well in a humidified incubator at 37 °C and 5% CO_2. Similar number of cells was seeded in wells without PET samples to be used as control. Cellular viability was determined by the MTS assay that evaluates the reduction of 3-(4,5-dimethylthiazol-2-yl)-5-(3-carboxymethoxyphenyl)-2-(4-sulfophenyl)-2H-tetrazolium (MTS) to formazan by enzymatic activity (mitochondrial dehydrogenases) of viable cells. After 48 h exposure, cells were washed twice with phosphate-buffered saline buffer (PBS) and 120 µL MTS reagent (CellTiter 96 Aqueous One Solution Cell Proliferation Assay; Promega, Madison, WI, USA) was added to each well. After 1 h incubation in the dark at 37 °C with a 5% CO_2 atmosphere, 100 µl of the MTS containing media was transferred to a new plate to avoid interference of all PLLA samples. The formazan absorbance was measured at 490 nm. To determine the viability, the background values of the wells without cells were subtracted from the values of the tested wells. The mean absorbance of the cells grown without PLLA and PLLA-Indo served as the reference for calculating 100% cellular viability. The results were expressed as a percentage of the viability of the untreated cells.

2.2.3.12. In vitro inflammatory and anti-inflammatory assay

THP-1 human monocytic cells were cultured in RPMI with 10% FBS (v/v), 100 µg/mL streptomycin, 100 U/mL penicillin and L-glutamine. Then, cells were differentiated to a macrophage phenotype by incubating with 20 µM phorbol myristate acetate (PMA) diluted in complete culture medium for 24 h. Differentiated cells were washed with serum-free RPMI-1640 medium, cells were detached from the culture plate and subsequently reseeded by adding a 50 µL drop containing 40 × 10^3 cells in the different pristine PLLA and PLLA-Indo samples (2 mm diameter). Cells were allowed to attach during 1 h at 37 ˚C and at 5% CO_2. Then, all PLLA surfaces were transferred to a 96-well culture plate and cells were maintained in the tissue culture plates for 24 h. The cells were then stimulated with 2.5 µg/mL of LPS and the levels of human IL-6 were determined at 48, 72 and 96 h by ELISA (Abcam, Spain), according to the manufacturer's protocol.

2.3. Results and discussion

For a better comprehension this section will be divided into types of click reactions.

2.3.1. Copper (I)-catalyzed azide alkyne click approach

To enhance the reactivity of PLLA surface, the initial step involved a hydrolysis reaction followed by amidation with propargylamine (pathway A, PA) or 3-azidopropan-1-amine (pathway B, PB), this way alkyne and azide moieties, key functional groups for the click reaction, were introduced (**Scheme 2.1**). This preactivation approach allowed PLLA surface for subsequent functionalizations, notably facilitating the azide-alkyne click reaction.

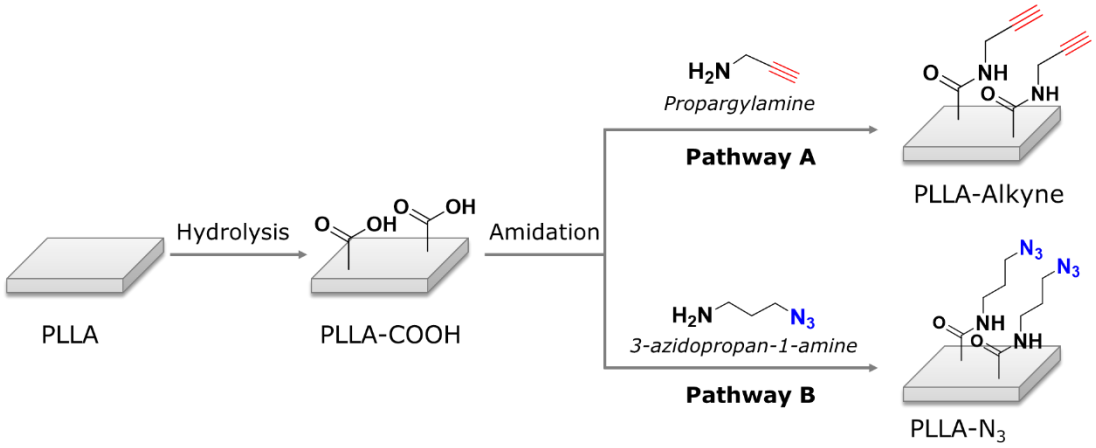

Scheme 2.1. Representative scheme of hydrolysis and amidation reactions onto PLLA film through two different pathways

The amount of carboxylic group was quantitatively determined by a colorimetric method based on the ionic interaction between the TBO cation and carboxylate anions generated during PLLA basic hydrolysis. As can be seen in **Scheme 2.1**, after the hydrolysis, PLLA films were submitted to amidation conditions with propargylamine or, alternatively, with previously synthesized 3-azidopropan-1-amine. Therefore, it was proposed the conjugation of the fluorophore to the polymer surface through two alternative pathways. In pathway A, the alkyne functional group was linked to the surface. Whereas, in pathway B the azido moiety was the one linked to the polymer surface, and the alkyne to the fluorophore compound. After amidation conditions, colorimetric method was again employed, as amide group cannot be deprotonated, it cannot link with the cationic TBO, only unreacted acid group can interact with it indicating (**Scheme 2.2**). This way, it can be estimated the amount of propargylamine or 3-azidopropan-1-amine bound to the surface. Employing equation

(1), mentioned in materials and methods section, it was calculated that approximately 15% of the acid groups were successfully amidated with propargylamine by going through pathway A, while in pathway B the conversion of amidation was approximately of 7% (**Figure 2.5**). The amidation values were obtained by using the following calibration plot Abs= 75,301xM; R^2 = 0.9984, measuring the mol quantity of COOH group before and after amidation.

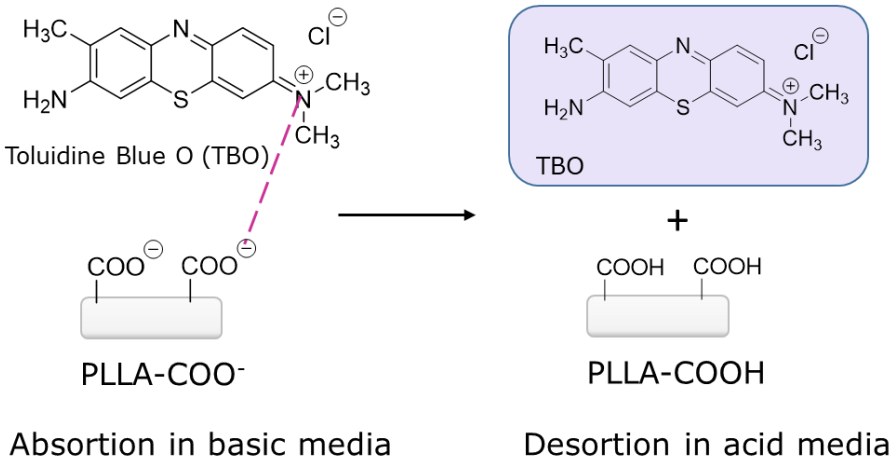

Scheme 2.2. Illustrative mechanism of the absortion and desortion of TBO onto hydrolyzed and amidated PLLA surfaces.

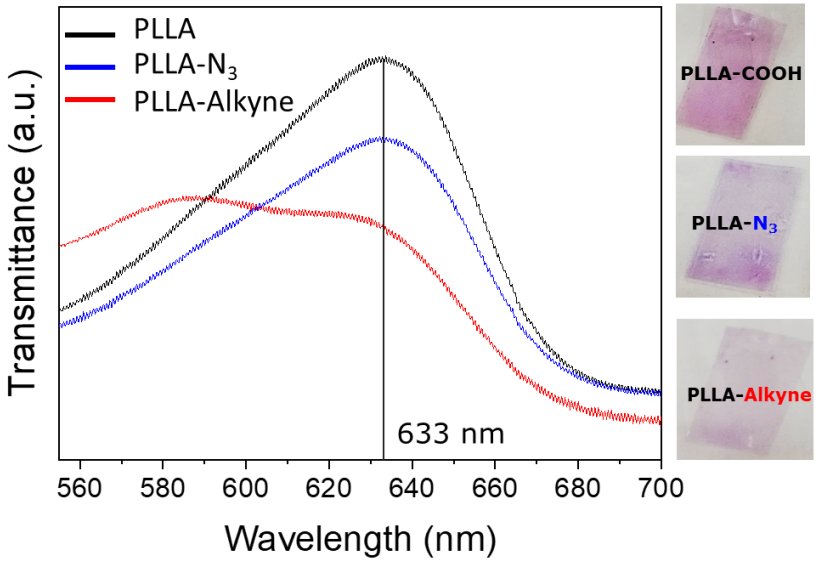

Figure 2.5. UV-Vis transmittance spectra of hydrolyzed and amidated PLLA.

As it is known, surface reactions such as hydrolysis only affect the physical-chemistry properties of the surface, while the bulk properties of the material, in this case, polymer, remain intact. To validate the chosen method for film preparation and

functionalization, it is crucial to ascertain whether these processes influence the mechanical properties of the polymer. Equally important is understanding if these mechanical properties, in turn, alter surface functionalization. For this purpose, differential scanning calorimetry assays were performed (**Figure 2.6**).

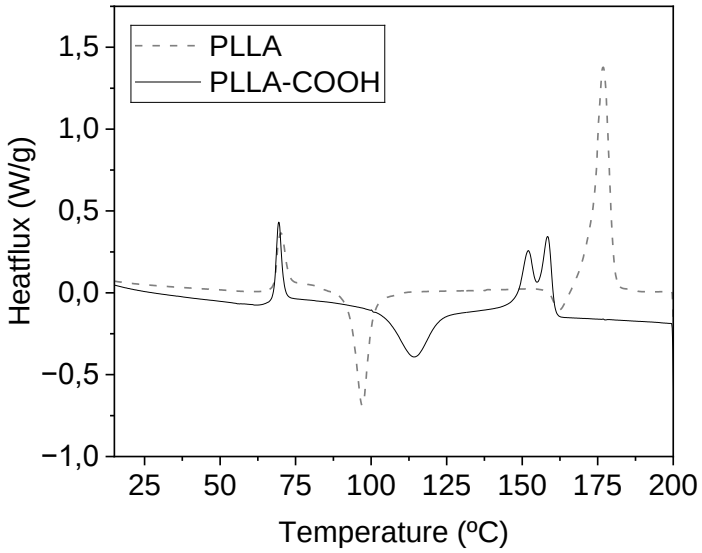

Figure 2.6. DSC spectra of pristine PLLA and hydrolyzed PLLA surfaces.

As can be seen in **Figure 2.6**, no significance difference can be apreciated in both PLLA and PLLA-COOH spectra. While the T_g value remained constants after hydrolysis, a slight decrease in the T_m value could be observed. These results suggested a modest reduction in crystallinity, conssistently associated with the hydrolysis process. Overall, this modification did not alter the bulk properties of the material.

After both amidation reactions were carried out, the next step was the immobilization of a drug. In this case, to validate the proposed methodogy, a fluorophore was employed. Dansyl stands out as one of the most effective derivatization reagent, being extensively employed in the field of biology for fluorescence labeling of of cells and aminoacids [90]. Although, in this work dansyl derivatives has been used only for the control of the conjugation owing to its fluorescence, it is worth mentioning that sulfonamides are known as broad spectrum antimicrobial agents, which can inhibit the growth of both Gram-positive and Gram-negative bacteria [91]. Thus, the proposed methodology would be a suitable alternative to carry out the immobilization of this type of compounds. In this context, the immobilization of two derivatized dansyl compounds **2a** and **2b** was carried out onto PLLA surfaces. For this, a previous

modification of dansyl chloride was performed. For comparative purposes, and in order to carry out the two alternative click reactions, two different fluorophore derivatives of dansyl were prepared: one with alkyne and othe other with the azide moiety (**Scheme 2.3**, **Table 2.3**).

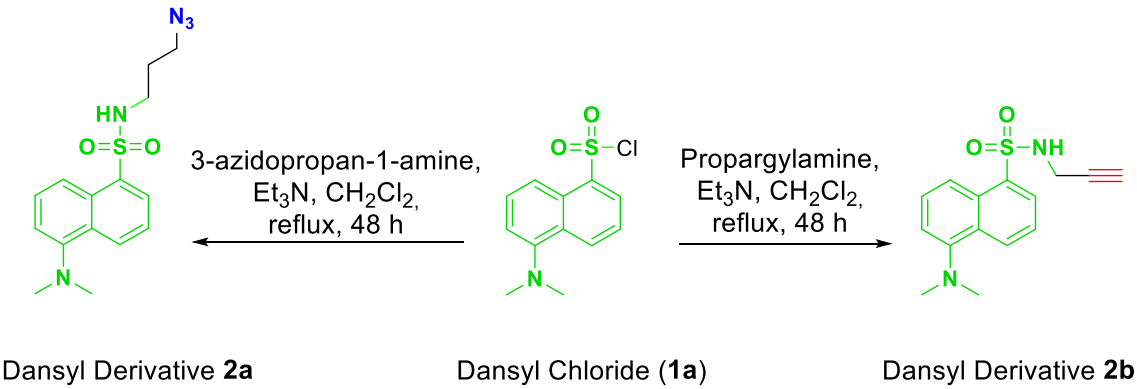

Scheme 2.3. Synthesis of two different dansyl derivatives.

Table 2.1. Reactions conditions for the derivatization of dansyl chloride (**1a**)

Entry	Amine	Base	Solvent	T (ºC)	t (h)	Product	Yield (%)
1	3-azidopropan-1-amine	Et_3N	CH_2Cl_2	r.t.	24	**2a**	[a]
2	3-azidopropan-1-amine	Et_3N	CH_2Cl_2	r.t	48	**2a**	[a}
3	3-azidopropan-1-amine	Et_3N	CH_2Cl_2	Reflux, 40	48	**2a**	94
4	Propargylamine	Et_3N	CH_2Cl_2	Reflux, 40	48	**2b**	89

[a] starting substrate was obtained

As can be seen in **Table 2.1**, when the reaction was initially conducted at room temperature to produce dansyl derivative **2a**, only starting substrate was detected (**Entry 1**). Subsequently, when reaction time was prolonged to 48 h, yet no promising results were obtained. Consequently, temperature was increased until solvent reflux. Fortunately, this heating allowed to acces the corresponding sulfonamide **2a** with excellent yield, 94% specifically. Same reactions conditions were employed for the synthesis of dansyl derivative **2b**, resulting again in the desired product with similar yield (89%).

As it has been commented before, in order to validate the proposed azide alkyne click reaction, the surfaces were submitted to CuAAC click reaction conditions with two different dansyl derivatives (**2a-b**) (**Scheme 2.4**), these fluorescent agents were

analyzed by means of a fluorescent microscope. As it can be seen in **Figure 2.7**, only the conjugation of dansyl derivative **2a** onto PLLA *via* pathway A showed an intense green fluorescence (**Figure 2.7C**), whereas fluorescent microscope revealed that the amount of dansyl derivative **2b** attached to the PLLA *via* pathway B was not enough to obtain a good fluorescence. Additionally, as it was expected, hydrolyzed PLLA did not show any type of fluorescence at the same power (20 W). Consequently, these results revealed that the pathway A reaction, which implies the alkyne group linked to the polymeric surface and the azido to the modified fluorophore (**2a**), is more effective to link drugs on PLLA. According to these results, indomethacin drug was proved to link to the surface *via* PA, with the azido moiety introduced on the drug.

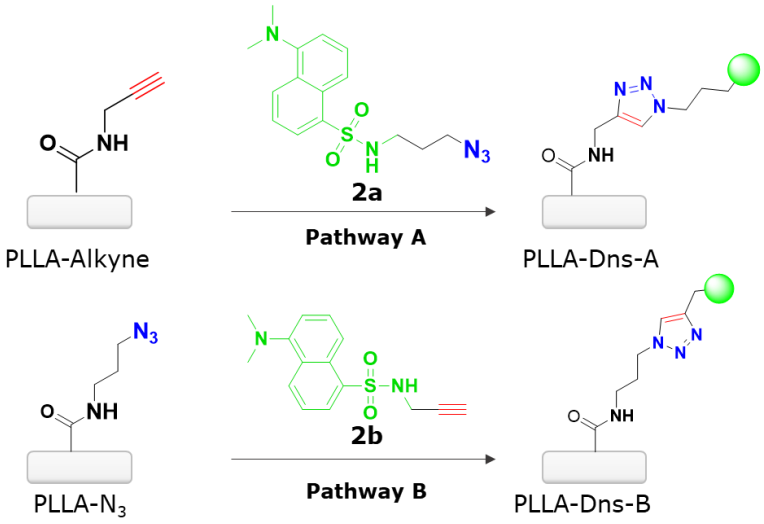

Scheme 2.4. A schematic representation of two ways to immobilize the fluorophore derivative.

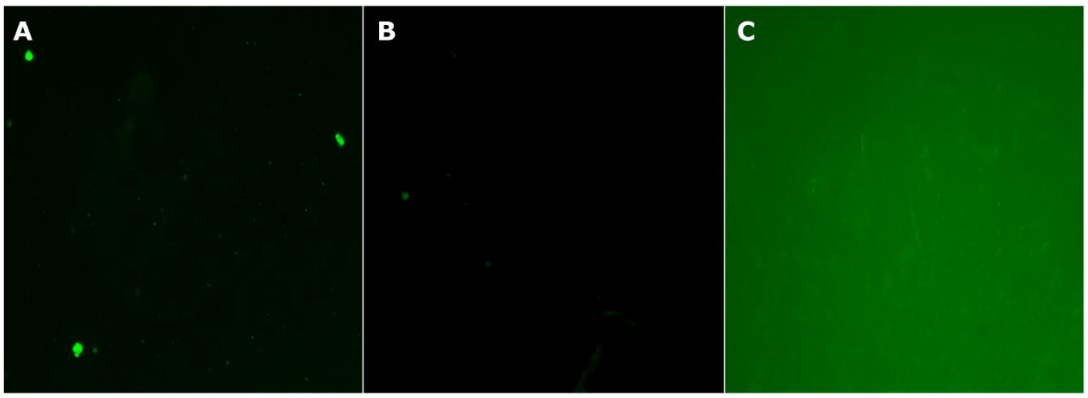

Figure 2.7. Representative fluorescence images of (A) PLLA-COOH, (B) conjugation of dansyl derivative **2b** onto PLLA film *via* PB (PLLA-Dns-B), and (C) conjugation of dansyl derivative **2a** onto PLLA film *via* PA (PLLA-Dns-A).

The analysis of surface chemical compositions of dansyl functionalized PLLA surfaces were carried out by XPS in order to asses the efficacy of the proposed approach. The

XPS spectra (**Figure 2.8**) corresponding to PLLA-COOH films showed two main contributions of C1s peak at 285 eV and O1s at 533 eV. After amidation and PA click reaction, an increase in the C1s peak could be clearly observed because of the attachment of more carbon containing molecules. Moreover, small peaks that corresponding to the contribution of nitrogen N1s, with a binding energy of 395 eV, and sulphur S2p, with a binding energy of 167 eV, were also observed in PLLA samples (PLLA-Dns-A), which anchored dansyl derivative **2a**. However, in PB click reaction with dansyl derivative **2b** onto PLLA appear neither nitrogen nor sulphur atoms. Once again, these findings corroborated the observations made through fluorescent microscopy, highlighting PA as the most effective method for immobilizing the fluorophore. To avoid hindering the coherency of this Doctoral Thesis, the proportional distribution of each element will be outlined in **Table 2.3**, along with data related to the bioconjugation of indomethacin derivative **3a**.

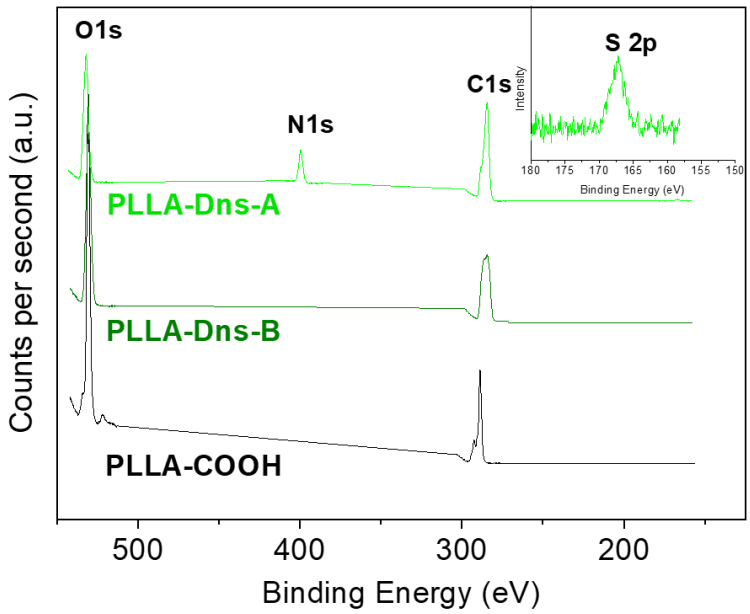

Figure 2.8. XPS spectra of CuAAC functionalized PLLA surfaces, including PLLA-COOH, PLLA-Dns-A and PLLA-Dns-B.

After confirming the effectiveness of the proposed methodology, the same process was applied using the drug indomethacin. Newly, prior structural modifications were necessary to introduce the required functional group essential for CuAAC reaction. In this case, in order to introduce the azido moiety an amidation reaction with 3-azidopropan-1-amine of carboxylic acid of indomethacin was proposed (**Scheme 2.5**). **Table 2.2** shows the results of the experiments carried out to optimize the amidation reaction.

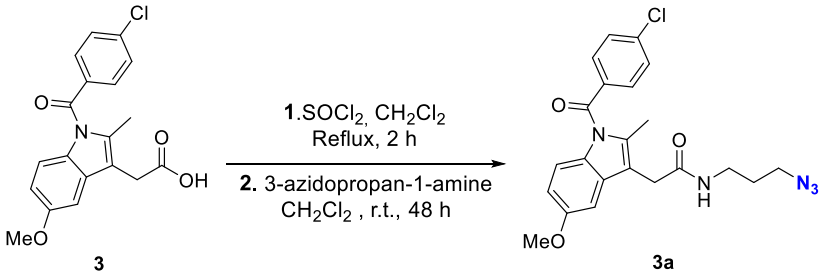

Scheme 2.5. Synthesis of indomethacin derivative **3a**.

Table 2.2. Reaction condition used for the amidation reaction of indomethacin.

Entry	3-azide-1-propyl-amine (eq.)	Base (eq.)	Active agent (eq.)	Solvent	T (°)	t (h)	Yield (%)
1	(1.5)	Et_3N (1.5)	EDC·HCl (1.5) /HOBT (1.4)	CH_2Cl_2	Reflux	48	-[a]
2	(1.5)	Et_3N (1.5)	EDC·HCl (1.5) /NHS (1.4)	CH_2Cl_2	Reflux	48	-[a]
3	2	-	DCC (2.1)	CH_2Cl_2	Reflux	48	-[a]
4	4	-	DCC (4.1)	CH_2Cl_2	Reflux	48	-[a]
5	5	-	DCC (5.1)	CH_2Cl_2	Reflux	48	-[a]
6	2	-	DCC (2.1)	Toluene	Reflux	48	-[b]
7	4	-	DCC (4.1)	Toluene	Reflux	48	-[b]
8	4	-	DCC (4.1)	Toluene	80	48	Traces[c]
9	1.5	DIPEA (1.5)	EDC·HCl (1.5) /NHS (1.4)	Toluene	80	48	Traces[c]
10	4	-	DCC (4.1)	DMF	85	48	-[b]
11	4	Et_3N (4)	DCC (4.1)	DMF	85	48	-[b]
12	1	-	DCC (1) /DMAP (0.05)	CH_2Cl_2	r.t	24	Traces[c]
13	1	-	$SOCl_2$(1.1)	CH_2Cl_2	Reflux/r.t	2+72	71

[a]starting substrate was recovered [b] complex mixtures of compounds due to decomposition were observed [c] only traces of **3a** were observed by ^{1}H-NMR along with the starting substrate

As can be seen in **Table 2.2**, no carbodiimide, neither EDC·HCl, nor DCC, was effective in the amidation reaction although different reaction conditions were tested (**Entry 1-12**). Fortunately, when more drastic reaction conditions were employed (**Entry 13**) the desired derivative was obtained with very good yields (71%) and analyzed by NMR (**Figure 2.9**).

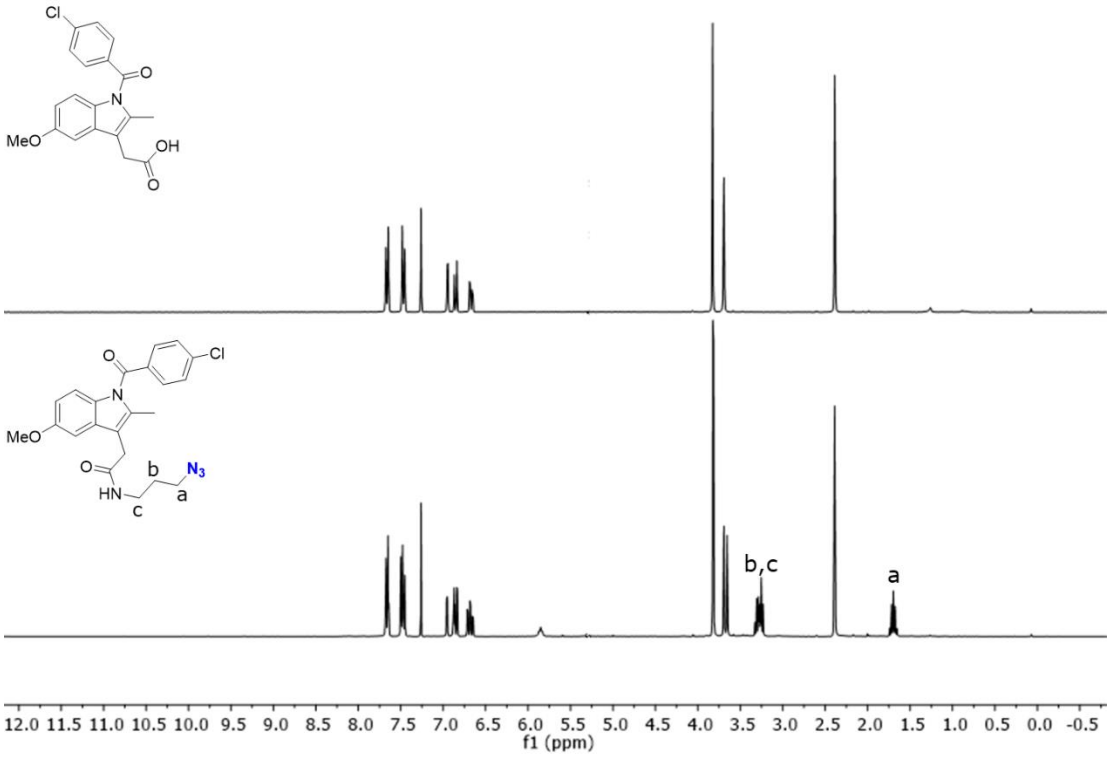

Figure 2.9. ^{1}H-NMR spectra of indomethacin and its derivative **3a**.

By means of NMR, the conversion of indomethacin into *N*-(3-azidopropyl)-2-(1-(4-chlorobenzoyl)-5-methoxy-2-methyl-1H-indol-3-yl)acetamide was observed, concluding that the reaction was carried out successfully. As can be seen in **Figure 2.9**, two new signals at 1.70 and 3.23 ppm can be observed corresponding to the protons of the introduced 3-azidopropan-1-amine. These signals along with the amine signal at 5.84 ppm corroborated that the obtained product was the desired indomethacin derivative **3a.**

Once indomethacin derivative **3a** was synthesized the immobilization onto PLLA surfaces was performed followig pathway A (**Scheme 2.6**).

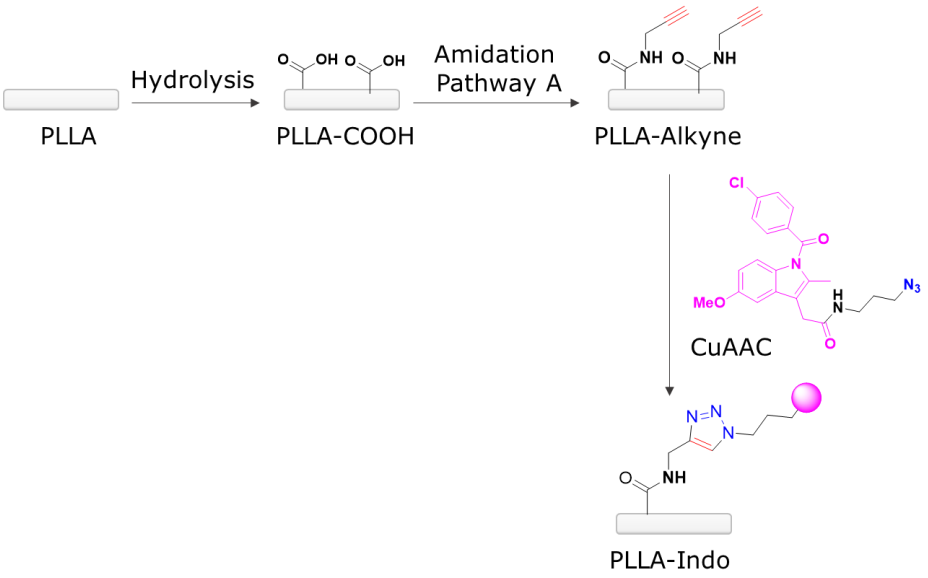

Scheme 2.6. Indomethacin derivative **3a** bioconjugation on PLLA surface.

Again, XPS was employed to determine the elemental composition of modified surface. In fact, in this case, the appearance of a peak with a binding energy of 200 eV corroborated the presence of chloride element (**Figure 2.10**). As consequence, we could corroborate that the immobilization of indomethacin derivative **3a** through the click reaction had been successful.

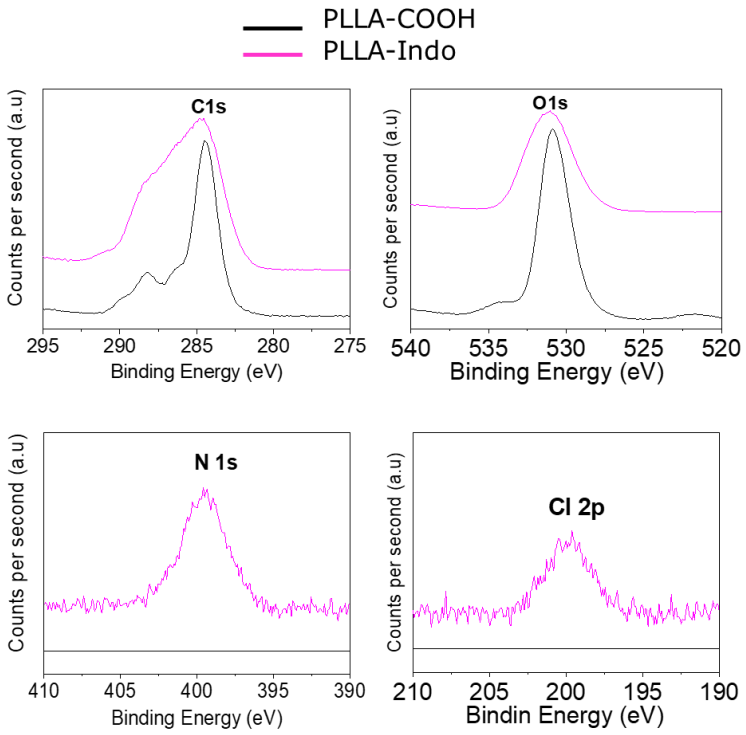

Figure 2.10. XPS spectra of PLLA-COOH and PLLA-Indo.

The surface composition of functionalized PLLA samples is summarized in **Table 2.3**. According to the chemical structure of PLLA, the hydrolyzed films show that the surface is mostly made by carbon (38.7%) and oxygen (46.4%). This result suggests that the amount of oxide functional groups on the surface is highly significant. As shown in the table, before click reactions PLLA films had neither nitrogen, nor sulphur or chloride elements, as it can be expected. After the immobilization of dansyl derivatives, only in pathway A (PA) appeared nitrogen (1,2,3-triazole) and sulphur (S=O) elements. Nevertheless, in reaction pathway B (PB), appeared carbon and oxygen in a higher amount comparing to nitrogen, which suggests again that immobilization of dansyl derivative **2b** is not the most appropriate for this surface. As it is previously commented, the indomethacin drug was modified to link to the surface *via* PA. The content of these elements shows a success of the copper (I) catalyzed azide alkyne click reaction when the azido group is attached to the drug. In all samples, a content of silicon is shown which is caused by the contamination of a glass.

Table 2.3. The atomic weight percentage of hydrolyzed and functionalized PLLA samples.

	Composition (%)					
Sample type	**C**	**O**	**N**	**S**	**Cl**	**Si**
PLLA-COOH	38.7	46.4	-	-	-	14.9
PLLA-Dns-A	61.2	25.7	8.8	0.6	-	1.7
PLLA-Dns-B	62.5	37.4	0.06	-	-	-
PLLA-Indo	59.4	36.6	2.8	-	0.3	0.6

Finally, through contact angle measurements the surface modifications were also followed by analizing hydrophilicity changes induced in each step (**Figure 2.11**). As could be observed, the static water contact angle of untreated PLLA was 111.1±7.2°, which is highly hydrophobic and difficult for further surface treatment due to a lack of polar functional groups on the PLLA surface. The value of the contact angle decreased significantly to 79.4±4.2° after the hydrolysis process as a result of the presence of polar groups (-COOH). Subsequent to the amidation reaction with propargylamine, the contact angle decreased again (56.8±10.7°). Nevertheless, the amidation with 3-azidopropan-1-amine did not change drastically the contact angle (80.5±8.1°). Although the polarity of the attached functional groups diminished, the significantly important roughening of the surface could explain the decline in the contact angle value in case of the propargylation [92]. The covalent immobilization of both dansyl derivative **2a** and anti-inflammatory indomethacin enhanced contact angle (84.5±4.1° and 86.4±4.7°, respectively). This result could be connected to the increase in hydrophobicity due to the presence of 1,2,3-triazole ring generated

through the click reaction and the aromatic rings presented in both immobilized substances [93]. In contrast, the covalent immobilization of dansyl derivative **2b** did not change too much comparing to the propargylation process (81.4±6.1°). These results suggested, again, successful modification of the polymer surfaces using pathway A, which is supported by the difference between the morphology of untreated and modified PLLA surfaces.

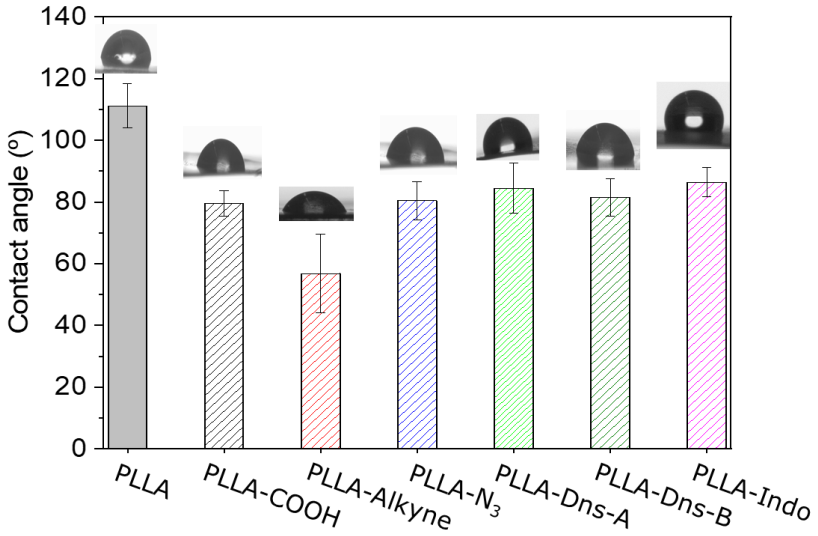

Figure 2.11. Water contact angles of untreated and modified PLLA.

Overall, these findings concluded that copper (I) catalyzed azido-alkyne click reaction is an effective approach for immobilizing biologically active drugs.

In order to demonstrate the efficacy of the obtained surfaces, anti-inflammatory analyses were conducted. To achieve this, PLLA-Indo surfaces were immersed in a biological medium with human monocytic cells THP-1 and lipopoyisaccharide (LPS), known to the release of interleukin 6 (IL-6), an inflammatory cytokine. The pro-inflammatory marker IL-6 was analyzed by ELISA at different time intervals on PLLA-Indo surfaces. As seen in **Figure 2.12**, these assays demonstrated that the immobilization of indomethacin derivative **3a** resulted in a reduction in the synthesis of IL-6 pro-inflammatory marker triggered by LPS, thereby mitigating the inflammation even after 96 h.

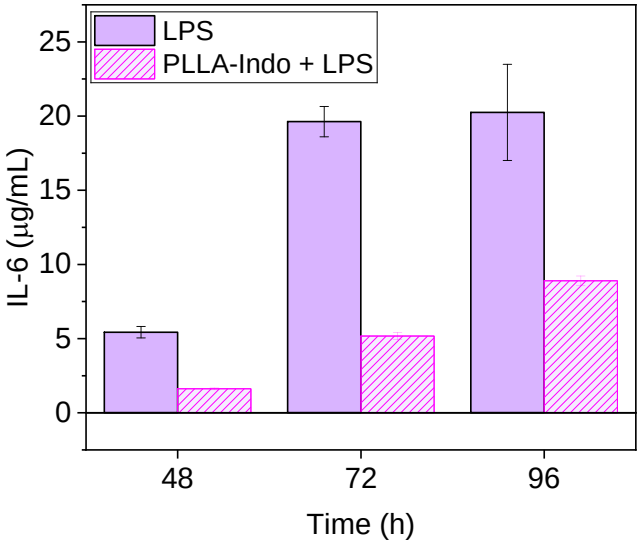

Figure 2.12. Anti-inflammatory response of PLLA-Indo *in vitro*.

As mentioned previously, the use of copper can exhibit cytotoxic effects on cells, thus impeding good biocompatibility and biointegration of the biomaterial. However, it is important to clarify that thorough washes of the surfaces were conducted with water and ethanol. Nevertheless, traces of copper were indeed observed in the experiments conducted *via* XPS. Hence, cytotoxic assays, using HEK293 cells, and inflammatory response of these materials were carried out. THP-1 human monocytic cells were differentiated into a macrophage phenotype and cultured on PLLA and PLLA-Indo. The levels of pro-inflammatory marker IL-6 were examined at 0, 48, 72 and 96 h. Both samples (Pristine PLLA and PLLA-Indo) exhibited non inflammatory production (**Figure 2.13**).

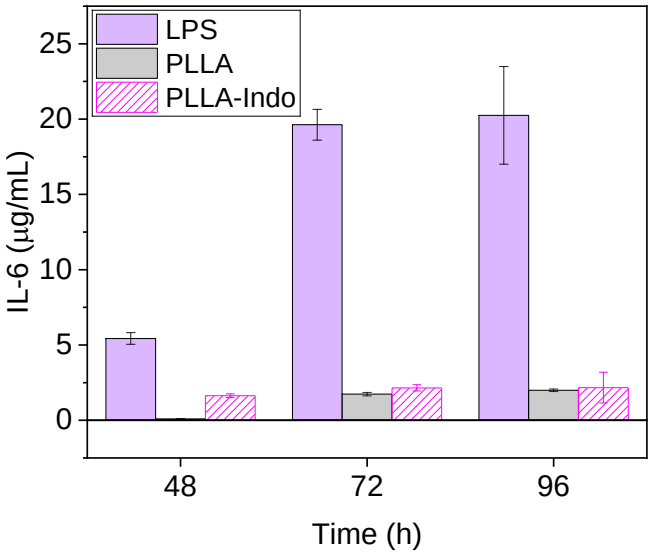

Figure 2.13. Inflammatory Activity of pristine PLLA and PLLA-Indo assessed *in vitro*. Error bars represent standard deviations from three independent experiments.

As shown in **Figure 2.14**, the cellular viability, assessed using the MTS assay, after 48 h of growing in 96-weel culture wells, pristine PLLA and PLLA-Indo was similar. No statistically significant differences were determined between the cells cultured with pristine PLLA and PLLA-Indo samples and those without control cells. Overall, both pristine PLLA and PLLA-Indo have demonstrated non-cytotoxic effect with high cell viability content after 48 h. These results suggested that the obtained PLLA-Indo surfaces did not pose any harm to cells, rendering these materials attractive for applications in the biomedical field.

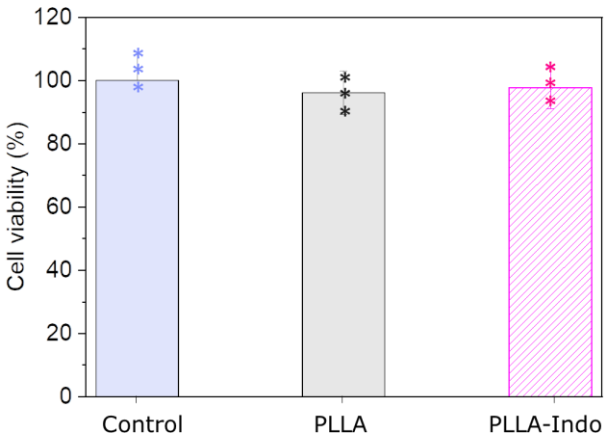

Figure 2.14. Assessment of cytotoxicity induced by pristine PLLA and indomethacine derived functionalized PLLA samples in HEK293 Cells. HEK293 cells (40 × 10^3) were seeded on PLLAs

in a 96-well culture plate and maintained for 48 h in complete DMEM. Cellular viability was evaluated using the MTS assay as described in Materials and Methods. Results are expressed as a percentage of viability relative to untreated cells (Control). Statistical analysis was performed by the Student's t-test. Incubation with the pristine PLLA and PLLA-Indo surfaces did not produce statistically significant differences.

2.3.2. Copper (I) azide alkyne click dual approach

After the covalent immobilization of indomethacin derivative **3a**, we decided to proceed with a second conjugation to verify if this strategy is capable of immobilizing different compounds on the same PLLA surface. For this purpose, the dansyl derivative **2a** was again used (**Scheme 2.7**).

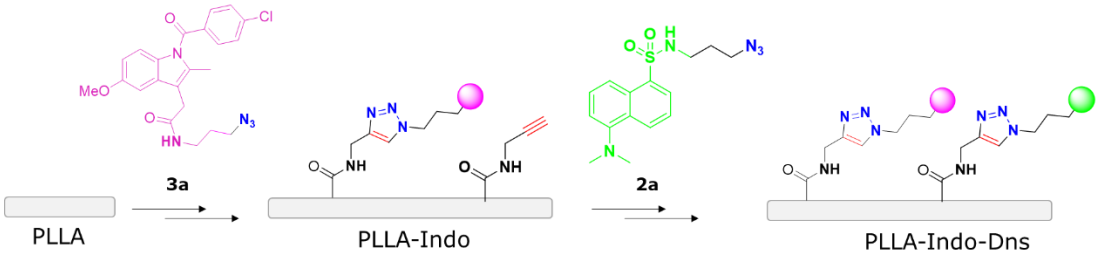

Scheme 2.7. Dual immobilization *via* copper catalyzed azide-alkyne click reaction onto PLLA surfaces.

The surface obtained after the second immobilization of the dansyl derivative **2a** (PLLA-Indo-Dns) was analyzed by XPS, confocal fluorescence, and water contact angle. Following the elemental surface analysis, characteristic peaks of both compounds were observed. As can be seen in **Figure 2.15**, the nitrogen (6.9%) and chlorine (0.44%) elements corresponding to the indomethacin derivative **3a** were detected, and on the other hand, the sulfur element (1.7%) was perceived at 187 eV respectively.

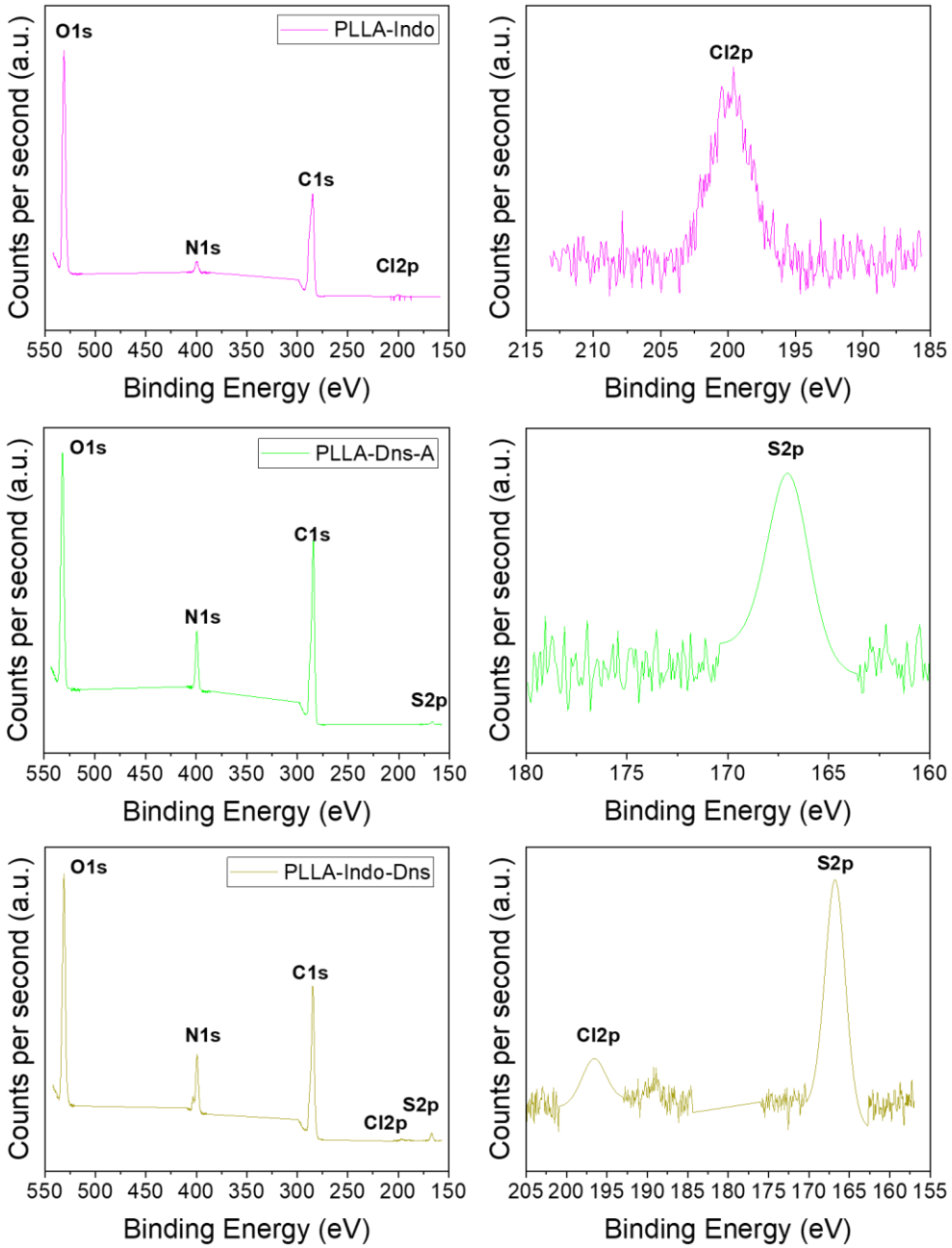

Figure 2.15. Total XPS spectra of PLLA-Indo, PLLA-Dns and PLLA-indo-Dns surfaces.

On the other hand, when PLLA-Indo-Dns surface was subjected to same fluorescence excitacion as previous section, as can be seen in **Figure 2.16**, a green fluorescence emission was perceived, addressing the immobilization of dansyl derivative **2a**.

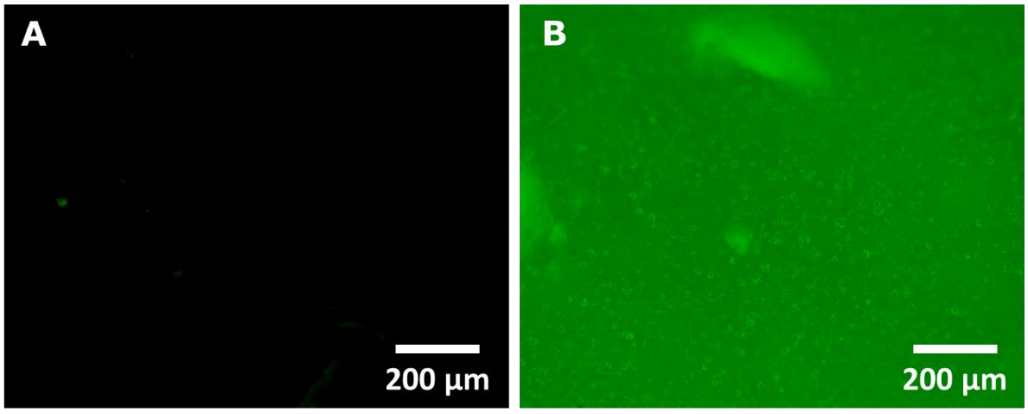

Figure 16. Confocal fluorescence microscopy image of (A) PLLA-Indo and (B) PLLA-Indo-Dns.

In this way, minor changes in wettability were observed on the PLLA-Indo-Dns (79.7±10.4°) surface compared to surfaces immobilized independiently with indomethacin and dansyl derivatives. Notably, both the indomethacin derivative **3a** and dansyl derivative **2a** possess aromatic rings in their structures, and their respective water contact angle values were very similar. Hence, an analogous water contact angle value was anticipated for the PLLA-Indo-Dns surface (**Figure 2.17**).

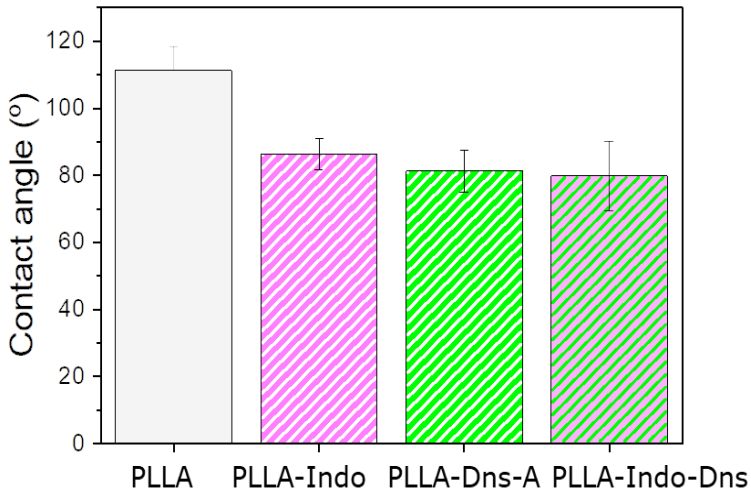

Figure 2.17. Contact angle measurements of PLLA, PLLA-Indo, PLLA-Dns and PLLA-Indo-Dns.

Overall, these results once again demonstrated the effectiveness of the copper-catalyzed azide-alkyne reaction. Not only is it capable of immobilizing one biologically active compound, but also, by conducting a second stage, it can enable the conjugation of another agent. For this purpose, it is essential for the surface to

contain alkyne groups, in this case, available for subsequent modification. This methodology presents an opportunity to bioconjugate sequentially various biological compounds through a unified technique.

2.3.3. Copper free azide-yne click approach employing activated acetylene

As mentioned in the *Chapter 1*, the copper used in CuAAC reeactions have demonstrated cytotoxic effect on cells, inducing hypoxia and leding to their death. Consequently, in recent years, innovative methodologies have been developed to mitigate the use of copper and, consequently, its cytotoxic effects. Among these, the use of activated alkyne with electron attractive groups, such as propiolic acid, has revolutionized materials science. In this Section, the use of propiolic acid is proposed in order to immobilize various drugs.

Again, the first step of the PLLA surface functionalization was the hydrolysis reaction. Indeed, hydrolysis reaction of PLLA was carried out in basic media, employing NaOH 1M during 30 min at 50 °C. As a result, carboxylic acids were generated on the surface of PLLA and, subsequently, were amidated using ethylendiamine (ETDA), obtaining an amide with NH_2 as ending group (PLLA-NH_2, **Scheme 2.8**). Then, further functionalization of the terminal amine was performed in order to incorporate the alkyne group on PLLA surface, which is essential for the conjugation of the fluorophore compound. This is, in fact, the main difference between this work and the one described in the previous section. Indeed, the first amidation of PLLA with a diamine, allowed carrying out a second amidation with propiolic acid, thus achieving an electron-deficient alkyne, which could be used to accomplish the 1,3-dipolar cycloaddition click reaction with the azide moiety of the fluorophore compound in the absence of catalyst. Finally, previously synthesized dansyl derivative was immobilized onto PLLA by copper free azide alkyne cycloaddition reaction (**Scheme 2.8**).

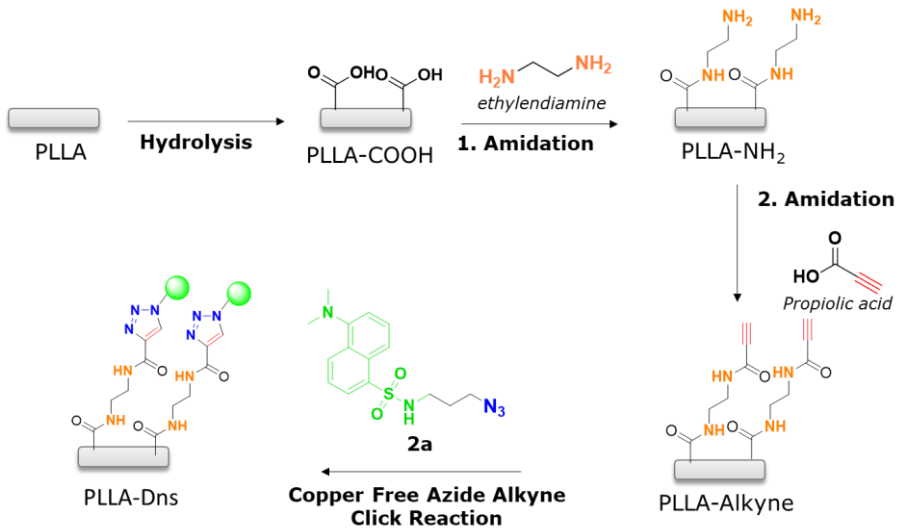

Scheme 2.8. Several steps of PLLA modification and conjugation of dansyl derivative **2a**.

The ATR-FTIR spectra of pristine PLLA, hydrolyzed PLLA (PLLA-COOH), both amidated PLLA (PLLA-NH_2 and PLLA-Alkyne) and clicked PLLA (PLLA-Dns) are shown in **Figure 2.18**. After 30 min of being submerged on NaOH solution, PLLA-COOH samples presented a band at 3250 cm^{-1}, corresponding to the stretching vibrations of O-H bonds, as well as the peak at 2900 cm^{-1} related to stretching $C_{sp}{}^3$-H bond slightly increased. These changes in ATR-FTIR spectrum evidenced the success of hydrolysis reaction on PLLA surface. After further grafting with ethylendiamine (PLLA-NH_2), the intensity of the band around 3250-3300 cm^{-1} enhanced due to the presence of NH and NH_2 on the surface, which indicated that amidation reaction was carried out successfully. The incorporation of alkyne group through a second amidation reaction with propiolic acid was validated by observing distintive stretching bands at 2090 cm^{-1} and 3350 cm^{-1} in PLLA-alkyne samples. These bands corresponds to the stretching vibration of C_{sp}-C_{sp} and C_{sp}-H bonds, respectively. Additionally, the presence of a peak at 1700 cm^{-1} corresponding to the stretching of C=O was slightly shifted to 1650 cm^{-1}. This signal aligns with the common appearance of C=O in amides, providing strong evidence that the second amidation reaction occurred successfully. Finally, after dansyl derivative **2a** conjugation *via* copper-free azide-yne click reaction (PLLA-Dns), the C_{sp}-C_{sp} stretching signal disappeared, concluding that dansyl derivative was effectively immobilized onto PLLA.

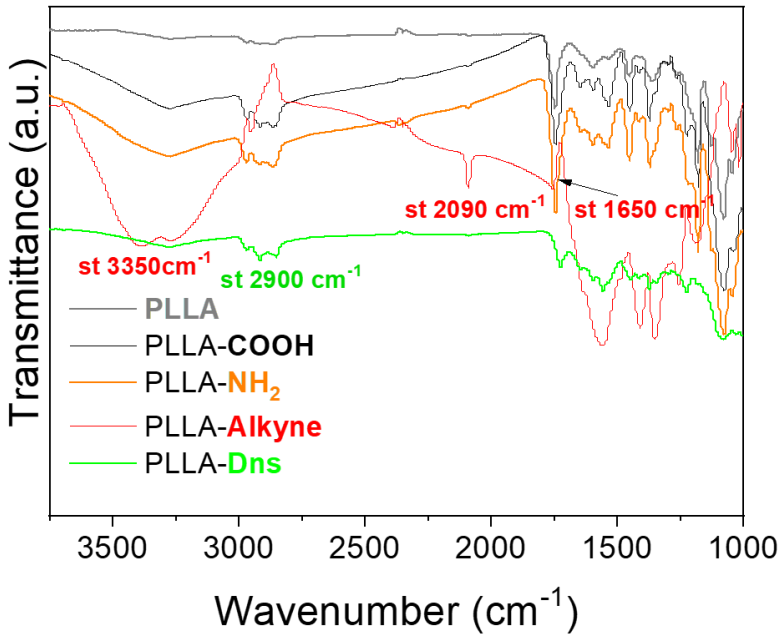

Figure 2.18. ATR-FTIR spectra of pristine PLLA and functionalized PLLA samples.

Chemical compositions of functionalized surfaces were measured by XPS and the results are resumed in **Figure 2.19** and **Table 2.4**. As expected, PLLA-COOH only exhibited two major peaks at 284 eV and 535 eV attributing to C1s and O1s, respectively. In addition, the element composition of C and O were 69.9% and 29.8%, respectively. Meanwhile, high resolution spectra of C1s showed three peaks corresponding to C-C/C-H (284.6 eV), C-O (286.3 eV) and C=O (288.8 eV) bonds as it is an ester based polymer and also agreed with literature [94–96]. After amidation with ethylendiamine, a new peak at 400 eV attributing to N1s appeared in the spectrum of PLLA-NH_2, confirming the successful amidation of hydrolyzed PLLA. Additionally, high-resolution carbon spectra also corroborated the introduction of nitrogen due to the enhanced peak of C-O/C-N contribution at 285.8 eV. The content of C, O and N elements on PLLA-NH_2 was 63.1%, 31.5% and 1.8%, respectively. Following the second amidation process employing propiolic acid (PLLA-Alkyne), similar C, O and N content values were obtained when compared to PLLA-NH_2, 62.0 %, 26.0% and 3.2%, respectively. However, notable changes were detected in the nitrogen high-resolution spectra of PLLA-NH_2 and PLLA-Alkyne. Indeed, the contributions observed at 398.9 eV, 399.7 eV and 400.6 eV corresponding to the emergence of NH_2, N-C=O and C-NH, respectively on PLLA-NH_2 surfaces disappeared, while NH-C=O contribution increased on PLLA-Alkyne surfaces. These findings confirmed the introduction of propiolic acid, a terminal alkyne ester crucial for facilitating not only catalyst free azide-yne, but also amino-yne and thiol-yne click

reactions, which will be further discussed. After further functionalization with dansyl derivative, the presence of new peak around 169 eV was observed, corresponding to S2p element. Additionally, high resolution spectra of sulfur exhibited two contributions at 164 eV and 168 eV, corresponding to C-NH/S-NH and S=O species, which agrees with literature [97,98]. Furthermore, high resolution spectra of nitrogen also confirmed the presence of sulfur at 402 eV, by exposing N-S binding [99]. These results confirmed again the immobilization of dansyl derivative onto PLLA surface through a copper free click methodology.

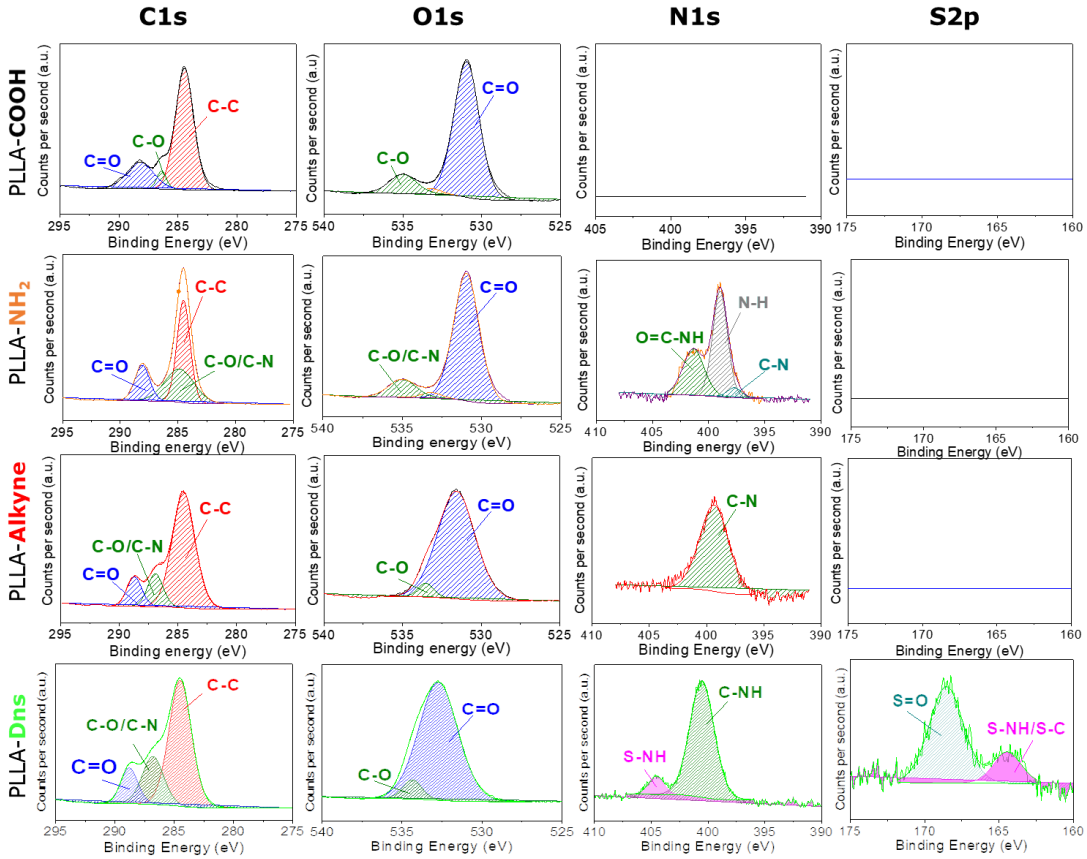

Figure 2.19. Deconvolution XPS spectra of PLLA-COOH, PLLA-NH_2, PLLA-Alkyne and PLLA-Dns.

Table 2.4. C, O, N and S content of functionalized PLLA surfaces.

Sample	C (%)	O (%)	N (%)	S (%)
PLLA	69.9	29.8	-	-
PLLA-COOH	71.6	27.5	-	-
PLLA-NH_2	63.1	31.5	1.8	-
PLLA-Alkyne	61.0	26.5	3.2	-
PLLA-Dns	67.2	26.0	3.6	0.5

The morphology and wettability of the surface were determined by SEM and water contact angle measurements respectively. As can be seen in **Figure 2.20**, the hydrolysis and subsequent functionalization reactions resulted in notable changes in the hydrophobicity of the surfaces which is reflected in the changes in the water contact angles. As expected, pristine PLLA presented high static water contact angle value (111.1±7.2°) due to its lack of polar functional groups on the top of the surface, which implies that the surface is hydrophobic. After hydrolysis, the water contact angle decreased to 72.4±13.5°, which indicated that carboxylic acid and hydroxyl groups are successfully formed on the surface. The amidation reaction with ETDA supposed only a slight change in the contact angle (54.2±8.7°). In fact, similar polarities of involved moieties, such as amine or hydroxyl group, imply similar interactions with water. Nevertheless, the second amidation, once the alkyne group was incorporated, resulted in a drastic decrease in the water contact angle (18.7±4.6°). Although the polarity of the attached functional groups diminished, the significantly important roughening of the surface could explain the decline in the contact angle value in this case [100,101]. Moreover, after the click reaction, once the fluorophore compound was conjugated onto PLLA, the water contact angle increased again to 100±8.7°, this result could be connected to the increase in hydrophobicity due to the presence of aromatic ring of dansyl derivative, specially, the naftyl group.

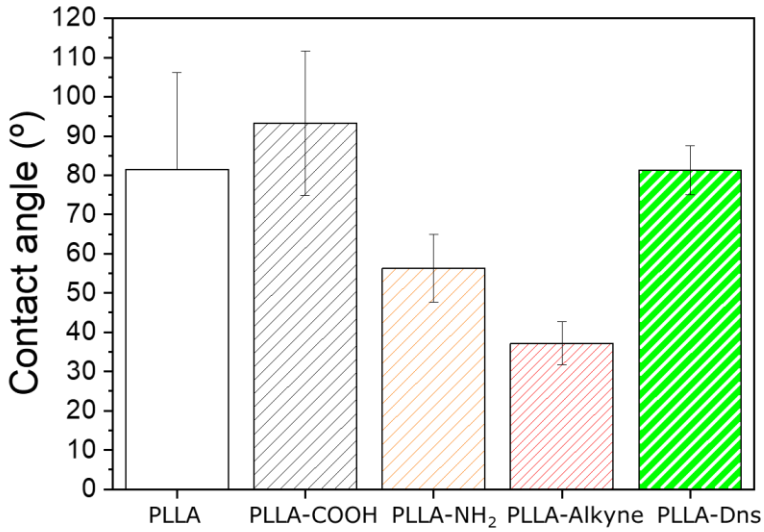

Figure 2.20. Contact angle values of functionalized PLLA surfaces.

SEM images indicated the surface morphologies of different PLLA samples, as can be seen in **Figure 2.21**. For pristine PLLA, the surface was smooth with no obvious

defect. Nevertheless, after hydrolysis, PLLA-COOH sample showed some clear scratches, even flaking, which can be related to the degradation of the surface on the first step of functionalization. After first amidation, the morphology continued changing, becoming more heterogeneous with round areas. Once the alkyne was incorporated, the surface roughness increased, which is closely related with the above mentioned water contact results, since a rougher surface with a larger area is more hydrophilic [100,101].

Pristine PLLA surfaces were quite flat and smooth, but some breaks appeared due to the pressing process suffered in films fabrication. After hydrolysis, the surface became rougher and slightly changes were exhibited after amidation with ethylendiamine. Once amidated with propiolic acid, new protrusions appeared on the surface

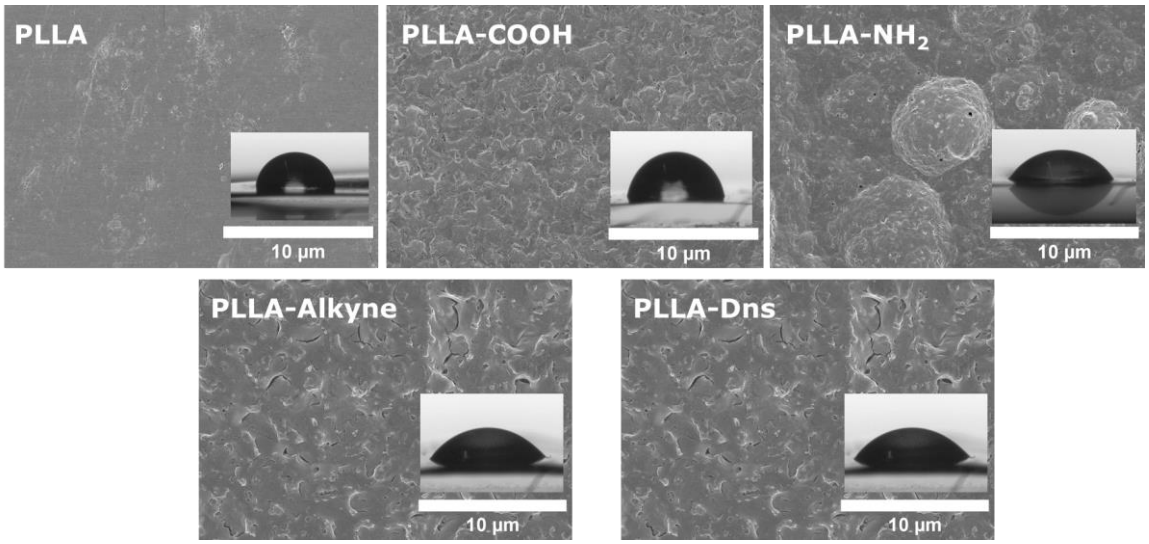

Figure 2.21. SEM images of functionalized PLLA A) pristine PLLA, B) PLLA-COOH, C) PLLA-NH_2, D) PLLA-Alkyne and E) PLLA-Dns were analyzed in 10 µm.

Finally, verification of dansyl derivative immobilization *via* copper-free azide-alkyne click reactions was conducted using both a fluorescent microscope and fluorescence spectroscopy, focusing in the characteristic emission peak at 500 nm of the fluorophore. Pristine PLLA and dansyl derivative clicked PLLA (PLLA-Dns) were compared in this study. As can be seen in **Figure 2.22A,** as expected**,** PLLA-Dns surface exhibited a fluorescence maximum peak at 495 nm, specifically attributed to the dansyl compound. Meanwhile, pristine PLLA did not present any maximum at the same emission wavelength. On the other hand, confocal microscopy analysis (**Figure 2.22B**) indicated that pristine PLLA presented no fluorescence emission across various wavelengths, even when excited at dansyl derivative's optimal excitation

point around 340 nm. However, PLLA-Dns displayed a green fluorescence, attributing this emission to the fluorescence region of the dansyl derivative **2a**. These results definitively confirmed the successful immobilization of the fluorophore compound onto PLLA surfaces.

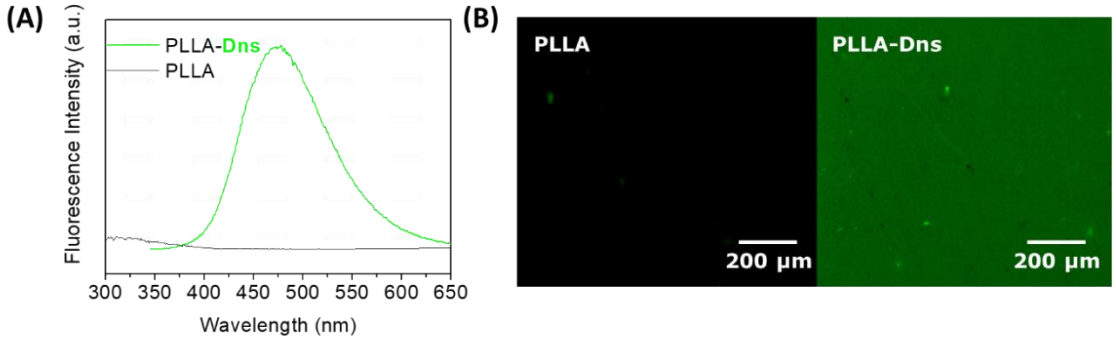

Figure 2.22. (A) Steady state fluorescence of PLLA and PLLA-Dns; (B) Fluoresce microscopy images of Pristine PLLA and PLLA-Dns.

2.3.4. Catalyst free amino-yne click aproach employing acetylenic activator

Due to the discovery of activated alkynes, similar to the azide-yne copper free click reaction, the amine-yne Michael-type reaction has garnered significant interes in recent years. This reaction enables the conjugation of complex structures, such as peptides or proteins, in a straightforward manner. This Section describes the use of this reactions for the covalent immobilization of tryptophan and amoxicillin. Both molecules contain tha amino-functional group required for the click reaction. While amoxicillin is widely recognized for its antibacterial effect, the use of tryptophan in antimicrobial peptides has increased at it has demonstrated an enhanced antimicrobial capacity. Furthermore, in this case, due to its fluorescent capability, it was employed as a fluorophore to validate the proposed methodology.

Before performing the bioconjugation of the amino-containing molecules, that is tryptophan and amoxicillin, it was necessary to accomplish some modifications to the PLLA surfaces. The incorporation of alkyne group was carried out followed the same procedure described in the previous Section. Once amidated with propiolic acid, PLLA-Alkyne surfaces were directly reacted with tryptophan *via* amino-yne click reaction. (**Scheme 2.9**).

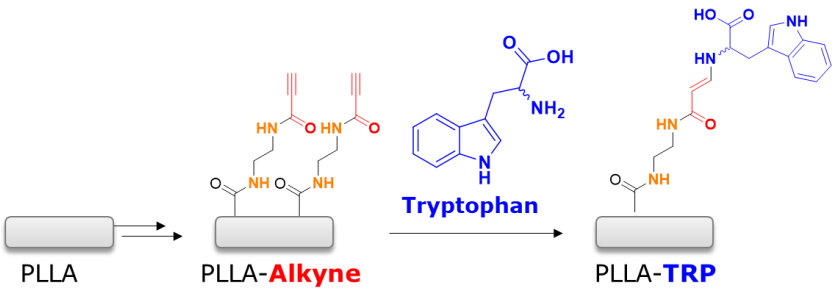

Scheme 2.9. Chemical PLLA surface modification steps for tryptophan bioconjugation.

After every functionalization step, surface chemical structure was determined by means of ATR-FTIR technique (**Figure 2.23**). The hydrolysis and amidation reactions results were previously discussed. In this case, after conjugation reaction with tryptophan, the signals corresponding to alkyne moiety (at 2100 cm^{-1} and 3300 cm^{-1}) disappeared on PLLA-TRP surfaces, corroborating that the amino-yne click reaction between tryptophan and functionalized PLLA was successfully carried out. Moreover, due to the presence of tryptophan at the top of the surface, the signals corresponding to O-H and N-H suffered a slight decrease. Thus, it confirms, again, that reaction took place successfully.

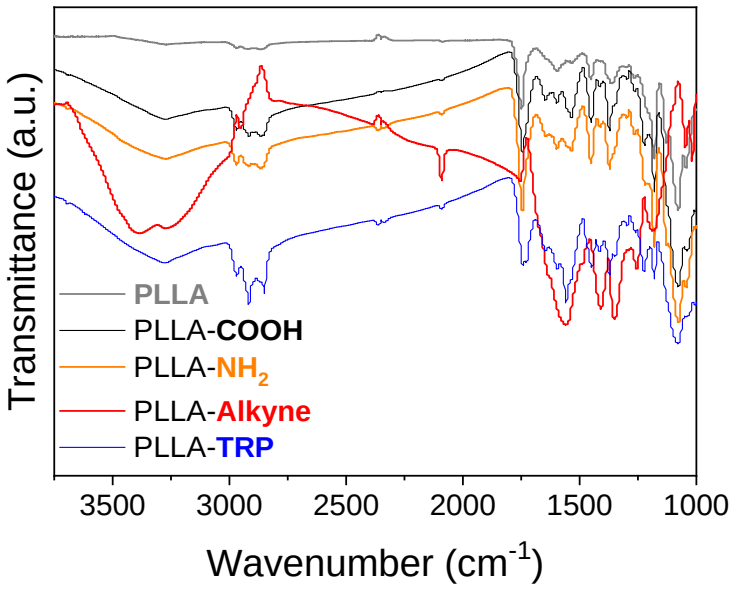

Figure 2.23. ATR-FTIR spectra of pristine PLLA and functionalized PLLA surfaces, including PLLA-TRP.

Many studies, including our previous works, confirmed that surface chemical modification can alter the morphology and wettability properties of a surface [62,102,103]. Therefore, SEM and contact angle techniques have been employed after every modification step in order to determine the topographical changes and water affinity of the surface (**Figure 2.24**). According to static water contact angle

values (WCA), after tryptophan immobilization, WCA value increased to 78.9±4.5°. The increment corroborated the presence of aromatic groups on the polymer surface. Therefore, this enhanced wettability change in WCA value indicated that tryptophan bioconjugation was successfully carried out.

On the other hand, SEM images indicated the surface morphologies of different PLLA samples, as can be seen in **Figure 2.24**. Regarding topographical properties, as commented before, hydrolysis process became the surface rougher, and amidation with ethylendiamine did not suppose major topographical changes. Upon the aminoacid immobilization, surface becomes smoother, although the presence of some cavities was observed. These particular surface variations indicated again that surface functionalization and tryptophan immobilization were actually achieved.

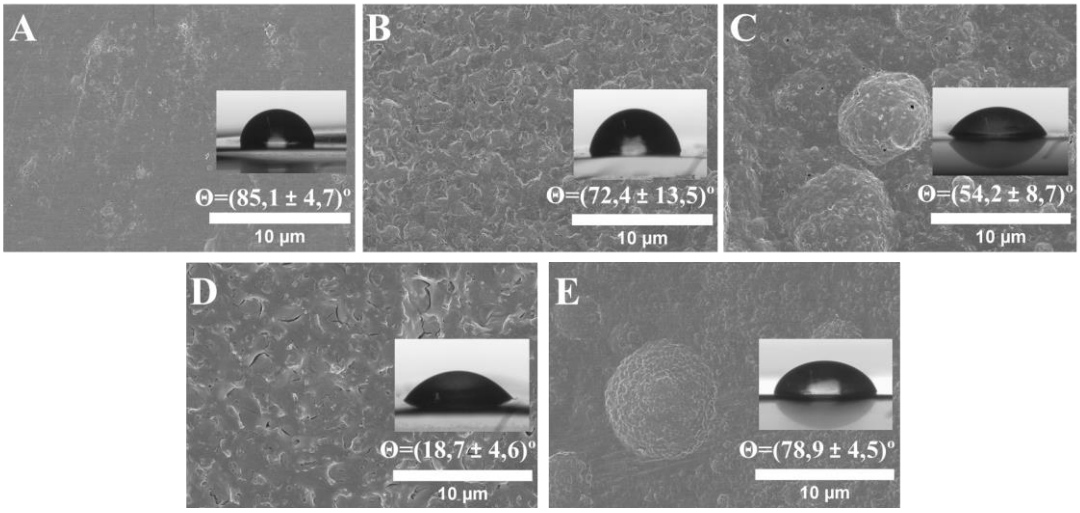

Figure 2.24. SEM images of functionalized PLLA A) pristine PLLA, B) PLLA-COOH, C) PLLA-NH_2, D) PLLA-Alkyne and E) PLLA-TRP were analyzed in 10 µm.

Finally, by means of confocal fluorescence and fluorescence spectroscopy the bioconjugation of tryptophan *via* amino-yne click reaction was corroborated (**Figure 2.25**). Both experiments demonstrated the successful immobilization of tryptophan when sample was irradiated under different wavelength. This fluorophore present an excitation peak at 225-280 nm and emission around 320-370 nm. When both pristine PLLA sample and PLLA-TRP sample were excited under the same energy value, only PLLA-TRP emitted a significant blue light, corresponding to the emission fluorescence range of tryptophan, indicating that the amino acid had been successfully immobilized. Moreover, fluorescence spectroscopy corroborated previous fluorescence emission. In this experiment, both samples pristine PLLA and PLLA-TRP were excited at the same wavelength, but only PLLA-TRP showed an emission peak around 310 nm, resulting from the tryptophan immobilization on surface.

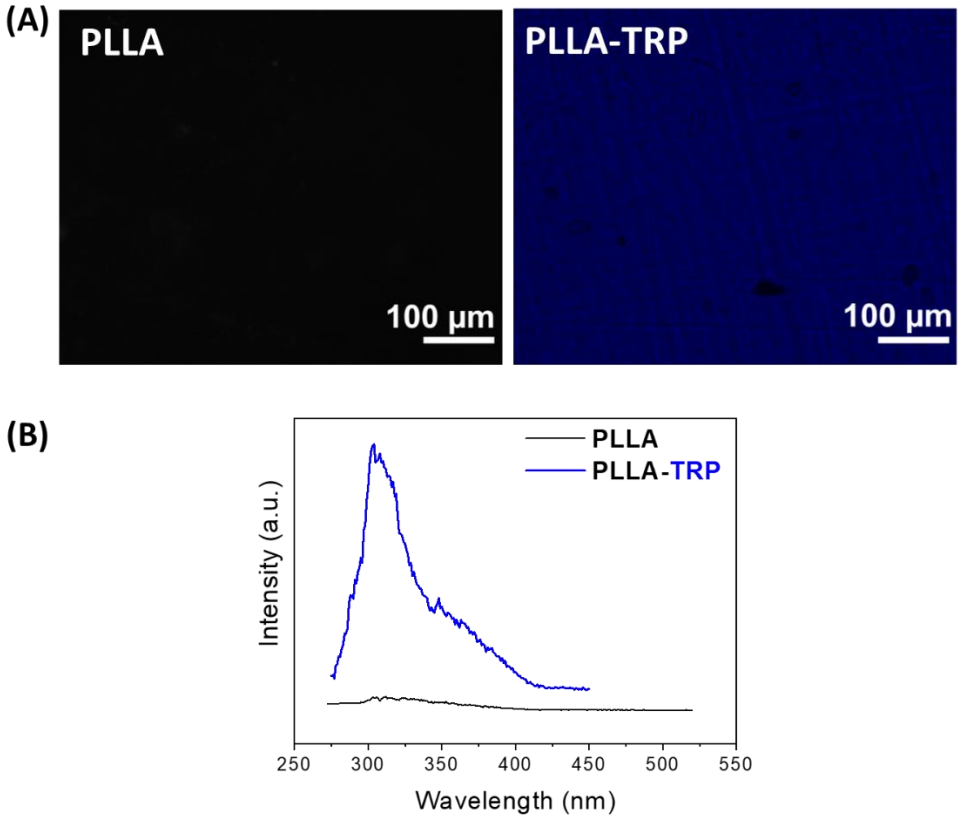

Figure 2.25. (A) Fluorescence microscopy images of Pristine PLLA and tryptophan functionalized PLLA, (B) fluorescence spectroscopy spectra of PLLA and PLLA-TRP.

The excellent results obtained in the immobilization of the fluorophore encouraged us to use the same methodology to bioconjugate the antibiotic amoxicillin on the polymeric surface (**Scheme 2.10***).*

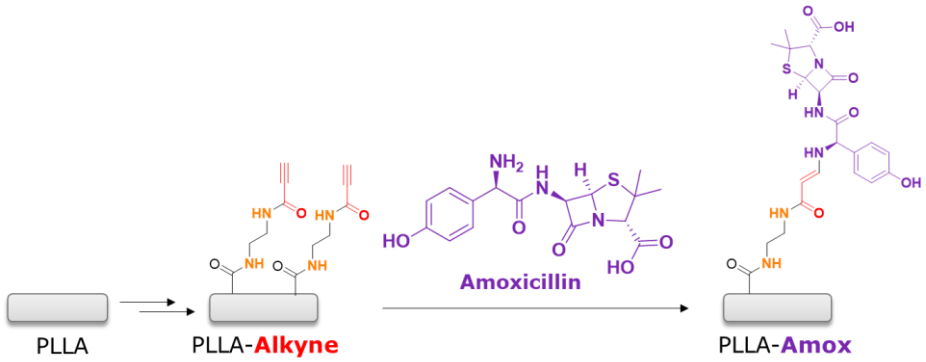

Scheme 2.10. Amoxicillin immobilization *via* amino-yne click onto PLLA surface.

As tryptophan immobilization, amoxicillin bioconjugation required previous surface functionalization including hydrolysis, amidation and propiolic acid chemical introduction. When incorporating amoxicillin to the surface wettability and topographical analysis were also studied (**Figure 2.26**).

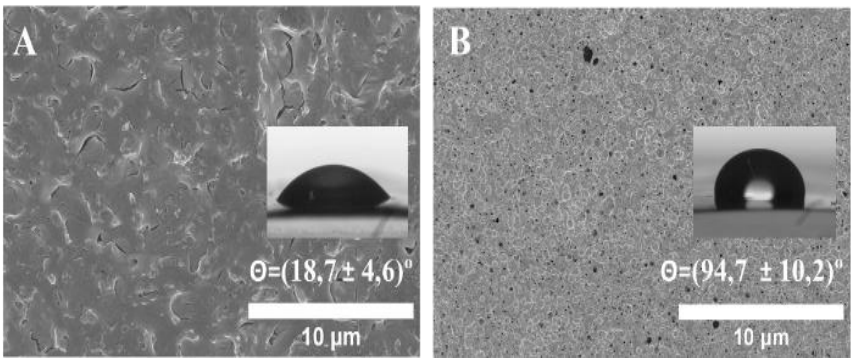

Figure 2.26. SEM images and WCA value of (A) PLLA-Alkyne and (B) PLLA-Amox.

Indeed, when comparing WCA value of propiolated (PLLA –Alkyne) and amoxicillin bioconjugated (PLLA-Amox) differences can be observed (**Figure 2.26**). WCA value significantly increased to 94.7±10.2° making the surface more hydrophophic than tryptophan-immobilized surface. In fact, amoxicillin presents an aminopenicillanic acid ring (APA), two fused rings, and phenyl functional group. These structural elements render the surface less susceptible to forming hydrogen bonds. Therefore, the hydrophobic interactions on amoxicillin are higher compared to tryptophan, which only poses the indole-aromatic group. On the other hand, granular roughness can be observed on amoxicillin functionalized PLLA surfaces, but making them smoother than previous functionalization. These changes in wettability and topography indicated that amoxicillin immobilization was carried out.

Further analysis were performed to corroborate the chemical bioconjugation of amoxicillin. Indeed, ATR-FTIR and fluorescence spectroscopy were employed. As commented before, the introduction of the alkyne onto PLLA surface was confirmed by twos characteristic signals observed at 2100 cm^{-1} and 3300 cm^{-1}. In fact, once amoxicillin was immobilized onto modified PLLA surface *via* amino-yne click reaction, these signals related to C_{sp}-C_{sp} and C_{sp}-H bonds disappeared, confirming that the alkyne reacted with the amino moiety of the antibiotic (**Figure 2.27**). These findings indicate that bioconjugation of amoxicillin *via* amino-yne click reaction was obtained.

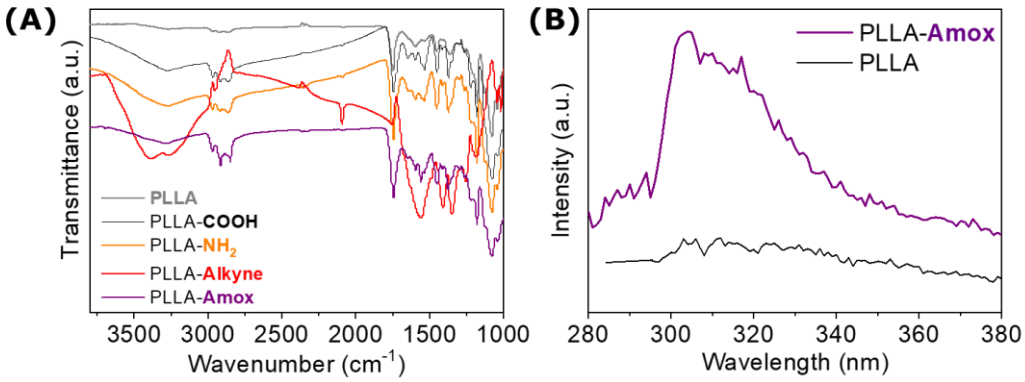

Figure 2.27. (A) ATR-FTIR analysis of pristine PLLA and functionalized PLLA, including PLLA-Amox; (B) fluorescence spectroscopy spectra of pristine PLLA and PLLA-Amox.

Moreover, fluorescence assays performed by spectroscopic methods confirmed again the immobilization of the antibiotic. In fact, non-functionalized PLLA and PLLA-Amox samples were excited in the same wavelength-range, but only emission spectra of PLLA-Amox exhibited a significant signal at 310 nm, indicating that amoxicillin has been successfully bioconjugated on PLLA surfaces (**Figure 2.27**).

2.3.6. Catalyst free thiol-yne click reaction with activated acetylene

Taking into account the good results obtained in the bioconjugation of nitrogen cointaining biomolecules, tryptophan and amoxicillin, through Michael-type reaction, we considered extending the methodology to the use of other nucleophiles, for example, thiol groups. In fact, as commented, thiol-yne reaction is a broad employed protocol in diverse fields. The purpose of this section is to bioconjugate the anticoagulant warfarin drug onto PLLA surfaces employing copper-free thiol-yne click reaction. For this purpose, the functional groups required for the click reaction were introduced onto PLLA and warfarin. Indeed, warfarin, one of the most recognized anticoagulant drug, inhibits vitamin K epoxide reductase enzyme and therefore decreases the synthesis of glutamic acid moiety, essential for blood clotting process.

As the introduction of alkyne moeity into PLLA surfaces was already obtained we consider that the most appropiate approach would be to introduce the essential thiol into warfarin. In this case, we considered that the optimal strategy to introduce the thiol group was through a reductive amination reaction, where the carbonyl group of the ketone would react with cysteamine. As in previous sections, the use of a fluorophore, dansyl again, has been proposed in order to validate and monitor the proposed methodology (**Scheme 2.11**). It has to be noted that this reaction presents

a particularity in comparison with already explained click reactions, the use of a photoinitiator, and consequently specific light, are required for the photoimmoblization of the agents.

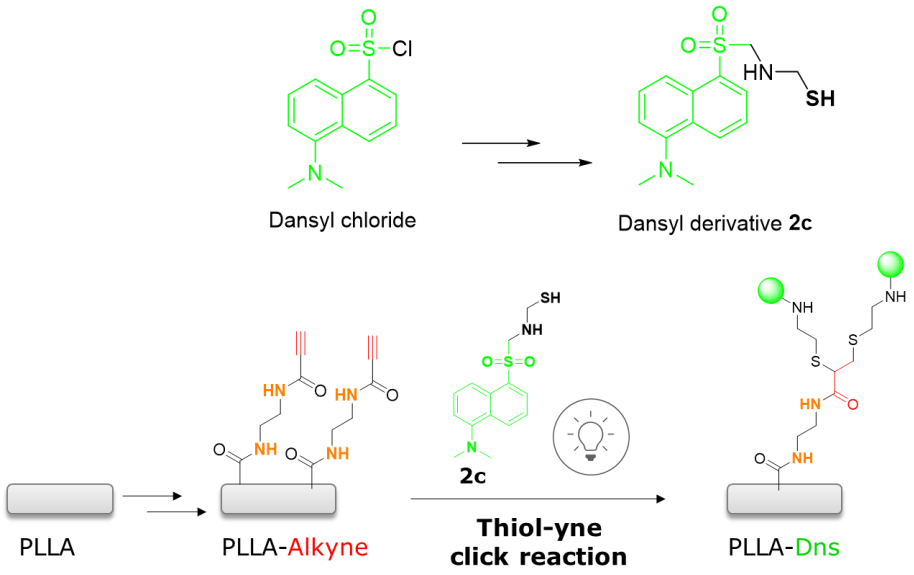

Scheme 2.11. Dansyl derivative **2c** photoimmobilization *via* thiol-yne click reaction.

The initial step of this section involved the chemical modifications of dansyl chloride and warfarin. It has to be noted that despite obtaining dansyl derivative **2c** product, it was not totally pure. Nevetheless, it was still used for surface conjugation.

For this thiol-yne click reaction Irgacure 651 photoinitiator was utilized to photoimmobilize the dansyl derivative **2c**. PLLA-alkyne samples carrying the dansyl derivative were exposed to irradiation for 1 and 4 h across a broad spectrum, ranging from 260 to 400 nm. Notably, the UV maximum absorption peak of the photoinitiator lies between 310-350 nm. Through confocal microscopy (**Figure 2.28**), the fluorescence emission from the PLLA-Dns surface was observed. Upon light excitation to both pristine PLLA and PLLA-Dns, only PLLA-Dns exhibited a green emission, corresponding to the dansyl region. These findings confirm the completion of the immobilization of dansyl derivative **2c** *via* the thiol-yne click reaction.

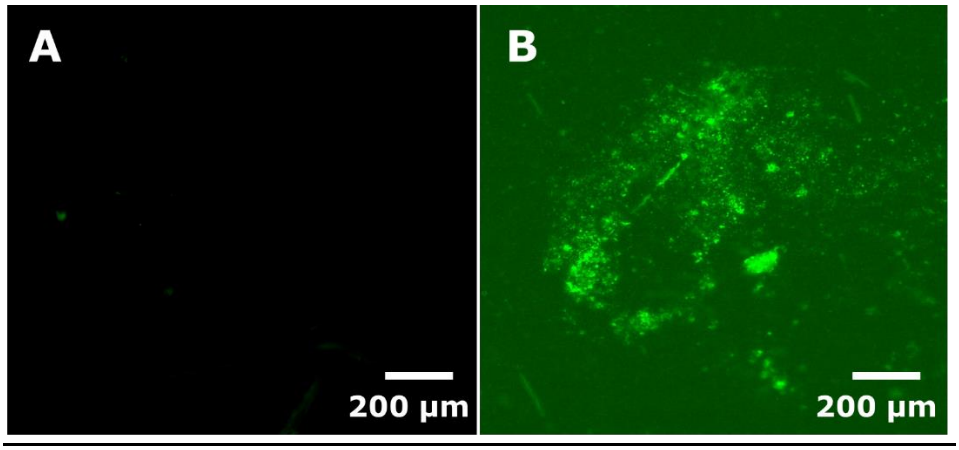

Figure 2.28. Confocal fluorescence emission images of PLLA-COOH and PLLA-Dns.

Similarly, steady state fluorescence spectroscopy was also employed for the corroboration of the fluorophore immobilization (**Figure 2.29**). Pristine PLLA and PLLA-Dns were excited at the same wavelengths, but only PLLA-Dns smple exhibited a maximum peak at 405 nm, which could be related with dansyl derivative **2c** fluorescence emission. These findings along with the confocal fluorescence emission confirmed the successful photoimmobilization of dansyl derivative **2c** using thiol-yne click reaction.

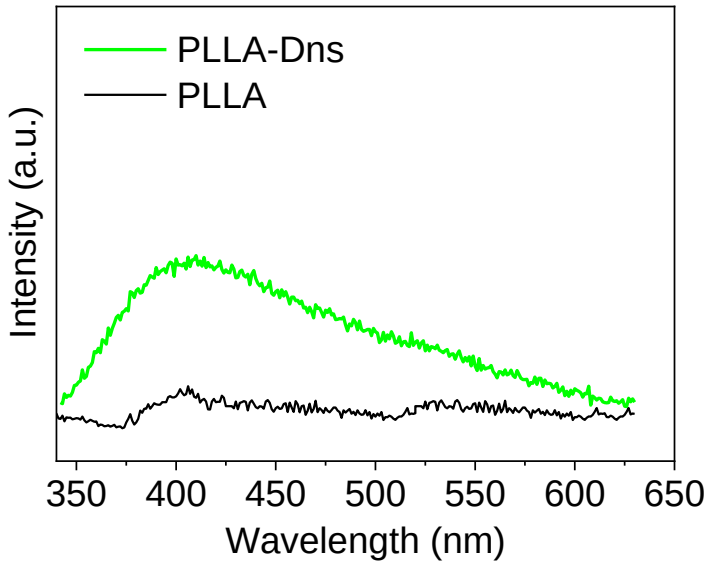

Figure 2.29. Steady state fluorescepce spectroscopy spcectra of pristine PLLA and PLLA-Dns.

On the other hand, SEM images indicated the surface morphologies of different PLLA samples, as can be seen in **Figure 2.30**. Regarding topographical properties, after

dansyl derivative **2c** immobilization, surface exhibited non heterogeneous protrusions. These particular surface variations indicated again that surface functionalization and tryptophan immobilization were actually achieved.

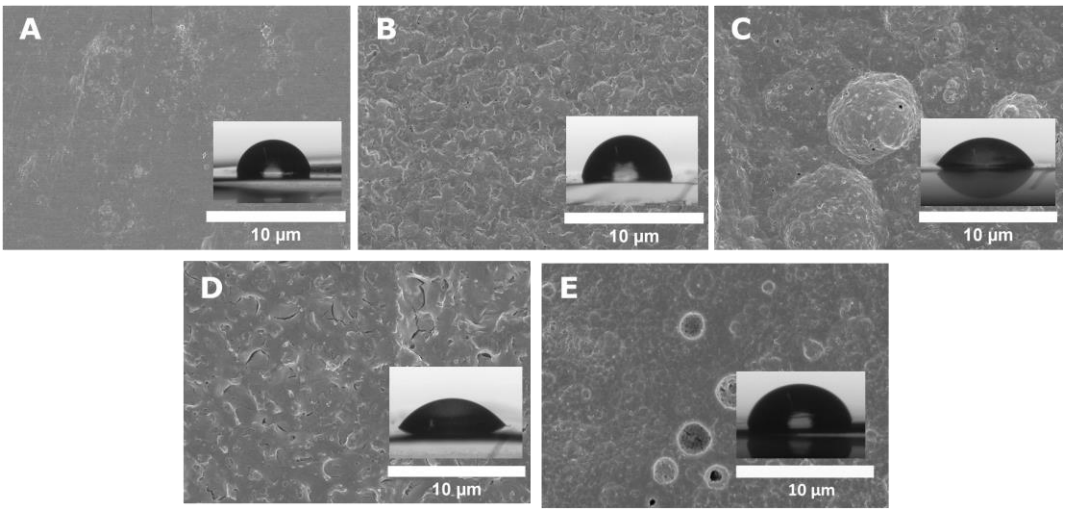

Figure 2.30. SEM images of (A) pristine PLLA, (B) PLLA-COOH, (C) PLLA-NH_2, (D) PLLA-Alkyne and (E) PLLA-Dns.

Moreover, wettability properties of the surface were analyzed after each functionalization step (**Figure 2.31**). Again, the hydrolysis and amidation reactions carried out on PLLA were previously described and their WCA values were discussed in *2.3.3. Section*. After the photoimmobilization of the dansyl derivative **2c**, the WCA valye increased to 81.3±6.3°. This augmentation corroborated the presence of aromatic groups on the polymer surface. These findings, consistent with those obtained in other sections, align with the aromatic functional groups present in dansyl, which render the surface less prone to forming hydrogen bonds with water. This change in WCA value reaffirmed the successful immobilization of the dansyl derivative **2c** through the thiol-yne click reaction.

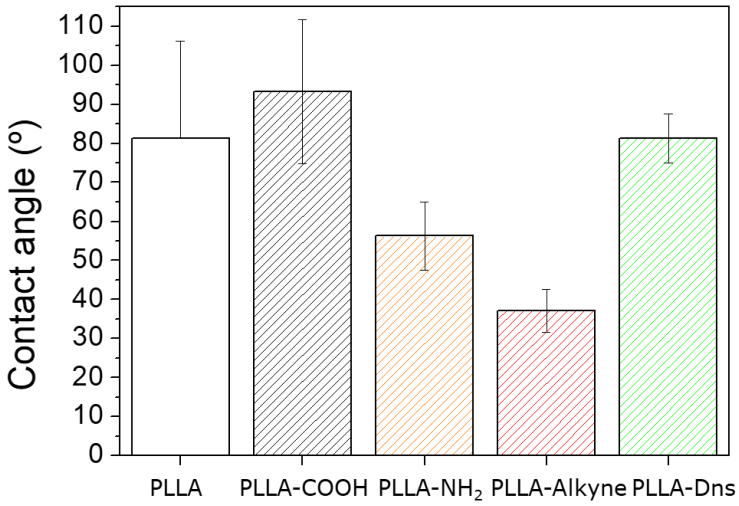

Figure 2.31. Contact angle values of pristine PLLA, PLLA-COOH, PLLA-NH_2, PLLA-Alkyne, PLLA-Dns *via* thiol-yne click reaction.

The success we achieved in immobilizing the fluorophore inspired us to apply the same methodology for bioconjugating the anticoagulant warfarin onto the polymeric surfaces (**Scheme 2.12**). However, prior drug modifications were required. As commented before, amination reductive reaction was proposed to introduce the neccessary thiol functional group within warfarin's structure (**Scheme 2.13**). Several reaction conditions were employed as can be seen in **Table 2.5**.

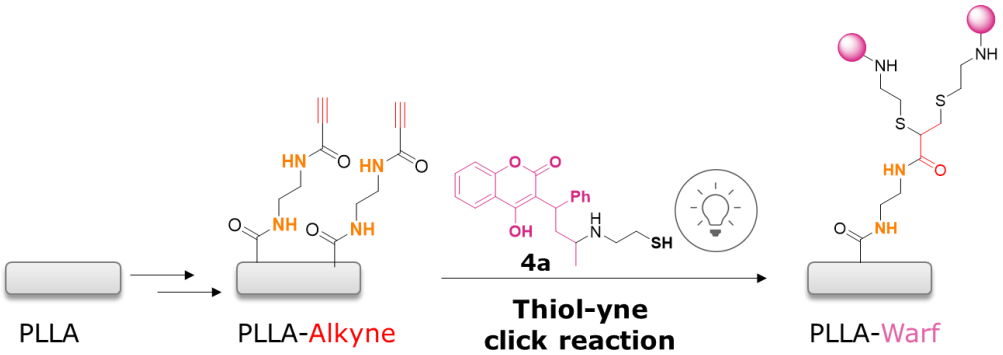

Scheme 2.12. Warfarin derivative **4a** photobioconjugation *via* thiol-yne click reaction.

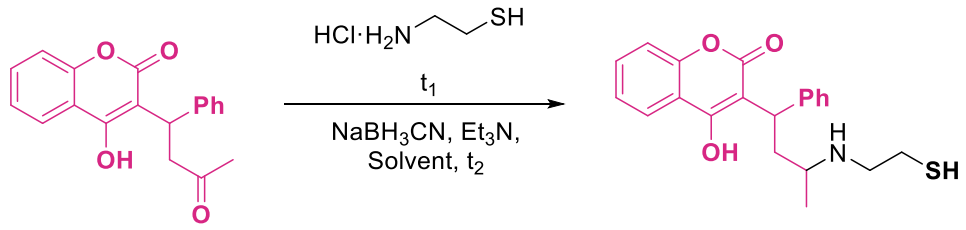

Warfarin

Warfarin derivative **4a**

Scheme 2.13. Synthesis of wafarin derivative **4a**.

Table 2.5. Reaction conditions employed for the introduction of thiol functional group onto warfarin.

Entry	Cystemine hydrochloride eq.	Warfarin eq.	Et_3N eq.	$NaBH_3CN$ eq	Solvent	t (h)
1	1.5	1	1.5	1.5	EtOH	24,48
2	1.5	1	1.5	1.5	EtOH	48,72
3	3	1	1.5	1.5	EtOH	24,48
4	3	1	3	3	EtOH	24,48
5	3	1	3	3	EtOH	24,48
6	2	1	-	1.5	DMF+ AcOH	24,48
7	2	1	-	1.5	DMF+ AcOH	24,120
8	2	1	2	1.5	DMF+ AcOH	24,120

Despite perfomed several trials involving variation in solvents and reaction times, the synthesis of warfarin derivative **4a** was not achieved. Further reaserach is neccessary to explore alternative methods for functionalizing warfarin and subsequently immobilizing into PLLA.

2.3.5. Plasma functionalized PLLA surfaces for propiolic activated click reactions

This research was primarily conducted at Politecnico di Torino (Italy), where the main objective was to understand and develop the plasma technique for the functionalization of polymeric surfaces, followed by their bioconjugation through click reactions.

One of the main objective of this work was to immobilize amino-containing or azido-containing biomolecules, such as, peptides on polymeric surfaces using the copper-free version of azido-yne or amino-yne click reactions. As previous works, the immobilization of the biomolecules required required prior activation and surface preparation. As in previous sections, the use of a fluorophore compound has been crucial to validate the methodological proposal. In this case, it was decided to once again employ tryptophan since it bears greater similarity to peptides, being recognized as an amino acid. Therefore, the functional group that can be find in this fluorophore will be the amino group, while the alkyne group will be present on PLLA surface. To incorporate the alkyne group onto PLLA, the methodology of self-assembled monolayers based on silane-anchor but using an innovative plasma technique was chosen. For this purpose, PLLA films were synthesized by solvent casting and were subjected to further plasma functionalization in order to generate the silane-based SAM (**Scheme 2.14**). For plasma treatment, PLLA surface was initially activated with Ar plasma and, then subjected to (3-aminopropyl)triethoxysilane (APTES) plasma. Among plasma parameters, when surfaces activation, Ar power and time were changed and, during APTES plasma, power, flow rata and time (**Table 2.6**).

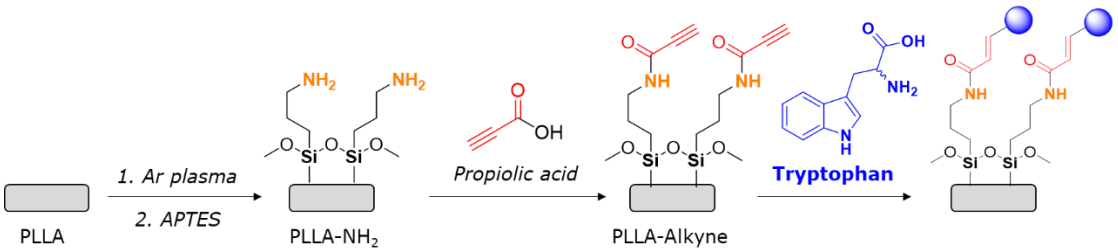

Scheme 2.14. PLLA surface plasma functionalization and tryptophan immobilization.

Table 2.6. Parameters employed for APTES plasma treatment onto PLLA surface

Experiments	Ar Power (W)	C/P*	Time (min)	APTES Power	APTES flow rate (mL/min)	C/P*	time (min)	Distance (mm)
1	20	C	1	10	1	P	5	5
2	10	C	1	10	2	P	5	5
3	10	C	1	20	1	P	5	5
4	10	C	1	20	2	P	5	5
5	10	C	1	20	1	P	10	5
6	10	C	1	20	2	P	10	5
7	10	C	1	20	1	P	15	5
8	10	C	1	20	2	P	15	5

*C: Continous phase, P: pulsed phase

As can be seen in **Table 2.6**, 8 experiments were perfomed where the power and time parameters are the most significant. As mentioned above, before APTES plasma treatment, a preactivation of the surface is required in order to generate radical on the top of the surface. For generating radicals, argon plasma is employed. Surface damage and, even, minor melting could be observed when the power of the argon plasma, employed for generating radicals, was above 20 W. It occurred the same when the time exposure of the plasma was above 1 min, since the flame generated was in a continuous mode.

The successful introduction of amino terminated silane by APTES plasma treatment on PLLA was further proved by Orange II colorimetric assay. After overnight incubation in Orange II solution, plasma treated PLLA samples were submerged in basic media to release the Orange II and measured in a plate reader was employed in order to monitor the proper progress of the modification process, and this way surface density of appropriate functional group, in this case NH_2, was estimated. Non-modified PLLA was used as a control material (**Figure 2.32**).

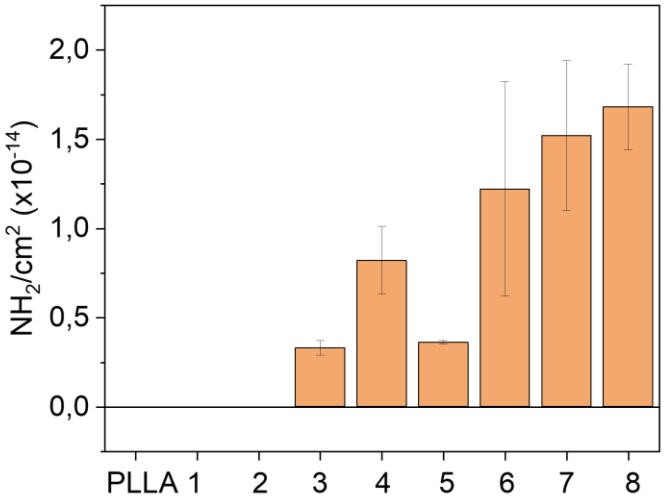

Figure 2.32. NH_2 density determination after APTES plasma treatment in PLLA sample. (*the results obtained from plasma 1 and 2 were not conclusive).

The number of amino groups on PLLA surface over the different experiments is very varied. However, experiments 7 and 8 presented the higher content of amino groups, which showed a similarity corresponding with the following obtained contact angle results. Therefore, the parameters employed in experiment 8 (PLLA-8) for the APTES plasma treatment of PLLA proved to be optimal, as reflected in the enhanced presence of amino groups.

After the next modification step, propiolic acid coupling, this value decreased and amounted to $2.31x10^{13}$ indicating that less amino groups are on the surface. Confirming that at least 86% of amino groups were amidated with propiolic acid.

In this case, ATR-FTIR technique could not be used to corroborate that the modifications carried out on the polymeric surfaces had taken place (**Figure 2.33**). That it probably due to the different orders of the penetration depth of the technique (0.5-2 μm) and the thickness of the deposited layers (a few nanometers). Therefore, the only appreciable signals in all samples were those corresponding to polymeric substrate regardless of the modification carried out in the surface.

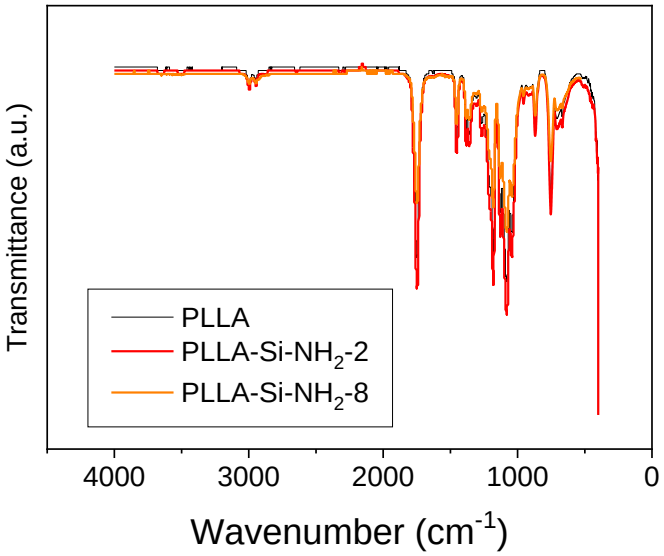

Figure 2.33. ATR-FTIR spectra of pristine PLLA, PLLA-Si-NH_2-2 and PLLA-Si-NH_2-8.

After plasma activated approach, PLLA surfaces were reacted with propiolic acid in order to have the desired functional group for the copper free Click Chemistry. Different concentrations of EDC·HCl, NHS and propiolic acid were employed as well as a variation of the reaction time (**Table 2.7**)

Table 2.7. Propiolic acid coupling reaction conditions.

Experiments	EDC·HCl (M) x10^5	NHS (M) x 10^5	Propiolic (M) x10^5	Stage 1	Stage 2
1	1.31	2.62	1.31	24 h	24 h
2	1.31	2.62	1.31	48 h	24 h
3	1.31	2.62	1.31	48 h	48 h
4	2.62	5.23	2.62	24 h	24 h
5	2.62	5.23	2.62	48 h	24 h
6	2.62	5.23	2.62	48 h	48 h

The wettability of the surface was determined by contact angle measurements. Indeed, contact angle measurements plasma triggered modifications have been followed by analyzing any hydrophilicity changes induced in each experiment. Static contact angle analysis is reported in **Figure 2.34**. Non modified PLLA sample showed a contact angle of 88.8 ± 0.44°. However, after plasma treatment with APTES static contact angle values decrease in all cases. Since APTES shows an amino terminal group, it is expected that the surface is more hydrophilic compared to the untreated surface. As can be seen, experiments 7 and 8 (PLLA-7 and PLLA-8) show the lowest

contact angle values, 59.0 ± 10.6° and 34.3 ± 13.1° respectively, which indicates that there are more hydrophilic groups anchored to the surface, *ergo* more active amino groups on the surface. This result is not surprising, since in experiments 7 and 8 both the exposure time and the power used are higher. The only difference is the flow rate applied when APTES is deposited, in PLLA-8 the flow rate is 2 mL/min higher than PLLA-7. This value increase is higher enough to obtain a much more hydrophilic, and consequently, more active surface, confirming more amino terminal groups on the surface. For that, the parameters employed in experiment 8 are considered optimal for further functionalization.

After optimizing APTES plasma treatment, modified PLLA surface was submitted to amidation conditions in order to react with propiolic acid by employing EDC/NHS coupling strategy. As can be seen in Figure **2.34** after propiolic acid coupling, contact angle value increased, indicating less hydrophilic groups on the surface, which demonstrated that terminal amino groups had reacted with propiolic acid successfully.

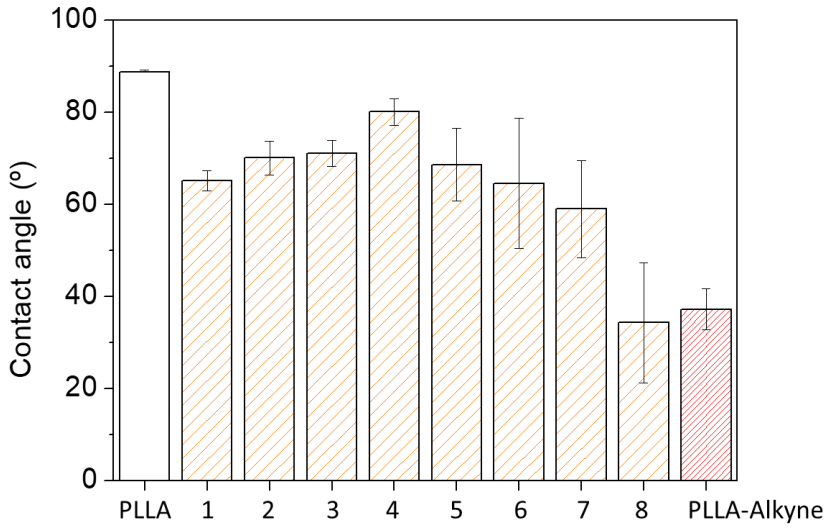

Figure 2.34. Water contact angles of pristine PLLA, plasma functionalized PLLAs and PLLA-Alkyne.

These results indicated that further analysis are required, focusing firstly on optimizing plasma treatment conditions and secondly, on introducing the alkyne moiety for posterior tryptophan immobilization. It is important to note that this study is still ongoing.

2.4. Conclusions

This study developed a surface treatment strategy for the conjugation of biological compounds onto polymer surfaces using copper catalyzed azide alkyne click reaction, copper-free azide alkyne clik reaction, copper-free aminoyne click rection and copper-free thiol-yne click rection. The success of surface prefunctionalization was confirmed through several techniques often used for surfae characterization as ATR-FTIR, XPS, water contact angles, SEM and fluorescence analysis. This work provides a new route to conjugate biological compounds by click reactions, which can also overcome the drawbacks of the cytotoxic metal. This innovative approaches for bioconjugation using latest copper-free Click Chemistry could have great potential in the biomedical field. By combining simple amidation reactions and advanced copper-free click reactions, it is possible to create bioactivated materials that can be used for a wide range of biomedical applications, such as implants coatings, biosensors or tissue engineering. In fact, this study highlights the potential of copper-free Click Chemistry in developing novel conjugation strategies and paves the way for future research to explore the practical applications of this technique in biomedical research.

2.5. Bibliography

1. Arciola, C.R.; Campoccia, D. Implant infections: adhesion, biofilm formation and immune evasion. *Nat. Rev. Microbiol.* **2018**, *16*, doi:10.1038/s41579-018-0019-y.

2. Campoccia, D.; Montanaro, L.; Renata, C. The significance of infection related to orthopedic devices and issues of antibiotic resistance. *Biomaterials* **2006**, *27*, 2331–2339, doi:10.1016/j.biomaterials.2005.11.044.

3. Sheikh, Z.; Brooks, P.J.; Barzilay, O.; Fine, N.; Glogauer, M. Macrophages, foreign body giant cells and their response to implantable biomaterials. *Materials (Basel).* **2015**, *8*, 5671–5701, doi:10.3390/ma8095269.

4. Franz, S.; Rammelt, S.; Scharnweber, D.; Simon, J.C. Immune responses to implants - A review of the implications for the design of immunomodulatory biomaterials. *Biomaterials* **2011**, *32*, 6692–6709, doi:10.1016/j.biomaterials.2011.05.078.

5. Anderson, J.M. Exploiting the inflammatory response on biomaterials research and development. *J. Mater. Sci. Mater. Med.* **2015**, *26*, 1–2, doi:10.1007/s10856-015-5423-5.

6. Zhou, G.; Groth, T. Host Responses to Biomaterials and Anti-Inflammatory Design—a Brief Review. *Macromol. Biosci.* **2018**, *18*, 1–15, doi:10.1002/mabi.201800112.

7. Bridges, A.W.; García, A.J. Anti-Inflammatory Polymeric Coatings for Implantable Biomaterials and Devices. *Surf. Coatings Technol.* **2008**, *2*, 984–994, doi:https://doi.org/10.1016/j.surfcoat.2006.09.088.

8. AlKhoury, H.; Hautmann, A.; Erdmann, F.; Zhou, G.; Stojanović, S.; Najman, S.; Groth, T. Study on the potential mechanism of anti-inflammatory activity of covalently immobilized hyaluronan and heparin. *J. Biomed. Mater. Res. - Part A* **2020**, *108*, 1099–1111, doi:10.1002/jbm.a.36885.

9. Al-Khoury, H.; Espinosa-Cano, E.; Aguilar, M.R.; Román, J.S.; Syrowatka, F.; Schmidt, G.; Groth, T. Anti-inflammatory Surface Coatings Based on Polyelectrolyte Multilayers of Heparin and Polycationic Nanoparticles of Naproxen-Bearing Polymeric Drugs. *Biomacromolecules* **2019**, *20*, 4015–4025, doi:10.1021/acs.biomac.9b01098.

10. Zhang, L.; Chen, D.; Wang, K.; Yu, F.; Huang, Z.; Pan, S. Blood compatibility improvement of titanium oxide film modified by doping La2O3. *J. Mater. Sci. Mater. Med.* **2009**, *20*, 2019–2023, doi:10.1007/s10856-009-3784-3.

11. Jingrun, R.; Jin, W.; Hong, S.; Nan, H. Surface modification of polyethylene terephthalate with albumin and gelatin for improvement of anticoagulation and endothelialization Ren. *Appl. Surf. Sci.* **2008**, *255*, 263–266, doi:10.1016/j.apsusc.2008.06.181.

12. Jing, F.J.; Wang, L.; Fu, R.K.Y.; Leng, Y.X.; Chen, J.Y.; Huang, N.; Chu, P.K. Behavior of endothelial cells on micro-patterned titanium oxide fabricated by plasma immersion ion implantation and deposition and plasma etching. **2007**, *201*, 6874–6877, doi:10.1016/j.surfcoat.2006.09.088.

13. Jaffer, I.H.; Weitz, J.I. The blood compatibility challenge . Part 1 : Blood-contacting medical devices : The scope of the problem. *Acta Biomater.* **2019**, *94*, 2–10, doi:10.1016/j.actbio.2019.06.021.

14. Cai, K.; Rechtenbach, A.; Hao, J.; Jandt, K.D. Polysaccharide-protein surface modification of titanium via a layer-by-layer technique : Characterization and cell behaviour aspects. *Biomateri* **2005**, *26*, 5960–5971, doi:10.1016/j.biomaterials.2005.03.020.

15. Al-mayouf, A.M.; Al-swayih, A.A.; Al-mobarak, N.A.; Al-jabab, A.S. Corrosion behavior of a new titanium alloy for dental implant applications in fluoride media. *Mater. Chem. Phys.* **2004**, *86*, 320–329, doi:10.1016/j.matchemphys.2004.03.019.

16. Hwang, M.; Lim, J.K.; Abdalla, A. In vitro bioactivity of titanium implants coated with bicomponent hybrid biodegradable polymers. *J. Sol-Gel Sci. Technol.* **2012**, *64*, 756–764, doi:10.1007/s10971-012-2912-6.

17. Kim, S.; Kang, M.; Kim, H.; Lim, H.; Byun, S.; Lee, J.; Lee, S. Innovative micro-textured hydroxyapatite and poly (L -lactic) -acid polymer composite fi lm as a fl exible , corrosion resistant , biocompatible , and bioactive coating for Mg implants. *Mater. Sci. Eng. C* **2017**, *81*, 97–103, doi:10.1016/j.msec.2017.07.026.

18. Narayanan, G.; Vernekar, V.N.; Kuyinu, E.L.; Laurencin, C.T. Poly (lactic acid)-based biomaterials for orthopaedic regenerative engineering. *Adv. Drug Deliv. Rev.* **2016**, *107*, 247–276, doi:10.1016/j.addr.2016.04.015.

19. Lichter, J.A.; Vliet, K.J. Van; Rubner, M.F. Design of Antibacterial Surfaces and Interfaces : Polyelectrolyte Multilayers as a Multifunctional Platform. *Macromolecules* **2009**, *42*, 8573–8586, doi:10.1021/ma901356s.

20. Mukherjee, T.; Kao, N. PLA Based Biopolymer Reinforced with Natural Fibre : A Review. *J. Polym. Environ.* **2011**, *19*, 714–725, doi:10.1007/s10924-011-0320-6.

21. Rebelo, R.; Fernandes, M.; Fangueiro, R. Biopolymers in Medical Implants : A Brief Review. *Procedia Eng.* **2017**, *200*, 236–243, doi:10.1016/j.proeng.2017.07.034.

22. Bergström, J.S.; Hayman, D. An Overview of Mechanical Properties and Material Modeling of Polylactide (PLA) for Medical Applications. *Ann. Biomed. Eng.* **2016**, *44*, 330–340, doi:10.1007/s10439-015-1455-8.

23. da Silva, D.; Kaduri, M.; Poley, M.; Adir, O.; Krinsky, N.; Shainsky-Roitman, J.; Schroeder, A. Biocompatibility, biodegradation and excretion of polylactic acid (PLA) in medical implants and theranostic systems. *Chem. Eng. J.* **2018**, *340*, 9–14, doi:10.1016/j.cej.2018.01.010.

24. Baran, E.H.; Yildirim Erbil, H. Surface modification of 3d printed pla objects by

fused deposition modeling: A review. *Colloids and Interfaces* **2019**, *3*, 43–68, doi:10.3390/colloids3020043.

25. Tyler, B.; Gullotti, D.; Mangraviti, A.; Utsuki, T.; Brem, H. Polylactic acid (PLA) controlled delivery carriers for biomedical applications. *Adv. Drug Deliv. Rev.* **2016**, *107*, 163–175, doi:10.1016/j.addr.2016.06.018.

26. Lorenzo, M.L. Di; Androsch, R. *Industrial Applications of Poly(lactic acid)*; Springer International Publishing: Cham, 2018; ISBN 9783319754581.

27. Lv, Y.; Xu, Y.; Sang, X.; Li, C.; Liu, Y.; Guo, Q.; Ramakrishna, S.; Wang, C.; Hu, P.; Nanda, H.S. PLLA-gelatin composite fiber membranes incorporated with functionalized CeNPs as a sustainable wound dressing substitute promoting skin regeneration and scar remodeling. *J. Mater. Chem. B* **2022**, *10*, 1116–1127, doi:10.1039/d1tb02677a.

28. Bu, Y.; Ma, J.; Bei, J.; Wang, S. Surface Modification of Aliphatic Polyester to Enhance Biocompatibility. *Front. Bioeng. Biotechnol.* **2019**, *7*, 1–10, doi:10.3389/fbioe.2019.00098.

29. Ujino, D.; Nishizaki, H.; Higuchi, S.; Komasa, S.; Okazaki, J. Effect of plasma treatment of titanium surface on biocompatibility. *Appl. Sci.* **2019**, *9*, doi:10.3390/app9112257.

30. Sasmazel, H.T.; Alazzawi, M.; Alsahib, N.K.A. Atmospheric pressure plasma surface treatment of polymers and influence on cell cultivation. *Molecules* **2021**, *26*, 1–25, doi:10.3390/molecules26061665.

31. Mai-Prochnow, A.; Murphy, A.B.; McLean, K.M.; Kong, M.G.; Ostrikov, K. Atmospheric pressure plasmas: Infection control and bacterial responses. *Int. J. Antimicrob. Agents* **2014**, *43*, 508–517, doi:10.1016/j.ijantimicag.2014.01.025.

32. Pasini, D. The Click Reaction as an Efficient Tool for the Construction of Macrocyclic Structures. *Molecules* **2013**, *18*, 9512–9530, doi:10.3390/molecules18089512.

33. Li, X.; Xiong, Y. Application of "Click" Chemistry in Biomedical Hydrogels. *ACS Omega* **2022**, *7*, 36918–36928, doi:10.1021/acsomega.2c03931.

34. Suárez, A. Reacciones de cicloadición 1,3-dipolares a alquinos catalizadas por cobre. *An. Quím* **2012**, *108*, 306–313.

35. Wang, C.; Ikhlef, D.; Kahlal, S.; Saillard, J.Y.; Astruc, D. Metal-catalyzed azide-alkyne "click" reactions: Mechanistic overview and recent trends. *Coord. Chem. Rev.* **2016**, *316*, 1–20, doi:10.1016/j.ccr.2016.02.010.

36. Lutz, J. 1 , 3-Dipolar Cycloadditions of Azides and Alkynes : A Universal Ligation Tool in Polymer and Materials Science. *Angew. Chemie - Int. Ed.* **2007**, *46*, 1018–1025, doi:10.1002/anie.200604050.

37. Barbosa, M.; Martins, C.; Gomes, P. "Click" chemistry as a tool to create novel biomaterials: A short review. *U.Porto J. Eng.* **2015**, *1*, 22–34, doi:10.24840/2183-6493_001.001_0004.

38. Arslan, M.; Tasdelen, M.A. Click Chemistry in Macromolecular Design : Complex Architectures from Functional Polymers. *Chem. Africa* **2019**, *2*, 195–214, doi:10.1007/s42250-018-0030-8.

39. Xi, W.; Scott, T.F.; Kloxin, C.J.; Bowman, C.N. Click Chemistry in Materials Science. *Adv. Funct. Mater.* **2014**, *24*, 2572–2590, doi:10.1002/adfm.201302847.

40. Lahann, J. *Click Chemistry for Biotechnology and Materials Science*; Lahann, J., Ed.; John Wiley & Sons Ltd: The Atrium, Southern Gate, Chichester, West Sussex, PO19 8SQ, United Kingdom, 2009; ISBN 9780470699706.

41. O'Hern, C.I.Z.; Djoko, K.Y. Copper Cytotoxicity: Cellular Casualties of Noncognate Coordination Chemistry. *MBio* **2022**, *13*, 1–4, doi:10.1128/mbio.00434-22.

42. Agard, N.J.; Prescher, J.A.; Bertozzi, C.R. A Strain-Promoted [3 + 2] Azide - Alkyne Cycloaddition for Covalent Modification of Biomolecules in Living Systems. *J. Am. Chem. Soc.* **2004**, *126*, 15046–15047.

43. Dommerholt, J.; Rutjes, F.P.J.T.; van Delft, F.L. Strain-Promoted 1,3-Dipolar Cycloaddition of Cycloalkynes and Organic Azides. *Top. Curr. Chem.* **2016**, *374*, 1–20, doi:10.1007/s41061-016-0016-4.

44. Kim, E.; Koo, H. Biomedical applications of copper-free click chemistry:: In vitro, in vivo, and ex vivo. *Chem. Sci.* **2019**, *10*, 7835–7851, doi:10.1039/c9sc03368h.

45. Yoon, H.Y.; Lee, D.; Lim, D.K.; Koo, H.; Kim, K. Copper-Free Click Chemistry: Applications in Drug Delivery, Cell Tracking, and Tissue Engineering. *Adv.*

Mater. **2022**, *34*, 1–24, doi:10.1002/adma.202107192.

46. Pickens, C.J.; Johnson, S.N.; Pressnall, M.M.; Leon, M.A.; Berkland, C.J. Practical Considerations, Challenges, and Limitations of Bioconjugation via Azide-Alkyne Cycloaddition. *Bioconjug. Chem.* **2018**, *29*, 686–701, doi:10.1021/acs.bioconjchem.7b00633.

47. Manova, R.; Vanbeek, T.A.; Zuilhof, H. Surface functionalization by strain-promoted alkyne-azide click reactions. *Angew. Chemie - Int. Ed.* **2011**, *50*, 5428–5430, doi:10.1002/anie.201100835.

48. Azagarsamy, M.A.; Anseth, K.S. Bioorthogonal click chemistry: An indispensable tool to create multifaceted cell culture scaffolds. *ACS Macro Lett.* **2013**, *2*, 5–9, doi:10.1021/mz300585q.

49. He, B.; Su, H.; Bai, T.; Wu, Y.; Li, S.; Gao, M.; Hu, R.; Zhao, Z.; Qin, A.; Ling, J.; et al. Spontaneous Amino-yne Click Polymerization: A Powerful Tool toward Regio- and Stereospecific Poly(β-aminoacrylate)s. *J. Am. Chem. Soc.* **2017**, *139*, 5437–5443, doi:10.1021/jacs.7b00929.

50. Zhang, J.; Zhang, Z.; Wang, J.; Zang, Q.; Sun, J.Z.; Tang, B.Z. Recent progress in the applications of amino-yne click chemistry. *Polym. Chem.* **2021**, *12*, 2978–2986, doi:10.1039/d1py00113b.

51. Worch, J.C.; Stubbs, C.J.; Price, M.J.; Dove, A.P. Click Nucleophilic Conjugate Additions to Activated Alkynes: Exploring Thiol-yne, Amino-yne, and Hydroxyl-yne Reactions from (Bio)Organic to Polymer Chemistry. *Chem. Rev.* **2021**, *121*, 6744–6776, doi:10.1021/acs.chemrev.0c01076.

52. Stump, B. Click Bioconjugation: Modifying Proteins Using Click-Like Chemistry. *ChemBioChem* **2022**, *23*, 1–9, doi:10.1002/cbic.202200016.

53. Amna, B.; Ozturk, T. Click chemistry: a fascinating method of connecting organic groups. *Org. Commun.* **2021**, *78*, 97–120, doi:10.25135/ACG.OC.100.21.03.2006.

54. Lucas, S. The Pharmacology of Indomethacin. *Headache Curr.* **2016**, *56*, 436–446, doi:10.1111/head.12769.

55. Vijay K. Tammara, Milind M. Narurkar, A. Michael Crider, M.A.K. Synthesis and Evaluation of Morpholinoalkyl Ester Prodrugs of Indomethacin and Naproxen. *Pharm. Res.* **1993**, *10*, 1191–1198.

56. Gliszczyńska, A.; Nowaczyk, M. Lipid formulations and bioconjugation strategies for indomethacin therapeutic advances. *Molecules* **2021**, *26*, 1576–1594, doi:10.3390/molecules26061576.

57. Nalamachu, S.; Wortmann, R. Role of indomethacin in acute pain and inflammation management: A review of the literature. *Postgrad. Med.* **2014**, *126*, 92–97, doi:10.3810/pgm.2014.07.2787.

58. Touhey, S.; Connor, R.O.; Plunkett, S.; Maguire, A.; Clynes, M. Structure – activity relationship of indomethacin analogues for MRP-1 , COX-1 and COX-2 inhibition : identification of novel chemotherapeutic drug resistance modulators. *Eur. J. Cancer* **2002**, *38*, 1661–1670.

59. Kalgutkar, A.S.; Marnett, A.B.; Crews, B.C.; Remmel, R.P.; Marnett, L.J. Ester and Amide Derivatives of the Nonsteroidal Antiinflammatory Drug , Indomethacin , as Selective Cyclooxygenase-2 Inhibitors. *J. Med. Chem.* **2000**, *43*, 2860–2870.

60. Silakari, O.; Kohli, D. V.; Chaturvedi, S.C. Quantitative structure activity relationship analysis of ester and amide derivatives of indomethacin. *Indian J. Pharm. Sci.* 2003, *65*, 471–476.

61. Kalgutkar, A.S.; Marnett, A.B.; Crews, B.C.; Remmel, R.P.; Marnett, L.J. Ester and amide derivatives of the nonsteroidal antiinflammatory drug, indomethacin, as selective cyclooxygenase-2 inhibitors. *J. Med. Chem.* **2000**, *43*, 2860–2870, doi:10.1021/jm000004e.

62. Sánchez-Bodón, J.; Ruiz-Rubio, L.; Hernáez-Laviña, E.; Vilas-Vilela, J.L.; Moreno-Benítez, M.I. Poly(L-lactide)-based anti-inflammatory responsive surfaces for surgical implants. *Polymers (Basel).* **2021**, *13*, 1–15, doi:10.3390/polym13010034.

63. Bodey, G.P.; Nance, J. Amoxicillin : In Vitro and Pharmacological Studies. *Antimicrob. Agents Chemother.* **1972**, *1*, 358–362.

64. de Marco, B.A.; Natori, J.S.H.; Fanelli, S.; Tótoli, E.G.; Salgado, H.R.N. Characteristics, Properties and Analytical Methods of Amoxicillin: A Review with Green Approach. *Crit. Rev. Anal. Chem.* **2017**, *47*, 267–277, doi:10.1080/10408347.2017.1281097.

65. Salvo, F.; De Sarro, A.; Caputi, A.P.; Polimeni, G. Amoxicillin and amoxicillin

plus clavulanate: A safety review. *Expert Opin. Drug Saf.* **2009**, *8*, 111–118, doi:10.1517/14740330802527984.

66. Neu, H.C. Antimicrobial Activity and Human Pharmacology of Amoxicillin. *J. Infect. Dis.* **1974**, *129*, S123–S131.

67. Goldstein, E.C.; Citron, D.M. Comparative In Vitro Activities of Amoxicillin-Clavulanic Acid and Imipenem against Anaerobic Bacteria Isolated from Community Hospitals. *Antimicrob. Agents Chemother.* **1986**, *29*, 158–160.

68. Geddes, A.M.; Klugman, K.P.; Rolinson, G.N. Introduction: historical perspective and development of amoxicillin/clavulanate. *Int. J. Antimicrob. Agents* **2007**, *30*, 109–112, doi:10.1016/j.ijantimicag.2007.07.015.

69. Ghisaidoobe, A.B.T.; Chung, S.J. Intrinsic tryptophan fluorescence in the detection and analysis of proteins: A focus on förster resonance energy transfer techniques. *Int. J. Mol. Sci.* **2014**, *15*, 22518–22538, doi:10.3390/ijms151222518.

70. Gebauer, M. Synthesis and structure – activity relationships of novel warfarin derivatives. *Bioorg. Med. Chem.* **2007**, *15*, 2414–2420, doi:10.1016/j.bmc.2007.01.014.

71. Porter, W.R. Warfarin: History, tautomerism and activity. *J. Comput. Aided. Mol. Des.* **2010**, *24*, 553–573, doi:10.1007/s10822-010-9335-7.

72. Jain, P.K.; Joshi, H. Coumarin : Chemical and Pharmacological Profile. *J. Appl. Pharm. Sci.* **2012**, *02*, 236–240, doi:10.7324/JAPS.2012.2643.

73. Pirmohamed, M. Warfarin: Almost 60 years old and still causing problems. *Br. J. Clin. Pharmacol.* **2006**, *62*, 509–511, doi:10.1111/j.1365-2125.2006.02806.x.

74. Liu, Y.; Mahara, A.; Kambe, Y.; Hsu, Y.I.; Yamaoka, T. Endothelial cell adhesion and blood response to hemocompatible peptide 1 (HCP-1), REDV, and RGD peptide sequences with free N-Terminal amino groups immobilized on a biomedical expanded polytetrafluorethylene surface. *Biomater. Sci.* **2021**, *9*, 1034–1043, doi:10.1039/d0bm01396j.

75. Ren, X.; Feng, Y.; Guo, J.; Wang, H.; Li, Q.; Yang, J.; Hao, X.; Lv, J.; Ma, N.; Li, W. Surface modification and endothelialization of biomaterials as potential scaffolds for vascular tissue engineering applications. *Chem. Soc. Rev.* **2015**,

44, 5680–5742, doi:10.1039/c4cs00483c.

76. Mahara, A.; Kitagawa, K.; Otaka, A.; Nakaoki, T.; Ishihara, K.; Yamaoka, T. Impact of REDV peptide density and its linker structure on the capture, movement, and adhesion of flowing endothelial progenitor cells in microfluidic devices. *Mater. Sci. Eng. C* **2021**, *129*, 112381, doi:10.1016/j.msec.2021.112381.

77. Zhao, S.; Liu, J.; Lv, Z.; Zhang, G.; Xu, Z. Recent updates on 1,2,3-triazole-containing hybrids with in vivo therapeutic potential against cancers: A mini-review. *Eur. J. Med. Chem.* **2023**, *251*, 115254, doi:10.1016/j.ejmech.2023.115254.

78. Carlucci, R.; Di Gresia, G.; Mediavilla, M.G.; Cricco, J.A.; Tekwani, B.L.; Khan, S.I.; Labadie, G.R. Expanding the scope of novel 1,2,3-triazole derivatives as new antiparasitic drug candidates. *RSC Med. Chem.* **2022**, *14*, 122–134, doi:10.1039/d2md00324d.

79. Malah, T. El; Nour, H.F.; Satti, A.A.E.; Hemdan, B.A.; El-Sayed, W.A. Design, synthesis, and antimicrobial activities of 1,2,3-triazole glycoside clickamers. *Molecules* **2020**, *25*, 1–17, doi:10.3390/molecules25040790.

80. Brik, A.; Alexandratos, J.; Lin, Y.C.; Elder, J.H.; Olson, A.J.; Wlodawer, A.; Goodsell, D.S.; Wong, C.H. 1,2,3-Triazole as a Peptide Surrogate in the Rapid Synthesis of HIV-1 Protease Inhibitors. *ChemBioChem* **2005**, *6*, 1167–1169, doi:10.1002/cbic.200500101.

81. Assis, S.P.D.O.; Silva, M.T. Da; De Oliveira, R.N.; Lima, V.L.D.M. Synthesis and anti-inflammatory activity of new alkyl-substituted phthalimide 1 H -1,2,3-triazole derivatives. *Sci. World J.* **2012**, *2012*, 1–8, doi:10.1100/2012/925925.

82. Kumar, A.; Alam, M.S.; Hamid, H.; Chugh, V.; Tikla, T.; Kaul, R.; Dhulap, A.; Sharma, S.K. Design and synthesis of anti–inflammatory 1,2,3–triazolylpyrrolobenzodiazepinone derivatives and impact of molecular structure on COX–2 selective targeting. *J. Mol. Struct.* **2023**, *1272*, 134151, doi:10.1016/j.molstruc.2022.134151.

83. Agalave, S.G.; Maujan, S.R.; Pore, V.S. Click chemistry: 1,2,3-triazoles as pharmacophores. *Chem. - An Asian J.* **2011**, *6*, 2696–2718, doi:10.1002/asia.201100432.

84. Matin, M.M.; Matin, P.; Rahman, M.R.; Ben Hadda, T.; Almalki, F.A.; Mahmud, S.; Ghoneim, M.M.; Alruwaily, M.; Alshehri, S. Triazoles and Their Derivatives: Chemistry, Synthesis, and Therapeutic Applications. *Front. Mol. Biosci.* **2022**, *9*, 1–8, doi:10.3389/fmolb.2022.864286.

85. Ji Ram, V.; Sethi, A.; Nath, M.; Pratap, R. Five-Membered Heterocycles. In *The Chemistry of Heterocycles*; 2019; pp. 149–478 ISBN 9780081010334.

86. Andrade-Del Olmo, J.; Pérez-Álvarez, L.; Ruiz-Rubio, L.; Vilas-Vilela, J.L. Antibacterial chitosan electrostatic/covalent coating onto biodegradable poly (L-lactic acid). *Food Hydrocoll.* **2020**, *105*, doi:10.1016/j.foodhyd.2020.105835.

87. Lao, L.; Tan, H.; Wang, Y.; Gao, C. Colloids and Surfaces B : Biointerfaces Chitosan modified poly (l -lactide) microspheres as cell microcarriers for cartilage tissue engineering. **2008**, *66*, 218–225, doi:10.1016/j.colsurfb.2008.06.014.

88. Chollet, C.; Chanseau, C.; Remy, M.; Guignandon, A.; Bareille, R.; Bordenave, L.; Durrieu, M.; Labruge, C.; Cedex, F.-B.; Bordeaux, U.; et al. Biomaterials The effect of RGD density on osteoblast and endothelial cell behavior on RGD-grafted polyethylene terephthalate surfaces. *Biomaterials* **2009**, *30*, 711–720, doi:10.1016/j.biomaterials.2008.10.033.

89. Uchida, E.; Uyama, Y.; Ikada, Y. Sorption of Low-Molecular-Weight Anions into Thin Polycation Layers Grafted onto a Film. *Langmuir* **1993**, *9*, 1121–1124.

90. Takeuchi, T. HPLC of Amino Acids as Dansyl and Dabsyl Derivatives. *J. Chromatogr. Libr.* **2005**, *70*, 229–241.

91. Lal, J.; Gupta, S.K.; Thavaselvam, D.; Agarwal, D.D. European Journal of Medicinal Chemistry Biological activity , design , synthesis and structure activity relationship of some novel derivatives of curcumin containing sulfonamides. *Eur. J. Med. Chem.* **2013**, *64*, 579–588, doi:10.1016/j.ejmech.2013.03.012.

92. Alberti, G.; Desimone, A.; A, P.R.S. Wetting of rough surfaces : a homogenization approach Wetting of rough surfaces : a homogenization approach. **2005**, *461*, 79–97, doi:10.1098/rspa.2004.1364.

93. Kantheti, S.; Narayan, R.; Raju, K.V.S.N. The impact of 1,2,3-triazoles in the

design of functional coatings. *RSC Adv.* **2015**, *5*, 3687–3708, doi:10.1039/c4ra12739k.

94. Renò, F.; D'Angelo, D.; Gottardi, G.; Rizzi, M.; Aragno, D.; Piacenza, G.; Cartasegna, F.; Biasizzo, M.; Trotta, F.; Cannas, M. Atmospheric pressure plasma surface modification of poly(D, L -lactic acid) increases fibroblast, osteoblast and keratinocyte adhesion and proliferation. *Plasma Process. Polym.* **2012**, *9*, 491–502, doi:10.1002/ppap.201100139.

95. Sourkouni, G.; Kalogirou, C.; Moritz, P.; Gödde, A.; Pandis, P.K.; Höfft, O.; Vouyiouka, S.; Zorpas, A.A.; Argirusis, C. Study on the influence of advanced treatment processes on the surface properties of polylactic acid for a bio-based circular economy for plastics. *Ultrason. Sonochem.* **2021**, *76*, 105627, doi:10.1016/j.ultsonch.2021.105627.

96. De Geyter, N.; Morent, R.; Desmet, T.; Trentesaux, M.; Gengembre, L.; Dubruel, P.; Leys, C.; Payen, E. Plasma modification of polylactic acid in a medium pressure DBD. *Surf. Coatings Technol.* **2010**, *204*, 3272–3279, doi:10.1016/j.surfcoat.2010.03.037.

97. Bunge, A.; Magerusan, L.; Morjan, I.; Turcu, R.; Borodi, G.; Liebscher, J. Diazonium salt-mediated synthesis of new amino, hydroxy, propargyl, and maleinimido-containing superparamagnetic Fe@C nanoparticles as platforms for linking bio-entities or organocatalytic moieties. *J. Nanoparticle Res.* **2015**, *17*, 379–395, doi:10.1007/s11051-015-3167-2.

98. Herrmann, I.; Kramm, U.I.; Radnik, J.; Fiechter, S.; Bogdanoff, P. Influence of Sulfur on the Pyrolysis of CoTMPP as Electrocatalyst for the Oxygen Reduction Reaction. *J. Electrochem. Soc.* **2009**, *156*, B1283, doi:10.1149/1.3185852.

99. He, M.; Yuan, T.; Dong, W.; Li, P.; Jason Niu, Q.; Meng, J. High-performance acid-stable polysulfonamide thin-film composite membrane prepared via spinning-assist multilayer interfacial polymerization. *J. Mater. Sci.* **2019**, *54*, 886–900, doi:10.1007/s10853-018-2847-6.

100. Xiao, Y.; Zheng, J.; He, Y.; Wang, L. Droplet and bubble wetting behaviors: The roles of surface wettability and roughness. *Colloids Surfaces A Physicochem. Eng. Asp.* **2022**, *653*, 130008, doi:10.1016/j.colsurfa.2022.130008.

101. Ubuo, E.E.; Udoetok, I.A.; Tyowua, A.T.; Ekwere, I.O.; Al-Shehri, H.S. The direct cause of amplified wettability: Roughness or surface chemistry? *J. Compos. Sci.* **2021**, *5*, 1–9, doi:10.3390/jcs5080213.

102. Sánchez-Bodón, J.; Diaz-Galbarriatu, M.; Pérez-Álvarez, L.; Moreno-Benítez, I.; Vilas-Vilela, J.L. Strategies to Enhance Biomedical Device Performance and Safety : A Comprehensive Review. *Coatings* **2023**, *13*, 1981–2005, doi:https://www.mdpi.com/2079-6412/13/12/1981/review_report.

103. Sánchez-Bodón, J.; Andrade-Del Olmo, J.; Alonso, J.M.; Moreno-Benítez, I.; Vilas-Vilela, J.L.; Pérez-Alvarez, L. Bioactive Coatings on Titanium: A Review on Hydroxylation, Self-Assembled Monolayers (SAMs) and Surface Modification Strategies. *Polymers (Basel).* **2022**, *14*, 165, doi:10.3390/polym14010165.

CHAPTER 3

PET-BASED SURFACES WITH MULTIBIOLOGICAL PROPERTIES BY EMPLOYING CONVENTIONAL CLICK CHEMISTRY

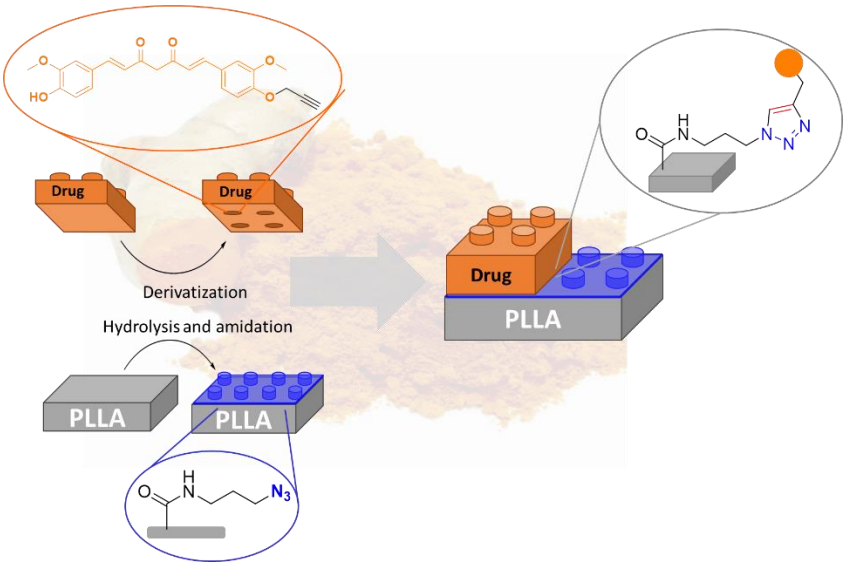

Implants are typically classified into three main groups: ceramic, metal and polymers. Among these materials, polymers offer advantages due to their diverse monomer combination and manufacturing methods. Particularly, polyethylene terephthalate (PET) has become a promising alternative for prosthesis or implants coating because of its high uniformity, excellent mechanical properties and exceptional resistance to chemical reactions. However, its surface properties are limited due to a lack of active functional groups. This major drawback makes this polymer unattractive for use in biomedical devices, mainly due to undesirable interactions with surrounding living tissue, including the possible formation of biofilms on the surface. For this reason, functionalization of PET surface with active molecules is essential in order to avoid bacterial contamination and to enhance bio-and hemocompatiblity of blood-contacting devices. This chapter will describe the use of traditional click chemistry for the immobilization of biological active compound, in this case curcumin, onto PET surfaces in order to overcome biofilm formation and improve inflammation and coagulation responses from the body.

CHAPTER 3

PET-BASED SURFACES WITH MULTIBIOLOGICAL PROPERTIES BY EMPLOYING CONVENTIONAL CLICK CHEMISTRY

3.1. Introduction

Polymers have been widely applied in the medical field for centuries [1–3]. From poly(methyl)methacrylate (PMMA) to silicone, these versatile materials have predominantly served as implants, facilitating the restoration of function in affected organs, joints or ligaments. Furthermore, owing to their diverse compositions and structure, their use is not restricted to implants and extends to all kinds of medical devices such as sutures, catheters, ocular lens or heart valves. In such devices, the polymeric material may serve as either a subcomponent or constitute the bulk of the entire device [4]. These materials exhibit controllable biological, chemical and physical properties, which can be precisely tailored to suit the specific requirements of a given area. Polymers offer numerous advantages that make them as promising biomaterials when compared to metals and ceramics. These advantages include ease of processing, compatibility with tissues and blood, biological stability, robustness and impressive mechanical properties for *in vivo* applications [3,5–7]. In particular, polyethylene terephthalate (PET), a commonly utilized polymer in the healthcare

field, stands out due to its biocompatibility, exceptional uniformity, robust mechanical strength and resistance to chemical and abrasion damage. Nevertheless, the inherent hydrophobic nature of PET results in a persistent vulnerability to bacterial contamination, making its mitigations and prevention an ongoing challenge [8]. In fact, one of the main drawbacks related to biomaterials is the incidence of implant-associated infection (IAI), which is increasing over the years. Long-term antibiotic administration is often required for the treatment of this serious complication. However, once bacterial colony is formed, drugs tend to fail biofilm penetration and, consequently, the effectiveness in killing bacteria decreases drastically. Thus, patients affected with biofilm formation on or near implants cannot be treated and additional surgery is frequently required to eliminate, drain, or, even, remove the implant. Consequently, further modifications are required to prevent such bacterial contamination [9,10].

Additionally, it is essential to highlight the pivotal role played by the implant surface in facilitating rapid integration with host tissues [11]. An early integration of the biomaterial has shown to be crucial for preventing bacterial adhesion and colonization. Upon implantation, not only bacteria but also host cells and proteins tend to adhere rapidly to biomaterial's surface providing prompt healing [11]. This intriguing phenomenon is often referred to as "race for the surface" [12,13], where host cells and bacteria compete to adhere onto the surface of biomaterial [14]. The adhesion of plasma proteins triggers subsequent events such as fibrin formation, coagulation cascade and the recruitment of inflammatory cells [11,12,15]. However, these events can be altered causing an increment on blood clotting, which provides an inflammation and resulting in a prosthesis failure [14]. Recently, the field of polymeric biomaterials has advanced toward the design and development of new materials with enhanced biological or mechanical functionality for specific purposes.

As previously commented, the physicochemical properties of a biomedical device's surface are crucial not only for a good biocompatibility but also for its capacity to exhibit antibacterial, anticoagulant and anti-inflammatory behavior [16,17]. For this purpose, recent advancements in surface modification strategies, including surface functionalization, grafting, surface topography modification and coating techniques have demonstrated their efficacy in reducing or preventing bacterial contaminations [18–20]. Furthermore, they offer control over the adhesion of cell and proteins on biomaterial surfaces [9,21,22]. Regarding surface topography modification, simple physical variation in surfaces can offer anti-adhesive properties to plastic materials since surface properties such as roughness, hydrophilicity and surface energy may be altered [17,23]. On the other hand, methodologies based on chemical surface

modification has demonstrated also excellent protection against bacteria and other microorganism, resulting in both anti-adhesive and biocidal effects. This way, drug immobilization approaches have emerged as a promising strategy to provide significant antibacterial, anti-inflammatory and anticoagulant activity [24].

Numerous methods can be found in the literature for enhancing surfaces properties [25], endowing them with antibacterial, anti-inflammatory and anticoagulant characteristics through chemical modification [10,26]. For instance, plasma treatment [27,28], ozone treatment [29], radiation, hydrolysis[30], oxidation and enzymatic modification are frequently employed due to the simplicity of the procedures. It is important to notice that the selected functionalization method can change the microstructure and nanostructure of a polymeric surface, which, therefore, may change surface roughness [17]. Additionally, several studies have proven surface roughness, by itself, can affect the hydrophilicity of the surface. Regarding surface wetting, this phenomenon can be either homogeneous or heterogeneous, which has different impact in bacterial adhesion. According to the Wenzel's phenomenon [31], on homogenously wetted surfaces, both hydrophilicity and hydrophobicity properties are enhanced by an increasing roughness. In this case, hydrophilic surface will become more hydrophilic, whereas the hydrophobicity of a hydrophobic surface will increase. However, one of the main drawback of biocidal methodologies is that they tend to modify the bulk of polymers and lead to a loss of mechanical strength. Therefore, designing and developing platforms that can improve both biocompatibility and hemocompatibility as well as provide anti-inflammatory effect without compromising the properties of the material is highly desirable.

Since it was first introduced in 1999, the use of Click Chemistry has been rising over years due to its mild reaction conditions required and easily available reagents [32]. Moreover, comparing to traditional cross-linking reactions (e.g., carbodiimide), click chemistry shows higher efficiency [33,34]. On the other hand, the use of Click Chemistry with drugs is especially advantageous as there are rarely any nonaromatic double bonds for undesirable side reactions to take place [35]. Among click reactions, the Copper (I)-Catalyzed Azide Alkyne cycloaddition reaction (CuAAC) has gained prominence as the preferred method for conjugating diverse biomolecules, due to its orthogonal nature. The reaction exhibits exceptional chemoselectivity, particularly as azide groups demonstrate remarkable reactivity with alkyne moieties. Importantly, when drug are immobilized using click reactions, there is no discernible impact on the biological acitivity of the molecule. In fact, the pharmacophore functional groups remain unaltered in the compound [35]. Additionally, obtained 1,2,3-triazole is

considered as peptide mimetic, but being inert to enzymatic hydrolysis [36,37]. This reaction has been widely employed for the immobilization of not only drugs, but also nanoparticles, biomolecules, proteins, overall different agents with anti-inflammatory and bactericidal properties [38–41].

Among innovative biomolecules, curcumin has garnered attention in recent years due to their beneficial biological properties. Curcumin, also known as diferuloylmethane with the chemical name of 1,7-*bis*(4-hydroxy-3-methoxyphenyl)-1,6-heptadiene-3,5-dione, constitutes the main phytochemical of *Curcuma longa* L. rhizome [42]. This natural polyphenol has been traditionally used in Asian countries as a remedy to treat different disorders, owing to its diverse biological activities, which encompass antioxidant effects [43], anti-inflammatory properties, anti-mutagenic attributed, antimicrobial and antifungal capabilities [44], as well as its potential in anticancer applications [45,46]. Turmeric is a spice that has received much interest from both medical, scientific and culinary worlds. It is derived from the *rhizomatus herbaceous perennial* plant, known as *Curcuma longa*, a member of the ginger family [47]. The medical properties of turmeric, which is the source of curcumin, have been recognized for thousand years, however the precise mechanism of actions as well as the bioactive components have been recently researched.

Regarding the chemical structure, unlike other mentioned drugs, curcumin undergoes a phenomenon known as keto-enol tautomerism, where the molecular structure can shift between two forms depending on the acidity of the media. In acidic and neutral environments, the keto form is the more prevalent tautomer, while in alkaline conditions, the equilibrium is shifted to the enolic tautomer (**Figure 3.1**) [43,48]. The enol form is stabilized by resonance-assisted hydrogen bonds. This phenomenon hinders the typical characterization and isolation of curcumin and its analogs. According to Payton *et al.*, curcumin exists mostly in mixture of the keto-enol tautomers in variety of solvents (chloroform, mixture of DMSO and water, buffered aqueous DMSO solutions) [49].

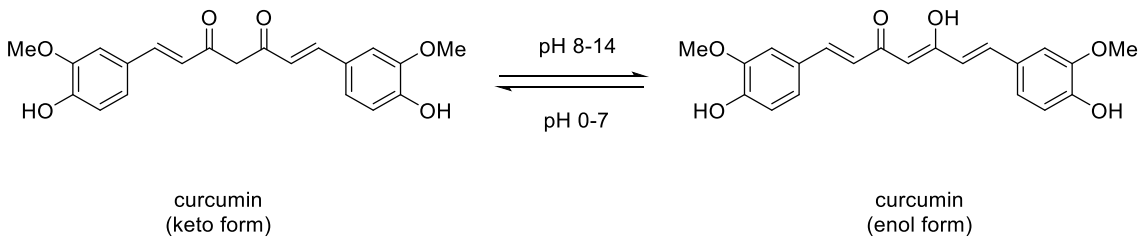

Figure 3.1. Curcumin tautomers.

As commented, curcumin exhibits a wide range of biological activities and interacts with numerous biological targets [46]. To understand the biological activity of the curcumin and its analogs, the relationship between their chemical structures and biological activities, the SAR, will be described.

Regarding anti-inflammatory activity, current studies suggest that this turmeric compound exhibits anti-inflammatory effects through a range of mechanisms, targeting multiple sites within the inflammation pathway [50]. Similarly to other anti-inflammatory drugs, numerous studies have shown that curcumin can also modulate inflammation by inhibiting the activity of COX2 as well as lipoxygenase enzyme (LOX), which are the responsible for the production of pro-inflammatory mediators like prostaglandins and leukotrienes [51]. By blocking these enzymes, curcumin helps to reduce the production of inflammatory molecules. Beside enzyme inhibition, it has shown to modulate several signaling pathways involved inflammation such as nuclear factor-kappa β (NF-kβ) and mitogen-activated protein kinases (MAPKs). NF-kB is a key transcription factor that regulates the expression of many pro-inflammatory genes, whereas MAPKs are proteins involved in cellular responses to inflammation. Overall, curcumin can inhibit the activation of NF-kB and MAPKs by suppressing the expression of pro-inflammatory genes and reducing inflammation. Additionally, curcumin has been found to inhibit the production of inflammatory cytokines, such as tumor necrosis factor-α (TNF-α), interleukin-1-β (IL-1β) and interleukin-6 (IL-6). Furthermore, curcumin has been shown to modulate immune cell function, including the regulation of immune cell proliferation, differentiation and activation. It can also influence the expression of adhesion molecules involved in immune cell trafficking and migration to sites of inflammation.

With reference to the chemical structure and anti-inflammatory activity, some studies concluded that the β-diketone moiety plays a crucial role in this biological activity [52]. Additionally, no substitutions on the phenyl groups led to a decrease in the inhibitory activity. Therefore, proper substitution of the phenyl rings is required. Moreover, the substitution in *para* position with hydroxy groups is essential, since its absence shown weak or no anti-inflammatory effects. Similarly, the introduction of substituents at adjacent positions to the phenolic hydroxy group (or *meta* to phenyl rings) has a significantly impact in the anti-inflammatory activity. Among the substitutions tested, dimethyl substitution displayed the highest enhancement in activity, followed by diethyl, dimethoxy and diisopropyl. However, longer ramifications such as ditetrabutyl resulted in a reduction of the anti-inflammatory activity likely due to its bulky nature. Additionally, it is worth noting that di-substitution enhanced the ability to inhibit COX more than mono substitution.

Curcumin also manifests antioxidant properties [45,53], which play a crucial role in its anti-inflammatory effects. Oxidative stress is closely associated with inflammation and this turmeric compound acts as a potent scavenger of reactive oxygen species (ROS), thereby reducing oxidative damage and dampening the inflammatory response. Natural antioxidative compounds can generally be categorized into two types: phenolic compounds and β-diketone compounds. Although curcumin fall into β-diketone compounds, its chemical structure presents both moieties, therefore both groups protect cells from oxidative damage by neutralizing free radicals. Regarding again the chemical structure of curcumin, it has been proved that the dimethoxy substitution on *meta* position is essential to maintain this activity. Indeed, absence of one or both methoxy groups resulted in decreased antioxidant activity. Several models suggest that the phenolic moieties are important to obtain potent antioxidant activity.

Additionally, it has been proved that curcumin exhibits a remarkable range of antimicrobial activities, including potent antibacterial and antiviral properties [54]. Studies have demonstrated that it is effective as an antibacterial agent against both Gram-positive and Gram-negative bacteria by disrupting their cell membranes. Additionally, the antibacterial activity of mono- and di-glucoside derivatives of curcumin agains *Streptococcus pneumonia* has been described by Adamczak *et al*. [54]. The multifaceted antimicrobial potential of curcumin makes it an intriguing candidate for further research and development as natural therapeutic agent against microbial infections.

All these properties make curcumin a powerful candidate to use in medical field. However, one of the main drawbacks of this compound is its poor overall oral bioavailability mainly due to its very low solubility in aqueous media, in fact, only 0.391 g/mL is soluble in water [55]. According to pharmacokinetic investigations, curcumin displays minimal absorption, undergoes metabolism, and is rapidly eliminated. Furthermore, this natural polyphenol is susceptible to degradation *via* acidic and alkaline hydrolysis, oxidation, and even light exposure [48]. As a consequence of the great therapeutic importance of curcumin, it has prompted extensive research to enhance its performance. Various approaches have been explored, including direct covalent modification and encapsulation in molecular containers. For example, materials such as chitosan [56,57] or cellulose [58], surfactants or cyclodextrins [59] have been employed as encapsulation systems for curcumin. Another strategy to enhance bioavailability is immobilizing curcumin on material surfaces. In this sense, various works of curcumin immobilization on metallic surface have been described, such as the modification of titanium with

curcumin by He *et al.* [60], employing a catechol approaching to combat fibrous encapsulation. However, immobilizing curcumin on polymeric surface remains a challenge.

Thus, considering the numerous advantages of click reactions and the unique characteristics exhibited by curcumin, we aim to employ CuAAC for modifying PET surfaces with curcumin as a potential solution for combating bacterial adhesion, inflammation prevention and coagulation inhibition. To the best of our knowledge, this study describes the pioneering bioconjugation of curcumin to a polymeric surface. In addition, *in vitro* biological test have been carried out corroborating diverse activities of curcumin in modified PET surfaces.

3.2. Materials and methods

3.2.1. Materials

Polyethyeleneterephthalate (PET, HIFI film Industry) films were employed as substrate with an average thick around 75 µm. Ethanol (EtOH, 99%, Macron Fine Chemicals, Gliwice, Poland), acetonitrile (CH_3CN, 99%, Panreac, Darmstadt, Germany), dichloromethane (CH_2Cl_2, 99%, Macron Fine Chemicals, Gliwice, Poland), acetic acid (99%, Sigma Aldrich, St. Louise, MO, USA), ethyl acetate (EtOAc, 99%, Sigma Aldrich, St. Louise, MO, USA), deuterated chloroform ($CDCl_3$, 99.8 %, Sigma Aldrich, St. Louise, MO, USA), deuterated acetone ($(CD_3)_2CO$), 99.8 % Sigma Aldrich, St. Louise, MO, USA) and Milli Q water were used as a solvents. Sodium hydroxide (NaOH, 99%, Panreac, Darmstadt, Germany), *N*-(3-dimethylaminopropyl)-*N'*-ethylcarbodiimide hydrochloride (EDC·HCl, 98%, Sigma Aldrich, St. Louis, MO, USA), *N*-hydroxysuccinimide (NHS, 98%, Sigma Aldrich, St. Louis, MO, USA), 3-bromo-1-propyne (97.5%, Sigma Aldrich, St. Louis, MO, USA), 3-bromopropan-1-amine hydrobromide (98%, Sigma Aldrich, St. Louis, MO, USA), triethylamine (Et_3N, 99%, St. Louis, MO, USA), sodium azide (NaN_3, 99.5%, St. Louis, MO, USA), copper (II) sulfate pentahydrate ($CuSO_4 \cdot 5H_2O$, 98%, St. Louis, MO, USA), sodium ascorbate (98%, St. Louis, MO, USA), sodium sufate anhydrous (Na_2SO_4, 96%, Panreac, Darmstadt, Germany), sodium chloride (NaCl, 98%, Panreac, Darmstadt, Germany), O-toluidine blue (TBO, dye content 80%, Sigma Aldrich, St. Louis, MO, USA), dansyl chloride (<99%, Sigma Aldrich, St. Louis, MO, USA), curcumin (<99%, Sigma Aldrich, St. Louis, MO, USA).

For *in vitro* biological tests various reagents and solvents were purchased from: For *in vitro* biological tests various reagents and solvents were employ: DMEM (Merck, Sigma-Aldrich, Darmstadt, Germany), fetal bovine serum (FBS) (Thermo Fisher

Scientific, Carlsbad, CA, USA), streptomicyin (Thermo Fisher Scientific, Invitrogen, Carlsbad, CA, USA), penicillin (Thermo Fisher Scientific, Invitrogen, Carlsbad, CA, USA), L-glutamine (Thermo Fisher Scientific, Invitrogen, Carlsbad, CA, USA), HEK293 cells (Sarstedt, Hildesheim, Germany), phorbol myristate acetate (PMA) (Merck, Sigma-Aldrich, Darmstadt, Germany), RPMI-1640 medium (Merck, Sigma-Aldrich, Darmstadt, Germany) lipopolyssacharide (LPS, Merck, Sigma-Aldrich, Darmstadt, Germany) , *Escherichia coli* (ATCC25922), *Staphylococcus aureus* (ATCC29213) and *Staphylococcus epidermidis* (ATCC35984)(Thermo Fisher Scientific, Invitrogen, Carlsbad, CA, USA), PBS^{Mg} (Merck, Sigma-Aldrich, Darmstadt, Germany). The blood was taken from a healthy donor in accordance with a protocol approved by the Basque Committee of Ethics and Clinical Research PS2022025.

3.2.2. Experimental procedure

3.2.2.1. General procedure for synthesis of 3-azidopropan-1-amine

3-bromopropan-1-amine hydrobromide (2.28 g, 10.4 mmol) was dissolved in a mixture of water/acetonitrile (1:1) (15 mL) and NaN_3 (2.78 g, 42.8 mmol) was added. Then, the mixture was refluxed for 48 h. After cooling to room temperature, the solution was basified by addition of NaOH (2 M) aqueous solution, and the mixture was extracted with dichloromethane (3x15 mL) and washed with a saturated solution of sodium chloride (2 x 15 mL). Organic layers were collected, dried over anhydrous Na_2SO_4 and the solvent was evaporated to afford 3-azidopropan-1-amine as a yellowish oil (0.77 g, % 77).[61] ^{1}H-NMR (300 MHz, $CDCl_3$) (δ, ppm): 2.92 (t, *J* = 6.6 Hz, 2H, CH_2, H_3), 2.33 (t, *J* = 6.6 Hz, 2H, CH_2, H_1), 1.99 (bs, 2H, NH_2), 1.29 (q, *J* = 6.6 Hz, 2H, CH_2, H_2); ^{13}C-NMR (75 MHz, $CDCl_3$) (δ, ppm): 48.8 (N_3-CH_2, C_1), 38.5 (NH-CH_2, C_3), 31.5 (CH_2, C_2).

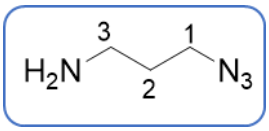

*3.2.2.2. Synthesis of dansyl derivative **2b***

Dansyl chloride (2.00 g, 7.40 mmol) was dissolved in dichloromethane (20 mL) and propargylamine (0.48 mL, 7.40 mmol) and triethylamine (0.75 g, 7.40 mmol) were added. The reaction was refluxed for 48 h. After cooling to room temperature, a portion of water was added to the reaction and the solution was extracted with CH_2Cl_2 (3x10 mL) and washed with a saturated solution of sodium chloride (2x10 mL). Organic layers were collected, dried over anhydrous Na_2SO_4 and the solvent was evaporated under *vacuum* to afford 5-(dimethylamino)-*N*-(prop-2-yn-1-yl)naphthalene-1-sulfonamide (**2b**) as a yellowish oil (0.95 g, 89%). ^{1}H-NMR (300 MHz, $CDCl_3$) (δ, ppm): 8.52 (d, *J* = 8.5 Hz, 1H, CH_{arom}, H_7), 8.30-8.28 (m, 2H,

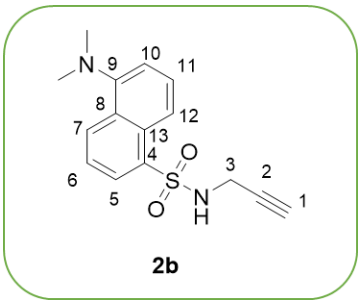

2b

CH_{arom}, H_5 and H_{12}), 7.54-7.51 (m, 2H, CH_{arom}, H_6 and H_{11}), 7.18 (dd, *J* = 7.5 Hz, *J* = 0.54 Hz, 1H, CH_{arom}, H_{10}), 5.26 (s,1H, NH), 3.77 (d, *J* = 2.5 Hz, 2H, CH_2, H_3), 2.86 (s, 6H, 2xCH_3), 1.91 (t, *J* = 2.5 Hz, 1H, ≡CH, H_1); ^{13}C-NMR (75 MHz, $CDCl_3$) (δ, ppm): 152.0 (C_{arom}-N, C_9), 135.5 (C_{arom}-S, C_4), 132.6 (C_{arom}-H, C_7), 131.3 (C_{arom}-C, C_{13}), 129.5 (C_{arom}-H, C_5), 129.2 (C_{arom}-H, C_6), 128.5 (C_{arom}-H, C_{11}), 123.2 (C_{arom}-H, C_{12}), 118.9 (C_{arom}-C, C_8), 115.3 (C_{arom}-H, C_{10}), 84.3 (C≡C, C_2), 71.2 (≡CH), 45.2 (N-(CH_3)$_2$), 33.2 (CH_2).

*3.2.2.3. Synthesis of curcumin derivative **5a***

Curcumin (2.10 g, 5.60 mmol) was dissolved in acetonitrile (20 mL) and potassium carbonate (0.80 g, 6.20 mmol) and propargyl bromide (0.70 mL, 6.60 mmol) were added. Then, reaction was stirred during 48 h at room temperature. After that, the reaction was stopped by adding water and dichloromethane, the phases were separated, and the aqueous phase was extracted with ethyl acetate (3x30 mL). Then, combined organic phases were washed with a saturated solution of sodium chloride (2x30 mL). Finally, organic phase was collected, dried over anhydrous Na_2SO_4 and solvent was evaporated under *vacuum* to afford (1*E*,6*E*)-1-(4-hydroxy-3-methoxyphenyl)-7-(3-methoxy-4-(prop-2-yn-1-loxy)phenyl)hepta-1,6-diene-3,5-dione (**5a**) as a yellowish oil (1.5 g, 71%). ^{1}H-NMR (300 MHz, $CDCl_3$) (δ, ppm): 7.61

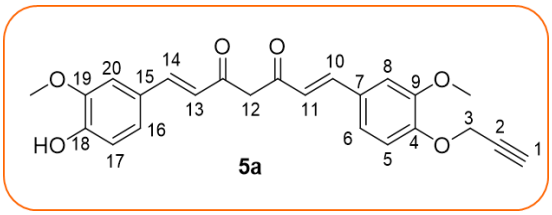

5a

(d, *J* = 15.8 Hz 2H, CH, H_{10} and H_{14}), 7.18 (d,*J*= 15.8 Hz, 1H, CH, H_{11} or H_{13}), 7.15-6.88 (m, 4H, CH_{arom}), 6.81 (d, *J* = 2.4 Hz, 2H, CH_{arom}, H_8 and H_{20}), 6.46 (d, *J*= 15.8 Hz, 1H, CH, H_{11} or H_{13}), 6.21 (s, 1H, OH), 4.81 (d, *J*= 1.2 Hz, 2H, OCH_2, H_3), 3.64 (s, 2H, CH_2, H_{12}), 3.95 (s, 3H, OCH_3), 3.92 (s, 3H, OCH_3), 2.54 (t, *J*= 1.2 Hz, 1H, ≡CH, H_1),); ^{13}C-NMR (75 MHz, $CDCl_3$) (δ, ppm): 183.7 (C=O), 182.6 (C=O), 149.7 (C_{arom}-OCH_3, C_{19}), 149.4 (C_{arom}-OCH_3, C_9), 148.6 (C_{arom}-OCH_2, C_4), 147.2(C_{arom}-OH, C_{18}), 139.9 (C=C, C_{10} and C_{14}), 130.9 (C=C, C_{11} and C_{13}), 127.8 (C_{arom}-C), 127.2 (C_{arom}-C), 122.9 (C_{arom}-H), 122.2 (C_{arom}-H), 121.3 (C_{arom}-H), 122.0 (C_{arom}-H), 115.14 (C_{arom}-H), 109.4 (C_{arom}-H), 78.7 (C≡C, C_2), 76.4 (≡CH, C_1), 48.8 (2xOCH_3), 38.5 (OCH_2, C_3), 31.5 (CH_2, C_{12}).

3.2.3. Preparation of PET films

3.2.3.1. Hydrolysis of PET samples

In this chapter polyethylene terephthalate sheets 20x20 mm dimensions were used as a polymeric substrate. All PET films were thoroughly cleaned in ultrasound bath with distilled water and ethanol three times. Then, samples were dried overnight at 30 ºC before surface modification. Hydrolysis process was performed by the immersion of PET films in NaOH 4 M at 70 °C during 3 h. After that, samples were washed with an aqueous solution of HCl 1M. Finally, they were immersed in deionized water for 90 min, sonicated in EtOH and dried overnight at 40 °C under *vacuum* for further modifications [62].

3.2.3.2. Amidation of hydrolyzed PET samples

After activating PET substrates by chemical hydrolysis, samples were exposed to amidation conditions following the procedure employed in a first work [63,64]. Briefly, PET-COOH samples were introduced in an acetic/acetate buffer solution with EDC·HCl and NHS for 24 h. In this case, 3-azidopropan-1-amine (2.00 g, 19. mmol) was employed as amine.

3.2.3.3. Immobilization of drug derivatives onto modified PET samples

Once dried, corresponding dansyl derivative **2b** or curcumin derivative **5a** (1 mmol) was dissolved in a mixture of EtOH/H_2O 1:1 (v/v), then $CuSO_4 \cdot 5H_2O$ (0.025 g, 0.10 mmol) and sodium ascorbate (0.025 g, 0.13 mmol) were added to solution. Once the solution was homogeneous, previously amidated PET films were immersed on it during 72 h at room temperature. Finally, the samples were removed from the solution vials, thoroughly washed with distilled water to eliminate non-immobilized drug species and dried at room temperature for 24 h.

3.2.4. Physicochemical characterization of biomolecules and PET samples

3.2.4.1. Nuclear Magnetic Resonance (NMR)

The proton (^{1}H-NMR) and carbon thirteen (^{13}C-NMR) nuclear magnetic resonance spectra were performed at room temperature in a Bruker AV-300 (300 MHz for ^{1}H and 75.4 MHz for ^{13}C) using deuterated chloroform as solvent. Chemical shifts (δ) are expressed in parts per million (ppm) relative to TMS using the residual signal of

the solvent [7.26 ppm (^{1}H) and 77.0 (^{13}C)] as internal reference. Coupling constants (*J*) are expressed in Hertz (Hz).

3.2.4.2. Colorimetric Quantification via UV-Vis Spectroscopy

The amount of grafted carboxylic groups (-COOH) in the hydrolysis process can be determined by a colorimetric method using TBO as a colorant. Chollet *et al.* described this method as an ionic interaction between the cationic colorant and the carboxylate groups [65]. Hydrolyzed PET films were immersed in a TBO $5x10^{-4}$ M basic solution for 5 minutes. Then, the films were removed and washed in a NaOH 2 M solution, so that the excess of TBO could be removed. Subsequently, the films were immersed in an acetic acid 50% aqueous solution in order to release the attached TBO and the solution was measured by UV-VIS (Shimadzu MultiSpec-1501 spectrophotometer). The concentration of the carboxyl groups was determined using a calibration plot (Abs= 75301 x M; R^2 = 0.9984) by measuring the optical absorbance at 633 nm and based on the assumption that the stoichiometry of the interaction between TBO and –COOH groups is 1:1 [66]. The amidation was determined employing equation (1).

$$\% \text{ Surface Amidation} = \frac{\text{nPET-COOH-nPET-Amidated COOH}}{\text{nPET-COOH}} x\ 100 \quad (1)$$

3.2.4.3. X-ray Photoelectron Spectroscopy (XPS)

The elemental analysis of modified PET films was determined by X-ray photoelectron spectroscopy SPECS system (XPS, SPECS Surface Nano Analysis, Berlin, Germany) using focus monochromatic radiation source 500 with dual anode Al/Ag and it is equipped with a Phoibos 150 1D-DLD analyser (Berlin, Germany). During the measurements stainless steel holders and carbon tape were used to fix samples. Additionally, all measurements were determined by using carbon reference.

3.2.4.4. Epifluorescent Microscopy

The fluorescence analysis of PET surfaces were performed before and after click reaction using an epifluorescence microscope Zeiss Axioskop (Jena, Germany).

3.2.4.5. Water Contact Angle (WCA)

The change in hydrophobicity in PET films caused by surface modifications was analyzed using contact angle method (NEURTEK Instruments OCA 15 EC, Eibar, Spain). Milli-Q water was used as a testing liquid and sessile drop method (3 µL per

drop) was carried out at room temperature to do the measurements. The average values were calculated using 10 measurements of each composition.

3.2.4.6. Scanning Electron Microscope (SEM)

Surface morphology of all samples was monitored by a Fine coat ion sputter JFC-1100 Scanning electron microscope (SEM). The micrographs were taken using a Hitachi 4800 (Singapore) and operated at 15 kV, 20 mA, 150 and zoom at nm. All SEM images were analyzed and processed by image analysis freeware Fiji.

3.2.4.7. Compressive stress/strain tests

The study of the mechanical properties of 20x20 mm sized films was performed in an AGS-X Universal Testing Machine from Shimadzu at a constant jack speed of 5 mm/s with a load cell of 500 N until fracture.

3.2.4.8. Mass loss measurements

The study of the loss of mass of the films after hydrolysis, amidation and click reactions was performed by weighting the functionalized samples after each process.

3.2.4.9. Differential Scanning Calorimetry (DSC)

The glass transition temperature of the pristine PET and PET-Cur were measured by differential scanning calorimeter (DSC) with a DSC METTLER TOLEDO 822^{e} instrument (Greifensee, Switzerland) equipped with STAR© v14.0 software. The samples (~10 mg) were placed in 100 µL aluminum crucibles. Samples were heated from 0 °C to 300 °C, employing a scanning rate of 10 °C·min^{-1} under a nitrogen atmosphere with a flow rate of 20 mL/min.

3.2.4.10. Dynamic Mechanical Thermal Analysis (DMTA)

Dynamic mechanical thermal analysis (DMTA) was carried out in the tensile mode by a DMA1-METTLER TOLEDO instrument (Greifensee, Switzerland) equipped with STAR© v14.0 software for curve analysis. Storage modulus (E'), loss modulus (E") and loss factors (tan δ) values were collected at 3 °C·min^{-1} heating rate from 0 to 250 °C, displacement of 20 µm, and 1, 3 and 10 Hz frequencies. Samples of 2 x 1 cm and thickness of 80-90 µm were prepared. The glass transition was assigned at the maximum of the loss factor (tan δ = E"/E').

3.2.4.11. Cytotoxicity assay

HEK293 cells (40 $\times 10^3$) in DMEM supplemented with 10% FBS (v/v), 100 µg/mL streptomycin, 100 U/mL penicillin and L-glutamine were seeded by adding a 50 µL drop in the different pristine PET and PET-Curcumin surfaces (2 mm diameter) and allowed to attach during 1 h at 37 °C and at 5% CO_2. Then, pristine PET and curcumin functionalized PETs were transferred to a 96-well culture plate and cells were maintained for 48 h in complete DMEM 150 µL/well in a humidified incubator at 37 °C and 5% CO_2. Similar number of cells was seeded in wells without PET samples to be used as control. Cellular viability was determined by the MTS assay that evaluates the reduction of 3-(4,5-dimethylthiazol-2-yl)-5-(3-carboxymethoxyphenyl)-2-(4-sulfophenyl)-2H-tetrazolium (MTS) to formazan by enzymatic activity (mitochondrial dehydrogenases) of viable cells. After 48 h exposure, cells were washed twice with phosphate-buffered saline buffer (PBS) and 120 µL MTS reagent (CellTiter 96 Aqueous One Solution Cell Proliferation Assay; Promega, Madison, WI, USA) was added to each well. After 1 h incubation in the dark at 37 °C with a 5% CO_2 atmosphere, 100 µl of the MTS containing media was transferred to a new plate to avoid interference of all PET samples. The formazan absorbance was measured at 490 nm. To determine the viability, the background values of the wells without cells were subtracted from the values of the tested wells. The mean absorbance of the cells grown without PET and PET-Curcumin served as the reference for calculating 100% cellular viability. The results were expressed as a percentage of the viability of the untreated cells.

3.2.4.12. Analysis of pristine PET and PET-Curcumin on Inflammatory Response in vitro

THP-1 human monocytic cells were cultured in RPMI with 10% FBS (v/v), 100 µg/mL streptomycin, 100 U/mL penicillin and L-glutamine. Then, cells were differentiated to a macrophage phenotype by incubating with 20 µM phorbol myristate acetate (PMA) diluted in complete culture medium for 24 h. Differentiated cells were washed with serum-free RPMI-1640 medium, cells were detached from the culture plate and subsequently reseeded by adding a 50 µL drop containing 40 $\times 10^3$ cells in the different pristine PET and PET-Curcumin samples (2 mm diameter). Cells were allowed to attach during 1 h at 37 °C and at 5 % CO_2. Then, all PET surfaces were transferred to a 96-well culture plate and cells were maintained in the tissue culture plates for 24 h. The cells were then stimulated with 2.5 µg/mL of LPS and the levels of human IL-6 were determined at 48, 72 and 96 h by ELISA (Abcam, Spain), according to the manufacturer's protocol.

3.2.4.13. Determination of bacterial growth by spectrophotometry and viable CFU/mL

Firstly, strains and culture conditions were prepared.For this purpose, *Escherichia coli* (ATCC25922), *Staphylococcus aureus* (ATCC29213) and *Staphylococcus epidermidis* (ATCC35984) were used as test microorganism in this study. All the strains were stored as frozen stocks with 15% glycerol at -80 °C. The bacteria were cultured in Luria Bertani (LB) broth or LB agar.

Overnight bacterial cultures from single colonies grown on agar plates were diluted 10-fold in fresh medium and incubated at 37 °C until the turbidity reached an optical density between 0.08 -0.100 ($1.5x10^8$ CFU/mL) corresponding to 0.5 McFarland, measured by spectrophotometry at 600 nm. The inoculum (200 µL) containing $5x10^5$ CFU/mL of each strain was added to wells of microtiter plate containing either pristine PET or PET-Cur. The plates were incubated at 37 ºC for 24 or 48 h. Bacterial growth was evaluated by measuring the turbidity at 600 nm in a plate Reader (Bio-Tek Instruments, USA). The effect PET-Cur on bacterial growth was determined by the percentage reduction in bacterial growth compared to the bacterial growth in the presence of pristine PET.

To determine viable bacterial colony-forming units (CFUs/mL) after 24 and 48 h incubation with PET pristine or PET-Curcumin, bacterial cultured in microtiter plate were ten-fold serially diluted, and plated on nutrient agar plates. The plates were then incubated overnight at 37 ºC, and bacterial colonies were counted.

3.2.4.14. In vitro hemolysis analysis

The entire assay was meticulously conducted at a controlled temperature of 4 °C to ensure optimal preservation of biological components. Blood samples were collected in citrate extraction tubes through the Basque Biobank (http://www.biobancovasco.org) in accordance with a protocol approved by the Basque Committee of Ethics and Clinical Research PS2022025. Subsequently, 1 mL of citrated blood was transferred to 1.5 mL Eppendorf tubes. Following this, red blood cells (RBCs) were isolated by centrifugation at 500 x *g* for 5 minutes, and the resulting supernatant was carefully removed. The pelleted RBCs were then resuspended in 1 mL PBS^{Mg} ice-cold solution and, they were resuspended in ice cold PBS^{Mg} at a 30 % (v/v) concentration. Various volumes of this concentrated solution were employed for reactions with PBS^{Mg} and Triton X-100. Specifically, for pristine PET and PET-Cur samples, 33.3 µL PBS^{Mg} and 3.7 µL of RBCs (30 % v/v) were used. For 100 % hemolysis control 30.3 µL of PBS^{Mg}, 3.7 µL of RBCs (30 % v/v) and 3 µL

of Triton X-100 (10 % v/v) were combined. These reactions underwent a precisely timed incubation of 1 hour at 37°C to simulate physiological conditions. After the incubation, the reactions were place on ice for 20 min. Subsequently, RBCs were centrifuged at 500 x *g* for 5 min and the supernatant (20 µL) was placed on a new 96-well plate. Finally, each transferred supernatant was diluted with 80 µL of PBS^{Mg}, and the released hemoglobin was quantified by measuring the absorbance of the diluted supernatants at 405 nm using a microplate reader Infinite M nano (Tecan).

3.2.4.15. In vitro whole blood clotting time

Blood samples were collected in accordance with a protocol approved by the Basque Committee of Ethics and Clinical Research PS2022025. Pristine PET and PET-Cur samples were then placed on a 24-well plate, preparing one plate for each time point (15, 30 and 45 min). Immediately after the blood draw, 7 µL of blood was dispensed onto each sample. 500 µL of distilled water (DI) was deposited onto the 24-well plate and 7 µL of the drawn blood was then added for free hemoglobin positive control. After each time point, the materials with the blood drop were taken to a different 24 well plate and 500 µL of DI were added to each well. The plate was positioned on a horizontal shaker for 30 seconds at 100 rpm. After, it was moved to a bench for the release of free hemoglobin. After waiting 5 min, 200 µL of each solution was transferred to a new 96-well plate, and the absorbance of free hemoglobin was measured using a microplate reader Infinite M nano (Tecan) set at 540 nm. The statistical analysis was performed using SPSS version 27.0 (IBM). The statistical comparison between the two conditions was conducted by U by Mann-Whitney. The confidence intervals were fixed at 95 % ($p \leq 0.05$).

3.3. Results and discussion

As commented before, the aim of this work is provide antibacterial and anti-inflammatory properties to PET by employing copper catalyzed azide alkyne click reaction. For this purpose, PET sample was submitted to different surface reactions in order to immobilized modified curcumin. To test the effectiveness of the methodology, a dansyl derivative **2b** was immobilized whose fluorescence would allow us to conclude that the conjugation reaction had taken place successfully (**Scheme 3.1**)

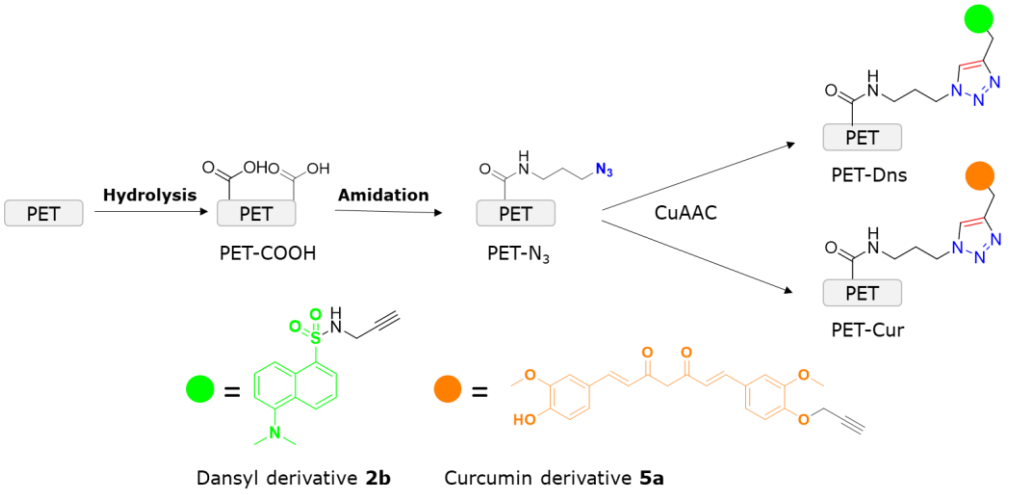

Scheme 3.1. General illustration of dansyl derivative **2b** and curcumin derivative **5a** immobilization onto PET.

3.3.1. Synthesis of curcumin derivative 5a

As commented before, this chapter will describe the immobilization of curcumin derivative employing copper catalyzed azide alkyne click reaction. This reaction required two significant main groups, azide and alkyne functional groups. Thus, one of the functional group, the alkyne, was proposed to be introduced onto the structure of curcumin by S_N2 reaction (**Scheme 3.2**).

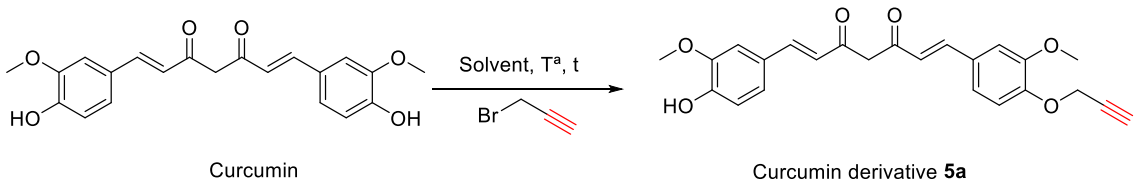

Scheme 3.2. Representative scheme of the synthesis of curcumin derivative **5a**.

In order to obtain (1*E*,6*E*)-1-(4-hydroxy-3-methoxyphenyl)-7-(3-methoxy-4-(prop-2-yn-1-yloxy)phenyl)hepta-1,6-diene-3,5-dione product several changes in reaction conditions were proposed, they are sum up in **Table 3.1**.

Table 3.1.Reaction condition employed for the synthesis of curcumin derivative **3a**

Entry	propargyl bromide (eq.)	Solvent	Tª (ºC)	t (h)	Yield (%)
1	1	acetonitrile	r.t.	24	[b]
2	1	acetonitrile	80	24	[b]
3	1	acetonitrile	80	48	71
4	1	DMF	r.t.	48	[b][c]
5	1	DMF	45	48	23
6	1	DMF[a]	45	48	43
7	1	DMF[a]	45	73	30

[a] solvents were purged with nitrogen and the reaction was performed under inert conditions [b] starting product [c] no total conversion of curcumin derivative **5a.**

After several changes in solvent, reaction time and molar ratio, the conditions employed in **entries 3,5,6** and **7** resulted in curcumin derivative **5a.** As can be seen in **Table 3.1**, the increase in temperature allowed to yield the product. However, the main problem of this reaction was the solubility of curcumin in the media. All and the products obtained were analyzed by NMR. ^{1}H-NMR spectra of curcumin and curcumin derivative **3a** are presented in **Figure 3.2**.

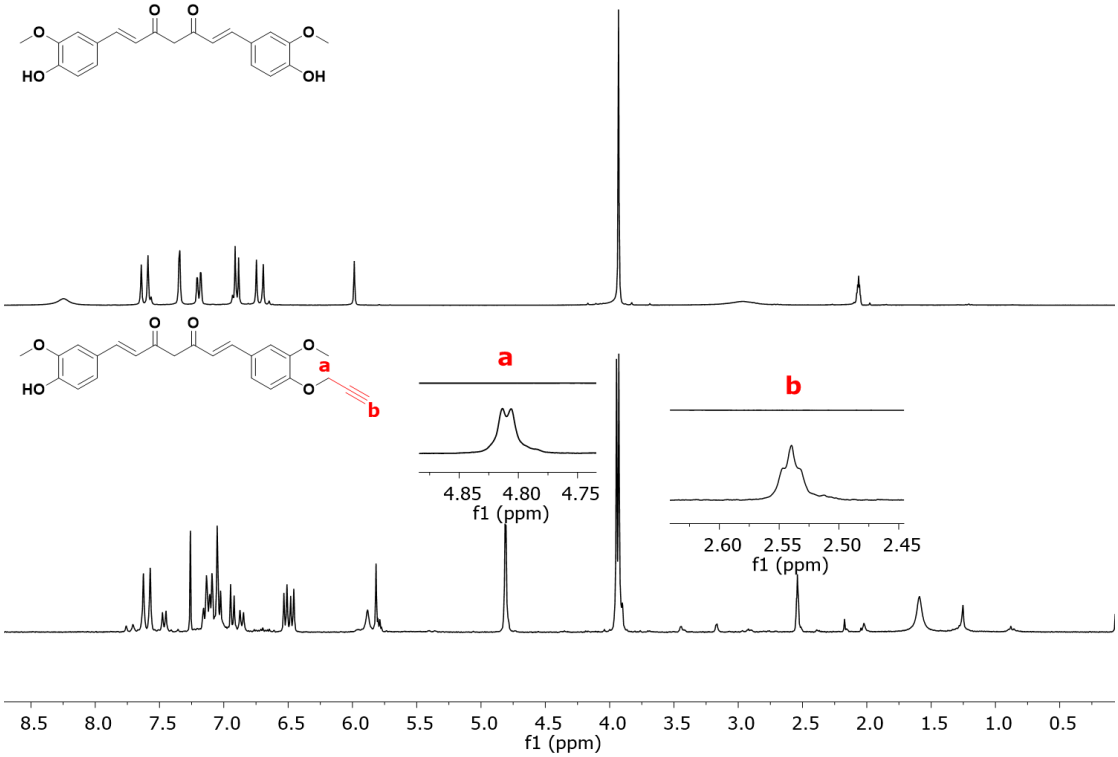

Figure 3.2. 1H-NMR spectra of curcumin (above) and curcumin derivative (**5a**)(below).

As depicted in **Figure 3.2**, the ^{1}H-NMR spectra of curcumin derivative **5a** exhibited two distinctive signals at 2.54 and 4.81 ppm, attributed to the CH_2 and CH of the propargyl moiety, respectively. Moreover, it has to be noted that curcumin exhibits symmetry, but, when the mono-functionalization occurred, this symmetry was lost. Consequently different signals can be appreciated for both aromatic rings and even the methoxide groups. This resulted in the observation of two signals with similar chemical shits in the curcumin derivative **5a** spectra.

3.3.2. *Colorimetric cuantification by Uv-Vis*

As mentioned above, the first steps of surface modification was a hydrolysis reaction and the subsequent amidation of the so-obtained carboxylic acid moieties (**Scheme 3.3**). The amount of carboxylic groups was quantitatively determined by a colorimetric method based on the ionic interaction between the TBO cation and carboxylate anions generated during PET basic hydrolysis. As can be seen in **Scheme 3.3**, after hydrolysis, PET films were submitted to amidation conditions with previously synthesized 3-azidopropan-1-amine. After amidation reaction, colorimetric method was again employed, as amide group cannot link with the cationic TBO, only unreacted acid groups can interact with it. The number of total amidated acids was determinted employing equation 1.

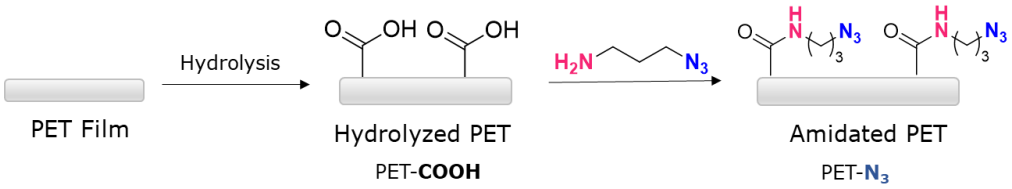

Scheme 3.3. Representative scheme of hydrolysis and amidation reactions onto PET samples.

The efficiency of hydrolysis and amidation reaction was confirmed through UV-Vis analysis. in **Figure 3.3**, the TBO solution of hydrolyzed PET (PET-COOH) analysis revelead a prominent peak at 633 nm, the absorption maximun peak of TBO specifically. After amidation reaction, the TBO content in the modified PET (PET-N_3) markedly decreased, nearly to the point of zero absorption. This observation suggested that approximately 64% of the acid groups had successfully undergone amitation with 3-azidopropan-1-amine.

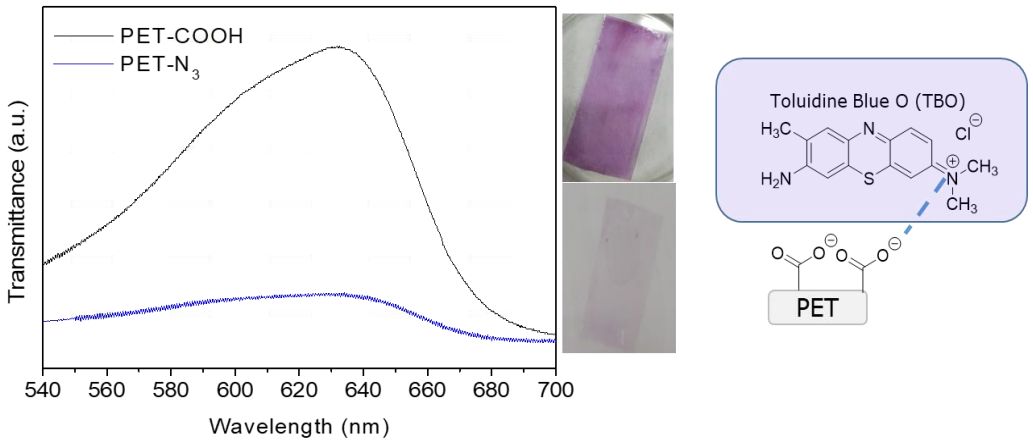

Figure 3.3. UV-Vis transmittance spectra of hydrolyzed and amidated PET.

3.3.3. XPS, fluorescence and ATR-FTIR analysis

Building upon our preliminary research [64], we aimed to validate the effectiveness of the click reaction for drug conjugation, specifically with curcumin. To do so, we first carried out the process employing a fluorescent dansyl derivative. (**Scheme 3.4**). Consequently, this fluorophore was subjected to a comprehensive analysis through both X-ray photoelectron spectroscopy (XPS) and fluorescence microscopy.

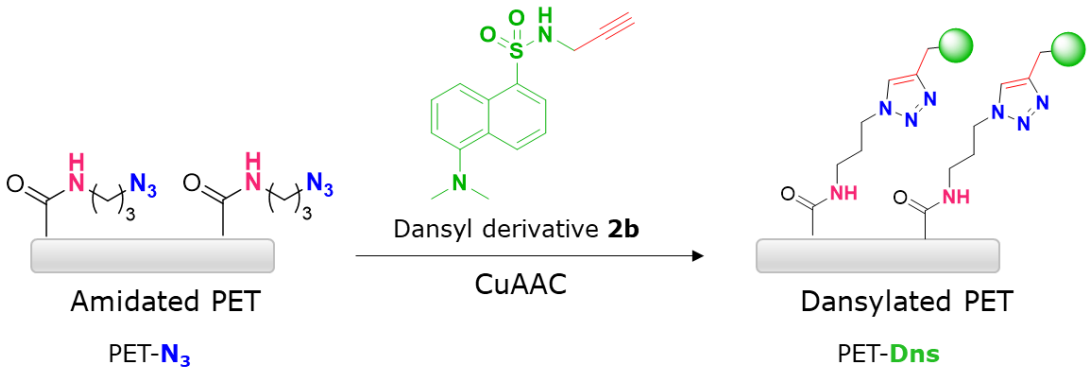

Scheme 3.4. Illustration of dansyl derivative **2b** immobilization onto amidated PET surface.

For the analysis of surface chemical compositions of the functionalized PET surfaces, XPS measurements were carried out before and after different chemical surface modifications (**Figure 3.4**). The XPS spectra corresponding to PET-COOH exhibited two main contributions C1s peak at 285 eV and O1s located at 533 eV. Meanwhile, in the high resolution spectra of C1s, three peaks appeared corresponding to C-C (284.6 eV), C-O (285.8 eV) and C=O (288.4 eV) groups, which agreed with references [67–69]. In addition, peaks at 534.8 eV and 533.3 eV in the high resolution O spectrum can also be attributed to C-O and C=O bonds, respectively, confirming the presence of these groups in PET-COOH surface. After amidation and click reaction, a noticeable increase in the C1s peak was evident due to the attachment of additional carbon-containing molecules. Moreover, discernible small peaks are presented in the dansyl modified PET sample (PET-Dns), corresponding to the contribution of nitrogen N1s with a binding energy of 395 eV, and sulphur S2p, with a binding energy of 167 eV. Additionally high resolution XPS spectra of carbon and oxygen presented some changes as depicted in **Figure 3.4A**, which further confirmed that dansyl derivative was successfully immobilized on the surface. Indeed, in C high resolution XPS spectra the signal corresponding to C-O contribution disappeared, as less content of C-O species were visible on the surface after amidation and click reaction. On the other hand, O high resolution XPS spectra exhibited a new peak at 530 eV, which can correspond to S-O bond according to references [68]. These results indicated that Copper-Catalyzed Azide-Alkyne click reaction had been efficient in the conjugation of the dansyl derivative, and therefore, the methodology had been successfully validated.

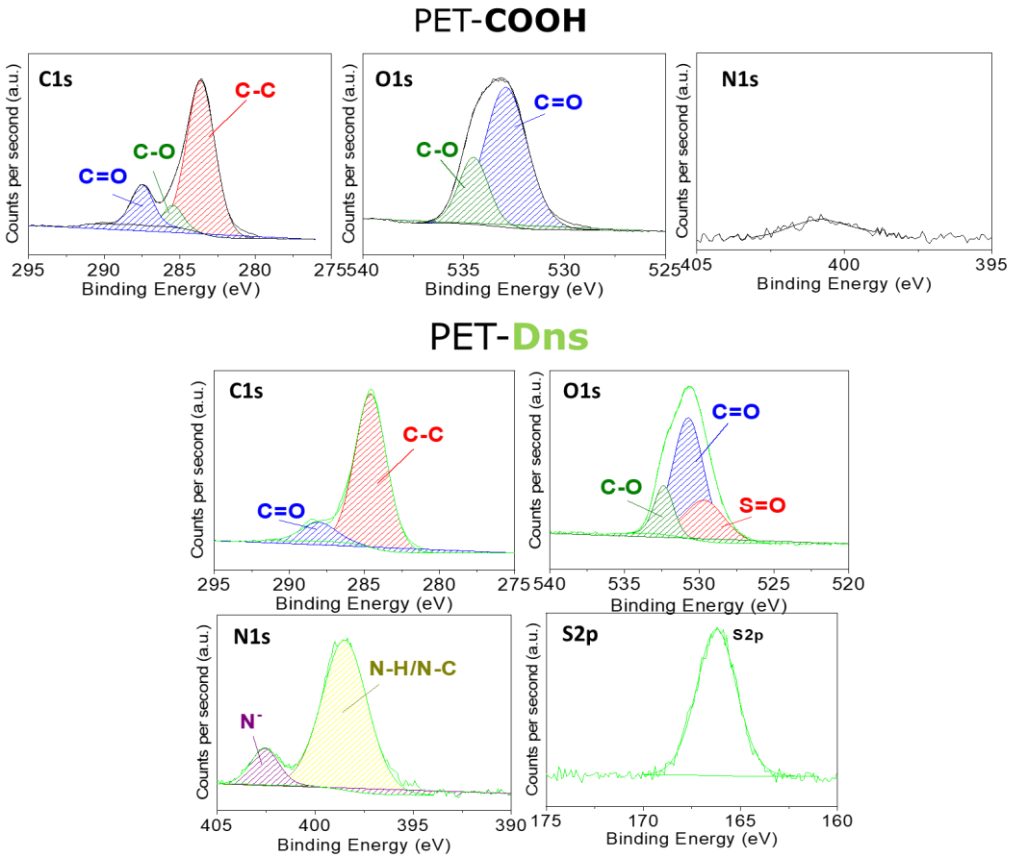

Figure 3.4. XPS spectra of PET-COOH and PET-Dns samples

As can be seen in **Figure 3.5**, the immobilization of dansyl derivative **2b** onto PET surface was further substantiated through fluorescence analysis. The fluorescent microscope revealed an intense green fluorescence owing to dansyl fluorophore onto PET-Dns surface. In addition, as it was expected, hydrolyzed PET did not show any type of fluorescence at the same power (20W).

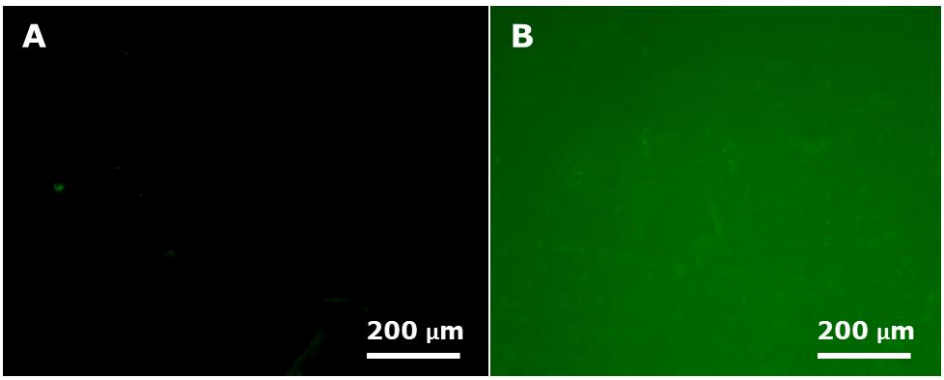

Figure 3.5. Representative fluorescence images of (A) PET-COOH and (B) PET-Dns

After validating the click conjugation process, immobilization of curcumin was carried out employing the same procedure (**Scheme 3.5**). Analysis *via* XPS revealed subtle

surface chemical alterations on carbon, oxygen and nitrogen spectra after amidation and curcumin derivative immobilization. Notably, after amidation with 3-azidopropan-1-amine (PET-N_3) a discernible peak attribute to nitrogen elements emerged at 395 eV (average value), differentiating from hydrolyzed PET (PET-COOH) (**Figure 3.6**), which indicated the presence of azido and amine in the PET surface. Additionally, the variation on contributions of nitrogen high resolution spectra after curcumin derivative immobilization confirmed the successful bioconjugation of this natural polyphenol.

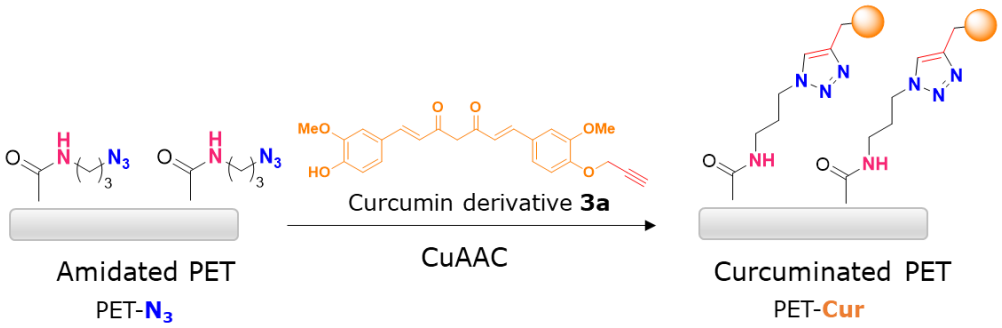

Scheme 3.5. Curcumin derivative **3a** immobilization onto modified PET surface.

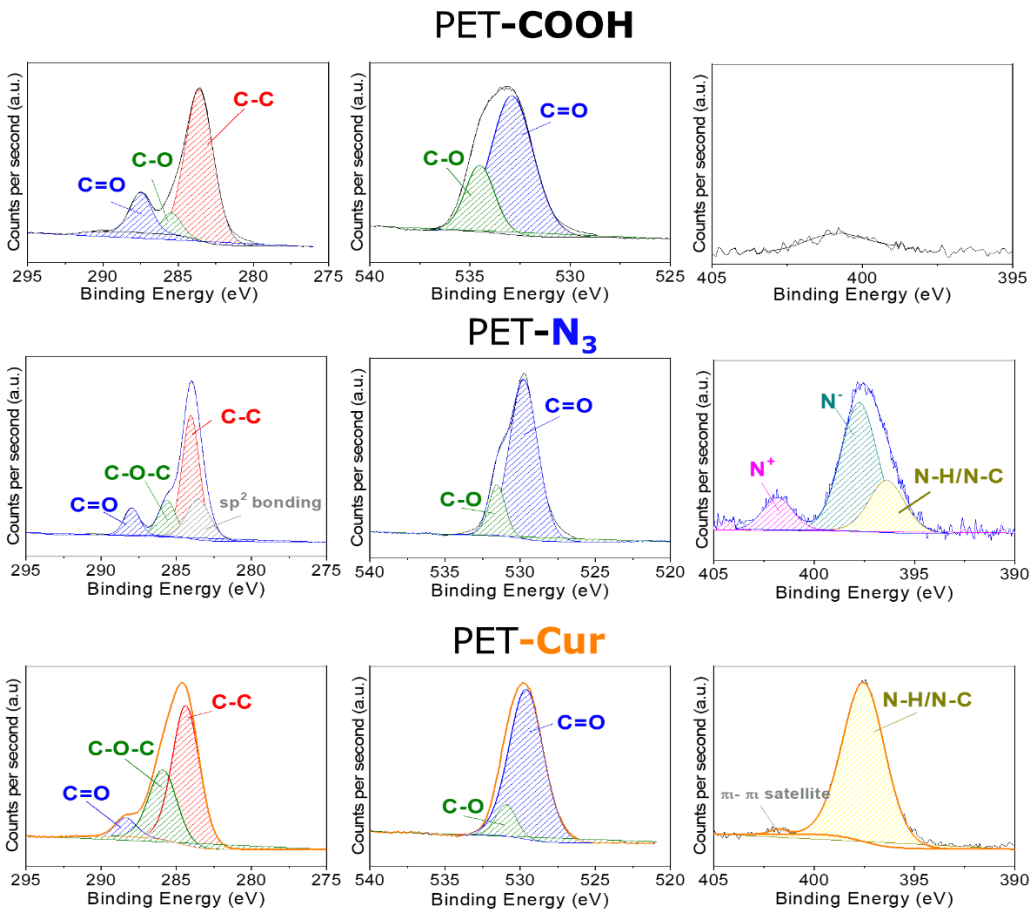

Figure 3.6. XPS spectra of modified PET-COOH, PET-N_3 and PET-Curcumin samples.

Indeed, as can be seen in **Figure 3.6**, high resolution XPS spectra of carbon and oxygen presented no significant variations. However, nitrogen high resolution XPS spectra exhibited three peaks at 396.2 eV, 398.6 eV and 402.0 eV corresponding to N-N/N-C, N^- and N^+ groups. The N^+ atom is the central nitrogen atom found in the azido functional group, which can exist in two mesomeric forms $-N=N^+=N^- \leftrightarrow -N^- - N^+\equiv N$. At the same time, N^- corresponds to the external atoms of the azido group, as the negative charge is placed onto two atoms the contribution of these peak is higher. As can be seen, the ratio of N^-/N^+ contributions is 2/1, which agrees with the chemical structure of the azido group [70]. However, it has to be noted that longer exposure of X-ray can alter N^-/N^+ ratio, since azido groups suffer from degradation. These finding further confirmed the introduction of azido group on PET surfaces. After curcumin derivative immobilization, once 1,2,3-triazole functional group is formed, the only dominant contribution is N-H/N-C peak that appeared at 398.3 eV, indicating that click reaction was carried out successfully.

Elemental compositions of carbon, oxygen, nitrogen and sulphur in each sample (PET-COOH, PET-Dns and PET-Cur) are summarized in **Table 3.2**. As expected, according to the chemical structure of PET, the hydrolyzed films are mostly made by carbon (38.7%) and oxygen (46.4%). This result suggests that the amount of oxidized functional groups on the surface is highly significant. After the click reaction carried out with dansyl derivative **2b** nitrogen and sulphur elements appeared. On the other hand, when curcumin derivative **5a** was immobilized the nitrogen amount increased. The presence of these elements indicated the successful completion of the conjugation reactions involving both dansyl and curcumin derivatives.

Table 3.2. The atomic weight percentage of hydrolyzed and functionalized PET samples.

Sample	C (%)	O (%)	N (%)	S (%)	Si (%)*
PET-COOH	70.00 ± 0.96	29.27 ± 0.58	-	-	0.73 ± 0.09
PET-N_3	69.20 ± 0.33	22.9 ± 0.54	2.1 ± 0.07	-	4.5 ± 0.12
PET-Dns	72.16 ± 0.26	26.11 ± 0.28	1.26 ± 0.12	0.86 ± 0.01	0.36 ± 0.05
PET-Cur	70.00 ± 0.53	20.65 ± 0.66	6.97 ± 0.43	-	1.88 ± 0.19

*In all samples, a small content of silicon was present due to possible contamination of glass

On the other hand, ATR-FTIR results also corroborated that all steps involved in the proposed methodology had occurred successfully (**Figure 3.7**). In fact, after hydrolysis two characteristics signals were observed corresponding to the vibration

of C=O and O-H bonds at 1760 and 3350 cm^{-1}, respectively. After amidation step with 3-azidopropan-1-amino, a remarkable peak corresponding to $-N=N^{+}=N^{-}$ was observed at approximately 2100 cm^{-1}, indicating that azido compound was successfully linked to the surface. However, as expected, this signal disappeared due to its participation in the click reaction with the alkyne residue of the curcumin derivative, resulting in a successful click reaction and drug immobilization.

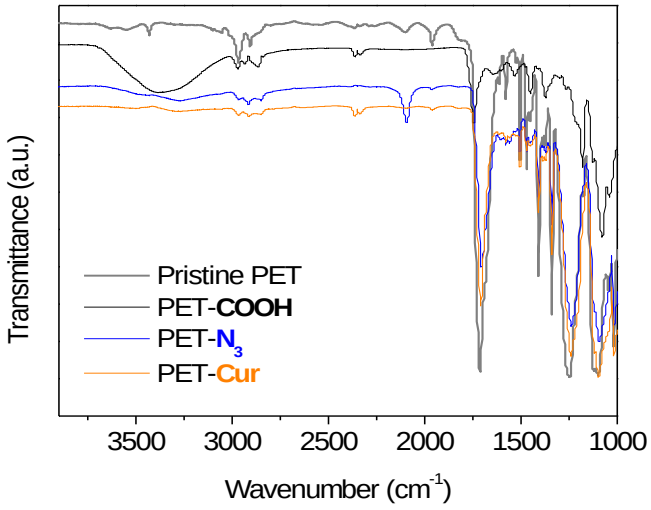

Figure 3.7. ATR-FTIR spectra of different functionalized PET surfaces.

3.3.4. Surface wettability and morphology

Surface wettability results of modified samples were obtained by water contact angle and are summarized in **Figure 3.8**. As can be seen, the static water contact angle of pristine PET was 82.0±6.7°. This value refers to as a hydrophobic nature of PET surface, which difficult further surface treatment because of lacking polar and functional groups on the PET surface. As expected, after the hydrolysis process by NaOH treatment the value of the contact angle decreased significantly to 52.5±3.1° as a result of the presence of polar groups and the increased area. The success of the subsequent amidation reaction with 3-azidopropan-1-amine was demonstrated by a further change in the contact angle. In fact, the contact angle increased to 63.3±4.4º. In this case, although the polarity of the attached functional groups diminished, the significantly important roughening of the surface could explain the small increase in the contact angle value [71]. After the immobilization of dansyl and curcumin derivatives, contact angle measurements showed similar values within a range of 74.0±2.4º to 80.8±4.2º. After both immobilizations, the WCA value increased due to the presence of aromatic rings and the formation of 1,2,3-triazole,

which are slightly hydrophobic functional groups making the surface less render to form H-bonds with water. Overall, these results indicated the successful immobilization of both dansyl derivative **2b** and curcumin derivative **5a** [72].

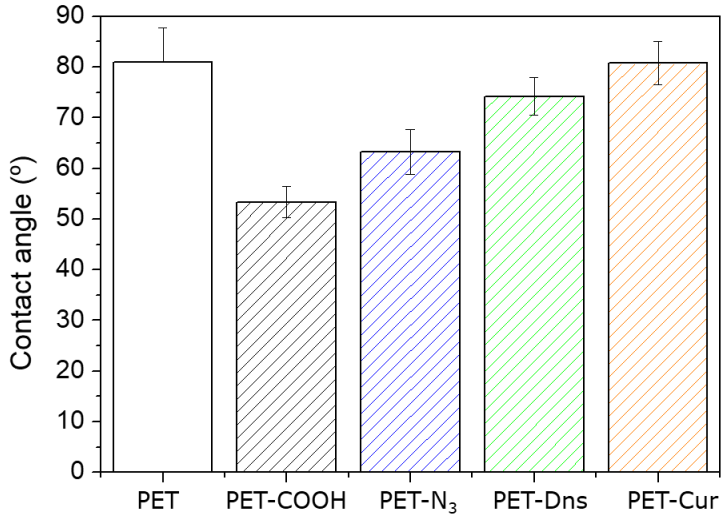

Figure 3.8. Contact angle values for different PET functionalization.

Preliminary results suggested successful modification of the polymer surfaces, which was supported by different morphologies of untreated and modified PET surfaces. SEM microscopy was employed to carry out the studies of the morphology of the surfaces (**Figure 3.9**). The reference pristine PET surface was smooth without impurities. However, after alkali treatment it became relatively rough due to the increased surface area. Moreover, after amidation process, as chemical reaction took place, fissures appeared heterogeneously along the surface and cracking and flaking made more evident due to the surface degradation of the material. Nevertheless, the particle size and distribution of immobilized dansyl and curcumin derivatives were slightly different for each sample. In PET-Dns figure, more homogeneous and shapeless surface could be observed, otherwise in PET-Cur figure, an increase on particle size could be perceived, similar to hydrolyzed PET surface.

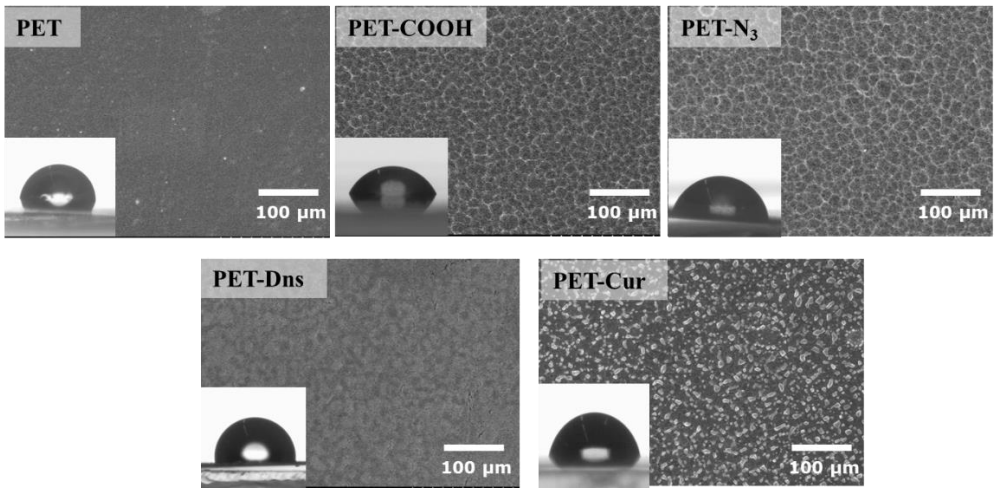

Figure 3.9. SEM images of pristine PET and functionalized PET samples.

3.3.5. Loss mass and mechanical properties

It is important to note that alkali and acid treatments can induce the cleavage of polymeric chains, transforming them into oligomers and yielding low molecular weight fragments [22]. Nevertheless, these smaller fragments are typically removed during the purification process, resulting in a decrease in the mass of the films. Mass loss measurements, performed though a weighing process, revealed the basic hydrolysis of PET led to polymer scission, resulting in an approaximate 7% reduction in mass. In fact, this phenomenon was consistent with the SEM images presented in **Figure 3.9**, where fisures and cracking were observed due to the degradation of the materials, which also agree with literature [67]. On the other hand, subsequent reactions did not produce significant mass losses, mainly due to the stability of the polymer chains under the mild reaction conditions. In fact, as shown in **Figure 3.10A**, the masses remained relatively constant.

On the other hand, the study of the mechanical properties of the modified PET was performed. Stress–strain curves of the films are shown in **Figure 3.10B**. Initially, all the films exhibited a very similar initial modulus. However, a significant in the strain percentage at the point of break was observed when comparing pristine PET with hydrolyzed and curcumin clicked PET samples. According to literature, this can be due to the fact that after hydrolysis and subsequent click reaction, macromolecular scission takes place mainly in the interlamellar amorphous regions, which determines the material elastic properties in films, and, subsequently, varies notoriously the strain at break of the films [22].

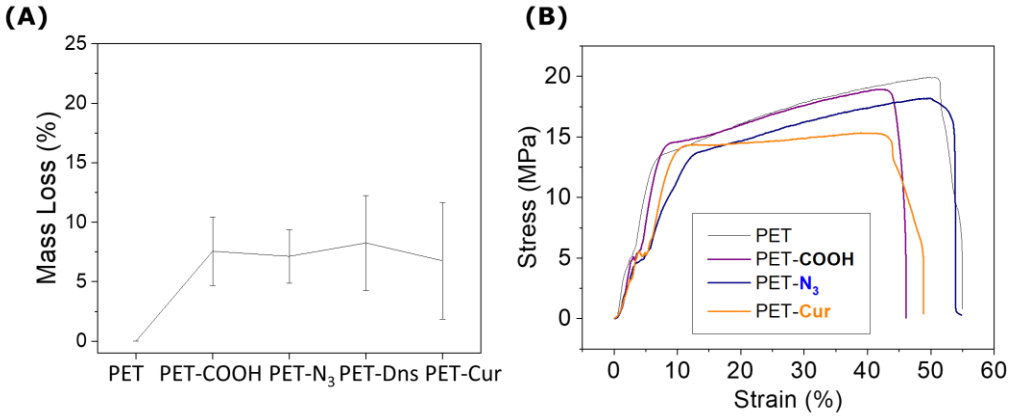

Figure 3.10. (A) Mass loss diagram of pristine PET and functionalized PET samples, (B) mechanical behaviour of pristine PET and functionalized PET samples,

This biofunctionalization was also followed by DSC and DMTA assays (**Figure 3.11**) in order to prove that only superficial physical chemistry properties had been modified while the bulk properties of the material remained unchanged.

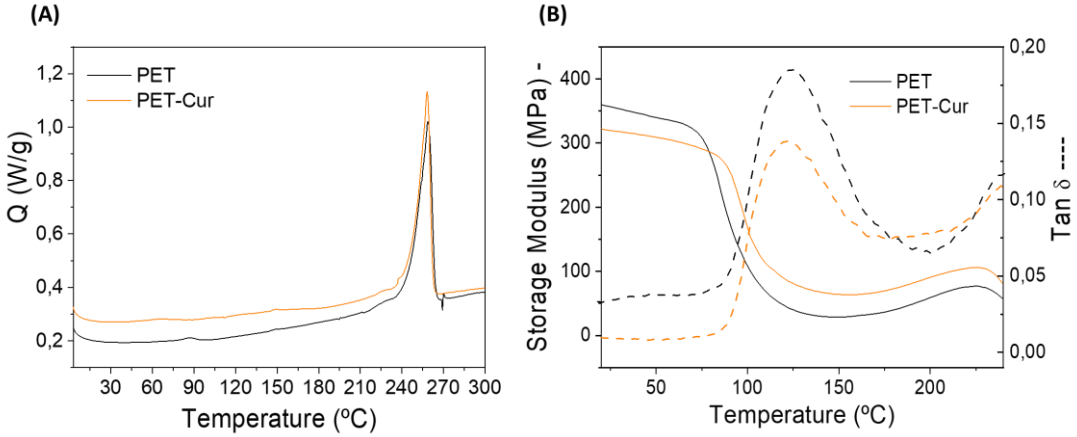

Figure 3.11. (A) DSC measurment of pristine PET and PET-Cur samples, (B) DMTA assays of Prisine PET and PET-Cur samples.

Both assays, DSC and DMTA, revealed that pristine PET and curcumin derivative modified PET exhibited similar T_g value, indicating that the intrinsic properties of the bulk material are nearly the same. Additionally, the storage modulus (E') refers to the elasticity (stiffness) of a material and is proportional to the energy that is stored during one period under load. It can be observed that both pristine PET and PET-Cur films obtained maximum storage modulus (E') value at the glassy region due to the

characteristics of the bulk material, PETexhibits excellent mechanical strength [73]. In the vicinity of the Tg, a sharp decrease in storage modulus (E') value was observed which indicates that the films are going through glass/rubbery transition (**Figure 3.11**). Furthermore, it has to be noted that PET-Cur sample exhihbits lower E' value when comparing to pristine PET, indicating a higher hardness in the curcumin-modified polymer surface, probably due to the increase in crystallinity transmitted by the aromatic compound linked to the polymer surface.

3.3.6. Biological activity analysis

3.3.6.1. In vitro cytotoxicity assay

As shown in **Figure 3.12**, the cellular viability, assessed using the MTS assay, after 48 h of growing in 96-weel culture wells, pristine PET and PET-Cur was similar. No statistically significant differences were determined between the cells cultured with pristine PET and PET-Cur samples and those without control cells. Overall, both pristine PET and PET-Cur have demonstrated non-cytotoxic effect with high cell viability content after 48 h.

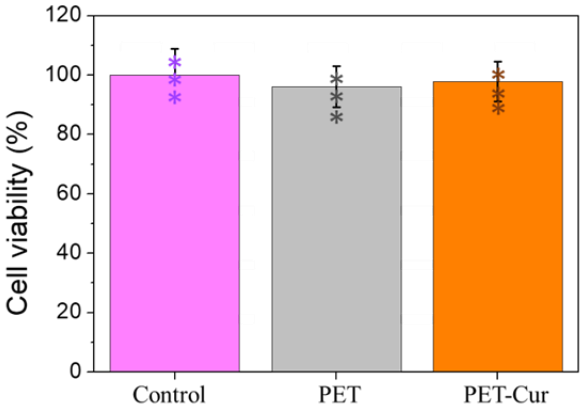

Figure 3.12. Assessment of cytotoxicity conducted by pristine PET and curcumin derived functionalized PET samples in HEK293 Cells. Results are expressed as a percentage of viability relative to untreated cells (Control). Statistical analysis was performed by the Student's t-test. Incubation with the pristine PET and PET-Cur surfaces did not produce statistically significant diffeences.

3.3.6.2. In vitro effect of pristine PET and PET-Cur on Inflammatory Response

THP-1 human monocytic cells were differentiated into a macrophage phenotype and cultured on pristine PET and PET-Cur. As can be seen in **Figure 3.13**, incubation of PET and PET-Cur with macrophages did not induce a pro-inflammatory response. IL-

6 remained at baseline levels during the examined incubation times (0, 48, 72, and 96 hours) compared to the control (monocytes cultured in the well without PET and also treated with LPS). These findings suggest that PET and PET-Cur do not stimulate an inflammatory reaction when in contact with macrophages

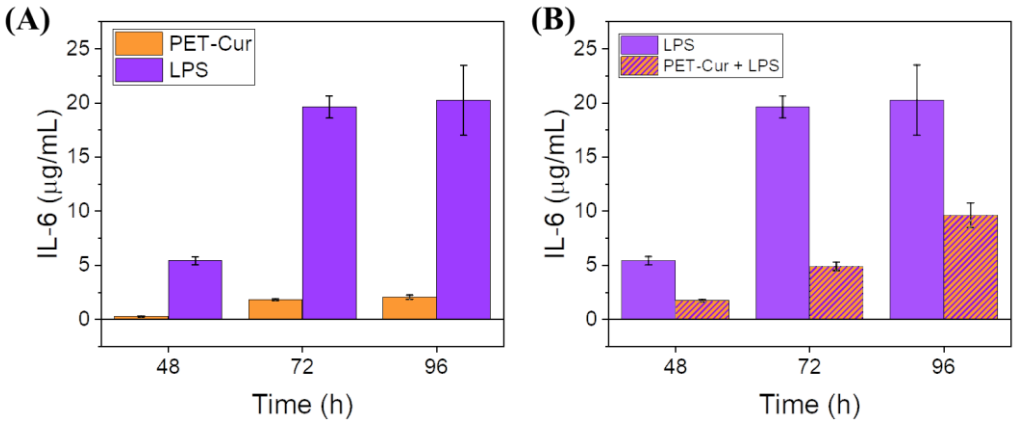

Figure 3.13. (A) Effect of PET-Cur on Inflammatory Response in vitro. Error bars represent standard deviations from three independent experiments. (B) Anti-Inflammatory Activity of pristine PET and PET-Curcumin assessed in vitro. THP-1 human monocytic cells were differentiated into a macrophage phenotype and cultured on pristine PET and PET-Cur. Incubation with these materials reduced the pro-inflammatory response induced by LPS at the tested incubation times (0, 48, 72, and 96 h). IL-6 levels were determined by ELISA at 48, 72, and 96 hours. Error bars represent standard deviations from three independent experiments.

On the other hand, this pro-inflammatory marker was added PET-Cur solutions and was examined at incubation times (0, 48, 72, and 96 h) compared to control (monocytes cultured in the well without PET-Cur and also treated with LPS). IL-6 levels were determined by ELISA at 48, 72, and 96 h. The results demonstrated that the presence of PET-Cur inhibits the pro-inflammatory response triggered by LPS, highlighting their potential anti-inflammatory properties (**Figure 3.13**).

3.3.6.3. Inhibition of Bacterial Growth and bactericidal effect of pristine PET and PET-Cur

Upon assessment through spectrophotometry at 600 nm, the growth of *Escherichia coli*, *Staphylococcus aureus*, and *Staphylococcus epidermidis* was markedly inhibited by PET-Cur compared to pristine PET. A significant reduction in turbidity at both 24 and 48 h, underscoring the efficacy of PET-Cur in impeding bacterial proliferation (**Figure 3.14**).

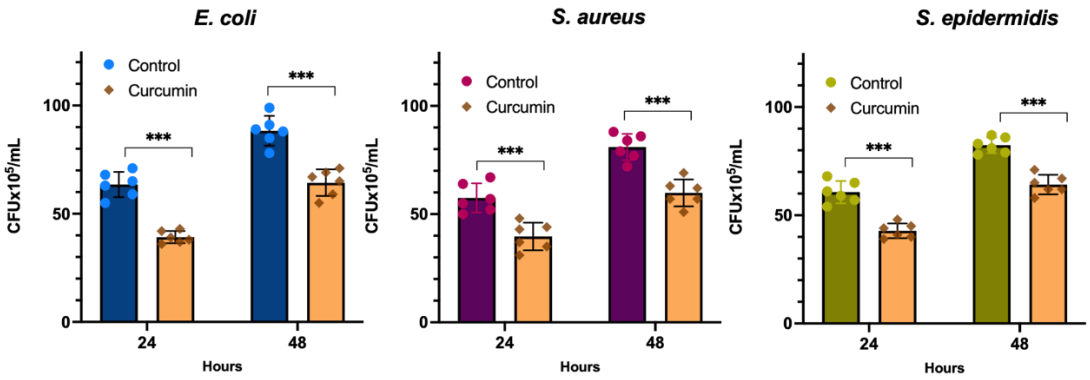

Figure 3.14. Inhibition of bacterial growth by PET-Curcumin**.** *Escherichia coli*, *Staphylococcus aureus*, and *Staphylococcus epidermidis* growth was significantly inhibited after 24 and 48 h of incubation with PET-Cur. Error bars represent standard deviations from independent experiments. Statistical significance was determined using Student's t-test (***p < 0.001).

To further elucidate the antimicrobial potential, viable colony-forming units (CFUs/mL) were enumerated after 24 and 48 hours of incubation. As shown in **Figure 3.15**, PET-Cur samples exhibited a substantial reduction in viable CFUs compared to pristine PET, indicating a pronounced bactericidal effect against *Escherichia coli*, *Staphylococcus aureus*, and *Staphylococcus epidermidis*. These findings underscore the bactericidal efficacy of curcumin derivative functionalized PET surfaces, reinforcing its potential as a promising antimicrobial agent with implications for diverse applications.

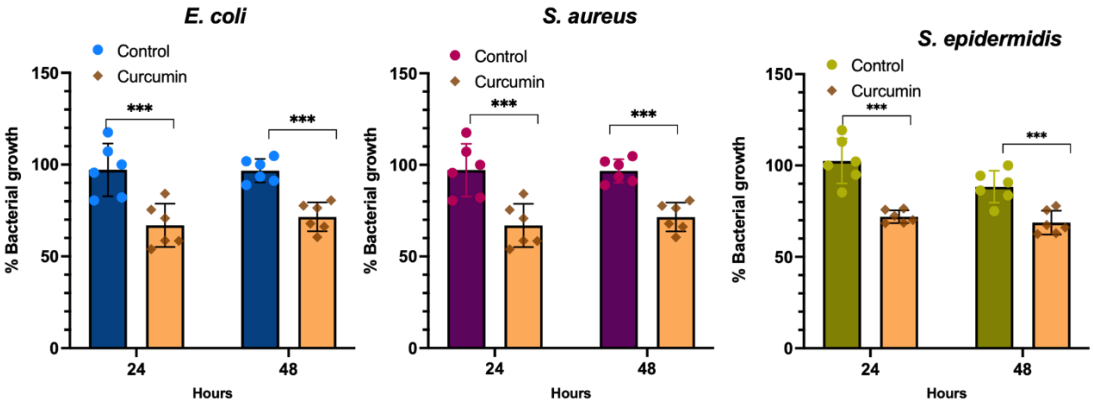

Figure 3.15. Bactericidal effect of PET-Cur. *Escherichia coli*, *Staphylococcus aureus*, and *Staphylococcus epidermidis* viability was significantly inhibited after 24 and 48 h of incubation with PET-Cur. Error bars represent standard deviations from independent experiments. Statistical significance was determined using Student's t-test (***p < 0.001).

3.3.6.4. In vitro hemolysis analysis

The hemolysis rate, that is the extent of red blood cell (RBC) rupture, serves as a critical indicator of hemocompatibility in assessing blood-contacting medical devices.

In these experiments, the release of hemoglobin, is used as a readout for RBC membrane disruption. This analysis is instrumental in the comprehensive evaluation of medical device's compatibility with blood, providing valuable insights into its performance and safety in clinical applications, being a rate below 5% the necessary standard for clinical utilization. The obtained results show that after 1 h incubation, the hemolysis ratio for PET-Cur was lower than for pristine PET (**Figure 3.16**). This suggests that PET-Cur surfaces do cause less hemolysis, however there were not significant statistical differences.

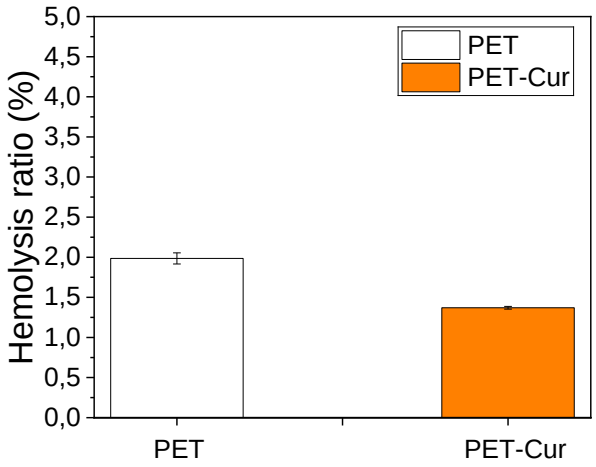

Figure 3.16. Hemolysis ratio of pristine PET and PET-Cur samples.

3.3.6.5. In vitro whole blood clotting time assay

The interaction of medical devices with blood can lead to thrombus formation and device failure. Therefore, for their clinical use it is essential to evaluate the interaction of biomaterials with whole blood and their ability to promote blood clotting. This assay uses the lytic resistance of RBCs as an indirect readout of blood clotting on the surfaces of the biomaterials. Thus, a higher hemoglobin release indicates less blood clotting on the surface. In these experiments, we incubated the samples with blood for up to 45 minutes and then placed them in deionized water, which caused the rupture of non-clotted RBCs. As can be seen in **Figure 3.17**, the hemoglobin concentration after 30 and 45 minutes is significantly higher for PET-Cur samples compared to pristine PET. These findings indicate that the surfaces with immobilized curcumin display antithrombogenic properties.

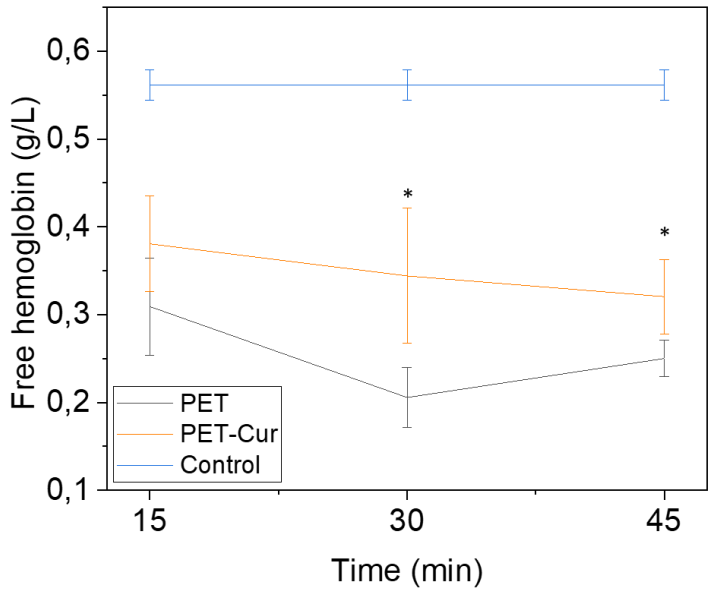

Figure 3.17. Whole blood clotting analysis of pristine PET and PET-Cur surfaces. Statistical significance was set at (*p ≤ 0.05).

3.4. Conclusions

Curcumin, a natural compound known for its diverse biological benefits, faces a challenge due to its low solubility in water, limiting its effectiveness as therapeutic drug. This study introduces an innovative methodology based on Click Chemistry reactions aiming to bioconjugate drugs onto polymeric substrates. By activating and functionalizing PET through a copper-catalyzed azide-alkyne click reaction, biologically active multifunctional polymers with promising biomedical applications can be achieved. The proposed methodology was firstly validated employing a fluorescent dansyl derivative, confirming its immobilization primarily through fluorescence microscopy. Similarly, the bioconjugation of curcumin derivative was verified through SEM and contact angle measurements, revealing significant changes in surface properties, including both topographical and wettability characteristics, after each surface functionalization step. Furthermore, the identification of different nitrogen species on XPS and ATR-FTIR analysis confirmed the covalent immobilization of the natural drug derivative. This method not only demonstrated the efficacy of attaching covalently a drug onto a polymeric surface, but also overcame the bioavailability limitation, showcasing remarkable biological activity in various in vitro experiments. Specifically, curcumin-derived PET surfaces exhibited improved biocompatibility and hemocompatibility without inducing inflammation response despite using copper as catalyst. Moreover, these functionalized surfaces offer

bactericidal protection against Gram-negative and Gram-positive bacteria, coupled with sustained anti-inflammatory properties even after 72 h. Additionally, PET-Cur samples have demonstrated excellent antithrombogenic effect when expose to human health blood at 30 and 45 min. The obtained results indicate that curcumin exhibits promise as a multifunctional drug, and more importantly, the employed modifications and click reactions did not suppress its intrinsic biological activity. This underscored the potential viability of curcumin as a versatile therapeutic agent. Indeed, these surfaces exhibit exceptional characteristics suitable for various medical applications, particularly as coatings for implants, showcasing their potential in advancing medical treatments.

3.5. Bibliography

1. Junter, G.A.; Thébault, P.; Lebrun, L. Polysaccharide-based antibiofilm surfaces. *Acta Biomater.* **2016**, *30*, 13–25, doi:10.1016/j.actbio.2015.11.010.

2. Wendels, S.; Avérous, L. Biobased polyurethanes for biomedical applications. *Bioact. Mater.* **2021**, *6*, 1083–1106, doi:10.1016/j.bioactmat.2020.10.002.

3. Helary, G.; Migonney, V. *Bioactive polymer coatings to improve bone repair*; Woodhead Publishing Limited, 2009; ISBN 9781845693855.

4. Teo, A.J.T.; Mishra, A.; Park, I.; Kim, Y.J.; Park, W.T.; Yoon, Y.J. Polymeric Biomaterials for Medical Implants and Devices. *ACS Biomater. Sci. Eng.* **2016**, *2*, 454–472, doi:10.1021/acsbiomaterials.5b00429.

5. Festas, A.J.; Ramos, A.; Davim, J.P. Medical devices biomaterials – A review. *Proc. Inst. Mech. Eng. Part L J. Mater. Des. Appl.* **2020**, *234*, 218–228, doi:10.1177/1464420719882458.

6. Dang, T.T.; Nikkhah, M.; Memic, A.; Khademhosseini, A. *Polymeric Biomaterials for Implantable Prostheses*; Elsevier Inc., 2014; ISBN 9780123969835.

7. He, W.; Benson, R. *Polymeric Biomaterials*; Elsevier Inc., 2014; ISBN 9780323221696.

8. Wang, S.; Ge, Y.; Ai, C.; Jiang, J.; Cai, J.; Sheng, D.; Wan, F.; Liu, X.; Hao, Y.; Chen, J.; et al. Enhance the biocompatibility and osseointegration of polyethylene terephthalate ligament by plasma spraying with hydroxyapatite in vitro and in vivo. *Int. J. Nanomedicine* **2018**, *13*, 3609–3623,

doi:10.2147/IJN.S162466.

9. Swar, S.; Zajícová, V.; Rysová, M.; Lovětinská-Šlamborová, I.; Voleský, L.; Stibor, I. Biocompatible surface modification of poly(ethylene terephthalate) focused on pathogenic bacteria: Promising prospects in biomedical applications. *J. Appl. Polym. Sci.* **2017**, *134*, 1–11, doi:10.1002/app.44990.

10. Sánchez-Bodón, J.; Diaz-Galbarriatu, M.; Pérez-Álvarez, L.; Moreno-Benítez, I.; Vilas-Vilela, J.L. Strategies to Enhance Biomedical Device Performance and Safety : A Comprehensive Review. *Coatings* **2023**, *13*, 1981–2005, doi:https://www.mdpi.com/2079-6412/13/12/1981/review_report.

11. Arciola, C.R.; Campoccia, D. Implant infections: adhesion, biofilm formation and immune evasion. *Nat. Rev. Microbiol.* **2018**, *16*, doi:10.1038/s41579-018-0019-y.

12. Subbiahdoss, G.; Kuijer, R.; Grijpma, D.W.; van der Mei, H.C.; Busscher, H.J. Microbial biofilm growth vs. tissue integration: "The race for the surface" experimentally studied. *Acta Biomater.* **2009**, *5*, 1399–1404, doi:10.1016/j.actbio.2008.12.011.

13. Szaraniec, B.; Pielichowska, K.; Pac, E.; Menaszek, E. Multifunctional polymer coatings for titanium implants. *Mater. Sci. Eng. C* **2018**, *93*, 950–957, doi:10.1016/j.msec.2018.08.065.

14. Williams, D.F. On the mechanisms of biocompatibility. *Biomaterials* **2008**, *29*, 2941–2953, doi:10.1016/j.biomaterials.2008.04.023.

15. Campoccia, D.; Montanaro, L.; Renata, C. The significance of infection related to orthopedic devices and issues of antibiotic resistance. *Biomaterials* **2006**, *27*, 2331–2339, doi:10.1016/j.biomaterials.2005.11.044.

16. Zhang, H.; Wu, X.; Wang, G.; Liu, P.; Qin, S.; Xu, K.; Tong, D.; Ding, H.; Tang, H.; Ji, F. Macrophage polarization, inflammatory signaling, and NF-κB activation in response to chemically modified titanium surfaces. *Colloids Surfaces B Biointerfaces* **2018**, *166*, 269–276, doi:10.1016/j.colsurfb.2018.03.029.

17. Mu, M.; Liu, S.; DeFlorio, W.; Hao, L.; Wang, X.; Salazar, K.S.; Taylor, M.; Castillo, A.; Cisneros-Zevallos, L.; Oh, J.K.; et al. Influence of Surface Roughness, Nanostructure, and Wetting on Bacterial Adhesion. *Langmuir*

2023, *39*, 5426–5439, doi:10.1021/acs.langmuir.3c00091.

18. Rana, D.; Ramasamy, K.; Leena, M.; Pasricha, R.; Manivasagam, G.; Ramalingam, M. *Surface Functionalization of Biomaterials*; Elsevier Inc., 2017; ISBN 9780128027561.

19. Li, W.; Thian, E.S.; Wang, M.; Wang, Z.; Ren, L. Surface Design for Antibacterial Materials: From Fundamentals to Advanced Strategies. *Adv. Sci.* **2021**, *8*, 1–23, doi:10.1002/advs.202100368.

20. Chouirfa, H.; Bouloussa, H.; Migonney, V.; Falentin-Daudré, C. Review of titanium surface modification techniques and coatings for antibacterial applications. *Acta Biomater.* **2019**, *83*, 37–54, doi:10.1016/j.actbio.2018.10.036.

21. Bridges, A.W.; García, A.J. Anti-Inflammatory Polymeric Coatings for Implantable Biomaterials and Devices. *Surf. Coatings Technol.* **2008**, *2*, 984–994, doi:https://doi.org/10.1016/j.surfcoat.2006.09.088.

22. Del Hoyo-Gallego, S.; Pérez-Álvarez, L.; Gómez-Galván, F.; Lizundia, E.; Kuritka, I.; Sedlarik, V.; Laza, J.M.; Vila-Vilela, J.L. Construction of antibacterial poly(ethylene terephthalate) films via layer by layer assembly of chitosan and hyaluronic acid. *Carbohydr. Polym.* **2016**, *143*, 35–43, doi:10.1016/j.carbpol.2016.02.008.

23. Garay, A.T.; Bousquet, A.; Ibarboure, E.; Teran, F.J.; Ruiz, L.; Laza, M.; Vilas, L.; Papon, E.; Rodri, J. pH Responsive Surfaces with Nanoscale Topography. *J. Polym. Sci. Part A Polym. Chem.* **2010**, *48*, 2982–2990, doi:10.1002/pola.24076.

24. Ozaltin, K.; Lehocky, M.; Humpolicek, P.; Pelkova, J.; Di Martino, A.; Karakurt, I.; Saha, P. Anticoagulant polyethylene terephthalate surface by plasma-mediated fucoidan immobilization. *Polymers (Basel).* **2019**, *11*, 1–12, doi:10.3390/polym11050750.

25. Bu, Y.; Ma, J.; Bei, J.; Wang, S. Surface Modification of Aliphatic Polyester to Enhance Biocompatibility. *Front. Bioeng. Biotechnol.* **2019**, *7*, 1–10, doi:10.3389/fbioe.2019.00098.

26. Valverde, A.; Pérez-Álvarez, L.; Ruiz-Rubio, L.; Pacha Olivenza, M.A.; García Blanco, M.B.; Díaz-Fuentes, M.; Vilas-Vilela, J.L.J.L. Review of titanium surface

modification techniques and coatings for antibacterial applications. *Carbohydr. Polym.* **2020**, *10*, 37–54, doi:10.1016/j.actbio.2018.10.036.

27. Immobilization, P.F.; Ozaltin, K.; Lehocky, M.; Humpolicek, P.; Pelkova, J.; Martino, A. Di; Karakurt, I.; Saha, P. Anticoagulant Polyethylene Terephthalate Surface by Plasma-Mediated Fucoidan Immobilization. *Polymers (Basel).* **2019**, *11*, 1–12.

28. Ujino, D.; Nishizaki, H.; Higuchi, S.; Komasa, S.; Okazaki, J. Effect of plasma treatment of titanium surface on biocompatibility. *Appl. Sci.* **2019**, *9*, doi:10.3390/app9112257.

29. Yang, Y.; Zhang, H.; Komasa, S.; Morimoto, Y.; Sekino, T.; Kawazoe, T.; Okazaki, J. UV/ozone irradiation manipulates immune response for antibacterial activity and bone regeneration on titanium. *Mater. Sci. Eng. C* **2021**, *129*, 112377, doi:10.1016/j.msec.2021.112377.

30. Liu, Y.; He, T.; Gao, C. Surface modification of poly (ethylene terephthalate) via hydrolysis and layer-by-layer assembly of chitosan and chondroitin sulfate to construct cytocompatible layer for human endothelial cells. *Colloids Surfaces B Biointerfaces* **2005**, *46*, 117–126, doi:10.1016/j.colsurfb.2005.09.005.

31. Ray, S.S.; Lee, H.K.; Kwon, Y.N. Review on blueprint of designing anti-wetting polymeric membrane surfaces for enhanced membrane distillation performance. *Polymers (Basel).* **2020**, *12*, doi:10.3390/polym12010023.

32. Lutz, J. 1 , 3-Dipolar Cycloadditions of Azides and Alkynes : A Universal Ligation Tool in Polymer and Materials Science. *Angew. Chemie - Int. Ed.* **2007**, *46*, 1018–1025, doi:10.1002/anie.200604050.

33. Thorek, D.L.J.; Elias, D.R.; Tsourkas, A. Comparative analysis of nanoparticle-antibody conjugations: Carbodiimide versus click chemistry. *Mol. Imaging* **2009**, *8*, 221–229, doi:10.2310/7290.2009.00021.

34. Bolley, J.; Guenin, E.; Lievre, N.; Lecouvey, M.; Soussan, M.; Lalatonne, Y.; Motte, L. Carbodiimide versus click chemistry for nanoparticle surface functionalization: A comparative study for the elaboration of multimodal superparamagnetic nanoparticles targeting αvβ3 integrins. *Langmuir* **2013**, *29*, 14639–14647, doi:10.1021/la403245h.

35. Best, M.D. Click Chemistry and Bioorthogonal Reactions: Unprecedented

Selectivity in the Labeling of Biological Molecules. *Biochemistry* **2009**, *48*, 6571–6584, doi:10.1021/bi9007726.

36. Ramapanicker, R.; Chauhan, P. Click Chemistry : Mechanistic and Synthetic Perspectives. In *Click reactions in Organic Synthesis*; 2016; pp. 1–24.

37. Li Li 1, 2 and Zhiyuan Zhang Development and Applications of the Copper-Catalyzed Azide-Alkyne Cycloaddition (CuAAC) as a Bioorthogonal Reaction. *Molecules* **2016**, *21*, 1–22, doi:10.3390/molecules21101393.

38. Lin, W.; Junjian, C.; Chengzhi, C.; Lin, S.; Sa, L.; Li, R.; Yingjun, W. Multi-biofunctionalization of a titanium surface with a mixture of peptides to achieve excellent antimicrobial activity and biocompatibility. *J. Mater. Chem. B* **2015**, *3*, 30–33, doi:10.1039/c4tb01318b.

39. Chen, J.; Zhu, Y.; Xiong, M.; Hu, G.; Zhan, J.; Li, T.; Wang, L.; Wang, Y. Antimicrobial Titanium Surface via Click-Immobilization of Peptide and Its in Vitro/Vivo Activity. *ACS Biomater. Sci. Eng.* **2019**, *5*, 1034–1044, doi:10.1021/acsbiomaterials.8b01046.

40. Lahann, J. *Click Chemistry for Biotechnology and Materials Science*; Lahann, J., Ed.; John Wiley & Sons Ltd: The Atrium, Southern Gate, Chichester, West Sussex, PO19 8SQ, United Kingdom, 2009; ISBN 9780470699706.

41. Watson, M.A.; Lyskawa, J.; Zobrist, C.; Fournier, D.; Jimenez, M.; Traisnel, M.; Gengembre, L.; Woisel, P. A "clickable" titanium surface platform. *Langmuir* **2010**, *26*, 15920–15924, doi:10.1021/la102688m.

42. Mahmood, K.; Zia, K.M.; Zuber, M.; Salman, M.; Anjum, M.N. International Journal of Biological Macromolecules Recent developments in curcumin and curcumin based polymeric materials for biomedical applications : A review. *Int. J. Biol. Macromol.* **2015**, *81*, 877–890, doi:10.1016/j.ijbiomac.2015.09.026.

43. Lestari, M.L.A.D.; Indrayanto, G. Chapter three - Curcumin. In *Profiles of Drug Substances, Excipients and Related Methodology*; Elsevier Inc, 2014; Vol. 39, pp. 113–204 ISBN 9780128001738.

44. Reddy, R.C.; Vatsala, P.G.; Keshamouni, V.G.; Padmanaban, G.; Rangarajan, P.N. Curcumin for malaria therapy. *Biochem. Biophys. Res. Commun.* **2005**, *326*, 472–474, doi:10.1016/j.bbrc.2004.11.051.

45. Vera-Ramirez, L.; Pérez-Lopez, P.; Varela-Lopez, A.; Ramirez-Tortosa, M.;

Battino, M.; Quiles, J.L. Curcumin and liver disease. *BioFactors* **2013**, *39*, 88–100, doi:10.1002/biof.1057.

46. Zhou, H.; Beevers, C.S.; Huang, S. The Targets of Curcumin. *Curr. Drug Targets* **2011**, *12*, 332–347.

47. Hewlings, Susan J. , Kalman, D.S. Curcumin : A Review of Its ' Effects on Human Health. *Foods* **2017**, *6*, 92–103, doi:10.3390/foods6100092.

48. Kharat, M.; Du, Z.; Zhang, G.; Mcclements, D.J. Physical and Chemical Stability of Curcumin in Aqueous Solutions and Emulsions: Impact of pH, Temperature, and Molecular Environment. *J. Agric. Food Chem* **2017**, *65*, 1525–1532, doi:10.1021/acs.jafc.6b04815.

49. Payton, F.; Sandusky, P.; Alworth, W.L. NMR study of the solution structure of curcumin. *J. Nat. Prod.* **2007**, *70*, 143–146, doi:10.1021/np060263s.

50. Reddy, A.R.; Achanta, P.S.; Kulandaivelu, U.; Boyapati, S. A Comprehensive Review on SAR of Curcumin. *Mini Rev Med Chem* **2013**, *13*, 1769–1777, doi:10.2174/1389557511313120007.

51. Lin, L.I.; Lee, K. Structure-Activity Relationships of Curcumin and Its Analogs with Different Biological Activities. *Stud. Nat. Prod. Chem.* **2006**, *33*, 785–812, doi:10.1016/S1572-5995(06)80040-2.

52. Elguero, J. Curcumin and curcuminoids : chemistry , structural studies and biological properties.

53. Nimiya, Y.; Wang, W.; Du, Z.; Sukamtoh, E.; Zhu, J.; Decker, E. Redox modulation of curcumin stability : Redox active antioxidants increase chemical stability of curcumin. *Mol. Nutr. Food Res.* **2016**, *60*, 487–494, doi:10.1002/mnfr.201500681.

54. Adamczak, A.; Ożarowski, M.; Karpiński, T.M. Curcumin, a natural antimicrobial agent with strain-specific activity. *Pharmaceuticals* **2020**, *13*, 1–12, doi:10.3390/ph13070153.

55. Zhang, Y.; Rauf Khan, A.; Fu, M.; Zhai, Y.; Ji, J.; Bobrovskaya, L.; Zhai, G. Advances in curcumin-loaded nanopreparations: improving bioavailability and overcoming inherent drawbacks. *J. Drug Target.* **2019**, *27*, 917–931, doi:10.1080/1061186X.2019.1572158.

56. Ejaz, S.; Ejaz, S.; Shahid, R.; Noor, T.; Shabbir, S.; Imran, M. Chitosan-curcumin complexation to develop functionalized nanosystems with enhanced antimicrobial activity against hetero-resistant gastric pathogen. *Int. J. Biol. Macromol.* **2022**, *204*, 540–554, doi:10.1016/j.ijbiomac.2022.02.039.

57. Liu, Y.; Ma, Y.; Liu, Y.; Zhang, J.; Hossen, M.A.; Sameen, D.E.; Dai, J.; Li, S.; Qin, W. Fabrication and characterization of pH-responsive intelligent films based on carboxymethyl cellulose and gelatin/curcumin/chitosan hybrid microcapsules for pork quality monitoring. *Food Hydrocoll.* **2022**, *124*, 107224, doi:10.1016/j.foodhyd.2021.107224.

58. Yuan, Y.; Zhang, S.; Ma, M.; Wang, D.; Xu, Y. Encapsulation and delivery of curcumin in cellulose nanocrystals nanoparticles using pH-driven method. *Lwt* **2022**, *155*, 112863, doi:10.1016/j.lwt.2021.112863.

59. Cabrera-Quiñones, N.C.; López-Méndez, L.J.; Ramos, E.; Rojas-Aguirre, Y.; Guadarrama, P. Mono-Dendronized β-Cyclodextrin Derivatives as Multitasking Containers for Curcumin. Impacting Its Solubility, Loading, and Tautomeric Form. *J. Phys. Chem. B* **2022**, doi:10.1021/acs.jpcb.1c09811.

60. Ronghan He,ab Xuefeng Hu,a Hark Chuan Tan,a Jason Feng,c Chris Steffi, a K.W. and W.W. Surface modification of titanium with curcumin: a promising strategy to combat fibrous encapsulation. *J. Mater. Chem. B* **2015**, *3*, 2137–2146, doi:10.1039/C4TB01616E.

61. Zeng, D.; Kuang, G.; Wang, S.; Peng, W.; Lin, S.; Zhang, Q.; Su, X.; Hu, M.; Wang, H.; Tan, J.; et al. Discovery of Novel 11-Triazole Substituted Benzofuro[3,2 - b]quinolone Derivatives as c - myc G - Quadruplex Speci fi c Stabilizers via Click Chemistry. *J. Med. Chem.* **2017**, *60*, 5407–5423, doi:10.1021/acs.jmedchem.7b00016.

62. Valverde, A.; Pérez-Álvarez, L.; Ruiz-Rubio, L.; Pacha Olivenza, M.A.; García Blanco, M.B.; Díaz-Fuentes, M.; Vilas-Vilela, J.L. Antibacterial hyaluronic acid/chitosan multilayers onto smooth and micropatterned titanium surfaces. *Carbohydr. Polym.* **2019**, *207*, 824–833, doi:10.1016/j.carbpol.2018.12.039.

63. Andrade-Del Olmo, J.; Pérez-Álvarez, L.; Ruiz-Rubio, L.; Vilas-Vilela, J.L. Antibacterial chitosan electrostatic/covalent coating onto biodegradable poly (L-lactic acid). *Food Hydrocoll.* **2020**, *105*, doi:10.1016/j.foodhyd.2020.105835.

64. Sánchez-Bodón, J.; Ruiz-Rubio, L.; Hernáez-Laviña, E.; Vilas-Vilela, J.L.; Moreno-Benítez, M.I. Poly(L-lactide)-based anti-inflammatory responsive surfaces for surgical implants. *Polymers (Basel).* **2021**, *13*, 1–15, doi:10.3390/polym13010034.

65. Chollet, C.; Chanseau, C.; Remy, M.; Guignandon, A.; Bareille, R.; Bordenave, L.; Durrieu, M.; Labruge, C.; Cedex, F.-B.; Bordeaux, U.; et al. Biomaterials The effect of RGD density on osteoblast and endothelial cell behavior on RGD-grafted polyethylene terephthalate surfaces. *Biomaterials* **2009**, *30*, 711–720, doi:10.1016/j.biomaterials.2008.10.033.

66. Uchida, E.; Uyama, Y.; Ikada, Y. Sorption of Low-Molecular-Weight Anions into Thin Polycation Layers Grafted onto a Film. *Langmuir* **1993**, *9*, 1121–1124.

67. Cao, W.; Wei, D.; Jiang, Y.; Ye, S.; Zheng, A.; Guan, Y. Surface chemical bonding with poly(hexamethylene guanidine) for non-leaching antimicrobial poly(ethylene terephthalate). *J. Mater. Sci.* **2019**, *54*, 2699–2711, doi:10.1007/s10853-018-2966-0.

68. Herrmann, I.; Kramm, U.I.; Radnik, J.; Fiechter, S.; Bogdanoff, P. Influence of Sulfur on the Pyrolysis of CoTMPP as Electrocatalyst for the Oxygen Reduction Reaction. *J. Electrochem. Soc.* **2009**, *156*, B1283, doi:10.1149/1.3185852.

69. Tudino, T.C.; Nunes, R.S.; Mandelli, D.; Carvalho, W.A. Influence of Dimethylsulfoxide and Dioxygen in the Fructose Conversion to 5-Hydroxymethylfurfural Mediated by Glycerol's Acidic Carbon. *Front. Chem.* **2020**, *8*, 1–11, doi:10.3389/fchem.2020.00263.

70. Saad, A.; Abderrabba, M.; Chehimi, M.M. X-ray induced degradation of surface bound azido groups during XPS analysis. *Surf. Interface Anal.* **2017**, *49*, 340–344, doi:10.1002/sia.6113.

71. Alberti, G.; Desimone, A.; A, P.R.S. Wetting of rough surfaces : a homogenization approach Wetting of rough surfaces : a homogenization approach. **2005**, *461*, 79–97, doi:10.1098/rspa.2004.1364.

72. Kantheti, S.; Narayan, R.; Raju, K.V.S.N. The impact of 1,2,3-triazoles in the design of functional coatings. *RSC Adv.* **2015**, *5*, 3687–3708, doi:10.1039/c4ra12739k.

73. Nisticò, R. Polyethylene terephthalate (PET) in the packaging industry. *Polym. Test.* **2020**, *90*, 106707, doi:10.1016/j.polymertesting.2020.106707.

CHAPTER 4

ANTICOAGULANT Ti6Al4V SURFACES BY EMPLOYING CONVENTIONAL CLICK CHEMISTRY

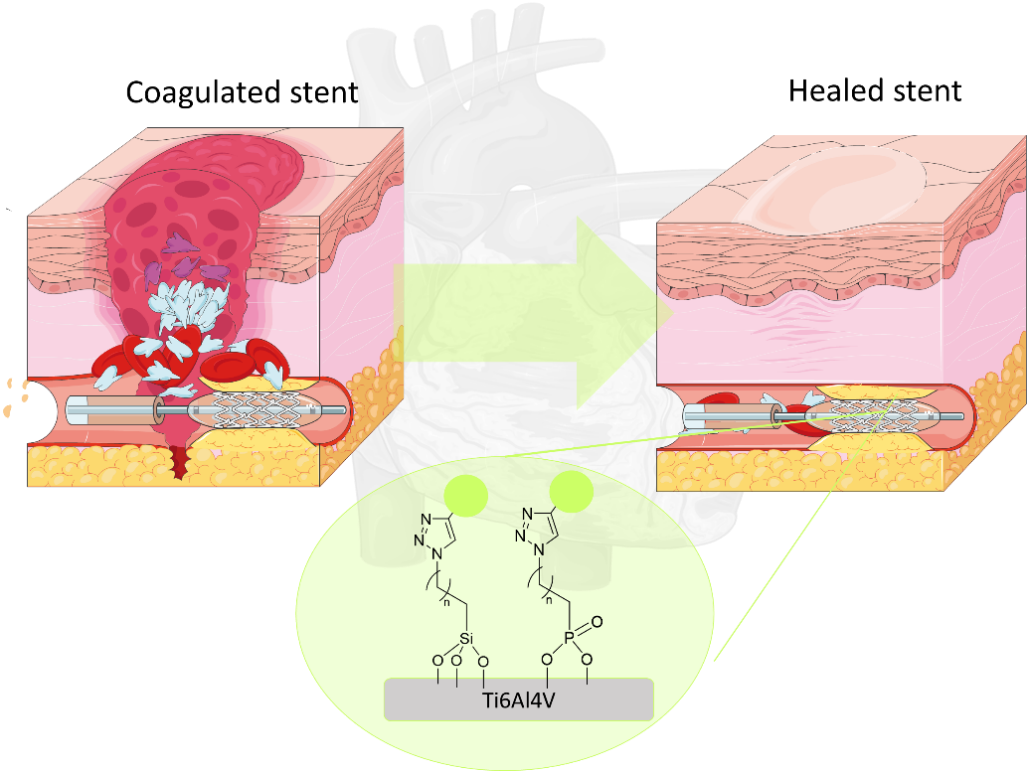

Among all different materials and composites employed as implants, titanium and its alloys are, by far, the most widely used. Specifically, Ti6Al4V alloys is widely employed in joint replacements, bone plates and screws, in dental implants. In fact, they have excellent properties to use in biomedical area such as excellent biocompatibility, high durability, good strength, low elastic modulus and low density among others. However, the osseointegration ability, bacteria resistance and hemocompatibility of this type of materials remain a challenge. Therefore, designing and producing surfaces that promote blood contact interactions along with avoiding bacterial contamination have become a priority line of research in the 21st century. For this purpose, in this chapter the employment of SAMs and click reactions for the immobilization of active drugs onto Ti6Al4V surfaces has been proposed in order to prevent any implant-associated infections and to improve the hemocompatibility.

CHAPTER 4

ANTICOAGULANT TITANIUM ALUMINIUM VANADIUM ALEATION SURFACES BY EMPLOYING TRADITIONAL CLICK CHEMISTRY

4.1. Introduction

Problems related to circulatory system such as cardiovascular diseases remain being the primary cause of mortality in Spain. In spite of the fact that the number of deaths has decreased over the years, still more than 120,000 people died in 2018. In fact, in 2018, they constituted 28.3 % of fatalities, notably being the leading cause of death among women. By 2021, despite a slight decrease to 26.4 % circulatory issues remained the primary cause of mortality in Spain. This trend persisted into 2022, with circulatory diseases causing 26.0 % of deaths [1–3]. In this context, artery bypass graft is the primary surgery for patients with advanced cardiovascular disease worldwide, which generates tremendous economic costs in all countries [4].

Several cardiovascular implants are approved by Food and Drug Administration (FDA) to treat cardiovascular diseases, however, a good tissue regeneration of these devices implantation is still a challenge [5]. Concerning endovascular stents, and in particular bare metal stents (BMS), the principal disadvantage of this type of implants, beside the typical inflammatory response, is the release of toxic ions such

as Cr, Ni or Co, which limits hemocompatibility and results in restenosis [6]. Therefore, implant failure occurs and additional surgeries are required. Despite that drug-eluting stent (DES) resulted to be an advance in stent design, it cannot be employed in long-term clinical studies as release of the drug has shown to cause an endothelization delay and late thrombosis [6,7]. Surface properties of these medical devices is the main issue associated with blood-compatibility. In order to improve the interaction between tissue and surface, cardiovascular devices have been chemically modified, allowing independent tailoring of surface and bulk properties [8]. Blood compatibility, compatible inflammatory reaction and re-endotheliazation are the key issues which have to be highlighted in order to design an optimum endovascular device [9]. Since, in blood vessels, blood compatibility is naturally guaranteed by the presence of the endothelial layer [10].

Metals, particularly titanium (Ti) alloys, have been widely used in biomedical field because of their beneficial properties such as strength, stiffness, corrosion resistance and blood compatibility [11,12]. The most common used Ti-based materials are commercially pure titanium (CP-Ti) and Ti6Al4V (titanium-aluminium-vanadium) alloy. One of the main advantages of these ones is their lightly weight. Nevertheless, as commented before, BMS stents have some limitations, since they can generate thrombosis, change the geometry of vessels and obstruct side branches [13]. An improvement of the surface chemistry of Ti, which enhances thromboresistance, would represent a significant technological advance that might contribute to more widespread adoption of these devices. Nowadays, several methods are known to prevent a thrombogenesis [14]. The use of functional groups on material surface to form covalent bonds between the substrate and active molecules, such as silanes or phosphonates, is an economical and often employed approach for constructing surface chemical modification.

The creation of a self-assembled monolayer (SAM) on the surface of a Ti6Al4V alloy is a way to change the properties of the tested material that is relatively quick, simple, and does not require high production costs [15,16]. It is also a kind of barrier between the material and the human body, which is extremely important from a biomedical point of view. Additionally, by using this method of modification, it is possible to control the surface composition, as well as to create an oriented, well-ordered, and stable layer [17,18]. Although chemically different SAMs have been reported such a carboxylic, hydroxyl or amine based coatings, only silane and phoshorous based SAMs will be described in this chapter [19,20]. In fact, due to their versatility and effectiveness these approaches are the most widely used to modify metal surfaces [21–23].

Silanization has proven to be an economical and effective strategy to modify covalently surfaces [24]. In fact, this methodology has been used to modify not only a large variety of metallic or metal oxide surfaces, but also minerals such us hydroxyapatite. For this strategy, all type of surfaces required previous surface activation, which incorporated hydroxyl groups so that silane-coupling agents can link with them. These silanes introduce active groups along with them, such as amino, carboxyl or bromide groups in order to be accessible for further modifications (**Figure 4.1**). For instance, Zhou *et al*. grafted antimicrobial peptide GL13K onto titanium by silanization to enhance an anti-inflammatory response, which promotes the process of osseointegration [25]. For that, titanium surface was previously activated with NaOH, then silanizated with 3-(chloropropyl)-triethoxysilane (CPTES) and modified with the antimicrobial peptide through nucleophilic aliphatic substitution of the chloride atom. Despite being the silanization process a simple and effective method for modification, the reaction conditions such as concentration of the silane and reaction time must be carefully controlled to prevent forming thick polymerized silane network on the surface (**Figure 4.1**).

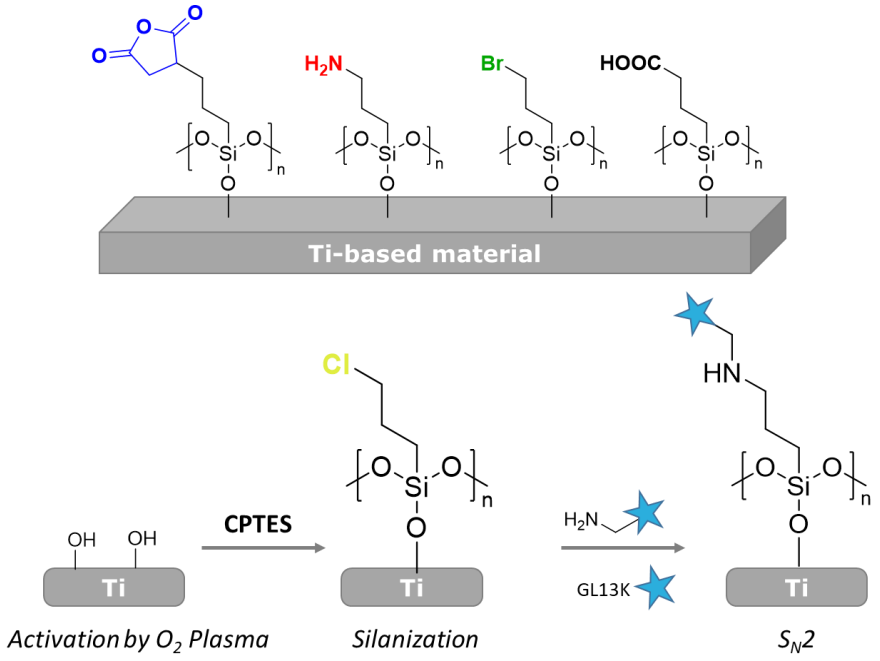

Figure 4.1. Schematic illustration of silane-based anchor with different terminal functional groups and GL13K peptide immobilization description.

Phosphorilation is a similar covalent coating method that has been used to obtain biologically active surfaces. However, compared to silanes, phosphonic acid-terminated small molecules have been shown to form stable Ti−O−P bonds on Ti surfaces with better surface coverage and improved hydrolytic stability under physiological conditions [19,26,27]. Phosphonates, which are phosphonic acid

precursors, are at the same time biologically active phosphate derivatives, characterized by a substitution of a carbon atom instead of an oxygen atom. This chemical change increases the stability against enzymatic hydrolysis of the molecule. When they are used as a surface coating, phosphonates have been demonstrated to enhance surface hydrophilicity. This suggests beneficial effects for the healing process following implant insertion, as hydrophilic surfaces exhibit improved adsorption of proteins and enhanced angiogenesis during early implant osseointegration [28].

Despite self-assembled monolayers (SAMs) have shown biological activity response, the effectiveness of passive coating is limited, especially reducing bacterial adhesion and promoting endothelization [28]. Thus, this limitations have endorsed the interest in active alternatives. Active approaches are based on the incorporation of biological active compounds on substrates for achieving improved biocompatibility and better protection against bacteria or other microorganisms. Although such active coatings can be designed employing several strategies, immobilization of active molecules by chemical linkage will be discussed in this chapter.

The immobilization of several drugs and biological active complexes can be carried out following different chemical reactions such as nucleophilic substitution, Click Chemistry or photochemical reactions. Lately, click reactions have proven to be a very useful approach for bioconjugating molecules on different surfaces. The Click Chemistry term was firstly introduced by K. Sharpless *et al.* and refers to a full class of reactions that are high yielding stereospecific and wide in scope [29–31]. Moreover, the reaction conditions as well as the purification processes are simple, due to the use of solvents that are easy to remove or even, in some cases, the reactions are carried out in the absence of them. The discovery of Cu(I)-catalyzed azide-alkyne cycloaddition in 2001 revolutionized this process, elevating it from a mere concept to a practical reality. This reaction, conducted under mild conditions and employing various available substrates, yields 1,4-regioisomers of 1,2,3-triazoles as exclusive products, a remarkable feat aligning precisely with the fundamental principles of Click Chemistry [30,32]. This nearly flawless reaction has become synonymous with Click Chemistry and is often refered as "The Click Reaction”. Azide-based reactions predominantly find application in bioconjugation, offering several distinct advantages. These advantages include: (i) the scarcity of azide moieties in naturally occurring compounds, and (ii) despite their inherent reactivity, azides allow for selective ligation with a very limited set of reaction moieties [33,34].

Among drugs, salicylic acid (SA) is well-known recognized painkiller with widespread use around the world. It is a phenolic compound that is synthesized by various organisms, including both prokaryotes and eukaryotes, such as plants. In fact, the leaves and bark of the willow tree (Salix species) are rich in SA [35,36]. Throughout history, due to its therapeutic properties, SA has been widely used as a medicinal substance for pain relief. In 1828, J.A.Buchner successfully isolated salicin from willow bark. Salicin, SA derivative, is a glucoside of salicyl alcohol [35]. A decade later, Raffaele Piria performed a chemical conversion of salicin into an acidic aromatic compound, obtaining for the first time in a laboratory salicylic acid. However, the first chemical synthesis described for SA was performed by H. Kolbe and coworkers in 1859. Nevertheless, its bitter taste and associated side effects limited its prolonged medicinal use. Years later, the acetylation of salicylic acid was obtained, achieving the known Aspirin® (ASA), which exhibited improved pharmacokinetics properties. (**Figure 4.2**)[35].

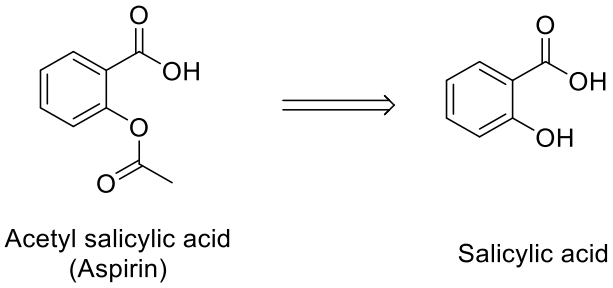

Figure 4.2. Chemical structure of acetyl salicylic acid (Aspirin®) and its precursor salicylic acid.

Similarly to indomethacin and curcumin, salicylic acid is able to inhibit prostaglandin synthesis. Initially, it was considered that the inhibition of prostaglandins carried out through COX inhibition. However, in 1999, Xu *et al.* proposed a novel pathway for prostaglandins inhibition by SA and aspirin [35,37]. Their research demonstrated that SA and ASA act as anti-inflammatory agents by suppressing the transcription of genes responsible for COX production. Moreover, some studies have revealed that salicylic acid exerts additional effects independent of COX inhibition, as it does not inhibit COX considerably, the anti-inflammatory effect is not mediated through direct inhibition of COX activity, indicating that it possess other mechanisms of action beyond COX pathway. Indeed, it has demonstrated significant inhibition of both leukocyte function and some expression of different pro-inflammatory genes. Additionally, it has exhibited inhibition on nitric oxide synthase (iNOS), which is induced by cytokines and lipopolysacharides (LPS). Moreover, high concentration of salicylic acid can affect kinases and, particularly, mitogen-activated protein kinase

(MAPK). In fact, Kopp and Gosh proved the inhibition of NF-kB by salicylic acid, which is a nuclear factor crucial in cellular response to inflammatory stimulus [38].

On the other hand, one of the most extensively studied characteristics of salicylic acid is its antioxidative property. Due to its ability to act as a chemical trap for hydroxyl radicals, salicylic acid has been reported to effectively reduce tissue damage caused by hypoxia/reoxigenation [38].

According to SAR studied performed on salicylic acid, reducing the acidity of the carboxyl group can significantly impact the potency of its activity. For instance, the conversion of the acid group to amide, obtaining salicylamide concluded that the analgesic action is still remain, but a decrease in anti-inflammatory properties is noted. However, research made by Jung *et al.* concluded that salicylamide showed greater inhibition potency on NFkB factor [38]. On the other hand, substitution of either the carboxyl or hydroxyl moieties in the molecule affects the activity and toxicity. Indeed, benzoic acid itself shows only week activity. Additionally, the *ortho* position of the hydroxyl group is essential, in fact, *meta* and *para* regioisomers lack activity.

Aspirin, as salicylic acid, has demonstrated inhibition of COX through two pathways direct dependent and independent COX inhibition. This is because aspirin is hydrolyzed in the blood some groups of proteins, including Lys, Arg, , Ser, Thr, Tyr and Cys, resulting in irreversible deacetylation and transforming into salicylic acid [36]. Hence, both salicylic acid and aspirin have demonstrated significant interest for immobilization strategies as multifunctional properties can be obtained [38].

This Doctoral thesis aims to bioconjugate aspirin or salicylic acid derivative to enhance anti-inflammatory and anti-platelet effect of Ti6Al4V samples. Leveraging the proven efficacy of the CuAAC click reaction in bioconjugating various drugs, this research studied the integration of two strategies for drug immobilization. This involves the formation of a SAM, exploring silane based and phosphonate based monolayers, through chemical functionalization followed by a subsequent click reaction.

4.2. Materials and Methods

4.2.1 Materials

The reagents used for the synthesis of different compounds are the following: Dansyl chloride (Sigma Aldrich, St. Louise, MO, USA), aspirin (Sigma Aldrich, St. Louise, MO,

USA), salicylic acid (Sigma Aldrich, St. Louise, MO, USA), toluene (Sigma Aldrich), thionyl chloride ($SOCl_2$, Sigma Aldrich, St. Louise, MO, USA), propargylamine (Sigma Aldrich, St. Louise, MO, USA), dichloromethane (CH_2Cl_2, Macron Fine Chemicals), potassium carbonate (Sigma Aldrich, St. Louise, MO, USA), hydrochlorihidric acid (HCl, % 37, Panreac, Darmstadt, Germany) sodium chloride saturated solution (prepared, Common salt for food use), diethyl (3-bromopropyl)phosphonate (Sigma Aldrich, St. Louise, MO, USA), bromotrimethylsilane (BTMS, Sigma Aldrich, St. Louise, MO, USA), anhydrous methanol (MeOH, Panreac, Darmstadt, Germany).

Ti6Al4V surfaces were obtained from Sigma Aldrich (St. Louise, MO, USA) and cut in 1x1 cm pieces by lasher ablation. The modifications of this samples were performed employing: sulfuric acid (H_2SO_4, 96%, Panreac, Darmstadt, Germany), hydrogen peroxide (H_2O_2, Foret, Alicante, Spain), sodium azide (NaN_3, Sigma Aldrich, St. Louise, MO, USA), acetonitrile (98%, Panreac, Darmstadt, Germany), acetone (99%, Panreac, Darmstadt, Germany), ethanol (EtOH, 98%, Panreac), (3-bromopropil)trimethoxysilane (Sigma Aldrich, St. Louise, MO, USA), sodium ascorbate (Sigma Aldrich, St. Louise, MO, USA), triethylamine (Et_3N, Sigma Aldrich, St. Louise, MO, USA), copper (II) sulfate pentahydrate ($CuSO_4 \cdot 5H_2O$, Sigma Aldrich, St. Louise, MO, USA)

4.2.2. Experimental procedure

*4.2.2.1. Synthesis of dansyl derivative **2b***

Dansyl chloride (2.00 g, 7.40 mmol) was dissolved in dichloromethane (20 mL) and propargylamine (0.48 mL, 7.40 mmol) and Et_3N (0.75 g, 7.40 mmol) were added. The reaction was refluxed for 48 h. After cooling to room temperature, a portion of water was added to the reaction and the solution was extracted with dichloromethane (3x10 mL) and washed with a saturated solution of sodium chloride (2x10 mL). Organic layers were collected, dried over anhydrous Na_2SO_4 and the solvent was evaporated under *vacuum* to afford 5-(dimethylamino)-*N*-(prop-2-yn-1-yl)naphthalene-1-sulfonamide (**2b**) as a yellowish oil (0.95 g, 89%). ^{1}H-NMR (300 MHz, $CDCl_3$) (δ, ppm): 8.52 (d, *J* = 8.5 Hz, 1H, CH_{arom}, H_7), 8.30-8.28 (m, 2H, CH_{arom}, H_5 and H_{12}), 7.54-7.51 (m, 2H, CH_{arom}, H_6 and H_{11}), 7.18 (dd, *J* = 7.5 Hz, *J* = 0.54 Hz, 1H, CH_{arom}, H_{10}), 5.26 (s,1H, NH), 3.77 (d, *J* = 2.5 Hz, 2H, CH_2, H_3), 2.86 (s, 6H, 2xCH_3), 1.91 (t, *J* = 2.5 Hz, 1H, ≡CH, H_1); ^{13}C-NMR (75 MHz, $CDCl_3$) (δ, ppm): 152.0 (C_{arom}-N, C_9), 135.5 (C_{arom}-S, C_4), 132.6

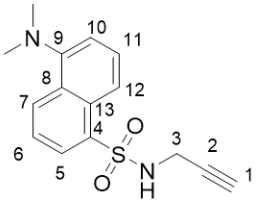

2b

(C_{arom}-H, C_7), 131.3 (C_{arom}-C, C_{13}), 129.5 (C_{arom}-H, C_5), 129.2 (C_{arom}-H, C_6), 128.5 (C_{arom}-H, C_{11}), 123.2 (C_{arom}-H, C_{12}), 118.9 (C_{arom}-C, C_8), 115.3 (C_{arom}-H, C_{10}), 84.3 (C≡C, C_2), 71.2 (≡CH), 45.2 (N-$(CH_3)_2$), 33.2 (CH_2).

*4.2.2.2. Synthesis of 2-hydroxy-N-(prop-2-yn-1-yl)benzamide (**6a**) from aspirin*

Acetylsalicylic acid (aspirin, 0.53 g, 2.94 mmol) was dissolved in toluene (15 mL) and thionyl chloride (1.00 mL, 13.9 mmol) was added to the solution. Then, the reaction was refluxed for 24 h. After cooling, solvent was evaporated under *vacuum*. After, a solution of propargylamine (0.88 mL, 13.9 mmol) in dichloromethane (10 mL) was added). The solution was stirred for 48 h at room temperature. After that time, the reaction was stopped by adding water, the phases were separated, and the aqueous phase was extracted with dichloromethane (3x20 mL). Combined organic phases were washed with a solution of potassium carbonate (2 M, 2x10 mL), chlorhydric acid (10%, 2x10 mL) and sodium chloride saturated solution (3x20 mL). Finally, organic layer was dried over anhydrous Na_2SO_4 and solvent was evaporated under *vacuum*. After that, 2-hydroxy-*N*-(prop-2-yn-1-yl)benzamide (**6a**) was obtained as a orangish oil (0.43 g, 81%). Thin layer chromatography (TLC) was employed to follow the reaction using Hexane:EtOAc (7:3) as eluent. ^{1}H-NMR (300 MHz, $CDCl_3$) (δ, ppm):

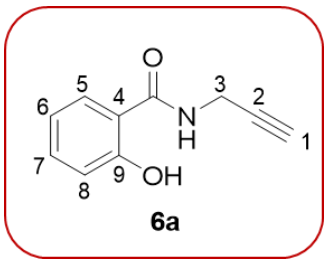

6a

12.00 (s, 1H, OH), 7.39 (m, 2H, CH_{arom}, H_5 and H_7), 6.99 (dd, *J*= 8.2 Hz, *J*= 1.2 Hz, CH_{arom}, H_8), 6.86 (td, *J*= 8.2 Hz, *J*=1.2 Hz, 1H, CH_{arom}, H_6), 6.49 (s, 1H, NH), 4.25 (d, *J*= 2.6 Hz, 2H, CH_2, H_3), 2.32 (t, *J*= 2.6 Hz, 1H, ≡CH, H_1); ^{13}C-NMR (75 MHz, $CDCl_3$) (δ, ppm): 169.7 (C=O), 161.5 (C_{arom}-OH, C_9), 134.6 (C_{arom}-H, C_5), 125.6 (C_{arom}-H, C_7), 118.9 (C_{arom}-H, C_6), 118.6 (C_{arom}-H, C_8), 112.3 (C_{arom}-C, C_4), 78.8 (C≡, C_2), 72.3 (≡CH, C_1), 24.4 (CH_2, C_3). FTIR (cm^{-1}): 3450 (R-N-H), 3200 (C_{sp}-H), 2100 (C_{sp}-C_{sp}), 1650 (C=O).

Same procedure was employed with salicylic acid (0.51 g, 3.70 mmol). Obtaining 2-hydroxy-*N*-(prop-2-yn-1-yl)benzamide (**6a**) as an orangish oil (0.38 g, 73%).

4.2.2.3. Synthesis of (3-azidopropyl)trimethoxysilane

(3-bromopropyl)trimethoxysilane (2 mL, 10.8 mmol), NaN_3 (1.76 g, 27.2mmol), tetrabutylammonium bromide (0.64 g, 2 mmol) and dry acetonitrile (35 mL) were added to a three-necked round-bottomed flask. Under nitrogen atmosphere, the reaction mixture was stirred for 48 h at 82 °C. After the flask is cooled in air, the unreacted sodium azide was filtered and the solvent was removed under *vacuum*. Cyclohexane (15 mL) was added to the mixture and subsequently filtered.

Cyclohexane was evaporated under *vacuum* and the colorless liquid was obtained.

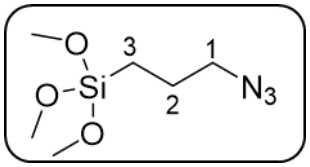

^{1}H-NMR (300 MHz, $CDCl_3$) (δ, ppm): 3.57 (s, 9H), 3.24-3.28 (m, 2H, N_3-CH_2, H_1), 1.68-1.72 (m, 2H, CH_2, H_2), 0.67-0.71 ppm (m, 2H, Si-CH_2, H_3).

4.2.2.4. Synthesis of (3-bromopropyl)phosphonic acid

Diethyl (3-bromopropyl)phosphonate (0.50 g, 1.58 mmol) was dissolved in anhydrous dichloromethane (20 mL) and BTMS (0.80 mL, 6 mmol) was added to the solution. Then, the reaction was stirred at room temperature for 12 h under nitrogen atmosphere. After that time, the solvent was evaporated under *vacuum*. Then, anhydrous methanol (15 mL) was added and the solution was stirred for 4 days at room temperature under nitrogen atmosphere. Finally, the solvent was evaporated under *vacuum*, obtaining (3-bromopropyl)phosphonic acid as orangish liquid (0.38 g, 96%). ^{1}H-NMR (300MHz, $CDCl_3$) (δ, ppm): 5.48 (sz, 2H, OH), 3.59 (t, 2H, *J*=6.0Hz,

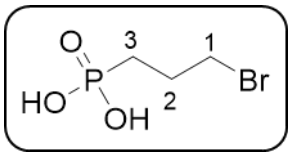

CH_2Br, H_1), 2.00 (m, 2H, P-CH_2, H_3), 1.60 (m, 2H, CH_2, H_2); ^{31}P-NMR (32 MHz, $CDCl_3$) (δ, ppm): 26.11 (s, 1P, $(OH)_2$**P**O-CH_2-R).

4.2.2.4. Hydrolysis of Ti6Al4V samples

1x1 cm square Ti6Al4V samples were ultrasonically cleaned for 20 min in acetone, deionized water and ethanol (5 times for each solvent). Then, samples were dried overnight at 60 ºC before surface modification. Once dried, Ti6Al4V samples were submerged in a mixture (3:1 v/v) of sulfuric acid (98% w/w) and hydrogen peroxide (30% w/w) for 1h at room temperature.

4.2.2.5. Formation of Self-Assembled Monolayers (SAMs) onto Ti6Al4V samples

a) Silane-based SAM strategy

Similar to Liu *et al*., Ti6Al4V-OH samples were submerged in an aqueous solution of 5 % (v/v) (3-bromopropyl)trimethoxysilane for 1h at room temperature. To remove unreacted silane the samples were washed ultrasonically with acetone for 5 min (x 5) and dried in *vacuum* at 40 ºC overnight [39].

b) Phosphonate-based SAM strategy

Similar methodology was employed for the anchoring of (3-bromopropyl)phosphonic acid. Ti6Al4V-OH samples were submerged in an aqueous solution of 5% (v/v)

modified (3-bromopropyl)phosphonic acid for 1 h at room temperature. To remove unreacted phosphonic acid the samples were washed ultrasonically with acetone for 5 min (x 5) and dried in *vacuum* at 40 ºC overnight.

c) Azidation

Sodium azide (0.20 g, 3.07 mmol) was dissolved in acetonitrile/water (1:1 v/v, 10 mL) mixture. After, the previously modified Ti6Al4V samples (Ti6Al4V-Si-Br and Ti6Al4V-P(OH)-Br) were submerged in the solution for 24 h at room temperature under constant stirring. Finally, samples were washed ultrasonically with water and acetone (x3) and dried under *vacuum* overnight for subsequent reactions.

4.2.2.6. Immobilization of dansyl derivative **2b** or salicylic acid derivative **6a** through copper (I) catalyzed azide-alkyne click reaction

Sodium ascorbate (0.08 g, 0.40 mmol) and copper (II) sulfate pentahydrate (0.033 g, 0.13 mmol) were dissolved in ethanol/water (6:4 v/v, 10 mL) mixture. Then, triethylamine (0.75 mL, 5.34 mmol) was added along with dansyl derivative **2b** or salicylic acid derivative **6a** (0.52 g, 2.97 mmol). Then, modified Ti6Al4V-P(OH)-N_3 or Ti6Al4V-Si-N_3 surfaces were submerged onto the solution and stirred for 48 h at room temperature. Finally, samples were washed with water and dried under *vacuum* for further characterization.

4.2.3. Physicochemical compound and surface characterization

4.2.3.1. Nuclear Magnetic Resonance (NMR)

The proton (^{1}H-NMR), carbon thirteen (^{13}C-NMR) and phosphorus thirty one (^{31}P-NMR) nuclear magnetic resonance spectra were performed at room temperature in an AV-300 spectrometer (300 MHz for ^{1}H, 75.4 MHz for ^{13}C and 32 MHz for ^{31}P) (Bruker, Rheinstetten, Germany) using deuterated chloroform and dimethylsulfoxide as solvent. Also, some ^{1}H and ^{31}P experiments were performed at room temperature in an AV-500 spectrometer (500 MHZ for ^{1}H and 125.8 MHz for ^{31}P), employing same deuterated solvents. Chemical shifts are expressed in parts per million (ppm) relative to TMS using the residual signal of the solvent [in $CDCl_3$:7.26 ppm (^{1}H) and 77.0 (^{13}C) and in DMSO-d_6: δ=2.50 ppm (^{1}H) and 39.5 ppm (^{13}C)] as internal reference. Coupling constants (*J*) are expressed in Hertz (Hz).

4.3.2.2. Fourier transformed infrared spectroscopy (FTIR)

By means of Fourier Transformed Infrared 2-hydroxy-*N*-(prop-2-yn-1-yl)benzamide (**6a**), salicylic acid and acetylsalicylic acid were analyzed. For this purpose, NICOLET Nexus FT-IR spectrophotometer (Thermo Electron Corporation, Thermo Scientific, Loughborough, UK) was employed. Each sample was measured between 4000 cm^{-1} and 500 cm^{-1} wavelength, with a resolution of 4 cm^{-1} and 32 scans per spectrum.

4.3.2.3. X-ray photoelectron spectroscopy (XPS)

The elemental analysis of modified Ti6Al4V samples was carried out by X-ray photoelectron spectroscopy SPECS system (XPS, SPECS Surface Nano Analysis, Berlin, Germany) using focus monochromatic radiation source 500 with dual anode Al/Ag and it is equipped with a 150 1D-DLD analyzer (Phoibos, Berlin, Germany). Ti6Al4V samples were fixed with stainless steel holders and carbon tape during the measurements. Moreover, a carbon reference was used to do the measurements.

4.3.2.4. Scanning electron microscopy (SEM)

Surface morphology of all samples was monitored by a Fine coat ion sputter JFC-1100 Scanning electron microscope (SEM). The micrographs were taken using a S-Hitachi 4800 (Singapore, Japan) and operated at 2 kV, 20 mA, 150s and 50.000x zoom). All SEM images were analyzed and processed by image analysis freeware Fiji.

4.3.2.5. Water Contact angle (WCA)

The change in hydrophobicity in Ti6Al4V samples caused by surface modifications was analyzed using contact angle method (NEURTEK Instruments OCA 15 EC, Eibar, Spain). Milli-Q water was used as a testing liquid and sessile drop method (2 µL per drop) was carried out at room temperature to do the measurements. The average values were calculated using 3 measurements of each composition.

4.3. Results and discussion

As discussed in the introduction, this chapter described the utilization of copper (I) catalyzed azide-alkyne reaction to immobilize biologically active compounds onto Ti6Al4V. Again, to validate the proposed methodology, the use of a fluorophore, specifically the well-known dansyl, was considered. It is important to highlight that immobilizing both dansyl and drug derivatives required prior modifications, as does Ti6Al4V surfaces, aimed to introduce the necessary functional groups for the click reaction.

Among surface functionalization, two distinct strategies involving SAMs were chosen: silane anchor monolayer and phosphonate anchor monolayer. As can be seen in **Scheme 4.1 and 4.2**, the azide functional group was incorporated on SAM, and therefore, on Ti6Al4V surface. This incorporation was be performed by two approaches, both involving the substitution of the bromide functional group into azide group. In the first approach, the commercially available silane was initially anchored, followed by the nucleophilic substitution. Conversely, in the second approach, the (3-azidopropan)trimethoxysilane monomer was previously synthesized and subsequently anchored to the surface. Although both approaches led to same surface functionalization, the first approach resulted in more homogeneous SAM formation as contact angle values demonstrated, which agrees with literature [40]. That why, only the results obtained from first approach will be discussed in this Section.

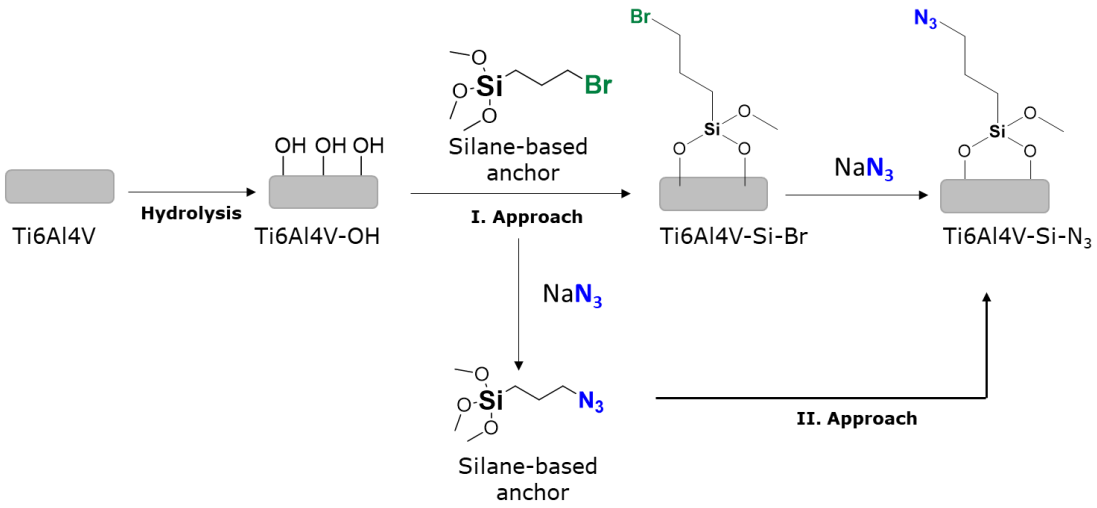

Scheme 4.1. Ti6Al4V hydrolysis and the proposed two silanization approaches.

Same approach was employed for phosphonate based SAM (**Scheme 4.2**), but in this case the commercially available phosphonate required from a previous hydrolysis reaction for better anchoring.

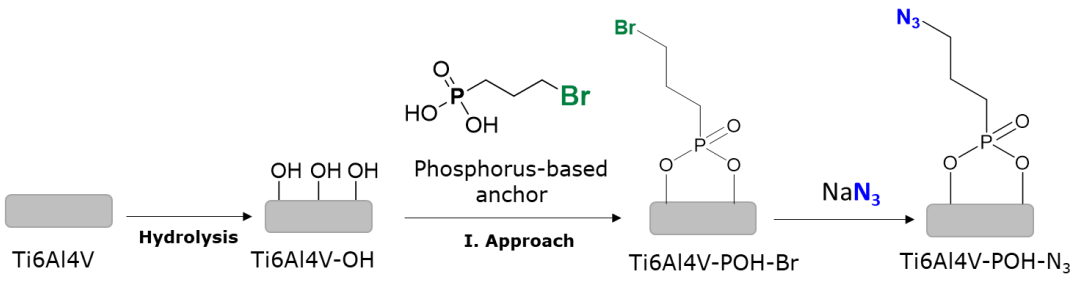

Scheme 4.2. Phosphonate-based SAM formation with incorporated azide moiety.

For better understanding of the work, this chapter will separately detail the results obtained from the modification of the compounds and the surface modifications, along with their characterization techniques.

4.3.1. Derivatization of chemically active compounds and NMR and FTIR analysis

4.3.1.1. Salicylic acid and its derivatives

In this chapter, the conventional azide alkyne click reaction and SAM strategy represent the preferred methods for bioconjugating anticoagulant drugs to the surface of Ti6Al4V. To implement this methodology, specific surface and drug functionalization were required.

Initially, the proposition to employ a widely recognized drug, acetylsalicylic acid (commonly referred to as aspirin) for immobilizing anti-inflammatory and anticoagulants onto metallic surfaces was considered. As aspirin is a prodrug, converting to salicylic acid in physiological conditions, both aspirin and salicylic acid were presented as potential options for bioconjugation. Given the inherent significance of azide and alkyne functional groups on click reactions, the focus was on introducing one of these two groups onto the structure of the drugs. Specifically, the alkyne moiety was introduced through amidation reaction, employing propargylamine as nucleophile (**Scheme 4.3**). It has to be noted that the amidation reaction required two steps, (I) the activation of the carboxylic acid group by using thionyl chloride to generate the corresponding acyl chloride and (II) the nucleophilic addition of propargylamine. Different reaction conditions were employed in order to carry out the required functionalization (**Table 4.1**).

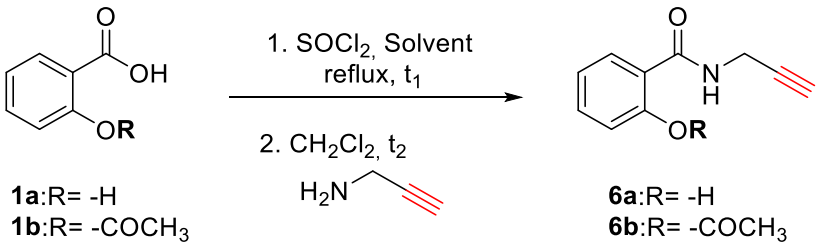

Scheme 4.3. Modification of acetylsalicylic acid and salicylic acid.

Table 4.1. Reaction conditions used for the amidation reaction of acetylsalicylic acid and salicylic acid.

Entry	R	$SOCl_2$ (eq.)	Propargylamine (eq.)	Solvent	t_1 (h)	t_2 (h)	Product	Yield (%)
1	-$COCH_3$	1	1	CH_2Cl_2	2	24	[c]	-
2	-$COCH_3$	1	1	CH_2Cl_2	12	24	[c]	-
3	-$COCH_3$	2	2	CH_2Cl_2	12	24	[c]	-
4	-$COCH_3$	2	2	CH_2Cl_2	24	24	[c],[d]	
5	-$COCH_3$	2	2	CH_2Cl_2	48	24	[c]	
6	-$COCH_3$	2	2	CH_2Cl_2	48	72	[c]	
7	-$COCH_3$	2	2	Toluene	4	24	[c},[d]	-
8	-$COCH_3$	1.5	1.5	Toluene	4	24	[c]	-
9	-$COCH_3$	1.5	1.5	Toluene	4	72	[c]	-
10	-$COCH_3$	1.5	1.5	Toluene	24	48	[c]	-
11	-$COCH_3$	3	3	Toluene	24	48	[c]	-
12	-$COCH_3$	3	3	Toluene	24	72	[c]	-
13	-$COCH_3$	5	5	Toluene	24	48	6a	81
14	-$COCH_3$	10	10	Toluene	24	48	6a	81
15	-H	5	5	Toluene	24	72	6a	64
16	-H	2.5	2.5	Toluene	24	72	6a	73

[c] Starting substrate recovered [d] propargylamine traces observed (no total conversion)

As can be seen in **Table 4.1**, after several trials, only four experiments concluded successfully. In the first five experiments, acetylsalicylic acid was employed as starting material and dichloromethane as solvent. After several changes in reaction time and molar ratios, desired product was not obtained. Therefore, it was decided to increase the reflux temperature of the first stage. For this purpose, a solvent with a higher boiling point was chosen, such as toluene, which, in addition, had already

been used in previous amidation reactions giving good results. Again, several changes in reaction time and molar equivalence were performed, but in this case, resulting in most cases, **6a** product with traces of propargylamine. Only when the molar equivalence of $SOCl_2$ and propargylamine was up to 5 complete conversion was achieved (**Entry 13**). It has to be noted that despite employing different drugs, aspirin and salicylic acid, the same product was obtained on both reactions, specifically 2-hydroxy-*N*-(prop-2-yn-1-yl)benzamide (**6a**). In fact, in these conditions, when aspirin was used as starting material, the deacetylation of the phenolic group occurred. In fact, the excess of thionyl chloride caused the hydrolysis of the ester group of aspirin, obtaining salicylic acid derivative, which was further functionalized with propargylamine. All reactions were followed by TLC and analyzed by NMR (**Figure 4.3**).

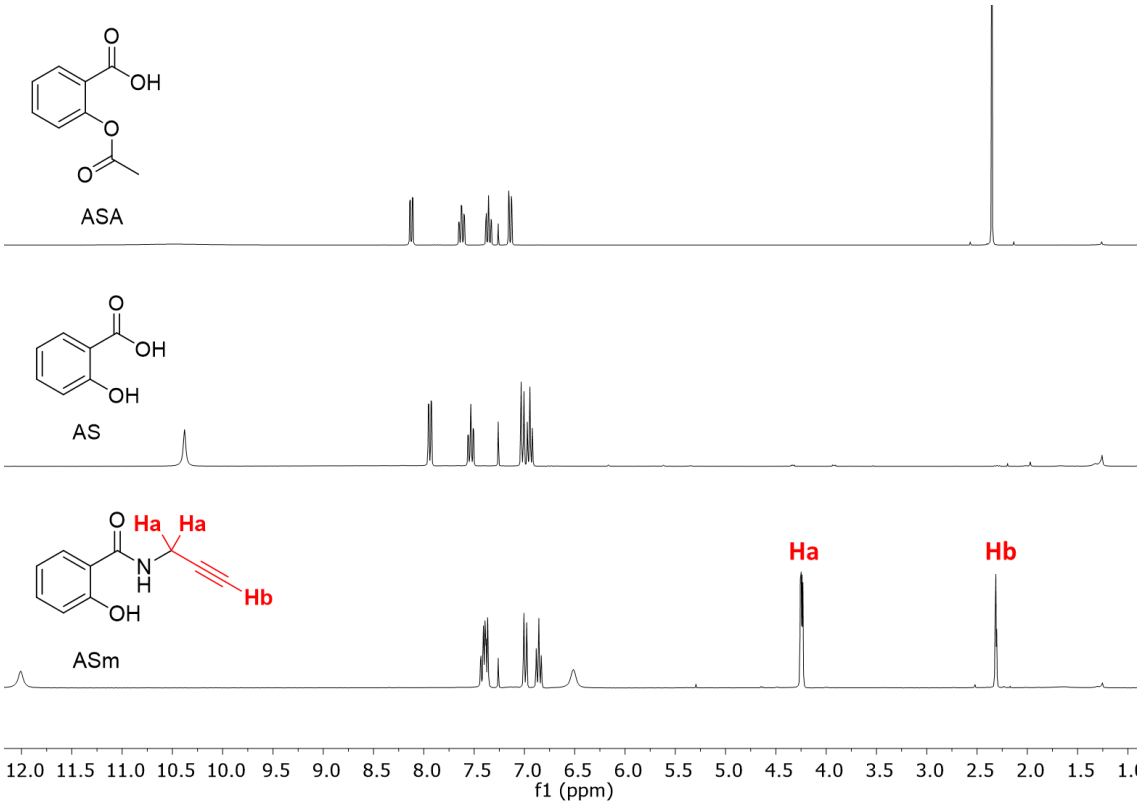

Figure 4.3. NMR spectra of acetylsalicylic acid, salicylic acid and its derivative **6a.**

By means of NMR, the conversion of salicylic acid into 2-hydroxy-*N*-(prop-2-yn-1-yl)benzamide was observed, concluding that the reaction was carried out successfully. As can be seen in **Figure 4.3**, three new signals appear in the obtained product, which corresponded to the protons of the introduced propargyl group. Indeed, at 2.32 ppm chemical shift a triplet integrating for 1 proton can be observed, corresponding to the terminal alkynic hydrogen of the propargyl moiety. Moreover,

there is another signal with two hydrogen integration corresponding to methylenic appeared at 4.26 ppm. Finally, at 6.54 ppm and 12.00 ppm two broad signals can be observed corresponding to amide proton and hydroxyl group. These findings concluded that the obtained product was, indeed, 2-hydroxy-*N*-(prop-2-yn-1-yl)benzamide (**6a**).

Based on the finding from FTIR analysis, the results consistently indicated the successful incorporation an alkyne functional group into the molecular structure of salicylic acid (**Figure 4.4**).

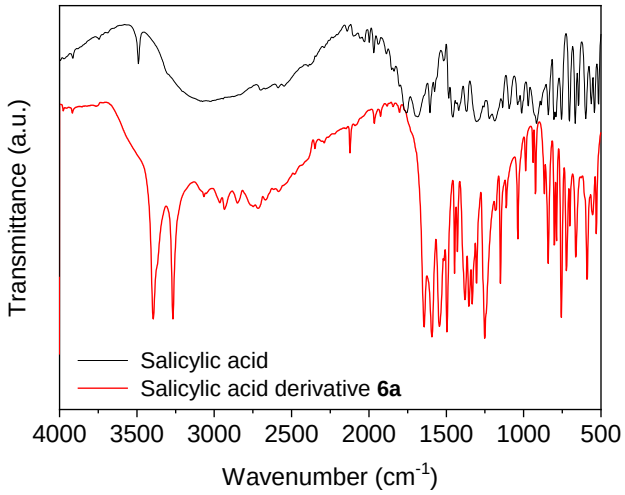

Figure 4.4. FTIR spectra of salicylic acid and salicylic acid derivative **6a**.

The FTIR spectra analysis of both compounds revealed distinctive features. In both spectra, the characteristic signal of an OH bond could be seen around 3200 cm^{-1}. However, in the case of the salicylic acid derivative **6a**, an additional band emerged at approximately 3400 cm^{-1}, indicating the NH stretching vibration. Contrarily, salicylic acid spectra displayed the typical C=O bond stretching vibration at 1700 cm^{-1}, representing the carboxylic acid moiety of SA. After amidation reaction, the salicylic acid derivative **6a** spectra exposed C=O bond at 1650 cm^{-1} of amide group, often characterized by two head peaks. Moreover, the salicylic acid derivative **6a** spectra exhibited two characteristics bands corresponding to C_{sp}-C_{sp} and C_{sp}-H bonds at 2100 cm^{-1} and 3300 cm^{-1} respectively. These results validated, again, the success of the amidation reaction.

4.3.1.2. Synthesis of (3-bromopropyl)phosphonic acid

To carry out the formation of phosphonate-based SAMs on the metallic surface a previous hydrolysis reaction was required to obtain the phosphonic acid (**Scheme 4.4**). The transformation of phosphonate to phosphonic acid through hydrolysis required a two-step process as well. Notably, the singular variable altered on both was the reaction time as can be seen in **Table 4.2**.

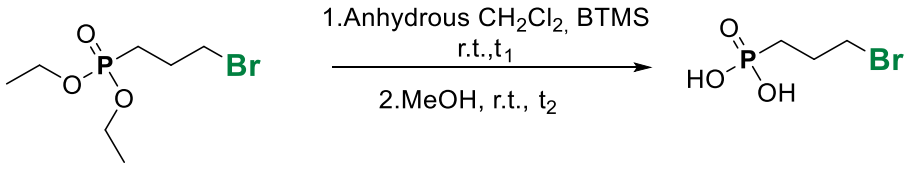

Scheme 4.4 Synthesis of (3-bromopropyl)phosphonic acid.

Several reaction conditions were employed until afford the desired product, in **Table 4.2** are summarized all the changes.

Table 4.2. Reaction conditions of the hydrolysis reaction of diethyl (3-bromopropyl)phosphonate.

Entry	t_1 (h)	t_2 (h)	Yield (%)
1	24	24	[a]
2	96	24	[a]
3	144	24	[a]
4	96	72	96

[a] only starting product was recovered with traces of (3-bromopropyl)phosphonic acid

The obtained product was analyzed by ^{1}H-NMR and ^{31}P-NMR as can be seen in **Figure 4.5 and Figure 4.6**. The first three trial did not show any product, despite increases reaction time to 6 days. However, to our delight the increase in the time of the second reaction step caused a drastic increase in the conversion of the reaction (**Entry 4**, **Table 4.2**).

By means of ^{31}P-NMR spectra the successfulness of the hydrolysis reaction of diethyl (3-bromopropyl)phosphonate was corroborated. **Figure 4.5** displays the spectra for

both diethyl (3-bromopropyl)phosphonate and (3-bromopropyl)phosphonic acid. The presence of a single phosphorus species (at 26.21 ppm), displayed at a lower chemical shift compared to diethyl (3-bromopropyl)phosphonate, confirmed the singular product formation, thereby implying the synthesis of the acid product.

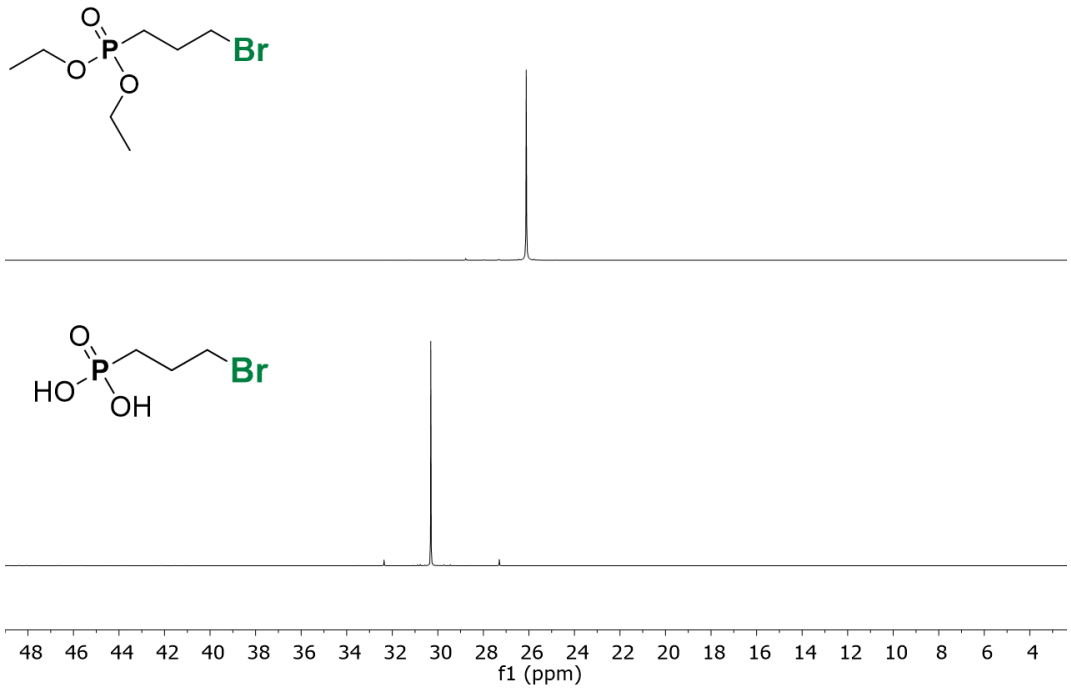

Figure 4.5. ^{31}P-NMR spectra of diethyl (3-bromopropyl)phosphonate and (3-bromopropyl)phosphonic acid.

^{1}H-NMR analysis provided additional confirmation of the success of the hydrolysis reaction (**Figure 4.6**). Notably, the signals corresponding to ethyl group, at 1.27 (-OCH_2) and 4.04 (-CH_3) ppm, disappeared in the product spectra ((3-bromopropyl)phosphonic acid). Instead, a distinctive broad singlet emerged at 5.48 ppm was observed, corresponding to the two hydroxyl groups of the product.

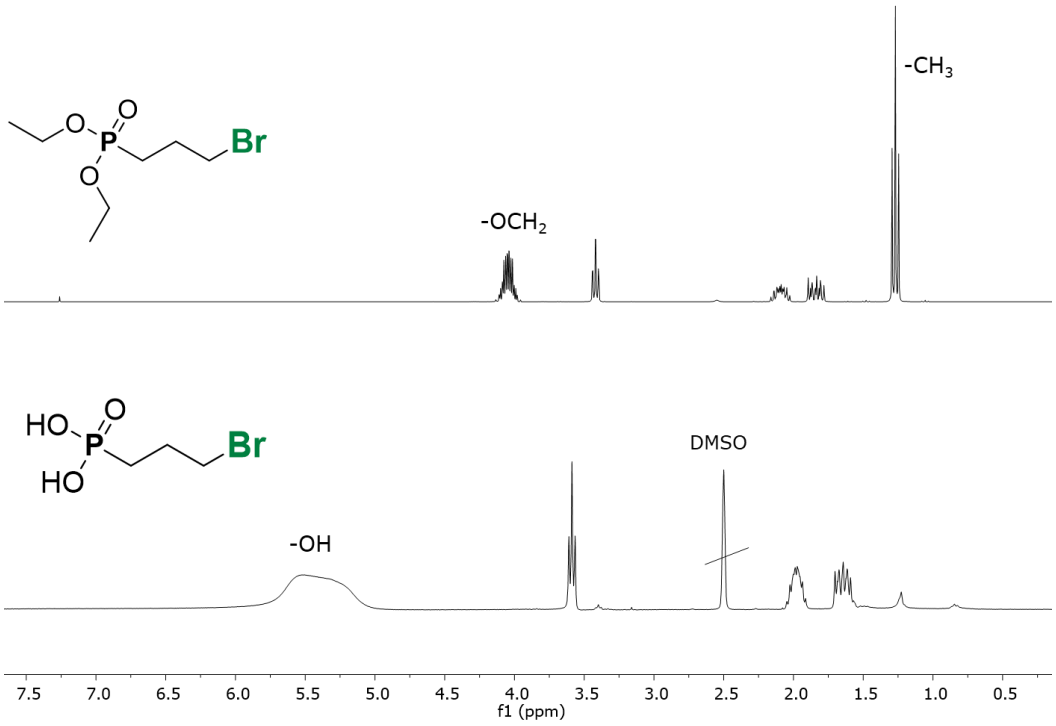

Figure 4.6. ^{1}H-NMR spectra of diethyl (3-bromopropyl)phosphonate and (3-bromopropyl)phosphonic acid.

Once all the reagents necessary for the immobilization of the dansyl derivative **2b** and salicylic acid derivative **6a** were synthesized, we proceeded to the functionalization of the Ti6Al4V surface.

4.3.2. Surface physicochemical characterization

As commented, again, the validation of the proposed two SAM methodologies was corroborated with dansyl fluorophore. As can be seen in **Scheme 4.5**, the fluorophore was derivatized with the required alkyne moiety and immobilized onto Ti6Al4V surfaces through CuAAC reaction.

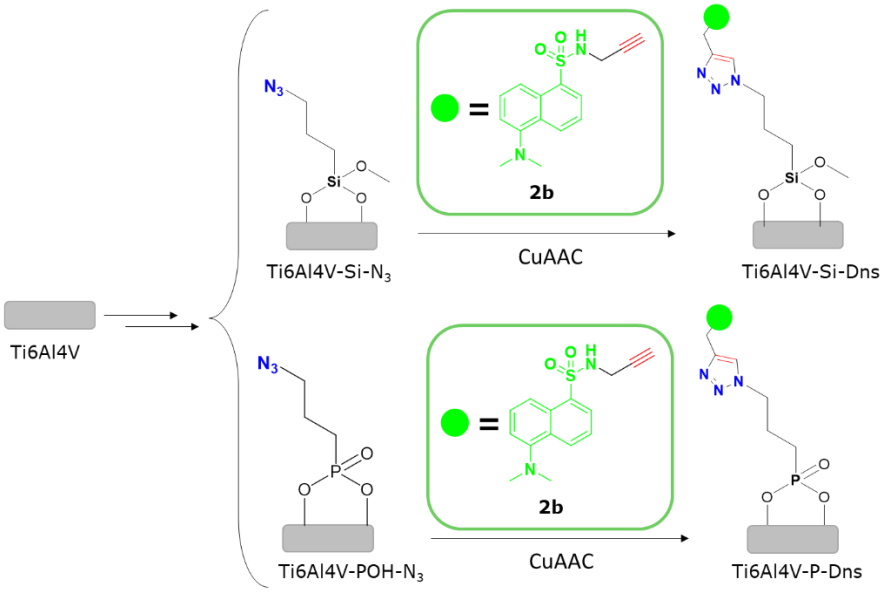

Scheme 4.5. Dansyl derivative **2b** immobilization onto Ti6Al4V *via* CuAAC reaction.

Overall, Ti6Al4V surfaces were subjected to four different functionalizations: hydrolysis, silanization or phosphorylation, azidation and click reaction. XPS, SEM, epifluorescence and contact angle techniques were employed to perform the physicochemical characterization of the obtained samples in each transformation. In the next sections the results obtained with each of those techniques will be commented.

4.3.2.1. XPS and epifluorescence analysis of pristine and functionalized Ti6Al4V samples

In order to monitor each step of functionalization onto Ti6Al4V surfaces, the analysis of surface chemical composition was carried out by XPS (**Figure 4.7**). Moreover, a deconvolution of each elemental was performed to determine in more detail the generated and broken bonds. In **Table 4.3** atomic chemical compositions of the following surfaces are shown: pristine Ti6Al4V and functionalized Ti6Al4V-Si-Br, Ti6Al4V-OH, Ti6Al4V-Si-Br, Ti6Al4V-Si-N3, Ti6Al4V-Si-Dns and Ti6Al4V-Si-D-ASm.

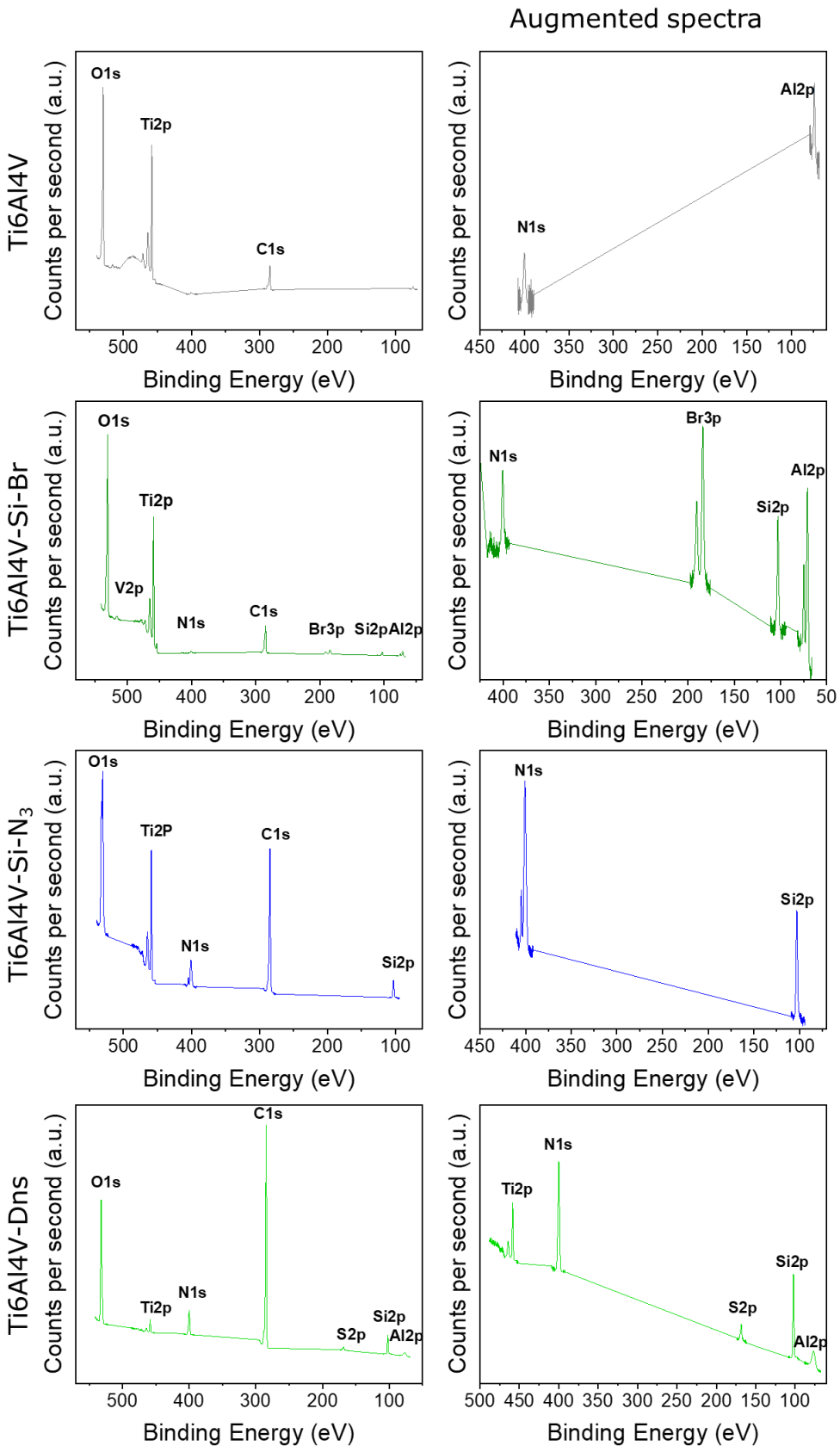

Figure 4.7. XPS total spectra of Ti6Al4V, Ti6Al4V-Si-Br, Ti6Al4V-Si-N_3 and Ti6Al4V-Si-Dns samples.

Table 4.3. Chemical atomic composition of Ti6Al4V surface modification route 1.

	Elemental chemical composition (%)									
Sample	**Ti**	**Al**	**V**	**C**	**O**	**N**	**Si**	**P**	**Br**	**S**
Ti6Al4V	7.9	1.6	1.9	11.9	74.5	1.1	-	-	-	-
Ti6Al4V-Si-Br	13.4	2.9	0.4	24.1	51.6	0.9	2.8	-	1.2	-
Ti6Al4V-Si-N_3	6.7	0.9	0.1	44.6	31.8	5.6	7.5	-	-	-
Ti6Al4V-Si-Dns	0.9	-	-	67.7	17.1	9.9	1.5	-	-	2.8

As can be seen in **Table 4.3**, the major components in the unmodified titanium surface are carbon and oxygen, followed by titanium, aluminum and vanadium. The high percentage of carbon and oxygen may be due to external contamination of the sample, since despite being stored under vacuum systems, the transport and handling of the sample were carried out at atmospheric pressure. However, a small percentage of these elements is not surprising, since the manufacturers described the material with these small impurities and even the appearance of the nitrogen. In addition, it can also be highlighted, as expected, that titanium appeared in higher concentration compared to the other two metals in this alloy.

Regarding Ti6Al4V-Si-Br surface, the compositions of before mentioned elements varied considerably and, as expected, new elements such as silicon and bromide appeared. First, it has to be considered that the irradiation employed in XPS technique is only capable of penetrating a few nanometers of the surface, and the formation of the SAM hinders the penetration of the irradiation to the metal surface. This is why elements such as aluminum or vanadium appear in lower concentrations compared to pristine Ti6Al4V.

On the other hand, the atomic composition of oxygen decreased, while that of carbon, as expected, increased since C is the major component of anchored (3-bromopropyl)trimethoxysilane. Moreover the appearance of silicon and bromine again confirmed the successful anchoring of the silane layer on Ti6Al4V. Thus determining that a silane SAM had been achieved onto Ti6Al4V alloy.

After successful silanization of the surface, a S_N2 reaction was carried out using sodium azide. Newly, in this case, the success of the reaction could be observed by XPS. In this case, a disappearance of bromine and an increase in nitrogen content was observed.

The deconvolution of the signals allowed to determine the species exposed on the surface. Firstly, the species found in pristine Ti6Al4V surface were studied (**Figure 4.8**).

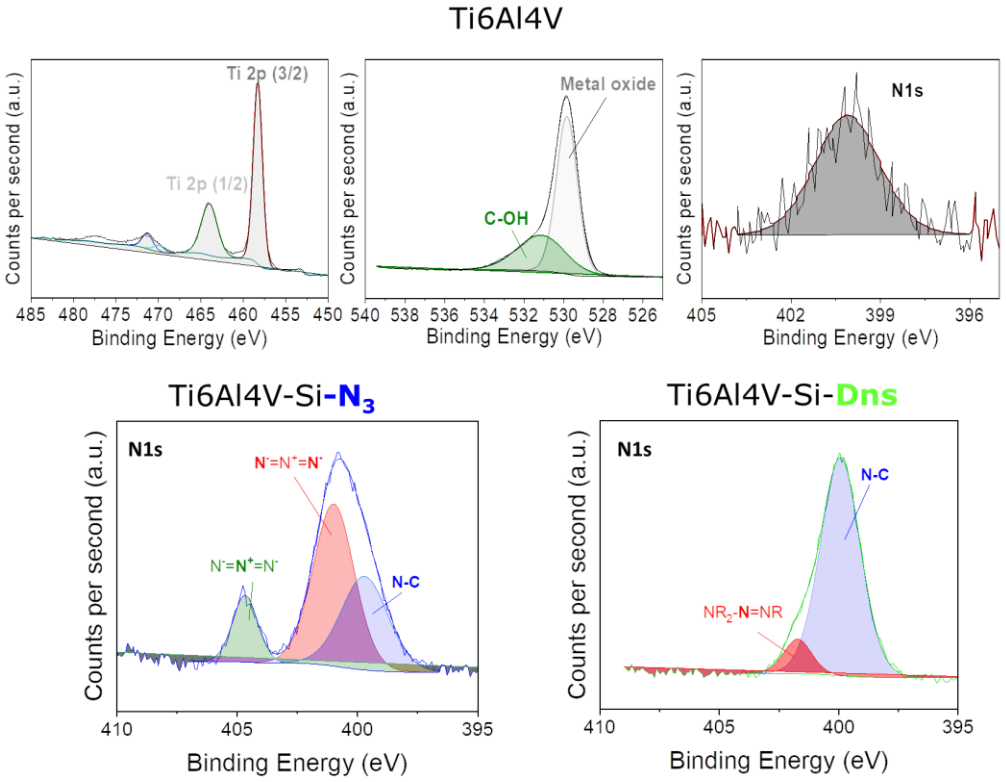

Figure 4.8. Ti, O and N deconvolution XPS spectra of pristine Ti6Al4V, N deconvolution XPS spectra of Ti6Al4V-Si-N_3 and Ti6Al4V-Si-Dns samples.

As can be seen in **Figure 4.8**, the carbon and oxygen species confirmed the passivation of the unmodified Ti6Al4V sample. The carbon deconvolution spectra of pristine T6Al4V confirmed that the majority species in carbon is C_{sp3}. These results agree with the composition described by the manufacturers.

As expected, after hydroxylation metal-OH species appeared in higher concentration compared to unmodified Ti6Al4V and limiting the passivation of the surface. Once the surface was activated, further functionalization, as silanization, was possible. Both Ti6Al4V-Si-Br and Ti6Al4V-Si-N_3 showed similar species composition on C, O, Ti, Al, Si elements, the only difference was bromine and nitrogen elements spectra. It has to be highlighted that unexpected signals were found in nitrogen spectra. Due to the X-ray photoelectron energy used for the characterization, the cleavage of the $^{-}N=N^{+}=N^{-}$ azide compound was confirmed by the presence of N_2 and N^{-} in the XPS spectra of nitrogen (**Figure 4.8**) [41].

Similar results were obtained when Ti6Al4V surface was functionalized with phosphonic acid derivative (**Scheme 4.2**). The elemental analysis of each sample are summarized in **Table 4.4**. In the XPS spectra depicted in **Figure 4.9**, after surface phosphorylation, the emergence of two distinct peaks corresponding to P2p and Br2p at 164 eV and 180 eV, respectively, was observed. These results strongly indicated the successful anchoring of (3-bromopropyl)phosphonic acid onto Ti6Al4V surface. Adopting silane-based approach, after surface phosphorylation, an interconversion of bromide moiety to azide functional group was carried out. This transformation was clearly evident in the Ti6Al4V-P-N_3 XPS spectra, where not only did the bromide element disappear, but the increase of nitrogen contribution, along with the deconvolution of N spectra, confirmed the presence of azide on the surface. Upon immobilization dansyl derivative **2b**, the characteristic element of dansyl, S2p, was observed. These findings corroborated the conjugation of dansyl derivative **2b** employing phosphonate based SAM formation.

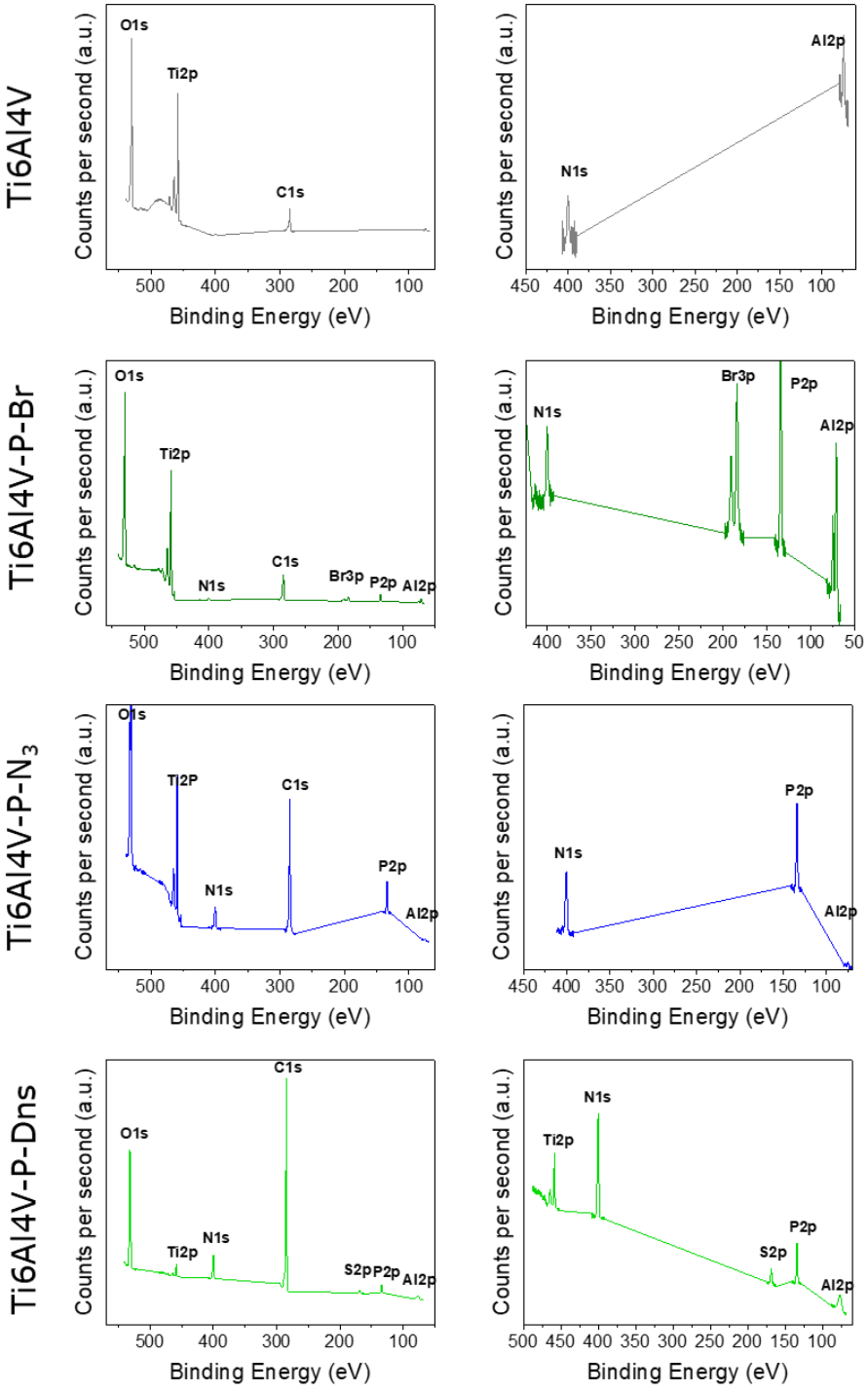

Figure 4.9. XPS spectra of pristine Ti6Al4V, Ti6Al4V-OH, Ti6Al4V-P-OH-Br, Ti6Al4V-P-N_3 and Ti6Al4V-Dns surfaces.

Table 4.4. Chemical atomic composition of Ti6Al4V surface modification based on phosphonate anchoring.

	Atomic chemical composition (%)									
Sample	**Ti**	**Al**	**V**	**C**	**O**	**N**	**Si**	**P**	**Br**	**S**
Ti6Al4V	7.9	1.6	1.9	11.9	74.5	1.1	-	-	-	-
Ti6Al4V-POH-Br	16.3	1.3	0.4	15.0	59.4	0.6	0.8	3.8	1.6	-
Ti6Al4V-POH-N_3	12.6	1.4	0.4	21.9	46.0	1.7	0.5	1.7	-	-
Ti6Al4V-POH-Dns	1.2	-	-	43.1	12.8	2.3	0.5	0.9	-	1.8

As commented before, carbon and oxygen elements were found in higher concentration compared to Ti, Al o V. In contrast to silane, in this strategy the titanium signals are not so compromised and its value remains stable throughout the different reactions step.

Additionally, the surfaces of pristine Ti6Al4V, Ti6Al4V-Si-Dns and Ti6Al4V-P-Dns were meticulously examined using fluorescence microscopy to further validate the effective immobilization of the dansyl fluorophore. **Figure 2.10** illustrates that upon excitation at 305 nm wavelengths, only Ti6Al4V-Si-Dns and Ti6Al4V-P-Dns surfaces exhibited a distinct green fluorescence, unequivocally associated with the presence of dansyl. These observations serve to further confirm the successful immobilization of dansyl derivative **2b** on both TI6Al4V surfaces.

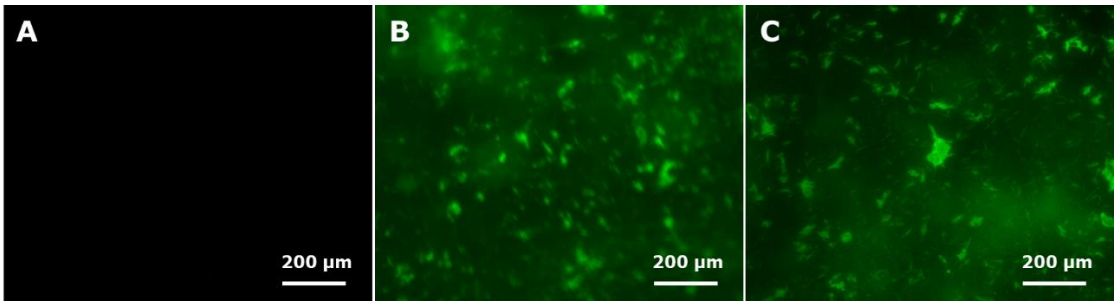

Figure 2.10. Fluorescence emission of (A) Pristine Ti6Al4V, (B) Ti6Al4V-Si-Dns and (C) Ti6Al4V-P-Dns surfaces.

4.3.2.2. SEM and contact angle of pristine and functionalized Ti6Al4V samples

After demonstrating the successful immobilization of dansyl derivative **2b** onto Ti6Al4V, we proposed to employ the same methodology to bioconjugate salicylic acid derivative **6a** (**Scheme 4.6**). For a better comprehension of the work, the SEM and contact angle results obtained from the immobilization of dansyl derivative **2b** will be combined with the results of salicylic acid derivative **6a** immobilization. The changes

on the topography of metallic surfaces occurred after each functionalization step were studied by means of SEM.

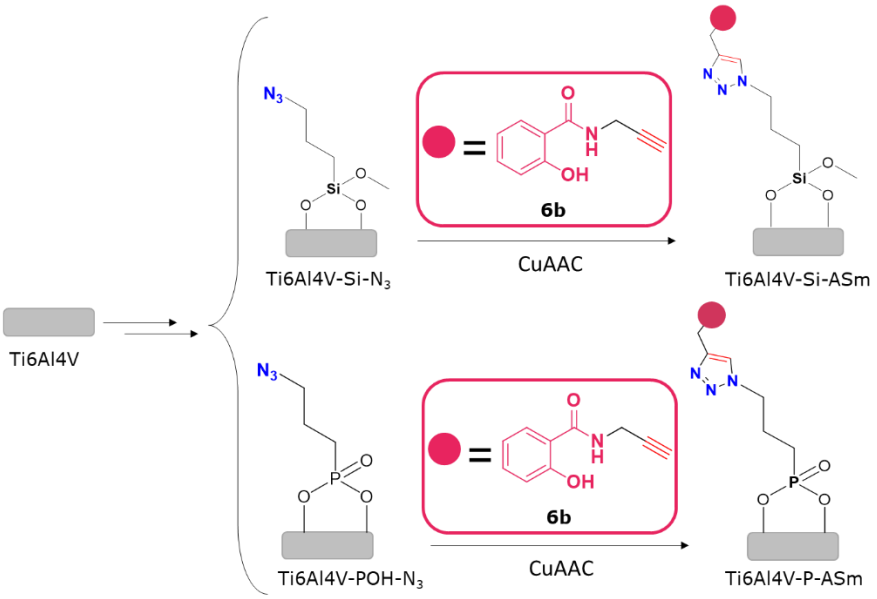

Scheme 4.6. Ti6Al4V surface functionalizations for salicylic acid derivative **5a** immobilization.

As can be seen in **Figure 4.11** and **Figure 4.12**, as anticipated, pristine Ti6Al4V exhibited a flat and smooth surface. After hydrolysis process, noticeable cracking and fissures were observed in Ti6Al4V-OH surfaces. In fact, these findings are not surprising, given the relatively harsh hydrolysis conditions (H_2SO_4:H_2O_2 piranha solution) applied, a factor that is typically associated with causing minor degradations on the surface. Notably, significant alteration in topography occurred after each silane and phosphonate anchoring. Both, Ti6Al4V-Si-Br and Ti6Al4V-P-Br surfaces exhibited some minor protrusions, with pronounced ridges and valleys, suggesting a complex topography, being more notorious on silane based surfaces. The transformation of bromide to azide did not led significant changes in topography. Conversely, dansil derivative **2b** and salicylic acid derivative **6a** immobilization resulted in rougher surfaces, especially in phosphonate based approach. Ti6Al4V-P-Dns and Ti6Al4V-P-ASm surfaces presented like crystalline grains, more distributed on salicylic acid derivative **6a** immobilized Ti6Al4V surface.

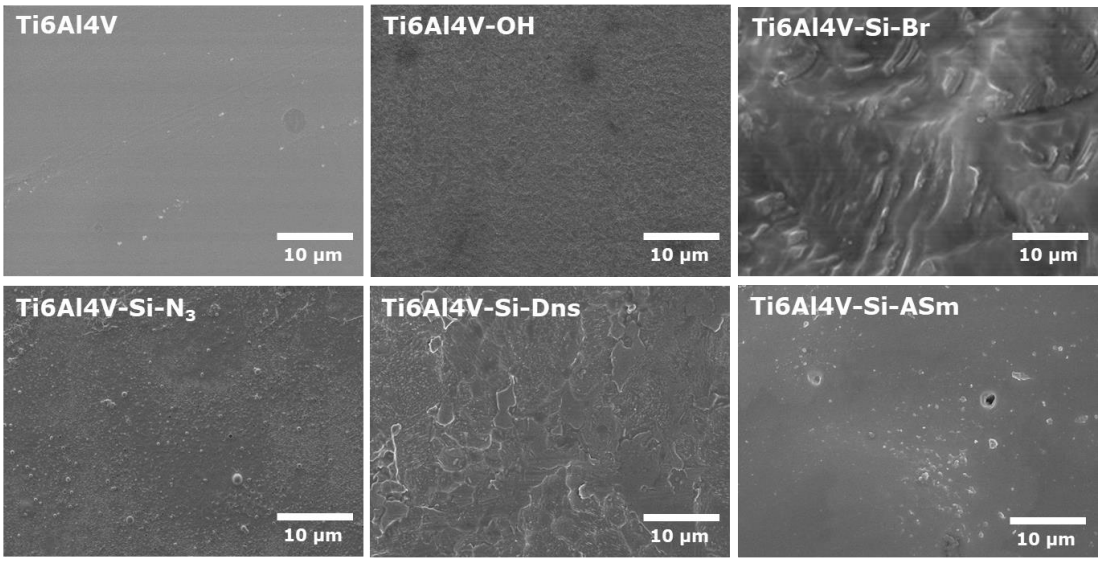

Figure 4.11. SEM images of silane based Ti6Al4V functionalizations.

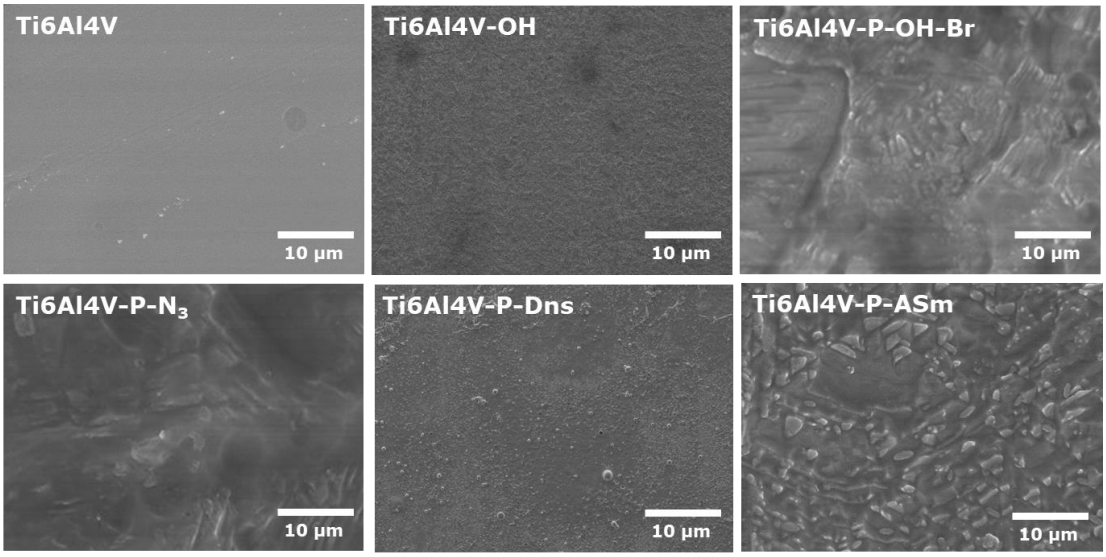

Figure 4.12. SEM images of phosphonate based Ti6Al4V functionalizations.

The change in surface wettability after each reaction step was analyzed using the contact angle technique (**Figure 4.13 and Figure 4.14**). As could be observed, the static water contact angle of pristine Ti6Al4V was 111º. In fact, the high hydrophobicity due to the lack of functional groups on the surface of this metal alloy hinders the subsequent functionalization of the surface. As commented on other sections, both polymeric and metallic surfaces required initial surface pre-activation, where hydrolysis or oxidation approaches are typically employed. In this case, piranha solution was used to form hydroxyl groups on Ti6Al4V surfaces. After hydrolysis reaction, the obtained sample shown to be super hydrophilic, indeed, the contact angle value was near to zero, that the system did not express measurable

value. This drastic change in contact angle values, corroborated the presence of polar groups (-OH), capable of making H-bonds with water, obtaining hydrolyzed Ti6Al4V activated surfaces prepared for posterior functionalization with SAMs.

Once Ti6Al4V surfaces were preactivated with hydroxyl groups, Ti6Al4V-OH samples were submitted to SAM formation, this is, to silanization or, alternatively, phosphorylation. After forming the self-assembled monolayer with silane and phosphonic acid derivatives, both Ti6Al4V-Si-Br and Ti6Al4V-POH-Br presented similar contact angle values. As it was expected, comparing with the precursor surface Ti6Al4V-OH, the angle increased to 112º and 92º, respectively, due to the attachment of carbon backbones on the surface of each sample. These trends align wih the observed alterations in SEM topography. After incorporating the functional group azide, new changes on the contact angle value were observed on both silanizated and phosphorylated Ti6Al4V surfaces. Particularly, the functionalization with azide decreased the contact angle value to 98° in silanizated surfaces, whereas increased to 102° on phosphorylated surfaces. Either way, this changes along with SEM and XPS results confirmed the transformation of Br to azide group. Finally, after the covalent immobilization of either dansyl derivative **2b** or salicylic acid derivative **6a** through CuAAC reactions decreased slightly the contact angle value, specifically to 92º and 90º in silane based surfaces and 98º and 75º in phosphonate based surfaces. It has to be noted that the contact angle value changes were more predominant in phosphonate based surfaces, but, at the same time, the surfaces obtained were more heterogeneous. These findings concluded again that the immobilization of fluorophore and drug derivative was obtained employing copper (I) catalyzed azide-alkyne click reaction.

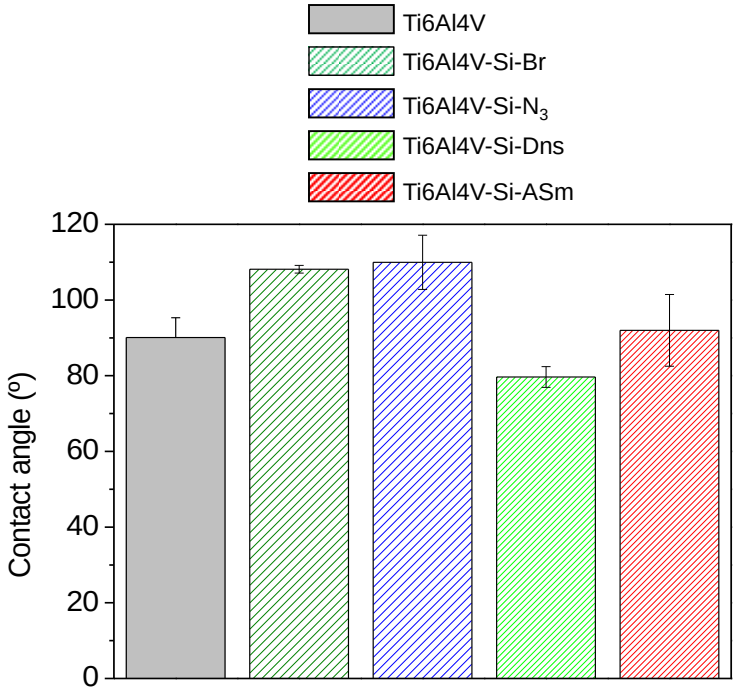

Figure 4.13. Contact angle values of silane-based Ti6Al4V functionalizations.

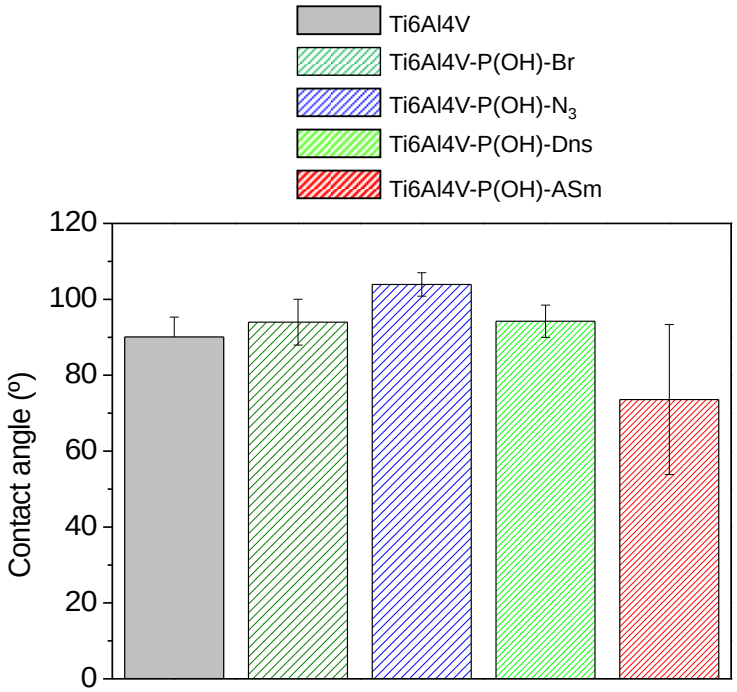

Figure 4.14. Contact angle values of phosphonate based Ti6Al4V functionalizations.

4.4. Conclusions

In this chapter, the combination of SAM strategy with Click Chemistry is detailed. Indeed, both strategies led to covanlent and durability surface functionalization. To achieve this, the surface was previously activated through an acidic hydrolysis reactions and, then, commercially available silane and phosphorus monomers were covalently assembled to the surface. In this case, the immobilization of a salicylic acid derivative was proposed. As in all other chapters, a fluorophore compound was employed to validate the proposed methodology. Once, again, dansyl was used as te fluorophore. The successful immobilization of dansyl was confirmed by XPS, observing the characteristic S element in both silane and phosphonate SAMs. Fluorescence analysis revealed green fluorescence corresponding to dansyl, while slight variations in topography and wettability, confirmed through contact angle and SEM, further corroborated this immobilization. On the other and, the effectiveness of anchoring drugs through the proposed SAM approach and click methodology was again proved by employing salicylic acid as a drug. The immobilization was corroborated by changes in topography and wettability.

4.5. Bibliography

1. Intituto Nacional de Estadística *Defunciones según la causa de muerte - año 2022 (datos provisionales)*; 2023; Vol. 2022;.

2. INE Defunciones según la Causa de Muerte Año 2021 (datos definitivos) y primer semestre 2022 (datos provisionales). *Notas de prensa* **2021**, *2021*, 19.

3. INE *Defunciones según la Causa de Muerte Año 2018*; 2019; Vol. 2018;.

4. Quint, C.; Arief, M.; Muto, A.; Dardik, A.; Niklason, L.E. Allogeneic human tissue-engineered blood vessel. *J. Vasc. Surg.* **2012**, *55*, 790–798, doi:10.1016/j.jvs.2011.07.098.

5. Sapirstein, W.; Alpert, S.; Callahan, T.J. The role of clinical trials in the food and drug administration approval process for cardiovascular devices. *Circulation* **1994**, *89*, 1900–1902, doi:10.1161/01.CIR.89.4.1900.

6. Martin, D.M.; Boyle, F.J. Drug-eluting stents for coronary artery disease: A review. *Med. Eng. Phys.* **2011**, *33*, 148–163, doi:10.1016/j.medengphy.2010.10.009.

7. Boccafoschi, F.; Fusaro, L.; Cannas, M. Immobilization of peptides on

cardiovascular stent. In *Functionalised Cardiovascular Stents*; Elsevier Ltd., 2017; pp. 305–318 ISBN 9780081004968.

8. Meyers, S.R.; Grinstaff, M.W. Biocompatible and bioactive surface modifications for prolonged in vivo efficacy. *Chem. Rev.* **2012**, *112*, 1615–1632, doi:10.1021/cr2000916.

9. Jaffer, I.H.; Weitz, J.I. The blood compatibility challenge . Part 1 : Blood-contacting medical devices : The scope of the problem. *Acta Biomater.* **2019**, *94*, 2–10, doi:10.1016/j.actbio.2019.06.021.

10. Butruk-Raszeja, B.A.; Dresler, M.S.; Kuźmińska, A.; Ciach, T. Endothelialization of polyurethanes: Surface silanization and immobilization of REDV peptide. *Colloids Surfaces B Biointerfaces* **2016**, *144*, 335–343, doi:10.1016/j.colsurfb.2016.04.017.

11. Irena Gotman, P.D. Characteristics of Metals Used in Implants. *J. Endourol.* **1997**, *11*, 383–389.

12. Li, Y.; Yang, C.; Zhao, H.; Qu, S.; Li, X.; Li, Y. New developments of ti-based alloys for biomedical applications. *Materials (Basel).* **2014**, *7*, 1709–1800, doi:10.3390/ma7031709.

13. Sidambe, A.T. Biocompatibility of advanced manufactured titanium implants-A review. *Materials (Basel).* **2014**, *7*, 8168–8188, doi:10.3390/ma7128168.

14. Manivasagam, V.K.; Sabino, R.M.; Kantam, P.; Popat, K.C. Surface modification strategies to improve titanium hemocompatibility: A comprehensive review. *Mater. Adv.* **2021**, *2*, 5824–5842, doi:10.1039/d1ma00367d.

15. Sánchez-Bodón, J.; Diaz-Galbarriatu, M.; Pérez-Álvarez, L.; Moreno-Benítez, I.; Vilas-Vilela, J.L. Strategies to Enhance Biomedical Device Performance and Safety : A Comprehensive Review. *Coatings* **2023**, *13*, 1981–2005, doi:https://www.mdpi.com/2079-6412/13/12/1981/review_report.

16. Sánchez-Bodón, J.; Andrade-Del Olmo, J.; Alonso, J.M.; Moreno-Benítez, I.; Vilas-Vilela, J.L.; Pérez-Alvarez, L. Bioactive Coatings on Titanium: A Review on Hydroxylation, Self-Assembled Monolayers (SAMs) and Surface Modification Strategies. *Polymers (Basel).* **2022**, *14*, 165.

17. Hähner, G.; Hofer, R.; Klingenfuss, I. Order and orientation in self-assembled

long chain alkanephosphate monolayers adsorbed on metal oxide surfaces. *Langmuir* **2001**, *17*, 7047–7052, doi:10.1021/la010713a.

18. Cichomski, M.; Prowizor, M.; Kowalczyk, D.A.; Sikora, A.; Batory, D.; Dudek, M. Comparison of the physicochemical properties of carboxylic and phosphonic acid self-assembled monolayers created on a ti-6al-4v substrate. *Materials (Basel).* **2020**, *13*, 1–17, doi:10.3390/ma13225137.

19. Hasan, A.; Pandey, L.M. *Self-assembled monolayers in biomaterials*; Elsevier Ltd., 2018; ISBN 9780081007167.

20. Faucheux, N.; Schweiss, R.; Lützow, K.; Werner, C.; Groth, T. Self-assembled monolayers with different terminating groups as model substrates for cell adhesion studies. *Biomaterials* **2004**, *25*, 2721–2730, doi:10.1016/j.biomaterials.2003.09.069.

21. Freitas, S.C.; Correa-Uribe, A.; Martins, M.C.L.; Pelaez-Vargas, A. Self-Assembled Monolayers for Dental Implants. *Int. J. Dent.* **2018**, *2018*, doi:10.1155/2018/4395460.

22. Casalini, S.; Bortolotti, C.A.; Leonardi, F.; Biscarini, F. Self-assembled monolayers in organic electronics. *Chem. Soc. Rev.* **2017**, *46*, 40–71, doi:10.1039/c6cs00509h.

23. Nicosia, C.; Huskens, J. Reactive self-assembled monolayers: From surface functionalization to gradient formation. *Mater. Horizons* **2014**, *1*, 32–45, doi:10.1039/c3mh00046j.

24. Senna, P.M.; Mourão, C.F. de A.B.; Mello-Machado, R.C.; Javid, K.; Montemezzi, P.; Cury, A.A.D.B.; Meirelles, L. Silane-coating strategy for titanium functionalization does not impair osteogenesis in vivo. *Materials (Basel).* **2021**, *14*, 1–9, doi:10.3390/ma14071814.

25. Zhou, L.; Xing, Y.; Ou, Y.; Ding, J.; Han, Y.; Chen, J. Prolonged release of an antimicrobial peptide GL13K-loaded thermosensitive hydrogel on a titanium surface improves its antibacterial and. *RSC Adv.* **2023**, *13*, 23308–23319, doi:10.1039/d3ra03414c.

26. Han, X.; Sun, X.; He, T.; Sun, S. Formation of highly stable self-assembled alkyl phosphonic acid monolayers for the functionalization of titanium surfaces and protein patterning. *Langmuir* **2015**, *31*, 140–148,

doi:10.1021/la504644q.

27. Silverman, B.M.; Wieghaus, K.A.; Schwartz, J. Comparative properties of siloxane vs phosphonate monolayers on a key titanium alloy. *Langmuir* **2005**, *21*, 225–228, doi:10.1021/la0482271.

28. Lan, W.C.; Huang, T. Sen; Cho, Y.C.; Huang, Y.T.; Walinski, C.J.; Chiang, P.C.; Rusilin, M.; Pai, F.T.; Huang, C.C.; Huang, M.S. The potential of a nanostructured titanium oxide layer with self-assembled monolayers for biomedical applications: Surface properties and biomechanical behaviors. *Appl. Sci.* **2020**, *10*, doi:10.3390/app10020590.

29. Kolb, H.C.; Finn, M.G.; Sharpless, K.B. Click Chemistry : Diverse Chemical Function from a Few Good Reactions. *Angew. Chemie - Int. Ed.* **2001**, *40*, 2004–2021.

30. Lutz, J. 1 , 3-Dipolar Cycloadditions of Azides and Alkynes : A Universal Ligation Tool in Polymer and Materials Science. *Angew. Chemie - Int. Ed.* **2007**, *46*, 1018–1025, doi:10.1002/anie.200604050.

31. Binder, W.; Kluger, C. Azide/Alkyne-“Click” Reactions: Applications in Material Science and Organic Synthesis. *Curr. Org. Chem.* **2006**, *10*, 1791–1815, doi:10.2174/138527206778249838.

32. Rostovtsev, V. V; Green, L.G.; Fokin, V. V; Sharpless, K.B. A Stepwise Huisgen Cycloaddition Process : Copper (i) -Catalyzed Regioselective ™ Ligation ∫ of Azides and Terminal Alkynes **. *Angew. Chemie - Int. Ed.* **2002**, *41*, 2596–2599.

33. Kaur, J.; Saxena, M.; Rishi, N. An Overview of Recent Advances in Biomedical Applications of Click Chemistry. *Bioconjug. Chem.* **2021**, *32*, 1455–1471, doi:10.1021/acs.bioconjchem.1c00247.

34. Stump, B. Click Bioconjugation: Modifying Proteins Using Click-Like Chemistry. *ChemBioChem* **2022**, *23*, 1–9, doi:10.1002/cbic.202200016.

35. Jin, J.B.; Cai, B.; Zhou, J.M. *Salicylic acid*; Jiayang Li, Chuanyou Li and Steven Smith, 2017; ISBN 9780128115633.

36. Fijałkowski, Ł.; Skubiszewska, M.; Grześk, G.; Koech, F.K.; Nowaczyk, A. Acetylsalicylic Acid–Primus Inter Pares in Pharmacology. *Molecules* **2022**, *27*, doi:10.3390/molecules27238412.

37. Xu, X.M.; Sansores-Garcia, L.; Chen, X.M.; Matijevic-Aleksic, N.; Du, M.; Wu, K.K. Suppression of inducible cyclooxygenase 2 gene transcription by aspirin and sodium salicylate. *Proc. Natl. Acad. Sci. U. S. A.* **1999**, *96*, 5292–5297, doi:10.1073/pnas.96.9.5292.

38. Kim, J.; Kang, S.; Hong, S.; Yum, S.; Kim, Y.M.; Jung, Y. Structure-activity relationship of salicylic acid derivatives on inhibition of TNF-α dependent NFκB activity: Implication on anti-inflammatory effect of N-(5-chlorosalicyloyl)phenethylamine against experimental colitis. *Eur. J. Med. Chem.* **2012**, *48*, 36–44, doi:10.1016/j.ejmech.2011.11.030.

39. Liu, P.; Domingue, E.; Ayers, D.C.; Song, J. Modification of Ti6Al4V substrates with well-defined zwitterionic polysulfobetaine brushes for improved surface mineralization. *ACS Appl. Mater. Interfaces* **2014**, *6*, 7141–7152, doi:10.1021/am501967y.

40. Wang, L.; Schubert, U.S.; Hoeppener, S. Surface chemical reactions on self-assembled silane based monolayers. *Chem. Soc. Rev.* **2021**, *50*, 6507–6540, doi:10.1039/d0cs01220c.

41. Gouget-Laemmel, A.C.; Yang, J.; Lodhi, M.A.; Siriwardena, A.; Aureau, D.; Boukherroub, R.; Chazalviel, J.N.; Ozanam, F.; Szunerits, S. Functionalization of azide-terminated silicon surfaces with glycans using click chemistry: XPS and FTIR study. *J. Phys. Chem. C* **2013**, *117*, 368–375, doi:10.1021/jp309866d.

CHAPTER 5

CONCLUSIONS AND FUTURE WORK

In this chapter, the overall conclusions drawn from the thesis according to objectives outlined in *Chapter 1* are presented. Additionally, various potential avenues for future research endeavors are proposed.

CHAPTER 5

CONCLUSIONS AND FUTURE WORK

5.1. Conclusions

Based on the finding obtained throughout this Doctoral Thesis, the following conclusions have been derived:

- This Doctoral Thesis has proven the remarkable versatility of click reactions in bioconjugating distinct drugs onto various polymeric and metallic surfaces.
- The use of the CuAAC click reaction has facilitated the bioconjugation of indomethacin onto PLLA, curcumin onto PET and salicylic acid onto Ti6Al4V, upon the prior derivatization of the respective drugs and surfaces.
- It is possible to bioconjugate any drug containing sufficient amino nucleophilic groups in the absence of metal catalyst through amino-yne reaction.
- Prior to the bioconjugation of any drug it is extremely important to perform a comprehensive Structure-Activity Relationship (SAR) study of the drugs so that immobilization does not compromise their bioactivity.
- The efficacy of the proposed methodology in mitigating implant rejection has been well-established. Rigorous *in vitro* biological assays have unequivocally demonstrated that the surfaces not only enhance compatibility but also exhibit noteworthy anti-inflammatory, antibacterial and anticoagulant properties.

6.2. Future works & trends

This doctoral thesis has pioneered diverse Click Chemistry strategies for the immobilization of drugs onto both polymeric and metallic surfaces, showcasing promising biomedical applications. Notably, the bioconjugation of anti-inflammatory, antibacterial, and anticoagulant drugs such as indomethacin, curcumin, amoxicillin, and aspirin have been accomplished through diverse click reactions. Additionally, it has been verified that a sequential addition is possible through CuAAC reaction. However, there remain unexplored properties and novel drug-material combinations can be further investigated in order to get enhanced functionalities for tailored applications.

The potential incorporation of a second or even a third drug, each with distinct activities, onto any of the studied surfaces emerges as a promising strategy to confer multifunctional capabilities to the material. On the other hand, despite demonstrating the effectiveness in drug immobilization, in some cases, their biological activity has not been proven post-bioconjugation. Therefore, the relevant assays are intended to be conducted.

Additionally, unlike azide-yne and thiol-yne click reactions, the C-N bond obtained after amino-yne click reaction can be reversible under specific conditions. This could potentially release the immobilized biomolecule or drug from the surface. The study of the releasing profile associated with this reactions is essential for a comprehensive understanding and effective utilization.

Regarding Ti6Al4V material, the formation of a functional coatings involved the use of self-assembled monolayers (SAMs), silane-based and phosphonate-based monolayers specifically. As discussed in this work, phosphonates exhibit greater hydrolytic resistance to basic or physiological media than silanes, prompting the assessment of the duration of this coverage on surfaces. Therefore, studying the degradation rate of these coatings and conducting a comparative analysis of both strategies over the long term would be intriguing, offering deeper insights into their potential future applications.

The imperative need for rapid wound healing has prompted the development of active and multifunctional coatings, integrating antibacterial properties, real-time sensing, wireless communication and tailored treatment features. It has been demonstrated that growth factors can enhance wound healing properties. Therefore, the immobilization of peptides and growth factors offers promising advancements in enhancing implant functionalities, implying a significant step forward in the realm of biomedical implants.

eman ta zabal zazu

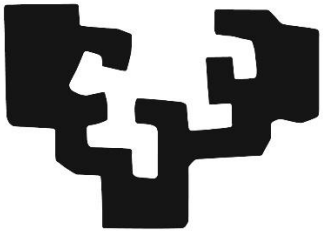

Universidad del País Vasco

Euskal Herriko Unibertsitatea

Click Reactions: An Efficient Tool Towards Biofunctional Materials

Klik Erreakzioak: Material Biofuntzionalen Biderako Metodo Eraginkorra

Julia Sánchez Bodón

2024

Zuzendariak: Dra. Isabel Moreno Benítez

Prof. José Luis Vilas Vilela

1. KAPITULUA

SARRERA

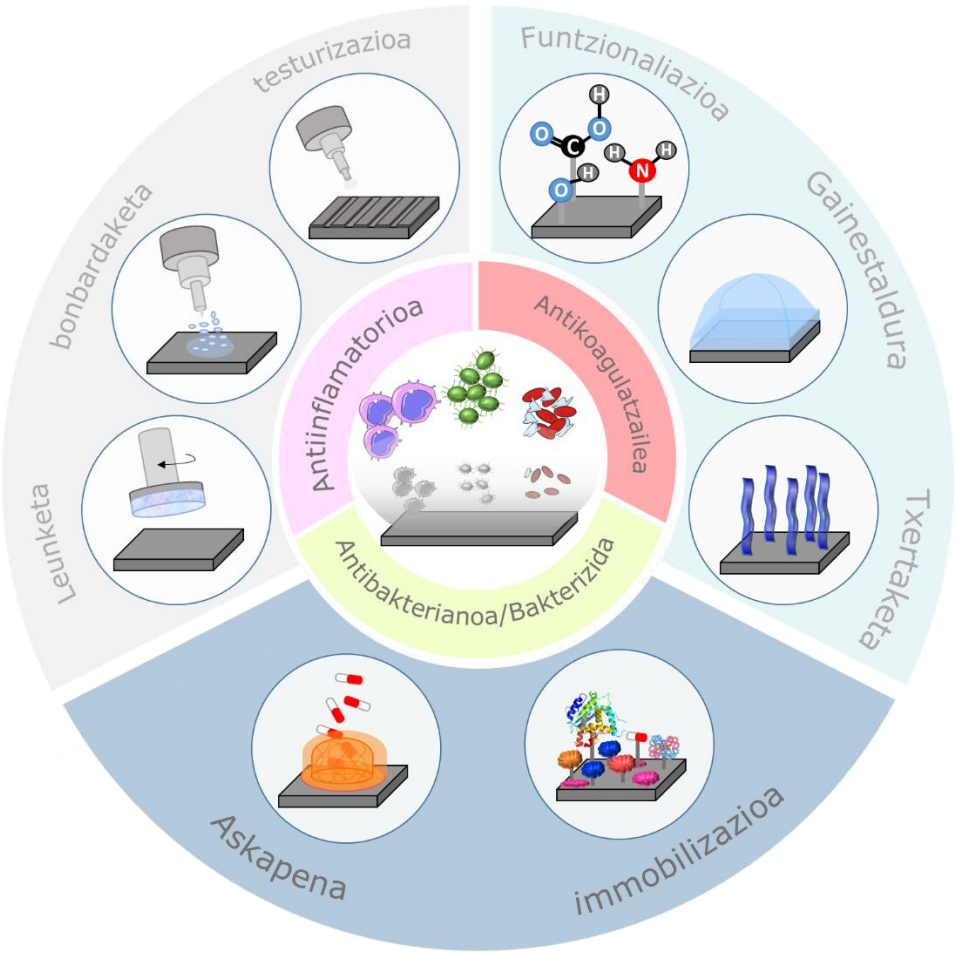

Kapitulu honen helburua gailu biomedikoen erabilera aztertzea eta haien mugei buruzko argia ematea da, besteak beste biofilmen eraketa eta biointegrazioarekin lotutako erronkak. Gai horieri aurre egiteko proposatutako estrategiak eztabaidatuko dira, hala nola, gainaleko eraldaketak, gainestaldura bioaktiboak eta farmakoak askatzeko edo immobilizatzeko teknikak. Izan ere, biointegrazioa eta pazienteen arreta hobetzeko irtenbideak azalduko dira. Gailu horiekin lotutako erronkei aurre egiteaz gain, kapitulu honetan Klik Kimikaren kontzeptua eta farmakoen immobilizazioan duen aplikazioa sakonduko da. Gainera, Klik Kimikaren oinarriak deskribatuko dira, inplikatutako erreakzio motak eta bakoitzaren funtsezko printzipioak azalduz. Azkenik, lan honen helburu orokorrak eta lan-plana aurkeztuko dira.

1. KAPITULUA

SARRERA

1.1. Biomaterialei buruzko sarrera

1987an, Europako Biomaterialen Elkarteak (European Society for Biomaterials) honela definitu zuen "biomaterial" terminoa: sistema biologikoekin elkarregiten duen material mediko ez-biologikoa. Denborarekin, biomaterialen definizioa aldatu egin da, eta hainbat testuingurutara egokitu da [1]. Gaur egun, biomaterialak sistema biologikoekin zenbait elkarrekintza pairatzen dituzten materialak dira, ehunen edo gorputzaren edozein funtzio ebaluatzeko, tratatzeko, sendatzeko edo ordezkatzeko erabiltzen direnak [2,3].

Biomaterial baten ezaugarri nagusia biobateragarritasuna da, hau da, materialak egoera jakin batean ostalariaren erantzun egokia lortzeko duen gaitasuna [4–6]. Berriro ere, biobateragarritasunaren interpretazioa zabalki deskribatu da, materialaren eginkizunaren edo funtzioaren arabera. Chen *et al.* lanean biobateragarritasuna honako parametroen hauen bidez ebalua daitekeen faktoretzat definitu zuten: zelulen bideragarritasuna, ehunen erantzuna, tumoreen eraketa, osotasun genetikoa, erreakzio immuneak eta odolaren koagulazio potentziala [7]. Faktore horiek kontuan hartuta, Elikagai eta Sendagaien Administrazioaren Agentziaren arabera (*Food and Drug Administration, FDA*), material bat

biobateragarritzat hartzeko, ezin izango dio inolako kalterik eragin pazienteari [8]. Horrenbestez, gailu mediko baten biobateragarritasuna ebaluatzean, erabilitako materialen bateragarritasun biologikoa ez ezik, beste faktore batzuk ere kontuan hartu behar dira, hala nola materialaren diseinua, geometria, kontrol elektrikoa eta jarduera mekanikoa [7,9]. Faktore horien ebaluazioak aplikazio zehatzak dituen gailu medikoaren segurtasuna eta eraginkortasuna bermatzen ditu, pazientearen ongizateari lehentasuna emanez.

Reinwaldek eta kolaboratzaileek deskribatutako biobateragarritasunaz gain, biomaterial guztiek zenbait eginkizun funtzional bete behar dituztela postulatu zuten. Besteak beste: segurtasuna, gailu mediko baten alderdirik garrantzitsuena; iraunkortasuna, ebakuntza kirurgikoen kopurua minimizatzeko; biofuntzionalitatea, biomateriala funtzionalki optimizatu behar baita proposatutako helbururako, eta gailuaren errendimendua bermatu behar baita, haren eraginkortasuna arriskuan jar dezakeen interferentziarik gabe. Horretaz gain, biomaterial biodegradagarriak berez deskonposatzen dira denborarekin, honek gailuak kentzeko beharra eliminatzen du. Hala, zenbait aplikaziotan, biodegradagarritasunak onura nabarmenak ekar ditzake. Izan ere, biobateragarritasuna hobetzen baita eta gaixoaren erantzun immune negatiboak murrizten baititu [10].

Toxikologiari dagokionez, biomaterialak ematen duten erantzun motaren arabera sailka daitezke [2]: (I) biomaterial toxikoak, zelulen heriotza edo inguruko ehunetan kalteak eragin ditzaketenak; (II) biomaterial ez-toxikoak eta biologikoki ez-aktiboak, erantzun toxikorik eragiten ez dutenak, baina, horren ordez, inplantearen lekuan lodiera aldakorreko zuntz gainestaldura sortzen duten materialak; (III) biomaterial ez-toxikoak eta biologikoki aktiboak, inplantearen eta inguruneko ehunen arteko lotura sendoa eratzen dutenak; eta (IV) ez-toxikoak eta biodegradagarriak, biomateriala degradatu ahala inguruko ehuna birsortzen duena, inplantea ordezkatuz [2,11,12].

Azken hamarkadetan, giza zelulekin epe luzean elkarreragin onak izan ditzaketen material biomedikoen garapena sakon aztertu da [10,13,14]. Aurrerapen hauek giza osasunaren zenbait alderdi irauli dituzte, aplikazio ugari eskainiz. Gailu biomedikoak gero eta garrantzitsuagoak dira, eta inplanterik gabeko forma askotan erabiltzen dira, hala nola finkapen ortopedikoko torlojuetan, baita inplante moduan ere, hala nola josturetan, kateterretan, hortzetako gailuetan eta gailu kardiobaskularren barnean, stentetan, bihotz balbuletan edo injerto baskularretan [15,16]. Material ortopedikoek hezur hausturak eta bestelako egoera muskuloeskeletikoak egonkortzen eta sendatzen laguntzen duten bitartean, finkapen torlojuek euskarri

sendoa eta lerrokatze segurua eskaintzen dute sendatze prozesuan. Era berean, josturak, kateterrak, hortzetako gailuak, gailu kardiobaskularrak edo antzeko inplanteek hainbat helburutarako balio dute, hala nola, zauriak ixteko edota gorputzeko funtzioak leheneratzeko.

Material biomedikoak etengabe garatzen eta hobetzen joan direnez, aurrerapen nabarmenak egin dira pazientearen arretan. Material horien propietate paregabeak direla eta, materialaren eta zelulen arteko elkarrekintzak kontrolatu eta hobetu daitezke. Gainera, material biomedikoen etengabeko ikerketak eta aurrerapenak aplikazio berrietarako bidea hedatu dute, baita pazieententzako emaitza onuragarriagoak lortzeko aukera ere hainbat arlo medikotan. Ikertzaileak eta ingeniariak etengabe saiatu dira material horien biobateragarritasuna, erresistentzia mekanikoa eta bizitza denbora hobetzen, eta giza gorputzarekin epe luzeko elkarrekintza egokiak bermatzen.

Gailu biomedikoen diseinuan materialen hautaketa oso garrantzitsua da, irizpide zorrotzak bete behar baitituzte. Aipatu bezala, material horiek aparteko iraunkortasuna izateaz gain, ehun zelulekiko elkarrekintza onuragarria sustatu behar dute, ezin dute erantzun immunologiko edo alergikorik sortu, eskatutako funtziorako ezaugarri mekaniko egokiak izan behar dituzte eta korrosioarekiko erresistentzia frogatu behar dute, besteak beste. Baldintza horiek betetzen dituzten eta gehien fabrikatzen diren materialen artean, hiru dira nagusi: zeramika, polimeroak eta metalak eta haien aleazioak. Zeramikak nahi diren hainbat propietate betetzen dituzte, hala nola gogortasuna, biobateragarritasuna eta higadurarekiko erresistentzia, eta, propietate horiei esker, karga handiak behar diren aplikazioetarako egokiak dira. Polimeroak, berriz, oso moldakorrak dira, eta prozesatzeko erraztasuna eta biobateragarritasun bikaina eskaintzen dituzte. Metalek eta haien aleazioek propietate mekaniko nabarmenak dituzte, korrosioarekiko erresistentzia eta biobateragarritasuna; beraz, ezinbestekoak dira gailu biomediko askotarako. Laburbilduz, biomedikuntzan erabiltzen diren materialen hautaketa prozesu kritikoa da, eta zenbait propietate arretaz aztertu behar dira**. 1.1 taulan**, egun gehien erabiltzen diren biomaterialen multzoa biltzen da, eta biomaterial bakoitzaren ezaugarri nagusiak eta aplikazioak laburbiltzen dira [17].

1.1 taula. Biomaterialaren sailkapena materialaren, ezaugarrien eta aplikazioen arabera.

Materiala	Abantailak	Desabantailak	Erabilerak
Polimeroa	fabrikazio erraza, dentsitate txikia	Erresistentzia mekaniko txikia, degradatzeko erraza	Josturak, arteriak, zainak, tendoi artifizialak, inplanteak
Metala	Harikortasuna, higadurarekiko eta inpaktuarekiko erresistentzia handia	Biobateragarritasun txikia, korrosioarekiko erresistentzia txikia ingurune fisiologikoan	Grapak, plakak eta alanbreak, protesi artikularrak, hortzetako inplanteak, garezurreko plakak
Zeramikoa	Biobateragarritasun altua, korrosioarekiko erresistentea, geldoa, eroankortasun termiko eta elektriko baxua	Inpaktu txikiko erresistentzia, propietateak erreproduzitzeko zaila, fabrikatzeko eta prozesatzeko zaila	Estaldurak, ekipamendu eta tresna medikoak, hezur-betegarriak
Konpositea	Biobateragarritasun altua, geldoak, korrosioarekiko erresistentea	Aldakorrak eta erreplikatzeko zailak	Bihotz-balbulak, inplanteak, artikulazio artifizialak

Doktorego Tesi honetan, zientzian eta ingeniaritzan funtsezko eginkizuna duten materialak ikertu dira eta, besteak beste, metalak eta polimeroak nabarmentzen dira. Izan ere, dituzten ezaugarriengatik eta funtzionaltasunerako egokiak izateagatik aukeratu dira, zehazki, material horiek. Beraz, material horien azterketa sakona aurkeztuko da jarraian.

1.2. Metalak eta aleazioak

Menderik mende, biomaterial metalikoek zeregin erabakigarria izan dute kirurgiaren arloan. Hasierako gailu kirurgikoak, hala nola torlojuak eta orratzak, metalezkoak izaten ziren, hau da, burdina, urrea, zilarra edo platinoa erabiltzen ziren, besteak beste, horiek egiteko [7,18]. Duela bi mende baino gehiago, inplante kirurgikoetan

aleazioak erabiltzen hasi ziren, altzairua izanik lehen aleazio metalikoa. Gero, materialen zientzian eta ingeniaritzan izandako aurrerapenei esker, biomaterial metalikoen aniztasuna nabarmen areagotu zen. Testuinguru horretan, berrikuntzak aleazio sofistikatuak ekarri zituen, hala nola altzairu herdoilgaitza, kromo-kobaltoaren aleazioak, nikel aleazioak eta titanio aleazioak, aplikazio medikoen eskakizun zorrotzak betetzeko berariaz diseinatuak.

1.2.1. Ti6Al4V aleazioa

Titanioa (Ti) da inplante kirurgikoetan erabiltzen den material nagusia, batez ere ortopedian edo odontologian, dituen propietate bikainak direla eta. Horrela, bada, gorputzeko ingurunean korrosioarekiko erresistentzia bikaina izateak inplantearen egonkortasuna eta bizitza luzea bermatzen ditu, eta denboran zehar haren osotasun estrukturala eta izaera biogeldoa bermatzen ditu, bai eta oseointegrazio gaitasuna ere. Gainera, titanioak nekearekiko erresistentzia ona du (300 MPa 10^7 ziklotan), eta modulu elastiko txikia duenez (113 GPa), estresarekiko arriskua murrizten du. Izan ere, metal horrek pisu arina du, dentsitate txikia baitu (4.51 g/cm3). Ezaugarri horiek guztiak aintzat hartuta, titanioa material biobateragarrienetako bat da [19]. Gainera, oseointegrazioaren fenomenoa inplantearen, gainazalaren eta hezurren arteko interfaze baten eraketari dagokio, eta Ti-inplanteak inguruko hezur ehunarekin lotura sendoa eratzeko aukera ematen du, biobateragarritasuna hobetuz [20]. Hezurrarekin egindako fusio horrek inplantearen egonkortasuna eta funtzionaltasuna hobetzen ditu, sendatzeko eta kargak eramateko gaitasuna errazten duen lotura fidagarri eta iraunkorra sortuz [21].

Ti-aleazioen aldakortasuna dela eta, beste metal batzuen gainetik daude, aleazio kimikoen eta prozesatze termikoko/mekanikoko metodoen bidez lor daitezkeen mikroegitura ugari eskaintzen baitituzte. Horren ondorioz, aleazio horiek nahi diren propietateekin eta aplikazioekin doitu eta egokitu daitezke [22]. Ti-aleazioek ingurune tenperaturan aurkezten dituzten mikroegiturak eta faseak bi faktoreren menpe daude: konposizio kimikoa, bereziki α eta β egonkortzaileen ehunekoa, eta materialaren prozesamendua, tratamendu termiko eta mekanikoak barne. Konposizio kimikoa zehazki doituz, α eta β faseen arteko oreka aurki daiteke. Fase horiek funtsezkoak dira materialaren ezaugarri mekaniko eta funtzionaletarako [23]. Gainera, prozesatze termiko eta mekanikoko metodoen konbinazioak mikroegituraren kontrol zorrotza ahalbidetzen du, propietate pertsonalizatuak dituzten materialak lortuz. Kategorizazio eta aukeraketak erraztuz, Ti-aleazioak hainbat gradutan sailka daitezke mikroegiturazko orientazioaren eta faseen arabera; zehazki α, β eta α+β ezagutzen dira [24]. Sailkapen horri esker, materialaren

gaitasunak eta mugak uler daitezke, eta aplikazio jakin baterako aleazio egokienak aukeratzen laguntzen du.

Garrantzitsua da azpimarratzea inplante material bakar batek ere ez duela inolako eraginik gabeko profila erakusten. Hala ere, altzairu herdoilgaitzarekin eta Co-Cr aleazioekin alderatuta, titanioak eta haren aleazioek oseointegrazio errendimendu handiagoa dute eta, beraz, oso desiragarria da aplikazio medikoetan [25]. Gainera, oxigenoarekin kontaktuan dagoenean, titanio aleazioen gainazalean TiO_2 geruza egonkor bat sortzen da eta horrek materialaren biobateragarritasuna areagotzen du. Izan ere, TiO2 geruzak inplantearen eta inguruko ingurune biologikoaren arteko elkarrekintzak bultzatzen ditu, integrazioa sustatuz eta emaitza kirurgiko arrakastatsuak ekarriz. Hala ere, zenbait ikerlanetan, Ti6Al4Van dauden banadioa eta aluminioa toxikotasun arazo posibleekin lotu dituzte, ioi metaliko horiek metaletik askatzearen ondorioz, baina aplikazio mota ugarien dituenez eta titanioaren eta titaniodun aleazioen ezaugarriak aintzat hartuta, aukera fidagarriak dira berrikuntza kirurgikoetarako [26,27].

1.3. Polimeroak

Biomaterial polimerikoak ezinbesteko osagai bilakatu dira hainbat gailu medikotarako, diagnostiko sistemetarako eta formulazio farmazeutiko askotarako [28]. Azken hamarkadetan, ehun ingeniaritzan eta birsorkuntza medikuntzan izandako aurrerapen azkarraren ondorioz, biomaterial polimerikoen eremua nabarmen hazi da. Polimero sintetiko biodegradagarriz eta makromolekula naturalez osatutako biomaterial ugari garatzeak ehunen birsorkuntzaren bidea nabari erraztu du [28]. Biomaterial polimerikoen aldakortasunari esker, propietateak edozein aplikaziotara egokitu daitezke, hala nola zauriak sendatzera, ehunak txertatzera eta farmakoak askatzeko sistemetara, besteak beste. Gainera, material polimeriko gehienek nahi diren ezaugarriak dituzte, hala nola biobateragarritasuna, biodegradagarritasuna eta funtzioaren arabera alda daitezken propietate mekanikoak. Izan ere, propietate hauek material seguruak eta eraginkorrak bihurtzen dituzte biomaterialak medikuntza sistemetarako [29].

1.3.1. Azido Poli-L-laktikoa (PLLA)

Azido polilaktikoa (PLA) -polilaktida ere esaten zaio- poliester alifatikoa da, almidoitik lortzen den azido laktikotik (azido 2-hidroxipropanoikoa) eratorria. Polilaktida erabilera askoko polimero biodegradagarria da eta, propietate aldakorrak dituenez, material garrantzitsuenetako bat bihurtu da [30–32][33]. Ez da polimero berria, izan

ere, Carothers Dupontek 1932an prestatu zuen lehen aldiz eta, harrezkero, haren propietateak lortzeko eta optimizatzeko modu berriak garatu izan dira. Azido laktikoa L eta D isomeroetan aurkitzen den molekula kirala da. Azido polilaktiko terminoa polimero familia bati dagokio, azido poli-L-laktiko purua (PLLA), azido poli-D-laktiko purua (PDLA) eta azido poli-D,L-laktikoa (PDLLA) hain zuzen (**1.1 irudia**) [34,35]. L isomeroa metabolito biologikoa da, eta iturri berriztagarrietatik eratorritako PLAren osagai nagusia da; iturri biologikoetako azido laktiko gehiena PLLA bezala ezagutzen da. L- eta D,L-enantiomero optikoki aktiboen konposizioaren arabera, PLAk hiru modutan kristaliza dezake (α,β,γ).

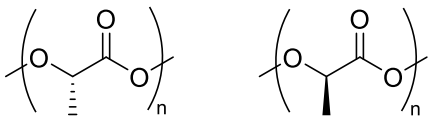

1.1 irudia. PLLA eta PDLA egituren eskema.

PLLAren biobateragarritasun eta propietate mekaniko nabarmenei esker, arreta handia jaso izan du. Hala ere, denbora luzea behar du degradatzeko, eta dituen zati kristalinoekin batera, hantura-erreakzioak eragin ditzake gorputzean. Isomero DL-laktikoa PLLAren egitura barnean sartuz, degradazio-tasa hobetu daiteke, degradazio luzeak eta zati kristalinoak eragindako hantura-erantzun potentziala arinduz [31,36].

PLAren propietateei dagokienez, estereokimikak eta propietate termikoek PLAren kristalinitatean eragiten dute. PLAn L-isomeroaren edukia (PLLA) %90 baino handiagoa denean, materialak egitura kristalinoa izateko joera du; purutasun optikoaren maila baxuagoetan, berriz, PLA amorfoa aurkitzen da. Era berean, PLAren urtze tenperaturak (T_m) eta beira trantsizioko tenperaturak (T_g) zuzeneko erlazioa dute PLLA kantitatearekin. PLLA edukia murriztu ahala, bai T_m, bai PLA T_g balioa txikitzen dira. PLAren trantsizio tenperaturak propietate fisikoetan eragiten du, hala nola, dentsitatean, bero ahalmenean eta propietate mekaniko eta erreologikoetan. Horren ondorioz, polimerizazio erreakzioan estereokimika kontrolatuz gero, zenbait aplikaziotarako egokitutako propietateak dituen PLAk lor daitezke [30,34].

PLAren degradazioari dagokionez, hezetasunaren eraginpean zenbait hilabete egon ondoren, deskonposizio hidrolitikoa jasaten du nagusiki. Degradazio prozesu hori bi etapatan gertatzen da: (I) ester taldeen kateak ausazko zatiketa ez-entzimatikoa pairatzen du, polimeroaren pisu molekularra murriztuz, (II) ondorengo fasean, pisu molekularra are gehiago murrizten da. Izan ere, sortutako azido laktikoa eta pisu molekular txikiko oligomeroak mikroorganismoen bidez metabolizatzen dira, karbono

dioxidoa eta ura emanez [37]. Polimeroak urarekin eta katalizatzailearekin duen erreaktibotasunak polimeroaren degradazio denboran eragiten du. Zenbait faktorek erreaktibotasun eta irisgarritasun horretan eragiten dute, besteak beste, partikulen tamaina eta forma, tenperatura, hezetasun maila, kristalinitatea, isomeroen edukia %-etan, azido laktikoaren hondar kontzentrazioa, pisu molekularra, uraren difusioa eta katalizatzailearen ezpurutasunak. Inplante kirurgikoetan erabiltzen den polilaktidaren degradazioa in vivo nahiz *in vitro* sakon ebaluatu da. *In vitro* egindako azterketek frogatu dute inguruneko pH-a funtsezkoa dela degradazio prozesuan [38].

1.3.2. Polietilen tereftalatoa (PET)

Polietilen tereftalatoa (PET) (**1.2 irudia**) polimero nahiko ekonomikoa da, eta propietate mekanikoengatik eta biobateragarritasun moderatuagatik da ezagun. Oso propietate onak ditu, besteak beste, gogortasuna, zurruntasuna, egonkortasun biokimikoa eta kimikoa. Hori dela eta, erabilera biomedikoetarako etorkizun handiko polimeroa da. Izan ere, hainbat gailu medikotan aurki daiteke, hala nola kateter baskular eta gernukoetan, bihotz balbuletan eta josturetan, besteak beste [39,40]. Hala ere, erabilerarekin lotutako infekzio tasa handiak mugatu egin du biomaterial horren aukera. PET materialen gainazalak nahiko hidrofobikoak direnez, bakterioen atxikimendua areagotzen da, infekzioa sortuz ehunen integrazio egokia gertatu aurretik [41].

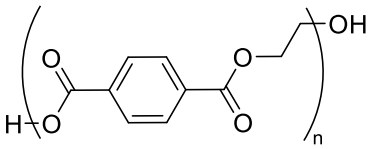

PET

1.2 irudia. PETaren egitura kimikoa.

PET egituraren kate nagusian eraztun aromatikoak eta talde polarrak egoteak polimeroaren egonkortasun termikoari eta zurruntasun hobeari laguntzen dio. Izan ere, PET erdikristalinoaren urtze puntua (T_m) nabarmentzen da, 255-265 ºC, material polimeriko batentzat nahiko handia. Gainera, kristalinitate mailaren eta orientazioaren arabera, T_g-aren balioa aldatu egiten da. PET amorfoek 67 °C inguruko T_g dute eta, erdikristalinoek, berriz, 80 °C ingurukoa. PET kristalinoen eta orientatuen kasuan, T_g balio handiagoak dituzte, 125 °C inguru. Joera horrek erakusten du polimeroaren egituraren barruko ordenamendu graduak T_g balio altuagoak emango dituela [42].

Egonkortasun kimikoari eta mekanikoari dagokionez, PET nahiko polimero geldoa da hainbat disolbatzaile eta erreaktiboen aurrean. Hala ere, baseak, baita ahulak ere, azido sendoak eta hidrokarburoak erabiltzen direnean desegonkortu daiteke. Zenbait faktorek, hala nola polimeroaren kristalinitatea, prozesamendua edo fabrikazioa (botilak, filmak, zuntzak), PET aurkezten duen erresistentzia mekanikoan eragiten dute. Oro har, PETak aparteko indar mekanikoa erakusten du polimero tradizionalekin (dentsitate altuko poletilenoa HDPE, polipropilenoa PP) konparatuta, izan ere 3,000 GPa inguruko Young-en modulu altua du. Gainera, behatu egin da kristalinitate graduak polimeroaren elongazioan ere eragina duela, elongazio balio altuagoak lortu egiten dira, kristalinitate gradua zenbat eta txikiagoa izan [42].

PET, poliester bezala, hidrolisi erreakzioak jasan ditzake bere Tg baino tenperatura altuagotan ipintzean hezetasun baldintza zehatzetan. Degradazio hidrolitikoak zati amorfoan dauden kate nagusiko ester loturei eragiten die bereziki [43]. Prozesu horren ondorioz, ester loturak apurtzen dira, eta ondorioz, funtzio talde azidoak eta hidroxidoak sortzeaz gain, pisu molekular txikiagoa duten polimeroak eratzen dira. Polimeroak ur molekulekiko duen iragazkortasuna dela-eta erreakzio hidrolitikoa ematen da. Hala ere, PETaren egituraren barnean dauden fase kristalinoek hesi moduan jokatzen dute, ur-molekulekiko iragazgaitz bihurtuz eta, beraz, hidrolisi prozesua motelduz. Hala ere, prozesu hori bizkortu daiteke PETa ingurune azido edo alkalinoen eraginpean dagoenean [42].

Dracon® PET biomedikoaren izen komertziala da. Oso polimero aldakorra, eta kristalinitate handiko talde aromatiko hidrofobikoen presentziari esker egozten zaio haren bioegonkortasuna, degradazio hidrolitikoa zailduz. Hala ere, Dracon-en muga nagusia gainazalean funtzio-talde polarrik ez izatea da, ehun-ingeniaritzako aplikazioetan izan dezakeen potentziala murriztuz [44]. Hainbat ikerketa burutu dira PETaren propietateak hobetzeko gainazalen funtzionalizazio tekniketan oinarrituta. Infekzio tasa baxua eta gorputzarekin hobeto integratzen den PETean oinarritutako biomaterialak sortzea da azkeneko helburua, pazienteen ondorioak hobetuz eta polimero horrek duen potentzial aplikazio medikoak areagotuz.

Polimeroek eragin nabarmena izan dute ikerketa biomedikoan, eta biomaterial gisa jardungo dute XXI. mendean ere, gero eta garrantzi handiagoa izanik. Izan ere, material polimerikoen aplikazio biomedikoak icebergaren tontorra baino ez dira, bidean dauden aurrerapenek potentzial handiagoa baitute arlo horretan. Biomaterialek sortzen dituzten erantzun biologikoetan sakondu eta giza osaera nahiz gaixotasunen funtzioak, biomekanika eta etiologia hobeto ezagutu ahala, kimikariek eta polimeroen zientzialariek biologoekin, medikuekin eta ingeniariekin lan egin

behar dute aplikazio biomediko espezifikoetarako neurrira egokitutako polimeroak lortzeko. Etorkizunean polimero bioaktiboak, biomimetikoak eta adimendunak izango dira nagusi, eta aplikazio biomedikoetan funtsezko lekua hartuko dute. Polimero horiek gorputzarekin elkarreraginean aritzeaz gain, beharrei aktiboki erantzungo diete, tratamendu medikoak eta terapiak irauliz.

Polimeroak hainbat formatan aurki daitezke, hala nola *film* gainazal bezala, zuntzetan, hidrogeletan, nanopartikuletan, besteak beste. Kapitulu honetan, polimero gainazalen funtzionaltasunaren aurrerapena eta erronkak aztertuko dira, biomaterial gisa hobeto jarduteko.

1.4. Biomaterialekin erlazionatutako arazoak

Inplante biomedikoek (protesiak, kateterrak eta beste hainbat gailu) goitik behera aldatu dute medikuntza modernoa, eta nabarmen hobetu dute paziente askoren bizi kalitatea. Hala ere, material horiek giza gorputzean integratzeak berezko arriskua dakar, infekzioekiko sentsibilitate handiagoa pairatzen baita [45–47]. Izan ere, inplanteekin eta biointegrazioarekin lotutako infekzioak biomaterialen erabilerari lotutako konplikazio nagusiak eta larrienak dira. Infekzioek hainbat konplikazio sor ditzakete, lokalizatutako minarekin hasi eta osasun sistemikoko arazoekin bukatu. Konplikazio horiek gertatzen direnean, interbentzio kirurgikoa ezinbestekoa izaten da eta, gainera, gaixoen emaitzak arriskuan jartzen dira [48].

Edozein biomaterial gorputzean ezartzen denean, ehun ostalariak erantzun bat sorrarazten du [49]. Erantzun hori sortu egiten da, biomateriala txertatzeko metodoa edozein dela ere, hau da, injekzio bidez edo kirurgia bidez. Izan ere, gorputzerako ezezaguna den biomaterialaren ezarpenak ostalariaren ehunaren ingurunea eraldatzen baitu [49]. Ostalariaren erantzunaren magnitudea inplantea txertatzeko garaian eragindako lesioaren araberakoa da, hau da, homeostasi edo desoreka mailaren araberakoa. Desoreka horrek, kanpoko inplantearen ezarpenaz gain, materialaren biobateragarritasuna baldintzatzen du. Biomaterial eta gailu mediko asko arrakastaz ezarri diren arren, oraindik ez dago giza gorputzaren zaintza sistema erabat saihestu duen materialik. Inplantea ezartzen denean, ostalariak materialaren gainazalera bidaltzen ditu proteinak, proteinen adsortzioa emanez eta, horren ondorioz, kolagenozko geruza lodi bat eratzen da inplantearen inguruan [50]. Enkapsulazio horrek inplanteak inguruko ehunarekin elkarreragitea eragozten du, prozesu horri *biofouling* esaten zaio [49,51].

Gorputz arrotzaren erantzunaren etapak (FBR) prozesu dinamikoak dira, eta hainbat azpietapatan banatzen dira. Etapa horietan sartzen dira zauria, odol material

elkarrekintzak, behin-behineko matrizearen eraketa, hantura akutua, hantura kronikoa, ehun pikortsuaren garapena eta zuntz kapsularen garapena (**1.3 irudia**) [49]. Odolaren bateragarritasuna edo hemobateragarritasuna materialak odolarekin kontaktuan egotean gainazalak eragindako erantzun tronbotikoa edo inflamatorioa doitzeko duen gaitasunari dagokio. Odolarekin kontaktuan egongo diren materialen diseinuan ezinbesteko baldintza da hemobateragarritasuna [52]. Odolaren eta gailu medikoen arteko elkarrekintza horiek gertaera konplexuak eragiten dituzte, besteak beste, proteinen adsortzioa, plaketen atxikimendua eta aktibazioa, koagulazioa eta tronbosia. Proteina plasmatikoen xurgapen azkarra odolaren eta materialaren arteko elkarrekintzaren hasierako gertaera izaten da [51]. Adsortzio hori biomaterialaren ondorengo erantzun biologikoa katalizatu, erregulatu edo kontrola dezaketen proteina aktibatuetan datza [51]. Epe luzeko odol ukipeneko gailu medikoen garapenean, gainazalak eragindako tronbosia da arazo larriena. Gainazaleko tronboen formazioa bi faktoreren ondorio da: plaketek eragindako erreakzioak eta odol plasmatikoaren koagulazioa [52].

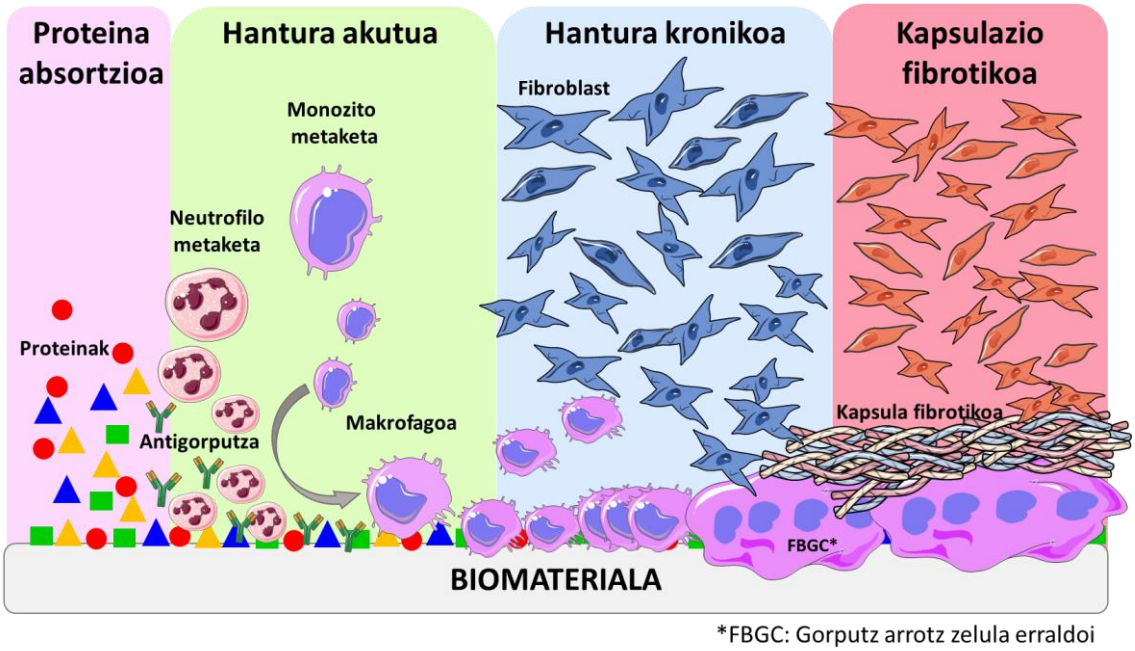

1.3 irudia. Ehun ostalariaren erantzunaren etapak inplantea ezartzen denean.

Prozesu honen bidez, zelula inflamatorioen, mitogenoen, kimioatraktoreen, zitokinen eta beste agente bioaktibo batzuen arteko interakzio konplexua gertatzen da erantzun moduan [11]. Gertaera horietako bakoitza ulertzea funtsezkoa da, eragin nabarmena baitute FBRaren emaitza globalean. Immunitate sistemaren eta material arrotzaren arteko interakzioek hantura akutua eragiten dute, behin-behineko matrizeak sortuz. Hasierako hantura erantzun hori hantura kronikoa bilakatzen da,

ehun pikortsuaren garapena sustatuz. Azkenik, material arrotza zuntz kapsula batek inguratzen du, inguruko ehunak materiala isolatuz eta kalte posibleetatik babestuz [6].

Urteetan zehar, "gainazaleraranzko lasterketa" kontzeptua proposatu da zelula ostalarien eta bakterio kutsatzaileen arteko lehia deskribatzeko. Inplante askoren eraginkortasuna lortzeko, biomaterialak ostalariaren ehunetan arrakastaz integratzea funtsezkoa dela behatu da [53]. Gainera, azterketa gehienetan ondorioztatu da integrazio azkarra funtsezkoa dela bakterioen atxikimendua eta kolonizazioa saihesteko. Ortopedian, hezur ehuna inplantearen inguruan sendatzen da, hezurraren aposizioa eraginez eta inplantearen integrazioan lagungarri izanik; prozesu horri oseointegrazioa esaten zaio [54]. Osteosarkoma zelulekin egindako *in vitro* azterketen arabera, kolonizatu aurreko bakterioek ostalariaren zelulen atxikimenduan eragiten dutela frogatu da. Bakterioen adhesioa ehuna konpondu aurretik gertatzen bada, azpimarratu behar da ostalariaren defentsa-mekanismoak ezingo duela bakterioen gainazaleko kolonizazioa eragotzi eta, beraz, biofilma eratzea posiblea izango dela [47,55].

Kapitulu honetan, inplante ortopedikoetan sakontzea da helburua. Gorputzean protesi moduan sartzen direnez, tronbosia, hantura eta, batez ere, infekzioak jasateko aukera areagotu egiten da, eta horrek erronka handiak suposatzen ditu. Izan ere, inplanteekin erlazionatutako konplikazio horien ondorioz gailuek sarritan huts egiten dute eta, kasu batzuetan, aldatu ere egin behar izaten dira, eta gaixotasun kronikoak ere eragin ditzakete. Inplante ortopedikoetan gertatzen diren infekzioak identifikatzea eta diagnostikatzea nahiko zaila izaten da, eta agente infekziosoa zehazteak eta haren mikrobioen aurkako sentsibilitatea aztertzeak ere zailtasun nabarmenak dakartza. Horrez gain, infekzio horiek tratatzea zaila izan daiteke, izan ere zenbait faktore hartu behar dira kontuan, hala nola mikrobioen aurkako erresistentzia, tolerantzia eta/edo iraunkortasuna. Nahiz eta *Staphylococcus aureus* bakterioa arrunta izan inplante ortopedikoen infekzioaren inguruan [47,48] funtsezkoa da onartzea infekzio horiek beste patogeno askok ere eragin ditzaketela.

Inplanteen infekzioak prozesu konplexuak dira, izan ere patogenoen, biomaterialen eta ostalariaren sistema immunearen arteko elkarrekintzak eragiten ditu. Gorputz arrotzik ez dagoenean, sistema immunearen defentsek patogeno oportunistak kanporatu ohi dituzte. Hala ere, aurretiaz aipatu denez, inplanteekin erlazionatutako infekzioen kasuan, biomaterialak ehunaren erantzun lokalizatua eragiten du, eta horrek hantura akutua eta kronikoa, gorputz arrotzaren erreakzioa, ehun pikortsuaren eraketa eta, batzuetan, materialaren zuntz enkapsulazioa eragiten ditu.

Ingurune bakar horrek depresio immuneko nitxo bat sortzen du, *locus minoris resistentiae* izenekoa, non inplantea mikrobioz errazago kolonizatzen eta infektatzen den. Gainera, biomaterialaren gainazalak bakterioak atxikitzeko eta biofilma eratzeko substratu bezala jokatzen du [47]. Bakterioen atxikipena biomaterialarekin lotutako infekzioen hasierako urratsa da, eta inplantea kolonizatzeko oinarri izaten da. Behin atxikita, patogenoek mikrokoloniak sortzen dituzte eta bakterioei babesa ematen dieten biofilmak garatzen dituzte. Horri esker, ostalariaren ingurunean luzaro irauten dute. Hala, bakterioen atxikimendua eta biofilmaren eraketa prozesu kritikoak dira, izan ere inplanteen guneetan infekzioak ezartzen eta mantentzen laguntzen baitiete patogenoei. Estrategia eraginkorrak garatzeko, interakzio konplexu horiek ulertzea funtsezkoa da, inplanteekin erlazionatutako infekzioak saihestu eta tratatu ahal izango direlako [56,57].

Bakterioen atxikimendua etapa askotan gertatzen den prozesu konplexua da, hala ere bi etapa nagusi desberdintzen dira (**1.4 irudia**). Lehenengo etapan, atxikimendu ez espezifikoa enitzulgarria ematen da; bigarrenean, berriz, atxikimendu espezifiko itzulezina. Hasieran, bakterioak eraldatu gabeko gabeko gainazaletara atxikitzen dira, lotura hau ez espezifikoa izaten da. Hala ere, ehunekin lotzen direnean, lektina eta adhesina bezalako proteinekin interakzionatzen dute elkarrekitza espezifikoen bitartez [47]. Biofilmaren eraketa zenbait etapetan burutzen da (**1.4 irudia**): (I) lehenengo etapa atxikimendua da; (II) mikrokolonien eraketa, eta kasu honetan bakterioak multzokatu egiten dira zelulaz kanpoko matrizea eratuz; (III) makrokoloniak eratzen dira, dore modura, bakterioen birmoldaketa eta heltzearen ondorioz biofilm egituraren barruan; (IV) azkeneko etapan biofilma sakabanatu egiten da, eta biofilma apurtzean askatzen diren bakterioek gune berriak kontaminatzen eta kolonizatzen dituzte [47].

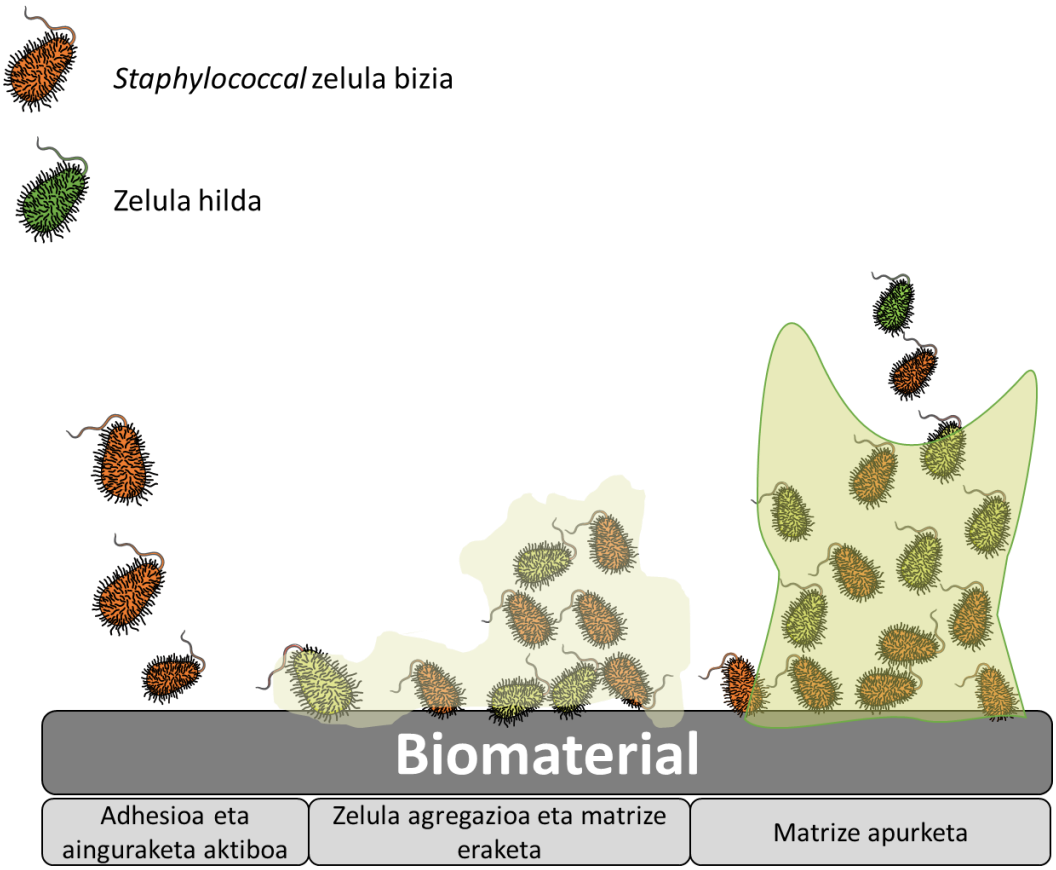

1.4 irudia. *Staphylococcal* bakterioaren biofilmaren eraketa.

Erantzun biologikoak eta bakterioen atxikitzea faktore askoren eraginpean daude; hala ere, esan beharra dago gainazalaren propietateek eragina dutela erantzun horietan [58]. Izan ere, gainazalaren zenbait ezaugarrik (hala nola kimikak, topografiak, gainazaleko energiak, elastikotasunak eta kargak) funtsezko zereginak dituzte proteinen eta zelulen elkarreraginen modulazioan eta, horrenbestez, baita ostalariaren erantzunean ere.

1.5. Biomaterialen gainazal propietateak

Esan bezala, zenbait ikerketaren ondorioen arabera, gainazaleko propietateek, hala nola topografiak, bustigarritasunak, kargak eta propietate kimikoek, funtsezko zeregina dute proteinen, zelulen eta bakterioen atxikimenduan eta hazkuntzan eta, hortaz, hemo eta biobateragarritasunean ere eragiten dute. Atal honetan, gainazal batek izan behar dituen ezaugarri nagusietan sakonduko dugu, eta biointegrazio ezin hobea lortzeko funtsezko faktoreak aztertu. Halaber, gorputzaren erantzun egokia sustatzeko eta bakterioen aurkako babes sendoa ezartzeko behar diren propietateak azalduko dira.

Gainazaleko topografia eta zimurtasuna sakonki azalduko dira, izan ere, funtsezkoak baitira material arrotzei eta bakterioen atxikimenduari emandako erantzun biologikoen zehaztapenean. Ikerketa zabal baten arabera, mikro eta nano eskalako egiturak dituzten gainazalek eragin nabarmena dute zenbait zelula eta bakterioren portaeran. Gainazalak duen patroiak eragina du, alde batetik, bakterio, zelula edo proteinen eta, bestetik, substratuaren arteko bai ukipen azaleran, bai atxikitze indarrean. Izan ere, gainazalaren ezaugarri horiek zelularen orientazioa, morfologia, atxikitzea, ugaritzea, baita zelula funtzioak eta gene adierazpena ere modulatu ditzakete [59]. Adibidez, Yang *et al*. lanean bakterio Gram-positiboen eta Gram-negatiboen atxikipena alderatu zuten gainazal patroi desberdinak erabiliz (**1.5 irudia**) [60]. Zenbait faktorek, hala nola geometriak, patroiekin egindako azalera tamainak eta altuerak, eragina dute bakterioen eta gainazalen arteko elkarrekintzetan. Proportzio handiko nanoegiturek, hala nola nanozutabeak eta nanoespigek, jarduera bakterizida aparta erakutsi zuten [61]. Izan ere, bakterio lotura gertatzen denean, bakterioaren mintz zelularra nanoegituratutako patroi barrunbeen barnean geratzen da, mintza hautsi arte. Bestalde, bai nanohodiek bai nanouhinek bakterioen atxikipena modu eraginkorrean murrizten dutela frogatu da. Gainera, nanohodien kasuan, diametro handiagoak erabiltzeak bakterio erredukzioa zekarrela demostratu zen eta, aldiz, nanohodietan eta nanouhinetan ukipen txikiagoa eragin zuen. Era berean, mikroeskalan egindako patroiei dagokienez, hala nola mikroputzuak, azpimikrozutabeak, mikrozutabeak eta mikroprotrusioak, bakterio hazkundean eta kolonizazioaren inhibizioan eraginkorrak direla frogatu zuten. Izan ere, bakterioak haran sakonetan harrapatzen zituzten, fluidoaren ebaketa indarretik babestuz; gainazal leun batek, berriz, atxiki edo itsatsitako bakterioen mugimendua errazten du eta, horren ondorioz, bakterioak atxikitzeko probabilitatea handitzen da.

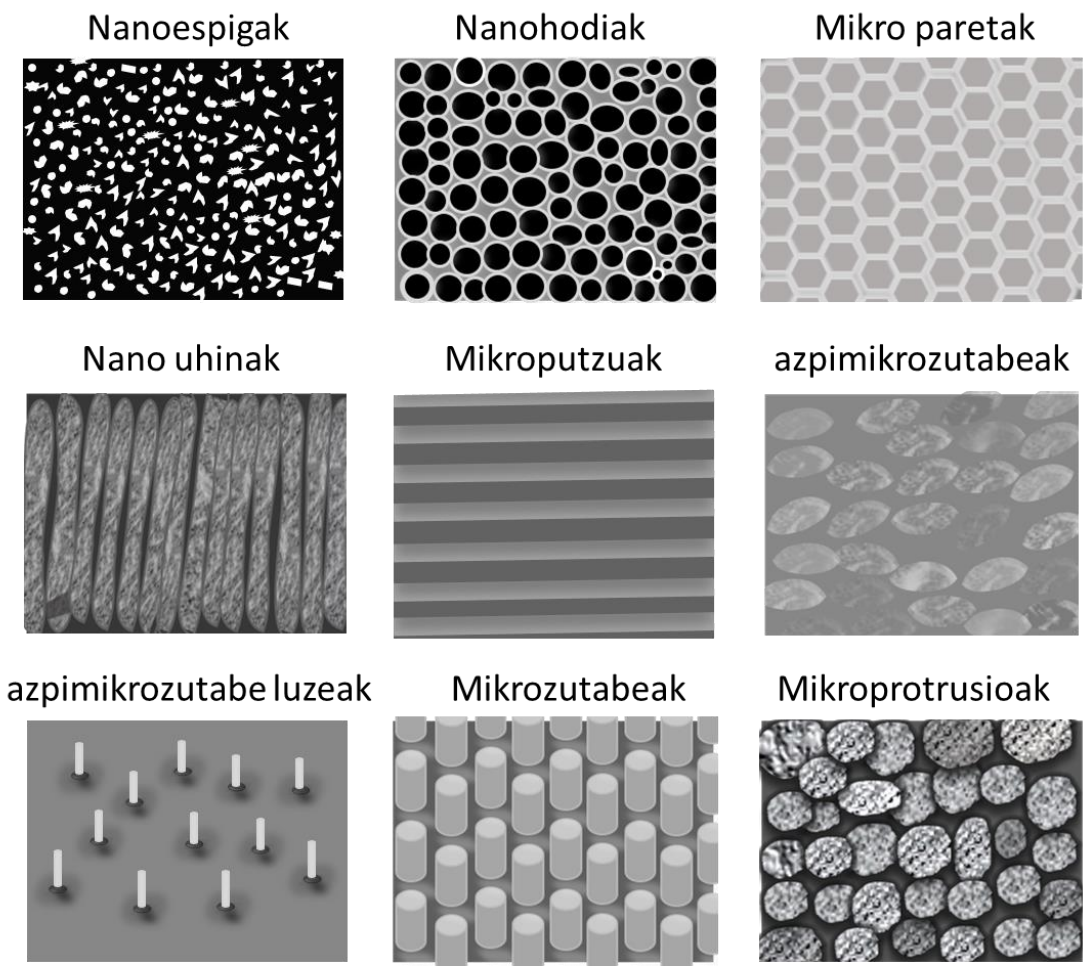

1.5 irudia. Patroi desberdineko gainazalen errepresentazio eskematikoa.

Esan bezala, bakterioak ez dira topografiaren eraginpean dauden mikoorganismo bakarrak. Gainazalen testurizazioak ere proteinen modulazio estrategikoa dakar. Teknika horrek proteina adsortzioaren guztizko mailen kontrol zehatza eskatzen du, eta zenbait proteinaren proportzioan, banaketa espazialean, konformazioan eta gainazalarekiko lotura afinitatean eragina du. Nanoeskalako topografiek proteinen adsortzioan duten eragina bereziki esanguratsua da, gainazaleraren ezaugarriak proteinen dimentsioekin bat datozenean. Izan ere, proteinen dimentsioak baino askoz handiagoak diren topografiak edo testurizazioak, hala nola mikrometroen eskala, gainazal lautzat hartzen dituzte proteinek, normalean [62]. Gainera, inplante gainazal lauak gorputz arrotzeko zelula erraldoien (FBGC) atxikitzea dakar, eta horrekin batera kapsula fibrotikoa sortzen da [63].

Zimurtasunaren (Ra) batez besteko balioa baxua denean, hau da 0,23 eta 6,13 nm bitarte, gainazala nahiko laua izaten da. Kasu horretan, bakterioek gainazal lauetan itsasteko probabilitatea altuagoa da gainazal zimurrekin konparatuz. Bestalde, balio horiek 6 eta 30 nm bitarteko tartean handitu ahala, bakterioek gainazal

zimurtsuetara itsasteko joera dute [60,64]. Zimurtasunaren egokigarritasun hori Mu *et al*. lanean aztertu zuten [65]. Kuartzozko gainazalak hainbat zimurtasunekin prestatu eta *Salmonella enterica* kultiboarekin tratatu zituzten. Gainazaleko zimurtasunak bakterioen atxikimenduan duen eragina nabarmena da 1.6 irudiko aurkikuntzetatik abiatuta. Zimurtasuna txikia denean (RMS < 10 nm), mikrokolonia isolatuak sortzen dira, eta bertan itsatsitako bakterioen populazioa nahiko txikia da. Zimurtasun ertaineko balioetara (RMS 10 eta 40 nm tartean) aurreratuz gero, atxikitako bakterioen hazkundea nabarmena da, eta isolatutako mikrokolonien ordez gutxi konektatutako bakterio monogeruzak azaltzen dira. Gainera, bakterioek deformazio/zapaltze erlazio handiagoa pairatu zuten gainazal horietan, eta horrek erakarpen handiagoa adierazten du bakterioen eta gainazalaren artean. Zimurtasun balio handiekin (RMS > 45 nm), atxikitako bakterioen azaleraren dentsitatea txikiagoa da, eta ez da mikrokoloniarik ikusten. Gainazal horietan bakterioak nagusiki banakako organismo isolatuak dira, eta zati txiki batean agregatu dimerikoak eta trimerikoak osatzen dituzte.

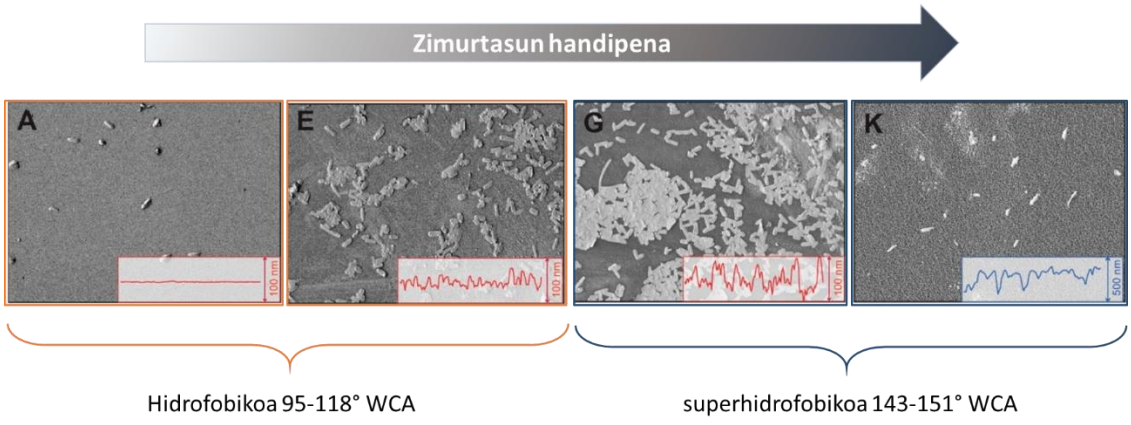

1.6 irudia. *Influence of Surface Roughness, Nanostructure, and Wetting on Bacterial Adhesion. Copyright 2023 American Chemical Society* aldizkaritik moldatutako SEM irudiak [65].

Gainazalaren bustigarritasuna gainazalaren zimurtasunarekin eta kimikarekin lotuta dago. Esan beharra dago gainazal zimurtsuen uraren ukipen angelua (WCA, "itxurazko" WCA esaten zaiona) ez datorrela bat gainazal lauen ukipen angeluarekin (WCA "intrintsekoa" esaten zaionarekin). Wenzelen ereduaren arabera, gainazal hidrofilo zimurtsu baten itxurazko WCAren balioa intrintsekoa baino txikiagoa da. Bestalde, gainazal hidrofobo lau baten itxurazko WCAren balioa intrintsekoa baino handiagoa da [66]. Zenbait ikerketak ondorioztatu zuten bakterioek nahiago dutela gainazal hidrofobikoetara atxikitzea. Hala ere, gainazal superhidrofilikoek eta superhidrofobikoek bakterioen kontrako portaera erakutsi dute [67,68]. Hain zuzen,

150°-tik gorako itxurazko WCA bat duten gainazal superhidrofobikoek aire burbuilak harrapatzen dituzte nanoegitura edo mikroegituren barruan, Cassie eta Bexterren ereduak azaltzen duen bezala [68]. Proteinei eta makrofagoei dagokienez, material hidrofobikoek proteina adsortzioa handitzen dute, baina makrofagoen atxikimendua ere handiagoa da; horrek enkapsulazio fibrotikoa sustatzen du. Bestalde, material hidrofiloen kasuan, makrofagoek karga positiboko inplanteekiko atxikimendu handiagoa erakusten dute, alternatiba anioniko edo nonionikoekin alderatuta [63].

Erronka kritiko horri aurre egiteko, materialen zientzia eta inplanteen diseinua ikertzea beharrezkoa da.

1.6. Biomaterialen propietate fisiko-kimikoen eraldaketak

1.5 atalean xeheki deskribatzen den moduan, biomaterialen propietate fisikokimikoek (hau da, gainazalaren topografiak, bustigarritasunak, karga dentsitateak eta gainazalaren kimikak) funtsezko zeregina dute proteinen adsortzioan eta horren ondoriozko zelula portaeran, bai eta bakterioen atxikitzean ere. Horren ondorioz, ikerketek onartu dute oso garrantzitsua dela ezarritako biomaterialetan gainazal propietate horiek eraldatzea, biobateragarritasun eta hemobateragarritasun hobea lortzeko, hanturazko erantzuna hobetzeko, baita bakterioen atxikitzea murrizteko ere.

Duela gutxi egindako azterketa batzuen arabera, hezur-ehunaren erantzunean eta zenbait materialen bakterioen aurkako propietateetan egindako hobekuntzek agerian utzi dute gainazala eraldatzeko teknologien potentziala, bakterio-kontaminazioa mugatzeko eta prebenitzeko, bai eta zelulak eta proteinak egoki atxikitzea sustatzeko ere [69,70]. Azpimarratu behar da biomaterialen aldaketa fisikoak eta kimikoak, farmakoen askatzea eta sistema immunearen osagaien jarduera zuzenean edo zeharka kontrola dezaketen molekula bioaktiboak immobilizatzea ikuspegi eraginkor gisa sortu direla.

Bakterioen kontrako gainazaletarako estrategiak eztabaidatzen direnean, sailkapen asko erabiltzen dira, izan ere gainazalaren gaitasunarekin zerikusia duten bi jarduera mota nagusi bereizten dira: gainazal biopasiboak eta bioaktiboak. Gainazal biopasiboek bakterioen gainazalarekiko atxikipena murrizten dute, baina bakterioa hil gabe; gainazal bioaktiboek, berriz, bakterioak hil ditzakete atxikipena gertatu aurretik [58]. Definizio horiek kontuan hartuta, termino horiek zabaldu egin daitezke, bakterioen aurka egiteaz gain, biobateragarritasuna eta hemobateragarritasuna

hobetzea eta hantura murriztea helburu duten estrategiak barneratzeko. Lan honetan, sailkapen orokor batean, propietate antiinflamatorioak eta antikoagulatzaileak dituzten gainazaletara ere estrapolatuko dira biopasibo eta bioaktibo terminoak. Gainazal biopasibotzat hartuko dira, halaber, hantura eta koagulazio prozesuak eragiten dituzten zelula edo proteinak desaktibatzen edo suntsitzen ez dituzten metodoak, baizik eta, zeharka, biomolekula horien atxikiduran, bereizketan edo hazkundean eragiten dutenak. Aldiz, edozein prozesu metaboliko aktiboki inhibitzen duten gainazalei edo hantura eta koagulazio faktoreen sintesian parte hartzen duten elementuak ezabatzen dituzten gainazalei gainazal bioaktiboak deritze (**1.7 irudia**).

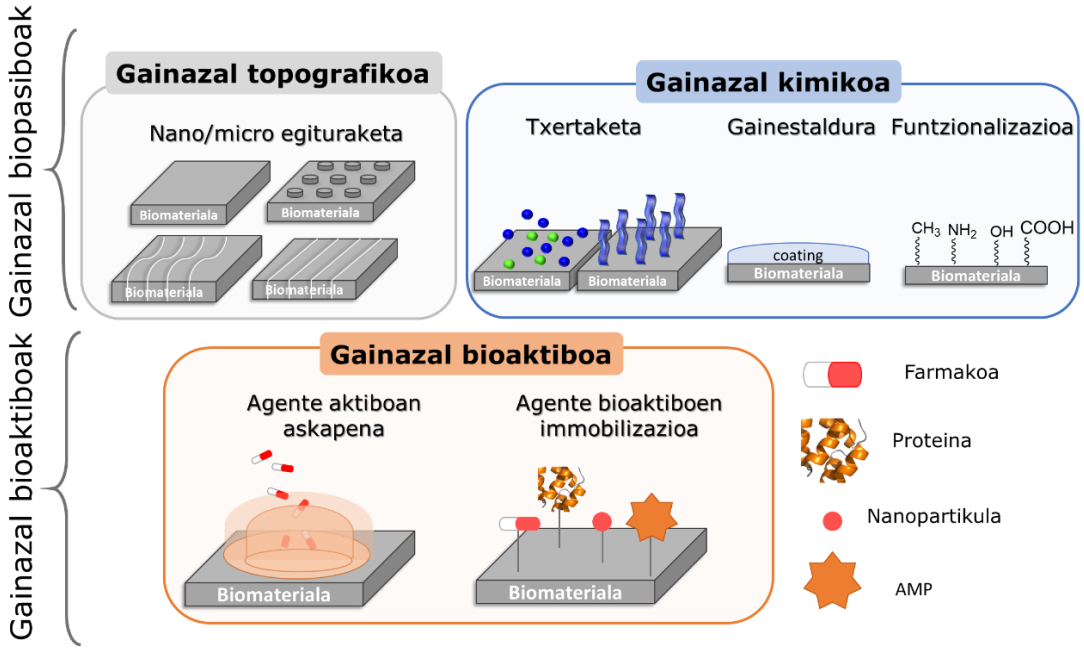

1.7 irudia. Gainazal biopasiboen eta bioaktiboen errepresentazio eskematikoa.

Aldaketa fisiko eta kimikoen artean, estrategia asko ezagutzen dira, hala nola nano eta mikro egituraketa, txertaketak, estaldurak eta gainazalaren funtzionalizazioa, besteak beste. Gainazaleko topografia eraldaketaren bidez material polimeriko edo metalikoek propietate anti-itsasgarriak izan ditzakete [71,72]. Zimurtasuna, hidrofilitatea eta gainazaleko energia eraldaketek bakterioen, zelulen edo proteinen atxikimenduan eragina izan dezakete. Hala ere, beste metodo batzuk erabili daitezke, hala nola farmakoen askapena edo immobilizazioa, bakterioen atxikipena saihesteaz gain, bakterioen hilketa eta hanturaren aurkako portaera duten materialen diseinua lortzeko. Horretaz gain, esan beharra dago txertaketa eta estaldura bidezko metodologiek bakterioen kontrako eta hanturaren kontrako jarduera garrantzitsua erakutsi dutela, biobateragarritasuna hobetuz, baina aurrerapen zientifikoak

beharrezkoak dira oraindik ere [73,74]. Izan ere, proposatutako teknika horiek materialaren gainazaleko kimika eta morfologia eraldatu ditzakete eta, horren ondorioz, propietate mekaniko, optiko, itsasgarri, elektriko eta morfologikoetan eragina izango dute; hala ere, materialaren propietate gehienak ez aldatzea bermatu behar da.

1.6.1. Gainazal biopasiboak

1.6.1.1. Gainazal topografia

Gainazaleko topografia eta zimurtasuna eraldatzeko egin behar izan diren azterketa fisikoek eraginkortasun handia erakutsi dute makrofagoen fenotiporen eta funtzioaren modulazioan eta, aldi berean, bakterioen atxikipena saihesteko bitarteko eraginkorra eskaintzen dute [75,76].

Gauza jakina da makrofagoek nahiago dutela gainazal zimurtsuetara itsastea, lauetara baino [77]. Izan ere, Refai *et al*. lanean makrofagoen aktibazioa eta zitokina proinflamatorioak diren zenbait interleukinen (IL)-1β, IL-6 eta tumore nekrosiaren (TNF)-α faktorean atxikipen eragina aztertu zituen topografia desberdineko Ti gainazaletan [78]. Horretarako, lau topografia erabili zituzten Ti gainazaletan, besteak beste, leunketa mekanikoa, hare lodiko zorrotada, azido bidezko grabazioa eta harea eta azido zorrotada. Gainera, hainbat saiakera egin zituzten eraldatutako titaniozko eta eraldatu gabeko titaniozko laginekin eta lipopolisakaridoekin (LPS), kontrol negatiboa eta positiboa izateko, hurrenez hurren. LPSrik ez zegoenean, zimurtutako eta azidoaren bidez grabatutako Ti gainazalek TNFa-α jariaketa handitu egin zuten. Aldiz, LPSak erabilitako titanio gainazal zimurtuek IL-1β, IL6 eta TNF-α maila altuak erakusten zituzten harea eta azidoarekin tratatutako gainazalekin konparatuz. Gainera, gainazaleko topografiek monozito kimioerakargarriak diren 1 proteina kimiotaktikoaren (MCP-1), eta makrofagoen hanturazko 1α proteinaren (MIP-1α) jariaketa RAW264.7 makrofagoetan modulatu zutela behatu zen. LPSrik gabeko kasuan, kimioerakargarriak diren proteinen ekoizpena murriztu egin zen; aldiz, LPSrekin estimulatutako gainazaletan proteina horien ekoizpena handitu egin zen. Nabarmendu behar da zimurtasunaren ondoriozko proteinen jariatze altuena bereziki 24 ordu eta 48 orduak igaro ondoren behatu zela, eta ez lehenengo 6 orduetan. Horrek esan nahi du efektu topografikoarekiko denborazko mendekotasuna dagoela, eta gainazalaren zimurtasunak RAW264.7 makrofagoen jariaketan duen eragina aldatu egin daitekeela denborarekin.

Halaber, makrofagoen portaerari dagokionez, Chen *et al*. lanean Poli(-kaprolaktona) (PCL), PLA eta poli(dimetil siloxanoa)(PDMS)aren gainazaletan topografia

eraldaketak eragin zituzten eskala biologikotik gertu 250 nm^{-2} zabalerako aztarna lerroak irudikatzearen ondorioz [79]. Horretarako, RAW 264.7 zelulak erabili ziren, eta ikusi zuten zelula horien atxikidura eta luzapena izan zirela nabarmenenak 500 nm-ko gainazal eraldaketan, kontrol planarrekin alderatuta. Nabarmenki, TNF-αlfak eta hodietako endotelio hazkuntzaren faktoreak (VEGF) eragin topografikoekiko sentsibilitate handiagoa erakutsi zuten eta, 48 ordu geroago, zitokin horiek neurri handiagoan murriztu zirela ikusi zen. Gainera, 21 egunen buruan, in vivo egindako azterketetan ikusi zen nabarmen jaitsi zela makrofagoen atxikitze dentsitatea, eta 2 μm gutxitu zela gainazal topografikoei egindako zelula fusioaren maila. Beraz, gorputz arrotzaren erantzuna kontuan hartuta, topografiak makrofagoen portaeran eragin handia duela ondorioztatu zuten.

Bakterioen aurkako propietateei dagokienez, Wang *et al*. lanean kuartzozko fotomasantearen bidezko PETezko gainazal mikropatroiak lortu zituzten, eta horiek bakterioen eskalarekin aldera daitezkeen mikropatroiak dira, zeluletan eragin handia dutenak. Gainera, eta garrantzitsuena, gainazalaren topografiak zelula atxikiduran eragin handia izan zuela ondorioztatu zuten, ukipen angeluak eta gainazalaren bustigarritasunak baino eragin handiagoa [80].

1.6.1.2. Eraldaketa kimikoak

Eraldaketa kimikoetan oinarritutako estrategiak nahiko konplexuak izan daitezke, izan ere eraldaketa sinpleak edo funtzio talde bakar baten sarrera inplikatzeaz gain, gainazaleko txertaketa metodoen erabilera ere suposa baitezake. Txertaketa estrategia horiek, askotan, gainazala aktibatzeko aurretiazko etapa bat eskatzen dute eta, etapa horietan, oso erreaktiboak diren funtzio taldeak sartzen dira, hala nola hidroxiloak, aminak, azido karboxilikoak, etab. Ondoren, erreakzio bat pairatzen da, intereseko molekula modu kobalentean gainazalarekin lotzeko.

Biomaterialen gainazaletan erreaktiboak diren funtzio taldeak sartzeko eraldaketa kimikoetan oinarritutako metodologia ugari erabili daitezke. Izan ere, metodo horien bidez gainazala "aktibatu" egiten da, eta prest uzten da ondorengo txertaketa erreakzioetarako. Bitxia bada ere, tratamendu horietako askok materialaren gainazalaren propietate espezifikoak alda ditzakete, eta horrek zelularen eta materialaren arteko elkarrekintzak edota bakterio eta materialaren arteko elkarrekintzak aldatzea dakar. Adibidez, teknika askoren bidez era daitezkeen talde hidroxiliko, karboxiliko edo amino taldeek gainazalaren hidrofilian/hidrofobizitatean eragiten dute, baita gainazaleko kargan eta energian ere. Horrek proteinen, zelulen eta bakterioen atxikiduran eragina du [81,82]. Gainazaletan eraldaketa kimikoak burutzen dituen funtzionalizazio metodo erabilienen artean, hidrolisia, oxidazioa,

aminolisia eta plasmaren bidezko tratamenduak aipatzen dira (**1.2 taula**). Teknika horietako bakoitzak abantaila bereziak ditu, eta biomaterialen berariazko baldintzetara egokitu daitezke.

1.2 taula. Material metaliko, zeramiko eta polimerikoen gainazal eraldaketaren deskribapena.

Teknika	Gainazala	Tratamendua	Abantailak	Erref.*
Hidrolisia eta aminolisia	PCL nanozuntzak	NaOH disoluzioa eta etilendiamina/isopropanol disoluzioa	Hobetutako zitobateragarritasuna Handitutako zelulen atxikipena, hedapena eta proliferazioa	[83]
	Ti6Al4V	Disoluzio azido eta basikoa (piraina)	Biobateragarritasun bikaina, zelulen ugalketa eta hemobateragarritasun bikaina Biofilmen aurkako eraketaren jarduera areagotzea	[84]
Oxidazioa	Titanioa	Ultramorea (UM)/Ozonoa	Bakterioen aurkako aktibitatearen hobekuntza and hezur-birsorkuntza	[85]
	Ti6Al7Nb	Anodidazio elektrokimikoa	Handitutako giza zelula mesenkialen atxikimendu eta proliferazioa	[86]
Plasma	Titanioa	Plasmaren bidezko alilaminaren polimierizazioa	Handitutako zelulen atxikimendu ahalmena	[87]
	Titanioa	Oxigenoaren murgiltze plasmatikoa	Areagotutako odol koagulazioa eta	[88]

		hobetutako bakterioen aurkako erresistentzia	
Poliuretanoa	Nitrogeno-ioien murgiltze plasmatikoa	Murriztutako bakterio Gram-positiboen (*Staphylococcus*) eta Gram-negatiboen Gram- (*Escherichia coli*) adhesioa	[89]
Titanium	Presio atmosferikoko plasma (PAP)	Zelula-hazkuntzaren atxikimendua eta bereizketa osteogenikoa ahalbidetzea	[90]
Titanium	Plasmaren bidezko fluor ioien askapena	Propietate bakterizidak	[91]

* Erref.: Erreferentzia bibliografikoak.

Hidrolisia

Tratamendu azidoaren edo basearen bidezko gainazaleko hidrolisia poliester alifatikoak (PLA, poli(azido glikolikoa) (PGA) edo PET) eta substratu metalikoak (Ti6Al4V barne) eraldatzeko erabili ohi den metodoa da. Hala ere, garrantzitsua da aipatzea polimeroen eta substratu metalikoen hidrolisi erreakzioaren mekanismoa desberdina dela. Polimeroetan, hidrolisiak polimeroaren katean eragiten du, ester loturen zorizko apurketa kimikoa pairatuz, baita hidroxilo eta karboxilo taldeak sortuz ere polimeroaren gainazalean. Bestalde, titanioan eta haren aleazioetan, hidrolisiak gainazal metalikoan aldez aurretik sortutako TiO_2 estaldura pasiboari bakarrik eragiten dio, eta oxidazioaren bidez talde hidroxiloak sortzen dira. Nolanahi ere, bi substratuetan tratamendu azidoak eta alkalinoak erabiltzen dira gehien industrian, aldakortasuna, sinpletasuna eta eraginkortasuna direla eta. Hainbat tratamendu eta nahasketa erabil daitezke, oinarrizko disoluzioak edo alkalinoak (NH_4/H_2O_2, NaOH, KOH…) eta disoluzio azidoak (HCl, HCl/H_2O_2, $H_2SO4/H2O_2$, H_2SO_4/HCl…) barne [16,84]. Hala ere, badira teknika kimiko honekin lotutako zenbait kezka. Polimeroen kasuan, garrantzitsua da ziurtatzea disoluzio azidoaren/alkalinoaren kontzentrazioak eta tratamenduaren iraupenak ez dituztela nabarmen aldatzen polimeroaren substratuaren propietateak. Eta bestetik, tratamenduaren izaera ez-espezifikoak gainazalaren degradazio irregularra eragin dezake, eta horrek lortutako materialaren

eta propietate orokorretan eragina izan dezake. Beraz, hidrolisi prozesua optimizatzea funtsezkoa da nahi diren aldaketak lortzeko, substratuaren oinarrizko propietateak aldatu gabe. Hala ere, lortzen diren funtzio talde berriak finkatze puntu moduan jarduten dute beste molekula batzuk polimeroaren gainazalarekin modu kobalentean lotzeko, zenbait konjugazio estrategien bidez. Hala ere, azpimarratu behar da hidrolisiak berak zenbait poliesterrekiko eta titanio aleazioekiko atxikipen zelularra erakutsi duela, materialaren hidrofilizitatea eta gainazalaren zimurtasuna handitzen baititu, eta, ondorioz, gainazalaren bustigarritasuna handitzen dela.

Testuinguru honetan, frogatu da hidrolisiaren ondoren Ti-OH eraketa gainazalaren hidrofilitatea handitzen duela, eta, hala, zitobateragarritasuna eta zelulen ugaritzea hobetzen direla, besteak beste. Izan ere, Andrade *et al*.-*ek* disoluzio azidoetan eta basikoetan oinarritutako hainbat tratamendu kimiko heze prestatu zituzten, H_2SO_4:H_2O_2, HCl:H_2O_2, NH_4OH: H_2O_2 eta NaOH tratamendueak, hain zuzen [84]. HCl:H_2O_2-rekin egindako tratamenduak gainazaleko aktibazio eraginkorrena suposatu zuen aldaketa topografikorik eragin gabe, eta funtzionalizazio biologikoak hobetu egin ziren.

Oxidazioa

Zenbait estrategia eta teknikaren bitartez, peroxido taldeak polimeroetan edo gainazal metalikoetan sar daitezke ondorengo txertatze erreakzioetarako; esate baterako, UV argiaren bidezko fotooxidazioaren edo ozonoaren oxidazioaren bitartez. UV argiak hidroperoxido taldeak oxigeno erreaktibo eta erradikal hidroxilo gisa deskonposa ditzake, eta ozonoaren bidezko tratamenduak peroxidoak, karboxiloa eta karbonilo taldeak sortzen ditu, eta horiek izan daitezke erabilienak gainazaleko polimerizazioak edo txertaketa erreakzioak hasteko [92]. Hala ere, bi ikuspegiek polimeroa degrada dezakete; beraz, garrantzitsua da substratuen propietateen aldaketa esanguratsuak kontrolatzea eta minimizatzea [93]. Bestalde, metalen kasuan, oxidazio anodiko elektrokimikoa hamarkada bat baino gehiagoan erabili da oxidazio geruza lodi eta uniformea lantzeko gainazal metalikoetan [94]. Teknika horrek asko hobetu du inplante metalikoen biobateragarritasuna, Huang *et al*. lanean zehazten dutenez [86]. Anodizazio elektrokimikoko tratamendu eraginkorraren bidez, aluminiorik gabeko oxido nanoporotsuzko geruza bat sortu zuten Ti-6Al-7Nb gainazalean. Gainazala oxidatzean, hobekuntza nabarmenak izan zituzten korrosioarekiko erresistentzian; izan ere, korrosio abiadura eta korronte pasiboa murriztu egin ziren, simulatutako odol plasman sartzean. Gainera, oxido nanoporotsuaren geruzak eragin positiboa izan zuen zelulen portaeran. Zehazki, giza hezur muineko zelula ama mesenkimalen atxikitzea eta ugaritzea areagotu egin zen,

garrantzi handia izanik aplikazio biomedikoetan. Aipatzekoa da oxidozko geruza ordenatuaren garapena zenbait parametroren erregulazioaren bidez egokitu daitekeela, hala nola elektrolitoen aukeraketa, aplikatutako korronte dentsitatea, elektrolitoen kontzentrazioa, elektrolitoen tenperatura, irabiatze abiadura, eta anodo eta katodoaren arteko gainazal eremuen erlazioa [95].

Aminolisia

Era berean, aminolisiaren bidez amina erreaktibo funtzio taldeak gainazal polimerikoetan eta metalikoetan eratzen dira. Aldaketa horietarako, poliuretanoa (PU), poli(kaprolaktona) (PCL) edo PLA bezalako polimeroak diamina disoluzioetan sartzen dira, hala nola 1,6-hexanodiamina edo etilendiamina, amidak osatuz eta gainazal polimerikoetan amina talde libreak lortuz [83,96]. Bestalde, amina taldeak eratzea substratu metalikoetan konplexuagoa izaten da, izan ere baldintza gogorragoak erabili behar izaten baitira, tratamendu plasmatikoa, esaterako. Hala ere, hidrolisiaren antzera, aminolisiak polimeroen degradazioa eragin dezake, polimeroen zimurtasuna eta bustigarritasuna handituz, eta horrek proteinen eta zelulen arteko interakzioak alda ditzake, baita bakterioen materialaren artekoak ere [81,97].

Horren adibidea Yaseri *et al*-ek deskribatu zuten bere lanean [83]. Izan ere, PCL nanozuntzen erabilera ehun ingeniaritzan analizatu egin zuten gainazaleko tratamendu desberdinak frogatuz, besteak beste, hidrolisia eta aminolisia. Behatu egin zen bi tratameduek PCL nanozuntzen gainazaleko ezaugarrietan eragina zutela, baina materialaren berezko propietateak kaltetu gabe. Aldaketa morfologiko txikiaz eta jarduera mekanikoaren leunki murriteaz gain, gainazal guztietan hidrofilitatea nabarmen handitu egin zela behatu zuten. In vitro egindako ikasketek frogatu zuten PCL nanozutzen gainazal eraldaketek ez zutela efektu zitotoxikorik eragiten, eta zelulen atxikimendua, hedapena eta proliferazioa sustatzeko substratu ezin hobeak zirela behatu zen L929 zelulak erabili zirenean.

Plasmaren bidezko tratamendua

Tratamendu plasmatikoa erabilera anitzeko metodoa da gainazal polimeriko eta metaliko geldoetan funtzio taldeak sartzeko, bai zuzenean, bai zeharka. Prozesuan presio txikiko gas bat (amoniakoa, oxigenoa edo argona) kitzikatzen da ganbera batean, hainbat energia iturriren bitartez, hala nola deskarga elektrikoa, korronte alternoa/zuzena, irrati-maiztasuneko energia, mikrouhinak edo beroa [98,99]. Gasaren ionizazio partzial horrek kargatutako molekulak sortzen ditu. Molekula horiek materialaren gainazala bonbardatzen dute, eta haren propietate kimikoak eta

fisikoak aldatzen dituzte. Substratuaren gainazalean sartutako funtzionaltasun mota gas plasmatikoaren hautaketaren eta eragiketa parametroen araberakoa da, hala nola presioa, potentzia, gas fluxua eta denbora. Adibidez, NH_3 plasma erreaktiboak aminak sartzen ditu, O_2 plasmak OH eta COOH funtzioen nahasketa bat sortzen du, eta plasma argonak erradikalak sortzen ditu. Beste bideen antzera, funtzio talde horiek erabil daitezke gainazala txertatzeko beste metodo batzuekin konbinatuta. Beste zenbait tratamendutan bezala, plasma bidezko tratamenduek zuzenean indartu ditzakete gainazaleko hidrofilitatea eta zelulen atxikimendua, hainbat abantaila eskainiz aplikazio biomedikoetan [100–102].

Testu inguru honetan, Ujino *et al*.-ek presio atmosferikoan burutzen den plasmaren tratamenduaren bitartez Ti gainazalak eraldatu zituzten hidrofilitatea handitzeko [90]. Azterketa horren helburua nagusia gainazalen hidrofiliate eta arratoizen hezur muinaren atxikimendua, eta ondorengo bereizketaren, eragina ebaluatzea zen. Plasma 30 s aplikatu ondoren, Ti gainazal puruek superhidrofilikoak bihurtu ziren. Emaitzen arabera, hobekuntza nabarmena behatu zen bai zelula atxikiduran, bai zelula bereizkea osteogenikoan plasmaren bidez tratamendua jasotako gainazaletan.

Era berean, Mian Chen *et al.*-ek plasmaren bidez Ti gainazalek fluoratu zituzten, fluoratutako Ti gainazal lortuz [91]. Esperimentuak fluorraen zenbait konposizio kimikoren arabera burutu ziren, hala nola, gainestaldurak. Staphylococcus aureus erabili ziren *in vitro* bakterioen aurkako entseguak egiteko eta zelulen bateragatarritasuna MC3T3-E1 zelulak erabiliz burutu zen. Emaitzen arabera, fluorokarbozko gainestadurek eta fluoruro metalikodunek hidrofiloak ziren nanoeskalako zimurtasunarekin. Bitxia bada ere, fluoruro metalikoz osatutako gainestaldurak propietate bakterizida bikainak erakutsi zituen, eta zitobateragarritasun oso ona erakutsi zuen baita ere. Aipatzekoa da bakterioen kontrako jarduera fluoruro metalikoen presentziari eta ioi fluoruroen askatzeari esleitu zitzaiola.

Testuinguru honetan, Lee eta kolaboratzaileek Ti laginak termikoa ez den eta presio atmosferikoan burutzen den plasmarekin (*Non-thermal atmospheris pressure plasma jet –NTAPPJ*) tratatu zituzten bakterioen aurkako propietateak izateko [103]. Bi bakterio pareta egitura desberdin ikasi zituzten: bakterio Gram-positiboak eta bakterio Gram-negatiboak. Helburu hori lotzeko, aire konprimitutako plasma erabili zuten, hidroxilo eta karboxilato ioien, ^{-}OH eta COO^{-}, hurrenez hurren, edukia handitu zuena. Horren ondorioz, erabilitako tratamenduak Ti gainazalen hidrofilitatea handitu zuen, gainazalaren propietate topografikoetan eragin gabe. Irudi fluoreszentearen teknikaren arabera, Ti gainazalean burututako eraldaketak, hala nola, gainazalaren

energiak, konposizio kimikoak eta NTAPPJ-ren bidezko erredukzio potentzialak, bakterioen atxikimendua murriztu eta biofilmaren eraketaren abiadura moteldu zuten. Gainera, bakterio Gram-positiboak bakterio Gram-negatiboekin konparatu zirenean, behatu zuten bai bakterioen atxikimendua eta biofilmaren eraketaren abiadura baxuagoa zela bakterio Gram-negatiboen kasuan, betiere laginen NTAPPJ-ren bidezko tratamendua luzeagoa zenean. Emaitza horien arabera, NTAPPJ tratamenduak oso metodo aproposa eta eraginkorra da bakterioen atxikimendua eta biofilmaren eraketak saihesteko Ti hortzetako inplanteetan.

Txertaketa Grafting

Erresistentzia fisiko eta kimiko handiagoa duten gainestaldurak garatzeko hainbat estrategia proposatu dira. Hala ere, estalduraren eta substratuaren artean ematen den lotura motak mugatzen ditu estrategia asko. Etorkizun handiko metodoalternatiboa txertaketa da, ingelesez grafting moduan deskribatzen dena, non materialaren gainazalean erresistentea den filma eratzen den zenbait konposaturen immobilizazio kobalentearen bitartez. Gaur egun, bi txertaketa metodo nagusi erabiltzen dira: "*grafting to*" eta "*grafting from*" [104].

"*Grafting to*" metodoaren bidez polimero kateak materialaren gainazalera lotzen dira, materialaren propietateak aldatzeko baliabide bat emanez. Aldiz, "*grafting from*" metodoaren kasuan, monomeroak atxikitzen dira materialaren gainazalera eta ondorengo polimerizazio erreakzioak pairatzen dituzte (**1.8 irudia**). Eratutako estalduraren egiturari eta propietateei erreparatuz, azken metodo horrek kontrol handiagoa eskaintzen du. Txertaketa tekniken bidez, propietate zehatzak dituzten estaldurak lor daitezke, hala nola higadurarekiko, korrosioarekiko eta inguruneareN degradazioarekiko erresistentzia hobetu daitezke. Gainera, polimeroen immobilizazio kobalenteak atxikidura eta iraunkortasun hobeak bermatzen ditu eta, beraz, baldintza gogorrak luzaroan jasaten dituzten estaldurak dira.

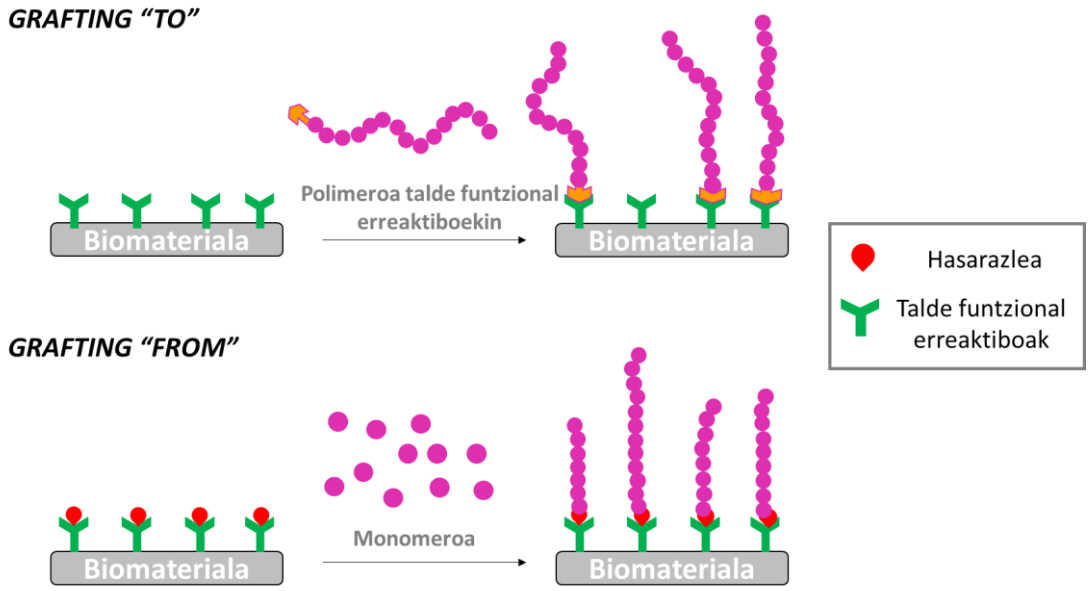

1.8. irudia. *grafting "to"* eta *grafting "from"* estrategien errepresentazio eskematikoa.

Testuinguru horretan, Huh *et al*. lanean hainbat esperimentu egin zituzten oxigeno plasmako gasak PET laginetan deskargatuz [105]. Plasmaren ondorioz, PETezko gainazalen testura hobetu egin zen, eta gainazaletan peroxidoak sortu ziren. Peroxido horiek katalizatzaile gisa erabili ziren azido akrilikoa txertatzeko eta polimerizatzeko eta, horrela, azido karboxilikoak sartu ziren gainazaletan. Ondoren, kitosano neutroa eta kuaternizatutako kitosanoa sartutako talde karboxilikoekin akoplatu ziren, txertatutako kitosano PET eta kuaternizatutako kitosan_PET gainazala lortuz. Eraldatutako PETaren bakterioen aurkako jarduera ebaluatzeko, irabiatutako matrazearen metodoa erabili zen. 6 orduz astindu ondoren, kobalenteki txertatutako kitosano-PET eta kitosano kuaternarioa PET gainazalak aztertu ziren, eta kitosanoak bakterio hazkuntza nabarmen inhibitu zuela ikusi zen. Testurizatutako PETa garbitu ondoren ere, bakterio hazkuntzaren inhibizioa % 48-58an mantendu zen, eta kitosanoarekin txertatutako PETezko testuren iraunkortasuna eta eraginkortasuna frogatu zen, nahiz eta gainazala sakonki garbitu.

Txertotzat har daitekeen beste estrategia bat egituren automuntaketa da. 1935ean, Blodgett *et al*. lanean, gainazal solidoetan kate luzeko azido karboxilikoak metatuz geruza organiko mehe baten prestaketa deskribatu zuten [106]. Aurreko lan horretan oinarrituta, hamarkada bat geroago, Zisman *et al*. lanean, platinozko eta pirexezko gainazal eraldatuetan, talde polarrak dituzten kate luzeko hidrokarburoen egitura automuntatzaileak ezarri zituzten [107]. Hala ere, Jacob Sagiv-ek ez zuen "monogeruza automuntatzaileak" (Self Assembled Monolayers, SAMs) terminoa 1983. urtera arte azaldu. Izan ere, monomeroen eta gainazalaren arteko

elkarrekintza espezifikoen ondorioz gainazal materialetan eratzen diren molekula multzo bidimentsional gisa deskribatu zituen SAMak. SAMen adibiderik ezagunenak dira, besteak beste, urrean sufrea duten molekulak eta oxidotan alkilsilanoak dituzten molekulak, baina sistema automuntatzaileen sorta zabal baten berri eman da. Izan ere, formazio mota horren sendotasun fisiko eta kimikoaren ondorioz, modu kontrolagarrian doi daitezke gainazaleko propietateak. Horren ondorioz, metodologia horrek aplikazio ugari ditu hainbat arlotan, hala nola biomaterialetan edo elektronikan [108–110].

Oinarrizko hiru osagai dituzten molekula anfifilikoek parte hartzen dute SAMetan. Lehenik eta behin, atxikitako taldeek substratuarekiko afinitate espezifikoa dute, eta eginkizun erabakigarria dute molekulen antolaketan. Bigarrenik, lotzaile edo espaziadore molekularrak buruaren eta amaierako taldearen artean kokatzen dira, izan ere lotzailearen luzerak SAM egituraren lodiera zehazten du; eskuarki, 1 nm-tik 3 nm-ra izaten da [16,108]. Azkenik, molekula anfifilikoaren beste muturrean, ondorengo eraldaketarako erabilgarria izango den funtzio taldea dago, eta eraldatutako substratuaren gainazalaren propietate fisiko eta kimikoak zehazten ditu. Azken funtzio talde hori gainazalaren propietateak finkatzeko baliagarria da, hala nola eroankortasuna, erreaktibotasun kimikoa, bustigarritasuna, marruskadura, korrosioarekiko erresistentzia eta, adierazgarriena, lan honen testuinguruan, biobateragarritasuna. SAMek zenbait substraturen propietateak eraldatzeko aukera paregabea eskaintzen ditu, besteak beste, beirarenak, silizearenak, polimeroenak eta metalenak, amaierako funtzio taldea trebeki egokituz [111]. Izan ere, gainazal horiek arrakastaz eraldatu dira baldintza espezifikoak betetzeko hainbat aplikaziotarako.

SAMak sei multzotan sailka daitezke atxikimendurako erabilitako akoplamendu talde kimikoan oinarrituta: karboxilatoak, alkenoak/alkinoak, aminak, silanoak, fosfonatoak eta katekolak [111]. Karboxilatoak, alkenoa/alkinoak, aminak eta katekolak SAMak prestatzeko asko erabili diren arren, kapitulu honetan Doktorego Tesian erabilitako silanoak eta fosfonatoak baino ez dira deskribatuko.

a) Silanoak

Alkilsilanoen bidezko gainazal eraldaketa teknika oso interesgarria da oxidatutako gainazaletan monogeruzak eratzeko. Organosilanoak honelako konposatuak dira: $RSiX_3$, R_2SiX_2 edo R_3SiX, non R alkilo talde bat den, eta X, berriz, doan talde bat, hala nola kloruroa, alkoxia edo hidruroa [108,112]. Organosilano horiek erabilera anitzeko aplikazioa aurkitu dute hainbat eremutan. Oxidatutako gainazaletan silanoen monogeruzaren formazioa erabiltzearen abantaila nagusia da substratuaren eta atxikitzen den taldearen arteko lotura kobalentea azkar ezartzen dela. Lotura

kobalente horrek egonkortasuna ematen dio monogeruzari, eta, aldi berean, hurrengo eraldaketa kimikoak errazten ditu, materialaren osotasuna arriskuan jarri gabe [113]. Monogeruza horien propietateak, hala nola osaera kimikoa, lodiera, orientazioa eta alkilo katearen alboko ordena, sakonki aztertu dira hainbat gainazaletan, titanio eta polimerozko gainazalak barne.

Bi bide jarrai daitezke Ti gainazaletan amaierako funtzio talde bat sartzeko: SAMa eratu ondoren, aurre-eraldatutako organosilanoaren lotura zuzena eratuz gainazal metalikoarekin edo gainazalaren eraldaketa kimikoa pairatuz. Bigarren estrategia hori bide eraginkorragotzat hartu da, hainbat arrazoi direla medio. Lehenik eta behin, gainazal eraldaketa gehigarriek ez dute monogeruzaren ordenan eragiten, baldin eta immobilizatutako SAM geruza egonkorra bada eta, beraz, baita ondorengo funtzionalizazioak ere. Bigarrenik, hainbat erreakzio kimiko erabil daitezke gainazal bera eraldatzeko, eta horrek zenbait funtzio talde sartzeko aukera gehiago eskaintzen ditu. Gainera, metodologia oso sinplea da, eta ez dira substratu berriak sintetizatu eta purifikatu behar; izan ere, molekula aitzindari erabilienak erraz eskura daitezke ongi definitutako monogeruza eratzeko [108].

Silanoen bidezko SAM eraketaren lehen urratsa gainazalean adsorbatutako ur molekulen bidezko organosilanoaren hidrolisia da. Gero, bigarren urratsean, eratutako hidroxisilanoak, Van der Waals indarren bitartez, gainazalean dauden oxido polarrei gehitzen zaizkie. Behin gehituta, Si-OH kondentsatu egiten da, eta ura kenduz, lotura berri bat sortzen da, Si-O-Si, alegia. Lotura berri hori gainazalean dauden silanoen artean gertatzen da, eta silanoen arteko sare bat sortzen da. Metodologia horren abantaila nagusia da merkatuan eskuragarri dauden silanoak aldakortasun handia dutela, zeren erreakzioen bidez eraldatu baitaitezke monogeruzaren egonkortasuna arriskuan jarri gabe (**1.1 eskema**). Doan talde bakarra duten organosilano monofuntzionalak, normalean R(CH3)2SiX, oso errepikakorrak dira, izan ere gainazalarekiko lotura mota bakarra era baitaiteke. Horien desabantaila bakarra bi metil taldeen bolumena da, titanio gainazalaren estaldura osoa mugatzen baitute. Aitzitik, organosilano trifuntzionalen kasuan (RSiX3), doazen hiru taldeak hidrolizatu daitezke, eta horrek geruza barneko eta geruza bakarreko lotura gurutzamendua sortzen du eta, ondorioz, monogeruzaren egonkortasuna handitzen du. Hala ere, kasu horretan, gainazalarekiko lotura kobalentearekin batera edo are lehenago, homokondentsazioaren ondorioz oligopolimerizazio erreakzioak gerta daitezke disoluzioan, egitura desordenatuak sortuz [108,111].

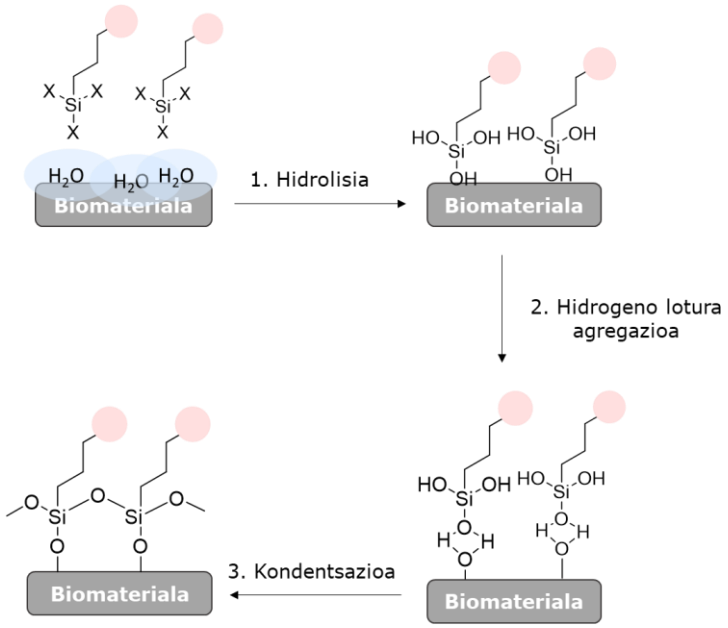

1.1. eskema. Silanoetan oinarritutako SAM eraketaren mekanismoa.

Bestalde, alkilo kateak gehien erabiltzen diren lotzaileak dira. Izan ere, horren arrazoi nagusia alkil kateen antolamendu erraza da, efektu hau molekula lipidikoen artean agertzen da hainbat egitura biologikoetan. Alkil kateen luzera faktore erabakigarria da elkarren artean ezartzen diren Van de Waals elkarrekintzen bidez ondo antolatutako SAMak lortzeko [114,115].

Amaierako funtzio taldeak baldintzatuko ditu SAMaren gainazal propietateak, hala nola erreaktibotasun kimikoa, eroankortasuna, bustigarritasuna, marruskadura, atxikidura eta ondorengo gainazalaren erabilerak [116]. Monogeruzan amaierako funtzio talde horiek sartzeari dagokionez, bi ikuspegi orokor daude. Bien arteko alde nagusia da titanio gainazalarekiko lotze puntua noiz emango den. (**1.9 irudia**). Lehenengo ikuspegiak (**1.9 irudiko A bidea**), aurrez sintetizatutako aitzindari baten adsortzioa suposatzen du. Protokolo horren desabantaila nagusia da sintetizatutako deribatu bakoitzaren automuntaketa etapa optimizatu behar dela. Bigarren metodologian (**1.9 irudiko B bidea**), berriz, lehen urratsean SAMa eratzen da, eta, ondoren, nahi den funtzionaltasuna lortzeko beharrezko erreakzioak burutzen dira. Metodologia horrek selektibitate altuko eta errendimendu handiko erreakzioak eskatzen ditu, baita ezpurutasunak eragiten dituzten albo erreakziorik eza ere, purifikazio aukera mugatua baita. Bestalde, ikuspegi horren abantaila nagusia sinpletasuna da, zeren, kasu horretan, gainazalari lotzeko emaitza onak dituzten eta monogeruza eraginkorra eratzen dituzten silanoak erabiltzen baitira. Izan ere, monogeruza ondoren, funtzionaltasun egokia lortzeko ondoren egin behar diren erreakzioek ez dute monogeruzaren egonkortasunean eragiten [115].

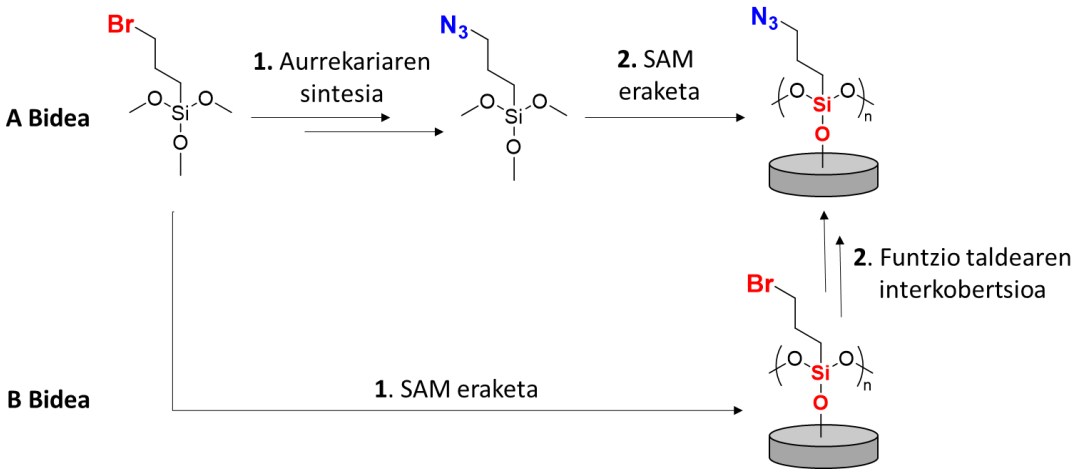

1.9. irudia. Desiratutako SAM eraketa bi bide desberdin jarraituz.

Testuinguru horretan, Hasan *et al*. lanean, silanoz egindako gainestalduraren prestaketa eta horrek titaniozko gainazaletan bakterioen aurkako jardueran duen eraginari buruzko azterketa egin zuten [117]. Ti6Al4V gainazal hezegarriak arrakasta handiz sortu zituzten, SAMs hidrofilikoak (karboxilikoak eta aminak), hidrofobikoak (oktil) eta erdi hidrofobikoak (mistoak eta hibridoak) sortuz. Konparaketa analisi sakona egin zen, eraldatutako gainazaletan proteina adsortzioa, zelula atxikitzea eta mikrobioen aurkako jarduera ebaluatzeko. Emaitzek erakutsi zuten mikrobioen atxikiduraren eta gainazaleko hidrofobitatearen artean lotura estua zegoela. Aminaz funtzionalizaturiko gainazalak, pH fisiologikoan protonatua dagoena, karga positiboa erakutsi zuen, eta karga horrek bakterio zelulak erakarri zituen, negatiboki kargatutako zelula-paretengatik. Horren ondorioz, *Escherichia coli* (Gram-positiboa) eta *Staphylococcus aureus* (Gram-negatiboa) bakterioak erabat atxikitu ziren. Gainazalen hidrofobitatea handitu ahala, bakterio-atxikidura nabarmen jaitsi zen; beraz, oktanozko gainazal oso hidrofobikoak bakterio-atxikimendu txikiagoa erakutsi zuen.

Silanoen bidezko beste adibide bat Abraham Rodríguezek eta lankideek azaldu zuten [118]. Polimero orrazi motako egiturak lortu zituzten aminoalkil silanoen lotura kobalenteak pairatuz Ti6Al4V-n gainazalean. Ti6Al4V aleazioa 3-aminopropiltrimetoxisilanoarekin (APTMS) funtzionalizatu zuten, bersilanizatu ahal zen dentsitate handiko gainazal estalia lortuz. Staphylococcus-en atxikipena eta biofilmaren eraketa aztertu zituzten eraldatu gabeko Ti6Al4V gainazal oxidatuan. Proba biologikoen arabera, eraldatutako Ti aleazioa egokia zen inplante eta protesi biomedikoetarako. Giza osteoblasto primarioaren portaeraren arabera, aminosilanizatutako laginek aleazioaren antzeko zitobateragarritasuna erakutsi

zuten. Gainera, *Staphylococcus epidermidis* espeziearekin egindako bakterio saiakuntzek aminosilano geruzek bakterio atxikitzearen aurkako babesa zutela adierazi zuten.

b) Fosfonatoak

Azido fosfonikoak (R-PO3H2), silanoen antzekoak, hidroxilatutako gainazaletarako erakargarriak dira. Hain zuzen, Ries eta Cook-ek 1954an egindako lan aitzindariaz geroztik, aurrerapen handiak egin dira fosfonato deribatu horiek monogeruzak eratzeko erabiltzean. Silverman *et al*. lanean fosfonatoen eta silanoen arteko konparaketa egin zen, eta egindako ikerketaren arabera, frogatu zen fosfonatozko monogeruzek silano monogeruzak baino egonkortasun hidrolitiko handiagoa dutela, batez ere, baldintza basikoetan edo fisiologikoetan [119]. Ezaugarri horri esker, azido fosfonikoak askoz erakargarriagoak dira medikuntzarekin lotutako aplikazioetarako. Izan ere, P-O-Ti loturen sendotasunari eta hidrolisiarekiko erresistentziari esker, monogeruza mota hori katekolean, alkalinoetan edo alkiletan oinarritutakoen monogeruzen antzekoa da, egonkortasunari eta funtzionaltasunari dagokienez. Aurkikuntza horiek agerian uzten dute azido fosfonikoan monogeruzen erabilera praktikoa, batez ere medikuntzaren arloan [120,121].

Alkilo-fosfonatozko monogeruzak lortzeko teknikarik erabiliena murgiltze bidezko estaldura da, fase likidoko erreakzio baldintzak dakartzana. Murgiltze denborak normalean minutu gutxi batzuetatik ordu batzuetara edo egun batzuetara aldatzen dira [16].

Zenbait faktorek gainazal metalikoen gaineko fosforo deribatuen kimisortzio mekanismoan eragiten dute, hala nola tenperaturak, pH balioak, kontzentrazioak edo disolbatzaileak. Aurretik aktibatutako titanio gainazalen Lewis azidotasuna dela eta, fosforo atomoaren koordinazioaren bidez gertatzen da loturaren hasierako urratsa. Horren ondorioz, fosforoaren elektroizaletasuna handitu egiten da, eta fosforoaren gaineko kondentsazio erreakzioa eragiten du gainazal metalikoan dauden hidroxilo taldeekin. Prozesu horren bidez geruza bakarreko atxikimendu kobalentea gertatzen da. Esan beharra dago, azido fosfonikoak ez ezik, fosfonato esterrek ere antzeko kondentsazio erreakzioak izaten dituztela baldintza leunetan, eta harrigarria da, izan ere P-O-C loturaren apurketak normalean baldintza sendoak eskatzen baititu disoluzioan (**1.2 eskema**). Nolanahi ere, gainazal metalikoan dauden hidroxilo taldeen kopurua funtsezkoa da fosfonatoen lotura arrakastatsua lortzeko [111,120].

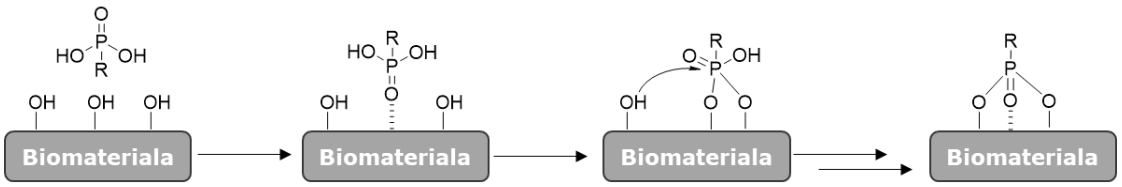

1.2 eskema. Fosfonatoetan oinarritutako SAM eraketaren mekanismoa.

Callies *et al*. lanean ikuspegi horren adibide bat deskribatzen dute. Lan horretan kopolimeroen sintesia aurkeztu zuten, 4- binilpiridina (VP) binilbentzilfosfonatoarekin (VBP) edo dimetil (2- metakriloxietil)fosfonatoarekin (DMMEP) konbinatua, erradikal askeen polimerizazioaren bidez [122]. Jarraian, 1-bromohexanoarekin *N*-alkilazioa burutu zen, *N*-hexilpiridinio bromuro (HexVP) taldeak sartzeko. Ondoren, kopolimeroak titanio oxidozko gainazalekin lotu ziren fosfonatozko estalduraren bidez. Estaldura prozesu horren ondorioz, ultrafinak diren film polimerikoak sortu ziren eskala nanometrikoan, 3 nm-tik eta 11 nm-era arteko lodierakoak. Ikerketak erakutsi zuen *Staphylococcus epidermisen* eta *Staphylococcus aureusen* banaketa ereduak desberdinak zirela estalitako gainazaletan, titanio kontrolekin alderatuta. Emaitza horiek argi erakutsi zuten DMMEP proportzio handiagoko estalduren eragin antimikrobianoa; izan ere, DMMEP monomero hidrofilikoa da, eta propietate anti-inkrustatzaileak dituen homopolimero bat sortzen du. Kopolimeroetan DMMEP egoteak lagundu egin zuen gainestalduren jarduera antimikrobianoa handitzen, eta mikrobioen aurkako gainazal eraginkorrak garatzeko material potentziala adierazi zuten.

1.6.1.3. Gainestaldurak

Gainestaldura polimerikoak eta zeramikoak gai interesgarriak dira aplikazio biomedikoetarako (**1.3 taula**). Estaldura horiek propietate onuragarri eta baliotsuak ematen dizkiote azpiko materialari, hala nola biobateragarritasuna handitzea, sendotasun mekanikoa hobetzea, higadurarekiko eta korrosioarekiko erresistentzia areagotzea eta gaitasun funtzionalak areagotzea.

1.3 taula. Biomaterialen artean erabiliak izan diren gainestaldura zeramikoen eta polimerikoen sailkapena.

Gainestaldura	Materiala	Abantailak/Aktibitatea	Erref.
Zeramikoa	Kaltzio fosfatoa	Oseoinegrazio abiadura handiagoa Korrosioarekiko erresistentzia Areagotutako atxikipen zelularra	[123–128]
	Hidroxiapatita	Faboratutako atxikipen eta proliferazio zelularrak Handiagotutako oseoeroankortasuna Hobetutako oseointegrazioa	[129–132]
	Bioactive glasses (BGs)	Oseoeroankortasun eta osteinduktibitate bikainak	[133,134]
Polymer	Kitosanoa Kolagenoa Azido hialuronikoa PEG	Propietate anti-inkrustatzaile eta antibakterianoa Hobetutako osteogenesia Handiagotutako biofilmaren saihespena	[135–141]

Gainestaldura zeramikoak

Zeramikazko gainestaldurak zeramikazko geruza meheak dira, eta hainbat substratuen gainazaletan aplika daitezke, hala nola metala, beira edo zeramika; propietateak hobetzeko edo funtzionalitate espezifikoak lortzeko erabiltzen dira gehienbat. Estaldura horiek aurkezten dituzten propietateak direla eta, industriann eta teknologian askotariko aplikazio izan dituzte. Propietateen artean hurrengoak nabarmentzen dira: tenperatura altuekiko, higadurarekiko eta korrosioarekiko erresistentzia, isolamendu elektriko eta termikoa, eta biobateragarritasuna [142].

Estaldura zeramikoen artean, hezur ehunarekin duen antzekotasuna dela eta, kaltzio fosfatoan (CaPs) oinarritutako estaldurak oso erabiliak dira. Izan ere, hezur birsorkuntzaren arloan etorkizun handiko materialak dira; hezur akatsen barnean, ehunen birsorkuntza errazteko eta indartzeko erabiltzen diren autoinjertoen eta aloinjertoen ordezko sendoak dira [143]. Hezur naturalean dagoen fase mineralarekin duten antzekotasunagatik, aparteko biobateragarritasun eta biodegradagarritasuna erakusten dute. Substratu metalikoen gaineko CaP estaldura zeramikoak garatzeko hainbat azterketa egin dira, hezur ehunaren propietate biologikoak erreplikatzeko eta inplanteen iraunkortasuna eta egonkortasuna hobetzeko asmoz.

Biomineralen eraketa eta zelulen eta proteinen atxikitzea arautu daitezke, CaP gainazaletan eskuratzen den zimurtasuna eta porositatearen bidez egokitutako gainazal propietateak modulatuz [143]. Bestalde, aipatu behar da fosfatoek, hala nola hidroxiapatitak (Hap) edo fosfato trikaltzikoak (TCP), biobateragarritasun desberdina dutela, izan ere kristalinitate, disolbagarritasun, egonkortasun, ioien askapen eta propietate mekaniko desberdinak baitituzte.

Komentatu denez, CaP estalduren artean, HAp-ak arreta berezia merezi du, hezur ehunaren osagai ez-organiko primarioa baita. Hain zuzen, zientziaren eta materialen prozesamenduaren arloetan izan diren aurrerapausoei esker, hidroxiapatitaz egindako txertoak hainbat eratan ekoitzi ahal izan dira, eta aplikazio kliniko ugariren eskaera bete da. Gainera, zenbait *in vitro* eta in vivo ikerketatan emaitza onak izan dituzte berrikuntza horiek [143].

Testuinguru horretan, Chen *et al*. lanean, HAp geruza nanoegituratu bat Ti gainazalean elektrojalkitzeko metodoa erabili zuten [132]. HAp estalduraren eta Ti gainazalaren arteko atxikidura hobetzeko asmoz, grabatu kimikoko eta oxidazioko tratamenduak erabili zituzten, eta TiO2 geruza mehe bat lortu zuten. Geruza horrek estres termikoa arindu eta estalduran pitzadura sortzea eragotzi zuen. HAp-en elektrojalkitzearen ondoren, nanoegituratutako HAp estaldura uniformea eta pitzadurarik gabea arrakastaz sortu zen Ti gainazalean. Horrez gain, MSC zelula kultiboen *in vitro* esperimentuek frogatu zuten HAp-Ti gainazal nanoegituratuaren biobateragarritasuna eta bioaktibitatea bikainak zirela. MSC zelulak ugariagoak izan ziren HAp- estaldura zuten Ti gainazaletan, eraladtu gabeko Ti gainazalarekin alderatuta.

Era berean, Hui Du *et al*. lanean, kaltzio silikatoz eta kaltzio fosfatoz osatutako gainestaldura fabrikatu zuten Mg-Zn-Mn-Ca aleazioaren gainean, NaSiO3 eta Ca(NO3)2 zituen erreakzio kimikoaren bidez [123]. Zelulen *in vitro* azterketen

ondorioz, osteoblastoek zelula atxikidura ona, hazkunde tasa handiak eta ugaltze ezaugarri handiak zituztela ikusi zuten. Emaitzetan ikusi zenez, gainazalaren zitobateragarritasuna nabarmen handitu zen kaltzio fosfatozko estaldurari esker.

Beste material zeramiko mota batzuk zirkonioan (ZrO_2) oinarritutako gainestaldurak dira. Material mota horiek tenperatura altuak eta tentsio handiak jasan ditzakete. Horren erabilera hainbat eremuetara hedatzen da, hala nola hortzetako inplanteak, eta metalezko inplanteen gaineko estalduraren korrosioarekiko erresistentzia hobetzeko babesle gisa. ZrO_2 zeramikak abantaila ugari eskaintzen ditu: erresistentzia mekaniko sendoa, egonkortasun kimikoa, biobateragarritasuna eta higadurarekiko erresistentzia handiagoa. Gainera, itrioarekin egonkortutako zirkonioak (YSZ) hortzetako inplanteen material gisa protagonismoa hartu du. YSZ gainestaldurek HAp gainestaldurek baino gogortasun eta erresistentzia handiagoa dute. Gainera, Saravan *et al*. lanean, YSZz estalitako Ti substratuek hemobateragarritasun hobetua dutela frogatu zuten, eta odoleko plaketak pseudopodoak garatzeko estimulatzen dituela [144].

Kristal bioaktiboak (BG) etorkizun handia duen beste material zeramiko mota bat da, batik bat, osteoeroankortasunagatik eta bioabsorbagarritutasunagatik, hezur ehunen ingeniaritzako aplikazioetarako material egokia baita. Idealki, aplikazio klinikoetan erabiltzen diren inplante bioaktiboek ehun ostalariaren antzeko propietateak izan behar dituzte, eta, aldi berean, ehun gogor eta bigunekin konexio interfazial sendoak ezarri behar dituzte. Kristal bioaktiboen osaera ez-organikoa eta ezaugarri mekanikoak direla-eta (hezur ehun "gogorren" ezaugarrien oso antzekoak dira), interes handia egon da hezurretan eta hortzetan egindako inplanteetan aplikatzeko. Hala ere, haren propietate mekaniko desegokiek nabarmen oztopatzen dute karga eremuetan erabiltzea. BG gehienek erresistentzia txikiagoa dute hausturarekiko, hezur naturalarekin konparatuz [142,145]. Izan ere, hausturaren erresistentziari dagokionez BGek, 0,2 eta 0,6 MPa arteko kargak jasaten dituzte; hezurrek, berriz, 2 eta 12 MPa arteko karga [146]. Beraz, BG estalduren erabilpena estrategia bideragarria da, ez bakarrik inplante metalikoen oseointegrazioa indartzeko, baita BGen berezko hauskortasuna arintzeko ere. Inplante metalikoen gaineko BG eta bitrozeramikazko estaldurak hainbat teknikaren bidez sor daitezke, hala nola lurruneztatze termikoa, irrati-maiztasuneko magnetroidun sputtering-a (RF-MS), pultsu laser bidezko jalkitzea (PLD), sol-gel estaldura eta jalkitze elektroforetikoa (EPD) [147].

Testuinguru horretan, Bargavi *et al*. lanean, BGko matrize batean sartutako eta komertzialki puruak diren Ti substratuetan (Cp-Ti) gordetako zirkonio oinarriko film

mehe bat aurkeztu zuten [148]. Zr kontzentrazio desberdinetan sartzearen helburua estalduraren egonkortasun mekanikoa hobetzea izan zen. Hemobateragarritasun azterketek bateragarritasun bikaina erakutsi zuten, hemolisi tasa % 2tik beherakoa izanik. Gainera, *in vitro* egindako zitobateragarritasun saiakuntzetan, osteoblastoen zelula lerroak erabiliz (MG-63), nabarmen handitu zen zelulen bideragarritasuna. Gainera, bakterioen aurkako saiakuntzen arabera, Zr eduki handiko Bg-Zr konposatuak erabili zirenean Cp-Ti substratuak estaltzeko, biofilm eraketa murriztu egin zela ikusi zen, gainazaleko zimurtasuna handitu egin zelako. Ondorioz, Cp-Ti inplante materialen gainazalean burutako BG-Zr estaldurak bioaktibitate hobea eta oseointegrazio hobea erakutsi zituen, aplikazio ortopedikoetarako estaldura mota egokia izanik.

Gainestaldura polimerikoak

Biomedikuntza aplikazioetan funtsezko papera duten gainestaldura mota bat polimerozko estaldurak dira. Gainestaldura horiek oso erabiliak dira biomaterialen errendimendua, biobateragarritasuna eta funtzionalitatea hobetzeko. Gainera, aurreko abantailak eskaintzeaz gain, ehunen eta fluido biologikoen arteko elkarrekintzak hobetu ditzakete [57,74]. Testuinguru horretan, nabarmentzekoa da propietate anti-inkrustatzaileak dituen polimero gainestalduraren erabilera.

Gainazalaren ezaugarriak eraldatzeko asko erabiltzen den beste estrategia bat gainestaldura anti-inkustatzaileen bidezko biomaterialen pasibazioa da. Adibidez, polietilenglikola (PEG), polihidroxietil metakrilatoa (PHEMA) eta fosfatidilkolina polimeroak gainestaldura moduan erabiltzen diren material polimerikoen adibide garrantzitsuenak dira [149–151]. Estaldura horiek aldarapen esteriko nagusiak aurkezten dituzte, hidratazio indarrak ezartzen dituzte, proteina eta bakterioen adsortzioa saihesteko. Mekanismo horiek erabiltzean, estaldura horiek ostalariaren immunitate sistemaren forma materiala babesten dute, eta, ondorioz, leukozito atxikidura eta ostalariaren hantura erantzuna mugatzen dituzte. Gainera, estaldura oso hidrofiliko horiek bakterioak erraz uxatzeko eta ostalariaren eta materialaren arteko interakzioa hobetzeko emaitzak eskaintzen dituzte.

Testuinguru horretan, Ungureanuk eta kolaboratzaileek Ti aleazioan Polopirrola (PPy) eta polietilenglikola (PEG) oinarri dituen estaldura konpositea elektrojalki zuten. PEG motako hiru kontzentrazio desberdin erabili ziren, zehazki %0,5, %2 eta %4 [152]. Gainestalduraren bakterioen aurkako propietateak ikertzean, %2ko PEG kontzentrazioa zuen estaldurak agertu zuen bakterioen aurkako efekturik onena, izaera hidrofilikoa eta zimurtasun txikiagoa baitzituen. Emaitza horiek bat datoz biomaterialaren eta bakterioaren arteko interakzio mekanismoarekin; mekanismo

horrek, bakterioen atxikidurari eta hazkundeari eragiten dien faktore den aldetik, interakzio fisiko-kimikoko hasierako etapa bat eragiten du, non zimurtasuna eta bustigarritasuna bakterio atxikidura eta biofilm metaketa arautzen ahal dituzten faktoreak baitira.

Azken urteotan, geruzen bidezko (Layer by Layer, LBL) metodologiak gero eta ospe handiagoa hartu du gainazal batean material polimerikoak jalkitzeko erabilera anitzeko teknika eraginkor gisa. Metodo berritzaile horrek polielektrolito kationikoen eta anionikoen geruzak sekuentzialki jalkitzea eskatzen du. Geruza horiek sendo elkar daitezke ioi elkarrekintzen bidez, estaldura mehe eta zehazki kontrolatuko film bat sortuz. Prozesu hori polimero bakoitzak pH baldintza espezifikoetan sortzen duen karga positiboetan eta negatiboetan oinarritzen da. LBL bide horrek aparteko malgutasuna eskaintzen du, eta hainbat funtzionaltasun eta propietate pertsonalizatuko estaldurak sortzeko aukera ematen du [153]. Erabilitako polielektrolito motak eta sekuentziak aldatuz, gainazal ezaugarri espezifikoak lor daitezke, hala nola karga, hidrofilitatea edo bioaktibitatea. Teknika hori hainbat eremutan aplikatu da, besteak beste, ingeniaritza biomedikoan, botikak askatzeko sistemetan eta inplante medikoen gainazalen eraldaketan [154–157] Askapen kontrolatua duten estaldura mehe eta uniformeak ekoizteko ahalmenak bide berriak ireki ditu biomaterialen biobateragarritasuna eta funtzionaltasuna hobetzeko.

Horren adibide bat Del Hoyo-Gallego *et al*. lanean deskribatu zuten [141]. Frogatu zuten positiboki kargatutako kitosanoak (CHI) eta negatiboki kargatutako azido hialuronikoak (HA) zituen PET filmean sortutako gainestaldurak arrakasta izan zuela. Geruzen bidezko estrategia bat erabili zuten polimero bakoitza PET gainazalean sartzeko, eta propietate anti-inkrusktatzaileak dituen eskala nanometrikoko lodiera duen geruza fabrikatu zuten interakzio elektrostatikoen bidez. CHIak gainazalaren contact killing propietateak hobetu zituen, eta HAren hidrofilitateak bakterioen aldarapena erraztu zuen, uraren xurgatzeak sortutako efektu esterikoen bidez.

Erresistentzia fisiko eta kimiko handiagoa duten estaldurak garatzeko hainbat estrategia proposatu dira. Hala ere, estalduraren eta substratuaren arteko lotura motek mugatzen dituzte askotan estrategiak horiek; izan ere, orain arte eztabaidatutako estaldurak materialaren gainean daude fisikoki, bi sistemen arteko interakzio egonkor eta kobalenterik gabe. Farmakoen askapena eta immobilizazioa barne hartzen dituzten ikerketek frogatu dute eraginkortasun handia dutela bakterioak eliminatzeko eta odolarekin kontaktuan egoteko interakzio egokia sustatzeko. Gainazala eraldatzeko teknika horiek optimizatzean, bakterioen aurkako portaera, propietate antiinflamatorioa eta antikoagulatzailea lor daitezke, hainbat

aplikaziotarako oso eraginkorra izanik, hala nola osasun inguruneetako gailu medikoetan, inplanteetan eta gainazaletan.

1.6.2. Gainazal bioaktiboak

1.6.2.1. Farmakoen askapena

Gainazal bioaktiboak garatzeko etorkizun handiko estrategiak zenbait agente aktiboen askapen kontrolatuan oinarritzen dira, hala nola farmakoak, hazkuntza faktoreak, proteinak, peptidoak, azido nukleikoak eta baita zilarrezko nanopartikulak ere [16]. Askapen kontrolatu hori hainbat plataformatan gertadaiteke, hala nola hidrogeletan eta nanogeletan, polimero multigeruzetan eta ziklodextrinetan, besteak beste [158–160]. Polimeroetan eta proteinetan oinarritutako egitura horiek molekula bioaktiboak askatzeko gai diren gordailu aldakorrak dira. Askapen kontrolatuko mekanismo horri esker, nahi den erantzuna lor daiteke gainazalean.

Lehenago esan denez, agente aktiboa kontrolpean askatzeko ahalmena duten estaldurak geruza anitzeko sistemen bidez era daitezke. Geruza anitzeko estaldurek gai aktiboen karga ahalmen txikiagoa izan dezakete hidrogelekin alderatuta, baina osaera kimikoan, egituran, lodieran, homogeneotasunean eta erantzun gaitasunean kontrol bikaina erakusten dute [161]. Konposatu aktiboen karga eraginkorra eta askapen iraunkorra lortzeko, funtsezkoa da polimeroen eta agente aktiboen arteko erresistentzia loturak edo elkarrekintzak izatea. Hidrogelen antzera, geruza anitzeko estalduren bidezko agente aktiboen askapena geruzaren difusio eta degradazio prozesuen bidez ematen da [162].

Kirurgia ortopedikoko inplanteei lotutako infekzioak kezka kritikoa sortzen du, izan ere hezur orbaintzea eragotzi dezake, inplanteen porrota eragin dezake eta osteomielitisa areagotu dezake. Farmakoak askatze dituzten inplanteak antibiotikoa leku lokalizatu batean askatzeko diseinatuta daude, eta infekzioak saihesteko prozedura erakargarri bihurtu dira. Li *et al*. lanean, bankomizina (antibiotikoa) enkapsulatu zuten PEG sisteman oinarritutako hidrogel film batean. Hidrogel hori kobalenteki finkatu zen Ti inplanteetan eta, ondoren, PEG-(poli(laktik-ko-kaprolaktona) (PEG-PLC) mintz baten bidez estali zen [163]. Horrez gain, elkargurutzatutako almidoia hidrogelari gehitu zitzaion, haren mikroegitura porotsua zela eta. Mikroegitura horrek hidrogelaren hantura murriztu zuen eta, ondorioz, agente aktiboaren askapena erregulatu zuen. Bankomizinaren askapen zinetika kontrolagarria zela behatu zen, bai gai aktiboaren kargaren bai estalduraren lodieraren araberakoa izanik. Azpimarratzekoa da bankomizinaz kargatutako Ti laginek farmakoen askapen profil iraunkorra erakutsi zutela, hasierako berehalako

askapenik gertatu gabe. *In vitro* egindako esperimentuek frogatu zuten agente aktiboa etengabe askatu zela ia 3 astez; in vivo egindako saiakuntzak, berriz, 4 astetik gora luzatu zuen askapen hori. Gainera, *Staphylococcus aureus*-ekin kutsatutako untxi eredu batean nabarmen murriztu zen hantura erantzuna, eta mikrobioen aurkako propietate sendoak erakutsi zituen 4 mg bankomizina zuten inplanteak erabili zirenean. Beraz, hezur infekzio lokalizatuak tratatzeko eta prebenitzeko estrategia eraginkorra dela zehazten dute.

Era berean, Karakurt *et al*. lanean bi estrategia aurkeztu zituzten PLLAn sakaridoen estaldura konbinatua sortzeko, bakterioen aurkako biomateriala garatzeko asmoz [164]. Hasieran, PLLA laginak presio txikiko plasmaren bidez tratatu ziren eta, gero, azido akrilikozko disoluzioarekin erreakzionatu ziren, COOH eta OH funtzio talde erreaktiboak lortzeko. Ondoren, PLLAren gainazalean azido poliakrilikozko (PAA) orraziak sortzeko "*grafting*" metodoa erabili zen. Gainera, kitosanoa (CS) gainazalean sartu zen karbodiimidarekin akoplamendu erreakzio kobalenteen bidez edo interakzio elektrostatikoekin zuzenean estaltzeko metodoaren bidez. Horren ondoren, lomefloxinaz betetako kondroitina sulfatozko sakaridoa (Chs) aurreko gainazalean estali zen, eta konplexu polielektrolitikoa (PEC) sortu zen. CS eta ChS artean PEC eratzen duten estaldurek bakterioen aurkako jarduera handiagoa agertu zuten banakako estaldurekin alderatuta. Horrez gain, interakzio horiek handitu egin zuten filmen estaldurei atxikitako lomefloxazina kantitatea, eta farmakoaren askatze profila handitu egin zuten. Azkenik, inhibizio probak baieztatu zuen CS-ChS estaldurak contact killing mekanismo bat erakutsi zuela; farmakoz betetako filmek, berriz, hilketa bikoitzeko mekanismo bat erakutsi zuten, ukipen bakterioen kontrako ekintzak zein askapen kontrolatuetan oinarritutakoak barne hartzen zituena.

Bakterioen kontrako propietateei buruzko beste adibide bat Chen *et al*. lanean deskribatu zuten [165]. Bakterioen aurkako propietateak dituen 3Dn inprimatutako PLA diskoak lortzeko estrategia arrakastatsua garatu zuten. Bi antibiotiko, anpizilina eta bankomizina, zuzenean adsorbatu zituzten PLA diskoaren gainazaletan. Gehieneko adsortzio ahalmena 75 mg/g PLA eta 65 mg/g PLA izan zen, hurrenez hurren. Antibiotikoen ur disoluzio kontzentrazioen aldaketak laginaren gainazaletan xurgatutako antibiotikoen kantitatea murriztea eragin zuen. Disoluzioan 50 mg/mL-ko antibiotiko kontzentrazioa erabili zutenean, farmakoak askatzeko profil egonkorrak lortu zituzten. Profil horiek sendo mantendu zuten disoluzio indargetzailean agente antibiotikoaren kontzentrazioa, Staphylococcus aureus-en gutxieneko inhibizio kontzentrazioaren (MIC90) gainetik. Gainera, antibiotikoak askatzeko zinetikak Korsmeyer-Peppas ereduari hurbiletik jarraitu zion. Anpizilinaren eta bankomizinaren bioaktibitateak, laginaren gainazaletan behar bezala xurgatu

zenean, eraginkor iraun zuen gutxienez 28 egunez. Praktikan, agente antibiotikoak zuzenean xurgatuta zituen PLA diskoak Staphylococcus aureus-en dentsitate optiko erlatiboa %40-ra murriztu zuen mililitro bakoitzeko 10^6 kolonia unitate (UFC/mL) zituen disoluzio batean, Staphylococcus aureus-ekin soilik egindako disoluzio batekin konparatuz, baldintza berdinetan.

Farmakoen askapen kontrolatuan oinarritutako eta propietate bioaktibo potentzialak dituzten Ti6Al4V substratuen gaineko geruza anitzeko estalduren adibide garrantzitsuak argitaratu dira literaturan. Testuinguru horretan, Valverde *et al*. lanean, geruza anitzeko azido hialuroniko(HA)/kitosano (CHI) geruza bat garatu zuten zenbait Ti6Al4V mikropatroi laginetan [166]. Horretarako, laser bidez egindako patroiak zituzten laginak eta lagin leunak erabili zituzten, eta hidrolisi azidoarekin aurrez aktibatu ziren, H_2SO_4/H_2O_2 nahastea erabiliz, eta, ondoren, APTESekin silanizatu ziren. Behin azken amino funtzio taldea lortuta, 5 HA eta CHI geruza jalki zituzten. Triklosana, agente antibiotiko moduan erabiliz, polisakaridoen geruzen artean sartu zen murgiltze prozesu bakoitzaren ostean. Gainera, eraldaketa horren ondorioz, hasiera batean hidrofoboa zen materiala hidrofiliko bihurtu zen, gainazal mikroegituratuen ukipen angeluaren balioak nabarmen murriztu baitziren. Bestalde, hasierako materialen ezaugarri topografikoak mantendu egin ziren gainazala eraldatu ondoren. Horrez gain, geruza anitzeko lagin leunek eta patroidunek bakteriziden gordailu eraginkor gisa jardun dezakete, inplantea egin ondoren kontrolpean askatzea erraztuz. Izan ere, geruza anitzeko material horiek gai izan ziren lehenengo 10 orduetan kargatutako triklosanaren % 25 inguru askatzeko. Kontrol hori dela eta, material horiek interesgarriak dira inplante osteko aldi kritikoan bakterioen atxikidura eta ugaltzea inhibitzeko. Eraginkortasun hori Staphylococcus aureus bakterio aurkako proben bidez berretsi zen.

Bestalde, arestian aipatu denez, inplantea ezarri ondoren makrofagoek biomaterialei ematen dieten erantzuna erregulatzea funtsezkoa da hantura arintzeko. Testuinguru horretan, Shenek eta kolaboratzaileek TiO_2 nanotutuak (TNTak) modu iraunkorrean askatzeko sistema bat diseinatu zuten, hanturaren kontrako propietateak zituzten titanio inplanteen osteogenesia hobetzeko [167]. Prozesu horretan, anodizazioaren bidez, titaniozko gainazaletan TNTak fabrikatu ziren. Ondoren, TNT horiek dexametasona (DEX) gai antiinflamatorioarekin kargatu ziren, eta, gero, geruza anitzeko kitosano geruzez (CHI) estali ziren. *In vitro* esperimentuetan, tratatutako eta tratatu gabeko titanio gainazaletan osteoblasto primarioko eta makrofagoetako (RAW 264.7) zelulak landu ziren. CHIz estalitako eta dexametasonaz betetako TNTen gainazaletan hazitako osteoblastoetan fosfatasa alkalino (ALP) gehiago eta mineralizazio handiagoa ikusi zuten, eta hori bat zetorren gene osteoblastikoen qRT-

PCR analisiekin, hala nola I motako kolagenoa (Col I), osteokaltzina (OCN), osteopontina eta runt-ekin lotutako 2. transkpizio faktorea (Runx2). Alderantziz, dexametasona duten TNTetan, CHI estaldura duten TNTetan, eta dexametasona eta CHI estaldura dituzten TNTetan makrofagoek sortutako oxido nitrikoaren (NO) eta zitokina proinflamatorioen (TNF-α eta IL-1β) proteina mailak askoz txikiagoak izan ziren. Murrizketa hori bereziki nabarmena izan zen dexametasona duten eta CHIz estalitako TNTen gainazaletan, titanioarekin eta TNTekin alderatuta. Emaitza horien arabera, dexametasona duten eta CHIz estalitako TNT gainazalek osteoblastoen bereizketa sustatzeaz gain, makrofagoen hantura erantzuna ere gutxitu zuten. Ikuspegi berritzaile horrek titanio oinarrizko inplanteak garatzeko TNTen aldaketari buruzko ezagutza berriak dakartza.

Baskularizazioa erronka esanguratsua da, oraindik ere, ehun ingeniaritzaren arloan. Aipatu bezala, biomateriala giza gorputzean ezartzen denean, gorputzak erantzun immunea sortzen du, eta horrek eragin handia izan dezake angiogenesi prozesuan, odol hodi berriak sortzeari dagokionez. Gertaera hori saihesteko, Yin *et al*. lanean interleukinaren askapena proposatu zuten. Izan ere, geruza anitzeko estaldura berritzaile bat sartu zuten T43BL-G Ti inplantearen gainazalerako, kitosanoa eta alginatoa funtsezko osagai gisa erabiliz [168]. Estaldura aurreratu horrek interleukina-4 (IL-4) zitokina eraginkortasunez enkapsulatzeko gaitasuna frogatu zuen. Nabarmentzekoa da IL-4 kontrolpean askatzeak osteogenesi sendoa erraztu zuela, bai *in vitro*, bai *in vivo*, eta hezur formazioa areagotu zuela. TNTan ipinitako geruza anitzeko ALG/CS filmek HUVEC atxiki eta hedatzea erraztu zuten, baina ez zuten eragin handirik izan zelulen ugaritzean, migrazioan eta hodien eraketan. Geruza anitzeko ALG/CS filmetatik askatutako IL-4ak are gehiago hobetu zuen HUVECen portaera angiogenikoa, eta markatzaile baskular goiztiarren adierazpena erregulatu zuen. Gainera, materialak eragindako makrofago polarizatuek (M1 edo M2) nabarmen handitu zuten HUVECetan markatzaile baskular berantiarren adierazpena. Hala, materialaren propietateek eta materialek eragindako makrofagoek eragina izan dezakete angiogenesiaren zenbait etapatan. In vivo azterketan, IL-4z kargatutako inplanteak odol hodi berri ugari eragin zituen epe labur batean; amaierako fasean, IL-4z kargatutako inplantearen inguruko ehuna egoera normalera itzuli zen. Beraz, IL-4z kargatutako inplanteak gaitasun bikaina erakutsi zuen angiogenesia eta ehun konponketa sustatzeko, bai endotelio zelulak zuzenean estimulatuz, bai makrofagoen fenotipo mesedegarriak zeharka induzituz.

1.6.2.2. Farmakoen immobilizazioa

Bide honetan, biomolekula edo agente bioaktiboa materialaren gainazalari atxikitzen zaio immobilizazio kobalentearen bidez. Bakterioen aurkako propietateari dagokionez, eragile bakterizidek, hala nola pisu molekular baxuko bakterioen kontrako botikek, bakteriofagoek, mikrobioen aurkako peptido kationikoek, lisozima edo amonio kuaternarioko polimeroek bakterioen heriotza eragin dezakete zuzeneko kontaktuan izatean [57,169]. Bakterioen heriotza, oro har, bakterio mintzaren perturbazioaren bidez gerta daiteke, edo immobilizatutako agenteen eta bakterioen mintzean dauden biomolekulen artean gertatzen diren elkarrekintza espezifikoengatik. Era berean, hanturaren kontrako propietateak eta propietate antikoagulatzaileak lor daitezke agente zehatzen immobilizazioaren bidez. Hala ere, ekintza horien atzean azaltzen diren mekanismoak intrintsekoak dira eta erabiltzen den agente espezifikoaren araberakoak dira. Adibidez, hanturaren kontrako propietateak dituzten biomolekulek –hala nola glikosaminoglikanoak (GAG), heparina (HEP), kondroitina sulfatoak (CS) edo azido hialuronikoak (HA)– hanturaren kontrako potentzia nabarmena erakutsi dute hainbat esperimentu eta saiakuntza klinikotan [138,170], eta hanturaren kontrako erantzun hori zenbait mekanismoren bidez pairatzen dute. Karga negatiboko polisakarido linealek zenbait proteinarekin elkartzeko gaitasun handia dute, esaterako MEC proteinekin (hala nola kolagenoa eta fibronektina), baita kimiozina, zitokina, hazkuntza faktore eta prozesu biologikoetan (esaterako, zelulen migrazioan, hazkuntzan eta bereizketan) parte hartzen duten entzima integralekin ere. Elkarrekintza ahalmen horri esker hanturarekin lotutako gertaerak modulatu daitezke.

Agente horiek materialen gainean immobilizatu baino lehen, material horien gainazala aurrez eraldatu edo aktibatu behar da. Horretarako, aipatutako estrategiak erabili ohi dira, hala nola txertaketa eta funtzionalizazioa. Izan ere, funtzio taldeak sartzeko aukera ematen dute, eta talde horiek gai izan behar dute biomolekulei konjugazio erreakzioen bidez atxikitzeko, besteak beste, amidazioaren, esterifikazioaren edo erreakzio konplexuagoen bidez, hala nola klik erreakzioen bidez.

Jarraian, bakterioen aurkako propietateak dituzten zenbait laginen adibideak aurkeztuko dira, zeinetan antibiotikoak edo agente bioaktiboak immobilizatu diren gainazalean.

Titanio gainazaletan peptido antimikrobianoen immobilizazio kobalentea erabili da bakterioen atxikidurari eta biofilm eraketari aurrea hartzeko estrategia gisa. Hala ere, oraindik ere zalantzan jartzen da lotzaile bat erabili behar ote peptidoa gainazalarekin

lotzeko, bakterioen atxikipenean biobateragarritasuna mantenduz. Nie-ren eta kolaboratzaileen azterlan batean, Ti gainazalek eta PEGilatutako Ti gainazalek (PEGez estalitako gainazala) eragindako bakterioen aurkako propietateak eta hantura erantzuna ikertu zituzten [171]. Ondoren, gainazal horiek KR-12 peptidoarekin funtzionalizatu ziren modu kobalentean. KR-12 peptidoa LL-37tik eratorritako peptidoa da, disoluzioan propietate bakterizida eta bakteriostatikoak aurkezten dituen substantzia. Horretarako, Ti gainazalak NaOH disoluzio alkalinoaren bidez aktibatu ziren, gainazalean OH funtzio taldeak sortzeko, eta, gero, (2-aminoetilamino)propiltrimetoxisilanoarekin silanizatu ziren. PEG konjugatzeko,

EDC eta NHS akoplamendu agenteak erabili ziren. Azkenik, KR-12 peptidoa silanizatutako Ti gainazaletan eta PEGilatutako Ti gainazaletan immobilizatu zen, berriz ere EDC eta NHS erabiliz akoplamendu agente gisa. KR-12 inkorporazioak eragin handia izan zuen bakterio atxikiduran. Izan ere, bi gainazaletan bakterio atxikidura nabarmen murriztea lortu zen. Hala ere, mikrobioen aurkako eraginkortasuna nabarmen handitu zen PEGiltatutako Ti gainazaletan, eta, horren ondorioz, nabarmen murriztu ziren Staphylococcus epidermis *in vitro* atxikidura eta biofilm eraketa, PEGilatu gabeko Ti gainazaletik konparatuz. Gainera, bai Ti PEGilatutako gainazaletan, bai PEGilatu gabeetan, TNFa-α eta IL-1β jariaketaren murrizketa behatu zen, eta, ondorioz, makrofagoak egoera ez-aktiboan egotea behartu zuten. Beraz, azterlan horrek KR-12 peptidoa immobilizatzeko PEG lotzailearen potentziala berresten du. Peptido horrek bakterioen aurkako propietate hobeak sustatzen ditu, eta makrofagoen aktibazio txikiagoa eragiten du, eta horrek hantura erantzun globala murriztu dezake.

Bestalde, Andras Heijink eta kolaboratzaileek titaniozko inplanteen gainazalaren biobateragarritasuna hobetzea proposatu zuten, Arg-Gly-Aps (RGD) tripeptidoarekin funtzionalizatuz [172]. Helburua osteoblastoen atxikimendua erraztea izan zen, inplanteen ezarpen hoberako funtsezko urratsa. Azterlan horren bidez, Ti inplanteen errendimendu histomorfometriko eta mekanikoaren azterketa sakona egin zen, eta RGD immobilizaziorako bi bide aztertu ziren: bata, fosfonatoen monogeruza automuntatzaileen bidezko immobilizazioa (RGD/SAMPS), eta bestea, tiolato/urrea interfase konbentzionalena (RGD/tiolato) erabiltzea. Emaitzen arabera, RGD/SAMPekin estalitako inplanteek hezurraren hazkundea eta inplanteen finkapena hobela zela erakutsi zuten, RGD/tiolate-urrearekin estalitako gainazalarekin alderatuta.

Testuinguru horretan, Hoyos-Nogues eta kolaboratzaileek peptido bikoitzaren eta PEG estalduraren estrategia erabili zuten komertzialki puruak diren Ti laginetan

[173]. Bakterioen kutsadura aldaratzeko, bakterio itsaskorrak hiltzeko eta osteoblastoen atxikitzea sustatzeko diseinatutako estaldura trifuntzionala garatzeko metodo bat aurkeztu zuten. Horretarako, titaniozko gainazalen funtzionalizazioari ekin zioten PEG geruza anti-inkrustatzaile baten elektrojalkitzearen bidez, eta, ondoren, propietate kimioitsaskorrak eta bakterizidak dituen RGD eta LF1-11 peptido plataforma lotu zuten. Emaitzek iradokitzen dutenez, PEG estaldurak eta biomolekulen immobilizazioak ez zuten morfologia eta topografia aldatu. Gainera, PEG estaldurak eta peptido immobilizazioak proteinen adsortzioa saihesteaz gain, osteoblasto zelulen atxikipena zaildu zuten. Hala ere, zelulekiko eremu itsasgarrien sarrerak osteoblastoen atxikidura berpiztu zuen, zelularen atxikitze eta hedatze maila nabarmen handiagoa izanik kontrol laginekin alderatuta. Bakterioen aurkako propietateei dagokienez, PEG geruzen presentziak bakterio atxikimendua nabarmen murriztea ekarri zuen gainazalean, eta peptido bakterizida gehitzeak are gehiago hobetu zuen bakterioen aurkako portaera hori, bakterioen atxikitze maila % 0,2 baino txikiagoa izanik. Sarrera atalean esan den bezala, infekzio arriskuaren eta biomaterial baten oseointegrazio optimoaren arteko oreka "gainazala lortzeko lasterketa" gisa deskribatzen da maiz, non bakterio kutsatzaileak eta ehun ostalariko zelulak kolonizatzeko lehian baitaude. Azterketa horretan, titaniozko gainazaletarako funtzio anitzeko estaldura garatu dute, zelula osteoblastikoen lotura eta hedapena sustatzeaz gain, bakterio kolonizazioa ere inhibitzen duena.

Antikoagulatzaile propietateei erreparatuz, Tan eta kolaboratzaileek heparina (HEP) eta fosforilkoline (PC) txertatu zuten poliuretano (PU) gainazaletan biobateragarritasuna handitzeko eta propietate antikoagulatzaileak izateko [174]. Polietilenimina (PEI) PU gainazalean txertatu ondoren, amino talde funtzional askeak aurkezten ziren gainazalean. Ondoren, heparina amina talde horieri ainguratu zen kobalenteki amidazio erreakzioren bidez, heparinak dituen azido karboxilikoak kontuan harturik. Jarraia, PC taldeak kobalenteki immobilizatu ziren PU-PEI gainazalera kondentsazio erreakzioen bidez, amino taldeak fosforilkolin glizeraldehido (PCGA) konposatuaren aldehido taldeekin erreakzionaraziz. Lortutako PU-HEP eta PU-PC filmek plaketen atxikimendua murriztu zuten, gertaera trombotikoa gutxituz. Gainera, material horiek odol bateragarritsun ona eta anti-tronbogenesia erakutsi zuten, esparru desberdintan erabilera anitzeko aukerak bihurtuz, hala nola, odol-hodi artifizialak, balbula-protesi artifizialak, bihotz-*stentak*. Emaitz horien arabera, PU-HEP eta PU-PC filmak etorkizun handiko hautagaik dira ondolarekin kontaktua dauden ehunen ingeniaritzarako.

Era berean, Ozaltinek eta kolaboratzaileek aire korronteko zuzeneko plasma tratamenduaren bidez PETaren gainazalean geruza oxidatzailea eratu zuten, eta

gainazal horretan itsasotik eratorria den sulfatozko polisakarido antikoagulatzailea, fukoidan, lotu zuten [175]. Lotura kimikoaren portaera optimizatzeko eta, ondorioz, antikoagulazioa jarduera, immobilizazio prozesua 3-7 bitarteko PH balioetan burutu zuten. Plasma tratamenduaren ondoren pH 5-ekin lortutako fukoidan immobilizazioak eraginkorrenak zirela ondorioztatu zuten. pH balio horietan fukoidan immobilizazioak jarduera antikoagulatzaile ona erakutsi zuen, erabakarria den muga (100 s) gaindituz. Jarduera nabarmen horrek xeheki erakusten du PETan oinarritutako materialak egokiak direla odola zuzenean ukitzeko gailuak diseinatzeko.

1.7. Klik kimika

Sharpless *et al*.-en lanean azaldu zuten lehen aldiz klik kimikaren kontzeptua, 2001. urtean, eta etekin altuko eta selektibitate altuko produktuak lortzen dira horren bidez, C-heteroatomo edo C-C lotura berriak eratuz [176]. Erreakzio moldakor eta eraginkor horien bidez, egitura konplexua duten molekulak sintetiza daitezke molekula txikietatik abiatuta [177]. Oro har, erreakzio bat klik erreakzio gisa hartuko da hurrengo baldintzak betetzen baditu [176]:

1. Abiapuntuko erreaktiboen ugaritasuna. Erreaktibo ugari onartzeaz gain, erabiltzen diren materialak eta substratuak erraz eskuratzeaz dira. Klik kimika beste sektore batzuetara hedatzen laguntzen du moldakortasun horrek; izan ere, molekula multzo desberdinak eraikitzea ahalbidetzen du.
2. Erreakzio baldintza sinpleak. Klik erreakzioetan erabiltzen diren baldintza ohikoenak sinpleak dira, erreakzioak giro tenperaturan eta oxigenoaren eta uraren presentzian egin baitaitezke. Hori dela eta, bateragarriak dira ingurune biologikoarekin. Baldintza horiek klik erreakzioen erabilgarritasuna hedatzen dute, besteak beste biokonjugazioan edo materialen zientzian erabil daitezke eta.
3. Eraginkotasun altua. Klkik erreakzioak oso ezagunak dira etekin eta konbertsio altuagatik, izan ere produktuaren eraketa azkarra izaten da.
4. Selektibitatea. Erreakzio mota hauek oso estereoselektiboak dira, izan ere ez dituzte albo-produkturik sortzen, funtzio taldeen arteko selektibitatea osoa altua delako. Orokorrean, albo-produkturik gabeko fusio erreakzioak dira, eta albo-produturik sortzekotan ura askatzen da normalean. Erreakzio hauek aurkezten duten espezifitate altuari esker, egitura konplexuak eta zehatzak lor daitezke. Horretaz gain, esan beharra dago klik erreakzio batzuk oso ortogonalak direla. Hau da, soilik funtzio talde batzuekin erreakzionatzeko joera dute, erreakzioa funtzio taldeerekiko oso selektiboa baita.

Irizpide hauek betetzen dituzten erreakzio ugari aurkitu arren, aipagarrienak hurrengoak dira (**1.10 irudia**) [178]:

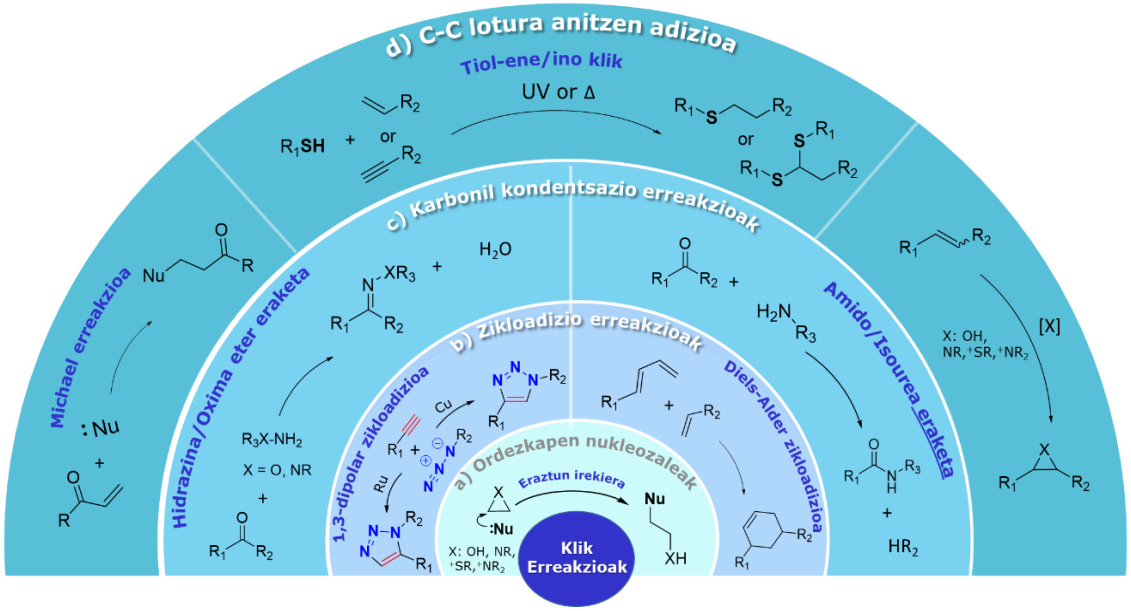

1.10 irudia. Erabilenak diren klik erreakzioen errepresentazio eskematikoa.

1. Nukleozalearen bidezko eraztunaren irekieran oinarritutako erreakzioak

Erreakzio hauetan heteroatomo tertziarioa duen funtzio taldeak aurkituko dira, hala nola, epoxi deribatua, aziridinak, sulfato ziklikoak, sulfamida ziklikoak, aziridinio-ioiak, ziklosulfonio ioiak, besteak beste. Eraztunaren barne tensioaren energia askatu egiten da, eraztuna irekitzen den heinean (**1.10 irudia**) [176].

2. Zikloadizio erreakzioak

Zikloadizio-erreakzioek klik kimikaren kontzeptua oso ondo deskribatzen dute. Izan ere, erreaktibo asegabeak konbinatuz bost eta sei atomo dituen heterozikloa lortu egiten da (**1.1. irudia**). Erreakzio honen adibiderik esanguratsuena azidaren eta alkinoaren arteko zikloadizioa da, Huisgenek 1960ko erreakzioan deskribatu baitzuen lehen aldiz [179].

3. Karbonil funtzio taldearen gaineko kondentsazio erreakzioak

Karboniloren bidezko kondentsazio erreakzioak hainbat transformazio-prozesu hartzen ditu, eta hauek aplikazio zabala aurkitu dute sintesi organikoan. Batez ere, aldehidoek eta zetonek 1,3-diolekin erreakzionatzean, sortutako 1,3-dioxolanoak; aldehidoek hidrazina edo hidroxilamina-eterrekin erreakzionatzean lortzen diren

hidrazonak edo oximak, eta α,β-karbonil aldehidoek eta zetonek esterrekin lortzen diren konposatu heterozikliKoak dira gehienbat erabiltzen diren kondentsazio erreakzioak (**1.10 irudia**). Erreakzio aldakor hauek bide eraginkorra eskaintzen dute hainbat talde funtzionalekin egokitutako konposatu kimiko baliotsu mota bat eraikitzeko, molekula konplexuen sintesian ezinbestekoak bihurtuz, produktu naturalak barne [176].

4. Karbono-karbono lotura anizkoitzen adizio erreakzioak

Tiol-eno/ino erreakzioa karbono lotura anizkoitzen adizio erreakzio ezagunena da (**1.10 irudia**), Huisgenen erreakzioaren ondoren aurkitu zena. Orokorrrean, erreakzio hau UM irradiazioaren bidez bururtzen da, non fotoiniziatzaile bat erabiltzen den- Fotoiniziatzaile honek lotura asegabearen eta tiolaren arteko klik erreakzioaren hasarazle moduan jokatzen du [180,181]. Klik erreakzio mota hau aplikazio ugari eskeintzen ditu. Klik erreakzio honek ez du katalizatzaile metalikorik behar, modu sinple batean erabili daiteke erreakzioak aurrera eramteko eta polimeroak eraldatzeko [182,183]. Gainera, alkino talde ordezkatzailea oso aporposa da klik kimika honetan, izan ere, egonkorrak dira eta hainbat egitura desberdin sor dezakete [184].

Arestian aipatutako ezaugarriek klik kimikaren erabilgarritasuna eta ospea hedatzen laguntzen dute. Egitura konplexuak lortzeko metodo eraginkor eta fidagarria eskaintzen duenez, klik kimika hori ezinbesteko estrategia bihurtu da hainbat arlotan, hala nola farmakoen diseinuan eta ikerkuntzan, materialen zientzian eta biokonjugazioan.

1.7.1. Kobrearen bidezko azida eta alkinoaren arteko zikloadizio erreakzioa (CuAAC)

Hainbat erreakzioren artean, azida eta alkinoaren arteko 1,3-zikloadizio dipolarra klik erreakzioen prototipo ezagunena da. Huisgenek azida eta alkino taldeen arteko lehenengo erreakzioa deskribatu zuen 1960an, 1,2,3-triazolak sintetizatzeko biderik eraginkorrena izanik [179]. Azida eta alkinoen arteko 1,3-zikloadizioa termodinamikoki egonkorra da, baina, normalean, tenperatura altuak eta errefluxu-baldintzak behar izaten dira, tolueno edo karbono tetrakloruro (CCl_4) bezalako disolbatzaileetan [179]. Erreakzioaren konbertsio totala lortzeko 12 eta 60 h arteko periodo luzea behar da. Baldintza termiko horietan, 1,2,3-triazol produktuaren bi erregioisomeroak (1,4 eta 1,5 erregioisomero) nahaste ia ekimolekularrean eratzen dira (**1.3 eskema**). Hala ere, erregioselektibitate-maila altuagoa lor daiteke, erreakzio-baldintzak kontu handiz kontrolatzen badira. Erreakzioaren

erregioselektibitatea erreakzioan parte hartzen duten funtzio taldeen propietate elektronikoak aldatuz hobetu daiteke. Elektroi-urriko azetileno taldeak lotura hirukoitzan dagoen karbonoaren elektroizaletasuna handitzen dute, karbono ordezkatuagoaren eraso nukleozalea erraztuz (1,4 adizio). Berriz, elektroietan aberastuak diren azetileno taldeak, eraso nukleozalea eragiten diote gutxien zailduta dagoen karbonoari (1,5 adizio). Laburbilduz, elektroi urriko azetileno taldeak 1,4-erregioisomeroa sortzen laguntzen duen bitartean, elektroietan aberatsak diren azetilenoek 1,5-isomeroaren eraketa faboratuko dute [185].

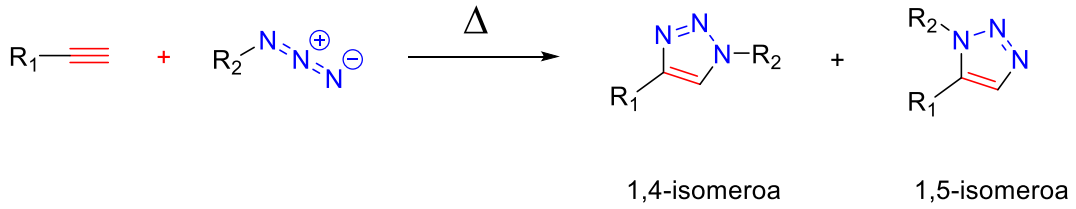

1.3 eskema. Huisgen erreakzioaren azida eta alkinoaren arteko zikloadizioa.

Bai alkino bai azida taldeek energia-eduki altuko funtzio taldeak dira. Hala ere, talde funtzional hauek konposatu organiko gutxitan aurki daitezke. Zikloadizioaren bidez eratzen den 1,2,3-triazolak egonkortasun nabarmena erakusten du. Triazolaren egonkortasun zinetikoari esker, erreakzio-baldintza ugari jasan ditzake; eta ondorioz, oso aldakorra da hainbat ingurune organiko eta biologikotan [176,177]. Talde funtzional horiek tolerantzia handia dute biomolekulekiko, oxigenoarekiko, urarekiko eta ingurune organiko eta biologikoetan aurkitutako baldintzekiko ere. Gainera, hainbat alkinoek eta azidek erakusten duten geldotsunari eskeri sistema biologikoetan aplikatzeko egokiak dira. Izan ere, biomolekulekin, hala nola proteinak edo azido nukleikoekin, batera egon daitezke interferentzia nabarmenik eta ondorio kaltegarririk sortu gabe. Bateragarritasun horrek bidea erraztu du biokonjugazio erreakzioetan eta material biobateragarrien garapenean [186,187]. Gainera, 1,2,3-triazolaren egitura propietate fisikokimiko apartak izateaz gain, propietate biologiko bikainak erakusten ditu. Izan ere, lotura peptikoaren mimetikoa da, baina abantaila honek ez du hidrolisi entzimatikorik pairatzen. 1,2,3-triazol horretan 1. eta 4. posizioetan dauden karbono atomoak 5,0 Å-eko distantzian kokatzen dira; amidaren loturak, berriz, 3,8 Å-etara kokatzen dira karbono atomoak. Gainera, 1,2,3-triazolean 2 eta 3 posiziotan dauden nitrogeno atomoek hidrogeno loturak onartzeko propietate ahulak dituzte. Amidarekiko atxikiduraren antzera, triazolak hidrogeno-loturen emaile izan daitezke, eta CH··X hidrogeno-loturak baimendu dezakete, triazol-eraztun batek berez duen momentu dipoloa dela eta (**1.11 irudia**). Gainera, beste

heterozikloekin konparatuz, heterozikloaromatiko horiek ez dira oso erreaktiboak ingurune oxidatzaile edo erreduzitzaileen [186,188].

Distantzia R_1-R_2 = 3.8 Å Distantzia R_1-R_2 = 5.0 Å

1.11 Irudia. Amida eta 1,2,3-triazolaren arteko antzekotasun elektroniko eta topologikoa.

Azida eta alkinoaren arteko erreakzioaren balio praktikoa konposatu organikoetan sartzeko erraztasunean oinarritzen den arren, erreakzio horien eragin handia ez zen behatu kobrearen bidezko katalizazioa agertu zen arte. Kobre (I) katalizatzailearen aurkikuntza, klik kimikaren eremua irauli zuen.Izan ere, zikloadizio erreakzioen erabilera nabarmen handitu zen. Kobre (I) katalizatzailaren bidezko azida eta alkinoaren arteko zikloadizio erreakzioak azkarragoak izateaz gain, erregioselektibitatea sustatzen du. Izan ere, kobrearen katalizazioaren bidez erreakzio abiadura 10^7 handiagotzen da, eta era daitezkeen bi erregioisomeroetatik, 1,4-isomeroa lortzen da esklusiboki. Meldal *et al*.-ek 2002an, kobre ioduroaren (CuI) eta *N,N*-isopropiletilaminaren erabilera proposatu zuen zenbait 1,2,3-triazol sintetizatzeko, fase solidoan immobilizatutako alkinoak erabiliz [189]. Urte berean, Sharpless eta laguntzaileek kobre sulfato pentahidratatuaren eta sodio askboratoaren erabilera uretan deskribatu zuten. Erreakzio oso exotermikoa izanik, ura bero disipatzaile moduan joatzen du [190]. Aurkitutako baldintza hauek, klik erreakzioaren potentziala hedatu zuten hainbat arlo desberdinetara.

Arestian aipatu den bezala, azida eta alkinoaren arteko zikloadizio erreakzioa kobre katalizatzailaren menpean burutzen da. Hori dela eta, erreaktibo hauen iturrien azterketa burutu da.

Alkinoen iturriari dagokionez, propargil talde funtzionalaren bidez amaierako alkinoa sar daiteke beste konposatu organikoetan. Izan ere propargilamina, propargil alkohola edo propargil halogenuroa sarritan erabili ohi dira. Esaterako, fenolaren propargilazioa Wiliamson erreakzioaren bidez lor daiteke erraz [191].

Bestalde, hiru estrategia desberdin ezagutzen dira CuAAC erreakzioan jokatzen duen Cu(I) espezia lortzeko: (1) Cu(II) gatzen *in situ* erredukzioa, CuSO4·5H2O eta sodio askorbatoa erabili ohi izan den kobinazioa da, oxigenoaren presentzian ere eraginkorra dena. (2) kobre metalikoaren oxidazioa, metodologia honetarako ezinbestekoa da Cu (II) gatzen erabilera. Izan ere, kobre metalikoa erreduzitzaile

moduan jokatzen du, Cu (II) ioia Cu (I) ioian bihurtuz. (3) Jadanik prestatutako Cu (I) gatzen adizioa, metdologiahonek Cu (I) gatzen gehipena deskribatzen du, nitrogeno baseen erabilrak, hala nola, trietilamina (Et_3N), piridina (Py), 2,2-bipiridina, 2,6-ludidina, DIPEA edo *N,N,N*-pentametiletilentetramina (PMDETA), metodo honen optimizazioan laguntzen dute [186,191–193].

Doktorego tesi honetan, lehen estrategia erabili izan da; izan ere Cu (II) gatzen *in situ* erredukzioaren produktua Cu (I) gatzak izaten dira normalean eta Cu (II) gatz komertzial gehiago ezagutzen dira. Gainera, $CuSO_4 \cdot 5H_2O$ kasuetan, sodio askorbatoa erreduzitzaile oso ona izaea erakutsi du, izan ere etekin altuko eta purutasuna altuko 1,4-triazol produktuen eraketan oso erkatalizatzaile eraginkorra izatea erakutsi du. Nahiz eta hainbat esperimentu pH neutroetan burutu, behatu egin da katalizatzaileak ondo jokatzen duela4-12 pH balio tartean. Oso katalizatzaile sendoa da eta baldinta erreakzio ugari jasan ditzake.

Azida eta alkinoen arteko zikloadizio erreakzioan kobrea katalizatzaile gisa erabiltzen denean, erreakzioan egon daitezkeen arazoak gainditzen dira; erreakzio denbora egunetatik orduetara murrizten da, eta erregioselektibitatea hobetzen da, soilik 1,4 triazolak lortuz. Bestelako katalizatzaileekin, rutenioarekin esaterako, 1,5-triazolak lor daitezke. 1,2,3-triazolaren propietate fisiko-kimiko eta biologikoei esker, lotura peptidikoaren mimetikoa edo antzekoa den heterozikloa lortzen da, baina hidrolisi entzimatikoaren aurrean ez da aktiboa. Azidak oso erreaktibo egokiak dira metodologia honetan erabiltzeko. Egia da, beste 1,3-dipolo batzuekin zikloadizioa azkarragoa eta selektiboagoa izan daitekeelako. Hala ere, azidek oso abantaila garrantzitsu bat dute: haien egonkortasuna baldintza anitzetan, hain zuzen ere [194].

Zikloadizioan ematen den ziklo katalitikoa hurrengo eskeman laburtuta dago, 5 etapetan ematen da (**1.4 eskema**) [190]. Lehenengo eta behin, kobre azetiluroaren (**I**) eraketa ematen da. Erreakzio hori amaierako alkinoetan soilik gertatzen dela behatu da, hots, barruko alkinoekin ez da baliagarria. Disolbatzaile organikoetan, hala nola azetonitriloan, beharrezkoa da konplexu horren formaziorako estekatzailearen disoziazio endotermikoa 0.6 kcal/mol). Aldiz, disoluzio urtsuetan konplexu horren formazioa exotermikoa da (11.7 kcal/mol), hots, faboratuago egonik estekatzailearen disoziazioa, erreakzioaren abiadura bizkortzen da. Horretaz gain, Density Functional Theory edota dentsitate funtzionalaren teoriaren arabera (DFT), zeina molekulen geometria eta haien loturen ezaugarriak ezagutzeko baliagarri den, behatu da alkinoaren pKa murriztu egiten dela kobrearekin koordinatzean, hau da, alkinoaren protoia azidoago bilakatzen da; ondorioz, disolbatzaile urtsuetan ez da

beharrezkoa izango base bat erabiltzea. Aldiz, bestelako disolbatzaile organikoetan, non alkinoak duen protoia ez den hain azidoa, komenigarria da base bat erabiltzea kobre eta alkinoaren arteko konplexua eratzeko. Kobre azetiluroaren formazioaren ondoren, azidan aurkitzen den estekatzaile baten desplazamendua dela eta, azida eta kobrezko azetiluro konplexua sortzen da (**II**). Behin konplexu hori eratuta, azidaren erreaktibotasuna handiagoa da, eta horren ondorioz hirugarren nitrogenoak eraso nukleozalea eragingo du azetiluroaren 3C-an, metaloziklo bat sortuz (**III**). Metaloziklo hori denborarekin eboluzionatu egiten da beste metaloziklo batera (**IV**) uzkurduraren ondorioz, eta azken hori protonolisi baten ondorioz nahi dugun produktua eta katalizatzailea askatzen dira ziklo katalitiko berri bat hasteko.

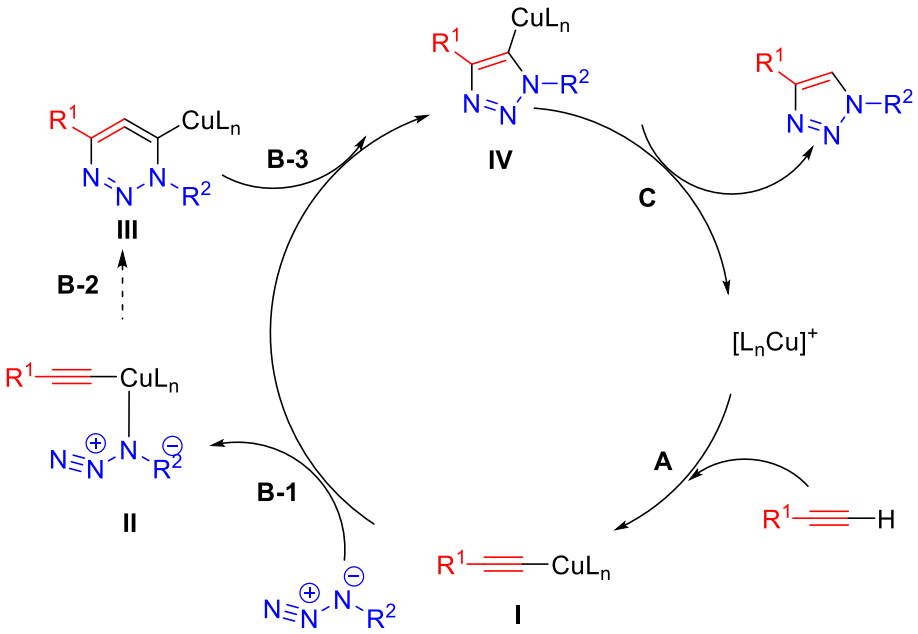

1.4 eskema. Kobre katalizaturiko azida eta alkinoaren arteko klik erreakzioaren mekanismoa.

Bestaldetik, ikerlan zinetikoek kobrez katalizaturiko erreakzioa bigarren ordenakoa dela adierazten dute. Kobrearen bigarren atomoaren jokaera oraindik ez dago guztiz frogatuta, atomo horrek azida funtzioa aktiba dezake edo beste azetiluro talde batekin konplexa daiteke, horrek ziklazioaren erreaktibitatea handituko baitu [195]. Aitzitik, kobre kontzentrazioa sobera erabiltzerakoan, erreakzioaren ordena alkinoan 1 edo 2 izan daitekeela ondorioztatu da. Alkinoaren kontzentrazio oso altuak erabiltzeak eragina du Cu (I)-ean, katalizatzailea asetuz eta zikloadizioa inhibituz. Horren ondorioz, komertzialak diren kobre azetiluro asetuek ez dute inolako aktibitate katalitikorik erakusten eta horrek frogatzen du estekatzailearen disoziazioa ziklo katalitikoan zehar oso garrantzitsua dela. Esan beharra dago ziklo katalitikoan inplikaturik dagoen I konplexuaren natura oraindik eztabaigai dela. Hala ere, horri

buruzko azken ikerkuntzek ondorioztatu dute konplexu horrek bi zentro metaliko dituela, non bi estekatzaile baino gehiago inplikaturik dauden: bi alkino eta azida talde bat.

Azken urteotan, frogatu da zikloadizioaren katalizazioa giro tenperaturan burutu daitekeela Ru, Ni, Pt, Pb eta antzeko gatz metalikoak erabiliz. Ikerkuntza horietatik nabarmendu behar da Ru-ren erabilerak 1,5-diordezkatutako triazol aduktua ematen duela erreakzioak; aldiz, Cu(I)-katalizatzailearen erabilerarekin 1,4-diordezkatua lortzen da [188].

1.7.2. Kobrerik gabeko azida eta alkinoaren arteko zikloadizio erreakzioa

1.7.2.1. Tentsio bidezko zikloadizio erreakzioak (SPAAC)

Ziklooktinoen tentsio bidezko azida zikloadizioa kobrerik gabeko aukera oso moldakorra da, sarri erabilitako CuAAC errekzioen alternatiba gisa [196]. Arrazoibide logiko baten emaitza da ziklooktinoei finkapen bat eratzea; izan ere, azida organikoen konjugazioa errazten du edozein disolbatzailetan [197]. Nabarmentzekoa da kobre bidez katalizatutako azida eta alkinoen ateko zikloadizioak (CAAC) zenbait muga dituela ingurune biologikoetan, kobre(I) espeziea toxikoa baita zelula eta organismo bizidunentzat [188].

Ziklooktinoen eta azida organikoen arteko berezko erreakzioa eraldaketa kimiko organiko oso erakargarria da, haren sinpletasunagatik. Nahasi eta astindu besterik ez da egin behar, eta katalizatzailerik edo erreakzio zehatzik behar ez duen aziden eta ziklooktinoen arteko erreakzioaren bidez azkar eta modu selektiboan sortzen da triazol produktu egonkor bat. Tentsio bidezko erreakzio hori aplikazio akademiko eta komertzial handiak dituen prozesu kimiko indartsu eta moldakor gisa ezarri da. Kimika horren gune nagusia tamaina ertaineko alkino zikliko oso tentsionatu batean oinarritzen da, bereziki ziklooktinoan. Alkino ziklikoen egonkortasuna azkar murrizten da eraztunaren tamaina handitu ahala. Ezegonkortasun hori zuzenean lotuta dago C-C lotura hirukoitzen angeluarekin, egitura ziklikoa dela eta angelu horrek ezin baitu iritsi sp hibridazioa duten karbono atomoen 180º-ko lotura angelu idealera [196,198]. Azpimarratu behar da ziklooktinoa isola daitekeen zikloalkino txikiena dela, eta azetilenoarekiko 163°-ko lotura angelua duela, hori ere linealtasunetik nabarmen desbideratuta. Azetileno linealek ez bezala, ziklooktinoen lotura hirukoitzaren deformazioak berezko erreakzioa ahalbidetzen du azida konposatuarekin, nahiz eta 1,3-dipolar hartzaile gisa jarduteko gaitasun eskasa izan.

Datu esperimentalek adierazten dute ziklooktinoek 18 kcal/mol-eko eraztun tentsioa dutela gutxi gorabehera; aldiz, ziklooktano aseek 12,1 kcal/mol-eko eraztun tentsioa dute. Horren ondorioz, tamaina ertaineko alkino ziklikoen berezko egonkortasuna eraztun tentsio adierazgarri baten presentziari egotz dakioke [198].

Arestian esan den bezala, ziklooktinoen eta aziden arteko erreakzio azkar eta espontaneo hori eraztunaren deformazioaren askapen entalpikoaren ondorioz gerta daiteke, deformazio eraztuna fusionatutako eraztun bihurtzen baita [199]. Triazolaren eraginez, bigarren eraztun horrek lotura bat du sp2 hibridazioa duten karbono atomoekin; beraz, eratutako angelua egokia da lotura mota horretarako. Hasiera batean, kimika biortogonalean aplikatzeko garatu zen erreakzio mota hori, hau da, sistema bizien barruan egin daitekeen edozein erreakzio kimikotan aplikatzeko, jatorrizko prozesu biokimikoak arriskuan jarri gabe. Nabarmendu behar da biortogonalitatearen termino hori Bertozzi *et al*.-en lanean azaldu zutela lehen aldiz. Erreakzio biortogonalen kontzeptu hori aminoazidoen (hala nola lisinaren eta zisteinaren) alboko katean dauden funtzio taldeen erreaktibotasun desberdina aprobetxatzen duten aurreko metodologietan oinarritzen da. Ikuspegi hori biokonjugazioan asko erabiltzen den arren, *in vitro* helburuetarako ezin da erabili, funtzio talde horiek ez baitira naturalki agertzen konposatuetan [200,201]. Hala ere, SPAAC erreakzioak tresna eraginkorrak dira zientziaren beste arlo batzuetan, hala nola biokonjugazio prozesuetan, polimero hibridoetan eta blokeetan, errendimendu handiko materialetan eta autokonponketan, sistema biologikoen ingeniaritza metabolikoan eta beste batzuetan [202–204]. SPAACen arrakastaren gakoetako bat da erreakzioaren osagai azidoa eskuragarria, txikia eta egonkorra dela. Hala ere, ziklooktinoen kimikak ahalmen handia erakutsi du azken urteetan, azido organikoen bidezko zikloadizioaz haratago. Lehen esperimentuak aldatu gabeko ziklooktinoekin egin ziren arren, elektroiak erakartzen dituzten funtzio taldeak erabiltzeak erreakzioa errazten du. Erabilitako lehen ziklooktinoak (OCT) (**1.12. irudia**), erreaktibo biortogonal gisa garatu zenak, bigarren ordenako abiadura konstantea zuen, $2{,}4\times10^{-3}$ $M^{-1}\cdot s^{-1}$, bentzil azidarekin erreakzionarazi zitzaionean. Gainera, abiadura hori handitu egin zen, $4{,}3\times10^{-3}$ $M^{-1}\cdot s^{-1}$-ra arte, ziklooktino monofluoratua (MOFO) erabili zenean (**1.12 irudia**), eta handitzen jarraitu zuen bi fluor atomo gehituta (ziklooktino difluoratua, DIFO) (**1.12 irudia**) propargil posizioan, eta $7{,}6\times10^{-2}$ $M^{-1}\cdot s^{-1}$ko abiadura konstantera iritsi zen, ziklooktinoa baino ordena bat bizkorrago. Azken urteetan, ziklooktino deribatuen garapena izugarri handia izan da. Azken hamarkadan, dibentzoziklooktinoak (DIBO) (**1.12 irudia**) eta haren deribatuek zikooktinoak baino abiadura konstante handiagoa erakutsi dute. Hala ere, material horiek garestiak eta sintetizatzen zailak direnez, beste estrategia batzuen diseinua oso garrantzitsua da [198,205–207].

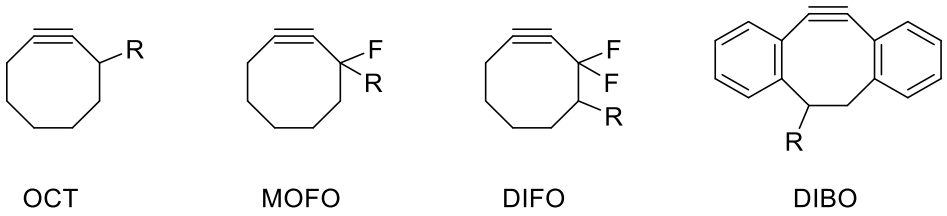

1.12 irudia. Ziklooktino deribatu erabilienak.

1.7.2.2. Azetileno aktibatuaren bidezko zikloadizio erreakzioak

Arestian aipatu den bezala, azidek gaitasun txikia dute dipolarofilo gisa jokatzeko, baina hori konpentsa liteke, ez tentsioaren bidez, Bertozzik proposatzen duen bezala, efektu elektronikoen bidez baizik. Hori dela eta, alkino taldeak eraldatzea eta erreaktiboago bihurtzea etorkizun handiko alternatiba izan daiteke.

Elektroiak erakartzen dituzten taldeak dituzten alkino deribatuak erabiltzea, hala nola azido propiolikoa eta bere deribatuak, azida eta alkinoen arteko zikloadizio erreakzioa bultzatzeko modu azkar eta eraginkorra dela frogatu da. Izan ere, erreakzioaren aktibazio energia murriztea lortzen da horrela (**1.5 eskema**). Metodologia berri hori Ju *et al*.-en lanean aztertu zuten lehen aldiz disoluzioan, aziden eta elektroi urriko alkinoen arteko lehen zikloadizio erreakzioa (1,3-dipolarra) egin baitzuten uretan [208]. Alkinoak (terminalak edo barnekoak) elektroiak erakartzen zituen funtzio talde bat, behintzat, baldin bazuen ondoko karbonoan, hala nola azido propolikoa, triazola giro tenperaturan ere era zitekeen uretan, katalizatzailerik gabe. Alkiloak SPAACaren alternatiba itxaropentsua izan arren, kobrerik gabeko erreakzio mota horien adibide gutxi batzuk baino ez dira ezagutzen. Adibidez, hidrogelen [209], aparren edo polimeroen sintesian erabili da [210,211], besteak beste. Potentzial handia izan arren, konposatuen biokonjugazioan edo immobilizazioan oraindik elektroi urriko alkinoa ez da oso ezaguna. Katalizatzailerik gabeko beste klik erreakzio batzuen antzeko estrategia izan arren (adibidez, SPAAC), eremu horietan duten aplikazioa nahiko berria da eta ikertu gabe dago. Hala ere, ikerketa gehiago egin eta metodologia optimizatu ahala, biomedikuntzarako gainazal polimerikoak aldatzeko tresna baliotsua bihur daiteke.

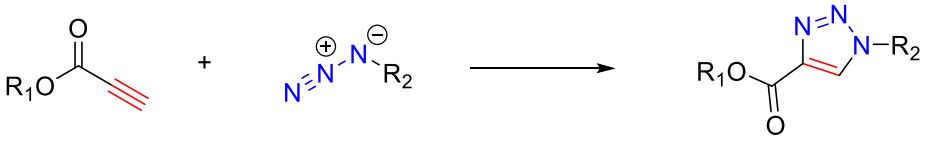

Azido propioliko deribatua

1.5 Eskema. Kobrerik gabeko azida eta alkino aktibatuaren zikloadizio erreakzioa.

1.7.3. Katalizatzaile gabeko amino-ino erreakzioa

Michael amino-ino erreakzioa tiol-ino erreakzioarekin antzekotasunak partekatzen dituen prozesu moldakorra da. Michaelen erreakzio horren bidez, amina primario edo sekundario batek elektroi gutxiko alkino taldeko β-karbonoari erasotzen dio. Kasu horretan, erreakzioak ez du katalizatzailerik behar; izan ere, espontaneoki gerta daiteke giro tenperaturan [212]. Erreaktibotasun hori aminari esker da, askotan tiol-ino erreakzioa baino eraginkorragoa izaten baita. Hori dela eta, materialen zientzietan eta biologia zientzietan erabil daitezke erreakzio horiek. Horretaz gain, esan beharra dago erreakzio horren bidez lortzen diren produktuak, Michael enaminak hain zuzen, oso erreaktiboak eta moldakorrak direla; horregatik, bitarteko baliotsua dira sintesi organikoan [213].

1899an, Ruhemann eta kolaboratzaileek lehen amino-ino erreakzioaren sintesia aurkeztu zuten [213,214]. Hain zuzen ere, dietilaminak (edo piperidinak) dietilazetileno dikarboxilatoarekin eta fenilpropiolatoarekin erreakzionatzean prozesu exotermiko bortitzak hauteman zituzten. Bitxia bazen ere, erreakzio horiek giro tenperaturan espontaneoki gertatzen ziren, katalizatzailerik behar izan gabe. Hala ere, orokorrean, erreakzio horiek baldintza sendoak eskatzen dituzte, hala nola, tenperatura altuak (> 300 ºC), presio altuak edo metal astunen erabilera.

Michaelen amino-ino erreakzioak metodo erraz eta eraginkorra dira produktu erregio- eta estereo-erregularrak lortzeko, etekin bikainekin eta katalizatzailerik erabili gabe [212]. Alkinoak eta aminak giro tenperaturan nahastuta, erreakzioa arazorik gabe garatzen da, **1.6 eskeman** deskribatzen den bezala. Gainera, erreakzio mekanismoa ondo ulertzen da, eta honela azal daiteke labur-labur: adizio nukleozalearen urratsean, aminaren elektroi pareak alkino funtzio taldearen azken karbonoari erasotzen dio. Izan ere, karbonilo taldeak elektroiak lapurtzen dizkio alkinoari, alkinoaren elektroizaletasuna faboratuz. Azken karbonoa erasotzen denez, erreakzio erregio-selektiboa da. Protoien transferentzia etapan, E isomeroak Z isomeroak baino egonkorragoak dira termodinamikoki. Izan ere, lotura bikoitzaren inguruan ematen den antolamendu geometrikoagatik egonkortu egiten da E isomeroa. Hala ere, esan

beharra dago giro tenperaturan Z isomeroak E isomero bihur daitezkeela, horiek egonkorragoak direlako. Transformazio hori "nitrogeno bidez aktibatutako lotura bikoitzeko erreakzioa" deritzon trantsizio egoera bakar baten bidez gertatzen da, eta egoera horrek estereoselektibitatea eragiten du erreakzioan [212].

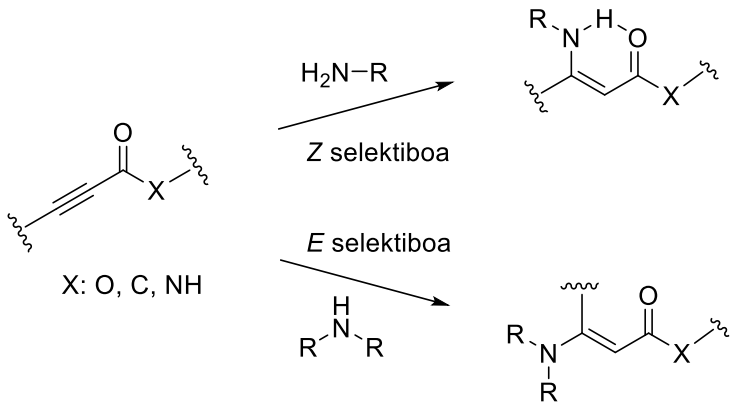

1.6 eskema. 1 eta 2 amina nukleozaleen 1,4 adizio konjokatua Michael hartzaileen gainean.

1.6.4. Katalizatzaile gabeko tiol-ino erreakzioa

2009an, Bowmanek eta laguntzaileek erradikal bidezko tiol-ino lotura eraketa azaldu zuten, elkargurutzatutako polimero sareak eraikitzeko [180]. Aintzat hartu gabeko zenbait ikerketa izan zituzten oinarri, alkinoen gainean egindako tiol erradikalen adizioari buruzkoak. Ikuspegi berritzaile horrek konbinatu egiten ditu kobre(I) bidez katalizaturiko azida eta alkinoen arteko erreakzioaren bidez eratzen diren bloke eraikuntzak eta tiol-eno erreakzioaren kimika, funtzio anitzeko materialak sortuz erreakzio baldintza sinpleetan [184].

Tiol-ino akoplamendu prozedurak zenbait abantaila ditu [215]. Lehenik eta behin, alkino funtzio talde bakarrekin akopla daitezke bi tiol, eta prozesu hori errazago egin daiteke erradikal iturri kimiko bat, UM erradiazioa edo eguzki argia erabiliz giro tenperaturan [188]. Moldakortasun horri esker eta baldintza sinpleetan lan egin daitekeenez, tiol-ino prozedura oso erakargarria da. Erreakzio horren funtsezko ezaugarrietako bat bere mekanismo erradikala da, metodoa sendoa eta moldakorra izatea ahalbidetzen du eta [180].

Tiol-ino erreakzio erradikal horien lehen urratsa tiol-eno erreakzioen antzekoa da (**1.7 eskema**). Alkino bati tiol bat gehituta (adizioa) hasten da prozesua, β-tioeter funtzioa duen erradikal binilikoa eratuz. Ondoren, azken erradikal horrek tiol molekula baten hidrogeno atomo bat harrapatzen du, tiil erradikala (RS·) sortuz.

Erradikal berri hori binil tioeterrari gehitzen zaio, eta karbonozko bigarren erradikal bat eratzen da. Horrek, aldi berean, beste tiol molekula baten hidrogeno atomo bat harrapatzen du, 1,2-ditioeterra sortuz. Erreakzioan eratutako tiil erradikalak katean jarraituko du prozesu, zikloa osatuz. Klik erreakzio erradikal horretan, alkinoari tiola gehitzea (adizioa) abiadura mugatzen duen pausoa da. Hala ere, tarteko tiol-alkenoari bigarren tiola gehitzeko urratsa azkarragoa da, gutxi gorabehera hasierako adizioa baino hiru aldiz azkarragoa [180,188].

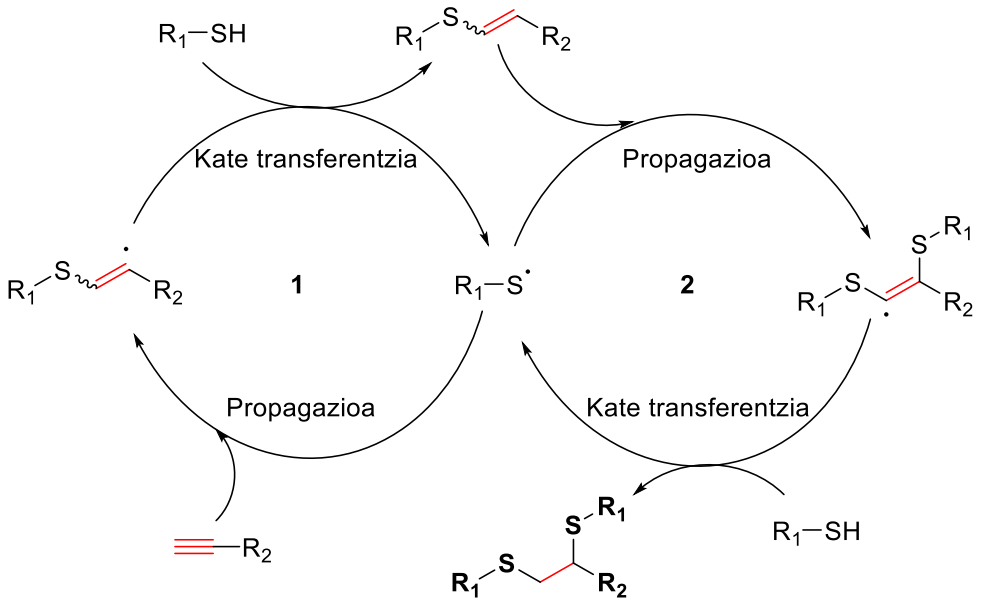

1.7 eskema. Tiol-ino adizio erreakzioaren mekanismoa.

Laburbilduz, tiol-ino klik erreakzioetan birritan eransten zaizkio tiolak alkino funtzio taldeari, 1,2-ditioeterra eratuz. Erreakzio hori asko erabiltzen da funtzio anitzeko polimero egiturak sortzeko [181,182]. Izan ere, tiol-ino erreakzioak behin eta berriz erabiliz gero, funtzio anitzeko molekulak sortzen dira, ondoren dendrimeroak edo polimero hiperadarkatuak sortzeko erabil daitezkeenak. Erreakzio horrek aukera interesgarriak eskaintzen ditu funtzionalitate pertsonalizatuak dituzten egitura polimerikoak diseinatu eta sintetizatzeko [213][216]. Horrez gain, erreakzio erradikal horrek funtzio talde ugari onartzen dituenez, zenbait funtzio talde kimiko sar daitezke polimeroen sareetan. Hala ere, erreakzio horretan ezin da oxigenorik erabili, erreakzio erradikala delako [217].

1.8. Helburu orokorrak eta antolatutako lana

Doktorego tesi honen helburua propietate bioaktiboak dituzten gainazalak eta materialak garatzea da, bakterioen aurkako funtzioak, hanturaren aurkako propietateak eta ezaugarri antikoagulatzaileak barne. Gainazalk eta materialak askotarikoak izango dira, eta hainbat estrategia erabiliko dira propietate bioaktibo horiek lortzeko. Hala ere, ikerketetan zehar, oso ohikoa da farmakoen edo biomolekula aktiboen biokonjugaziorako klik errekazioak erabiltzea. Klik Kimikaren bidez, nahi diren konposatu bioaktiboak polimeroekin (PLLA eta PET) eta metal-aleazioekin (Ti6Al4V) modu zehatz eta eraginkorrean lotzea erraztu nahi da, materialaren jarduera terapeutikoa hobetuz. Ikuspegi horrek aldakortasuna eta kontrola eskaintzen ditu, eta funtzionalitate bioaktibo egokituak dituzten biomaterial berriak garatzeko aukera ematen du. Ikerketa saiatzen da aplikazio biomedikoetan Aurrera egitea, soluzio berritzaileak ematen baititu zenbat materialen biobateragarritasuna eta eraginkorasun terapeutikoa hobetzek, eta gailu horien erabilerak izan ohi dituzten eragozpenak gutxitzen ditu.

Dokumentu honen egiturak garatu nahi diren materialak eta farmakoak immobilizatzeko erabili diren estrategiak banatzen ditu. *1. Kapituluak* gaur egungo egoeren ikuspegi orokorra ematen du, biomaterial motak eta haien erronka nagusiak, hala nola, biobateragarritasuna, hemobateragarritasuna eta bakterioen infekzioa, biltzen dituena. Arreta berezia jarri da bakterio atxikidurari eta biofilmaren eraketari aurre egiteko estrategietan, baita ostalariaren ehunaren kontrako erantzunak arintzeo biobatergarritasunean egindako aurrerapenetan ere. Kapituluak ere deskribatzen ditu klik erreakzioen moldakortasuna, batez ere kobrearen bidezko azida eta alkinoaren arteko zikloadizio erreakzioari arreta handia jarri zitzaion. Laburbilduz, sekuentzia horri jarraituz, lanak narrazio koherente eta informatiboa aurkeztu nahi du, gainazal bioaktiboak garatzeko materialak eta estrategiak erakutsiz, aplikazio biomediko hobetuak erabiliz.

2. Kapituluan PLLAren gainerako zenbait agenteen, besteak beste, indometazinaren eta amoxizilinaren biokonjugazioan sakontzen da klik erreakzioak erabiliz. Horretako, kapitulu honetan, hautatutako farmakoen eraginkortasuna eta material bioaktiboen testuinguruan izan dezakeen garrantzia ikasiko da. Erabbilitako farmakoen funtsezko ezaugarri farmakologikoetan sakonduz eta haien egitura eta jardueraren arteko erlazioa aztertuz. Izan ere, kapitulu hori 5 ataletan banatuko da, erabilitako klik erreakzioaren arabera. Kapitulu honetan, kobraren bidezko azida eta alkinoaren arteko zikloadizio erreakzioa deskribatzen da, zenbait konposatu immobilizatzeko eta funtzionalizazio sekuentzial bikoitza ahalbidetzeko gaitasuna erakutsiz. Gainera,

acetileno aktibatuan oinarritutako estrategia berritzaileak eztabaidatzen dira. Egokia den alkino aktibatua erabili izan da kobre gabeko zenbait klik erreakzio pairatzeko, besteak beste, azido-ino, amino-ino eta tiol-ino erreakzioak.

3.Kapituluak PETaren erabilera eta haren gainazaleko jarduera biologikoa hobetzeko estrategiak aztertzen ditu. Estrategia honen muina gainazalaren funtzionalizazioan oinarritzen da, zeina hidrolisi erreakzioaren ondoren multiaktiboa den kurkumina deribatua immobilizatzen da, kobrearen bidezko azida eta alkinoaren arteko klik erreakzioa erabiliz. Metodo horiek zehaztean, PET gainazalaren bioaktibitatearen hazkundea deskribatzen da, bereziki hanturaren kontrako ezaugarriak, antikoagulatzailea eta bakterioen aurkako propietateak, gainazal horiek aplikazio biomedikoetarako egokiagoak izan daitezen. Funtzionalizazio prozesuak funtseko zeregina du gainazal propietateetan eta kurkumina deribatua arrakastaz immobilizatzeko plataforma bat sortzeko. Kapituluak urratsez urrats erabiltzen diren prozedurei buruzko ezagutza baliotsuak ematen ditu, eta PETan oinarritutko gainazal bioaktiboak, besteak beste, gainestaldurak, zuntzak edo inplante medikoak, garatzen laguntzen du.

4 Kapituluan Ti6Al4V gainazal gisa erabiltzen da. Kasu honetan, oso nabargarriak diren bi estrategia desberdintzen dira: silanoetan oinarritutako eta fosfonatoetan oinarritutako SAMak. Bi kasuetarako, Ti aleazioa zehazki prestatu egin da aurretik. Gainera, kapitulu honek CuAAC erreakzio konbentzionala aztertzen du, azido salizilikoaren deribatuaren immobilizazioa burutuz. Berriro ere, ikuspegi horiekin, kapituluak klik erreakzioen modalkortasuna areagotzeaz gain, substratuaren propietate anti-inflamatorioak eta antikoagulanteak sustatu nahi ditu.

Tesi honen azken kapitulua, 5. Kapitulua, egindako ikerketaren ondorio orokorrak deskribatzen ditu. Kapitulu honek lan honen bidez lortutako aurkikuntzak eta ezagutza nagusien laburpen zehatza eskaintzen du. Horretaz gain, materialak hobetzeko eta eraldatzeko iradokizun baliotsuak eskaintzen ditu, etorkizuneko lanak sustatuz.

1.9. Bibliography

1. Williams, D.F. On the nature of biomaterials. *Biomaterials* **2009**, *30*, 5897–5909, doi:10.1016/j.biomaterials.2009.07.027.

2. Festas, A.J.; Ramos, A.; Davim, J.P. Medical devices biomaterials – A review. *Proc. Inst. Mech. Eng. Part L J. Mater. Des. Appl.* **2020**, *234*, 218–228, doi:10.1177/1464420719882458.

3. Crawford, L.; Wyatt, M.; Bryers, J.; Ratner, B. Biocompatibility Evolves: Phenomenology to Toxicology to Regeneration. *Adv. Healthc. Mater.* **2021**, *10*, 1–21, doi:10.1002/adhm.202002153.

4. Black, J. *Biological Performance of Materials: Fundamentals of Biocompatibility, Fourth Edition*; 2005; ISBN 9781420057843.

5. Ludovica Parisi; Carlo Galli; Alberto Neri; Andrea Toffoli; Elena Calciolari; Edoardo Manfredi; Simone Lumetti; Guido M Macaluso; Federico Rivara; Claudio Macaluso Aptamers improve the bioactivity of biomaterials. *Aptamers* **2017**, *1*, 3–12.

6. Williams, D.F. On the mechanisms of biocompatibility. *Biomaterials* **2008**, *29*, 2941–2953, doi:10.1016/j.biomaterials.2008.04.023.

7. Chen, Q.; Thouas, G.A. Metallic implant biomaterials. *Mater. Sci. Eng. R Reports* **2015**, *87*, 1–57, doi:10.1016/j.mser.2014.10.001.

8. Cber, C. FDA Guidance Document, 2023, Use of the International Standard ISO 10993-1, dated September 8, 2023 (Docket No. FDA-2013-D-0350) 2023, 1–66.

9. Ghasemi-Mobarakeh, L.; Kolahreez, D.; Ramakrishna, S.; Williams, D. Key terminology in biomaterials and biocompatibility. *Curr. Opin. Biomed. Eng.* **2019**, *10*, 45–50, doi:10.1016/j.cobme.2019.02.004.

10. Reinwald, Y.; Shakesheff, K.; Howdle, S. *Biomedical Devices*; 2011; ISBN 9780470390849.

11. Velnar, T.; Bunc, G.; Klobucar, R.; Gradisnik, L. Biomaterials and host versus graft response: A short review. *Bosn. J. Basic Med. Sci.* **2016**, *16*, 82–90, doi:10.17305/bjbms.2016.525.

12. BaoLin, GUO; MA, P.X. Synthetic biodegradable functional polymers for tissue engineering: a brief review. *Sci. China Chem.* **2014**, *57*, 490–500, doi:10.1007/s11426-014-5086-y.

13. Dang, T.T.; Nikkhah, M.; Memic, A.; Khademhosseini, A. *Polymeric Biomaterials for Implantable Prostheses*; Elsevier Inc., 2014; ISBN 9780123969835.

14. Wendels, S.; Avérous, L. Biobased polyurethanes for biomedical applications. *Bioact. Mater.* **2021**, *6*, 1083–1106, doi:10.1016/j.bioactmat.2020.10.002.

15. Guo, J.; Chai, R.; Li, H.; Sun, S. *Hearing Loss: Mechanisms, Prevention and Cure*; 2019; Vol. 1130; ISBN 978-981-13-6122-7.

16. Sánchez-Bodón, J.; Andrade-Del Olmo, J.; Alonso, J.M.; Moreno-Benítez, I.; Vilas-Vilela, J.L.; Pérez-Alvarez, L. Bioactive Coatings on Titanium: A Review on Hydroxylation, Self-Assembled Monolayers (SAMs) and Surface Modification Strategies. *Polymers (Basel).* **2022**, *14*, 165, doi:10.3390/polym14010165.

17. Sáenz, A.; Rivera-muñoz, E.; Brostow, W.; Castaño, V.M. Ceramic Biomaterials : an Introductory Overview. *J. Mater. Educ.* **1999**, *21*, 297–306.

18. Sidambe, A.T. Biocompatibility of advanced manufactured titanium implants-A review. *Materials (Basel).* **2014**, *7*, 8168–8188, doi:10.3390/ma7128168.

19. Özcan, M.; Hämmerle, C. Titanium as a reconstruction and implant material in dentistry: Advantages and pitfalls. *Materials (Basel).* **2012**, *5*, 1528–1545, doi:10.3390/ma5091528.

20. Liu, Y.; Rath, B.; Tingart, M.; Eschweiler, J. Role of implants surface modification in osseointegration: A systematic review. *J. Biomed. Mater. Res. - Part A* **2020**, *108*, 470–484, doi:10.1002/jbm.a.36829.

21. W. Nicholson, J. Titanium Alloys for Dental Implants: A Review. *Prosthesis* **2020**, *2*, 100–116, doi:10.3390/prosthesis2020011.

22. Sarraf, M.; Rezvani Ghomi, E.; Alipour, S.; Ramakrishna, S.; Liana Sukiman, N. A state-of-the-art review of the fabrication and characteristics of titanium and its alloys for biomedical applications. *Bio-Design Manuf.* **2022**, *5*, 371–395, doi:10.1007/s42242-021-00170-3.

23. Shen, X.; Shukla, P. A Review of Titanium Based Orthopaedic Implants (Part-

I): Physical Characteristics , Problems and the need for Surface Modification. *Int. J. Peen. Sci. Technol.* **2020**, *1*, 301–332.

24. Chopplet, M.; Theirry, J.P. *Biomedical materials*; 1990; Vol. 5; ISBN 9783030492052.

25. Eliaz, N. Corrosion of metallic biomaterials: A review. *Materials (Basel).* **2019**, *12*, doi:10.3390/ma12030407.

26. Wang, G.; Wan, Y.; Wang, T.; Liu, Z. Corrosion Behavior of Titanium Implant with different Surface Morphologies. *Procedia Manuf.* **2017**, *10*, 363–370, doi:10.1016/j.promfg.2017.07.006.

27. Karpagavalli, R.; Zhou, A.; Chellamuthu, P.; Nguyen, K. Corrosion behavior and biocompatibility of nanostructured TiO 2 film on Ti6Al4V. *J. Biomed. Mater. Res. Part A* **2007**, *83A*, 1087–1095, doi:10.1002/jbm.a.31447.

28. He, W.; Benson, R. *Polymeric Biomaterials*; Elsevier Inc., 2014; ISBN 9780323221696.

29. Teo, A.J.T.; Mishra, A.; Park, I.; Kim, Y.J.; Park, W.T.; Yoon, Y.J. Polymeric Biomaterials for Medical Implants and Devices. *ACS Biomater. Sci. Eng.* **2016**, *2*, 454–472, doi:10.1021/acsbiomaterials.5b00429.

30. Narayanan, G.; Vernekar, V.N.; Kuyinu, E.L.; Laurencin, C.T. Poly (Lactic Acid)-Based Biomaterials for Orthopaedic Regenerative Engineering. **2017**, 247–276, doi:10.1016/j.addr.2016.04.015.Poly.

31. Taib, N.A.A.B.; Rahman, M.R.; Huda, D.; Kuok, K.K.; Hamdan, S.; Bakri, M.K. Bin; Julaihi, M.R.M. Bin; Khan, A. *A review on poly lactic acid (PLA) as a biodegradable polymer*; Springer Berlin Heidelberg, 2022; ISBN 0123456789.

32. Gilding, D.K.; Reed, A.M. Biodegradable polymers for use in surgery-polyglycolic/poly(actic acid) homo- and copolymers: 1. *Polymer (Guildf).* **1979**, *20*, 1459–1464, doi:10.1016/0032-3861(79)90009-0.

33. Li, J.; Liu, F.; Qin, Y.; He, J.; Xiong, Z.; Deng, G.; Li, Q. crossmark. *J. Memb. Sci.* **2017**, *523*, 505–514, doi:10.1016/j.memsci.2016.10.027.

34. Garlotta, D. A Literature Review of Poly (Lactic Acid). *J. Polym. Environ.* **2019**, *9*, 63–84.

35. Mehta, R.; Kumar, V.; Bhunia, H.; Upadhyay, S.N. Synthesis of poly(lactic acid): A review. *J. Macromol. Sci. - Polym. Rev.* **2005**, *45*, 325–349, doi:10.1080/15321790500304148.

36. Lorenzo, M.L. Di; Androsch, R. *Industrial Applications of Poly(lactic acid)*; 2018; ISBN 9783319754581.

37. da Silva, D.; Kaduri, M.; Poley, M.; Adir, O.; Krinsky, N.; Shainsky-Roitman, J.; Schroeder, A. Biocompatibility, biodegradation and excretion of polylactic acid (PLA) in medical implants and theranostic systems. *Chem. Eng. J.* **2018**, *340*, 9–14, doi:10.1016/j.cej.2018.01.010.

38. Bone, P.-L.P. Long-term in vivo Degradation of Poly-. *21*, 395–411, doi:10.1177/0885328206065125.

39. Bhouri, N.; Debbabi, F.; Merghni, A.; Rohleder, E.; Mahltig, B.; Ben Abdessalem, S. New manufacturing process to develop antibacterial dyed polyethylene terephthalate sutures using plasma functionalization and chitosan immobilization. *J. Ind. Text.* **2021**, *0*, 1–24, doi:10.1177/15280837211050525.

40. Swar, S.; Zajícová, V.; Rysová, M.; Lovětinská-Šlamborová, I.; Voleský, L.; Stibor, I. Biocompatible surface modification of poly(ethylene terephthalate) focused on pathogenic bacteria: Promising prospects in biomedical applications. *J. Appl. Polym. Sci.* **2017**, *134*, 1–11, doi:10.1002/app.44990.

41. Çaykara, T.; Sande, M.G.; Azoia, N.; Rodrigues, L.R.; Silva, C.J. Exploring the potential of polyethylene terephthalate in the design of antibacterial surfaces. *Med. Microbiol. Immunol.* **2020**, *209*, 363–372, doi:10.1007/s00430-020-00660-8.

42. Nisticò, R. Polyethylene terephthalate (PET) in the packaging industry. *Polym. Test.* **2020**, *90*, 106707, doi:10.1016/j.polymertesting.2020.106707.

43. Lasoski, W. Kinetics of hydrolysis of polyethylese terephthalate filris. *J. Phys. Chem* **1960**, *64*, 895–898.

44. Subramaniam, A.; Sethuraman, S. *Biomedical Applications of Nondegradable Polymers*; Elsevier Inc., 2014; ISBN 9780123969835.

45. Agrawal, R.; Kumar, A.; Mohammed, M.K.A.; Singh, S. Biomaterial types, properties, medical applications, and other factors: a recent review. *J. Zhejiang*

Univ. Sci. A **2023**, doi:10.1631/jzus.A2200403.

46. Schierholz, J.M.; Beuth, J. Implant infections : a haven for opportunistic bacteria. **2001**, 87–93, doi:10.1053/jhin.2001.1052.

47. Arciola, C.R.; Campoccia, D. Implant infections: adhesion, biofilm formation and immune evasion. *Nat. Rev. Microbiol.* **2018**, *16*, doi:10.1038/s41579-018-0019-y.

48. Campoccia, D.; Montanaro, L.; Renata, C. The significance of infection related to orthopedic devices and issues of antibiotic resistance. *Biomaterials* **2006**, *27*, 2331–2339, doi:10.1016/j.biomaterials.2005.11.044.

49. Chandorkar, Y.; Ravikumar, K.; Basu, B. The Foreign Body Response Demystified. *ACS Biomater. Sci. Eng.* **2019**, *5*, 19–44, doi:10.1021/acsbiomaterials.8b00252.

50. Sheikh, Z.; Brooks, P.J.; Barzilay, O.; Fine, N.; Glogauer, M. Macrophages, foreign body giant cells and their response to implantable biomaterials. *Materials (Basel).* **2015**, *8*, 5671–5701, doi:10.3390/ma8095269.

51. Zhou, G.; Groth, T. Host Responses to Biomaterials and Anti-Inflammatory Design—a Brief Review. *Macromol. Biosci.* **2018**, *18*, 1–15, doi:10.1002/mabi.201800112.

52. Franz, S.; Rammelt, S.; Scharnweber, D.; Simon, J.C. Immune responses to implants - A review of the implications for the design of immunomodulatory biomaterials. *Biomaterials* **2011**, *32*, 6692–6709, doi:10.1016/j.biomaterials.2011.05.078.

53. Subbiahdoss, G.; Kuijer, R.; Grijpma, D.W.; van der Mei, H.C.; Busscher, H.J. Microbial biofilm growth vs. tissue integration: "The race for the surface" experimentally studied. *Acta Biomater.* **2009**, *5*, 1399–1404, doi:10.1016/j.actbio.2008.12.011.

54. López-Valverde, A.; López-Valverde, N.; Flores-Fraile, J. The unknown process osseointegration. *Biology (Basel).* **2020**, *9*, 1–3, doi:10.3390/biology9070168.

55. Stones, D.H.; Krachler, A.M. Against the tide: The role of bacterial Adhesion in host colonization. *Biochem. Soc. Trans.* **2016**, *44*, 1571–1580, doi:10.1042/BST20160186.

56. Benčina, M.; Mavrič, T.; Junkar, I.; Bajt, A.; Krajnović, A.; Lakota, K.; Žigon, P.; Sodin-Šemrl, S.; Kralj-Iglič, V.; Iglič, A. The Importance of Antibacterial Surfaces in Biomedical Applications. *Adv. Biomembr. Lipid Self-Assembly* **2018**, *28*, 115–165, doi:10.1016/bs.abl.2018.05.001.

57. Olmo, J.A. Del; Ruiz-Rubio, L.; Pérez-Alvarez, L.; Sáez-Martínez, V.; Vilas-Vilela, J.L. Antibacterial coatings for improving the performance of biomaterials. *Coatings* **2020**, *10*, doi:10.3390/coatings10020139.

58. Chouirfa, H.; Bouloussa, H.; Migonney, V.; Falentin-Daudré, C. Review of titanium surface modification techniques and coatings for antibacterial applications. *Acta Biomater.* **2019**, *83*, 37–54, doi:10.1016/j.actbio.2018.10.036.

59. Wu, S.; Zhang, B.; Liu, Y.; Suo, X.; Li, H. Influence of surface topography on bacterial adhesion: A review (Review). *Biointerphases* **2018**, *13*, 1–11, doi:10.1116/1.5054057.

60. Yang, K.; Shi, J.; Wang, L.; Chen, Y.; Liang, C.; Yang, L.; Wang, L.N. Bacterial anti-adhesion surface design: Surface patterning, roughness and wettability: A review. *J. Mater. Sci. Technol.* **2022**, *99*, 82–100, doi:10.1016/j.jmst.2021.05.028.

61. Francone, A.; Merino, S.; Retolaza, A.; Ramiro, J.; Alves, S.A.; de Castro, J.V.; Neves, N.M.; Arana, A.; Marimon, J.M.; Torres, C.M.S.; et al. Impact of surface topography on the bacterial attachment to micro- and nano-patterned polymer films. *Surfaces and Interfaces* **2021**, *27*, 101494, doi:10.1016/j.surfin.2021.101494.

62. Luong-Van, E.; Rodriguez, I.; Low, H.Y.; Elmouelhi, N.; Lowenhaupt, B.; Natarajan, S.; Lim, C.T.; Prajapati, R.; Vyakarnam, M.; Cooper, K. Review: Micro-and nanostructured surface engineering for biomedical applications. *J. Mater. Res.* **2013**, *28*, 165–174, doi:10.1557/jmr.2012.398.

63. Hernandez, J.L.; Park, J.; Yao, S.; Blakney, A.K.; Nguyen, H. V; Katz, B.H.; Jensen, J.T.; Woodrow, K.A. Effect of tissue microenvironment on fibrous capsule formation to biomaterial-coated implants. *Biomaterials* **2021**, *273*, 120806, doi:10.1016/j.biomaterials.2021.120806.

64. Crawford, R.J.; Webb, H.K.; Truong, V.K.; Hasan, J.; Ivanova, E.P. Surface topographical factors influencing bacterial attachment. *Adv. Colloid Interface*

Sci. **2012**, *179–182*, 142–149, doi:10.1016/j.cis.2012.06.015.

65. Mu, M.; Liu, S.; DeFlorio, W.; Hao, L.; Wang, X.; Salazar, K.S.; Taylor, M.; Castillo, A.; Cisneros-Zevallos, L.; Oh, J.K.; et al. Influence of Surface Roughness, Nanostructure, and Wetting on Bacterial Adhesion. *Langmuir* **2023**, *39*, 5426–5439, doi:10.1021/acs.langmuir.3c00091.

66. Ubuo, E.E.; Udoetok, I.A.; Tyowua, A.T.; Ekwere, I.O.; Al-Shehri, H.S. The direct cause of amplified wettability: Roughness or surface chemistry? *J. Compos. Sci.* **2021**, *5*, 1–9, doi:10.3390/jcs5080213.

67. Ellinas, K.; Kefallinou, D.; Stamatakis, K.; Gogolides, E.; Tserepi, A. Is There a Threshold in the Antibacterial Action of Superhydrophobic Surfaces? *ACS Appl. Mater. Interfaces* **2017**, *8*, 39781–39789, doi:10.1021/acsami.7b11402.

68. Zhang, X.; Wang, L.; Levänen, E. Superhydrophobic surfaces for the reduction of bacterial adhesion. *RSC Adv.* **2013**, *3*, 12003–12020, doi:10.1039/c3ra40497h.

69. Mariani, E.; Lisignoli, G.; Maria, R.; Pulsatelli, L. Biomaterials : Foreign Bodies or Tuners for the Immune Response? *Int. J. Mol* **2019**, *20*, 636–678, doi:10.3390/ijms20030636.

70. Anderson, J.M. Exploiting the inflammatory response on biomaterials research and development. *J. Mater. Sci. Mater. Med.* **2015**, *26*, 1–2, doi:10.1007/s10856-015-5423-5.

71. Hotchkiss, K.M.; Reddy, G.B.; Hyzy, S.L.; Schwartz, Z.; Boyan, B.D.; Olivares-Navarrete, R. Titanium surface characteristics, including topography and wettability, alter macrophage activation. *Acta Biomater.* **2016**, *31*, 425–434, doi:10.1016/j.actbio.2015.12.003.

72. Bhagwat, G.; O'Connor, W.; Grainge, I.; Palanisami, T. Understanding the Fundamental Basis for Biofilm Formation on Plastic Surfaces: Role of Conditioning Films. *Front. Microbiol.* **2021**, *12*, 1–10, doi:10.3389/fmicb.2021.687118.

73. Nathanael, A.J.; Oh, T.H. Biopolymer coatings for biomedical applications. *Polymers (Basel).* **2020**, *12*, 1–26, doi:10.3390/polym12123061.

74. Song, J.; Winkeljann, B.; Lieleg, O. Biopolymer-Based Coatings : Promising Strategies to Improve the Biocompatibility and Functionality of Materials Used

in Biomedical Engineering. **2020**, *2000850*, doi:10.1002/admi.202000850.

75. Mcwhorter, F.Y.; Davis, C.T.; Liu, W.F. Physical and mechanical regulation of macrophage phenotype and function. *Cell. Mol. Life Sci.* **2015**, *72*, 1303–1316, doi:10.1007/s00018-014-1796-8.Physical.

76. McNamara, L.E.; Burchmore, R.; Riehle, M.O.; Herzyk, P.; Biggs, M.J.P.; Wilkinson, C.D.W.; Curtis, A.S.G.; Dalby, M.J. The role of microtopography in cellular mechanotransduction. *Biomaterials* **2012**, *33*, 2835–2847, doi:10.1016/j.biomaterials.2011.11.047.

77. Rich, A.; Harris, A.K. Anomalous preferences of cultured macrophages for hydrophobic and roughened substrata. *J. Cell Sci.* **1981**, *50*, 1–7, doi:10.1242/jcs.50.1.1.

78. Refai, A.K.; Textor, M.; Brunette, D.M.; Waterfield, J.D. Effect of titanium surface topography on macrophage activation and secretion of proinflammatory cytokines and chemokines. *J. Biomed. Mater. Res. - Part A* **2004**, *70*, 194–205, doi:10.1002/jbm.a.30075.

79. Chen, S.; Jones, J.A.; Xu, Y.; Low, H.Y.; Anderson, J.M.; Leong, K.W. Characterization of topographical effects on macrophage behavior in a foreign body response model. *Biomaterials* **2010**, *31*, 3479–3491, doi:10.1016/j.biomaterials.2010.01.074.

80. Wang, L.; Chen, W.; Terentjev, E. Effect of micro-patterning on bacterial adhesion on polyethylene terephthalate surface. *J. Biomater. Appl.* **2015**, *29*, 1351–1362, doi:10.1177/0885328214563998.

81. Zhu, Y.; Mao, Z.; Gao, C. Aminolysis-based surface modification of polyesters for biomedical applications. *RSC Adv.* **2013**, *3*, 2509–2519, doi:10.1039/c2ra22358a.

82. Stewart, C.; Akhavan, B.; Wise, S.G.; Bilek, M.M.M. Progress in Materials Science A review of biomimetic surface functionalization for bone- integrating orthopedic implants : Mechanisms , current approaches , and future directions. *Prog. Mater. Sci.* **2019**, *106*, 100588, doi:10.1016/j.pmatsci.2019.100588.

83. Yaseri, R.; Fadaie, M.; Mirzaei, E.; Samadian, H.; Ebrahiminezhad, A. Surface modification of polycaprolactone nanofibers through hydrolysis and aminolysis: a comparative study on structural characteristics, mechanical properties, and

cellular performance. *Sci. Rep.* **2023**, *13*, 1–17, doi:10.1038/s41598-023-36563-w.

84. Andrade del Olmo, J.; Alonso, J.M.; Ronco-Campaña, A.; Sáez-Martínez, V.; Pérez-González, R.; Rothnie, A.J.; Tighe, B.J.; Vilas-Vilela, J.L.; Pérez-Álvarez, L. Effectiveness of physicochemical techniques on the activation of Ti6Al4V surface with improved biocompatibility and antibacterial properties. *Surf. Coatings Technol.* **2022**, *447*, doi:10.1016/j.surfcoat.2022.128821.

85. Yang, Y.; Zhang, H.; Komasa, S.; Morimoto, Y.; Sekino, T.; Kawazoe, T.; Okazaki, J. UV/ozone irradiation manipulates immune response for antibacterial activity and bone regeneration on titanium. *Mater. Sci. Eng. C* **2021**, *129*, 112377, doi:10.1016/j.msec.2021.112377.

86. Huang, H.H.; Wu, C.P.; Sun, Y.S.; Lee, T.H. Improvements in the corrosion resistance and biocompatibility of biomedical Ti-6Al-7Nb alloy using an electrochemical anodization treatment. *Thin Solid Films* **2013**, *528*, 157–162, doi:10.1016/j.tsf.2012.08.063.

87. Huang, M.S.; Wu, C.Y.; Ou, K.L.; Huang, B.H.; Chang, T.H.; Endo, K.; Cho, Y.C.; Lin, H.Y.; Liu, C.M. Preparation of a biofunctionalized surface on titanium for biomedical applications: Surface properties, wettability variations, and biocompatibility characteristics. *Appl. Sci.* **2020**, *10*, 1438–1449, doi:10.3390/app10041438.

88. Shiau, D.K.; Yang, C.H.; Sun, Y.S.; Wu, M.F.; Pan, H.; Huang, H.H. Enhancing the blood response and antibacterial adhesion of titanium surface through oxygen plasma immersion ion implantation treatment. *Surf. Coatings Technol.* **2019**, *365*, 173–178, doi:10.1016/j.surfcoat.2018.05.029.

89. Morozov, I.A.; Kamenetskikh, A.S.; Beliaev, A.Y.; Scherban, M.G.; Lemkina, L.M.; Eroshenko, D. V.; Korobov, V.P. The Effect of Damage of a Plasma-Treated Polyurethane Surface on Bacterial Adhesion. *Biophys. (Russian Fed.* **2019**, *64*, 410–415, doi:10.1134/S000635091903014X.

90. Ujino, D.; Nishizaki, H.; Higuchi, S.; Komasa, S.; Okazaki, J. Effect of plasma treatment of titanium surface on biocompatibility. *Appl. Sci.* **2019**, *9*, doi:10.3390/app9112257.

91. Chen, M.; Wang, X.Q.; Zhang, E.L.; Wan, Y.Z.; Hu, J. Antibacterial ability and biocompatibility of fluorinated titanium by plasma-based surface modification.

Rare Met. **2022**, *41*, 689–699, doi:10.1007/s12598-021-01808-y.

92. Diamanti, M.V.; del Curto, B.; Pedeferri, M. Anodic oxidation of titanium: From technical aspects to biomedical applications. *J. Appl. Biomater. Biomech.* **2011**, *9*, 55–69, doi:10.5301/JABB.2011.7429.

93. Celina, M.C. Review of polymer oxidation and its relationship with materials performance and lifetime prediction. *Polym. Degrad. Stab.* **2013**, *98*, 2419–2429, doi:10.1016/j.polymdegradstab.2013.06.024.

94. Huynh, V.; Ngo, N.K.; Golden, T.D. Surface Activation and Pretreatments for Biocompatible Metals and Alloys Used in Biomedical Applications. *Int. J. Biomater.* **2019**, *2019*, doi:10.1155/2019/3806504.

95. Minagar, S.; Berndt, C.C.; Wang, J.; Ivanova, E.; Wen, C. A review of the application of anodization for the fabrication of nanotubes on metal implant surfaces. *Acta Biomater.* **2012**, *8*, 2875–2888, doi:10.1016/j.actbio.2012.04.005.

96. Carmagnola, I.; Chiono, V.; Abrigo, M.; Ranzato, E.; Martinotti, S.; Ciardelli, G. Tailored functionalization of poly(L-lactic acid) substrates at the nanoscale to enhance cell response. *J. Biomater. Sci. Polym. Ed.* **2019**, *30*, 526–546, doi:10.1080/09205063.2019.1580954.

97. Jeznach, O.; Kołbuk, D.; Marzec, M.; Bernasik, A.; Sajkiewicz, P. Aminolysis as a surface functionalization method of aliphatic polyester nonwovens: impact on material properties and biological response. *RSC Adv.* **2022**, *12*, 11303–11317, doi:10.1039/d2ra00542e.

98. Mai-Prochnow, A.; Murphy, A.B.; McLean, K.M.; Kong, M.G.; Ostrikov, K. Atmospheric pressure plasmas: Infection control and bacterial responses. *Int. J. Antimicrob. Agents* **2014**, *43*, 508–517, doi:10.1016/j.ijantimicag.2014.01.025.

99. Cools, P.; De Geyter, N.; Vanderleyden, E.; Dubruel, P.; Morent, R. Surface analysis of titanium cleaning and activation processes: Non-thermal plasma versus other techniques. *Plasma Chem. Plasma Process.* **2014**, *34*, 917–932, doi:10.1007/s11090-014-9552-2.

100. Paredes, V.; Salvagni, E.; Rodriguez, E.; Gil, F.J.; Manero, J.M. Assessment and comparison of surface chemical composition and oxide layer modification

upon two different activation methods on a cocrmo alloy. *J. Mater. Sci. Mater. Med.* **2014**, *25*, 311–320, doi:10.1007/s10856-013-5083-2.

101. Pelleg, J. Surface Treatment. In *Structural Integrity*; 2022; Vol. 22, pp. 431–478 ISBN 9780323266987.

102. De Geyter, N.; Morent, R.; Desmet, T.; Trentesaux, M.; Gengembre, L.; Dubruel, P.; Leys, C.; Payen, E. Plasma modification of polylactic acid in a medium pressure DBD. *Surf. Coatings Technol.* **2010**, *204*, 3272–3279, doi:10.1016/j.surfcoat.2010.03.037.

103. Lee, M.; Kwon, J.; Jiang, H.B.; Choi, E.H.; Park, G.; Kim, K. The antibacterial effect of non- thermal atmospheric pressure plasma treatment of titanium surfaces according to the bacterial wall structure. *Sci. Rep.* **2019**, *9*, 1–13, doi:10.1038/s41598-019-39414-9.

104. Helary, G.; Migonney, V. *Bioactive polymer coatings to improve bone repair*; Woodhead Publishing Limited, 2009; ISBN 9781845693855.

105. Huh, M.W.; Kang, I.K.; Lee, D.H.; Kim, W.S.; Lee, D.H.; Park, L.S.; Min, K.E.; Seo, K.H. Surface characterization and antibacterial activity of chitosan-grafted poly(ethylene terephthalate) prepared by plasma glow discharge. *J. Appl. Polym. Sci.* **2001**, *81*, 2769–2778, doi:10.1002/app.1723.

106. Blodgett, B. Films Built by Depositing Successive Monomolecular Layers on a Solid Surface. *J. Am. Chem. Soc.* **1935**, *57*, 1007–1022.

107. Bigelow, W.C.; Pickett, D.L.; Zisman, W.A. Oleophobic monolayers: I. Films adsorbed from solution in non-polar liquids. *Joural Colloid Sci.* **1946**, *1*, 513–538.

108. Hasan, A.; Pandey, L.M. *Self-assembled monolayers in biomaterials*; Elsevier Ltd., 2018; ISBN 9780081007167.

109. Casalini, S.; Bortolotti, C.A.; Leonardi, F.; Biscarini, F. Self-assembled monolayers in organic electronics. *Chem. Soc. Rev.* **2017**, *46*, 40–71, doi:10.1039/c6cs00509h.

110. Kim, S.; Yoo, H. Self-assembled monolayers: Versatile uses in electronic devices from gate dielectrics, dopants, and biosensing linkers. *Micromachines* **2021**, *12*, doi:10.3390/mi12050565.

111. Pujari, S.P.; Scheres, L.; Marcelis, A.T.M.; Zuilhof, H. Covalent surface modification of oxide surfaces. *Angew. Chemie - Int. Ed.* **2014**, *53*, 6322–6356, doi:10.1002/anie.201306709.

112. Faucheux, N.; Schweiss, R.; Lützow, K.; Werner, C.; Groth, T. Self-assembled monolayers with different terminating groups as model substrates for cell adhesion studies. *Biomaterials* **2004**, *25*, 2721–2730, doi:10.1016/j.biomaterials.2003.09.069.

113. Sagiv, L.N. and J. A New Approach to Construction of Artificial Monolayer Assemblies. *J. Am. Chem. Soc.* **1983**, *105*, 674–676.

114. Singh, V.; Mondal, P.C.; Singh, A.K.; Zharnikov, M. Molecular sensors confined on SiOx substrates. *Coord. Chem. Rev.* **2017**, *330*, 144–163, doi:10.1016/j.ccr.2016.09.015.

115. Wang, L.; Schubert, U.S.; Hoeppener, S. Surface chemical reactions on self-assembled silane based monolayers. *Chem. Soc. Rev.* **2021**, *50*, 6507–6540, doi:10.1039/d0cs01220c.

116. Love, J.C.; Estroff, L.A.; Kriebel, J.K.; Nuzzo, R.G.; Whitesides, G.M. *Self-assembled monolayers of thiolates on metals as a form of nanotechnology*; 2005; Vol. 105; ISBN 2172440809.

117. Hasan, A.; Saxena, V.; Pandey, L.M. Surface Functionalization of Ti6Al4V via Self-assembled Monolayers for Improved Protein Adsorption and Fibroblast Adhesion. *Langmuir* **2018**, *34*, 3494–3506, doi:10.1021/acs.langmuir.7b03152.

118. Rodríguez-Cano, A.; Cintas, P.; Fernández-Calderón, M.C.; Pacha-Olivenza, M. ángel; Crespo, L.; Saldaña, L.; Vilaboa, N.; González-Martín, M.L.; Babiano, R. Controlled silanization-amination reactions on the Ti6Al4V surface for biomedical applications. *Colloids Surfaces B Biointerfaces* **2013**, *106*, 248–257, doi:10.1016/j.colsurfb.2013.01.034.

119. Silverman, B.M.; Wieghaus, K.A.; Schwartz, J. Comparative properties of siloxane vs phosphonate monolayers on a key titanium alloy. *Langmuir* **2005**, *21*, 225–228, doi:10.1021/la0482271.

120. Han, X.; Sun, X.; He, T.; Sun, S. Formation of highly stable self-assembled alkyl phosphonic acid monolayers for the functionalization of titanium surfaces

and protein patterning. *Langmuir* **2015**, *31*, 140–148, doi:10.1021/la504644q.

121. Adden, N.; Gamble, L.J.; Castner, D.G.; Hoffmann, A.; Gross, G.; Menzel, H. Phosphonic acid monolayers for binding of bioactive molecules to titanium surfaces. *Langmuir* **2006**, *22*, 8197–8204, doi:10.1021/la060754c.

122. Calliess, T.; Sluszniak, M.; Winkel, A.; Pfaffenroth, C.; Dempwolf, W.; Heuer, W.; Menzel, H.; Windhagen, H.; Stiesch, M. Antimicrobial surface coatings for a permanent percutaneous passage in the concept of osseointegrated extremity prosthesis. *Biomed. Tech.* **2012**, *57*, 467–471, doi:10.1515/bmt-2011-0041.

123. Du, H.; Wei, Z.; Wang, H.; Zhang, E.; Zuo, L.; Du, L. Surface microstructure and cell compatibility of calcium silicate and calcium phosphate composite coatings on Mg-Zn-Mn-Ca alloys for biomedical application. *Colloids Surfaces B Biointerfaces* **2011**, *83*, 96–102, doi:10.1016/j.colsurfb.2010.11.003.

124. Cunningham, B.W.; Hu, N.; Zorn, C.M.; McAfee, P.C. Bioactive titanium calcium phosphate coating for disc arthroplasty: analysis of 58 vertebral end plates after 6- to 12-month implantation. *Spine J.* **2009**, *9*, 836–845, doi:10.1016/j.spinee.2009.04.015.

125. Katić, J.; Krivačić, S.; Petrović, Ž.; Mikić, D.; Marciuš, M. Titanium Implant Alloy Modified by Electrochemically Deposited Functional Bioactive Calcium Phosphate Coatings. *Coatings* **2023**, *13*, doi:10.3390/coatings13030640.

126. Farjam, P.; Luckabauer, M.; de Vries, E.G.; Rangel, V.R.; Hekman, E.E.G.; Verkerke, G.J.; Rouwkema, J. Bioactive calcium phosphate coatings applied to flexible poly(carbonate urethane) foils. *Surf. Coatings Technol.* **2023**, *470*, 129838, doi:10.1016/j.surfcoat.2023.129838.

127. Heimann, R.B. Osseoconductive and corrosion-inhibiting plasma-sprayed calcium phosphate coatings for metallic medical implants. *Metals (Basel).* **2017**, *7*, 1–19, doi:10.3390/met7110468.

128. Yang, F.; Wolke, J.G.C.; Jansen, J.A. Biomimetic calcium phosphate coating on electrospun poly(ε-caprolactone) scaffolds for bone tissue engineering. *Chem. Eng. J.* **2008**, *137*, 154–161, doi:10.1016/j.cej.2007.07.076.

129. Lin, B.; Zhong, M.; Zheng, C.; Cao, L.; Wang, D.; Wang, L.; Liang, J.; Cao, B.

Preparation and characterization of dopamine-induced biomimetic hydroxyapatite coatings on the AZ31 magnesium alloy. *Surf. Coatings Technol.* **2015**, *281*, 82–88, doi:10.1016/j.surfcoat.2015.09.033.

130. Deplaine, H.; Lebourg, M.; Ripalda, P.; Vidaurre, A.; Sanz-Ramos, P.; Mora, G.; Prõsper, F.; Ochoa, I.; Doblaré, M.; Gõmez Ribelles, J.L.; et al. Biomimetic hydroxyapatite coating on pore walls improves osteointegration of poly(L-lactic acid) scaffolds. *J. Biomed. Mater. Res. - Part B Appl. Biomater.* **2013**, *101 B*, 173–186, doi:10.1002/jbm.b.32831.

131. Rigo, E.C.S.; Boschi, A.O.; Yoshimoto, M.; Allegrini, S.; Konig, B.; Carbonari, M.J. Evaluation in vitro and in vivo of biomimetic hydroxyapatite coated on titanium dental implants. *Mater. Sci. Eng. C* **2004**, *24*, 647–651, doi:10.1016/j.msec.2004.08.044.

132. Chen, F.; Lam, W.M.; Lin, C.J.; Qiu, G.X.; Wu, Z.H.; Luk, K.D.K.; Lu, W.W. Biocompatibility of Electrophoretical Deposition of Nanostructured Hydroxyapatite Coating on Roughen Titanium Surface : In Vitro Evaluation Using Mesenchymal Stem Cells. *J. Biomed. Mater. Res.* **2006**, *82B*, 183–191, doi:10.1002/jbmb.

133. Yuan, H.; De Bruijn, J.D.; Zhang, X.; Van Blitterswijk, C.A.; De Groot, K. Bone induction by porous glass ceramic made from Bioglass® (45S5). *J. Biomed. Mater. Res.* **2001**, *58*, 270–276, doi:10.1002/1097-4636(2001)58:3<270::AID-JBM1016>3.0.CO;2-2.

134. El-Fiqi, A.; Kim, J.H.; Kim, H.W. Osteoinductive fibrous scaffolds of biopolymer/mesoporous bioactive glass nanocarriers with excellent bioactivity and long-term delivery of osteogenic drug. *ACS Appl. Mater. Interfaces* **2015**, *7*, 1140–1152, doi:10.1021/am5077759.

135. D'Almeida, M.; Attik, N.; Amalric, J.; Brunon, C.; Renaud, F.; Abouelleil, H.; Toury, B.; Grosgogeat, B. Chitosan coating as an antibacterial surface for biomedical applications. *PLoS One* **2017**, *12*, 1–11, doi:10.1371/journal.pone.0189537.

136. Palla-Rubio, B.; Araújo-Gomes, N.; Fernández-Gutiérrez, M.; Rojo, L.; Suay, J.; Gurruchaga, M.; Goñi, I. Synthesis and characterization of silica-chitosan hybrid materials as antibacterial coatings for titanium implants. *Carbohydr. Polym.* **2019**, *203*, 331–341, doi:10.1016/j.carbpol.2018.09.064.

137. Xing, C.M.; Meng, F.N.; Quan, M.; Ding, K.; Dang, Y.; Gong, Y.K. Quantitative fabrication, performance optimization and comparison of PEG and zwitterionic polymer antifouling coatings. *Acta Biomater.* **2017**, *59*, 129–138, doi:10.1016/j.actbio.2017.06.034.

138. Ao, H.; Zong, J.; Nie, Y.; Wan, Y.; Zheng, X. An in vivo study on the effect of coating stability on osteointegration performance of collagen/hyaluronic acid multilayer modified titanium implants. *Bioact. Mater.* **2018**, *3*, 97–101, doi:10.1016/j.bioactmat.2017.07.004.

139. Guarise, C.; Maglio, M.; Sartori, M.; Galesso, D.; Barbera, C.; Pavan, M.; Martini, L.; Giavaresi, G.; Sambri, V.; Fini, M. Titanium implant coating based on dopamine-functionalized sulphated hyaluronic acid: in vivo assessment of biocompatibility and antibacterial efficacy. *Mater. Sci. Eng. C* **2021**, *128*, 112286, doi:10.1016/j.msec.2021.112286.

140. Guarise, C.; Barbera, C.; Pavan, M.; Pluda, S.; Celestre, M.; Galesso, D. Dopamine-functionalized sulphated hyaluronic acid as a titanium implant coating enhances biofilm prevention and promotes osseointegration. *Biofouling* **2018**, *34*, 719–730, doi:10.1080/08927014.2018.1491555.

141. Del Hoyo-Gallego, S.; Pérez-Álvarez, L.; Gómez-Galván, F.; Lizundia, E.; Kuritka, I.; Sedlarik, V.; Laza, J.M.; Vila-Vilela, J.L. Construction of antibacterial poly(ethylene terephthalate) films via layer by layer assembly of chitosan and hyaluronic acid. *Carbohydr. Polym.* **2016**, *143*, 35–43, doi:10.1016/j.carbpol.2016.02.008.

142. Montazerian, M.; Hosseinzadeh, F.; Migneco, C.; Fook, M.V.L.; Baino, F. Bioceramic coatings on metallic implants: An overview. *Ceram. Int.* **2022**, *48*, 8987–9005, doi:10.1016/j.ceramint.2022.02.055.

143. Fiume, E.; Magnaterra, G.; Rahdar, A.; Vern, E. Hydroxyapatite for Biomedical Applications : A Short Overview. *Ceramics* **2021**, *4*, 542–563.

144. Kaliaraj, G.S.; Bavanilathamuthiah, M.; Kirubaharan, K.; Ramachandran, D.; Dharini, T.; Viswanathan, K.; Vishwakarma, V. Bio-inspired YSZ coated titanium by EB-PVD for biomedical applications. *Surf. Coatings Technol.* **2016**, *307*, 227–235, doi:10.1016/j.surfcoat.2016.08.039.

145. Sergi, R.; Bellucci, D.; Cannillo, V. A review of bioactive glass/natural polymer composites: State of the art. *Materials (Basel).* **2020**, *13*, 1–38,

doi:10.3390/ma13235560.

146. Kaur, G.; Kumar, V.; Baino, F.; Mauro, J.C.; Pickrell, G.; Evans, I.; Bretcanu, O. Mechanical properties of bioactive glasses, ceramics, glass-ceramics and composites: State-of-the-art review and future challenges. *Mater. Sci. Eng. C* **2019**, *104*, 109895, doi:10.1016/j.msec.2019.109895.

147. Sergi, R.; Bellucci, D.; Cannillo, V. A comprehensive review of bioactive glass coatings: State of the art, challenges and future perspectives. *Coatings* **2020**, *10*, doi:10.3390/COATINGS10080757.

148. Bargavi, P.; Chitra, S.; Durgalakshmi, D.; Radha, G.; Balakumar, S. Zirconia reinforced bio-active glass coating by spray pyrolysis: Structure, surface topography, in-vitro biological evaluation and antibacterial activities. *Mater. Today Commun.* **2020**, *25*, doi:10.1016/j.mtcomm.2020.101253.

149. Ishihara, K. Blood-Compatible Surfaces with Phosphorylcholine-Based Polymers for Cardiovascular Medical Devices. *Langmuir* **2019**, *35*, 1778–1787, doi:10.1021/acs.langmuir.8b01565.

150. Peng, L.; Chang, L.; Si, M.; Lin, J.; Wei, Y.; Wang, S.; Liu, H.; Han, B.; Jiang, L. Hydrogel-Coated Dental Device with Adhesion-Inhibiting and Colony-Suppressing Properties. *ACS Appl. Mater. Interfaces* **2020**, *12*, 9718–9725, doi:10.1021/acsami.9b19873.

151. Zare, M.; Bigham, A.; Zare, M.; Luo, H.; Ghomi, E.R. pHEMA : An Overview for Biomedical Applications. *Int. J. Mol. Sci.* **2021**, *22*, 6376–6384.

152. Ungureanu, C.; Pirvu, C.; Mindroiu, M.; Demetrescu, I. Antibacterial polymeric coating based on polypyrrole and polyethylene glycol on a new alloy TiAlZr. *Prog. Org. Coatings* **2012**, *75*, 349–355, doi:10.1016/j.porgcoat.2012.07.015.

153. Tang, J.; Yan, D.; Chen, L.; Shen, Z.; Wang, B.; Weng, S.; Wu, Z.; Xie, Z.; Fang, K.; Hong, C.; et al. Enhancement of local bone formation on titanium implants in osteoporotic rats by biomimetic multilayered structures containing parathyroid hormone (PTH)-related protein. *Biomed. Mater.* **2020**, *15*, 045011, doi:10.1088/1748-605X/ab7b3d.

154. Wang, B.; Ren, K.; Chang, H.; Wang, J.; Ji, J. Construction of Degradable Multilayer Films for Enhanced Antibacterial Properties. *ACS Appl. Mater. Interfaces* **2013**, *5*, 4136–4143, doi:10.1021/am4000547.

155. Wu, C.; Shao, X.; Lin, X.; Gao, W.; Fang, Y.; Wang, J. Surface modification of titanium with collagen/hyaluronic acid and bone morphogenetic protein 2/7 heterodimer promotes osteoblastic differentiation. *Dent. Mater. J.* **2020**, *39*, 1072–1079, doi:10.4012/dmj.2019-249.

156. Jacob, J.; Haponiuk, J.T.; Thomas, S.; Gopi, S. Biopolymer based nanomaterials in drug delivery systems: A review. *Mater. Today Chem.* **2018**, *9*, 43–55, doi:10.1016/j.mtchem.2018.05.002.

157. Criado-Gonzalez, M.; Mijangos, C.; Hernández, R. Polyelectrolyte multilayer films based on natural polymers: From fundamentals to Bio-Applications. *Polymers (Basel).* **2021**, *13*, 1–30, doi:10.3390/polym13142254.

158. Li, J.; Mooney, D.J. Designing hydrogels for controlled drug delivery. *Nat. Rev. Mater.* **2016**, *1*, 1–18, doi:10.1038/natrevmats.2016.71.

159. Zafar, M.S.; Fareed, M.A.; Riaz, S.; Latif, M.; Habib, S.R.; Khurshid, Z. Customized therapeutic surface coatings for dental implants. *Coatings* **2020**, *10*, 1–37, doi:10.3390/coatings10060568.

160. Li, X.; He, L.; Li, N.; He, D. Curcumin loaded hydrogel with anti-inflammatory activity to promote cartilage regeneration in immunocompetent animals. *J. Biomater. Sci. Polym. Ed.* **2023**, *34*, 200–216, doi:10.1080/09205063.2022.2113290.

161. Ariga, K.; McShane, M.; Lvov, Y.M.; Ji, Q.; Hill, J.P. Layer-by-layer assembly for drug delivery and related applications. *Expert Opin. Drug Deliv.* **2011**, *8*, 633–644, doi:10.1517/17425247.2011.566268.

162. Pahal, S.; Gakhar, R.; Raichur, A.M.; Varma, M.M. Polyelectrolyte multilayers for bio-applications: recent advancements. *IET Nanobiotechnology* **2017**, *11*, 903–908, doi:10.1049/iet-nbt.2017.0007.

163. Li, D.; Lv, P.; Fan, L.; Huang, Y.; Yang, F.; Mei, X.; Wu, D. The immobilization of antibiotic-loaded polymeric coatings on osteoarticular Ti implants for the prevention of bone infections. *Biomater. Sci.* **2017**, *5*, 2337–2346, doi:10.1039/c7bm00693d.

164. Karakurt, I.; Ozaltin, K.; Pišťˇ, H.; Vesela, D.; Michael-lindhard, J.; Mozetiˇ, M. Effect of Saccharides Coating on Antibacterial Potential and Drug Loading and Releasing Capability of Plasma Treated Polylactic Acid Films. *Int. J. Mol.*

Sci **2022**, *23*, 8821.

165. Chen, C.; Yao, Y.; Tang, H.; Lin, T.; Chen, D.W.; Cheng, K. Long-term antibacterial performances of biodegradable polylactic acid materials with direct absorption of antibiotic agents. *RSC Adv.* **2018**, *8*, 16223–16231, doi:10.1039/C8RA00504D.

166. Valverde, A.; Pérez-Álvarez, L.; Ruiz-Rubio, L.; Pacha Olivenza, M.A.; García Blanco, M.B.; Díaz-Fuentes, M.; Vilas-Vilela, J.L. Antibacterial hyaluronic acid/chitosan multilayers onto smooth and micropatterned titanium surfaces. *Carbohydr. Polym.* **2019**, *207*, 824–833, doi:10.1016/j.carbpol.2018.12.039.

167. Shen, K.; Tang, Q.; Fang, X.; Zhang, C.; Zhu, Z.; Hou, Y.; Lai, M. The sustained release of dexamethasone from TiO 2 nanotubes reinforced by chitosan to enhance osteoblast function and anti-in fl ammation activity. *Mater. Sci. Eng. C* **2020**, *116*, 111241, doi:10.1016/j.msec.2020.111241.

168. Yin, X.; Li, Y.; Chen, Y.; Liu, P.; Feng, B.; Zhang, P.; Zeng, H. IL-4-loaded alginate/chitosan multilayer films for promoting angiogenesis through both direct and indirect means. *Int. J. Biol. Macromol.* **2023**, *232*, 123486, doi:10.1016/j.ijbiomac.2023.123486.

169. Birkett, M.; Dover, L.; Cherian Lukose, C.; Wasy Zia, A.; Tambuwala, M.M.; Serrano-Aroca, Á. Recent Advances in Metal-Based Antimicrobial Coatings for High-Touch Surfaces. *Int. J. Mol. Sci.* **2022**, *23*, doi:10.3390/ijms23031162.

170. Karakurt, I.; Ozaltin, K.; Vesela, D.; Lehocky, M.; Humpol, P. Antibacterial Activity and Cytotoxicity of Immobilized Glucosamine / Chondroitin Sulfate on Polylactic Acid Films. *Polymers (Basel).* **2019**, *11*, 1–12.

171. Nie, B.; Long, T.; Li, H.; Wang, X.; Yue, B. A comparative analysis of antibacterial properties and inflammatory responses for the KR-12 peptide on titanium and PEGylated titanium surfaces. *RSC Adv.* **2017**, *7*, 34321–34330, doi:10.1039/c7ra05538b.

172. Heijink, A.; Schwartz, J.; Zobitz, M.E.; Nicole Crowder, K.; Lutz, G.E.; Sibonga, J.D. Self-assembled monolayer films of phosphonates for bonding RGD to titanium. *Clin. Orthop. Relat. Res.* **2008**, *466*, 977–984, doi:10.1007/s11999-008-0117-7.

173. Hoyos-Nogués, M.; Buxadera-Palomero, J.; Ginebra, M.P.; Manero, J.M.; Gil,

F.J.; Mas-Moruno, C. All-in-one trifunctional strategy: A cell adhesive, bacteriostatic and bactericidal coating for titanium implants. *Colloids Surfaces B Biointerfaces* **2018**, *169*, 30–40, doi:10.1016/j.colsurfb.2018.04.050.

174. Tan, M.; Feng, Y.; Wang, H.; Zhang, L.; Khan, M.; Guo, J. Immobilized Bioactive Agents onto Polyurethane Surface with Heparin and Phosphorylcholine Group Immobilized Bioactive Agents onto Polyurethane Surface with Heparin and Phosphorylcholine Group. *Macromol. Res.* **2013**, *21*, 541–549, doi:10.1007/s13233-013-1028-3.

175. Ozaltin, K.; Lehocky, M.; Humpolicek, P.; Pelkova, J.; Di Martino, A.; Karakurt, I.; Saha, P. Anticoagulant polyethylene terephthalate surface by plasma-mediated fucoidan immobilization. *Polymers (Basel).* **2019**, *11*, 1–12, doi:10.3390/polym11050750.

176. Kolb, H.C.; Finn, M.G.; Sharpless, K.B. Click Chemistry : Diverse Chemical Function from a Few Good Reactions. *Angew. Chemie - Int. Ed.* **2001**, *40*, 2004–2021.

177. Devaraj, N.K.; Finn, M.G. Introduction: Click Chemistry. *Chem. Rev.* **2021**, *121*, 6697–6698, doi:10.1021/acs.chemrev.1c00469.

178. Amna, B.; Ozturk, T. Click chemistry: a fascinating method of connecting organic groups. *Org. Commun.* **2021**, *78*, 97–120, doi:10.25135/ACG.OC.100.21.03.2006.

179. Huisgen, R. 1,3-Dipolar Cycloadditions. *Angew. Chemie - Int. Ed.* **1963**, *2*, 565–598.

180. Fairbanks, B.D.; Scott, T.F.; Kloxin, C.J.; Anseth, K.S.; Bowman, C.N. Thiol - Yne Photopolymerizations : Novel Mechanism , Kinetics , and Step-Growth Formation of Highly Cross-Linked Networks. *Macromolecules* **2009**, *42*, 211–217.

181. Daglar, O.; Luleburgaz, S.; Baysak, E.; Gunay, U.S.; Hizal, G.; Tunca, U.; Durmaz, H. Nucleophilic Thiol-yne reaction in Macromolecular Engineering: From synthesis to applications. *Eur. Polym. J.* **2020**, *137*, 109926, doi:10.1016/j.eurpolymj.2020.109926.

182. Lowe, A.B. Thiol-yne 'click'/coupling chemistry and recent applications in polymer and materials synthesis and modification. *Polymer (Guildf).* **2014**, *55*,

5517–5549, doi:10.1016/j.polymer.2014.08.015.

183. Hensarling, R.M.; Doughty, V.A.; Chan, J.W.; Patton, D.L. "Clicking" polymer brushes with thiol-yne chemistry: Indoors and out. *J. Am. Chem. Soc.* **2009**, *131*, 14673–14675, doi:10.1021/ja9071157.

184. Lowe, A.B.; Hoyle, C.E.; Bowman, C.N. Thiol-yne click chemistry: A powerful and versatile methodology for materials synthesis. *J. Mater. Chem.* **2010**, *20*, 4745–4750, doi:10.1039/b917102a.

185. Huisgen, R. 1,3-Dipolar Cycloadditions Past and Future [*]. *Angew. Chemie - Int. Ed.* **1963**, *2*, 565–632, doi:10.1097/TP.0000000000001850.

186. Diaz Diaz, David; Finn, M.G; Sharpless, K.Barry, Fokin, Valery.V; Hawker, C.. Cicloadición 1,3-dipolar de azidas y alquinos. I: Principales aspectos sintéticos. *An. Química RSEQ* **2008**, *104*, 173–180.

187. Lutz, J. 1 , 3-Dipolar Cycloadditions of Azides and Alkynes : A Universal Ligation Tool in Polymer and Materials Science. *Angew. Chemie - Int. Ed.* **2007**, *46*, 1018–1025, doi:10.1002/anie.200604050.

188. Ramapanicker, R.; Chauhan, P. Click Chemistry : Mechanistic and Synthetic Perspectives. In *Click reactions in Organic Synthesis*; 2016; pp. 1–24.

189. Meldal, M.; Tornøe, C.W. Cu-Catalyzed Azide - Alkyne Cycloaddition. **2008**, 2952–3015.

190. Rostovtsev, V. V; Green, L.G.; Fokin, V. V; Sharpless, K.B. A Stepwise Huisgen Cycloaddition Process : Copper (i) -Catalyzed Regioselective ™ Ligation ∫ of Azides and Terminal Alkynes **. *Angew. Chemie - Int. Ed.* **2002**, *41*, 2596–2599.

191. Liang, L.; Astruc, D. The copper(I)-catalyzed alkyne-azide cycloaddition (CuAAC) "click" reaction and its applications. An overview. *Coord. Chem. Rev.* **2011**, *255*, 2933–2945, doi:10.1016/j.ccr.2011.06.028.

192. Molteni, G.; Bianchi, C.L.; Marinoni, G.; Santo, N.; Ponti, A. Cu/Cu-oxide nanoparticles as catalyst in the "click" azide-alkyne cycloaddition. *New J. Chem.* **2006**, *30*, 1137–1139, doi:10.1039/b604297j.

193. Himo, F.; Lovell, T.; Hilgraf, R.; Rostovtsev, V. V.; Noodleman, L.; Sharpless, K.B.; Fokin, V. V. Copper(I)-catalyzed synthesis of azoles. DFT study predicts

unprecedented reactivity and intermediates. *J. Am. Chem. Soc.* **2005**, *127*, 210–216, doi:10.1021/ja0471525.

194. Ben El Ayouchia, H.; Bahsis, L.; Anane, H.; Domingo, L.R.; Stiriba, S.E. Understanding the mechanism and regioselectivity of the copper(i) catalyzed [3 + 2] cycloaddition reaction between azide and alkyne: A systematic DFT study. *RSC Adv.* **2018**, *8*, 7670–7678, doi:10.1039/c7ra10653j.

195. Wang, C.; Ikhlef, D.; Kahlal, S.; Saillard, J.Y.; Astruc, D. Metal-catalyzed azide-alkyne "click" reactions: Mechanistic overview and recent trends. *Coord. Chem. Rev.* **2016**, *316*, 1–20, doi:10.1016/j.ccr.2016.02.010.

196. Agard, N.J.; Prescher, J.A.; Bertozzi, C.R. A Strain-Promoted [3 + 2] Azide - Alkyne Cycloaddition for Covalent Modification of Biomolecules in Living Systems. *J. Am. Chem. Soc.* **2004**, *126*, 15046–15047.

197. Best, M.D. Click Chemistry and Bioorthogonal Reactions: Unprecedented Selectivity in the Labeling of Biological Molecules. *Biochemistry* **2009**, *48*, 6571–6584, doi:10.1021/bi9007726.

198. Dommerholt, J.; Rutjes, F.P.J.T.; van Delft, F.L. Strain-Promoted 1,3-Dipolar Cycloaddition of Cycloalkynes and Organic Azides. *Top. Curr. Chem.* **2016**, *374*, 1–20, doi:10.1007/s41061-016-0016-4.

199. Bach, R.D. Ring strain energy in the cyclooctyl system. the effect of strain energy on [3 + 2] cycloaddition reactions with azides. *J. Am. Chem. Soc.* **2009**, *131*, 5233–5243, doi:10.1021/ja8094137.

200. Baskin, J.M.; Bertozzi, C.R. Bioorthogonal click chemistry: Covalent labeling in living systems. *QSAR Comb. Sci.* **2007**, *26*, 1211–1219, doi:10.1002/qsar.200740086.

201. Sletten, E.M.; Bertozzi, C.R. Bioorthogonal Chemistry : Fishing for Selectivity in a Sea of Functionality Angewandte. *Angew. Chemie - Int. Ed.* **2009**, *48*, 6974–6998, doi:10.1002/anie.200900942.

202. Vrabel, M.; Carell, T. *Cycloadditions in Bioorthogonal Chemistry*; 2016; ISBN 978-3-319-29684-5.

203. Kim, E.; Koo, H. Biomedical applications of copper-free click chemistry:: In vitro, in vivo, and ex vivo. *Chem. Sci.* **2019**, *10*, 7835–7851, doi:10.1039/c9sc03368h.

204. Wang, S.; Yang, X.; Zhu, W.; Zou, L.; Zhang, K.; Chen, Y.; Xi, F. Strain-promoted azide-alkyne cycloaddition " click " as a conjugation tool for building topological polymers. **2014**, *55*, 4812–4819, doi:10.1016/j.polymer.2014.08.003.

205. Li, W.; Zou, J.; Zhu, S.; Mao, X.; Tian, H.; Wang, X. Fluorodibenzocyclooctynes: A Trackable Click Reagent with Enhanced Reactivity. *Chem. - A Eur. J.* **2019**, *25*, 10328–10332, doi:10.1002/chem.201902834.

206. Gordon, C.G.; MacKey, J.L.; Jewett, J.C.; Sletten, E.M.; Houk, K.N.; Bertozzi, C.R. Reactivity of biarylazacyclooctynones in copper-free click chemistry. *J. Am. Chem. Soc.* **2012**, *134*, 9199–9208, doi:10.1021/ja3000936.

207. Sakata, Y.; Nabekura, R.; Hazama, Y.; Hanya, M.; Nishiyama, T.; Kii, I.; Hosoya, T. Synthesis of Functionalized Dibenzoazacyclooctynes by a Decomplexation Method for Dibenzo-Fused Cyclooctyne-Cobalt Complexes. *Org. Lett.* **2022**, doi:10.1021/acs.orglett.2c03832.

208. Li, Z.; Seo, T.S.; Ju, J. 1,3-Dipolar cycloaddition of azides with electron-deficient alkynes under mild condition in water. *Tetrahedron Lett.* **2004**, *45*, 3143–3146, doi:10.1016/j.tetlet.2004.02.089.

209. Truong, V.X.; Ablett, M.P.; Gilbert, H.T.J.; Bowen, J.; Richardson, S.M.; Hoyland, J.A.; Dove, A.P. In situ-forming robust chitosan-poly(ethylene glycol) hydrogels prepared by copper-free azide-alkyne click reaction for tissue engineering. *Biomater. Sci.* **2014**, *2*, 167–175, doi:10.1039/c3bm60159e.

210. Šarić, I.; Kolympadi Markovic, M.; Peter, R.; Linić, P.; Wittine, K.; Kavre Piltaver, I.; Jelovica Badovinac, I.; Marković, D.; Knez, M.; Ambrožić, G. In-situ multi-step pulsed vapor phase surface functionalization of zirconia nanoparticles via copper-free click chemistry. *Appl. Surf. Sci.* **2021**, *539*, doi:10.1016/j.apsusc.2020.148254.

211. Saric, I.; Peter, R.; Kolympadi Markovic, M.; Jelovica Badovinac, I.; Rogero, C.; Ilyn, M.; Knez, M.; Ambrožić, G. Introducing the concept of pulsed vapor phase copper-free surface click-chemistry using the ALD technique. *Chem. Commun.* **2019**, *55*, 3109–3112, doi:10.1039/c9cc00367c.

212. He, B.; Su, H.; Bai, T.; Wu, Y.; Li, S.; Gao, M.; Hu, R.; Zhao, Z.; Qin, A.; Ling, J.; et al. Spontaneous Amino-yne Click Polymerization: A Powerful Tool toward

Regio- and Stereospecific Poly(β-aminoacrylate)s. *J. Am. Chem. Soc.* **2017**, *139*, 5437–5443, doi:10.1021/jacs.7b00929.

213. Worch, J.C.; Stubbs, C.J.; Price, M.J.; Dove, A.P. Click Nucleophilic Conjugate Additions to Activated Alkynes: Exploring Thiol-yne, Amino-yne, and Hydroxyl-yne Reactions from (Bio)Organic to Polymer Chemistry. *Chem. Rev.* **2021**, *121*, 6744–6776, doi:10.1021/acs.chemrev.0c01076.

214. Ruhemann, Siegfried; Beddow, F. CII.—Condensation of phenols with esters of the acetylene series. Part II. Action of phenols on ethyl phenylpropiolate and ethyl acetylenedicarboxylat. *J. Chem. Soc., Trans.* **1900**, *77*, 1119–1125.

215. Yakubu, S.; Etim, E.E. Modern Advances in Click Reactions and applications. *J. Chem. React. Synth.* **2023**, *13*, 129–151.

216. Fu, X.; Qin, A.; Tang, B.Z. Dynamic covalent polymers generated from X-yne click polymerization. *J. Polym. Sci.* **2023**, 1–12, doi:10.1002/pol.20230383.

217. Fu, X.; Qin, A.; Tang, B.Z. X-yne click polymerization. *Aggregate* **2023**, *4*, 1–22, doi:10.1002/agt2.350.

4. KAPITULUA

Ti6Al4V GAINAZAL ANTIKOAGULATZAILEA KLIK ERREAKZIO ARRUNTA ERABILIZ

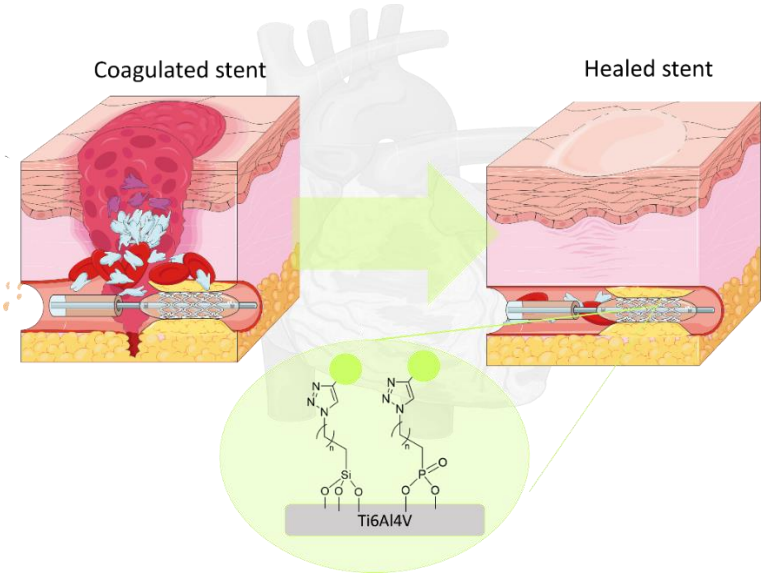

Inplante gisa erabili diren materialen eta konpositeen artean, titanioa eta bere aleazioak dira ezagunenak, askogatik. Ti6Al4V aleazioak erabiliak izan ohi dira giltzadura ordezkapenean. Izan ere, propietate oso onak dituzte biomedikuntzan erabili ahal izateko, hala nola biobateragarritasuna, iraunkortasun handia, gogortasuna, modulu elastiko baxua eta dentsitatea txikia. Hala ere, material horien erronka izaten jarraitzen dute hezur-bateragarritasunak, bakterioen aurkako erresistentziak edo hemobateragarritasunak Hori dela eta, odolarekin kontaktua hobetzen eta bakterioen kontaminazioa zailtzen duten materialen diseinu berritzaileak sustatzea ezinbestekoa da. Horretarako, kapitulu honetan SAM eta klik erreakzioen erabilera konbinatua proposatzen da farmakoen immobilizaziorako Ti6Al4V gainazaleetan, inplanteak egitean infekzioak prebenitzeko eta hemobateragaritasuna hobetzeko.

4. KAPITULUA

Ti6Al4V GAINAZAL ANTIKOAGUALATZAILEA KLIK ERREAKZIO ARRUNTA ERABILIZ

4.1. Sarrera

Zirkulazio sistemarekin erlazionatutako arazoak dira oraindik ere heriotza eragile nagusiak Espainian; besteak beste, gaixotasun kardiobaskularrak. Urteetan zehar hildakoen kopuruak behera egin duen arren, 2018an 120.000 pertsona baino gehiago hil ziren. Izan ere, 2018ko heriotzen %28,2 zirkulazio sistemarekin erlazionatuak izan ziren, eta horixe izan zen emakumeen heriotza kausa nagusia. 2021ean, zirkulazio arazoak %26,4ra jaitsi arren, Espainiako heriotza kausa nagusia izaten jarraitu zuen. Joera mantendu egin zen 2022an, eta zirkulazio gaixotasunek eragin zituzten heriotzen %26 [1–3]. Testuinguru horretan, arterien bypass injertoa gaixotasun kardiobaskular aurreratua duten pazienteen lehen mailako kirurgia da mundu osoan, eta izugarrizko kostu ekonomikoak ditu herrialde guztietan [4].

Elikagaien eta Sendagaien Administrazioa (*Food and Drug Administrarion*, FDA) erakundeak zenbait inplante kardiobaskular onartu ditu gaixotasun kardiobaskularrak tratatzeko. Hala ere, inplante horien ehun birsortzea prozesu luzea da oraindik ere [5]. *Stent* endobaskularren, eta zehazki metalezko stenten (bare metal stents, BMS deiturikoak) desabantaila nagusia da, ohiko erantzun inflamatorioaz gain, ioi toxikoak askatzen dituztela, hala nola Cr, Ni eta Co, hemobateragarritasuna zailduz [6].

Inplanteek sor ditzaketen arazok direla eta, beharrezkoa izan daiteke bigarren ebakuntza egitea. Farmakoak askatzen dituzten stentak diseinatu arren, mota horietako materialak ezin dira luzaroan erabili, farmakoaren askapenak endotelizazioaren atzerapena eta tronbosia eragin baititzake [6,7]. Hemobateragarritasunarekin lotutako arazo nagusiak gailu mediko horien gainazal propietateen araberako dira [8]. Ehunaren eta gainazalaren arteko elkarrekintza hobetzeko, gailu kardiobaskularrak kimikoki eraldatu dira, gainazalaren eta materialaren propietateen egokitzapen independentea ahalbidetuz [9]. Hemobateragarriasuna, hantura erreakzio bateragarriak eta bir-endotelizazioa funtsezko alderdiak dira, gailu endobaskular ezin hobea diseinatzeko nabarmendu beharrekoak [10].

Metalek eta bereziki titanio (Ti) aleazioek dituzten propietate onuragarriei esker, hala nola erresistentzia mekanikoa, korrosioarekiko erresistentzia kimikoa, zurruntasuna eta hemobateragarritasuna, asko erabili dira biomedikuntzan [11,12]. Titanioan oinarritutako material erabilienen artean daude titanio komertzial purua (Cp-Ti) eta Ti6Al4V, material arinak baitira. Hala ere, lehen komentatu den bezala, BMS gailuek zenbait muga dituzte. Tronbosia eragiteaz gain, zain hodien geometria aldatu edo hodiak buxatu ditzakete [13][14]. Titanioaren gainazalaren kimika hobetzeak tronbosiekiko erresistentzia handitzea dakar. Hori lortzea aurrerapen teknologiko garrantzitsua izango litzateke, tresna horien hedapena sustatuko luke eta. Gaur egun, tronbogenesia saihesteko zenbait metodo ezagutzen dira [14]. Esaterako, silizioan edo fosforoan oinarritutako funtzio taldeen erabilpena estrategia eraginkorra eta ekonomikoa bihurtu da, substratuaren eta molekula aktiboen lotura kobalentea ezartzeko.

Estrategia horren bidez, Ti6Al4V aleazioaren gainazalean monogeruza auto muntatzailea (Self-Assembled Monolayer, SAM) sortzen da. Materialaren gainazalaren propietateak eraldatzeko modu hori azkarra eta sinplea da [15,16], erlatiboki, eta ez du ekoizpen kostu handirik. Gainera, gainazalaren konposizioa kontrolatu daiteke bide horretatik, baita eratutako geruzaren antolamendua, noranzkoa edo egonkortasuna ere, besteak beste [17,18]. SAM mota asko ezagutu arren, hala nola karboxilo, hidroxilo edo aminetan oinarritutako gainestaldurak, kapitulu honetan soilik silizio eta fosforo taldeetan oinarritutako SAM egiturak deskribatuko dira [19,20]. Monogeruza horien eraginkortasunagatik eta aldakortasunagatik, erabilgarrienak dira gainazal metalikoak eraldatzeko [21–23].

Silanizazio prozesua gainazalak modu kobalentean eraldatzeko estrategia ekonomikoa eta eraginkorra dela frogatu da [24]. Izan ere, metodologia hori gainazal metaliko edo oxido metaliko mota asko eraldatzeko erabili ohi da, baita hidroxiapatita

bezalako mineralen gainazalak funtzionalizatzeko ere. Estrategi hori erabili ahal izateko, gainazal mota guztiek aurretiko aktibazioa behar dute. Izan ere, hidroxilo taldeak dituen gainazal bat behar da, silano konposatuak gainazalera lotzeko. Silano konposatu horiekin batera funtzio talde aktiboak sartzen dira, hala nola amino, karboxilo edo bromuro taldeak, eta ondorengo eraldaketa kimikoetan parte hartzen dute (**4.1. irudia**). Adibidez, Zhou *et al*.-ek GL13K mikrobioen aurkako peptidoa immobilizatu zuten Ti gainazalean, silanoetan oinarritutako estrategia erabiliz. Horrela, hanturaren kontrako erantzuna eta ondorengo oseointegrazio prozesua sustatzen zuten [25]. Horretarako, Ti gainazala NaOHarekin aktibatu zen aldez aurretik, ondoren 3-(kloropropil)trietoxisilanoarekin (CPTES) silanizatu zen, eta, azkenik, mikrobioen aurkako peptidoa gainazalean funtzionalizatu zen, kloruro atomoaren ordezkapen alifatikoaren bidez, amina nukleozalea erabiliz. Silanizazio prozesua metodo erraza eta eraginkorra izan arren, ezinbestekoa da zenbait erreakzio baldintza kontrolatzea, besteak beste silano kontzentrazioa eta erreakzio denbora, gainazalean polimerizatutako gainestalduran sare lodi bat sor ez dadin (**4.1. irudia**).

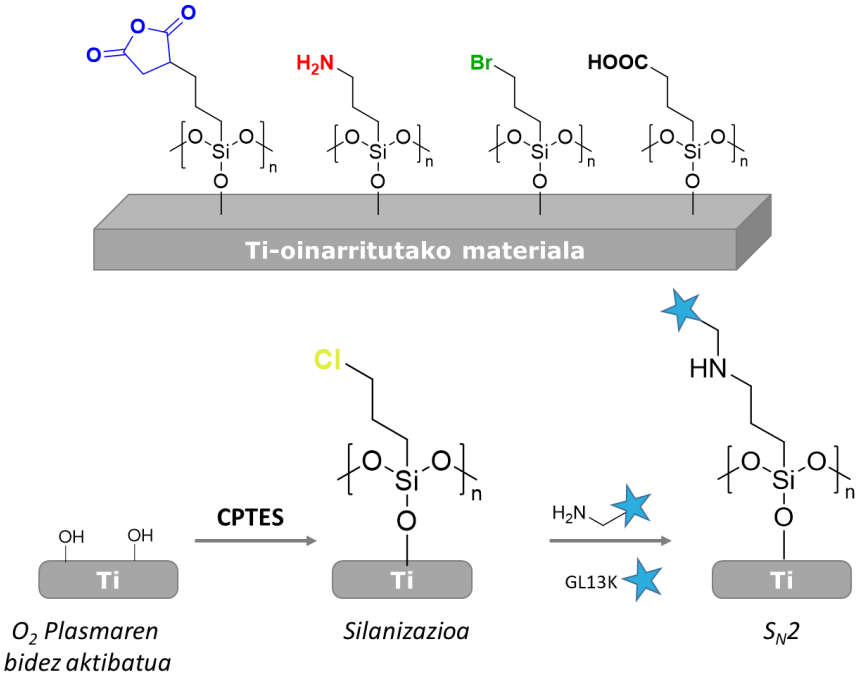

4.1. irudia. A) silano taldean oinarritutako monogeruza desberdinen eskema, B) GL13K peptidoaren immobilizazioaren deskribapena.

Fosforilazioa gainazal biologikoki aktiboak lortzeko erabili den beste gainestaldura kobalente bat da. Hala ere, silanoekin konparatuz, ikusi da azido fosfonikoetan oinarritutako gainestaldurek lotura egonkorragoa eratzen dutela materialaren gainazalarekin. Izan ere, baldintza fisiologikoetan, Ti-O-P loturek egonkortasun

hidrolitiko hobea dute [19,26,27]. Fosfonatoak azido fosforikoaren aitzindariak dira, eta, aldi berean, biologikoki aktiboak diren fosfato deribatuak. Kasu honetan, karbono atomo bat dute oxigeno atomo baten ordez, eta horrek egonkortasun kimikoa ematen dio gainestaldurari, hidrolisi entzimatikoaren aurrean. Horretaz gain, gainestaldura horiek substratuaren hidrofilitatea hobetzen dutela frogatu da, eta hori onuragarria da inplantea sartu ondorengo sendatze prozesurako; izan ere, gainazal hidrofilikoek proteina gehiago adsorbatzeko gaitasuna dute, angiogenesia eta inplantearen oseointegrazioa hobetuz [28].

SAM monogeruzek jarduera biologikoa duten arren, estaldura pasibo horien eraginkortasuna mugatua da, batez ere bakterioekiko atxikidura murriztu nahi bada edo endotelizazioa sustatu nahi bada. Horren ondorioz, piztu egin da muga horiek gainditzeko alternatiba aktiboak garatzeko interesa. Alternatiba aktibo horietan, biologikoki aktiboak diren konposatuak erabiltzen dira, biobateragarritasuna hobetuz eta bakterioen edo beste mikroorganismo batzuen aurkako babesa lortuz. Gainestaldura aktibo horiek diseinatzeko estrategia bat baino gehiago dauden arren, lotura kimikoen bidezko molekula aktiboen immobilizazioa ahalbidetzen duten estrategiak eztabaidatuko dira kapitulu honetan.

Farmakoak eta konplexu biologiko aktiboak immobilizatzeko hainbat motatako erreakzio kimikoak erabili daitezke, hala nola ordezkapen nukleozaleak, erreakzio fotokimikoak edo Klik Kimika. Azken estrategia horrek modu eraginkorrean ahalbidetzen du molekula biologikoen biokonjugazioa, hainbat substratutan. Klik Kimikaren terminoa K. Sharpless *et al*.-en lanean aipatu zen lehen aldiz, eta etekin handiko erreakzio estereoespezifikoak eta oso hedatuak batzen dituen terminoa da [29–31]. Gainera, erreakzio horien baldintzak eta purifikazio prozesuak nahiko sinpleak dira, disolbatzaileak erraz eliminatzen baitira, edo, batzuetan, erreakzioak disolbatzailerik gabe ere eman baitaitezke. Klik erreakzioen artean, Huisgenek deskribatutako azida eta alkinoen arteko zikloadizio 1,3-dipolarra da adierazgarriena. Huisgen *et al*.-en lanean 1970eko hamarkadan aurkeztutako erreakzio hori oso exotermikoa zen, baina erreakzioaren etekina eta konbertsioa oso baxuak ziren, erreakzioaren erabilgarritasuna mugatuz. Kobre katalizatzailearen erabilera proposatu zenean, erreakzioaren inflexio puntua izan zen hori. Izan ere, kobre(I) bidez katalizaturiko azida eta alkinoen arteko erreakzioaren erabilgarritasuna izugarri handitu zen, eta kontzeptu hutsa zen hori errealitate praktiko bihurtu zen. Erreakzioa baldintza sinpleetan burutzeaz gain, eskura dauden hainbat substratu erabili daitezke. Erreakzio horren bidez 1,2,3-triazol bakarra lortzen da, eta 1,4-erregioisomeroa isolatzen da produktu gisa, hain zuzen. Espezifikotasun horrek klik kimikaren oinarrizko printzipioekin bat egiten du [30–32]. Esan bezala, erreakzio hori

klik erreakzioen prototipo gisa ezagutzen da. Azida taldean oinarritutako erreakzioak nagusiki biokonjugazio estrategietan dira erabilgarriak, eta hainbat abantaila dituzte. Hona hemen abantaila horietako batzuk: (I) azida talde urria da konposatu naturaletan, eta (II) lotura oso selektiboak ahalbidetzen ditu soilik funtzio talde zehatzekin, funtzio taldearen erreaktibotasuna eta erreakzioaren selektibitatea areagotuz [33,34].

Farmakoen artean, azido salizilikoa (SA) mundu osoan erabili den analgesikoa da. Zenbait organismok, hala nola, prokariotak eta eukariotak, eta landareek sintetizatutako konposatu fenolikoa da. Izan ere, sahatsaren zuhaitzaren hostoak eta azala (Salix espezieak) aberatsak dira [35,36]. Historian zehar, SA mina arintzeko sendagai gisa erabili da, aurkezte dituen propietate terapeutikoak direla. 1828an, J.A.Buchner salizina konposatua, SAtik eratorritako alkohol salizilikoaren glukosa, arrakastaz isolatu zuen sahatza zuhatzairen azalatik [35]. Hamarkada bat geroago, Raffaele Piriak salizina konposatu aromatiko azidoa bihurtu zuen, azido salizilikoa lortuz lehen aldiz laborategi batean. Hala ere, deskribatutako SAren lehenengo sintesia Kolbe eta kolaboratzaileek aurkeztu zuten 1859an. Alabaina, sendagaiaren zapore mingatsak eta horri lotutako albo-ondorioak luzaroko erabilpena mugatu zuten. Urte batzuk geroago, azido salizilikoaren azetilazioaren bidez aspirina (ASA) lortu zen, erabilerarekin lotutako albo-ondorioak murrizten dituen sendagaia (**1.16 irudia**) [35].

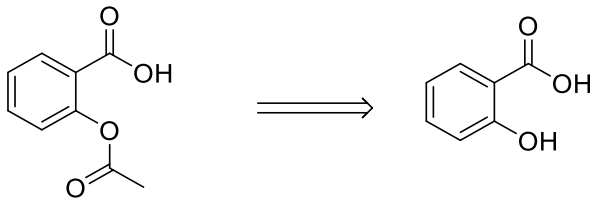

Azido azetil salizilikoa (Aspirin)

Azido salizilikoa

4.2 irudia. Azido azetil salizilikoaren (Aspirina ®) eta haren aitzindariaren, azido salizilikoaren, egitura kimikoak.

Indometazina eta kurkumina bezala, azido salizilikoa prostaglandinen sintesia inhibitzeko gai da. Hasieran, prostaglandinen inhibizioa COXaren inhibizioaren bidez egiten zela pentsatu zen [35]. Baina 1999an, Xu *et al.* ASak eta ASAk eragindako prostaglandinen inhibizio bide berri bat proposatu zuten [35,37]. Haien ikerketen arabera, AS eta ASAk COX ekoizten duten geneen transkripzioa ezabatzen dute, hanturaren kontrako farmako modura jokatuz. Horretaz gain, zenbait ikerketak erakutsi zuten azido salizilikoak ez duela soilik COXen inhibizioan parte hartzen,

baizik eta beste mekanismo batzuen bidez eragiten duela hantura kontrako efektua. Izan ere, inhibizio gaitasun nabarmena du leukozito funtzioan nahiz gene proinflamatorioen adierazpenean. Gainera, zitokinek eta lipopolisakaridoek (LPS) induzitutako oxido nitriko sintasa (iNOS) inhibitzen du. Gainera, azido salizilikoaren kontzentrazio handiak eragina izan dezake zenbait kinasatan, eta, bereziki, MAPK (*Mitogen-activated protein kinasa*) kinasan. Hain zuzen, Koppek eta Goshek frogatu zuten azido salizilikoak NFkB faktore nuklearraren inhibizioan parte hartzen duela; faktore nuklear hori erabakigarria da zelulak hanturazko estimuluarekiko duen erantzunean [38].

Bestalde, azido salizilikoaren ezaugarri nabarmenetakoena da propietate antioxidatzaileak dituela. Hidroxilo erradikalak harrapatzeko gaitasuna duenez, hipoxiak/biroxigenazioak eragindako ehun kaltea murrizten du [38].

Azido salizilikoaren egitura-aktibitate erlazioari behatuta, ikusi da karboxilo taldearen azidotasuna murrizteak eragin handia duela farmakoaren aktibitatean. Esate baterako, azido taldea amida bihurtuz, eta horrela salizilamida lortuz, jarduera analgesikoak iraun egiten duela behatu zen, baina hanturaren kontrako propietateak murriztu egiten direla. Hala ere, Jung-ek eta kolaboratzaileek ondorioztatu zuten salizilamidak NFkB faktorearen inhibizio potentzia handiagoa zuela [38]. Bestalde, karboxilo edo hidroxilo funtzio taldeen ordezkapenak farmakoaren jardueran eta toxikotasunean eragiten du. Izan ere, azido bentzoikoak aktibitate baxua du. Horretaz gain, hidroxilo taldea *meta* edo *para* posiziora aldatzen bada karboxilo taldearekiko, aktibitaterik gabeko konposatua lortzen da.

Aspirinak, azido saliziliko gisa, frogatu du COX inhibitzen duela bi bidetatik: inhibizio zuzenaren eta inhibizio independentearen bidez [36]. Izan ere, aspirina hidrolizatu egiten da odolean zenbait proteinaren bidez (besteak beste Lys, Arg, Ser, Thr, Tyr eta Zis), eta azetilazio prozesu itzulezina gertatu eta azido saliziliko bihurtzen da. Bai azido salizilikoak bai aspirinak interes nabarmena erakutsi dute immobilizazio estrategietan, funtzio anitzeko propietateak lor daitezkeelako [38].

Doktorego tesi honen helburua aspirinaren biokonjugazioan datza, Ti6Al4V laginen eragin antiinflamatorioa eta plaketarioa sustatzeko asmoarekin. Aspirina, edo azido azetilsalizilikoa, azido salizilikoaren profarmakoa da. Izan ere, bai azido salizilikoa bai aspirina antinflamatorio ez-esteoridetzat hartzen dira, COX1en jarduera entzimatikoa modulatzen baitute, inflamatorioak diren prostaglandinen kontzentrazioa murriztuz.

4.2. Materialak eta metodoak

4.2.1.Materialak

Konposatu desberdinen sintesirako hurrengo erreaktiboak erabili ziren: Dansil kloruroa (Sigma Aldrich, St. Louis, MO, EEUU), aspirina (Sigma Aldrich, St. Louise, MO, EEUU), azido salizilikoa (Sigma Aldrich, St. Louis, MO, EEUU), toluenoa (Sigma Aldrich, St. Louis, MO, EEUU), tionil kloruroa ($SOCl_2$, Aldrich, St. Louis, MO, EEUU), propargilamina (Sigma Aldrich, St. Louis, MO, EEUU), diklorometanoa (CH_2Cl_2, Macron Fine Chemical, Gliwice, Polonia), potasio karbonatoa (Sigma Aldrich, St. Louis, MO, EEUU), azido klorhidrikoa (HCl, % 37, Panreac, Dermstadts, Alemania) prestatutako sodio kloruaren disoluzio saturatua (prestatutako, etxeko gatza) dietil (3-bromopropil)fosfonatoa (Sigma Aldrich, St. Louis, MO, EEUU) bromotrimetilsilanoa (BTMS, Sigma Aldrich, St. Louis, MO, EEUU), metanol lehorra (MeOH, Panreac, Darmstadt, Alemania).

Ti6Al4V gainazalak Sigma Aldrich-en hartu ziren eta laser bidezko ablazioaren bidez 1x1 cm-ko pieza txikietan moztu ziren. Hurrengo erreaktiboak erabili ziren gainazalen eraldaketetan: azido sulfurikoa (H_2SO_4, %96, Panreac, Dermstadt), hidrogeno peroxidoa (H_2O_2, Foret, Alicante, Espainia), sodio azida (NaN_3, Sigma Aldrich, St. Louis, MO, EEUU), azetonitriloa (%98, Panreac, Dermstadt, Alemania), azetona (%99, Panreac, Dermstadt, Alemania), etanol (EtOH, %98, Panreac, Dermstadt, Alemania), trimetoxi(3-bromopropil)silanoa (Sigma Aldrich, St. Louis, MO, EEUU), sodio askorbatoa (Sigma Aldrich, St. Louis, MO, EEUU), trietilamina (Et_3N, Sigma Aldrich, St. Louis, MO, EEUU), kobre (II) sulfato pentahidratatua ($CuSO_4 \cdot 5H_2O$, Sigma Aldrich, St. Louis, MO, EEUU)

4.2.2.Prozedura esprimentala

*4.2.2.1. Dansil deribatu **2b**-ren sintesia*

Dansil kloruroa (2.00 g, 7.40 mmol) diklorometanoa (20 mL) disolbatu zen eta propargl amina (0.48 mL, 7.40 mmol) eta Et_3N (0.75 g, 7.4 mmol) disoluzioan gaineratu ziren. Erreakzioa birfluxutan berto zen 48 h. Epeldu ondoren, disoluzioari ura bota zen eta diklorometanoarekin (3x10 mL) erauzi zen. Ondoren, sodio kloruro disoluzio saturatuarekin (2x10 mL) garbitu zen. Fase organiko batu eta gero, Na_2SO_4 anhdiroarekin lehortu eta disolbatzailea hutsean lurrundu zen 5-(dimetilamino)-*N*-(prop-2-in-1-yi)nafataleno-1-sulfonamida (**3b**) lortuz kolore horizko olio gisa (0.95 g, % 89). ^{1}H-EMN (300 MHz, $CDCl_3$) (δ, ppm): 8.52 (d, *J* = 8.5 Hz, 1H, CH_{arom}, H_7), 8.30-8.28 (m, 2H, CH_{arom}, H_5 and H_{12}), 7.54-7.51 (m, 2H, CH_{arom},

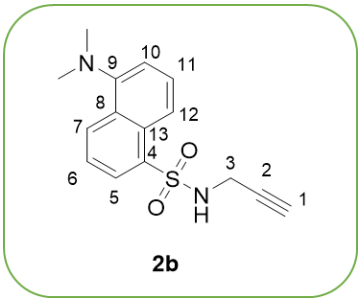

2b

H_6 and H_{11}), 7.18 (dd, *J* = 7.5 Hz, *J* = 0.54 Hz, 1H, CH_{arom}, H_{10}), 5.26 (s,1H, NH), 3.77 (d, *J* = 2.5 Hz, 2H, CH_2, H_3), 2.86 (s, 6H, 2xCH_3), 1.91 (t, *J* = 2.5 Hz, 1H, ≡CH, H_1); ^{13}C-EMN (75 MHz, $CDCl_3$) (δ, ppm): 152.0 (C_{arom}-N, C_9), 135.5 (C_{arom}-S, C_4), 132.6 (C_{arom}-H, C_7), 131.3 (C_{arom}-C, C_{13}), 129.5 (C_{arom}-H, C_5), 129.2 (C_{arom}-H, C_6), 128.5 (C_{arom}-H, C_{11}), 123.2 (C_{arom}-H, C_{12}), 118.9 (C_{arom}-C, C_8), 115.3 (C_{arom}-H, C_{10}), 84.3 (C≡C, C_2), 71.2 (≡CH), 45.2 (N-$(CH_3)_2$), 33.2 (CH_2).

*4.2.2.2. Aspirinaren bidezko 2-hidroxi-N-(prop-2-in-1-il)bentzamidaren (**2a**) sintesia*

Azido azetilsalizilikoa (aspirina, 0.53 g, 2.94 mmol) toluenoan (15 mL) disolbatu zen eta tionil kloruroa (1 mL, 13.9 mmol) disoluziora gaineratu zen. Ondoren, erreakzioa birfluxuan jarrri zen 24 h. Epeldu ondoren, disolbatzailea hutsean lurrudu zen. Jarraian, propargilamina (0.88 mL, 13.9 mmol) diklorometanoan (10 mL) dislbatu zen eta aurreko sisteman gaineratu zen. Errekazioa irabiatzen utzi zen 48 h ingurune tenperaturan. Denbora hori pasa ondoren, erreakzioa geldiarazteko disoluzioari ura bota zitzazaion. Faseak banatu ondoren, fase urtsua diklorometanoarekin (3x20 mL) erauzi zen. Gero, Fase oreganiko konbinatuak potasio karbonato disoluzio satuarekin (2 M, 2x10 mL), azido klorhidrikoarekin (%10, 2x10 mL) eta sodio kloruro disoluzio saturatuarekin (3x10 mL) garbitu ziren. Azkenik, fase organikoak batu ziren, Na_2SO_4 anhidroarekin lehortu eta disolbatzailea hutsean lurrundu zen 2-hidroxi-*N*-(prop-2-in-1-il)bentzamida (**2a**) lortuz, kolore horidun olio bezala (0.43 g, % 81). Geruza fineko kromatografia (GFK) erabili zen Hexano:Etil Azetato (7:3) eluitzaile gisa. ^{1}H-EMN (300 MHz, $CDCl_3$) (δ, ppm): 12.00 (s, 1H, OH), 7.39 (m, 2H, CH_{arom}, H_5 and H_7), 6.99 (dd, *J*= 8.2 Hz, *J*= 1.2 Hz, CH_{arom}, H_8), 6.86 (td, *J*= 8.2 Hz, *J*=1.2 Hz, 1H, CH_{arom}, H_6), 6.49 (s, 1H, NH), 4.25 (d, *J*= 2.6 Hz, 2H, CH_2, H_3), 2.32 (t, *J*= 2.6 Hz, 1H, ≡CH, H_1); ^{13}C-EMN (75 MHz, $CDCl_3$) (δ, ppm): 169.7 (C=O), 161.5 (C_{arom}-OH, C_9), 134.6 (C_{arom}-H, C_5), 125.6 (C_{arom}-H, C_7), 118.9 (C_{arom}-H, C_6), 118.6 (C_{arom}-H, C_8), 112.3 (C_{arom}-C, C_4), 78.8 (C≡, C_2), 72.3 (≡CH, C_1), 24.4 (CH_2, C_3). FTIR (cm^{-1}): 3450 (R-N-H), 3200 (C_{sp}-H), 2100 (C_{sp}-C_{sp}), 1650 (C=O).

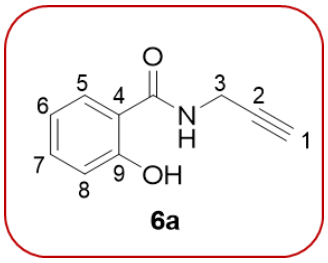

6a

Prozedura berdina erabili zen azido salizilikoarekin (0.51 g, 3.70 mmol). 2-hidroxi-*N*-(prop-2-in-1-il)bentzamida (**6a**) lortuz kolore horidun olio bezala (0.38 g, %73).

4.2.2.3. (3-azidopropil)trimetoxisilanoaren sintesia

(3-bromopropil)trimetoxisilanoa (2 mL, 10.8 mmol), NaN_3 (1.76 g, 27.2mmol), tetrabutilamonio bromuroa (0.64 g, 2 mmol) and azetonitrilo lehorra (35 mL) hiru buruko matraze boroboilera gaineratu ziren. Erreakzioa irabiatu zen nitrogenopean 82 ºC-tan 48 h. Ondoren matrazea epeldu zen, eta erreakzionatu gabeko sodio azida

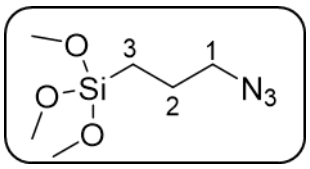

iragazi zen, jarraian disolbatzailea hutsean lurrundu zen. Ziklohexanoa (15 mL) nahastera gehitu zen eta ondoren iragazi egin zen. Azkenik, ziklohexanoa hutsean lurrundu zen kolore gabeko likidoa lortuz. ^{1}H-NMR (300 MHz, $CDCl_3$) (δ, ppm): 3.57 (s, 9H), 3.24-3.28 (m, 2H, N_3-CH_2, H_1), 1.68-1.72 (m, 2H, CH_2, H_2), 0.67-0.71 ppm (m, 2H, Si-CH_2, H_3).

4.2.2.3. azido (3-bromopropil)fosfonikoaren sintesia

Dietil (3-bromopropil)fosfonatoa (0.50 g, 1.58 mmol) diklorometano lehortuan (20 mL) disolbatu zen eta BTMS (0.8 mL, 6 mmol) disoluziora gaineratu zen. Ondoren, erreakzio irabiatzen utzi zen 12 h ingurune tenperaturan nitrogeno atmosferapean. Jarraian, disolbatzailea hutsean lurrundu zen. Ondoren, metanol lehorra (15 mL) gaineratu zen eta erreakzioa irabiatzen utzi zen 4 egunez ingurune tenperaturan nitrogeno atmosferapean. Azkenik, disolbatzailea hutsean lurrundu zen, azido (3-

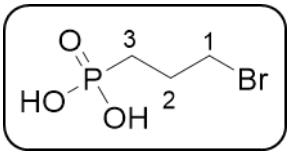

bromopropil)fosfonikoa lortuz likido laranja bezala (0.38 g, %96). ^{1}H-NMR (300MHz, $CDCl_3$) (δ, ppm): 5.48 (sz, 2H, OH), 3.59 (t, 2H, *J*=6.0Hz, CH_2Br, H_1), 2.00 (m, 2H, P-CH_2, H_3), 1.60 (m, 2H, CH_2, H_2); ^{31}P-NMR (32 MHz, $CDCl_3$) (δ, ppm): 26.11 (s, 1P, $(OH)_2$**P**O-CH_2-R).

4.2.2.4. Ti6Al4V lagineen hidrolisia

Ti6Al4V 1x1 cm-ko laukizuzenak azetonarekin, ur desionizatuarekin eta etanolarekin garbitu ziren ultrasoinuaren bidez 20 minutuz (prozedura hau 5 alditan errepikatu zen disolbatzaile bakoitzarekin). Ondoren, laginak lehortu egin ziren 60 ºC-tan 12 h. Behin lehortuta, Ti6Al4V laginak azido sulfuriko (%98, m/m) eta hidrogeno peroxido (%30, m/m) nahaste proportzioan (3:1 v/v) hondoratzen dira 1 h batez ingurune tenperaturan.

4.2.2.5. Monogeruza auto-muntatzaileen eraketa (Self-Assembly Monolayers-SAMs) Ti6Al4V laginetan

a) Silanoetan oinarritutako SAM estrategia

Ti6Al4V-OH laginak (3-bromopropil)trietoxisilano ur disoluzioan (%5) hondoratu ziren 1 h ingurune tenperaturan. Ondoren, erreakzionatu gabeko silano konposatua

azetonarekin garbitu zen ultrasoinuraren bidez (x 5) eta azkenik, materiala hutsean lehortu egin zen 40 ºC-tan gauez [39].

b) Fosfonatoetan oinarritutako SAM estrategia

Ti6Al4V-OH laginak azido (3-bromopropil)fosfoniko ur disoluzioan (%5) hondoratu ziren 1 h ingurune tenperaturan. Ondoren, erreakzionatu gabeko azido fosfoniko deribatua azetonarekin garbitu zen ultrasoinuraren bidez (x 5) eta azkenik, materiala hutsean lehortu egin zen 40 ºC-tan gauez.

c) Azidation

Sodio azida (0.20 g, 3.07 mmol) azetonitrilo/ura nahastean (1:1 v/v, 10 mL) disolbatu zen. Ondoren, aurretik eraldatutako gainazalak (Ti6Al4V-Si-Br eta Ti6Al4V-P(OH)-Br) disoluzioan hondoratu ziren 24 h giro tenperaturan. Azkenik, laginak ultrasoinu bidez garbitu ziren ur eta azetonatan, eta hutsean lehortu ziren 12 h.

4.2.2.6. Dansil fluoroforoaren edo salizilamida deribatuaren immobilizazioa kobrearen bidezko azida eta alkinoaren arteko klik erreakzioak

Sodio askorbatoa (0.08 g, 0.40 mmol) eta kobre (II) sulfato pentahidratua (0.033 g, 0.132 mmol) etanol/ur nahastean (6:4 v/v, 10 mL) disolbatu ziren. Ondoren, trietilamina (0.75 mL, 5.34 mmol) eta 2-hidroxi-*N*-(prop-2-in-1-il)bentzamida (0.52 g, 2.97 mmol) nahastera bota ziren. Jarraian, eraldatutako Ti6Al4V-P(OH)-N_3 or Ti6Al4V-Si-N_3 laginak prestatutako disoluzioan hondoratu ziren 48 h giro tenperaturan. Azkenik, laginak ura eta etanolarekin garbitu ziren eta hutsean lehortu ziren hurrengo karakterizazio urratsetarako.

4.2.3. Gainazalaren karakterizazio fisiko-kimikoa

4.2.3.1. Erresonantzia Magnetiko Nuklearraren (EMN) neurketak

Erresonantzia magnetiko nuklearreko espektroak (^{1}H-EMN) Bruker AC-300 eta AC-500 espektrofotometroetan burutu ziren 20-25 ºC-tan (^{1}H-rako 300 MHz, ^{13}C-rako 75.4 MHz eta 125.8 MHz, eta ^{31}P-rako 500 MHz), disolbatzaile gisa kloroformo deuteratua eta dimetilsulfoxido deuteratua erabiliz: $CDCl_3$ δ=7.26 ppm (^{1}H) eta 77.0 ppm (^{13}C), DMSO-d_6 δ=2.50 ppm (^{1}H eta ^{31}P) eta 39.5 ppm (^{13}C).

4.2.3.2. Fourier Transformadun Infragorri Espektroskopia (FTIR)

Fourier Transformadun Infragorri Espektroskopiaren (FTIR) bidez 2-hidroxi-*N*-(prop-2-in-1-il)bentzamidaren, azido salizilikoaren eta azido azetilsaliziloaren espektroak lortu ziren. Horretarako, NICOLET Nexus FT-IR espektrofotometroa (Thermo Electron Corporation) tresna erabili zen. Lagin bakoitza aztertzeko erabilitako baldintzak

ondorengoak izan ziren; 32 ekorketa, 4000 cm^{-1} – 500 cm^{-1} uhin zenbakien tartean eta 4 cm^{-1} bereizmena.

4.2.3.3. X-izpien bidezko Fotoelektroi Espektroskopia (XPS)

Ti6Al4V laginen konposizio elementalaren analisia XPS-ren bidez aztertu zen, SPECS (XPS, SPECS Surface Nano Analysis, Berlin, Germany) sistema erabiliz. Al/Ag anodo dualeko Focus 500 erradiazio monokromatikoko iturri bat erabili zen eta Phoibos 150 1D-DLD analizatzailean aztertu zen. Ti6Al4V laginak altzairu heldroilgatzezko euskarriekin eta karbono-zintarekin finkatu ziren. Gainera, karbono atomoa erabili zen erreferentzia moduan neurketa guztietan.

4.2.3.4. Elektroien Ekorketazo Mikroskopia (SEM)

Ti6Al4V plaken gainazalak ekortze-mikroskopia elektronikoaren bidez aztertu ziren, HITACHI S-4800 mikroskopioa erabiliz (150 s, 20 mA, 2 kV, 50.000x-ko zooma).

4.2.3.5. Kontaktu angelua

Tratatuko gainazalen kontaktu angelua Dataphysics OCA 15EC Neurtek Instruments sistema optikoarekin neurtu zen. Lagin bakoitzean ur-tantak jarri ziren (2 µL/tanta) eta lagin bakoitza 3 neurketen bidez analizau zen giro tenperaturan.

4.3. Emaitzak eta eztabaida

Sarreran aipatu den bezala, kapitulu honetan biologikoki aktiboak diren konposatuen biokonjugazioa azaltzen da Ti6Al4V gainazalean, kobre(I) bidezko azida eta alkinoen arteko zikloadizio erreakzioa erabiliz. Proposatutako metodologia balioztatzeko, fluoroforo bat erabiltzea pentsatu da; zehazki, jadanik beste kapituluetan erabilitako dansil konposatua. Azpimarratu behar da bai dansil eta bai farmakoen deribatuak immobilizatzeko aurre eraldaketak egin behar izan direla, baita Ti6Al4V gainazalen eraldaketak ere, klik erreakziorako behar diren funtzio taldeak sartu ahal izateko.

Gainazaleko funtzionalizazioen artean, SAM estrategia inplikatzen dituzten bi sistemak aukeratu ziren: silanoaren bidezko monogeruza eta fosfonatoen bidezko monogeruza. **4.1 eskeman** eta **4.2 eskeman** ikus daitekeen moduan, azida taldea SAM-an sartu zen, eta beraz, gainazalean. Azida taldearen sarrera bi modu desberdinetan burutu zen, bi aukeretan azida taldearen bidezko bromoaren ordezkapena deskribatzen da. Lehenengo aukeran, komertziala den silano taldea ainguratu zen, eta ondoren ordezkenapen nukleozalea eman zen. Bestalde, bigarren aukeran, aurretik prestatutako (3-azidopropano)trimetoxisilanoa ainguratu zen gainazalera. Nahiz eta bi aukerek gainazalaren funtzionalizazioa bideratu, kontaktu

angeluaren balioak demostratu zuten bezala, lehenengo aukeraren bidez lortzen den SAM gainazala homogenoagoa da, hori bilbiografiarekin bat dator [40]. Hori dela eta, lehenengo aukerarekin lortu diren datuak soilik azalduko dira.

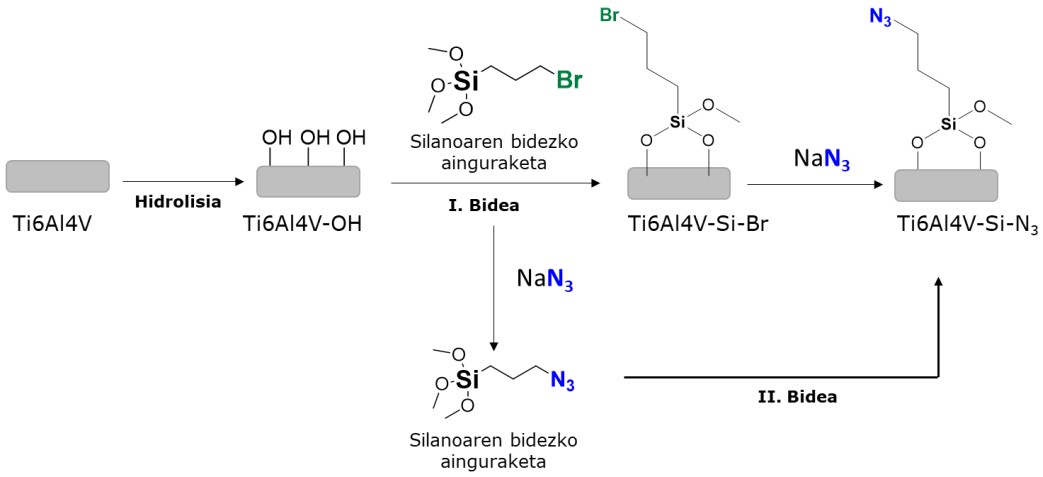

4.1 eskema. Ti6Al4V-ren hidrolisia eta proposatutako bi silanizazio aukerak.

Bide berdina erabili da fosfonatoetan oinarraitutako SAMak garatzeko (**4.2 eskema**), baina honetan komertziala den fosfonatoa aurretik hidrolizatu behar izan da ainguraketa on bat gertatzeko.

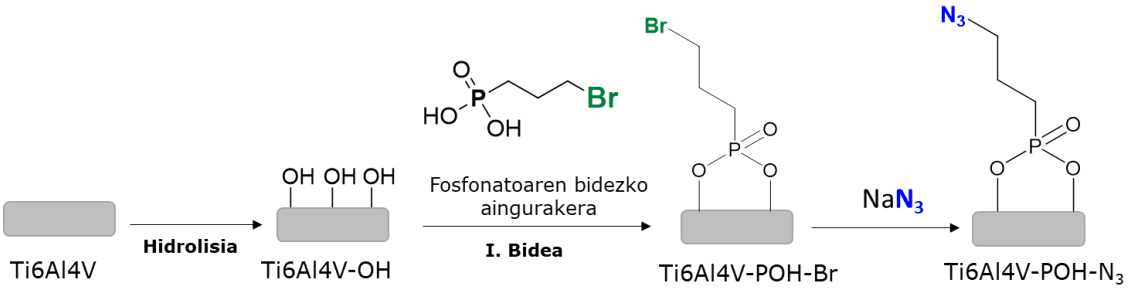

4.2 eskema. Fosfonatoan oinarritutako SAM eraketa azida taldearekin.

Lana hobeto ulertzeko, kapitulu honek konposatuetan egindako eraldaketak eta gainazalak pairatutako eraldaketak eta karakterizazioa teknikak desberdinduko dira.

4.3.1. Kimikoki aktiboak diren konposatuen deribatizazioa eta EMN eta FTIR analisia

4.3.1.1. Azido salizilikoa eta deribatuak

Kapitulu honetan, ezaguna den azida eta alkinoen arteko klik erreakzioa eta SAM estrategia konbinatu ziren farmako antikoagulatzailea biokonjugatzeko Ti6Al4V gainazalean. Metodologia hori erabiltzeko, beharrezkoa izan zen farmakoaren eta gainazalaren funtzionalizazio zehatzak egitea.

Lehenik eta behin, oso ezaguna den aspirina, azido azetilsalizilikoa deritzona, erabiltzea poposatu zen, hantura kontrako propietateak eta antikoagulatzaileak dituen gainazala lortzeko helburuarekin. Aspirinak azido salizilikoan bihurtzen da gorputzean, profarmako gisa jokatuz. Hori dela eta, aspirina eta azido salizilikoa biokonjugazioarako aukera potentzial gisa aukeztu ziren. Klik erreakzioan azida eta alkino funtzio taldeek berezko garrantzia dutenez, bi taldeetatik horietako bat farmakoen egituran sartzea zen lehenengo helburua. Zehazki, alkino talde funtzionala farmakoen egituran sartzea erabaki zen amidazio erreakzio baten bidez, propargilamina nukleozale gisa erabiliz (**4.3 eskema**). Esan beharra dago, amidazio-erreakzioak bi urrats izan zituela: (I) azido karboxilikoaren taldearen aktibazioa, tionil kloruroa erabiliz, dagokion azil kloruroa sortzeko, eta (II) propargilaminaren adizio nukleozalea. Horretarako, zenbait erreakzio baldintza frogatu ziren (**4.1. taula**)

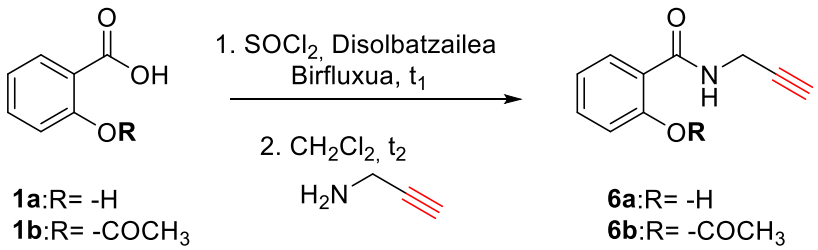

4.2. Eskema. Azido azetil salizlikoa eta azido salizilikoaren eraldaketa.

4.1. taula. Azido azetilsalizilikoaren eta azido salizilikoaren amidazio erreakziorako proposatutako erreakzio baldintza.

Sar.	R	$SOCl_2$ (bal.)	Propargilamina (bal.)	Disolb.	t_1 (h)	t_2 (h)	Produktua	Etekina (%)
1	-$COCH_3$	1	1	CH_2Cl_2	2	24	[c]	-
2	-$COCH_3$	1	1	CH_2Cl_2	12	24	[c]	-
3	-$COCH_3$	2	2	CH_2Cl_2	12	24	[c]	-
4	-$COCH_3$	2	2	CH_2Cl_2	24	24	[c],[d]	
5	-$COCH_3$	2	2	CH_2Cl_2	48	24	[c]	
6	-$COCH_3$	2	2	CH_2Cl_2	48	72	[c]	
7	-$COCH_3$	2	2	Toluenoa	4	24	[c},[d]	-
8	-$COCH_3$	1.5	1.5	Toluenoa	4	24	[c]	-
9	-$COCH_3$	1.5	1.5	Toluenoa	4	72	[c]	-
10	-$COCH_3$	1.5	1.5	Toluenoa	24	48	[c]	-
11	-$COCH_3$	3	3	Toluenoa	24	48	[c]	-
12	-$COCH_3$	3	3	Toluenoa	24	72	[c]	-
13	-$COCH_3$	5	5	Toluenoa	24	48	2a	81
14	-$COCH_3$	10	10	Toluenoa	24	48	2a	81
15	-H	5	5	Toluenoa	24	72	2a	64
16	-H	2.5	2.5	Toluenoa	24	72	2a	73

[c] hasierako erreaktiboaren lorpena [d] propargilaminaren aztarnak behatu ziren

4.1. taulan ikus daitekeen bezala, zenbait saiakuntza egin ondoren, lau esperimentu baino ez ziren arrakastatsuak izan. Lehenengo bost esperimentuetan, aspirina erreaktibo gisa erabili zen eta diklorometanoa disolbatzaile nagusia izan zen. Erreakzio denboran eta baliokidetasun molarrean zenbait aldaketa egin ondoren, ez zen lortu nahi zen produktua. Beraz, erreakzioaren lehenengo etaparen birfluxu tenperatura igotzea erabaki zen. Horretarako, irakite puntu altuagoa zuen disolbatzailea aukeratu zen, toluenoa hain zuen, zeina jadanik erabili zen beste

amidazio erreakzioetan. Berriro ere, zenbait aldaketa egin ziren erreakzio denboran eta erreaktiboen arteko baliokidetasunean, baina kasu honetan **6a** produktua eskuratu zen sarrera gehienetan propargilamina azpiprodukturu gisa. Soilik $SOCl_2$ eta propargilaminaren baliokidetasuna 5-ra aldatu zenean, erreakzioaren kobertsio totala eskuratu zen (**13. sarrera**). Hala ere, esan beharra dago produktu berdina, hots, 2-hidroxi-*N*-(prop-2-in-1-yl)bentzamida (**6a**) lortu zela bai azido azetilsalizilikoa edota azido salizilikoa erreaktibo gisa erabili zirenean. Izan ere, tionil kloruroak soberan izateak aspirinaren ester taldearen hidrolisia eragin zuen, propargilaminarekin funtzionalizatutako azido salizilikoaren deribatua lortuz. Erreakzio guztiak GFK-ren bidez jarraitu ziren eta lortutako emaitzak EMN-ren bidez analizatu ziren (**4.3 irudia**).

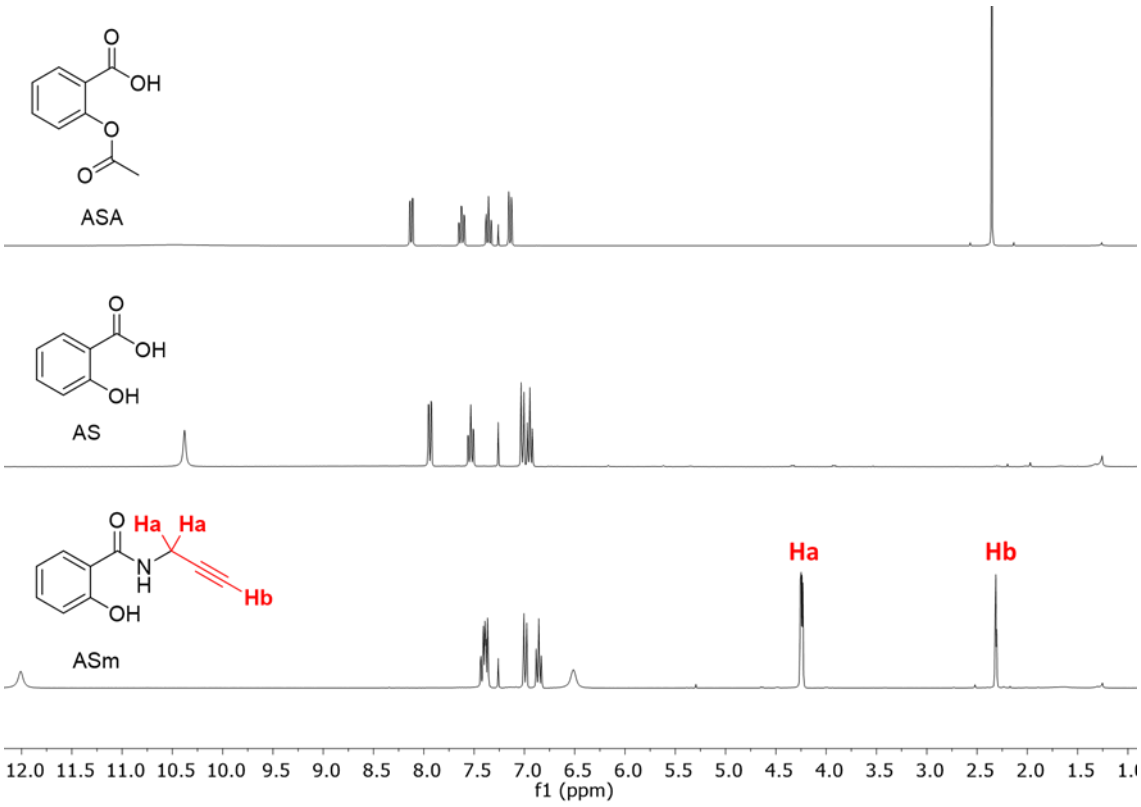

4.3. irudia. Azido azetil salizilikoa, azido salizilikoa eta **6a** deribatuaren EMN espektroak.

EMN bidez, azido salizilikoa eta azido azetilsalizilikoa 2-hidroxi-*N*-(prop-2-in-1-il)bentzamida bihurtu zirela ikusi zen, amidazio erreakzioa arrakastatsua izan zela ondorioztatuz. **4.2. irudian** ikus daitekeen bezala, lortutako produktuan hiru seinale

berri agertzen ziren; propargil funtzio taldeari zegozkion protoiak, hain zuzen ere. Izan ere, 2,32 ppm-ko lerrakuntza kimikoan protoi bat integratzen zuen hirukote bat nabarmentzen zen: propargil taldearen amaierako alkinoari dagokion hidrogenoa. Horretaz gain, 4.25 ppm-tan beste seinale bat ageri zen, bi hidrogeno integratzen zituena, metileno taldeari dagokiona. Azkenik, 6,54 ppm eta 12,00 ppm-tan bi seinale zabal ikus zitezkeen; amida eta hidroxilo taldeei zegozkien protoiak, hain zuzen. Emaitza horietatik ondorioztatzen da lortutako produktua, zehazki, 2-hidroxi-*N*-(prop-2-in-1- il)bentzamida (**6a**) dela.

FTIR analisiaren emaitzetan oinarrituz, berriro ere azido salizilikoan alkino taldea arrakastaz sartu zela frogatu zen (**4.4. irudia**).

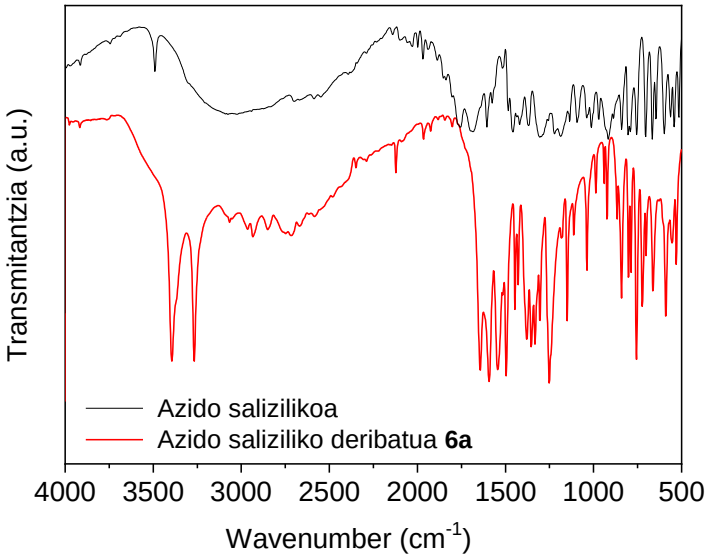

4.4. irudia. Azido salizilikoa eta azido saliziliko deribatuaren **6a** FTIR espektroak.

Bi konposatuen FTIR espektroek ezaugarri desberdinak adierazten zituzten. Bi espektroetan, OH loturari zegokion seinalea behatzen zen 3200 cm^{-1}-ean. Hala ere, azido salizilikoaren deribatura **6a**-ren kasuan, banda berrri bat agerian geratzen zen 3400 cm^{-1} inguruan, NH lotura bibrazioario zegokion seinalea hain zuzen. Bestetik, azido salizilikoaren espetroan, azido karboxilikoari zegokion C=O loturaren bibrazioa 1700 cm^{-1} ikusten zen bitartean, azido saliziliko deribatua **6a** espektroan, seinale horren eraldaketa behatzen zen. Amidazioaren ondoren, azido saliziliko deribatuaren 6a espektroa adierazte zuen C=O loturaren banda 1650 cm^{-1} uhin zenbakian, amida taldeari dagokion seinalea, hain zuzen. Izan ere, kasu horretan, amidaren karbonilo taldeak C=O lotura bibrazioa bi bandetan sakabanatu zen. Horretaz gain, C_{sp}-C_{sp} eta C_{sp}-H loturei dagozkion seinaleak behatzen ziren 2100 cm^{-1} eta 3300 cm^{-1} uhin

zenbakietan, hurrenez hurren. Emaitza hauek amidazio erreakzioaren berrespena konfirmatu egin zuten berriro ere.

4.3.1.2. Azido (3-bromopropil)fosfonikoaren sintesia

Aurretik komentatu bezala, fosfonato taldeetan oinarritutako SAM egonkorragoak dira degradazio hidrolitikoaren aurrean silizioan oinarritutako SAM baino. Hala ere, talde horiek gainazalera atxikitu aurretik, eraldaketa kimikoa jasan behar dute (**4.4. eskema**). Fosfonatoaren hidrolisiaren bidez azido fosfonikoa lortzen da, prozesu horretarako bi urratseko erreakzioa beharrezkoa izan zen. Nabarmentzekoa da bi urratsetan aldatutako aldagai bakarra erreakzio denbora izan zela, **4.2. taulan** ikus daitekeen moduan.

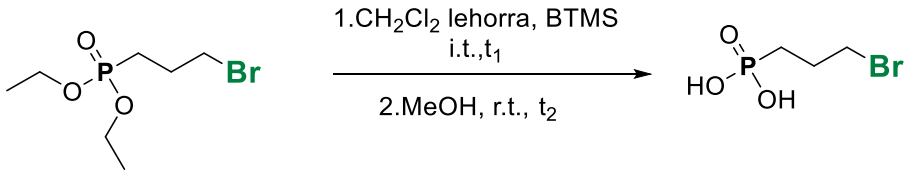

4.4. eskema. Azido (3-bromopropil)fosfonikoaren sintesia.

Zenbait erreakzio baldintza erabili izan ziren desiragarria zen produktua lortzeko, **4.2. taulan** laburbiltzen dira erabilitakoa baldintzak.

4.2. taula. Dietil (3-bromopropil)fosfonatoaren hidrolisi erreakzioaren baldintzak.

Sarrera	t_1 (h)	t_2 (h)	Etekina (%)
1	24	24	[a]
2	96	24	[a]
3	144	24	[a]
4	96	72	96

[a] azido (3-bromopropil)fosfonikoaren trazak aztertu ziren hasierako erreaktiboarekin

EMN-^{1}H eta EMN-^{31}Pren bidez hidrolisi erreakzioan lortutako produktua analizatu egin zen**, 4.5. eta 4.6. irudietan** ikus daitekeen moduan. Lehenengo hiru saiakuntzak ez zen produkturik lortu, nahiz eta erreakzio denbora 6 egunetara luzatu. Hala ere,

bigarren urratseko erreakzio denbora luzatzerakoan, erreakzioaren konbertsio totala lortu zen (**4. sarrera, 4.2. taula**).

EMN-^{31}P espektroaren bidez, dietil (3-bromopropil)fosfonatoaren hidrolisi erreakzioaren arrakasta egiaztatu zen. **4.5. irudian** dietil (3-bromopropil)fosfonatoaren eta azido (3-bromopropil)fosfonikoaren espektroak ikus daitezke. Fosfonato konposatuaren espektroak 30,3 ppm-tan fosforo taldeari dagokion seinal argia erakutsi zuen. Aldiz, hidrolisi prozesuaren ondoren, azido fosfoniko deribatuaren espektroan lerrakuntza kimiko baxuagotan, 26,2 ppm-tan, agertzen zen fosforo taldeari dagokion seinalea, emaitz hauek azido produktuaren formazioa iradokitzen dute.

EMN-^{1}H analisiek ere hidrolisi erreakzioaren arrakasta ziurtatu zuten. Izan ere, dietil (3-brmopropil)fosfonatoaren espektroan agertzen ziren bi seinale, etil taldeari dagozkion bi seinaleak hain zuzen, produktuaren espektroan desagertu ziren. Hau da, azido (3-bromopropil)fosfonikoaren espektroan ez diren etil taldeari dagozkion bi seinaleak antzematen. Horren ordez, 5,48 ppm-tan azido fosfonikoaren hidroxilo taldeari dagokion seina zabala eta bereizgarria behatzen zen. Esan beharra dago, seinale hauek literaturan azaltzen diren seinalekin bat egiten dutela. Beraz, emaitz hauek baieztatzen dute berriro ere nahi zen azido fosfonikoaren produktua lortu egin zela.

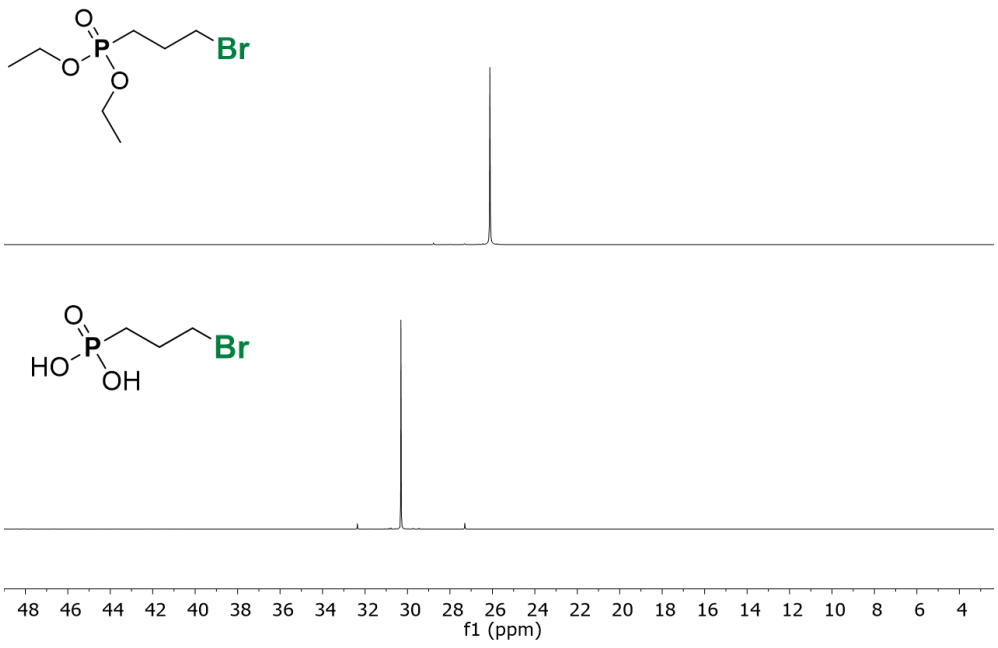

4.5. irudia. Dietill (3-bromopropil)fosfonatoaren eta azido (3-bromopropil)fosfonikoaren EMN-^{31}P espektroak.

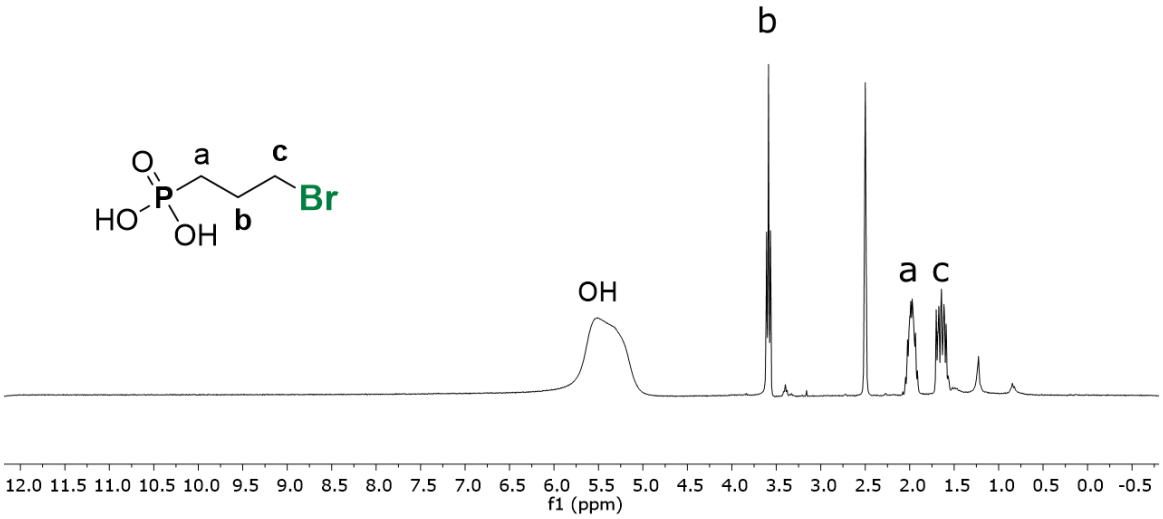

4.6. irudia. Dietill (3-bromopropil)fosfonatoaren eta azido (3-bromopropil)fosfonikoaren EMN-^{1}H espektroak.

Azido saliziliko deribatua immobilizatzeko beharrezkoak ziren erreaktibo guztiak sintetizatu ondoren, dansyl deribatua **2b**-ren eta azido salizilikoaren deribatu **6a**-ren immobilizazioak Ti6Al4V gainazalen burutu ziren.

4.3.2. Funtzionalizatutako gainazalen karakterizazio fisikokimikoa

Komentatu den bezala, berriro ere dansil fluoroaren erabilera proposatu zen bi SAM estrategietan metodoa baliozkotzeko. **4.5 eskeman** ikus daitekeen moduan, fluoroforoa beharrezkoa zen alkino taldearekin deribatizatu zen eta immobilizatu Ti6Al4V gainazalean CuAAC-ren bitartez.

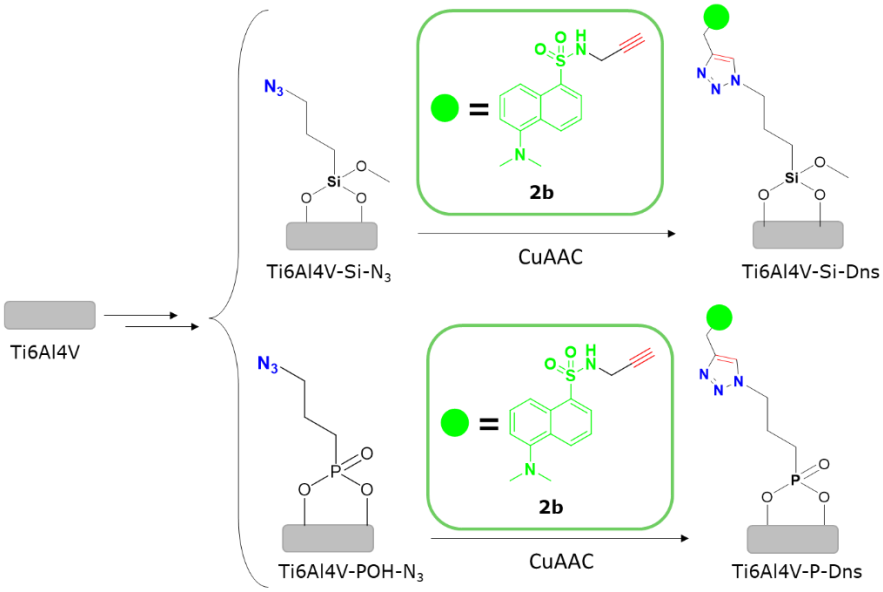

4.5. eskema. Dansil deribatu **2b**-ren immobilizazioa Ti6Al4V gainazalean CuAAC-ren bidez.

Ti6Al4V gainazalek lau funtzionalizazio-erreakzio desberdin pairatu zituzten: hidrolisia, silanizazioa edo fosforilazioa, azidazioa eta klik erreakzioa. Funtzionalizazio etapa bakoitzaren ostean lortutako gainazalen propietate fisiko kimikoa zenbait tekniken bidez analizatu ziren: XPS, SEM, fluoreszentzia eta kontaktu-angelua. Hurrengo atalean teknika horiekin lortutako emaitzak komentatuko dira.

4.3.2.1. Funtzionalizatutako Ti6Al4V eta funtzionalizatu gabeko Ti6Al4V-ren XPS eta epifluoreszentzia analisia

Funtzionalizazio etapa bakoitzaren osteko gainazalaren konposizio kimikoa XPS –ren bidez analizatu egin zen (**4.7 irudia**). Gainera, behatutako elementu bakoitzaren dekonboluzio espektroak burutu eta analizatu ziren, sortutako edo eliminatutako loturen determinazio zehatza lortzeko. **4.3. taulan** hurrengo laginen konposizio kimikoa zehazten da: funtzionalizatu gabeko Ti6Al4V, eta funtzionalizatutako Ti6Al4V-Si-Br, Ti6Al4V-OH, Ti6Al4V-Si-Br, Ti6Al4V-Si-N_3, Ti6Al4V-Si-Dns eta Ti6Al4V-Si-ASm.

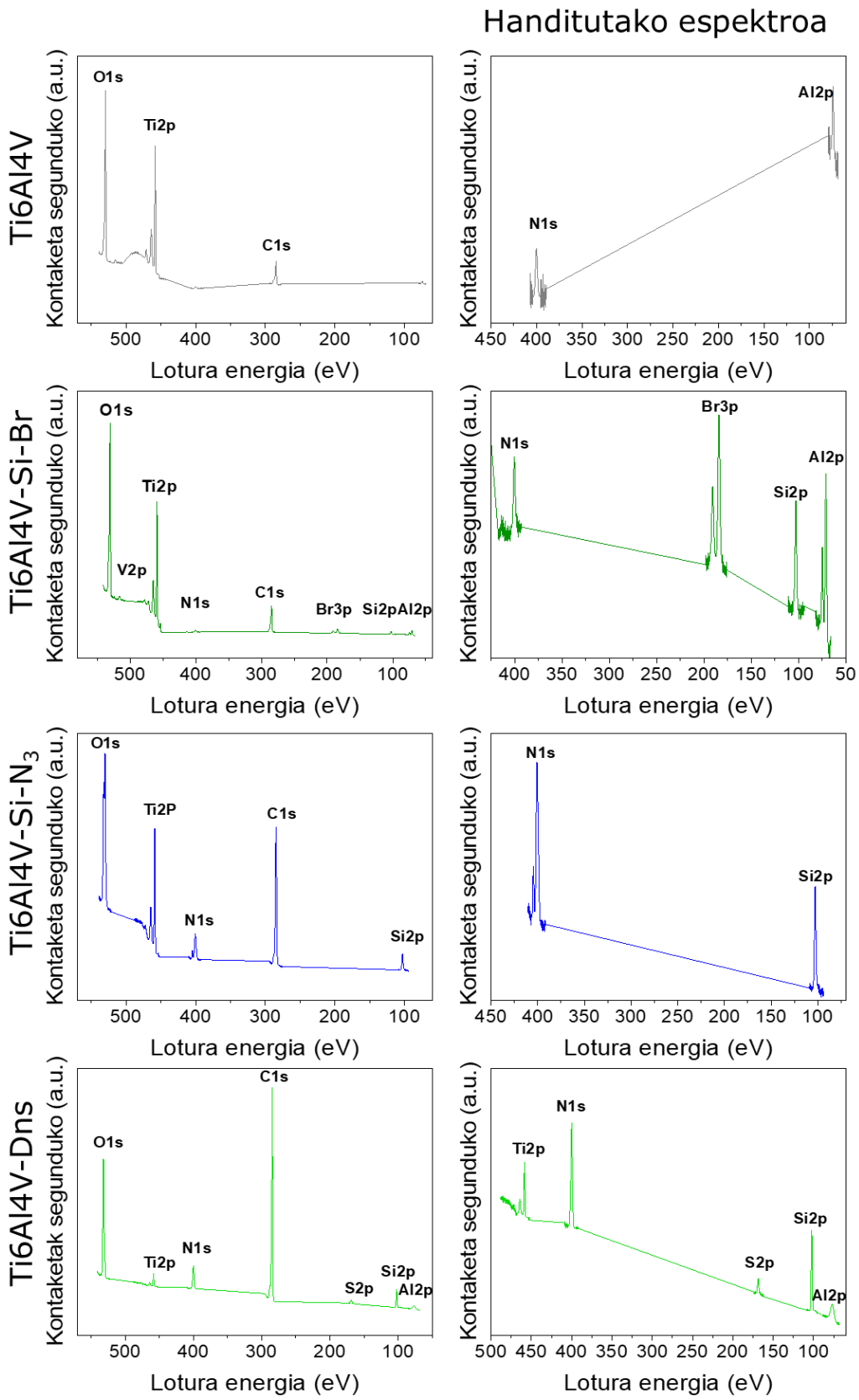

4.7. irudia. Ti6Al4V, Ti6Al4V-Si-Br, Ti6Al4V-Si-N_3 and Ti6Al4V-Si-Dns laginen XPS espektro totala.

4.3. taula. Funtzionalizatutako Ti6Al4V gainazalen konposizio kimiko atomikoa silanizazio prozesua jarraituz.

	Konposizio kimiko elementala (%)									
Lagina	**Ti**	**Al**	**V**	**C**	**O**	**N**	**Si**	**P**	**Br**	**S**
Ti6Al4V	7.9	1.6	1.9	11.9	74.5	1.1	-	-	-	-
Ti6Al4V-Si-Br	13.4	2.9	0.4	24.1	51.6	0.9	2.8	-	1.2	-
Ti6Al4V-Si-N_3	6.7	0.9	0.1	44.6	31.8	5.6	7.5	-	-	-
Ti6Al4V-Si-Dns	0.9	-	-	67.7	17.1	9.9	1.5	-	-	2.8

4.3 taulan ikus daitekeen moduan, funtzionalizaturik gabeko Ti6Al4V gainazalean, karbono eta oxigeno elementuak agertzen ziren nagusiki, titanio, aluminio eta banadioa konposizio horren joera jarraitzen zutelarik. Izan ere, laginak hutsean gorde izan arren, laginen manipulazioan edo garraioan egon ziitekeen kanpoko kontaminazioak karbono eta oxigenoaren gehiegizko kantitatearen agerpena azal dezake. Hala ere, elementu hauen portzentaia ez zen harritzekoa, fabrikatzaileek ezpurutasun txiki horiekin deskribatu baitzuten materiala, bai eta nitrogenoaren kontaminazioa ere. Gainera, espero bezala, titanio elementua kontzentrazio handiagoan agertu zen Al eta V metalekin alderatura.

Ti6Al4V-Si-Br gainazalari dagokionez, aurreko laginetan azaldutako elementuez gain, beste bi elementu berri agertu ziren, silizioa eta bromoa hain zuzen. Esan beharra dago, XPS teknikaren bidez ailegatzen den irradiazioa soilik gainazalaren nanometro batzuetara baino ez dela heltzen, eta eratutako SAM monogeruza zailtzen duela irradiazioa metal gainazalera heltzea. Horregatik, aluminio eta banadio bezalako elementuak kontzentrazio txikiagotan agertzen dira funtzionalizaturiko Ti6Al4V gainazaletan.

Bestalde, oxigenoaren kontzentrazioa murriztu egin zen eta karbonoarena, berriz, handitu. Izan ere, 3-bromopropilsilanoa konposatu karbonoduna denez, logikoa da karbono gehiago agertzea analisian. Horretaz gain, emaitza horiek silanizazioaren arrakasta ziurtatzen zuten.

Gainazalaren silanizazioaren ondoren, S_N2 erreakzioaren bidez bromo taldea azida taldearekin ordezkatu zen, sodio azida erabiliz. Kasu honetan, ikusi zen bromoa desagertu zela eta nitrogeno edukia handitu egin zela.

Dekonboluzioaren bidez, gainazal bakoitzean agertzen ziren espezieak determinatu egin ziren. Lehenengo eta behin, eraldatu gabeko Ti6Al4V gainazala aztertu egin zen (**4.8. irudia**).

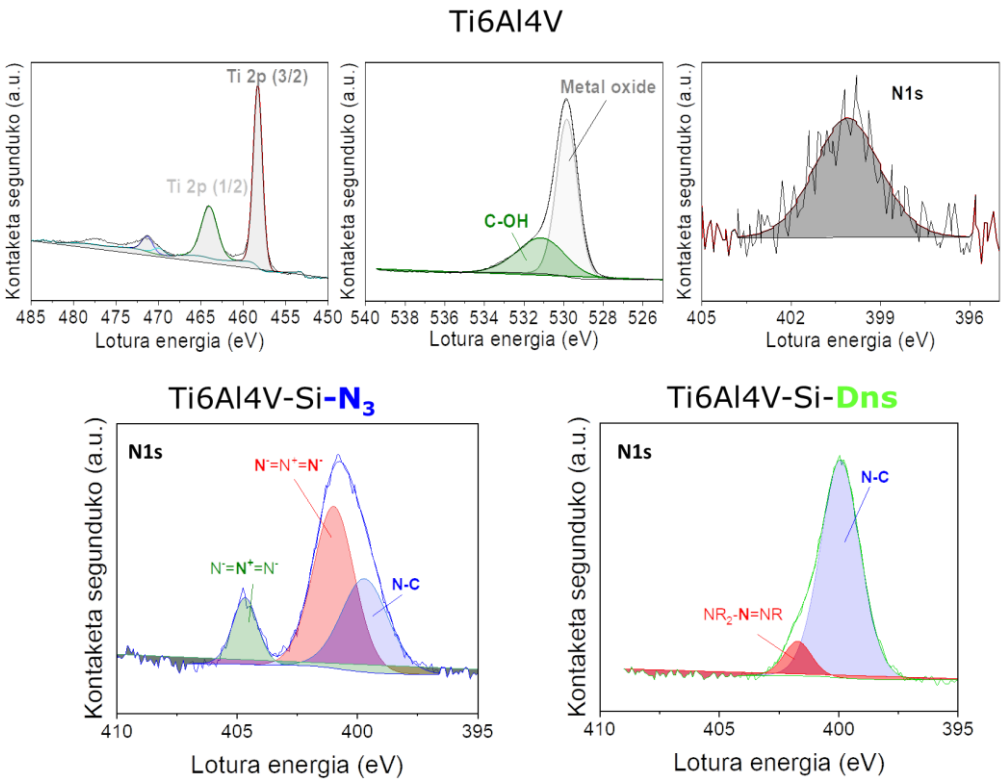

4.8. Irudia. Eraldatu gabeko Ti6Al4V gainazalean agertzen diren Ti, O eta N dekonboluzio XPS espektroak, Ti6Al4V-Si-N_3 eta Ti6Al4V-Si-Dns gainazalen N XPS dekonboluzio espektroa.

4.8. irudian ikus daitekeen moduan, karbono eta oxigeno espezieak eraldatu gabeko Ti6Al4V gainazalaren pasibazioa konfirmatu zuten. Hala ere, karbonoaren espektroan agertzen diren espezie gehienak C_{sp3}-ri dagokion konposatuak dira, hau da, karbono lotura bakunak egiten dituzten espezieak, beraz informazio hau bat dator fabrikatzaileek deskribatzen duten laginen konposizioarekin.

Espero zitekeen bezala, hidrolisi erreakzioaren ondoren metal-OH espezie hidroxilatuak ikusi ziren, eta eraldatu gabeko gainazaletan baino kontzentrazio handiagoan ageri ziren, gainazalaren pasibazioa mugatzen baitute. Behin gainazala aktibatu zenean, hurrengo funtzionalizazio erreakzioak egin ziren. Silanizazio erreakzioaren ondoren, Ti6Al4V-Si-Br gainazalek eta Ti6Al4V-Si-N_3 gainazalek antzeko espezie konposizioa zuten, eta aberatsak ziren C, O, Ti, Al eta Si elementuetan. Alde bakarra bromo eta nitrogeno elementuen espektroetan ikusi zen. Gainera, ustekabeko espezieak agertu ziren nitrogeno espektroan. Izan ere, XPS teknikan, X izpien irradiazioak azida taldea (-$N=N^+=N^-$) deskonposatu zuen, eta soilik N_2 and N^- espezieak ageri ziren espektroetan (**4.8. irudia**) [41].

Antzeko emaitzak lortu ziren Ti6Al4V gainazalak azido fosfoniko deribatuarekin funtzionalizatu zirenean (**4.2. eskema**). Lagin bakoitzaren analisi elemental **4.4. taulan** beha daiteke. **4.9. irudian** ikus daitekeen moduan, fosforilazioaren ondoren, bi seinale behatu ziren, S2p eta Br2p 164 eV eta 180 eV-etan, hurrenez hurren. Emaitza horiek konfirmatzen dute azido (3-bromopropil)fosfonikoa Ti6Al4V gainazalera ainguratu zela. Silanoan oinarritutako metodologiaren bezala, fosforilazioaren ostean bromooaren ordezkapena azida taldearekin eman zen. XPS-ren bidez ordezkapen hori behatu egin zen Ti6Al4V-P-N_3 gainazaletan. Izan ere, bromoaren seinalea desagertzeaz gain, nitrogenoaren edukia handitu zen. Gainera, nitrogenoaren dekonboluzio espektroak azida taldearen presentzia konfirmatu zuen.

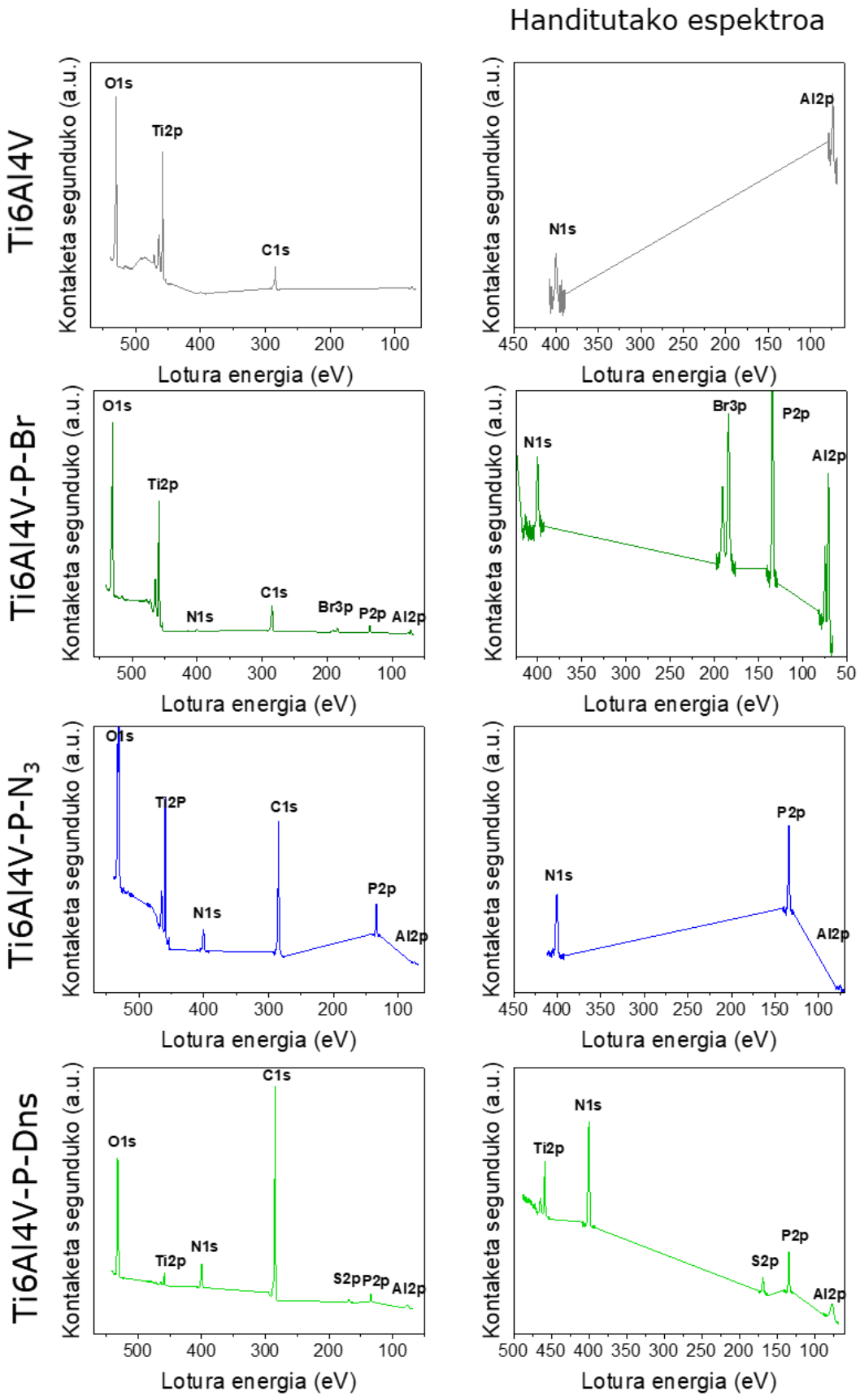

4.9. irudia. Eraldatu gabeko Ti6Al4V laginaren eta Ti6Al4V-POH-Br laginaren O dekonboluzio XPS spectra.

4.4 Taula. Ti6Al4V gainazalen konposizio kimiko atomikoa fosforilazioa prozesua jarraituz.

	Konposizio atomikoa (%)									
Lagina	**Ti**	**Al**	**V**	**C**	**O**	**N**	**Si**	**P**	**Br**	**S**
Ti6Al4V	7.9	1.6	1.9	11.9	74.5	1.1	-	-	-	-
Ti6Al4V-POH-Br	16.3	1.3	0.4	15.0	59.4	0.6	0.8	3.8	1.6	-
Ti6Al4V-POH-N_3	12.6	1.4	0.4	21.9	46.0	1.7	0.5	1.7	-	-
Ti6Al4V-POH-Dns	1.2	-	-	43.1	12.8	2.3	0.5	0.9	-	1.8

Esan bezala, karbono eta oxigeno espezieak kontzentrazio handiagoan aurkezten dira eraldatu gabeko Ti6Al4V gainazalean, Ti, Al edo V-rekin konparatuz. Hala ere, silanoarekin konparatuta, funtzionalizazio etapen ondoren espezie berriak agertu arren, titanio elementuaren kontzentrazioa nahiko konstante mantentzen da.

Horretaz gain, eraldatu gabeko Ti6Al4V, Ti6Al4V-Si-Dns eta Ti6Al4V-P-Dns gainazalak mikroskopia fluoreszentearen bidez xeheki analizatu ziren dansil fluoroforoaren immobilizazioa baieztatzeko. **2.10 irudian** adierazten den moduan, gainazalek 305 nm-ko uhinluzeran kitxikatu ondoren, soilik Ti6Al4V-Si-Dns eta Ti6Al4V-P-Dns gainazalek, dansil konpsatuari dagokion berde koloredun argia emititu zuten. Emaitza horiek berriro ere konfirmatu zuen dansil deribatu **2b**-ren immobilizazioa Ti6Al4V gainazaletan.

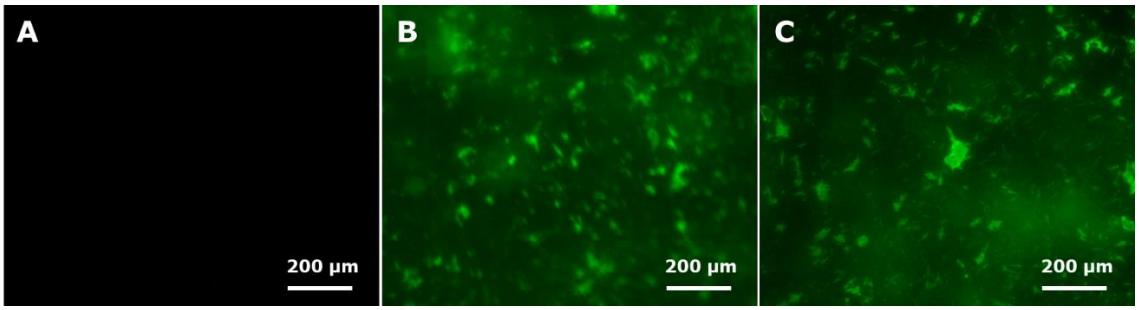

2.10. irudia. (A) eraldatu gabeko Ti6Al4V gainzala, (B)Ti6Al4V-Si-Dns eta (C) Ti6Al4V-P-Dns gainazalaren emisio fluoreszentea.

4.3.2.2. Funtzionalizaturik gabeko eta funtzionalizatutako Ti6Al4V laginen SEM eta angelu kontaktuaren analisia

Dansil deribatu **2b**-ren immobilizazio arrakastatsua Ti6Al4V gainazalean burutu ondoren, metodologia berdina erabiltzea proposatu genuen azido salizilikoaren deribatu **6a**-ren biokonjugaziorako (**4.6. eskema**). Lana hobeto ulertzeko, azido

salizilikoaren deribatu **6a**-ren SEM eta kontaktu angeluekin batera lortutako dansil deribatu **2b**-ren emaitzak komentatu egingo dira.

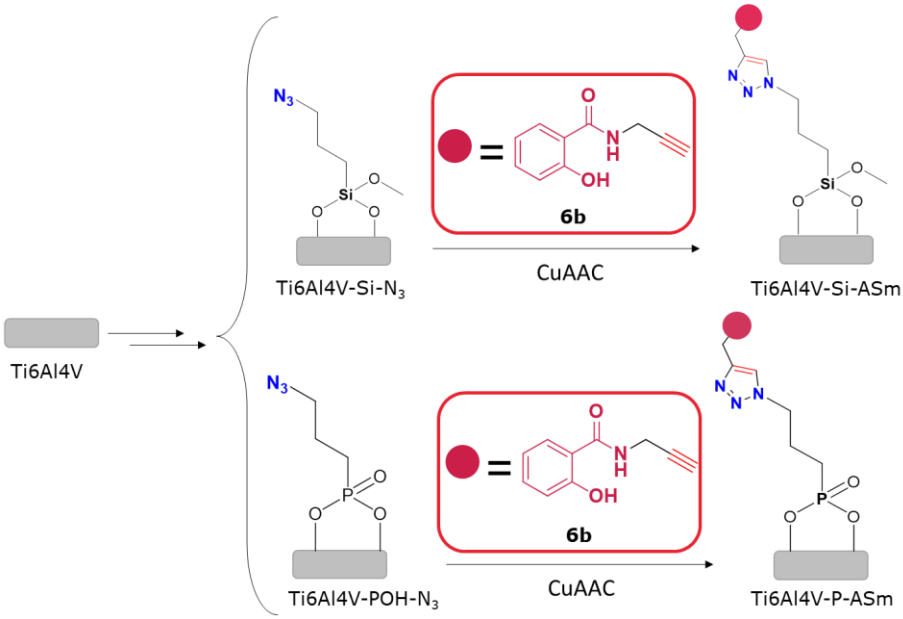

4.6. eskema. Azido saliziliko deribatu **6a**-ren immobilizazioa funtzionalizaturiko Ti6Al4V gainazaleetan.

4.11. irudian eta **4.12. irudian** ikus daiteken bezala, eraldatu gabeko Ti6Al4V laginek gainazal lau eta leuna zuten. Hidrolisi erreakzioaren ondren, gainazal apurketak behatu ziren Ti6Al4V-OH gainazaletan. Hain zuzen ere, aurkikuntza horiek ez dira harrigarriak, erabilitako hidrolisi baldintzak nahiko gogorrak direla kontuan hartuta (H_2SO_4/H_2O_2, piraina disoluzioa), normala da gainazalaren degradazio partziala eragitea. Silanoaren eta fosfonatoren inguraketa bakoitzaren ondoren, topografia nabarmen aldatu egin zen. Ti6Al4V-Si-Br eta Ti6Al4V-P-Br gainazalek zenbait protrusio txiki izan zituzten, gandor eta haran handiekin. Izan ere, topografia konplexua iradokitzen zuten, nabarmenagoa izanik silanoaren kasuan. Bromo taldearen ordezkapena azida taldearekin ez zuen eragin aldaketa nabarmenik gainazaletan. Bestalde, dansil deribatu **2b** eta azido saliziliko deribatu **6a** immobilizatu ostean, gainazalak zimurtsuagoak bilakatu ziren, batez ere fosfonato gainazalen kasuan. Izan ere, Ti6Al4V-P-Dns eta Ti6Al4V-P-ASm gainazalek pikor kristalino batzuk aurkeztu zituzten, banatuagoak azido saliziliko deribatu **6a**-ren kasuan.

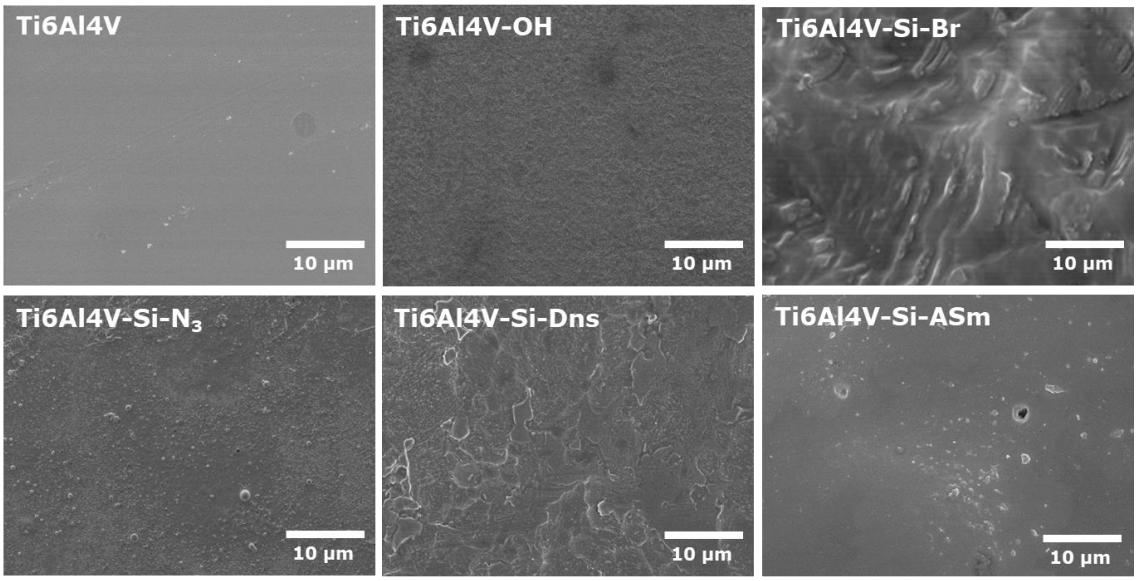

4.11. Irudia.Ti6Al4V lagin desberdinen SEM irudiak: pristine Ti6Al4V, Ti6Al4V-OH, Ti6Al4V-Si-Br, Ti6Al4V-Si-N_3, TI6Al4V-Si-Dns eta Ti6Al4V-Si-ASm

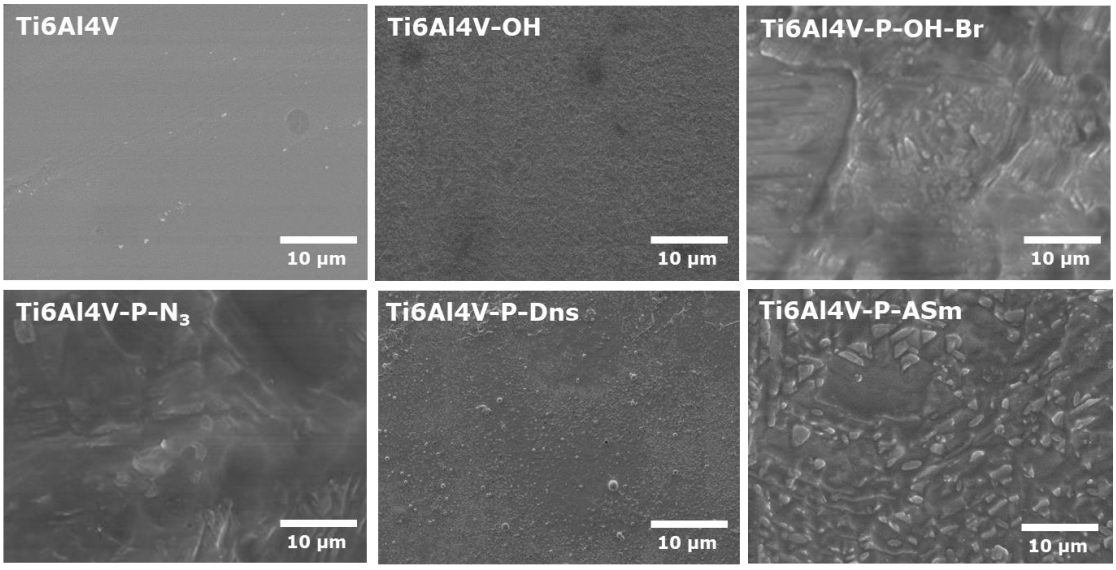

4.12. Irudia.Ti6Al4V lagin desberdinen SEM irudiak: pristine Ti6Al4V, Ti6Al4V-OH, Ti6Al4V-P(OH)-Br, Ti6Al4V-P-N_3, TI6Al4V-P-Dns eta Ti6Al4V-P-ASm

Funtzionalizazio etapa bakoitzaren ondoren jasandako hidrofilitate aldaketa kontaktu angelua teknikaren bidez aztertu zen (**4.13. irudia eta 4.14. irudia**). Ikus daitekeenez, eraldatu gabeko Ti6Al4V laginaren ur kontaktu angeluaren balioa 111º izan zen. Izan ere, aleazio metaliko horrek ez du funtzio talde aktiborik gainazalean, eta horren ondorioz nahiko hidrofoboa denez, gainazalaren funtzionalizazioa zaildu egiten da. Beste kapituluetan komentatu den bezala, gainazal polimerikoek eta

metalikoek aurreko aktibazioa eskatzen dute, eta hidrolisi edo oxidazio erreakzioak erabili ohi dira horretarako. Kasu honetan, piraina disoluzioa erabili zen Ti6Al4V laginaren gainazalean hidroxilo taldeak eratu ahal izateko. Hidrolisi erreakzioaren ostean, gainazala oso hidrofiliko bihurtu zen, kontaktu angeluaren balioa zerotik hurbil baitzegoen, eta sistemak ez zuen balio neurgarririk adierazten. Kontaktu angeluan izandako aldaketa bortitz horiek berretsi egin zuten talde polarren (-OH, hain zuzen) presentzia; izan ere, talde horiek hidrogeno loturak egin ditzakete urarekin.

Behin Ti6Al4V laginen gainazalak aktibatu ondoren, SAM erreakzioen bidez funtzionalizatu egin ziren, hau da, beharrezkoak ziren silizio edo fosforo taldeak atxikitu ziren monogeruza eratuz. Silano eta fosfonato monogeruza eratu ondoen, bai Ti6Al4V-Si-Br eta Ti6Al4V-POH-Br gainazalak kontaktu angelu antzekoa erakutsi zuten, hala ere kontaktu angeluaren balioa izugarri handitu egin zen hidrolizatutako gainazalekin konparatuz, 112º eta 92º balioetara igo zen, hurrenez hurren. Izan ere, gainazal hauetan H-loturarik egin ezin duten karbonodun kateak itsatsi baitziren. Azida talde funtzionala sartu ondoren, kontaktu angeluaren balioak aldaketa berriak adierazi zituen silanizatutako eta fosforilatutako gainazaletan. Zehazki, silanizautako gainazaletan angeluaren balioa 98º -ra murriztu egin zen bitartean, fosforilatutako gainazailetan 102º-tara heldu zen. Nolanahi ere, XPS eta SEM tekniken emaitzekin batera, bromo taldearen eraldaketa azida taldean berretsi egin zen. Azkenik, CuAAC-ren bidez dansil deribatua **2b** eta azido salizilikoaren deribatua **6a** eraldatutako Ti6Al4V gainazaletan immobilizatu ondoren, kontaktu angeluaren balioak murriztu egin ziren bai silano eta bai fosfonatoren bidez jarraitutako estrategietan. Hain zen, silanizatutako gainazalek 92º eta 90º angelu balioa erakutsi zuten dansil deribatua **2b** eta azido salizilikoaren deribatua **6a** immoilizatu ondoren. Aldiz, 98º eta 75º angeluak lortu ziren fosfonato taldea atxikitutako gainazaletan. Kontaktu angeluaren balioan izandako aldaketak nabariagoak izan ziren fosfonatodun gainazaletan, silanoekin konparatuz, baina aldi berean lortutako gainazalak heterogeneagoak ziren. Berriro ere, lortutako emaitza horiek berretsi egin zuten bai fluoroforoaren bai eraldatutako farmakoaren immobilizazioa Ti6Al4V gainazaletan, kobrez katalizaturiko azida eta alkinoen arteko erreakzioaren bidez.

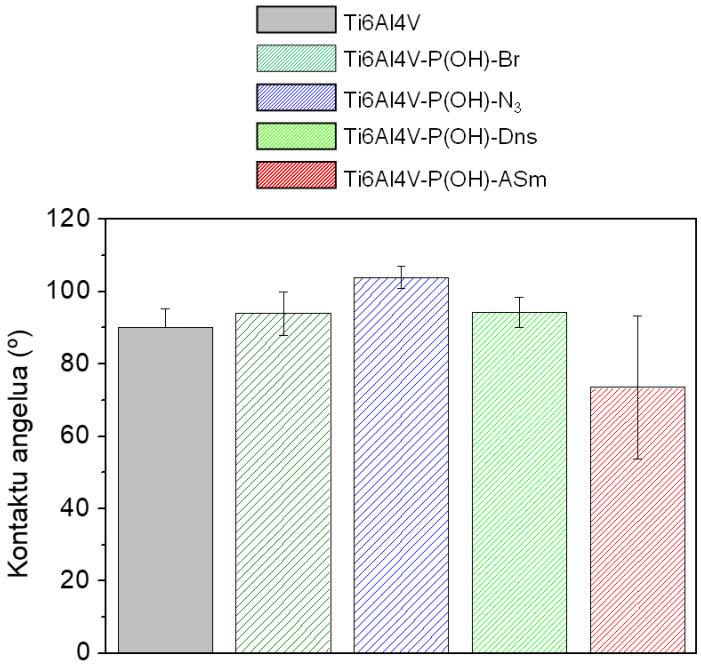

4.13. irudia. Eraldatu gabeko Ti6Al4V laginen eta funtzionalizatuako Ti6Al4V laginen kontaktu-angelua.

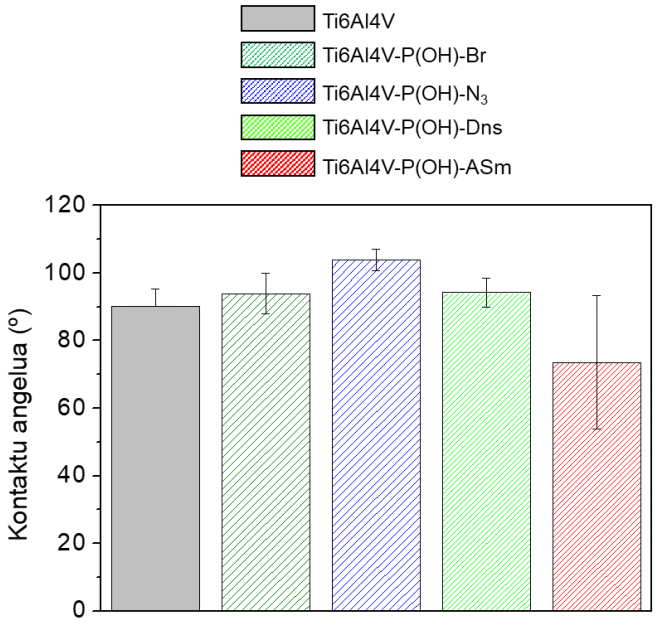

4.14. irudia. Eraldatu gabeko Ti6Al4V laginen eta funtzionalizatuako Ti6Al4V laginen kontaktu-angelua.

4.3. Ondorioak

Kapitulu honetan, SAM estrategiaren eta Klik Kimikaren arteko konbinazioa deskribatu egin da. Bi estrategiak gainazalen funtzionalizazio kobalente eta iraunkorrera bideratzen dira. Horrretako, gainazala hidrolisi azidoaren bidez aktibatu egin zen eta, ondoren, komertzialak diren silano eta fosfonato monomeroak ainguratu ainguratu ziren gainazalara. Kasu honetan, azido salizilikoaren deribauitua immobilizatu zen. Kapitulu guztietan gertatu den moduan, fluoroforo bat erabili da proposatutako metodologia berrespena izateko. XPS teknikaren bidez berretsi zen dansil deribatuaren **2b**-ren immobilizazioa, izan ere N eta S elementuak behatu ziren silano eta fosfonato SAMetan. Fluoreszentzia analisiek dansiloari dagokion kolore berdeko argiaren emisioa erakutsi zuten. SEM-aren bidez eta kontaktu angeluaren bidez behatutako topografia eta bustigarritasun aldaketek ere frogatu uten dansil deribatu **2b**-ren immobilizazioa. Bestalde, azido saliziliko deribatuaren **6a** biokonjugazioa kontaktu angeluaren eta SEM tekniken bidez berretsi zen, aukeratutako metodologiaren eraginkortasuna frogatuz.

4.4. Bibliografia

1. INE *Defunciones según la Causa de Muerte Año 2018*; 2019; Vol. 2018;.
2. INE Defunciones según la Causa de Muerte Año 2021 (datos definitivos) y primer semestre 2022 (datos provisionales). *Notas de prensa* **2021**, *2021*, 19.
3. Intituto Nacional de Estadística *Defunciones según la causa de muerte - año 2022 (datos provisionales)*; 2023; Vol. 2022;.
4. Quint, C.; Arief, M.; Muto, A.; Dardik, A.; Niklason, L.E. Allogeneic human tissue-engineered blood vessel. *J. Vasc. Surg.* **2012**, *55*, 790–798, doi:10.1016/j.jvs.2011.07.098.
5. Sapirstein, W.; Alpert, S.; Callahan, T.J. The role of clinical trials in the food and drug administration approval process for cardiovascular devices. *Circulation* **1994**, *89*, 1900–1902, doi:10.1161/01.CIR.89.4.1900.
6. Martin, D.M.; Boyle, F.J. Drug-eluting stents for coronary artery disease: A review. *Med. Eng. Phys.* **2011**, *33*, 148–163, doi:10.1016/j.medengphy.2010.10.009.
7. Boccafoschi, F.; Fusaro, L.; Cannas, M. Immobilization of peptides on cardiovascular stent. In *Functionalised Cardiovascular Stents*; Elsevier Ltd., 2017; pp. 305–318 ISBN 9780081004968.
8. Meyers, S.R.; Grinstaff, M.W. Biocompatible and bioactive surface

modifications for prolonged in vivo efficacy. *Chem. Rev.* **2012**, *112*, 1615–1632, doi:10.1021/cr2000916.

9. Jaffer, I.H.; Weitz, J.I. The blood compatibility challenge . Part 1 : Blood-contacting medical devices : The scope of the problem. *Acta Biomater.* **2019**, *94*, 2–10, doi:10.1016/j.actbio.2019.06.021.

10. Butruk-Raszeja, B.A.; Dresler, M.S.; Kuźmińska, A.; Ciach, T. Endothelialization of polyurethanes: Surface silanization and immobilization of REDV peptide. *Colloids Surfaces B Biointerfaces* **2016**, *144*, 335–343, doi:10.1016/j.colsurfb.2016.04.017.

11. Irena Gotman, P.D. Characteristics of Metals Used in Implants. *J. Endourol.* **1997**, *11*, 383–389.

12. Li, Y.; Yang, C.; Zhao, H.; Qu, S.; Li, X.; Li, Y. New developments of ti-based alloys for biomedical applications. *Materials (Basel).* **2014**, *7*, 1709–1800, doi:10.3390/ma7031709.

13. Sidambe, A.T. Biocompatibility of advanced manufactured titanium implants-A review. *Materials (Basel).* **2014**, *7*, 8168–8188, doi:10.3390/ma7128168.

14. Manivasagam, V.K.; Sabino, R.M.; Kantam, P.; Popat, K.C. Surface modification strategies to improve titanium hemocompatibility: A comprehensive review. *Mater. Adv.* **2021**, *2*, 5824–5842, doi:10.1039/d1ma00367d.

15. Sánchez-Bodón, J.; Diaz-Galbarriatu, M.; Pérez-Álvarez, L.; Moreno-Benítez, I.; Vilas-Vilela, J.L. Strategies to Enhance Biomedical Device Performance and Safety : A Comprehensive Review. *Coatings* **2023**, *13*, 1981–2005, doi:https://www.mdpi.com/2079-6412/13/12/1981/review_report.

16. Sánchez-Bodón, J.; Andrade-Del Olmo, J.; Alonso, J.M.; Moreno-Benítez, I.; Vilas-Vilela, J.L.; Pérez-Alvarez, L. Bioactive Coatings on Titanium: A Review on Hydroxylation, Self-Assembled Monolayers (SAMs) and Surface Modification Strategies. *Polymers (Basel).* **2022**, *14*, 165.

17. Hähner, G.; Hofer, R.; Klingenfuss, I. Order and orientation in self-assembled long chain alkanephosphate monolayers adsorbed on metal oxide surfaces. *Langmuir* **2001**, *17*, 7047–7052, doi:10.1021/la010713a.

18. Cichomski, M.; Prowizor, M.; Kowalczyk, D.A.; Sikora, A.; Batory, D.; Dudek, M. Comparison of the physicochemical properties of carboxylic and phosphonic acid self-assembled monolayers created on a ti-6al-4v substrate. *Materials (Basel).* **2020**, *13*, 1–17, doi:10.3390/ma13225137.

19. Hasan, A.; Pandey, L.M. *Self-assembled monolayers in biomaterials*; Elsevier Ltd., 2018; ISBN 9780081007167.

20. Faucheux, N.; Schweiss, R.; Lützow, K.; Werner, C.; Groth, T. Self-assembled monolayers with different terminating groups as model substrates for cell adhesion studies. *Biomaterials* **2004**, *25*, 2721–2730, doi:10.1016/j.biomaterials.2003.09.069.

21. Freitas, S.C.; Correa-Uribe, A.; Martins, M.C.L.; Pelaez-Vargas, A. Self-Assembled Monolayers for Dental Implants. *Int. J. Dent.* **2018**, *2018*, doi:10.1155/2018/4395460.

22. Casalini, S.; Bortolotti, C.A.; Leonardi, F.; Biscarini, F. Self-assembled monolayers in organic electronics. *Chem. Soc. Rev.* **2017**, *46*, 40–71, doi:10.1039/c6cs00509h.

23. Nicosia, C.; Huskens, J. Reactive self-assembled monolayers: From surface functionalization to gradient formation. *Mater. Horizons* **2014**, *1*, 32–45, doi:10.1039/c3mh00046j.

24. Senna, P.M.; Mourão, C.F. de A.B.; Mello-Machado, R.C.; Javid, K.; Montemezzi, P.; Cury, A.A.D.B.; Meirelles, L. Silane-coating strategy for titanium functionalization does not impair osteogenesis in vivo. *Materials (Basel).* **2021**, *14*, 1–9, doi:10.3390/ma14071814.

25. Zhou, L.; Xing, Y.; Ou, Y.; Ding, J.; Han, Y.; Chen, J. Prolonged release of an antimicrobial peptide GL13K-loaded thermosensitive hydrogel on a titanium surface improves its antibacterial and. *RSC Adv.* **2023**, *13*, 23308–23319, doi:10.1039/d3ra03414c.

26. Han, X.; Sun, X.; He, T.; Sun, S. Formation of highly stable self-assembled alkyl phosphonic acid monolayers for the functionalization of titanium surfaces and protein patterning. *Langmuir* **2015**, *31*, 140–148, doi:10.1021/la504644q.

27. Silverman, B.M.; Wieghaus, K.A.; Schwartz, J. Comparative properties of siloxane vs phosphonate monolayers on a key titanium alloy. *Langmuir* **2005**, *21*, 225–228, doi:10.1021/la0482271.

28. Lan, W.C.; Huang, T. Sen; Cho, Y.C.; Huang, Y.T.; Walinski, C.J.; Chiang, P.C.; Rusilin, M.; Pai, F.T.; Huang, C.C.; Huang, M.S. The potential of a nanostructured titanium oxide layer with self-assembled monolayers for biomedical applications: Surface properties and biomechanical behaviors. *Appl. Sci.* **2020**, *10*, doi:10.3390/app10020590.

29. Kolb, H.C.; Finn, M.G.; Sharpless, K.B. Click Chemistry : Diverse Chemical Function from a Few Good Reactions. *Angew. Chemie - Int. Ed.* **2001**, *40*, 2004–2021.

30. Lutz, J. 1 , 3-Dipolar Cycloadditions of Azides and Alkynes : A Universal Ligation Tool in Polymer and Materials Science. *Angew. Chemie - Int. Ed.* **2007**, *46*, 1018–1025, doi:10.1002/anie.200604050.

31. Binder, W.; Kluger, C. Azide/Alkyne-“Click” Reactions: Applications in Material Science and Organic Synthesis. *Curr. Org. Chem.* **2006**, *10*, 1791–1815, doi:10.2174/138527206778249838.

32. Rostovtsev, V. V; Green, L.G.; Fokin, V. V; Sharpless, K.B. A Stepwise Huisgen Cycloaddition Process : Copper (i) -Catalyzed Regioselective ™ Ligation ∫ of Azides and Terminal Alkynes **. *Angew. Chemie - Int. Ed.* **2002**, *41*, 2596–2599.

33. Kaur, J.; Saxena, M.; Rishi, N. An Overview of Recent Advances in Biomedical Applications of Click Chemistry. *Bioconjug. Chem.* **2021**, *32*, 1455–1471, doi:10.1021/acs.bioconjchem.1c00247.

34. Stump, B. Click Bioconjugation: Modifying Proteins Using Click-Like Chemistry. *ChemBioChem* **2022**, *23*, 1–9, doi:10.1002/cbic.202200016.

35. Jin, J.B.; Cai, B.; Zhou, J.M. *Salicylic acid*; Jiayang Li, Chuanyou Li and Steven Smith, 2017; ISBN 9780128115633.

36. Fijałkowski, Ł.; Skubiszewska, M.; Grześk, G.; Koech, F.K.; Nowaczyk, A. Acetylsalicylic Acid–Primus Inter Pares in Pharmacology. *Molecules* **2022**, *27*, doi:10.3390/molecules27238412.

37. Xu, X.M.; Sansores-Garcia, L.; Chen, X.M.; Matijevic-Aleksic, N.; Du, M.; Wu, K.K. Suppression of inducible cyclooxygenase 2 gene transcription by aspirin and sodium salicylate. *Proc. Natl. Acad. Sci. U. S. A.* **1999**, *96*, 5292–5297, doi:10.1073/pnas.96.9.5292.

38. Kim, J.; Kang, S.; Hong, S.; Yum, S.; Kim, Y.M.; Jung, Y. Structure-activity relationship of salicylic acid derivatives on inhibition of TNF-α dependent NFκB activity: Implication on anti-inflammatory effect of N-(5-chlorosalicyloyl)phenethylamine against experimental colitis. *Eur. J. Med. Chem.* **2012**, *48*, 36–44, doi:10.1016/j.ejmech.2011.11.030.

39. Liu, P.; Domingue, E.; Ayers, D.C.; Song, J. Modification of Ti6Al4V substrates with well-defined zwitterionic polysulfobetaine brushes for improved surface mineralization. *ACS Appl. Mater. Interfaces* **2014**, *6*, 7141–7152,

doi:10.1021/am501967y.

40. Wang, L.; Schubert, U.S.; Hoeppener, S. Surface chemical reactions on self-assembled silane based monolayers. *Chem. Soc. Rev.* **2021**, *50*, 6507–6540, doi:10.1039/d0cs01220c.

41. Gouget-Laemmel, A.C.; Yang, J.; Lodhi, M.A.; Siriwardena, A.; Aureau, D.; Boukherroub, R.; Chazalviel, J.N.; Ozanam, F.; Szunerits, S. Functionalization of azide-terminated silicon surfaces with glycans using click chemistry: XPS and FTIR study. *J. Phys. Chem. C* **2013**, *117*, 368–375, doi:10.1021/jp309866d.

5. KAPITULUA

ONDORIOAK ETA ETORKIZUNEKO LANA

Kapitulu honetan, *1. Kapituluan* azaldutako helburuen arabera tesitik ateratako ondorio orokorrak aurkezten dira. Horretaz gain, etorkizuneko ikerketarako aproposak diren lanak proposatzen dira.

5. KAPITULUA

ONDORIOAK ETA ETORKIZUNEKO LANA

5.1. ONDORIOAK

Doktorego tesi honetan lortutako ematzeetatik ondorio hauek atera dira:

- Doktorego tesi honek klik erreakzioen moldakortasuna frogatu egin du farmako desberdin biokongujatuz gainazal polimeriko eta metalikoren gainean.

- CuAAC klik erreakzioen erabilerak indometazinaren biokonjugazioa erraztu du PLLAn, kurkumina PETan eta aspirina Ti6Al4V gainazalean, farmako eta gainazalen aldez aurreko eraldaketen ondoren.

- Nukleozaleak diren amino talde funtzional nahikoak dituen edozein farmako biokonjugatu daiteke katalizatzailerik gabeko amino-ino erreakzioa erabiliz.

- Edozein farmakoren biokonjugazioa eman baino lehen, oso garrantzitsua da farmako bakoitzaren Egitura-Jarduera Erlazioaren (SAR) azterketa zehatza egitea, immobilizazioak farmakoaren bioaktibitatean eragin ez dezan.

- Proposatutako metodologiaren eraginkortasuna frogatu egin da inplanteen errefusaren minimizazioan. Izan ere, *in vitro* egindako entsegu biologikoek xeheki erakutsi dute eraldatutako gainazaleek, bateragarritasuna hobetzeaz gain, ezaugarri antiinflamatorioa, antikoagulatzailea eta bakterioen aurkako propietate nabarmenak dituztela.

6.2. ETORKIZUNEKO LANA

Doktorego tesi honek farmakoak immobilizatzeko gainaza polimeriko eta metalikoetan Klik Kimikan oinarritutako estrategia berritzaileak aurkeztu izan ditu, etorkizun handiko aplikazio biomedikoak erakutsiz. Nabarmentzekoa baita antiinflamatorioa, antibiotikoak eta antikoagulatzailea diren farmakoak, besteak beste, indometazina, kurkumina, amoxizilina eta aspirina, immobilizatu direla klik erreakzio desberdinak erabiliz. Gainera, frogatu egin da erreakzio sekuentzialak pairatu daitezkeela CuAAC erreakzioa erabiliz. Hala ere, oraindik aztertu gabeko propietateak daude eta aplikazio pertsonalizatuetarako funtzionalizazio hobetuak lortzeko farmako-material konbinaketa berriak garatu daitezke.

Funtzio anitzeko materiala lortzeko erabilitako edozein gainazalean jarduera biologiko desberdina duen bigarren edo hirugarren farmako bat immobilizatu daiteke. Bestalde, nahiz eta farmakoen immobilizazioa eraginkorra dela frogatu, haien jarduera biologikoa ez da egiaztatu immobilizatu ondoren, beraz beharrezkoak diren saiakuntza egokiak burutu nahi dira.

Horrez gain, azido-ino eta tiol-ino erreakzioak ez bezala, amino-ino klik erreakzioaren ondoren lortutako C-N lotura itzulgarria izan daiteke baldintza espezifikoetan. Horrek immobilizatutako biomolekularen askapena suposa dezake. Erreakzio horri lotutako askapen-profila aztertzea funtsezkoa da estrategiaren ulermen integral eta erabilera eraginkorra lortzeko.

Ti6Al4V materialari dagokionez, frogatu egin da gainestaldura funtzional baten garapena monogeruza automuntatzaileen (SAM) eraketaren bidez, hala nola, silanoetan oinarritutako monogeruza eta fosfonatoetan oinarrititutako monogeruza, lor daitekeela. Lan honetan eztabaidatzen den moduan, fosfonatoek erresistentzia hidrolitiko handiagoa dute ingurune fisiologikoan silanoek baino, eta, horren ondorioz, gainazalaren estalduraren iraupena ebaluatzea beharrezkoa da. Beraz, gainestaldura horien degradazio-tasa epe luzean aztertzea eta bi estrategien konparaketa burutzea intrigarria litzateke, etorkizunean izan ditzaketen aplikazioen ikuspegi sakonagoa eskaintzeko.

Zauriak azkar sendatzeko premia dela eta, funtzio anitzeko eta aktiboaren diren gainestaldurak garatu nahi dira, bakterioen kontrako propietateaz gain, zauri-sentsoreak, haririk gabeko komunikazio eta neurrira egindako tratamenduaren ezaugarriak integratuz. Izan ere, frogatu egin da hazkuntza faktoreek zaurien sendatzeko propietateak hobetu ditzaketela. Beraz, peptidoen eta hazkuntza faktoreen immobilizazioak aurrerapen nabarmenak dakartza inplanteen funtzionaltasunen hobekuntzan, eta ondorioz, biomedikuntza arloan.

ANEXOS/ERANSKINAK

NMR Spectra

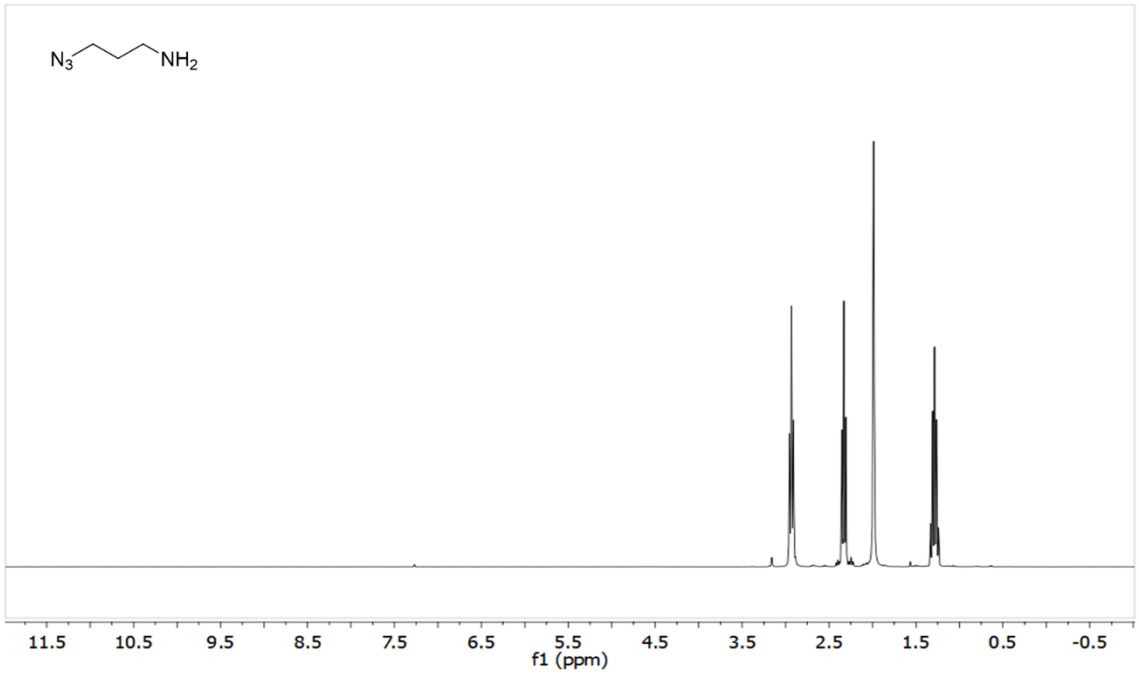

Figure SI-1. ^{1}H-NMR spectrum of 3-azidopropan-1-amine.

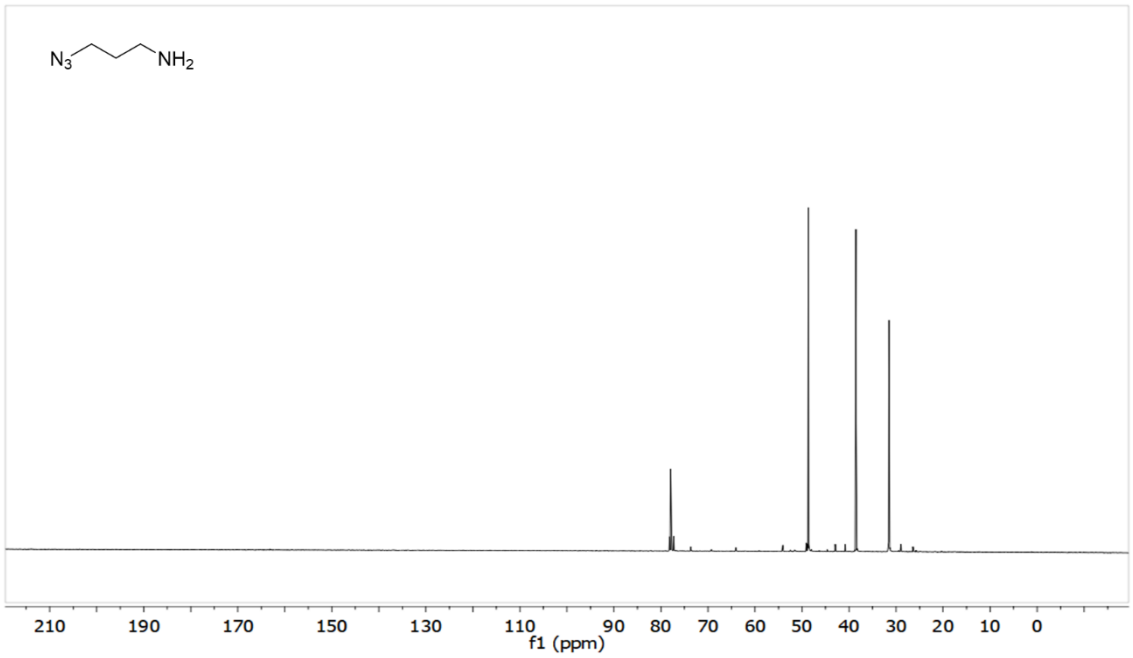

Figure SI-2. ^{13}C-NMR spectrum of 3-azidopropan-1-amine.

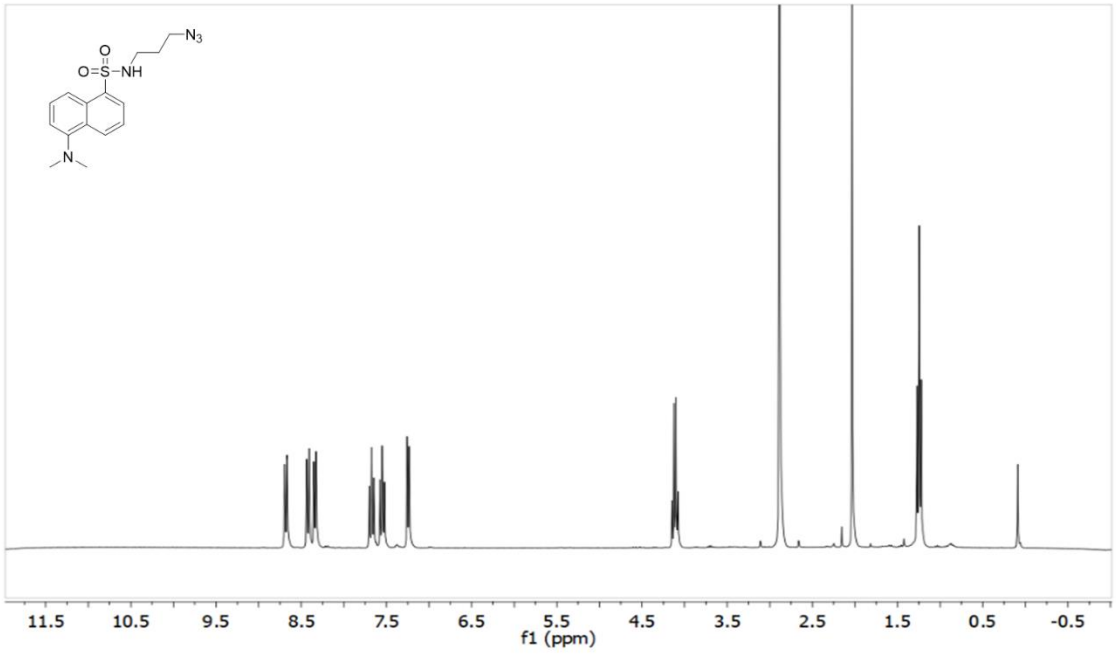

Figure SI-3. ^{1}H-NMR spectrum of *N*-(3-azidopropyl)-5-(dimethylamino)naphthalene-1-sulfonamide (**2a**).

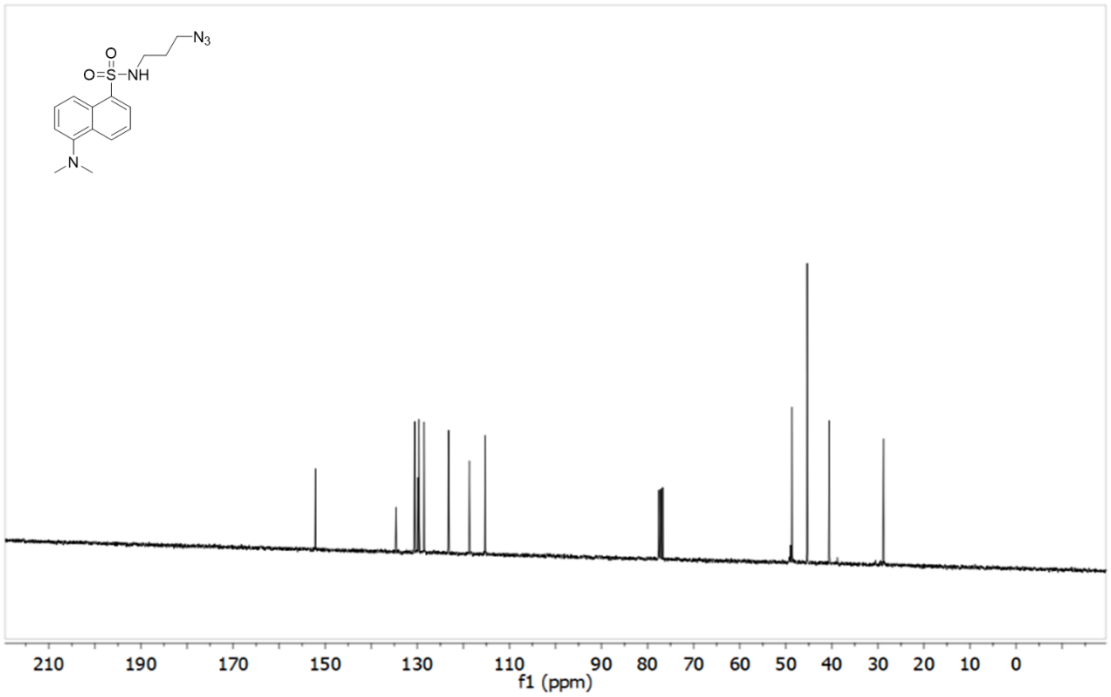

Figure SI-4. ^{13}C-NMR spectrum of *N*-(3-azidopropyl)-5-(dimethylamino)naphthalene-1-sulfonamide (**2a**).

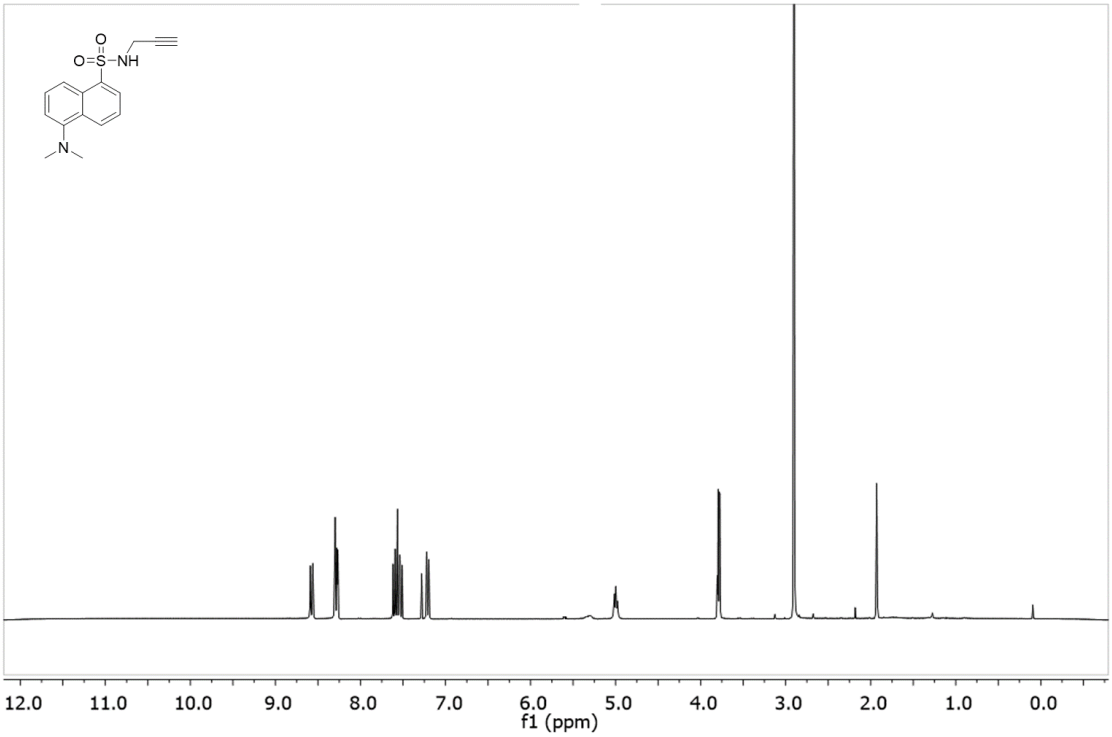

Figure SI-5. ^{1}H-NMR spectrum of 5-(dimethylamino)-*N*-(prop-2-yn-1-yl)naphthalene-1-sulfonamide (**2b**).

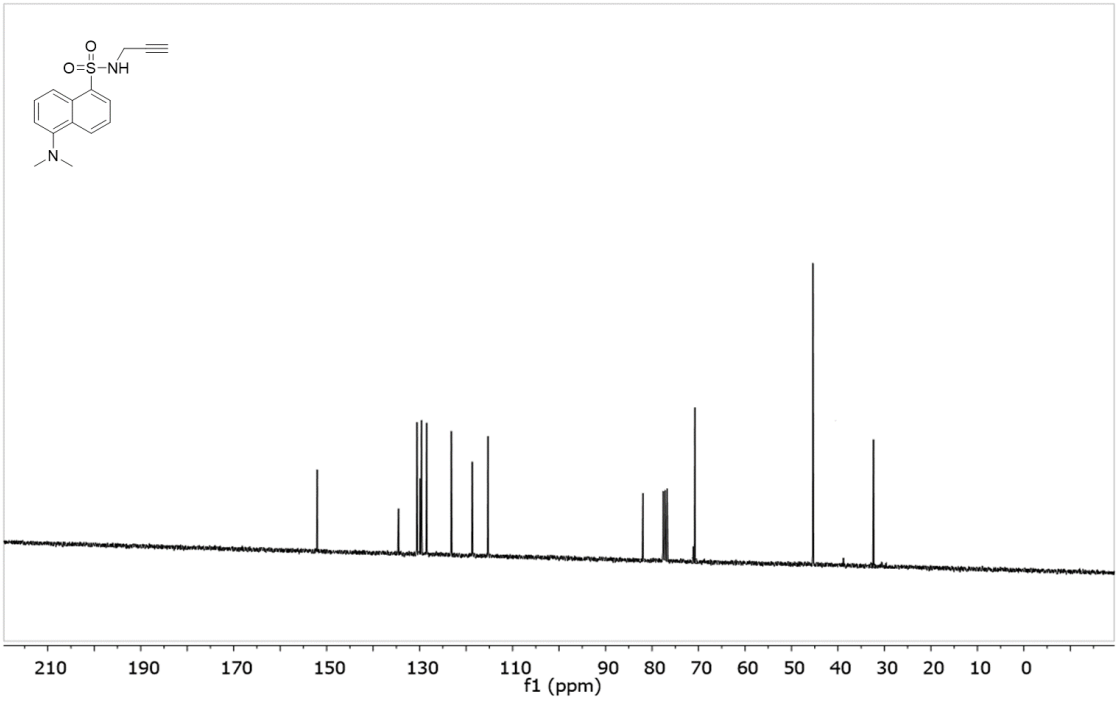

Figure SI-6. ^{13}C-NMR spectrum of 5-(dimethylamino)-*N*-(prop-2-yn-1-yl)naphthalene-1-sulfonamide (**2b**).

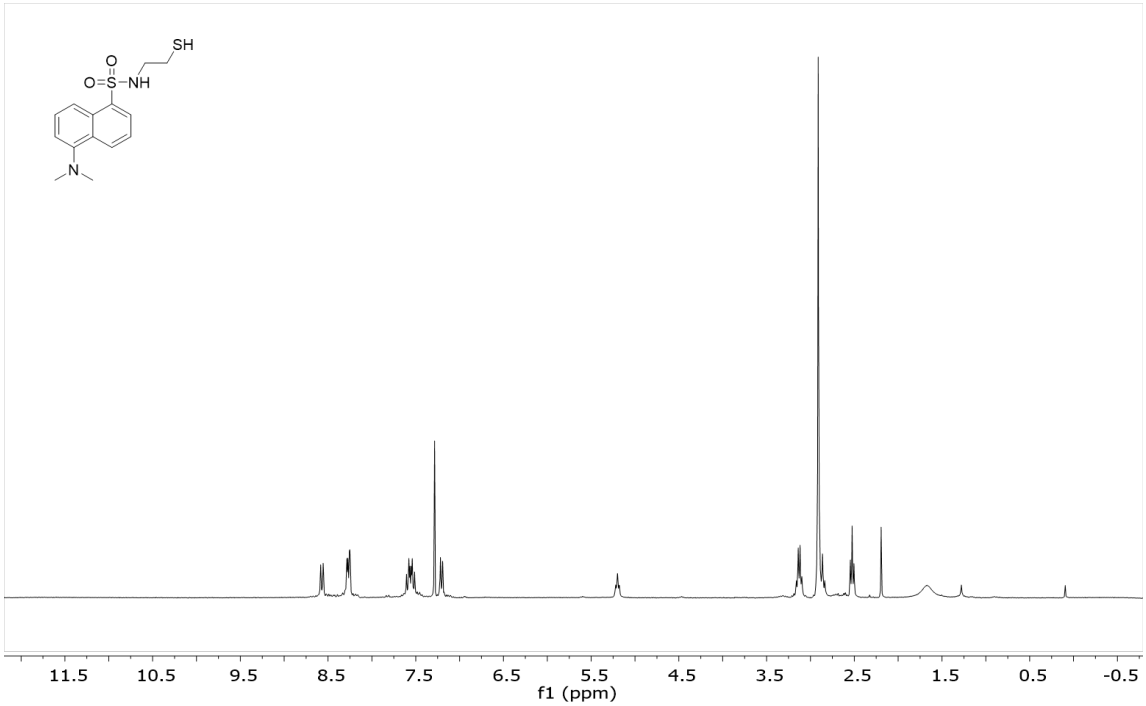

Figure SI-7. ^{1}H-NMR spectrum of 5-(dimethylamino)-*N*-(2-mercaptoethyl)naphthalene-1-sulfonamide (**2c**)

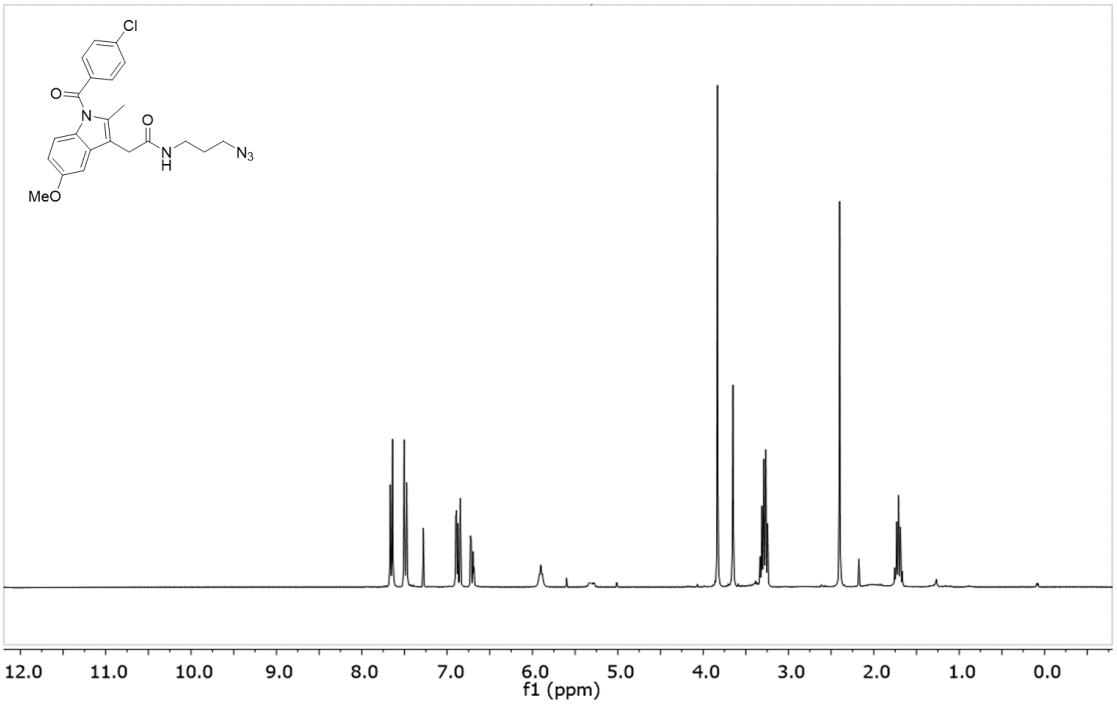

Figure SI-7.^{1}H-NMR spectrum of *N*-(3-azidopropyl)-2-(1-(4-chlorobenzoyl)-5-methoxy-2-methyl-1H-indol-3-yl)acetamide (**3a**).

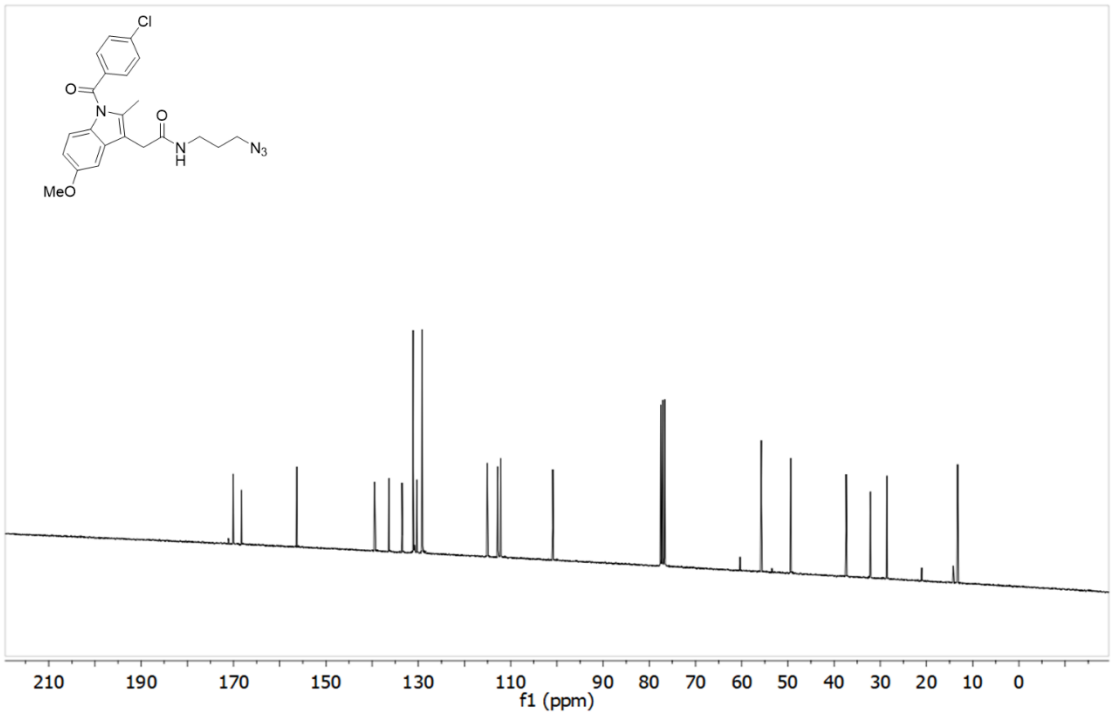

Figure SI-8. ^{13}C-NMR spectrum of *N*-(3-azidopropyl)-2-(1-(4-chlorobenzoyl)-5-methoxy-2-methyl-1H-indol-3-yl)acetamide(**3a**).

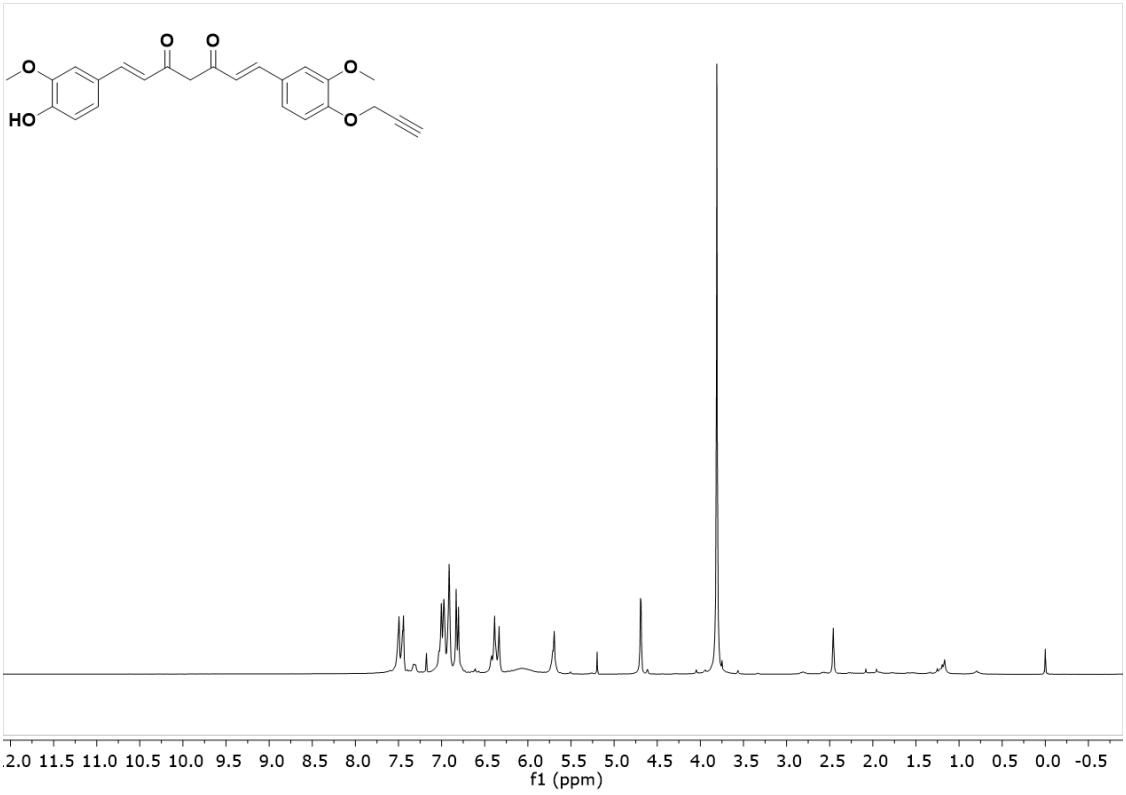

Figure SI-9. ^{1}H-NMR spectrum of (1*E*,6*E*)-1-(4-hydroxy-3-methoxyphenyl)-7-(3-methoxy-4-(prop-2-yn-1-yloxy)phenyl)hepta-1,6-diene-3,5-dione (**5a**).

Figure SI-10. ^{13}C-NMR spectrum of (1E,6E)-1-(4-hydroxy-3-methoxyphenyl)-7-(3-methoxy-4-(prop-2-yn-1-yloxy)phenyl)hepta-1,6-diene-3,5-dione (**5a**).

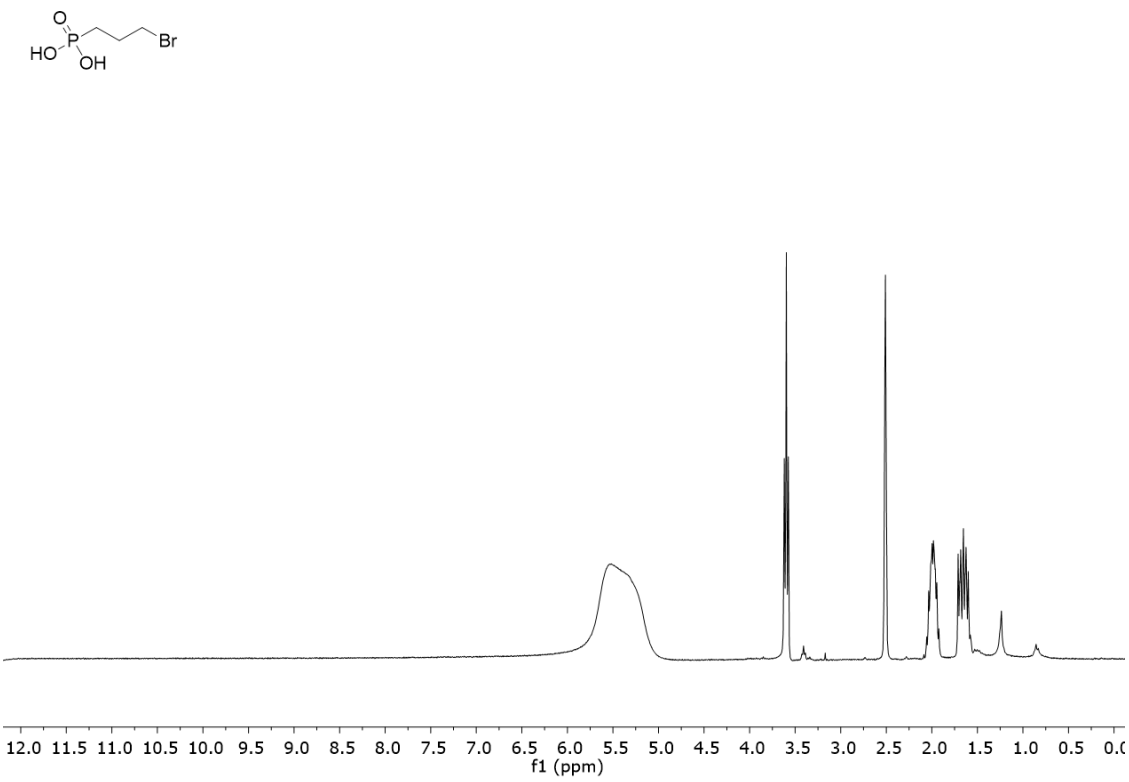

Figure SI-11. ^{1}H-NMR spectra of (3-bromopropyl)phosphonic acid.

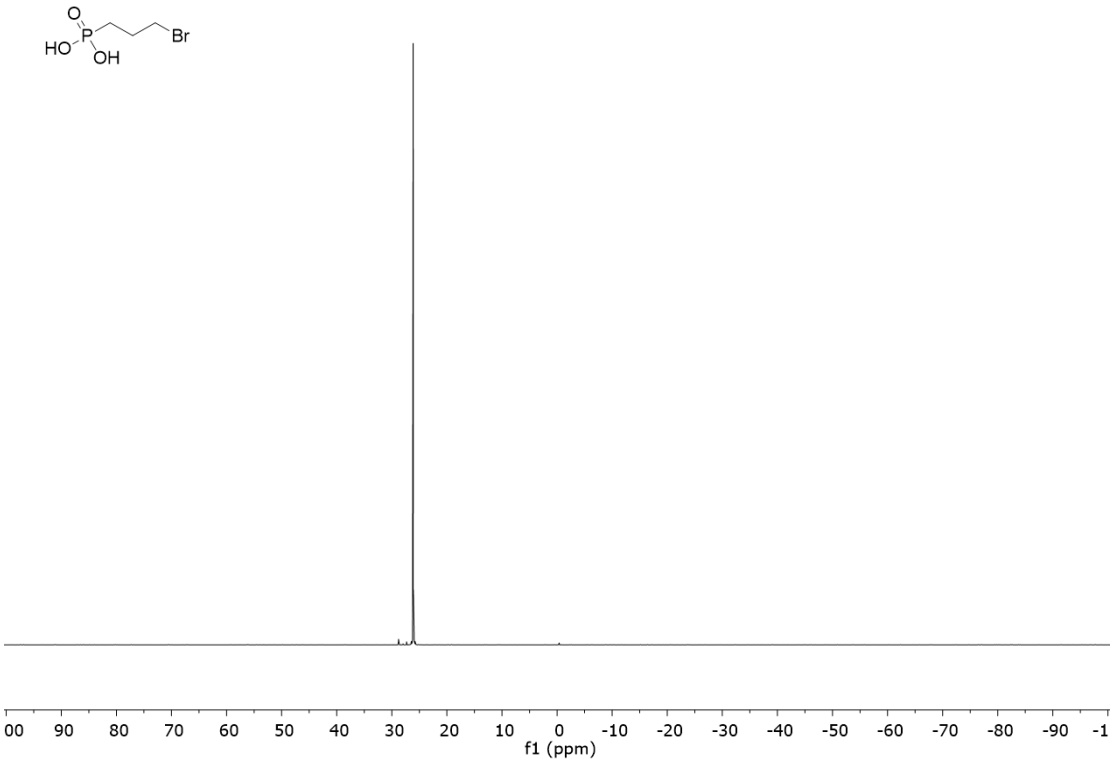

Figure SI-12. ^{31}P-NMR spectra of (3-bromopropyl)phosphonic acid.

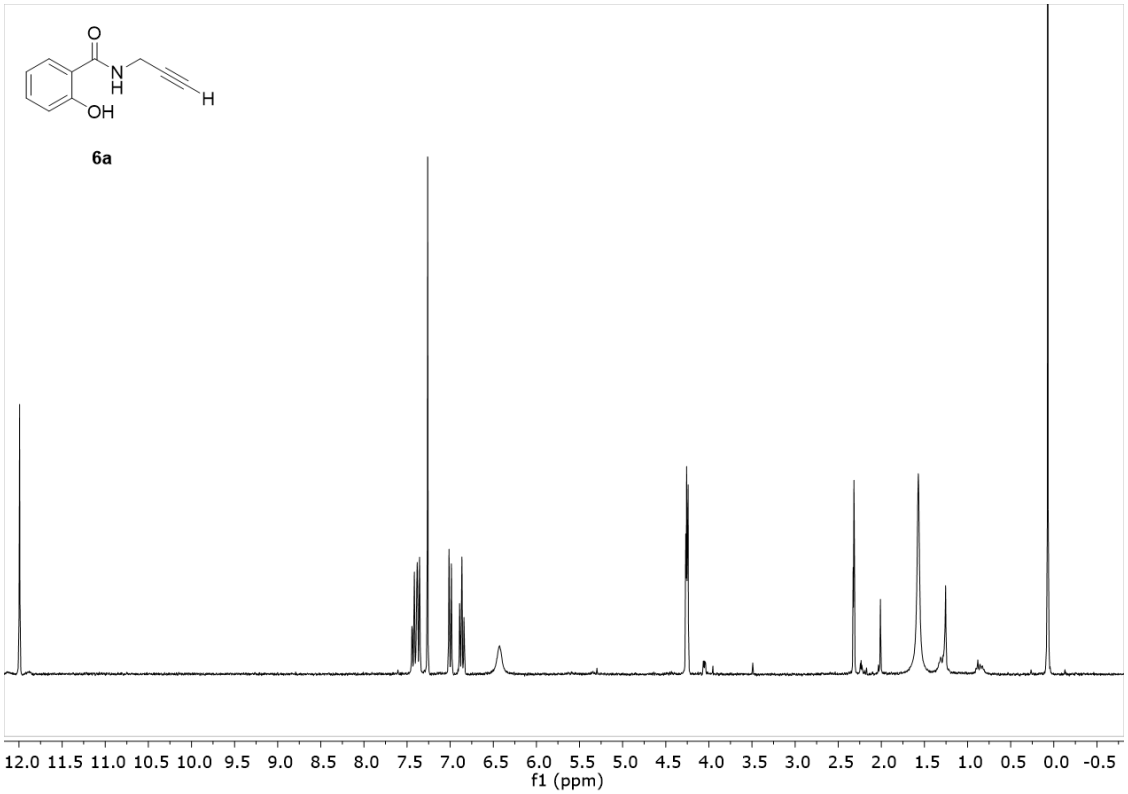

Figure SI-13. ^{1}H-NMR spectra of salicylic acid derivative **6a**.

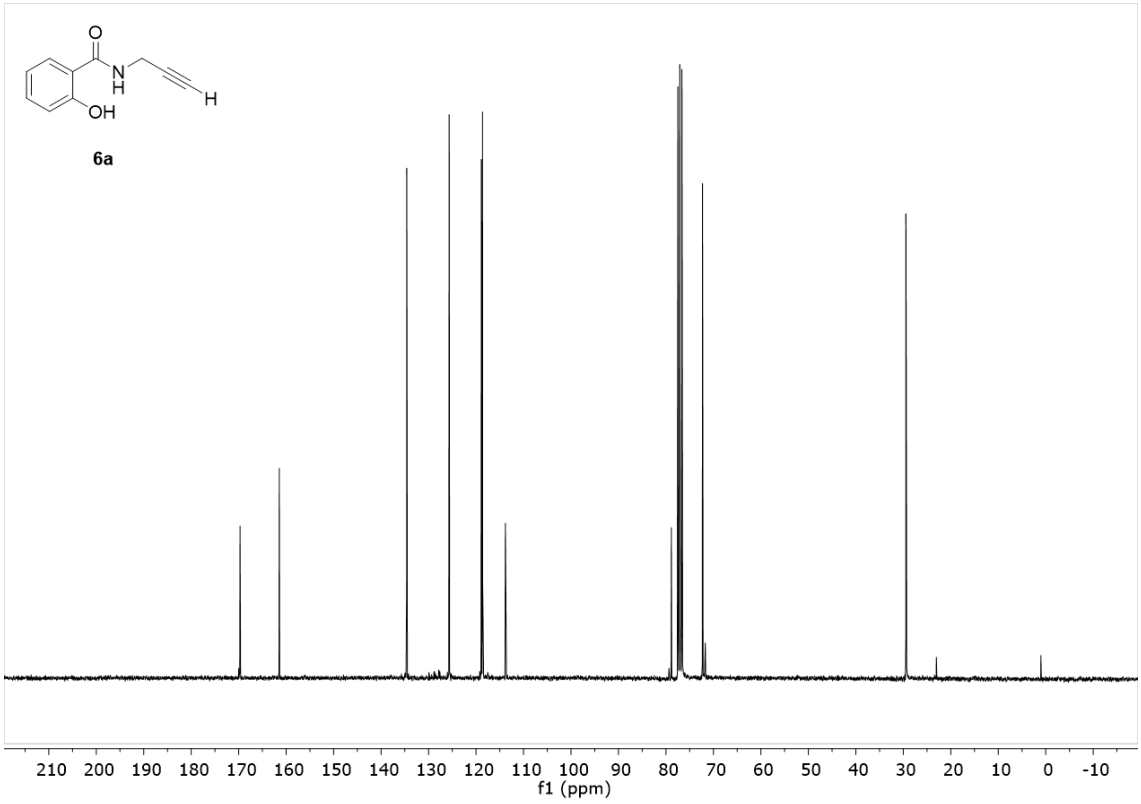

Figure SI-14. ^{13}C-NMR spectra of salicylic acid derivative **6a**.